

DECLARATION

This work has not previously been submitted for any degree and is not being concurrently submitted in candidature for any degree.

Signed _____



STATEMENT 1

This thesis is being submitted in partial fulfilment of the requirements for the degree of PhD.

**THE ROLES OF MAGMATISM, CONTAMINATION AND
HYDROTHERMAL PROCESSES IN THE DEVELOPMENT
OF PLATREEF MINERALIZATION,
BUSHVELD COMPLEX, SOUTH AFRICA**

STATEMENT 2

This thesis is being submitted in partial fulfilment of the requirements for the degree of PhD. Other sources are acknowledged by footnotes and giving explicit references. A reference list is appended.

Signed _____

David Holwell

STATEMENT 3

Submitted in partial fulfilment of the requirements for the degree of Ph.D.

Signed _____ (candidate)

Date, 3-11-06

November 2006

UMI Number: U584920

All rights reserved

INFORMATION TO ALL USERS

The quality of this reproduction is dependent upon the quality of the copy submitted.

In the unlikely event that the author did not send a complete manuscript and there are missing pages, these will be noted. Also, if material had to be removed, a note will indicate the deletion.



UMI U584920

Published by ProQuest LLC 2013. Copyright in the Dissertation held by the Author.
Microform Edition © ProQuest LLC.

All rights reserved. This work is protected against
unauthorized copying under Title 17, United States Code.



ProQuest LLC
789 East Eisenhower Parkway
P.O. Box 1346
Ann Arbor, MI 48106-1346

Acknowledgements

Firstly, many thanks to Iain, for his dedicated supervision of this project, for all his support, advice, technical expertise and especially his encouragement to continually publish the findings of this project. Thanks to all those in South Africa who were involved in the project and provided intellectual or logistical support, or entertainment, during the field seasons; in particular Anzie Jordaan, Richard Montjoie, Barry Jones, Alfred Sarila, Alan Bye, Robert Schouwstra, Jock Harmer and everyone at Wits Geosciences.

At Cardiff, thanks to Pete Fisher for his assistance in the SEM work, Tony Harris and Wes Gibbons for their assistance in unravelling metamorphic mineral assemblages, and to my office mates Alan and Rich for honing my indoor cricket skills, and to all the rest, for making the past three years such an enjoyable time.

Many thanks also to Adrian Boyce, another Glaswegian scholar and gentleman, for all his support, advice and logistical help in making trips to East Kilbride bearable.

Funding from the NERC and Anglo Platinum is greatly acknowledged through Industrial CASE project (NER/S/C/2003/11952), throughout the duration of the studentship, and for allowing me to return to South Africa to present the final thesis in person. Additional funding from the SEG and IOM³ are also acknowledged.

And finally, thanks to Jay, for all her support over the years, patient listening to my geological ramblings, and invaluable proof reading skills to make sure all the commas were put in the right place.

Abstract

The Platreef is a highly complex, pyroxenite-hosted Ni-Cu-PGE deposit. It is located at the base of the northern limb of the Bushveld Complex, South Africa, in direct contact with a variety of country rock sediments and Archaean basement. The interaction of the Platreef magma with these diverse country rock lithologies during emplacement had a profound effect on the style and distribution of the mineralization on both regional and local scales.

Geometrically, the Platreef was emplaced as a thin, sill-like intrusion, with pre-formed PGE-rich sulfide droplets entrained within the magma. Sulfur saturation is likely to have occurred in a deep staging chamber or conduit prior to emplacement, and where immiscible sulfide droplets became enriched in PGE, base metals and semi metals. After emplacement, the PGE and semi-metal rich sulfide liquid cooled to form 'primary' assemblages of IPGE-rich pyrrhotite, IPGE-, Rh- and Pd-rich pentlandite, chalcopyrite, Pt and Pd tellurides and bismuthides and electrum within the feldspathic pyroxenites of the Platreef.

Assimilation and metamorphism of some sedimentary footwall rocks, particularly the dolomites of the Malmani Subgroup, released large volumes of volatiles into the Platreef magma. This hydrothermal activity redistributed PGE and base metal sulfides (BMS) into the footwall rocks, and in places overprinted the 'primary' assemblages, and occasionally decoupled PGE from BMS, with the petrology of the reef and footwall, and the mineralogy of the platinum-group minerals, significantly affected. Each locality along the strike of the Platreef with a different footwall lithology has its own unique hydrothermal history directly related to the nature of the local floor rocks. For example, where the floor is composed of anhydrous basement gneiss, volatile activity was relatively insignificant, and partial melting of the floor allowed the percolation of PGE-rich sulfide liquid to penetrate the footwall.

The nature of the floor rocks also controls the type and amount of contamination in the Platreef. Sulfides in country rock shales, for example, are assimilated into the Platreef magma and locally upgrade the S content at such localities, although this did not trigger S saturation. Footwall sulfates, such as anhydrite, cannot be assimilated, but can interact with the Platreef sulfides through hydrothermal leaching when sufficient fluids had been released during assimilation.

After emplacement of the Platreef, a significant period of cooling occurred, such that the Platreef was almost completely crystallized, during which time some ductile deformation occurred. The gabbroic hangingwall magma was then emplaced, forming a magmatic unconformity over the Platreef, occasionally exploiting shear zones to intrude finger-like bodies down into the Platreef. Where the hangingwall magma assimilated mineralized Platreef thin zones of PGE mineralization developed at its base.

The magmatic intrusion of the Platreef can be considered to be distinct from that of other magmatic units in the northern limb of the Complex. Its Ni-Cu-PGE sulfide mineralization is orthomagmatic in origin; however, complex interaction with a variety of country rock lithologies has locally altered the style and distribution of the mineralization, to form unique mineralogical associations and assemblages along strike. The understanding of local country rock control on features such as the mineralogy of the ores and the extent of remobilization into the footwall is critical in optimizing exploration, mining and mineral processing techniques.

Contents

<u>Chapter 1. Introduction</u>	1
1.1 The platinum-group elements	2
1.2 Uses of PGE	3
1.3 Economic occurrences of PGE	4
1.4 Aims of the project	5
<u>Chapter 2. The Platreef</u>	6
2.1 The Bushveld Complex	7
2.1.1 Structural setting	8
2.1.2 Emplacement and magma source	10
2.2 The Northern limb	13
2.2.1 Stratigraphy of the northern limb	13
2.2.2. Age of the northern limb	16
2.3. The Platreef	17
2.3.1 Current state of research	17
2.3.2 Geology	19
2.3.2.1 Footwall lithologies	21
2.3.2.2 Platreef lithologies	21
2.3.3 Mineralization	25
2.3.4 Mineralization models and the role of contamination	26
2.3.5 Hydrothermal activity	29
2.3.6. Magmatic Emplacement	30
2.4 Introduction to and context of the papers in Chapters 3-8	32
<u>Chapter 3. Observations on the relationship between the Platreef and its hangingwall</u>	33
3.1 Abstract	34
3.2 Introduction	34
3.3 Methods	37
3.4 Lithological units	37
3.5 Observations	38
3.5.1 Macroscopic relationships	38
3.5.2 Petrography of the contact	40
3.5.3 PGE mineralization	40
3.5.4 Xenoliths	41
3.6 Discussion	41
3.6.1 Cross-cutting relationships	41
3.6.2 Chilling and erosion at the base of the hangingwall	42
3.6.3 PGE mineralization in the hangingwall	43
3.6.4 Source of calc-silicate xenoliths	44
3.6.5 Source of PGE in the Platreef	47
3.7 Conclusions	47
3.8 Acknowledgements	48
<u>Chapter 4. Three-dimensional mapping of the Platreef at the Zwartfontein South mine: implications for the timing of magmatic events in the northern limb of the Bushveld Complex, South Africa</u>	49
4.1 Abstract	50

4.2 Introduction	50
4.3 Geological setting of the Platreef	51
4.4 The Platreef at Zwartfontein South	53
4.4.1 Footwall lithologies	53
4.4.2 Platreef lithologies	53
4.4.3 Hangingwall lithologies	54
4.5 Mapping	54
4.6 Discussion	58
4.6.1 Timing of magmatic events:	58
4.6.2 Timing of deformation events	60
4.7 Conclusions	62
4.8 Acknowledgements	62
<u>Chapter 5. Platinum-group mineral assemblages in the Platreef at the Sandsloot Mine, northern Bushveld Complex, South Africa.</u>	63
5.1 Abstract	64
5.2 Introduction	64
5.3 Geology	66
5.3.1 Footwall lithologies	67
5.3.2 Igneous Platreef lithologies	68
5.3.3 Hangingwall lithologies	69
5.4 Mineralization	69
5.5 Platinum-Group Minerals	71
5.5.1 Grain size and morphology	73
5.5.2 Assemblages	74
5.5.2.1 Reef pyroxenites and pegmatites	75
5.5.2.2 Olivine-replaced reef	78
5.5.2.3 Reef clinopyroxenites	78
5.5.2.4 Footwall clinopyroxenites	79
5.5.2.5 Footwall calc-silicates	79
5.5.2.6 Footwall-reef hybrid	79
5.5.2.7 Footwall serpentinites	80
5.5.2.8 Hangingwall gabbro-norite	80
5.6 Discussion	82
5.7 Conclusions	86
5.8 Acknowledgements	88
<u>Chapter 6. Petrology, geochemistry and the mechanisms determining the distribution of Platinum-Group Element and Base Metal Sulphide mineralization in the Platreef at Overysel, northern Bushveld Complex, South Africa</u>	89
6.1 Abstract	90
6.2 Introduction	91
6.3 Materials and methods	93
6.4 Petrology	95
6.4.1 Footwall lithologies	95
6.4.2 Igneous Platreef lithologies	98
6.4.3 Hangingwall lithologies	103
6.5 Rare earth element geochemistry	103
6.6 PGE and BMS mineralisation	110
6.7 PGE geochemistry	113

6.8 Discussion	115
6.8.1 The PGE-S correlation	115
6.8.2 Distribution and fractionation of PGE into footwall	116
6.8.3 Hydrothermal redistribution	120
6.8.4 Chromitites	122
6.8.5 Comparison with other Platreef localities	123
6.9 Conclusions	125
6.10 Acknowledgements	127
<u>Chapter 7. Distribution of platinum-group elements in the Platreef at Overysel, northern Bushveld Complex: a combined PGM and LA-ICP-MS study.</u>	128
7.1 Abstract	129
7.2 Introduction	130
7.3 Samples and methods	131
7.4 Petrology and mineralogy	133
7.4.1 Footwall lithologies	133
7.4.2 Igneous Platreef lithologies	134
7.5 PGE mineralization	134
7.6 Platinum Group Mineralogy	135
7.6.1 Grain size and relative grain area	135
7.6.2 Assemblages	136
7.7 LA-ICP-MS analysis	141
7.8 PGE contents of BMS and other phases	144
7.8.1 Platreef feldspathic pyroxenites	144
7.8.2 Chromitites	146
7.8.3 Footwall gneisses	147
7.9 Mass balance	148
7.10 Discussion	150
7.10.1 The role of a sulfide liquid in Platreef PGE mineralization	150
7.10.2 Hydrothermal effects on PGM mineralogy	154
7.10.3 Chromitites and the timing of S saturation	155
7.10.4 Comparison with other Platreef localities and economic implications	157
7.11 Conclusions	158
7.12 Acknowledgements	159
<u>Chapter 8 Sulfur isotope variations within the Platreef: genetic implications for the origin of sulfide mineralization</u>	160
8.1 Abstract	161
8.2 Introduction	162
8.3 Sulfur Saturation and the use of Sulfur Isotopes	165
8.4 Previous Platreef S Isotope Work	166
8.5 Samples and Methods	169
8.6 Petrology and Mineralization	171
8.6.1 Sulfide mineralization	172
8.7 Analytical Results	175
8.7.1 Sandsloot	175
8.7.2 Zwartfontein	175
8.7.3 Overysel	175
8.7.4 Witrivier	179

8.7.5 La Pucella	181
8.8 Discussion	181
8.8.1 Magmatic S isotope signatures	181
8.8.2 Non-magmatic S isotope signatures	182
8.8.3 S isotope variations along strike	188
8.8.4 The sources of S in the Platreef	189
8.8.5 Mechanisms of S saturation in the Platreef	190
8.8.6 A genetic model for Platreef mineralization	192
8.9 Conclusions	196
8.10 Acknowledgements	197
<u>Chapter 9. Discussion and Conclusions</u>	198
9.1 Introduction	199
9.2 Magmatic emplacement	199
9.3 Source of sulfide	201
9.4 'Primary' Platreef mineralization	202
9.5 Contamination	203
9.6 Hydrothermal activity and redistribution of PGE into footwall rocks	204
9.7 Conclusions	206
<u>References</u>	209
<u>Appendices:</u>	
Appendix 1. Geological face maps from the Sandsloot and Zwartfontein South pits	222
Appendix 2. Whole-rock geochemical data	230
Appendix 3. LA-ICP-MS analyses of sulphides	239
Appendix 4. Mineral chemistry	242
Appendix 5. Geochemistry and mineralogy of the Platreef and "Critical Zone" of the northern lobe of the Bushveld Complex, South Africa: implications for Bushveld stratigraphy and the development of PGE mineralisation.	261

List of Figures

Figure 1.1. Demand by application of the Pt, Pd and Rh for 2005 (data from Kendall, 2006).	3
Figure 2.1. Geological map of the Bushveld Complex (after Kinnaird <i>et al.</i> , 2005).	8
Figure 2.2. Tectomagmatic evolution of the Kaapvaal Craton. After Silver <i>et al.</i> (2004).	9
Figure 2.3. Gravity map of the Bushveld Complex, showing the outline of surface outcrop, and the large gravity anomaly close to Mokopane (after Cawthorn and Webb, 2001).	11
Figure 2.4. Geological map of the northern limb of the Bushveld Complex (after Ashwal <i>et al.</i> , 2005).	14
Figure 2.5. Traditional correlation of stratigraphy of the eastern and western limbs of the Bushveld Complex, and the northern limb, with an inferred correlation between the Platreef with the Merensky Reef (after White, 1994).	15
Fig. 2.6. Geological map of the Platreef showing the different footwall units along strike and the farms referred to in the text. The map on the right hand side shows in detail the field area for this study, including the Sandsloot and Zwartfontein South pits.	18
Figure 2.7. Summary figure showing the geology and mineralization types along the strike of the Platreef.	20
Figure 3.1. Geological map of the Platreef showing localities referred to in the text. After Kinnaird and Nex (2003), von Gruenewaldt <i>et al.</i> (1989) Hammerbeck and Schürmann (1998).	36
Figure 3.2. Photograph and map showing a face in the south-western part of the Sandsloot pit showing an exposed section of olivine replaced reef, displaying a distinct darkening and different fracture pattern to the surrounding lithologies. The replaced reef is truncated at a magmatic contact with the hangingwall gabbronorite.	39
Figure 3.3. Composite photograph of a thin section showing the contact between fine-grained, hangingwall poikilitic leuconorite (upper half of photograph) and coarse-grained, mineralized Platreef feldspathic pyroxenite (lower half).	40
Figure 3.4. Schematic representation of the possible nature of the Platreef-hangingwall contact and the localization of hangingwall PGE mineralization in gabbronorite that directly overlies mineralized Platreef pyroxenite.	44
Figure 4.1. Geological map of the central portion of the Platreef showing the location of the Zwartfontein South pit.	51
Figure 4.2: Geological face maps and plan map from bench 222 at the Zwartfontein South pit. The plan map is the surface corresponding to the tops of the bench faces mapped.	55
Figure 4.3. Three dimensional schematic representation of the stages involved in the intrusion of the Platreef and hangingwall gabbronorite in the area mapped at Zwartfontein South.	60
Figure 5.1. Geological map of the central and southern sections of the northern limb of the Bushveld Complex, showing the Platreef and localities and lithologies referred to in the text.	

After Kinnaird and Nex (2003), von Gruenewaldt <i>et al.</i> (1989), Hammerbeck and Schürmann (1998).	65
Figure 5.2. Simplified stratigraphic representation showing all major rock units in the southwestern, central and northern parts of the Sandsloot pit.	67
Figure 5.3. A. Thin section of olivine replaced reef showing olivine overprinting orthopyroxene (opx); in cross-polarized transmitted light. B-D: Backscattered electron photomicrographs of: B and C, typical association of base-metal sulfides (BMS) intergrown with altered plagioclase (alt plag) at the edge of the interstitial region enclosing cumulus, sulfide-free orthopyroxene in Platreef pyroxenites at Sandsloot. D: typical association of discreet BMS grains with unaltered plagioclase (plag) from the Merensky Reef in the eastern Bushveld for comparison.	70
Figure 5.4. Range of PGM grain size (longest axis) in the various host rock lithologies at Sandsloot.	74
Figure 5.5. Backscattered electron photomicrographs of PGM found in Sandsloot Platreef samples.	77
Figure 6.1. Geological map of the Platreef, showing farms referred to in the text, together with a detailed map of the Sandsloot-Overysel area showing the locality of boreholes OY335 and OY387 and the 1980 shaft, based on field mapping and published maps of the Geological Survey of South Africa.	92
Figure 6.2. Stratigraphic logs of borehole cores OY335 and OY387 showing the positions of the samples and zones of visible BMS-PGE mineralization.	94
Figure 6.3. Thin section photographs of some of the lithologies present at Overysel.	97
Figure 6.4. Net-textured sulfides within the gneisses (sample OY387-378) showing concave boundaries of interconnected BMS blebs both at quartz and plagioclase grain boundaries (lower part of image), and within silicates (upper part of image).	97
Figure 6.5. Chromitites obtained from the underground workings on Overysel.	101
Figure 6.6. Chondrite-normalized REE plots for <i>a</i> : Platreef and hangingwall rocks from the OY335 core; <i>b</i> : footwall rocks from the OY335 core; <i>c</i> : Platreef and hangingwall rocks from the OY387 core; <i>d</i> : footwall rocks from the OY387 core; <i>e</i> : Platreef pyroxenites and footwall calc-silicates from Sandsloot (from McDonald <i>et al.</i> 2005); <i>f</i> : Upper, Middle and Lower Platreef rocks from Townlands (from Manyeruke <i>et al.</i> 2005). Normalising factors are from Taylor and McLennan (1985).	105
Figure 6.7. Distribution profiles with depth for <i>a</i> : S, Pd, Pt and Rh for the OY335 core; <i>b</i> : S, Cu and Ni for the OY335 core; <i>c</i> : S, Pd, Pt and Rh for the OY387 core; and <i>d</i> : S, Ni and Cu for the OY387 core.	111
Figure 6.8. Selected PGE ratios with depth through core OY387. Note the different logarithmic horizontal scales.	113
Figure 6.9. Chondrite-normalized PGE profile ranges of <i>a</i> : Overysel reef pyroxenite, upper gneisses, and lower gneisses and granite with individual profiles for the chromitiferous samples OY08C (chromitite band), OY16 (feldspathic chromitite) and OY335-303 (chromitiferous quartzo-feldspathic pyroxenite); and <i>b</i> : all reef, footwall and hangingwall at Sandsloot and Zwartfontein South.	115

Figure 6.10. Schematic model for the distribution of PGE-rich sulfides into the footwall at Overysel.	118
Figure 7.1. Geological map of the Platreef, showing the locality of boreholes OY335 and OY387, the 1980 shaft and farms referred to in the text. Based on field mapping and published maps of the Geological Survey of South Africa.	130
Figure 7.2. Stratigraphic logs of borehole cores OY335 and OY387 showing the positions of the samples and zones of visible BMS-PGE mineralization.	132
Figure 7.3. Backscattered scanning electron micrographs of: (a): typical association of PGM at the contact between BMS and silicates, (b): Enlarged area from A, (c): typical association of PGM located at the edge of BMS grains within footwall gneiss, (d): polyphase PGM enclosed within quartz in a sample of mineralized basement granite, (e): exsolution lamellae of pentlandite within pyrrhotite in a sample of massive sulfide. (f): enlarged view of massive sulfide showing the association of moncheite with exsolved pentlandite within pyrrhotite.	139
Figure 7.4. PGE contents of pyrrhotite and pentlandite grains plotted as: (a) Ir vs Os, (b) Ir vs Ru, (c) Ir vs Rh, (d) Ir vs Pd; (e) Ir vs Ni for pyrrhotite and (f) Pd vs Rh for pentlandite.	144
Figure 7.5. Selected TRA spectra for: (a) pyrrhotite, (b) pentlandite and (c) chalcopyrite with PGM from the Platreef pyroxenites; (d) pentlandite with PGM, (e) composite pyrrhotite-pentlandite, (f) composite pyrrhotite-pentlandite-chalcopyrite with PGM.	145
Figure 7.6. Chondrite normalized diagrams of average PGE in (a) pyrrhotite and bulk sulfide recalculated to 100% sulfide (po+pn) for Overysel Platreef pyroxenites, and (b) pentlandite and bulk sulfide recalculated to 100% sulfide (po+pn and pn only) for Overysel Platreef pyroxenites, (c) pyrrhotite and bulk sulfide recalculated to 100% sulfide (po+pn) for the Merensky Reef (d) pentlandite and bulk sulfide recalculated to 100% sulfide (po+pn) for the Merensky Reef. Merensky Reef data from Ballhaus and Sylvester (2000).	150
Figure 7.7. Schematic representation of the partitioning behaviour of the PGE within cooling droplets of sulfide within the Platreef magma.	154
Figure 8.1. Geological map of the Bushveld Complex showing the location of the northern limb and the Klipspringer kimberlite (after Kinnaird <i>et al.</i> , 2005).	162
Figure 8.2. Geological map of the northern limb of the Bushveld Complex showing the localities referred to in the text (after van der Merwe, 1978).	164
Figure 8.3. Summary of previous S isotope data on the Platreef and sulfide inclusions in diamonds from the nearby Klipspringer kimberlite.	167
Figure 8.4. Schematic cross section showing the major lithologies encountered along strike of the Platreef and the corresponding positions of the sample localities.	169
Figure 8.5. Backscattered electron photomicrographs of sulfides from the Platreef.	174
Figure 8.6. Range in $\delta^{34}\text{S}$ values for sulfides within each rock type and an indication on their paragenesis based on textural evidence and host rock lithology from (A): the Sandsloot pit; (B): the Zwartfontein South pit; (C): borehole cores OY335 and OY387 from Overysel; and (D): borehole core PR351 from Witrivier.	178

Figure 8.7. Variations in $\delta^{34}\text{S}$ for sulfides with depth in metres in the boreholes cores (A): OY335 from Overysel; (B): OY387 from Overysel; and (C): PR351 from Witrivier.	180
Figure 8.8. Genetic model for the intrusion and mineralization in the Platreef, with the presence of a deep, intermediate magma chamber.	194
Figure 8.9. Ni vs Fo content for Lower Zone olivines from the northern limb, from Hulbert (1983). Eastern Bushveld data from Cameron (1978). Field for layered intrusion from Simpkin and Smith (1970).	195
Figure 9.1. Model for the formation of the northern limb of the Bushveld Complex.	207

List of Tables

Table 1.1 Physical properties of the platinum-group elements (after Westland, 1981).	2
Table 5.1. Pt/Pd ratios and relative grade for selected hangingwall (HW), reef and footwall (FW) samples.	71
Table 5.2. Name and ideal formulae of all occurrences of PGM and Au-Ag minerals in the variety of host-rock types.	72
Table 5.3. Proportions of PGM type within each lithology in percentage of the total area of PGM.	75
Table 5.4. Textural associations of PGM (excluding Au/Ag alloy) in the variety of host-rock types in percentage number of grains.	76
Table 5.5. Compositions of unnamed Pd-germanide phase from the base of the hangingwall gabbronorite, together with the ideal compositions of Pd_2Ge and $\text{Pd}_{11}\text{Ge}_5$.	81
Table 6.1. Representative analyses of chromite grains within Platreef rocks from Overysel.	102
Table 6.2. Geochemical data for all samples from the OY335 and OY387 cores and chromitite samples from the underground workings on Overysel.	106
Table 6.3. Indications of PGE grade, PGE sloping profiles (Pt+Pd)/(Ir+Ru) and S contents of samples from the Overysel cores and chromitite grab samples, together with Ni/Cu, Ni/S and Cu/S ratios.	112
Table 7.1. List of all PGM identified, together with ideal formulae, and number of occurrences within the lithologies in the Overysel cores.	136
Table 7.2. Proportions of PGM type within each lithology in the Overysel cores, in percentage of the total area of 100% PGM.	137
Table 7.3. Associations of all PGM and Au, Ag phases, Pt dominant phases only, and Pd dominant phases only within each lithology in the Overysel cores in percentage of the number of grains.	137
Table 7.4. Compositions of base metal sulfides from the Platreef at Overysel and Sandsloot as determined by LA-ICP-MS analysis.	142
Table 7.5. Experimentally derived partition coefficients for the noble metals between monosulfide solid solution and sulfide liquid (900-1200°C).	151
Table 8.1. Results of all conventional (c) and laser (l) S isotope analyses for Platreef sulfides together with whole rock S concentrations where available from Sandsloot, Zwartfontein, Overysel and Witrivier, and Archaean basement rocks from Witrivier and La Pucella.	176

Chapter 1

Introduction

1.1 The platinum-group elements

The transition elements ruthenium (atomic number 44), rhodium (45), palladium (46), osmium (76), iridium (77) and platinum (78) occupy the second and third rows of Group VIII of the periodic table and are referred to as the platinum-group elements (PGE) and are often grouped together with gold and silver and termed 'precious' or 'noble' metals. They can be divided into a light triad (Ru, Rh and Pd) and a heavy triad (Os, Ir and Pt). The light triad have densities roughly half that of the heavy triad. Platinum and Pd are relatively soft and ductile. In contrast, Ru and Os are hard and brittle and are thus of limited industrial use. Table 1.1 shows some physical properties of the PGE.

Table 1.1 Physical properties of the platinum-group elements (after Westland, 1981).

Property	Ru	Rh	Pd	Os	Ir	Pt
Atomic number	44	45	46	76	77	78
Atomic weight	101.07	102.94	108.42	190.23	192.22	195.08
Density at 20°C (kgm ⁻³ *10 ⁻³)	12.2	12.4	12.0	22.5	22.4	21.5
Melting point (°C)	2334	1967	1555	3050	2454	1768
Boiling point (°C)	3900	3727	3140	5027	4130	3827
Resistivity at 0°C (μΩcm)	6.80	4.33	9.93	8.12	4.71	9.85
Hardness (annealed, VHN)	200-350	100-102	40-42	300-670	200-240	40-42
Atomic radius (cm ⁻⁸)	1.336	1.342	1.373	1.350	1.355	1.385
Oxidation state (common)	+3	+3	+2	+4	+3	+2
(highest)	+8	+6	+4	+8	+6	+6

Chemically, the PGE show highly siderophile tendencies in the presence of Fe metal, and are also mutually soluble in one another. The PGE are relatively unreactive in dilute acids and alkalis, but can be dissolved slowly in concentrated acid, in particular Pt and Pd are more reactive in this sense than the other PGE and are readily dissolved in aqua regia. At elevated temperatures, the PGE all react with oxygen to yield volatile oxides and with the halogens to produce PGE halide compounds such as hexafluorides and chlorides. In addition, and perhaps most importantly in the formation of natural platinum-group minerals (PGM), the PGE will dissolve in molten bases of the P block of the periodic table and form a wide range of sulfides, tellurides, arsenides, bismuthides, antimonides, and selenides.

1.2 Uses of PGE

The current principal uses for the most industrially important PGE: Pt, Pd and Rh, as stated by Kendall (2006), are shown in Fig. 1.1. Platinum is used principally as an autocatalyst and in jewellery, with industrial uses including the production of computer hard disks and liquid crystal displays (LCDs), and in petroleum refining. Other uses include dental alloys, spark plugs, turbine blades and in biomedical components and drugs, including the anti-cancer drug cisplatin. Around half of the demand for palladium is for autocatalysts, with jewellery, electronics and dental uses also important. Rhodium is also principally used as an autocatalyst, and also has minor demand in the glass industry for the manufacture of LCDs. Ruthenium is used in electronic applications such as computer hard disks, and the major use of iridium is in the manufacture of crucibles for the production of high quality single crystals, and together with ruthenium as a catalyst in the production of acetic acid.

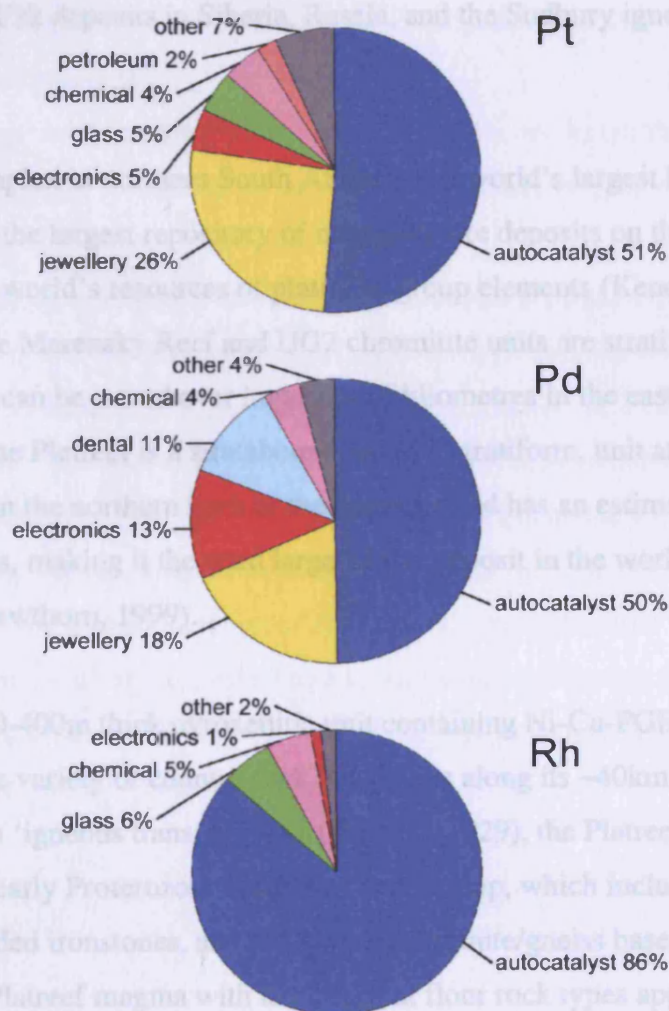


Figure 1.1. Demand by application of the Pt, Pd and Rh for 2005 (data from Kendall, 2006).

1.3 Economic occurrences of PGE

The PGE commonly occur together in nature and are among the scarcest of the metallic elements, usually present in concentrations of a few parts per billion, or less, in most rocks. This, together with their range of industrial and social applications outlined above make the PGE highly expensive commodities. Over the past five years the price of platinum has more than doubled, and throughout 2006, Pt was consistently trading at around the \$US1000 per troy ounce mark, double that of gold, with Pd around US\$300/oz and Rh approaching US\$5000/oz. There are very few major occurrences of PGE in the Earth's crust, and the most economic are in mafic layered igneous intrusions where they may attain concentrations around a few parts per million. By far the greatest of these deposits in terms of PGE content is the Bushveld Complex in South Africa, with the Great Dyke in Zimbabwe and the Stillwater Complex in Montana, USA, minor contributors. The PGE, and in particular Pd, are also significant by-products in large magmatic Ni-Cu sulfide deposits, the most significant of which are the Noril'sk deposits in Siberia, Russia, and the Sudbury igneous complex in Ontario, Canada.

The Bushveld Complex in northern South Africa is the world's largest layered igneous intrusion as is also the largest repository of magmatic ore deposits on the planet. It hosts around 75% of the world's resources of platinum-group elements (Kendall, 2006) in three major deposits. The Merensky Reef and UG2 chromitite units are stratiform layers located in mafic rocks which can be traced over hundreds of kilometres in the eastern and western limbs of the Complex. The Platreef is a stratabound, but not stratiform, unit at the base of the igneous sequence in the northern limb of the complex and has an estimated Pt+Pd reserve of 16.3 million ounces, making it the third largest PGE deposit in the world after the UG2 and Merensky Reef (Cawthorn, 1999).

The Platreef is a 10-400m thick pyroxenitic unit containing Ni-Cu-PGE mineralization that has intruded a wide variety of country rock lithologies along its ~40km strike length. In what has been termed an 'igneous transgression' (Wagner, 1929), the Platreef overlies sediments of the late Archaean-early Proterozoic Transvaal Supergroup, which include quartzites, shales, dolomites and banded ironstones, and the Archaean granite/gneiss basement complex. The interaction of the Platreef magma with the different floor rock types appears to have had

profound effects on the style and distribution of the mineralization on both a local and regional scale.

1.4 Aims of the project

This project aims to assess the roles that magmatism, contamination and hydrothermal activity have played during the development of Platreef mineralization. The research focuses on four main areas:

- Detailed geological mapping in open pit mines to provide the sound geological context to be able to apply any further petrological or geochemical interpretation to overall models. In particular the mapping provides a solid basis for determining the relative timings of events.
- Combined petrological and geochemical studies to assess the magmatic and hydrothermal processes involved in both the origin and nature of the Platreef magma, and the ore-forming sulfide liquid.
- Sulfur isotope work on the Platreef sulfides in order to determine the origin of the sulfur, the timing of S saturation and the extent of any contamination in the development sulfide mineralization.
- Detailed mineralogical studies and laser-ablation ICP-MS techniques on the mineralogy of the ore minerals to determine the mechanisms of precious metal enrichment in the Platreef, the partitioning behaviour of the PGE within the sulfides and to identify and assess to the effects of hydrothermal redistribution.

The nature of contamination and hydrothermal activity is directly dependant on the interaction of the variety of floor rock lithologies with the Platreef magma. The field area for this study encompasses a section of the Platreef where the floor rocks differ substantially and so all of the above factors can be assessed on a metre and kilometre scale, to determine the control that footwall lithology has on each aspect of the mineralization in this enigmatic deposit.

Chapter 2

The Platreef

2.1 The Bushveld Complex

The Bushveld Complex is located in the northeastern part of South Africa to the north of the city of Johannesburg. It is the world's largest layered igneous intrusion and is made up of a succession of mafic and ultramafic cumulates 7-8km thick and covers an area of approximately 65,000km². It is the largest repository of magmatic ore deposits on Earth, and currently produces around 75% of the world's platinum-group elements (PGE) (Kendall, 2006). It was intruded into the Kaapvaal Craton around 2.06Ga (Walraven *et al.*, 1990), and the country rocks in most parts of the complex are sediments of the 2.1-2.3Ga Pretoria Group, which is part of the lower Proterozoic Transvaal Supergroup. In the South African stratigraphic literature, the Bushveld Complex comprises of (Fig. 2.1):

- a suite of mafic sills intruded into the Transvaal Supergroup;
- the felsic and minor basic volcanics of the Rooiberg Formation;
- the layered mafic and ultramafic rocks of the Rustenburg Layered Suite;
- intrusive acid rocks of the Rashedoop Granophyre Suite, and;
- the Lebowa Granite Suite.

However, in much of the scientific literature and subsequently in this study also, the term Bushveld Complex refers to just the layered ultramafic/mafic sequence of the Rustenburg Layered Suite (RLS).

The RLS crops out in three distinct limbs: the western limb, around Rustenburg; the eastern limb, around Burgersfort; and the northern limb, from Mokopane (formerly Potgietersrus) to Villa Nora (Fig. 2.1). An extension of the western limb north of Zeerust, referred to as the far western limb, and an extension of the eastern limb beneath cover rocks, identified by gravity data in the south east, referred to as the southern, or Bethal limb, are also recognized (Eales and Cawthorn, 1996). The giant deposits of PGE, chromium and vanadium are all hosted in the RLS. The world class PGE deposits of the Merensky Reef and UG2 chromitite are located in the eastern and western limbs and the Platreef in the northern limb. The RLS in the western and eastern limbs is traditionally divided into five zones, originally defined by Hall (1932), comprising a Marginal Zone of norites, Lower Zone pyroxenites and harzburgites, Critical Zone chromitite-pyroxenite-norite cyclic units, Main Zone gabbronorites and Upper Zone anorthosites, gabbronorites and magnetites (Fig. 2.2). The similarity between the two limbs which includes the correlation of marker horizons such as the Merensky Reef chromitites led Hall (1932) to conclude they were originally connected. Meyer and de Beer (1987) used the

absence of a positive gravity anomaly between the two limbs as evidence for two discrete, inwardly-dipping sheets. Cawthorn and Webb (2001), however, showed that a mass of magma such as that in the BIC would have caused isostatic subsidence, thus cancelling out the expected gravity anomaly. This led the authors to favour the original interpretation of Hall (1932), stating that considering the remarkable similarities between limbs separated by over 100km, a much more petrologically plausible explanation is that the eastern and western limbs of the complex formed as a single lopolithic intrusion, that has been subsequently downwarped and is presently connected at depth.

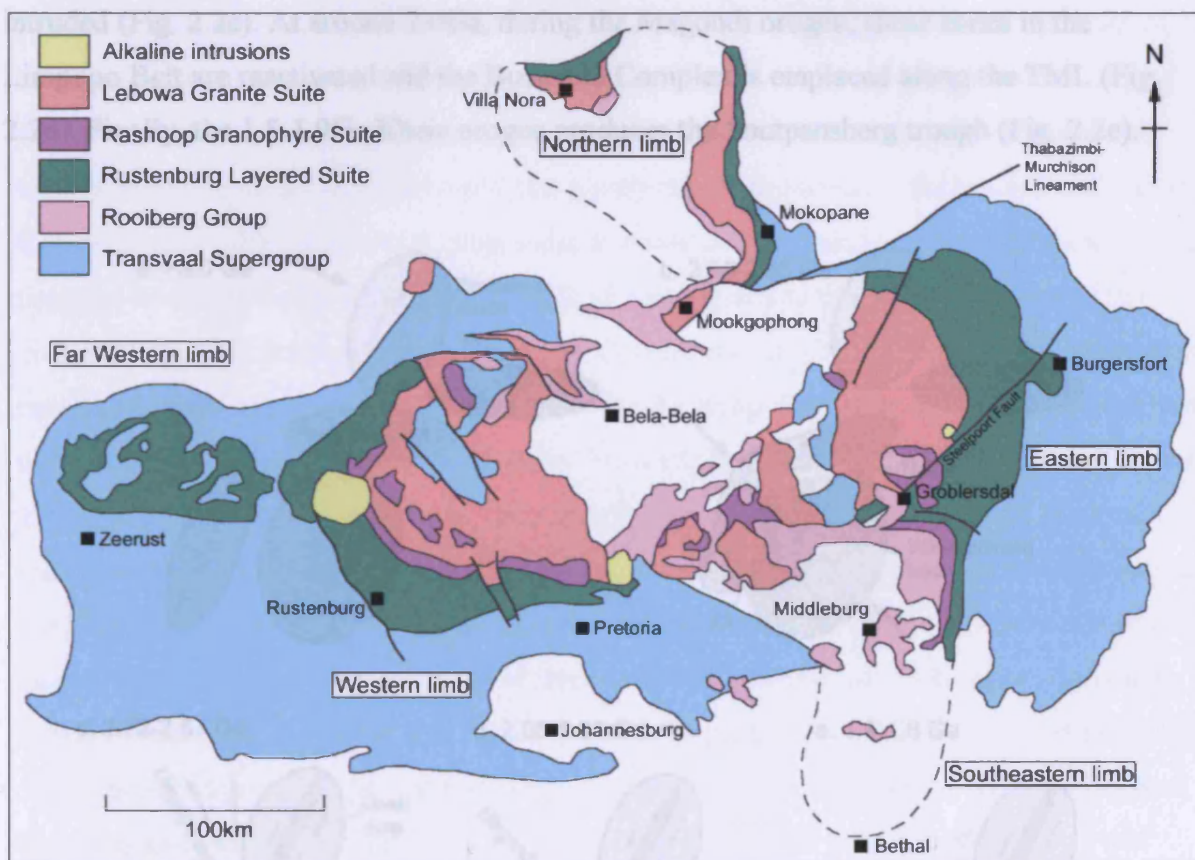


Figure 2.1. Geological map of the Bushveld Complex (after Kinnaird *et al.*, 2005).

2.1.1 Structural setting

The Bushveld Complex is located within the Kaapvaal Craton, which is comprised of a mosaic of crustal blocks that amalgamated between 3.7 and 2.6Ga, and can be subdivided into two periods (de Wit *et al.*, 1992). Between 3.7 and 3.1Ga, the initial separation of continental lithosphere from the mantle occurred through intraoceanic obduction and amalgamation

processes followed by within-shield melting, granite formation and chemical differentiation of the upper lithosphere to create the Kaapvaal shield. The second stage of Precambrian history of southern Africa was synthesized by Silver *et al.* (2004) using mantle fabrics revealed by seismic anisotropy and is summarized in Fig 2.2. Firstly, an unknown orogen imparts a mantle fabric on the Zimbabwe craton pre 2.9Ga (Fig. 2.2a). Around 2.9Ga, the Pietersburg and Kimberley blocks collide with the Kaapvaal Shield, which imparts an arc-like mantle fabric, and forms the Thabazimbi-Murchison Lineament (TML, Fig. 2.2b). During the Limpopo orogen at 2.6-2.7Ga, the Limpopo Belt is formed between the Kaapvaal and Zimbabwe cratons. During this time, the Great Dyke and Ventersdoorp Supergroup are intruded (Fig. 2.2c). At around 2.0Ga, during the Magondi orogen, shear zones in the Limpopo Belt are reactivated and the Bushveld Complex is emplaced along the TML (Fig. 2.2d). Finally, the 1.8-1.9Ga Kheis orogen produces the Soutpansberg trough (Fig. 2.2e).

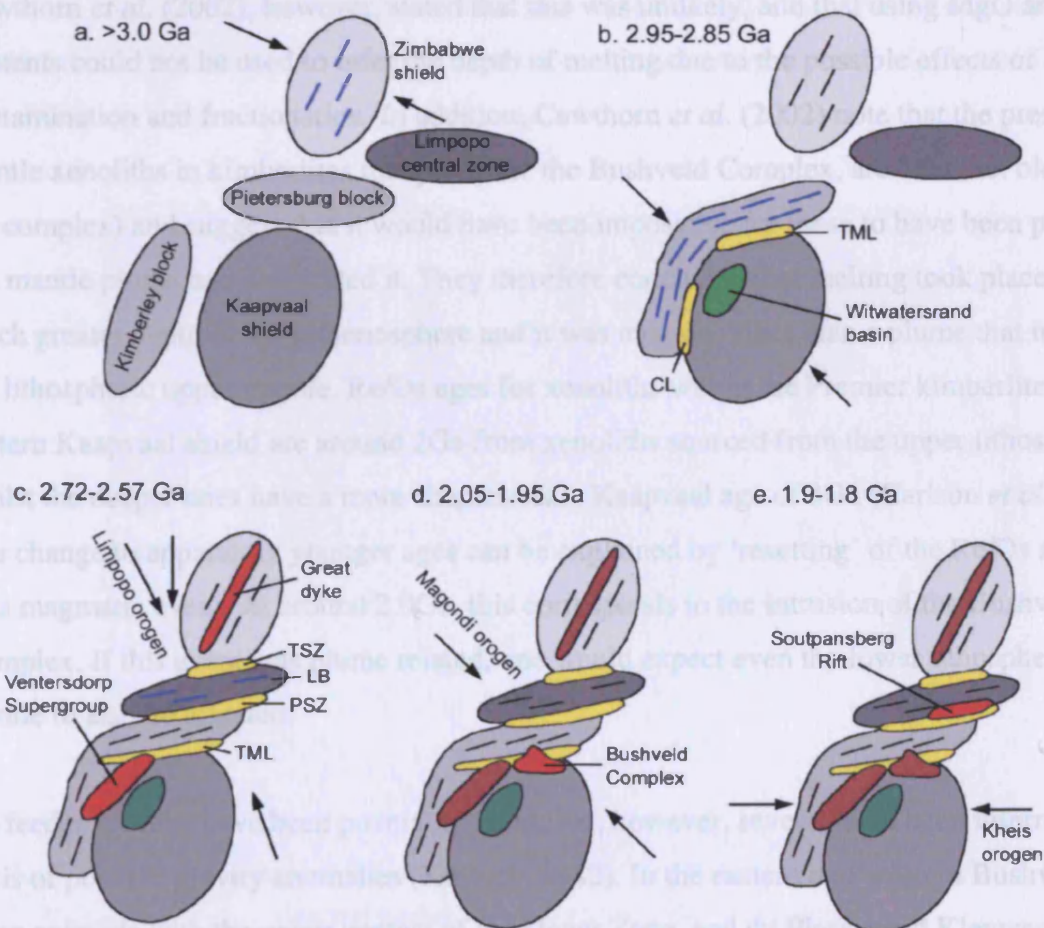


Figure 2.2. Tectomagmatic evolution of the Kaapvaal Craton. After Silver *et al.* (2004). See text for explanation. TML – Thabazimbi-Murchison Lineament, CL – Colesberg Lineament, PSZ – Palala Shear Zone, TSZ – Triangle Shear Zone, LB – Limpopo Belt.

2.1.2 Emplacement and magma source

The mechanism of emplacement for the Bushveld Complex remains unresolved. One of the earliest theories was described by Mills Davis (1925), who postulated “an active molten rock magma of common or normal composition deep down in the Central Transvaal area and its gradual advance upwards through thousands of feet of strata until it emerged through devious ways through the quartzites and shales of the Pretoria Group and...spread out like a colossal cake.” Wagner (1929) referred to its lopolithic nature and the likelihood of it being intruded into horizontal strata, but did not suggest a mechanism for the intrusion. Hatton (1995) considered the Bushveld Complex to be the intrusive equivalent of a continental flood basalt province, with the magma sourced from a mantle plume that impinged through the base of the crust. Using MgO and SiO₂ contents, he calculated that melting took place between 18 and 40km, and inferred that the only way to achieve melting at such depths in an intracratonic setting would be for a sufficiently buoyant mantle plume to penetrate the bottom of the crust. Cawthorn *et al.* (2002), however, stated that this was unlikely, and that using MgO and SiO₂ contents could not be used to infer the depth of melting due to the possible effects of contamination and fractionation. In addition, Cawthorn *et al.* (2002) note that the presence of mantle xenoliths in kimberlites that penetrate the Bushveld Complex, are 3Ga (i.e. older than the complex) and suggest that it would have been impossible for these to have been preserved if a mantle plume had penetrated it. They therefore concluded that melting took place at a much greater depth in the asthenosphere and it was magma rather than a plume that invaded the lithospheric upper mantle. Re/Os ages for xenoliths within the Premier kimberlite in the eastern Kaapvaal shield are around 2Ga from xenoliths sourced from the upper lithosphere, whilst the deeper ones have a more characteristic Kaapvaal age of 3Ga (Carlson *et al.*, 1999). The change to apparently younger ages can be explained by ‘resetting’ of the Re/Os system by a magmatic event. At around 2.0Ga, this corresponds to the intrusion of the Bushveld Complex. If this event was plume related, one would expect even the lower lithospheric mantle to also be affected.

No feeder systems have been positively identified; however, several have been inferred on the basis of positive gravity anomalies (Kinloch, 1982). In the eastern and western Bushveld, these coincide with the upper contact of the Upper Zone, and du Plessis and Kleywegt (1987) point out that this is where the thickness of the mafic rocks is greatest, and therefore a positive anomaly would be expected, thus these anomalies are unlikely to represent feeders. By far the

strongest gravity anomaly in the complex is located in the northern limb, just to the west of Mokopane, and does not in this case correspond to an area of the thickest mafic sequence. Van der Merwe (1976) interpreted this as a feeder vent, and also found no evidence of any physical link between the northern and eastern limbs of the complex on the basis of gravity data. The enormity of the Mokopane anomaly and the lack of connectivity with the eastern limb are shown in the gravity map in Fig. 2.3. The mafic rocks of the Bushveld Complex have a -60-70mGal Bouguer anomaly compared to the country rocks, which have an anomaly of -140mGal. The areas in the eastern and western Bushveld where feeders have been inferred have anomalies of around -45mGal, whereas the Mokopane anomaly is close to -10mGal. This obvious and much more convincing anomaly is surprisingly ignored by Cawthorn and Webb (2001), from where the map is reproduced. Kruger (2005a) used initial $^{87}\text{Sr}/^{86}\text{Sr}$ ratios to suggest that Main Zone magma for the whole complex was intruded north of the TML, from the Mokopane feeder, and flooded into the rest of the complex forming the Merensky Reef at the base. This model consequently implies that the Platreef and Merensky Reef are coeval and directly related, a view which is becoming increasingly questioned, (e.g. McDonald *et al.*, 2005)

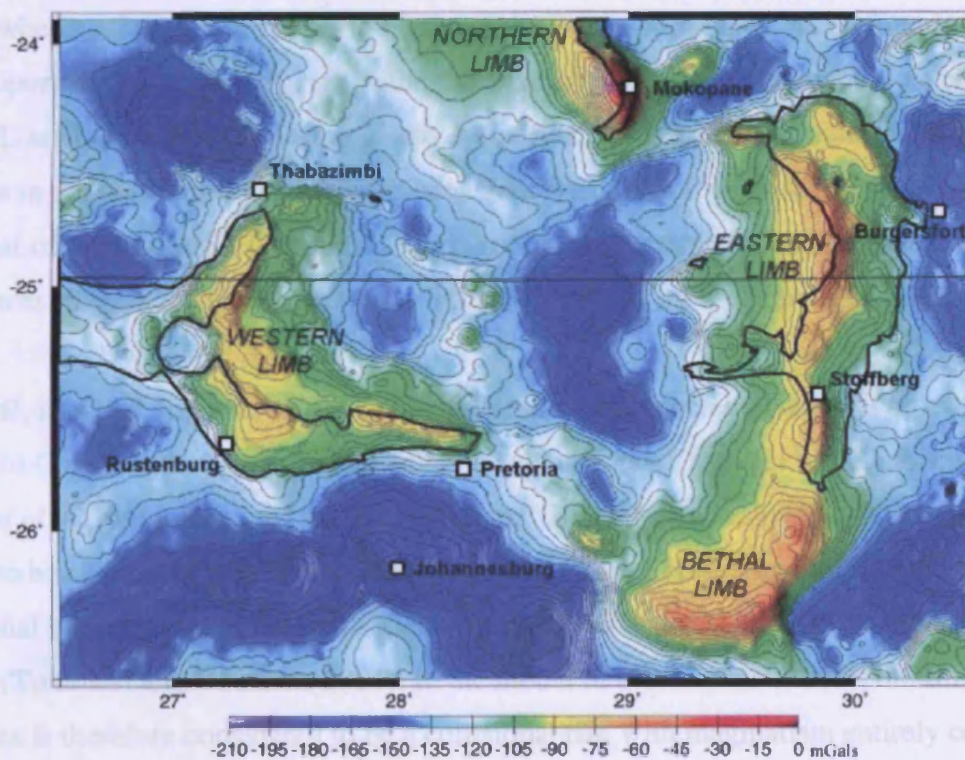


Figure 2.3. Gravity map of the Bushveld Complex, showing the outline of surface outcrop, and the large gravity anomaly close to Mokopane (after Cawthorn and Webb, 2001).

Linear feeders have been proposed by Cawthorn *et al.* (2002) and Friese (2004). The former authors considered the Steelpoort Fault (Fig. 2.1) to be a likely feeder zone. There are well known differences in stratigraphic thicknesses of individual units of the Lower and Critical Zones on either side of this lineament (e.g. Hatton and von Gruenewaldt, 1987). Cawthorn *et al.* (2002) explain these by proposing that magma flowing to the north and south of the linear feeder to greater or lesser degrees depending on the amount of subsidence on either side. This would therefore produce different depths of magma leading to the observed stratigraphic thicknesses. The authors also state that the Steelpoort Fault was unlikely to be the only feeder and many of the large faults that separate compartments of the Complex may have acted as feeders. Friese (2004), took an alternative view and considered the TML to be a likely feeder zone, with magmas ascending along the deep-seated shear zones until at a critical point in the crust where the magmatic pressure equalled lithostatic pressure and triggered the sill-like intrusion of the Complex. The TML is a 500km long, 25km wide ENE-WSW trending deformation belt, reactivated as a fault (McCourt and Vearncombe, 1987). It delineates a major cratonic subterranean boundary, and as such, represents a fundamental crustal and probably deep lithospheric-mantle break within the Kaapvaal Craton (Good and de Wit, 1997; Silver *et al.*, 2004). Figure 2.2 shows that the crust south of the TML belongs to the Kaapvaal shield, whereas the crust to the north is part of the Pietersburg block. Therefore the crust, and most importantly for magma genesis, the sub lithospheric continental mantle, on either side of the TML are fundamentally different, and as the Bushveld Complex straddles the TML, the magmas in the northern limb may have been generated from compositionally distinct mantle from that of the rest of the Complex. In doing so, this may explain the compositional differences in Bushveld rocks across the TML highlighted by McDonald *et al.* (2005).

The TML is also thought to be fundamentally important in the emplacement of not just the Bushveld Complex, but other large magmatic events in the Kaapvaal and Zimbabwe cratons. Silver *et al.* (2004) interpreted the Ventersdoorp, Great Dyke, Bushveld and Soutpansberg events to be collisional rifts. These develop during or after orogens parallel to the trend of the collisional belt in zones of far-field extensional stresses that reactivate pre-existing mantle fabrics (Tommasi and Vauchez, 2001). In the model of Silver *et al.* (2004), the Bushveld Complex is therefore considered to be a collisional rift, with magmatism entirely controlled by variations in lithospheric stress, rather than by the ascent of a plume from the deep mantle.

2.2 The Northern limb

The northern limb of the Bushveld Complex is separated from the rest of the complex by the Zebediela Fault, part of the TML (Fig. 2.1, 2.4). The northern limb is inferred to be triangular in shape, based on gravity surveys (van der Merwe, 1976). It crops out as a sinuous N-S trending, WSW-dipping body around 100km in length and up to 15km wide, which makes up the eastern edge of this triangle. In the Villa Nora area, around 100km NW of Mokopane (Fig. 2.1), it crops out again as the NW corner of the triangle, where the dips are to the S and SE (Grobler and Whitfield, 1970). The eastern edge of the limb is obscured by Waterberg sediments, though is inferred to run from Mookgophong (formerly Naboomspruit, Fig. 2.1) in the south to the Mogol River in the northwest, and is likely to have an easterly dip (Van der Merwe, 1976).

2.2.1 Stratigraphy of the northern limb

The stratigraphy of the northern limb differs from the RLS in the complex south of the TML. The traditional view of its relationship to the rest of the complex is summarized in Fig. 2.5, and a detailed map of the northern limb is shown in Fig. 2.4. There are also substantial differences in the stratigraphy on either side of the Ysterberg-Planknet fault, which trends NE-SW through Mokopane (Fig. 2.4). Lower Zone cumulates are developed most extensively south of Mokopane, and to the north only occur as isolated satellite bodies intruded into the floor rocks (Fig. 2.4). The sequence of Lower Zone cumulates comprises at least 1600m of 37 cyclic units of pyroxenites and harzburgites with chromitites (Hulbert, 1983; Hulbert and von Gruenewaldt, 1982). This sequence differs from the Lower Zone elsewhere in that it contains orthopyroxene with higher enstatite content and olivine with higher forsterite content (van der Merwe, 1976), chromitite layers with the highest Cr_2O_3 content and Cr# in the whole Bushveld Complex (Hulbert, 1983), and a PGE-rich sulfide horizon, which are not found in any of the Lower Zone cumulates in the rest of the complex (Hulbert and von Gruenewaldt, 1982). The area to the north of Mokopane contains several bodies of Lower Zone rocks, known as 'satellite bodies,' intruded into the floor rocks beneath the main Bushveld intrusion (Fig. 2.4), that are generally made up of orthopyroxene and orthopyroxene-olivine cumulates with occasional chromitite layers (van der Merwe, 1978).

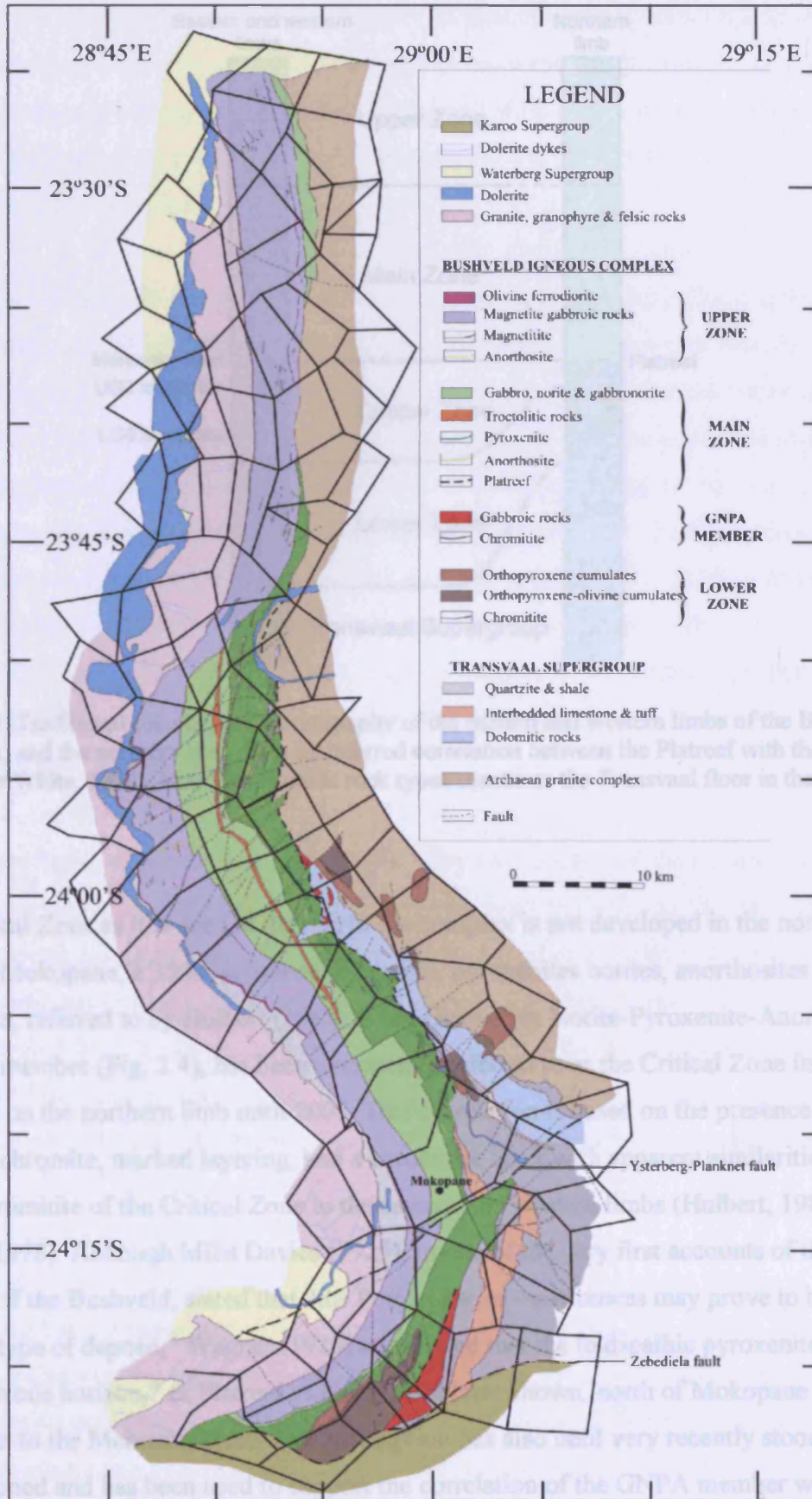


Figure 2.4. Geological map of the northern limb of the Bushveld Complex (after Ashwal *et al.*, 2005).

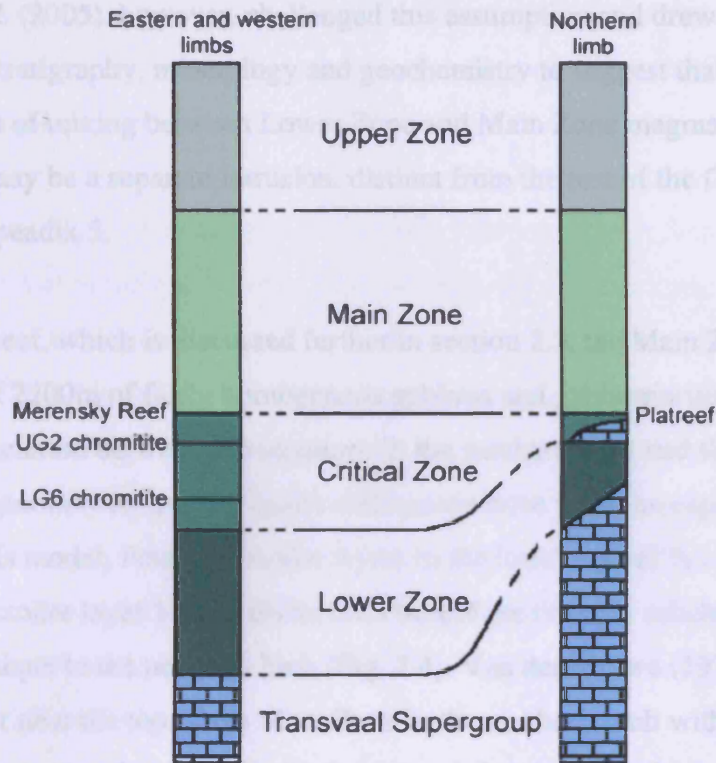


Figure 2.5. Traditional correlation of stratigraphy of the eastern and western limbs of the Bushveld Complex, and the northern limb, with an inferred correlation between the Platereef with the Merensky Reef (after White, 1994). Note that variable rock types constitute the Transvaal floor in the northern limb.

The Critical Zone as it is seen in the rest of the complex is not developed in the northern limb. South of Mokopane, a 350m sequence of layered, pyroxenites norites, anorthosites and a chromitite, referred to by Hulbert (1983) as the Grasvalley Norite-Pyroxenite-Anorthosite (GNPA) member (Fig. 2.4), has been uncritically referred to as the Critical Zone in the literature on the northern limb until 2005. This correlation is based on the presence of cumulus chromite, marked layering, and a chromitite layer with apparent similarities to the UG-2 chromitite of the Critical Zone in the eastern and western limbs (Hulbert, 1983; van der Merwe, 1978). Although Mills Davies (1925), in one of the very first accounts of the platinum deposits of the Bushveld, stated that “the Potgietersrust occurrences may prove to be a separate type of deposit,” Wagner (1929) considered that the feldspathic pyroxenite “platiniferous horizon,” or Platereef as it would be later known, north of Mokopane was analogous to the Merensky Reef. This assumption has also until very recently stood almost unquestioned and has been used to support the correlation of the GNPA member with the Upper Critical Zone.

McDonald *et al.* (2005), however, challenged this assumption and drew on the many differences in stratigraphy, mineralogy and geochemistry to suggest that the GNPA member was the product of mixing between Lower Zone and Main Zone magmas, and even that the northern limb may be a separate intrusion, distinct from the rest of the Complex. This paper is included as Appendix 5.

Above the Platreef, which is discussed further in section 2.3, the Main Zone in the northern limb consists of 2200m of fairly homogenous gabbros and gabbro-norites (van der Merwe, 1976). The correlation between the sequence in the northern limb and the rest of the complex has not been rigorously tested, and major differences have yet to be explained using a common genesis model. Four pyroxenite layers in the lower part of the succession and a 110m-thick troctolite layer 1100m above the Platreef are the only reliable marker horizons, all of which are unique to the northern limb (Fig. 2.4). Van der Merwe (1976) correlated a pyroxenite layer near the top of the Main Zone in the northern limb with the Pyroxenite Marker in the eastern and western limbs, however Ashwal *et al.* (2005) argue that the two horizons cannot be correlated on the basis of mineralogy and referred to the unit as the Pyroxenite Horizon to avoid confusion.

The Upper Zone of the northern limb more closely matches that of the eastern and western limbs, comprising alternating layers of gabbro, magnetite gabbro, anorthosite, magnetite and olivine diorite. However, only one of the magnetite layers can be reliably correlated with the Main Magnetite layer of the rest of the complex on terms of thickness and V₂O₅ content (Van der Merwe, 1976). The Upper Zone also crops out in the Villa Nora area (Fig. 2.1), where the main rock types are leuconorites, leucogabbros and anorthosites (Hattingh and Pauls, 1994). The lower zones in the Villa Nora compartment are faulted out by the Abbotspoort Fault.

2.2.2. Age of the northern limb

It has been almost unquestionably considered that all three limbs of the Bushveld Complex were formed at the same time, and the age of 2.06Ga (Walraven *et al.*, 1990), is taken to be age of the Complex by most workers. This date was confirmed by Buick *et al.* (2002) who used U-Pb dating of titanites within calc-silicate xenoliths in the RLS to provide a tight constraint on the minimum age for Bushveld intrusion at 2058.9±0.8Ma. However, in the light of the suggestion of McDonald *et al.* (2005), that the northern limb may possibly

represent a separate intrusion, it is necessary to reassess and test this assumption. Very few attempts have actually been made at determining the age of the northern limb, partly due to the assumption that it formed at the same time as the rest of the Complex, where most of the dating work has been done. However, there are two studies which may indicate a somewhat younger age for the intrusion of the northern limb. Palaeomagnetic data presented by Hattingh (1995) indicates that in the main part of the Complex, the Critical Zone's remnant magnetization was fixed before that of the Main and subsequent Upper Zones. Following this, magnetization of the Main Zones in the northern limb occurred and the youngest magnetization recorded is that of the Upper Zone in the northern limb. In addition to this intriguing data is a Re-Os isotope date by Ruiz *et al.* (2004), which provided a age of 2011 ± 50 Ma, which only just incorporates the assumed age of 2060 Ma into its error margin. A much more accurate date which would appear to give a minimum age to the Platreef at least is, provided by Hutchinson *et al.* (2004), who dated zircon in a granitic vein which cross-cut the Platreef at 2053.7 ± 3.2 Ma. If this is accurate it may imply a slightly younger age, however, it is in no way as great as that that could be inferred from the palaeomagnetic and Re-Os data.

2.3. The Platreef

The Platreef is one of the world's largest deposits of PGE, and also contains significant reserves of Ni and Cu. It is estimated to contain reserves of 16.3 million oz of Pt+Pd (Cawthorn, 1999), and with its thickness of up to 400 m and high grade, is amenable to open pit mining (Bye, 2001). Potgietersrus Platinums Ltd., a subsidiary of Anglo Platinum, currently operates two open-pit mines at Sandsloot and Zwartfontein South (Fig. 2.6), with others planned on the adjacent farms Overysel and Tweefontein. The activity of several other companies, including Anooraq Resources, Platreef Resources, Pan Palladium, Platinum Group Metals Ltd, Caledonia Mining and AfriOre has made the northern limb of the Bushveld Complex currently one of the most intensely explored areas for PGE in the world.

2.3.1 Current state of research

Platinum in the northern limb was originally found by a team of prospectors led by Hans Merensky in March 1925 (Mills Davies, 1925). By November of the same year, Potgietersrust Platinums Ltd (PPL) was formed, at which point Merensky himself (1925) stated, "I feel convinced that the Potgietersrust Platinums Ltd. will develop into a highly payable concern."

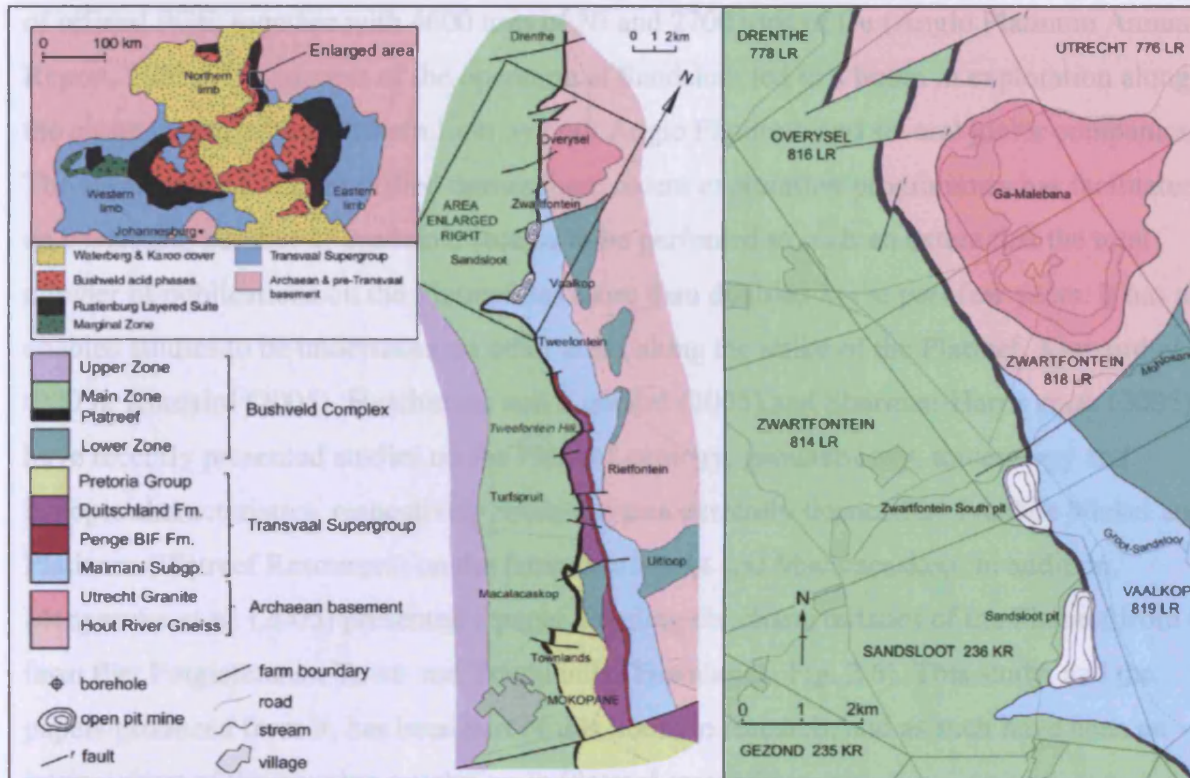


Fig. 2.6. Geological map of the Platreef showing the different footwall units along strike and the farms referred to in the text. The map on the right hand side shows in detail the field area for this study, including the Sandsloot and Zwartfontein South pits.

The first comprehensive account of the Platreef was by Wagner (1929). He stated that the Platreef was a 'platinum-bearing zone' and that it was a 'platinum-bearing zone' along the strike. The company was in production by 1926 (Cawthorn *et al.*, 2002) and much of the early work on the deposits was summarized by Wagner (1929) in his seminal volume: 'The platinum deposits of South Africa.' Despite early optimism, early mining results were poorer than expected and following the onset of the Great Depression in 1930, mining ceased. For the next six decades, Bushveld Complex mining and research was concentrated in the western and eastern limbs, with only a handful of investigations on the Platreef being published prior to 2000. In 1992, PPL, now fully owned by Anglo Platinum, opened the Sandsloot mine, which paved the way for a new wave of research on the deposit. Most of these, such as White (1994) and Viljoen and Schürmann (1998) have been undertaken on Anglo Platinum's property between the farms Tweefontein and Overysel (Fig 2.6). The subsequent studies of Harris and Chaumba, (2001), Armitage *et al.* (2002), Friese (2004), McDonald *et al.* (2005), Holwell *et al.* (2005, see Chapter 3) and Holwell *et al.* (2006, see Chapter 5) have all utilized data from the Sandsloot mine in their respective studies of Platreef contamination, mineralization, structure, geochemistry, emplacement and mineralogy. Merensky's prediction of 1925 had become realized and in 2005, Anglo Platinum's PPL produced some 443,000oz

of refined PGE, together with 4600 tons of Ni and 2700 tons of Cu (Anglo Platinum Annual Report, 2005). The success of the operation at Sandsloot led to a boom in exploration along the entire length of the northern limb by both Anglo Platinum and several junior companies. The sheer volume of core drilled during these recent exploration programmes has facilitated an expanding number of academic studies to be performed to such an extent that the total number of publications on the Platreef has more than doubled in the past few years. It has also enabled studies to be undertaken on other areas along the strike of the Platreef. Kinnaird *et al.* (2005), Kinnaird (2005), Hutchinson and Kinnaird (2005) and Sharman-Harris *et al.* (2005) have recently presented studies on the Platreef geology, geochemistry, mineralogy and isotopic characteristics, respectively, from the area currently licenced by Ivanhoe Nickel and Platinum (Platreef Resources) on the farms Turfspruit and Macalacaskop. In addition, Manyeruke *et al.* (2005) presented a paper detailing the characteristics of the Platreef from the farm Piet Potgietersrust Town and Townlands (Townlands, Fig. 2.6). This study, and the papers produced from it, has been part of this boom in research, and as such have been an intrinsic part of the ongoing revolution in Platreef research.

2.3.2 Geology

The first comprehensive account of the Platreef was by Wagner (1929). He stated that the Platreef can be generalized as a basal package of pyroxenites, norites, serpentinites and xenoliths of footwall rocks with PGE-Ni-Cu mineralization which transgresses a variety of floor rock lithologies and is overlain by gabbro-norites equated with the Main Zone. In detail however, the Platreef is a very complex zone of igneous and hybrid lithologies that vary along strike and whose differences are at least in part, directly related to the interaction of the Platreef magma with the local footwall type. Thickness varies from as little as 10m at Sandsloot (Armitage *et al.*, 2002) to 400m at Turfspruit (Kinnaird, 2005) and is thought to be controlled at least in part by structures in the floor rocks (Friese, 2004; Nex, 2005). The general geology, including footwall lithology, Platreef lithologies, xenolith types, together with a summary of the base metal sulfide (BMS) and platinum-group mineral (PGM) mineralogy of the Platreef with a comprehensive reference list for each farm along strike is shown in Fig. 2.7. The information in sections 2.3.2 and 2.3.3 are summarized in this figure.

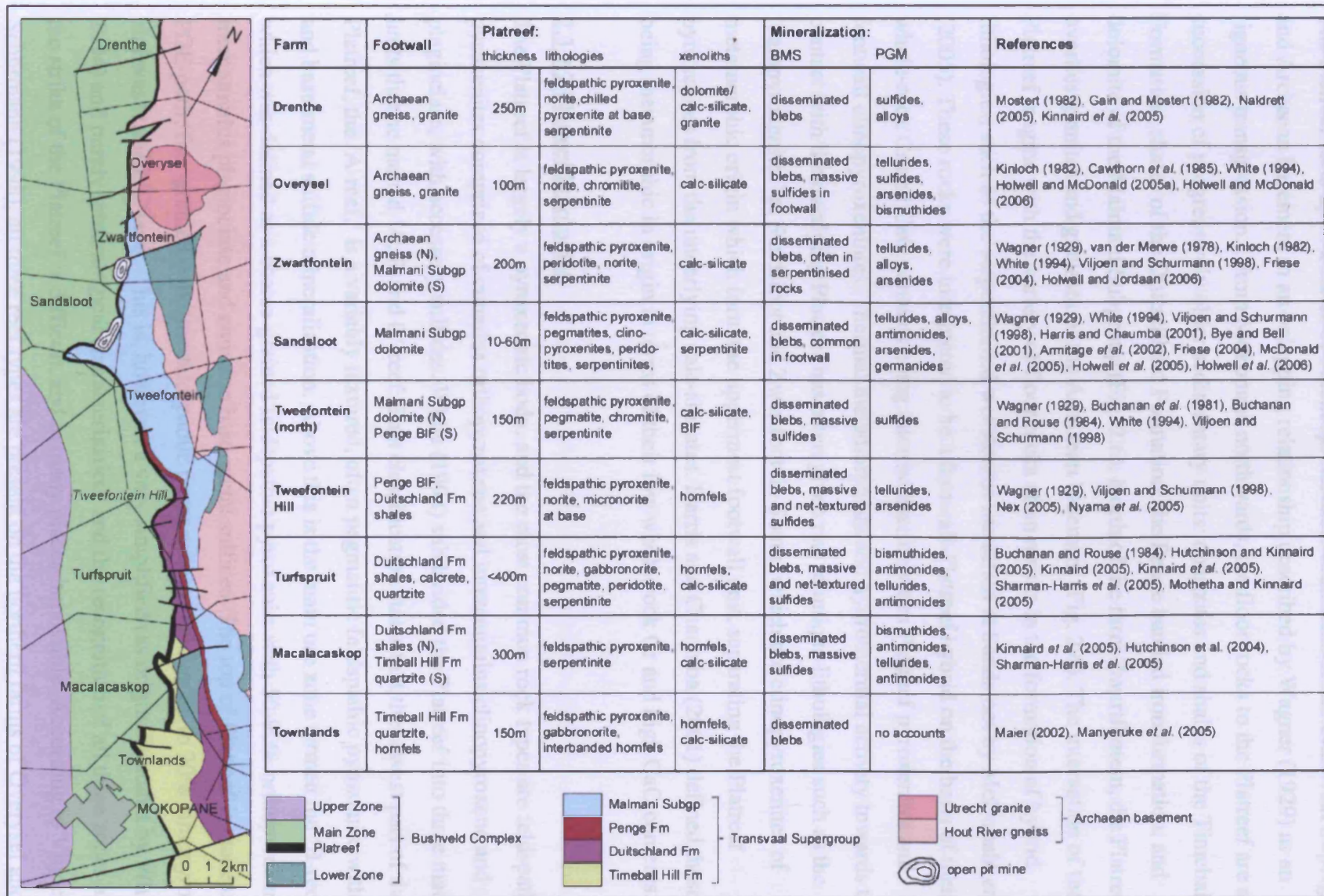


Figure 2.7. Summary figure showing the geology and mineralization types along the strike of the Platreef.

2.3.2.1 Footwall lithologies

The Platreef rests upon a series of Paleaeoproterozoic sediments of the Transvaal Supergroup, and Archaean basement in an onlapping relationship described by Wagner (1929) as an 'igneous transgression.' From Mokopane northwards, the floor rocks to the Platreef are a succession of progressively older sedimentary units: quartzites and shales of the Timeball Hill Formation; shales of the Deutschland Formation; the Penge banded iron formation, and dolomite of the Malmani Subgroup (Fig. 2.6). North of the farm Zwartfontein, the Platreef overlies granites and gneisses of the Archaean basement (Fig. 2.6). The interaction of the Platreef magma with the variety of floor rocks often results in the formation of hybrid lithologies, such as the serpentized websterites identified at Sandsloot by McDonald *et al.* (2005). These rocks were interpreted to be a footwall-Platreef hybrid on the basis of their whole-rock Cr and CaO contents being intermediate between Platreef pyroxenites and footwall clinopyroxenites. Thermal metamorphism and hydrothermal activity towards the contact with the overlying Platreef has often given rise to unique lithologies such as the 'parapyroxenites' at Sandsloot and Zwartfontein South, which are clinopyroxenites of metamorphic origin which form the uppermost footwall unit, separating the Platreef pyroxenites from the underlying calc-silicates. Harris and Chaumba (2001) defined these as being metamorphic in origin in terms of their low whole-rock Cr and high CaO contents.

2.3.2.2 Platreef lithologies

The Platreef is largely a pyroxenitic body, and the most common rock types are feldspathic pyroxenites comprised of cumulus orthopyroxene and intercumulus clinopyroxene and plagioclase, with accessory sulfides. White (1994) subdivided the Platreef into three main units that he named 'A, B and C' reef. This classification states that the lowest part of the Platreef, the 'A-reef,' is a variably textured, often pegmatitic feldspathic pyroxenite with PGE and base-metal sulfide mineralization. Above this is the main ore zone termed the 'B-reef' which was defined as a coarse-grained feldspathic pyroxenite with 50-90% orthopyroxene, intercumulus plagioclase and common base-metal sulfides. The top of Platreef is made up of a PGE-poor, fine-grained poikilitic feldspathic pyroxenite containing up to 70% clinopyroxene and was termed 'C-reef.' This is, however, a very simplified (as originally stated by White, 1994) and purely mineralogical characterization, and the recognition of all three zones along the strike of the Platreef is difficult, and in many places impossible. According to Viljoen and Schürmann (1998), all three reef types are present on the northern farms of Overysel and

Drenthe, and White (1994) notes that recognition of all three reef types is possible on Tweefontein Hill, due to the chemically less reactive nature of the banded ironstone footwall. Despite the very simplified nature of the classification, the terms have become entrenched in both the literature (e.g. Lee, 1996; Viljoen and Schürmann, 1998; Maier, 2002) and mining terminology. In 2004 and 2005, two Platreef workshops involving mining companies and academics have attempted to highlight the untenable nature of this classification in the light of the much wider knowledge that recent studies have produced and it is only now that this classification is staring to be dropped.

The most southerly farm on which the Platreef crops out is Townlands, where it overlies quartzites and shales of the Timeball Hill Formation. Manyeruke *et al.* (2005) described one core from the farm which appeared to be made up of a 150m package of three distinct intrusive phases based on geochemical constraints, separated by shales. The Platreef rocks are gabbronorites and feldspathic pyroxenites. However, a recent re-evaluation by Snowdon Mining Consultants for AIM Resources of drilling data generated during the 1990s by Thabex Exploration on Townlands revealed the Platreef to be a pegmatoidal pyroxenite, interfingered with pyroxenites, norites and melanorites, and containing xenoliths of footwall sediments, with no indication of intercalated sediments (AIM Resources, 2004).

There have been several recent studies on the Platreef in the Macalacaskop and Turfspruit areas, where the floor is comprized of hornfelses and dolomites of the Duitschland Formation, that have revealed a particularly thick Platreef sequence and a greater variety of rock types than were known from the Tweefontein-Overysel area (Kinnaird *et al.*, 2005; Kinnaird, 2005; Hutchinson and Kinnaird, 2005; Sharman-Harris *et al.*, 2005). Again, the Platreef is predominantly feldspathic pyroxenite, but also contains norites, melanorites, serpentinites and gabbronorites and micronorites classified as Marginal Zone. Xenoliths of quartzite are common at Macalacaskop. Buchanan and Rouse (1984) describe cores from one core from Turfspruit which has around 70m of peridotites towards the base of the succession. Kinnaird *et al.* (2005) and Mothetha and Kinnaird (2005) also note the presence of serpentinitized peridotites, which Kinnaird *et al.* (2005) classify as Lower Zone rocks. There are no further reports of such rocks north of Mokopane other than the satellite bodies.

North of Turfspruit, on Tweefontein Hill (Fig. 2.6) aluminous argillaceous shales of the Deutschland Formation form the immediate footwall to Platreef feldspathic pyroxenites which contain xenoliths of ironstone and shale on the southern side (Wagner, 1929). On the hill itself, the footwall is banded ironstone of the Penge Formation, which has been partially metamorphosed to magnetite-bearing hornfels (White, 1994). The Platreef sequence is relatively thick and appears to have developed in a structural downwarp, where the relatively inert nature of the footwall is thought to have allowed gravitational settling of a sulfide liquid, producing net-textured and massive sulfides (White, 1994; Viljoen and Schürmann, 1998; Nex, 2005). Nyama *et al.* (2005) describe the Platreef on Tweefontein as being a 220m thick package composed mainly of pyroxenites and some norites, with a basal micronorite.

Buchanan *et al.* (1981) describe a core from Tweefontein North that is made up of a basal pegmatoidal pyroxenite, and note a 6m thick massive sulfide in one borehole. The pegmatoid is overlain by pre-Bushveld sills and metamorphosed shales, in turn, overlain by 200m of Platreef gabbros. As this data come from cores, it is uncertain as to what the relationship of the massive-sulfide-bearing pegmatite to the overlying gabbros is. White (1994) documents the presence of a chromitite layer in 80% of boreholes drilled on Tweefontein North, and thus draws a parallel with the Merensky Reef. Chromitite layers are unusual in the Platreef, but discontinuous bands have been recorded at Sandsloot, Zwartfontein, and in particular, Overysel, and are described and discussed by Holwell and McDonald (2006, see chapter 6).

The Platreef in the Sandsloot area is probably the most well known due to the number of studies undertaken in the Sandsloot pit since it opened in 1992 (Harris and Chaumba, 2001; Bye and Bell, 2001; Armitage *et al.*, 2002; Friese, 2004; McDonald *et al.*, 2005; Holwell *et al.*, 2005, see Chapter 3; Holwell *et al.*, 2006, see Chapter 5). Medium- to coarse-grained feldspathic pyroxenites are the most common lithologies in a relatively thin reef package that also includes gabbros, peridotites, clinopyroxenites, serpentinites and calc-silicate xenoliths. The overlying gabbro-norites often have a mottled anorthosite at the base and the nature of this contact is described in detail by Holwell *et al.* (2005, see Chapter 3). The Platreef rests on metamorphic clinopyroxenites and calc-silicate hornfels, which are often serpentized and variably mineralized. At Zwartfontein South (Fig. 2.6), the footwall rocks are similar to those at Sandsloot, however the reef package is much thicker and contains a greater amount of serpentized lithologies, which are thought to be related to the alteration of rafts of calc-silicates within the Platreef (Holwell and Jordaan, 2006, see Chapter 4).

On the northern part of the farm Zwartfontein, the footwall changes from Malmani dolomite to Archaean granite/gneiss basement. Downdip to the west of the surface outcrop of the Platreef on Zwartfontein, deep drilling by AfriOre has intersected Platreef with a gneissic footwall that is made up of coarse grained feldspathic pyroxenites, occasionally chromitiferous, with calc-silicate xenoliths (Spies, 2005). On the adjacent farm to the north, Overysel (Fig. 2.6), Cawthorn *et al.* (1985) describe the Platreef as often having a thin medium-grained norite at the base which grades into a coarse pyroxenite. Holwell and McDonald (2006, see chapter 6) describe two cores drilled on the farm which contain feldspathic pyroxenites, serpentinized calc-silicate xenoliths, intrusive norites, some chromitite xenoliths and a basal hybrid zone of quartzo-feldspathic pyroxenite formed as a result of the invasion of a felsic melt derived from partial melting of the footwall. Trial mining on the farm also encountered some thick, but discontinuous bands of chromitite (White, 1994; Holwell and McDonald, 2006, see Chapter 6). A series of banded tonalitic gneisses underlie the Platreef on Overysel and are commonly referred to as granofels, particularly when brecciated by granitic veins, and beneath the gneisses, the domal body of the Utrecht granite is encountered (Fig. 2.6). Viljoen and Schürmann (1998) note the presence of large rafts of dolomite-derived calc-silicates within the Platreef pyroxenite, tens of metres across, although no xenoliths of granite or gneiss, despite these rocks being the immediate country rock. Cawthorn *et al.* (1985) suggest this may be due to granite fragments being totally assimilated, whereas dolomite, altered to olivine and pyroxene, remains refractory.

The most northerly section of Platreef with published accounts of the geology is on the farm Drenthe (Fig. 2.6). Mostert (1982) and Gain and Mostert (1982) describe the Platreef as being 250m and being made up of a basal 40-80m feldspathic pyroxenite that is chilled at the base against footwall granites. Chilling is not observed on Overysel by either Cawthorn *et al.* (1985) or Holwell and McDonald (2006). 170m of norites and melanorites with abundant calc-silicate xenoliths overly the pyroxenites, which are capped by a 10-30m feldspathic pyroxenite. Recent work by Naldrett (2005) identified intrusions of hangingwall gabbro-norites into the Platreef, particularly along horizons where altered calc-silicates were present at Drenthe. The norites in the centre of the Platreef succession that were described by Gain and Mostert (1982) are unlikely to correspond to such an intrusive body, as they contain cumulus orthopyroxenes with composition comparable to the Platreef, rather than the hangingwall.

Around 10km north of Drenthe, the Platreef disappears and Upper Zone cumulates cut down to rest upon the basement gneisses. Some 35km north of Drenthe, where the Main Zone reappears again (Fig. 2.4), a zone of significant PGE and BMS mineralization is developed between Main Zone gabbro and gabbro-norite cumulates and the basal contact of the Bushveld rocks (Harmer *et al.*, 2004). The host rocks are gabbro-norites and olivine gabbros, and orthopyroxene is very rare, and it is clear that the lithologies cannot be correlated with those of the Platreef.

2.3.3 Mineralization

Platreef PGE mineralization is generally associated with base-metal sulfides (BMS; pyrrhotite, pentlandite, chalcopyrite and minor pyrite) and is hosted by both the basal pyroxenitic igneous package and also the immediate footwall of metamorphosed sediments and Archaean basement (e.g. Wagner, 1929), although footwall mineralization is highly inconsistent in both width and grade (White, 1984). Some thin zones of mineralization at the base of the hangingwall have also been identified (Holwell *et al.*, 2005; see Chapter 3). In the feldspathic pyroxenites, the sulfides occur as interstitial blebs. The position of the mineralization is variable and may appear top-, middle- or bottom-loaded within the Platreef package (Viljoen and Schürmann, 1998; Kinnaird *et al.*, 2005), although the mechanisms controlling the stratigraphic position of the mineralization are as yet poorly understood.

Sulfide abundance is variable along strike and can locally reach up to 30 modal% in some cores (Kinnaird, 2004). The area around Turfspruit and Tweefontein Hill is known to commonly contain abundant sulfides, with net-textured and massive sulfides being common (White, 1994; Nex, 2005; Hutchinson and Kinnaird, 2005). At Tweefontein this is attributed to settling of a sulfide liquid in a structural downwarp (Viljoen and Schürmann, 1998; Nex, 2005) and at Turfspruit is likely to be a result of upgrading of the original S content of the magma by assimilation of sulfide from the footwall (Sharman-Harris *et al.*, 2005).

Serpentinized calc-silicate xenoliths and serpentinized zones in the footwall locally carry high grades of mineralization (Gain and Mostert, 1982; Armitage *et al.*, 2002). PGE grades (3PGE+Au) range from up to 15g/t (Lee, 1996), and can be as high as 26g/t (Hutchinson and Kinnaird, 2005) but are more commonly 2-4g/t. Nickel and copper abundances commonly range between 0.15-0.35% and 0.1-0.25% respectively (Lee, 1996), and although PGE are usually associated with BMS, there are many cases where decoupling of PGE from BMS

occur (e.g. Gain and Mostert, 1982; Hutchinson and Kinnaird, 2005; Kinnaird, 2005; Holwell *et al.*, 2006). This decoupling is likely to be a result of late-stage hydrothermal redistribution of PGE and/or BMS, and in particular serpentinites may contain variably high PGE and low BMS contents or vice versa (Armitage *et al.*, 2002; Holwell *et al.*, 2006). The average Pt/Pd ratio throughout the Platreef is generally around unity or slightly below (e.g. Kinnaird and Nex, 2003), however at Townlands, the Platreef appears to be relatively Pd-rich with the data of Manyeruke *et al.* (2005) indicating a Pt/Pd ratio of around 0.5.

As the footwall rock type changes along strike (Fig. 2.6), the interaction of the Platreef magma with the underlying rocks differs, which is reflected in the mineralization styles, and in particular, the platinum-group mineralogy. Until this study began in 2003, work on the platinum-group mineral (PGM) assemblages in the Platreef had been scarce, with only two papers covering Platreef PGM in any detail (Kinloch, 1982; Armitage *et al.*, 2002), and a brief overview by Viljoen and Schürmann (1998). In the past couple of years however, there have been three major PGM studies performed on the Platreef at Turfspruit (Hutchinson and Kinnaird, 2005), at Sandsloot (Holwell *et al.*, 2006, see Chapter 5) and at Overysel (see Chapter 7). The detailed assemblages and discussion of the changes along strike, together with a review of the current literature are described in these latter two papers and are therefore not discussed further here. Briefly, the most common types of PGM in the Platreef are tellurides, such as moncheite (PtTe₂) and kotulskite (PdTe), and sperrylite (PtAs₂) with antimonides, sulfides and bismuthides locally common, however, the abundances and presence of these PGM types appears to be directly controlled by footwall lithology (Viljoen and Schürmann, 1998; Holwell and McDonald, 2005a; Holwell *et al.*, 2006), and this is shown in summary Fig. 2.7.

2.3.4 Mineralization models and the role of contamination

Due to their highly chalcophile nature, the PGE, along with Cu and Ni, will be effectively collected by an immiscible sulfide liquid separating from a silicate magma. For this to occur, the magma must reach a state of S saturation, which it may attain in several different ways. For stratiform or reef PGE-sulfide deposits, which are generally S-poor, such as the Merensky Reef, or the J-M Reef in the Stillwater Complex, USA, S saturation is thought to have occurred through magma mixing (e.g. Campbell *et al.*, 1983), via extensive fractional crystallization of a tholeiitic parent magma (Hoatson and Keays, 1989), by chromatographic

separation as a magmatic fluid percolates upwards through a cumulate pile (Boudeau and Meurer, 1999) or by pressure fluctuations in the magma chamber (Cawthorn, 2005). The Platreef can be categorized as a 'contact-type' or 'marginal' PGE sulfide deposit, which are generally more S-rich than the stratiform deposits. Such deposits are common at the bases or margins of layered mafic intrusions, and are often 'stratabound' but not 'stratiform.' Examples include various deposits of the Penikat and Portimo Complexes of Finland and Federovo-Pansky intrusion in the Kola Peninsula, Russia (Alapieti and Lahtinen, 2002); the Muskox Intrusion in Canada (Irvine, 1988); the Dovirensky Layered Complex, Siberia (Papunen *et al.*, 1992); the East Bull Lake intrusion, Canada (Peck *et al.*, 2001) and the Duluth Complex, USA (Miller and Ripley, 1996). Similar deposits also occur in conduit systems such as the Uitkomst Complex, to the east of the Bushveld Complex (Gauert *et al.*, 1995) and the Voizey's Bay intrusion, Canada (Ripley *et al.*, 2002). For these deposits, sulfur saturation is often attributed to one or more contamination-related processes. The most obvious is an increase in fS_2 due to the assimilation of S-bearing country rock by the magma. Such a process is believed to have been significant in producing the mineralization in the Uitkomst Complex, with crustal S from the Malmani dolomites and Timeball Hill shales being assimilated by the magma (Li *et al.*, 2002), which has implications for Platreef mineralization due to the common country rock units. Silicic contamination, e.g. from the assimilation of granites, can also cause S saturation (Irvine, 1975), as can an increase in oxygen fugacity, for example as the result of devolatilization of assimilated country rocks within the magma. This can lower the FeO content and thus the S-carrying capacity of the magma and can therefore also induce economic sulfide mineralization (Buchanan and Nolan, 1979).

The Platreef has intruded a wide range of country rock lithologies and the interaction of the Platreef magma with these rocks has been considered by many workers to have been important in the generation and abundance of mineralization, by means of triggering sulfur saturation by silicic or sulfurous contamination. Cawthorn *et al.* (1985) showed the Platreef in the Overysel area to be contaminated with a partial melt from the gneissic footwall. Harris and Chaumba (2001) calculated that up to 18% dolomite had been assimilated by the Platreef magma in the Sandsloot area based on oxygen isotope studies. In particular, the addition of country rock sulfur to the magma through assimilation of S-bearing footwall rocks has been considered by some to have been an important trigger in initiating sulfur saturation in the

of S from anhydrite in country rocks such as the Malmani Subgroup, and silicic contamination from dolomite and granite triggered the precipitation of immiscible sulfides. Sharman-Harris *et al.* (2005) also attributed S saturation in the Turfspruit area to be the result of the assimilation of sulfide in the footwall Duitschland shales. Barton *et al.* (1986), however, considered the contamination at Overysel to post-date S saturation and Lee (1996) developed this by suggesting that the sulfide mineralization was of primary magmatic origin, with pre-formed PGE-enriched sulfides introduced from a staging chamber and settling out along the base of the intrusion to form the proto-Platreef, with contamination occurring as a post-emplacement event.

Sulfur isotope studies provide evidence for the source of sulfur and the potential role of any country rock S in upgrading the S budget. In the primary magmatic model advocated by Lee (1996), the S isotope signature of the early-formed sulfides should be magmatic (have a $\delta^{34}\text{S}$ value $0\pm 2\%$). In the contamination-driven hypothesis, the isotope signature will involve a component of crustal S, derived from the country rocks. Until very recently, the only sulfur isotope work that had been performed on the Platreef was by Buchanan *et al.* (1981) and Buchanan and Rouse (1984), who presented sulfur-isotope data for various metallic sulfides from the farms Tweefontein and Turfspruit that indicated a significant contribution from an isotopically heavy source of S in the footwall, that they thought was most likely to be anhydrite associated with the Malmani dolomites. It is from these early studies that anhydrite in the Malmani Subgroup came to be considered as the most likely source of country rock S added to the Platreef. More recent studies would suggest, however, that the Malmani was not the only source of additional S. For example, Manyeruke *et al.* (2005) presented data from the Platreef on Townlands, where Timeball Hill shales and quartzites make up the footwall, which also indicated a significant country rock contribution to the sulfur budget. A more detailed study by Sharman Harris *et al.* (2005) presented data from Rietfontein, Turfspruit and Macalacaskop, which identified pyrite in Duitschland shales to be a significant source of external sulfur in the area.

However, the work of Holwell *et al.* (Chapter 8) has shown that contamination by footwall S would appear to be strictly a localized process that upgrades the S content of the Platreef, but is not directly responsible for triggering S saturation. In addition, sulfate in the floor, for example in the Malmani Subgroup is unlikely to have had a major contribution to early

sulfide mineralization, and is more likely to have been incorporated into later-stage hydrothermal fluids. The details of these findings are presented in Chapter 8.

2.3.5 Hydrothermal activity

Platinum-group elements, and in particular Pt and Pd, are known to be mobile in aqueous fluids, and can be transported in a range of ways, including as chloride complexes, in bisulfide solutions, as hydroxides and in organic-ligand complexes (Wood, 2002). Aqueous fluids have the ability not just to modify economic PGE deposits by removing or upgrading PGE, but they can also be a primary concentration mechanism to some deposits. For example, the Pt deposits of the Waterberg, South Africa, are known to be hydrothermal in origin (McDonald *et al.*, 1995).

The interaction of the Platreef magma with the country rocks into which it intruded is also likely to have fundamentally influenced the nature and volume of hydrothermal fluids present at the time of mineralization, which in turn, are likely to have had significant effects on the style and distribution of the mineralization. Whilst the origin of the PGE is clearly magmatic, hydrothermal fluids have the potential to modify or redistribute PGE within the Platreef, and in particular, have the ability to transport PGE into the footwall. The changes in PGM mineralogy along strike as described by Kinloch (1982), Viljoen and Schürmann (1998), Armitage *et al.* (2002), Hutchinson and Kinnaird (2005), Holwell *et al.* (2006) and Holwell and McDonald (Chapter 7) show characteristic types of PGM species in areas of the same footwall lithology. In addition, Holwell *et al.* (2006, see Chapter 5) show that individual lithologies within the Platreef also host characteristic assemblages dominated by certain types and associations of PGM. These changes are directly related to the nature of fluids released by assimilation and metamorphism of the individual floor rocks on both a kilometre and metre scale, and the PGM mineralogy within individual rock types is a result of this. An effect of some of this hydrothermal activity is to cause decoupling of PGE from BMS, a feature which is particularly evident in the highly fluid-affected or serpentinized rocks such as calc-silicate floor rocks and xenoliths.

Hydrothermal activity is the most likely mechanism to have distributed mineralization into the footwall, and this certainly appears to be the case where the floor rocks are reactive sediments such as the dolomites at Sandsloot and Zwartfontein, where footwall mineralization is

such as the dolomites at Sandsloot and Zwartfontein, where footwall mineralization is common (e.g. Armitage *et al.*, 2002; Holwell *et al.*, 2006; Holwell and Jordaan, 2006). In other areas, however, such as where the floor rocks are hornfelses, distribution of PGE into the footwall is limited and grade falls off sharply into the footwall (Hutchinson and Kinnaird, 2005). Hydrothermal activity is, however, not the sole mechanism of distributing mineralization into the footwall. Where the floor rocks are Archaean basement gneisses, Holwell and McDonald (2006), note that the anhydrous nature of the floor rocks make the volumes of fluids released relatively small, and using textural evidence, suggest that mineralization penetrated the gneisses through an interconnected melt network in the partially melted footwall rocks.

2.3.6 Magmatic Emplacement

The timing of the emplacement of the Platreef and its position within Bushveld stratigraphy is currently contentious. Many workers such as Wagner (1929) and White (1994) have correlated the Platreef with the upper Critical Zone of the RLS primarily on the presence of the “Platinum Horizon” within pyroxenitic rocks, overlain by Main Zone rocks. Cawthorn *et al.* (2002) suggest that the magma which formed the UG2 chromitite layer in the eastern limb (where the Pt:Pd is closer to unity as in the Platreef) may have flown north, but without forming chromitite layers. Hulbert (1983) and van der Merwe (1978) regarded the GNPA member south of Mokopane as Critical Zone, but placed the Platreef at the base of the Main Zone. This is a view favoured by Kruger (2005a), who suggests that the Platreef and Merensky Reef are time equivalent and that the main pulse of Main Zone magma entered the chamber from north of the TML, spread out over the northern limb, picking up sulfur from the country rocks, before overtopping the TML, to flood into the rest of the complex, thus forming the Platreef as a basal unit in the north, and the Merensky Reef as the base to the Main Zone, overlying Upper Critical Zone rocks in the rest of the complex. On mineralogical, geochemical and textural grounds, McDonald *et al.* (2005) suggest that the GNPA member is not Critical Zone, but more likely a mixture of Lower Zone and Main Zone magmas, and that the Platreef and the GNPA member were formed in one or more of these mixing events. Field evidence from van der Merwe (1978) would suggest, though, that the Lower Zone was fully consolidated and tilted before emplacement of later magmas, however the transgressive relationships described are of the satellite bodies, and not the sequence south of Mokopane. It has been argued by Nell (1985) on the basis geothermobarometry data that the metamorphic

the emplacement of Lower Zone magma under estimated conditions of 750°C and 1.5kbar, and the second to the emplacement of Critical, Main and Upper Zone magmas at 900°C and 4-5kbar pressure. In a similar two-stage emplacement model, Kruger (2005b) used Cr/MgO ratios to suggest that the Platreef was intermediate between Main Zone and Lower Zone, but rather than a mixture of two magmas as suggested by McDonald *et al.* (2005), he suggests that the initial Main Zone magmas assimilated Lower Zone rocks, using the presence of chromitite schlieren in the Platreef as evidence for this.

One other possible explanation is that the Platreef was intruded post-lower Main Zone. Friese (2004) and Friese and Chunnet (2004) suggest that the Platreef was intruded as a syntectonic sheet-like intrusion along a thrust zone that formed along the contact between the Main Zone and the country rocks. The timing is suggested to correlate with that of the Pyroxenite Marker in the rest of the complex, though this seems unlikely due to the paucity of PGE within the Pyroxenite Marker (the highest 3PGE+Au concentration in any of the samples from the Pyroxenite marker in Maier *et al.*, 2001, is 109ppb; mean: 21ppb). There is a lack of evidence for a thrust contact at the base of the Main Zone or at the top of the footwall in all other studies (e.g. Armitage *et al.*, 2002). In addition, the nature of the contact between the Platreef and the overlying hangingwall rocks also do not support the post-lower Main Zone emplacement. This is discussed by Holwell *et al.* (2005) in Chapter 3.

2.4 Introduction to and context of the papers in Chapters 3-8

Chapters 3 and 4 present the results of geological mapping of the Platreef at Sandsloot and Zwartfontein and provide important constraints on the timing of magmatic and structural events related to the intrusion of the Platreef and the hangingwall magmas. Chapter 5 is a petrological and mineralogical study of the Platreef at Sandsloot that investigates the role of magmatic and hydrothermal processes on the distribution and style of mineralization. Chapter 6 follows this work up with a similar study at Overysel, where the floor rocks are dramatically different to those at Sandsloot, to investigate any footwall control on the mechanisms controlling the mineralization at that location. Chapter 7 is a detailed mineralogical investigation into the PGM mineralogy at Overysel coupled with laser ablation-inductively coupled plasma-mass spectrometry (LA-ICP-MS) analyses of the sulfide minerals and provides important evidence of the role of a sulfide liquid in the initial mineralising event. Finally, Chapter 8 uses S isotope data to assess the role of floor rock contamination in the generation of sulfide mineralization. This is used to constrain the source of mineralization in the Platreef and develop a more comprehensive model for its formation.

Chapter 3

Observations on the relationship between the Platreef and its hangingwall

Published as:

D. A. Holwell, P. E. B. Armitage and I. McDonald. 2005. Observations on the relationship between the Platreef and its hangingwall. *Applied Earth Science (Transactions of the Institute of Mining and Metallurgy B)*, **114**, 199–207.

Co-author roles:

P. E. B. Armitage undertook mapping of several faces within the southern part of the Sandsloot pit, which are described in Armitage *et al.* (2002), and subsequently produced Figure 3.2. Both P. E. B. Armitage and I. McDonald provided discussion during the preparation of the manuscript.

3.1 Abstract

Observations on the nature of the contact between the Platreef and its hangingwall have revealed that not only were the hangingwall gabbro-norites intruded after the Platreef, but that there appears to have been a significant time-break separating the two intrusive events. The hangingwall gabbro-norites truncate several features present within the Platreef pyroxenites but not in the hangingwall, such as shear zones and reef which have undergone alteration by Fe-rich fluids, implying that these features were formed prior to intrusion of the gabbro-norites. A fine-grained leuconorite at the base of the hangingwall exhibits textures showing erosion of Platreef orthopyroxene by fine-grained cumulus plagioclase, suggesting intrusion of a hot magma over cooled Platreef. Xenoliths of reef pyroxenite are also found in the hangingwall. PGE mineralization is present within basal zones of the hangingwall where the hangingwall overlies mineralized Platreef pyroxenite. We interpret the contact as a magmatic unconformity and, as the gabbro-norites do not appear to be PGE-depleted, suggest that PGE and S were scavenged or assimilated from the reef by the intruding magma, producing zones of orthomagmatic PGE mineralization in topographic depressions at the base of the crystallizing hangingwall. The presence of calc-silicate xenoliths in the hangingwall gabbro-norites can be explained by footwall anticlines or diapirism which the relatively thin Platreef had not overtopped, allowing footwall dolomite to be exposed to the main influx of hangingwall magma. The identification of a time-break between Platreef and hangingwall intrusion, and the most likely source of basal hangingwall PGE mineralization being the underlying Platreef, shows that the magma that formed the gabbro-norites could not have been the source of PGE for the Platreef as previously thought.

3.2 Introduction

The Platreef of the northern limb of the Bushveld Complex, South Africa, is currently one of the most extensively explored deposits of platinum-group elements (PGE) in the world. It is a pyroxenitic unit located between gabbro-norites attributed to the Main Zone of the complex, and floor rocks comprising Palaeoproterozoic metasediments and Archaean basement granite. PGE mineralization is heterogeneously distributed through the pyroxenite unit, and is usually present in the immediate footwall and occasionally in the immediate hangingwall (Armitage *et al.*, 2002; Holwell *et al.*, 2004; Lee, 1996; Viljoen and Schürmann, 1998). The northern limb of the Bushveld Complex comprises a succession of ultramafic-mafic lithologies, that have been broadly correlated by some authors with the Rustenburg Layered Suite (RLS)

present in the eastern and western limbs (Wagner, 1929; van der Merwe, 1976; von Gruenewaldt *et al.*, 1989; White, 1994). The well-defined igneous stratigraphy of the RLS comprises the Lower Zone of harzburgites and pyroxenites, the Critical Zone of cyclic chromitites, pyroxenites and norites, the Main Zone norites and gabbronorites, and the Upper Zone of magnetitites, gabbronorites and anorthosites. In the northern limb the stratigraphy differs in several important respects. The ultramafic Lower Zone is only developed south of the town of Mokopane, and as satellite bodies within the floor rocks north of the town (Fig. 3.1). Recent work has also shown that the Lower Zone extends for a limited distance north of Mokopane, with a series of serpentinized peridotites and pyroxenites present on Macalacaskop being attributed to the Lower Zone (Kinnaird *et al.*, 2005). The Critical Zone is not fully developed, and there is debate as to whether it is present at all (McDonald *et al.*, 2005). The Main Zone of the northern limb lacks correlatory horizons with the Main Zone in the rest of the complex, and includes a sequence of troctolites unique to the northern limb (van der Merwe, 1976). The Upper Zone has not been linked extensively with the rest of the complex, though one magnetite layer has been correlated with the Main Magnetite Layer on the basis of V_2O_5 content (van der Merwe, 1976, 1978). The footwall lithologies rest upon a succession of progressively older sedimentary units of the late Archaean - early Proterozoic Transvaal Supergroup, and Archaean granite basement, in what has been termed an 'igneous transgression' (Wagner, 1929). The footwall units are, north from Mokopane: quartzites and shales of the Timeball Hill Formation; sediments of the Deutschland Formation; the Penge banded iron formation; the Malmani dolomite and, north of Zwartfontein, the Archaean basement granites and gneisses (Fig. 3.1).

The timing of intrusion of the Platreef with respect to the units above it, and the general stratigraphy of the northern limb of the Bushveld Complex remain contentious issues. Traditionally, the Platreef pyroxenites north of Mokopane have been correlated with the Merensky Reef (Wagner, 1929; White, 1994), and a series of norite-pyroxenite-anorthosites with a chromitite layer (the GNPA member) south of Mokopane (Fig. 3.1), with the Critical Zone (Hulbert, 1983; van der Merwe, 1976; von Gruenewaldt *et al.*, 1989; White, 1994). Overlying gabbronorites have traditionally been correlated with the Main Zone. Kruger (2005a) suggests that the Platreef is the equivalent to the Merensky Reef and formed as a result of the first influx of Main Zone magma, therefore placing both reefs in the lower Main Zone. McDonald *et al.* (2005) suggest another alternative; that the Platreef and the GNPA

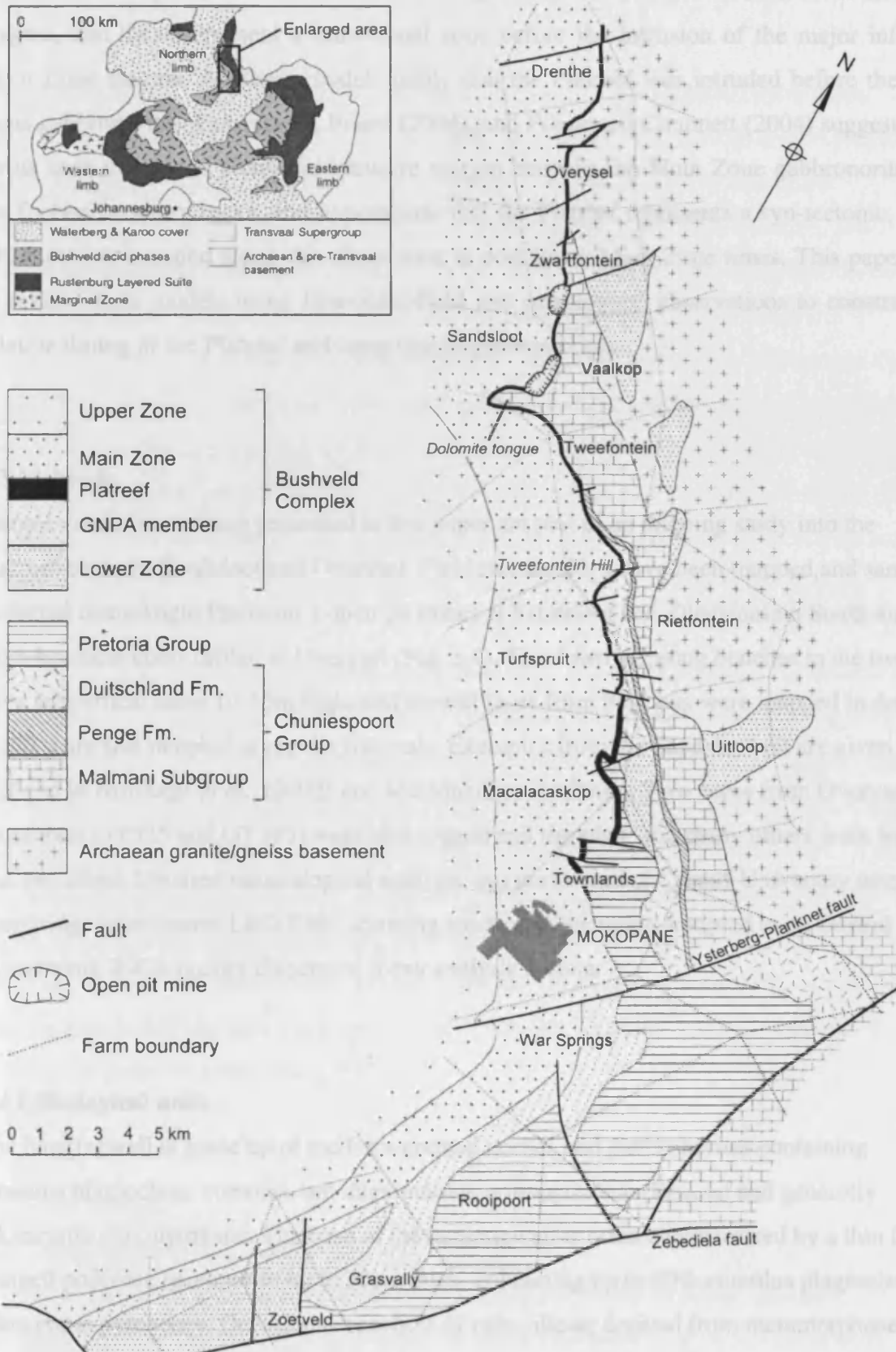


Figure 3.1. Geological map of the Platreef showing localities referred to in the text. After Kinnaird and Nex (2003), von Gruenewaldt *et al.* (1989) Hammerbeck and Schürmann (1998).

member are the products of one or more mixing events between Lower Zone and Main Zone magma, and these represent a transitional zone before the intrusion of the major influx of Main Zone magma. All these models imply that the Platreef was intruded before the Main Zone gabbro-norites. Conversely, Friese (2004), and Friese and Chunnnett (2004) suggest that a thrust zone developed along the intrusive margin between the Main Zone gabbro-norites and the footwall country rocks, and hypothesize that the Platreef represents a syn-tectonic, sheet-like intrusion intruded along this shear zone in post-lower Main Zone times. This paper aims to review these models using first-order field and petrological observations to constrain the relative timing of the Platreef and hangingwall gabbro-norites.

3.3 Methods

Samples and observations presented in this paper are part of an ongoing study into the Platreef between Sandsloot and Overysel. Field relationships have been mapped and samples collected from Anglo Platinum's open pit mines at Sandsloot and Zwartfontein South and from borehole cores drilled at Overysel (Fig. 3.1). The down-stepping benches in the two pits have subvertical faces 10-15m high, and several faces from both pits were mapped in detail at 1:100 scale and sampled at regular intervals. Examples from the Sandsloot pit are given Fig. 3.2, and in Armitage *et al.*, (2002) and McDonald *et al.* (2005). Two cores from Overysel (boreholes OY335 and OY387) were also logged and sampled, and many others were logged and described. Detailed mineralogical analysis was performed at Cardiff University using a Cambridge Instruments LEO S360 scanning electron microscope, coupled to an Oxford Instruments INCA energy dispersive X-ray analysis system.

3.4 Lithological units

The hangingwall is made up of medium-grained norites and gabbro-norites containing cumulus plagioclase, cumulus and intercumulus orthopyroxene (En₆₄₋₇₀) and generally oikocrystic clinopyroxene. The base of the hangingwall is often characterized by a thin fine-grained poikilitic leuconorite up to 30cm thick, containing up to 90% cumulus plagioclase and oikocrystic pyroxenes. Occasional xenoliths of calc-silicate derived from metamorphosed dolomite similar to that observed in the footwall are present in the hangingwall (Gain and Mostert, 1982; Kinnaird and Nex, 2003), and pyroxenites with petrographic and geochemical

characteristics similar to the Platreef are present within the hangingwall (McDonald *et al.*, 2005).

The Platreef is made up primarily of heterogeneously textured feldspathic pyroxenite, containing cumulus orthopyroxene (En₇₄₋₇₈), and intercumulus clinopyroxene and plagioclase. Base metal sulfide (BMS) and PGE mineralization is present within the interstitial assemblage. There is occasionally a fine-grained feldspathic pyroxenite, barren of BMS and PGE mineralization at the top of the Platreef succession. The maximum thickness observed for this unit in any of the faces mapped is 7m. In parts of the Sandsloot pit and at Zwartfontein, portions of the pyroxenites appear to have been affected by a late-stage Fe-rich fluid (McDonald *et al.*, 2005) which has removed plagioclase, and overprinted pyroxene with Fe-rich olivine (Fo₆₀₋₇₀) forming ultramafic lithologies that we have termed olivine-replaced reef (ORR). This has altered the normally telluride-dominant platinum-group mineral (PGM) assemblage to one dominated by alloys (Holwell *et al.*, 2004). Calc-silicate xenoliths are common within the reef and often extensively serpentinized (Armitage *et al.*, 2002).

The nature of the footwall varies along strike (Fig. 3.1). At Sandsloot and Zwartfontein South, the Platreef rests on dolomite of the Malmani Formation, which is metamorphosed to calc-silicates, which are variably serpentinized. At the transition from Platreef pyroxenite into calc-silicate, a unit termed 'parapyroxenite' is usually present which contains granoblastic clinopyroxene and is considered metamorphic in origin on the basis of whole-rock Cr and CaO content (Harris and Chaumba, 2001). Below this transitional zone, parapyroxenite also occurs as smaller lensoid bodies with gradational contact to the surrounding calc-silicate. At Overysel, where Archaen basement granite forms the floor rock, a hybrid unit of banded tonalitic gneisses of variable thickness termed 'granofels' is present, which separates the pyroxenites from the underlying granite.

3.5 Observations

3.5.1 Macroscopic relationships

In most of the faces studied, a planar magmatic contact is observed where poikilitic leuconorite or gabbronorite directly overlie the reef pyroxenites. Only a few faces show evidence for a sheared contact, and in these sections the uppermost pyroxenites are sheared

and subsequently altered by serpentine, sericite or carbonate; however, the overlying hangingwall rocks show no evidence of shearing or alteration.

In areas of the Sandsloot pit where the Platreef has undergone Fe-replacement, the rocks are visibly darker and the replaced zones display a greater degree of fragmentation in response to blasting than the rest of the reef and the hangingwall (Fig. 3.2). In all cases where these feldspar-poor ultramafic zones have been recognized, they are truncated by hangingwall lithologies that contain fresh plagioclase. The replacement event appears to be restricted to the Platreef and is not present in the hangingwall.

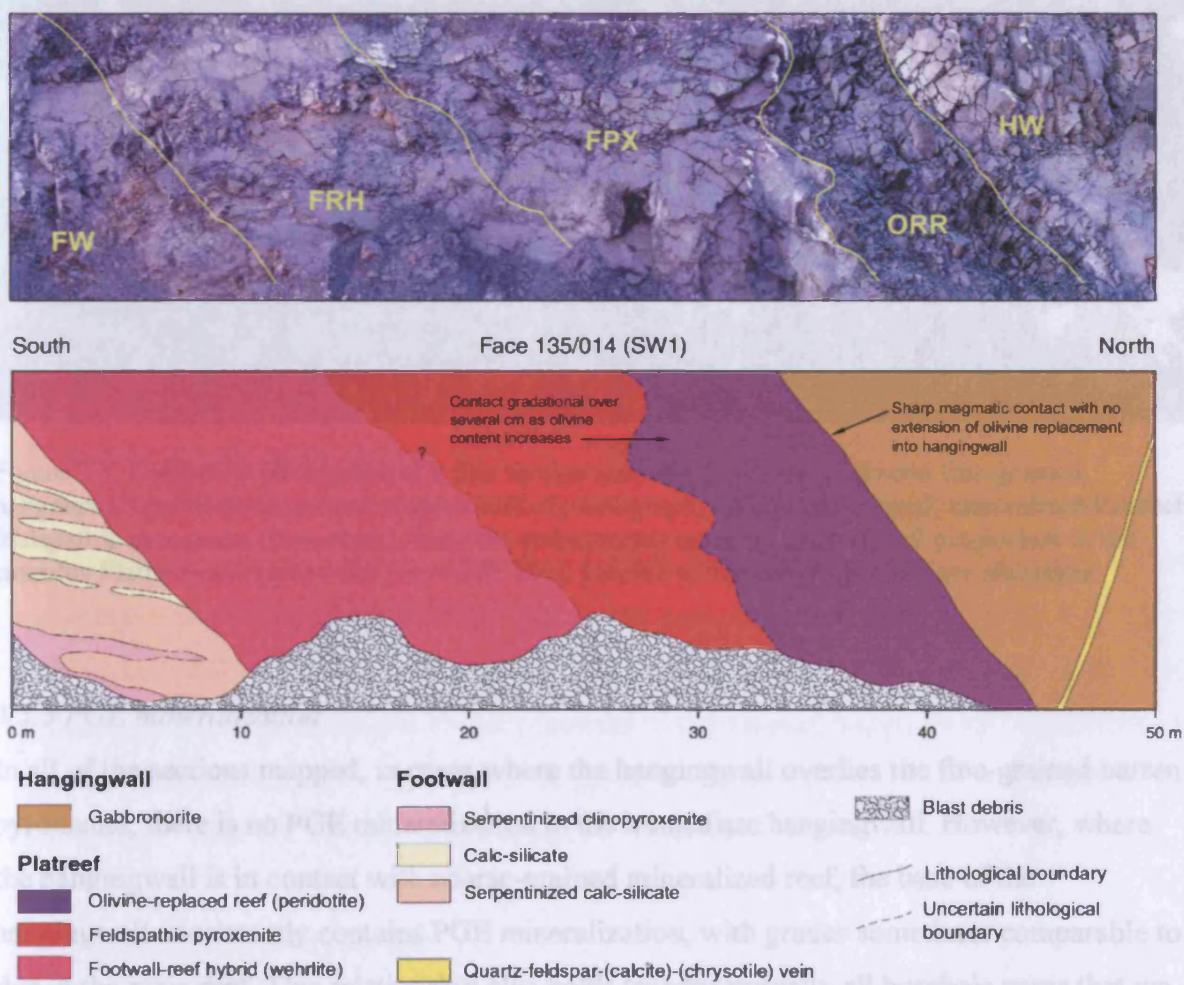


Figure 3.2. Photograph and map showing a face in the south-western part of the Sandsloot pit showing an exposed section of olivine replaced reef, displaying a distinct darkening and different fracture pattern to the surrounding lithologies. The replaced reef is truncated at a magmatic contact with the hangingwall gabbronorite. FW: footwall; FRH: footwall-reef hybrid; FPX: feldspathic pyroxenite; ORR: olivine-replaced reef; HW: hangingwall.

3.5.2 Petrography of the contact

Perhaps the most striking evidence for the nature of the contact is shown in Fig. 3.3, which shows the contact between hangingwall poikilitic leuconorite and coarse-grained, mineralized Platreef pyroxenite in thin section of a sample taken from the northern part of the Sandsloot pit. The cumulus orthopyroxene crystals at the top of the Platreef are visibly eroded and resorbed by cumulus plagioclase of the fine-grained poikilitic leuconorite. The leuconorite does not permeate the pyroxenite in any sense, and the embayments made by the small plagioclase crystals into the pyroxenes strongly suggest that the Platreef was completely or nearly completely solidified before intrusion of the overlying unit.

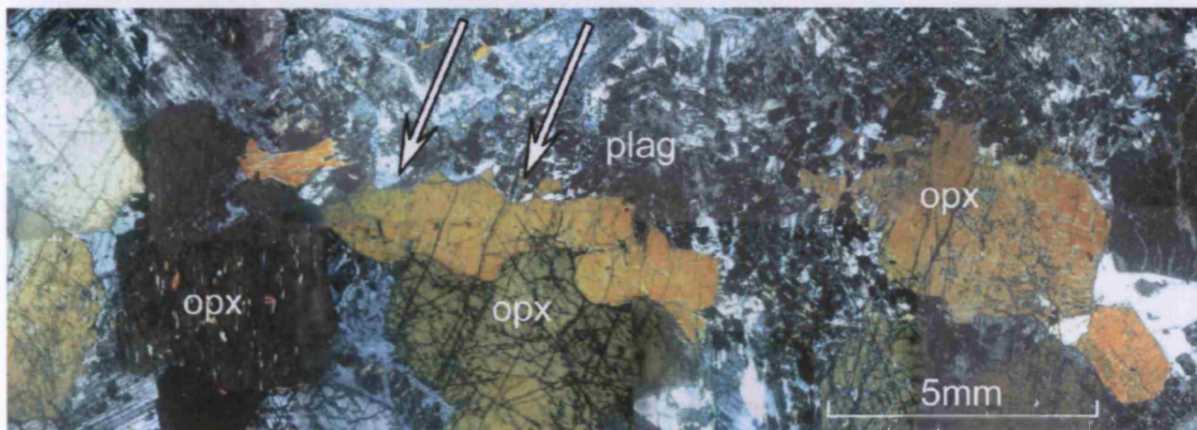


Figure 3.3. Composite photograph of a thin section showing the contact between fine-grained, hangingwall poikilitic leuconorite (upper half of photograph) and coarse-grained, mineralized Platreef feldspathic pyroxenite (lower half). Note the embayments made by hangingwall plagioclase in the cumulus Platreef orthopyroxenes (arrowed). Dark patches within the plagioclase are alteration.

3.5.3 PGE mineralization

In all of the sections mapped, in cases where the hangingwall overlies the fine-grained barren pyroxenite, there is no PGE mineralization in the immediate hangingwall. However, where the hangingwall is in contact with coarse-grained mineralized reef, the base of the hangingwall consistently contains PGE mineralization, with grades sometimes comparable to that in the main reef. This relationship also holds true for virtually all borehole cores that we have logged and described from the Sandsloot-Overysel section. Typically this zone of mineralization is in the lowermost metre of the hangingwall, and is rarely more than 3m thick. One such occurrence of hangingwall mineralization is described by Holwell *et al.* (2004) where an assemblage of Pd-bearing pentlandite, Pt-Fe alloy-BMS intergrowths and laurite is observed, which is characteristic of an orthomagmatic PGM association (Kinloch and Peyerl,

1990). Such assemblages have not been observed in the Platreef pyroxenites (Armitage *et al.*, 2002; Holwell *et al.*, 2004; Hutchinson *et al.*, 2004). The presence of mineralization appears to be very localized, and highly constrained by the nature of the reef on which the hangingwall rests.

3.5.4 Xenoliths

Xenoliths of calc-silicate are common throughout the Platreef and are also present in the hangingwall, up to 100m above the Platreef contact, and are also present further north several kilometres north of the last footwall outcrop of dolomite, e.g. at Drenthe (Gain and Mostert, 1982). At Sandsloot we have mapped rare occurrences of pyroxenite xenoliths in gabbronorites at the base of the hangingwall. These pyroxenites have whole-rock and cumulus orthopyroxene (En₇₈) compositions consistent with the Platreef. Intercumulus clinopyroxene showed evidence of partial recrystallization.

3.6 Discussion

In almost all current models for the formation of the Platreef and northern limb of the Bushveld Complex, the Platreef is taken to be the lowermost unit of the complex north of Mokopane, and the gabbronorites attributed to the Main Zone conformably overlie the Platreef. Prior to this study, most authors, with the exception of Friese (2004) have believed that the Platreef and the gabbronorites formed together, without any significant break in time and that the magma above the Platreef contributed some (or all) of the PGE to the reef (Buchanan and Rouse, 1984; Kruger, 2005a). The field relationships and mineralogical evidence presented in this paper identify features of the Platreef-hangingwall contact that have not been previously recognized and require a fundamental reassessment of these assumptions. Each line of additional evidence is considered in turn below.

3.6.1 Cross-cutting relationships

Some of the earliest work undertaken on the Platreef by Wagner (1929) describes veins of hangingwall norite intruding down into the Platreef, which would clearly imply a post-Platreef intrusion of the hangingwall. Evidence of a time-break between the emplacement of the Platreef and the gabbronorites lies in the truncation of certain features of the Platreef. For example, where the reef has been partially replaced by Fe-rich olivine, the olivine replacement is present directly below the hangingwall contact, but does not extend into the

hangingwall at all. The replacement is thought to be formed from the percolation of a late-stage, Fe-rich fluid through the reef (McDonald *et al.*, 2005) that post-dates formation of interstitial plagioclase and telluride-dominant PGM. Late Fe-rich ultramafic replacement bodies preferentially replace plagioclase-rich units in the RLS in the eastern and western Bushveld (Viljoen and Schoon, 1985), producing a Christmas-tree pattern of replacement and there seems no obvious reason why they should stop and not continue into the plagioclase-rich hangingwall at Sandsloot – unless it was not there. The obvious and consistent truncation of the Fe-rich olivine-replaced reef, and serpentinization in some of the pyroxenites, by the gabbronorites shows that the Platreef pyroxenites had both crystallized, and undergone alteration before the intrusion of the hangingwall gabbronorites.

Shear zones that are common in the Platreef pyroxenites, with associated alteration appear truncated by the hangingwall gabbronorites, with the hangingwall occasionally resting on sheared pyroxenite, but with no evidence of deformation or extension of alteration into the gabbronorites. This would imply that either the shearing took place before intrusion of the gabbronorites, or that competency contrasts between the pyroxenites and gabbronorites led to pyroxenites being sheared preferentially under conditions of deformation. In the first case, the gabbronorites must have been intruded after the Platreef and the shearing events. In the second case, it is not possible to constrain any relative timing, but preferential shearing of the reef is considered unlikely for shear zones which exhibit a high angle to the hangingwall contact.

We have mapped occurrences of pyroxenite xenoliths at the base of the hangingwall that have orthopyroxene compositions consistent with the Platreef. This relationship also provides evidence of a post-Platreef intrusion of the hangingwall magma.

3.6.2 Chilling and erosion at the base of the hangingwall

Perhaps the most compelling piece of evidence for this is shown in Fig. 3.3. The erosion of the Platreef orthopyroxene by fine-grained hangingwall plagioclase can only be explained by the intrusion of a hot magma onto cool, crystallized Platreef pyroxenite. The texture clearly demonstrates erosion of a solid pyroxenite with rigid properties, not a crystal mush. This inherently requires a significant time-break after the Platreef emplacement so as to cool the rock sufficiently for it to behave in this manner.

3.6.3 PGE mineralization in the hangingwall

The observation of hangingwall mineralization occurring exclusively in places where the gabbro-norites directly overlie mineralized reef is intriguing, and one that has not been previously recognized. The question is: where does the PGE in the mineralized zones of hangingwall come from? The Main Zone itself is a possible source of PGE. In the Merensky Reef, the overlying Main Zone is depleted of PGE (<10ppb Pt and Pd, Maier and Barnes, 1999); however, in the Platreef hangingwall, we have consistently found Pt and Pd concentrations to be around 10-15ppb, which indicates that the Main Zone in the northern limb is PGE fertile, and by implication did not have any of its PGE extracted to form the Platreef. The localization of hangingwall mineralization in anorthosite and gabbro-norite directly overlying mineralized Platreef pyroxenite and its corresponding absence above non-mineralized feldspathic pyroxenite strongly suggests incorporation of reef PGE into the basal zone of Main Zone magma by localized processes operating on a metre-scale. The barren, fine-grained feldspathic pyroxenite is stratigraphically higher than the coarser-grained, mineralized feldspathic pyroxenite, and is quite thin (maximum 7m in the sections mapped). It is possible that this barren, fine-grained unit was present continuously after the Platreef was intruded, and that the Platreef-hangingwall contact represents a magmatic unconformity surface, which has cut down through the uppermost barren pyroxenite and in places cut into mineralized reef, assimilating some PGE and enough sulfur and PGE to attain sulfur saturation, and producing very localized, basal zones of orthomagmatic PGE mineralization.

The 3-dimensional structure of the contact on a larger scale is uncertain due to the limited lateral distance exposed by the bench faces, but it is likely to be either an irregular, undulatory surface (Fig. 3.4A); or contain abrupt pothole-like structures (Fig. 3.4B); or it may be a planar surface, with the contact between fine-grained and coarse-grained pyroxenite undulatory (Fig. 3.4C). In either of the first two cases, PGE are scavenged from the reef and recrystallized virtually in-situ in depressions. The localization of mineralization within these depressions suggests that the overlying Main Zone magma was static, or had very low turbulence at the time of formation. Such a situation would support the pothole-like model, where the potholes may have formed after the hot Main Zone magma had been sitting on the cold Platreef for some time before melting the footwall, and creating a pothole-like structure. In such a model, one would expect to occasionally see the edges of such structures exposed in the bench faces, with the mottled anorthosite cutting down and truncating the fine-grained reef, although as yet, none of the faces we have mapped have shown such a relationship, and further mapping

is planned to attempt to confirm the true nature of the contact. It is important however to emphasize that there is an important genetic distinction between this contact and the unconformable contacts associated with the potholes of the Merensky Reef and UG2, which formed at magmatic or close to magmatic temperatures. There is no evidence of prior cooling of the footwall before their formation, such as chilling at the base. Here we use the term pothole as a morphological, rather than genetic analogue.

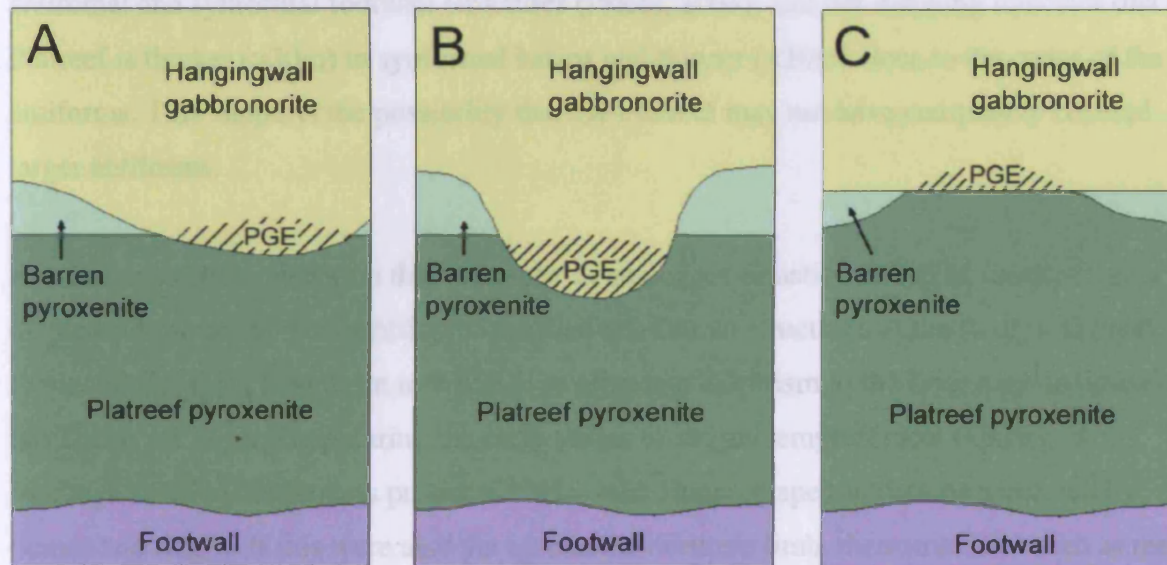


Figure 3.4. Schematic representation of the possible nature of the Platreef-hangingwall contact and the localization of hangingwall PGE mineralization in gabbronorite that directly overlies mineralized Platreef pyroxenite. A: the contact is an irregular, magmatic unconformity; B: the contact exhibits occasional pothole-like structures which cut down into the Platreef abruptly; C: the contact between mineralized and non-mineralized Platreef pyroxenite is undulatory, and the gabbronorite forms a planar contact, occasionally cutting mineralized Platreef.

3.6.4 Source of calc-silicate xenoliths

A prerequisite for any model which involves the Platreef being intruded before the hangingwall gabbronorites are emplaced is to explain the occurrences of calc-silicate xenoliths within the gabbronorites, which occur to heights up to 100m above the Platreef contact at Sandsloot (A. Bye, personal communication) and at Drenthe (Gain and Mostert, 1982). Friese (2004) used this as evidence of the Main Zone being intruded prior to intrusion of the Platreef, assuming that if the Platreef was formed first, it would have provided an impenetrable barrier between the footwall sediments and the Main Zone magma. This is not necessarily the case, and the occurrences of calc-silicate in the Main Zone can be explained in a number of ways, which still involve the Platreef being intruded first. An irregular floor

topography is one explanation: if structures such as the domal dolomite tongue, immediately to the south of the Sandsloot pit (Fig. 3.1) are pre-Bushveld, then the relatively thin Platreef may have intruded around such structures, thus leaving areas of exposed dolomite topographically higher than the Platreef. Such areas would therefore have been exposed to the Main Zone magma as it was intruded, and the incorporation of xenoliths of calc-silicate within the Main Zone is entirely possible. Pre-existing fold structures do appear to be influential in controlling the thickness of the reef. The Sandsloot pit shows some large antiformal and synformal footwall structures (Friese, 2004), and our mapping indicates that the Platreef is thicker (>30m) in synformal basins and thinner (<10m) close to the crests of the antiforms. This supports the possibility that the Platreef may not have completely covered larger antiforms.

Another possible explanation that produces an analogous situation is that of footwall diapirism initiated by the intrusion of the Platreef. Domal structures in the floor of the eastern Bushveld Complex have been interpreted to represent diapirism in the floor rock sediments of the Transvaal Supergroup during the early stages of magma emplacement (Uken and Watkeys, 1997). The process produces basins with finger-shaped intrusions separated by domes and ridges. If this were also the case in the northern limb, then structures such as the dolomite tongue (and presumably many unexposed structures) would represent syn-Bushveld structures, but would facilitate the exposure of footwall lithologies above the topographic level of the Platreef, as in the previous model.

A third possible explanation of calc-silicate xenoliths within the Main Zone is the possibility that they are xenoliths derived from country rocks that formed the roof of the Platreef. In the main part of the Bushveld Complex, the floor rocks are quartzites of the Magaliesburg Formation. These were unconformably capped by volcanic rocks of the 2061Ma Rooiberg Group, and the intrusion of the mafic suite of the Complex is thought to have immediately followed the eruption of the Rooiberg Group, and was intruded along the unconformable contact, with the Magaliesburg quartzites forming the floor rocks and the Rooiberg acting as a low-density carapace. Thus, the roof rocks in the main part of the complex are thought to have been the Rooiberg Group. This is not necessarily the case in the northern limb. It is clear from the transgressive nature of the Platreef-footwall contact that the Platreef was intruded obliquely to the country rock stratigraphy, as shown in the face maps in Fig. 3.2 and in

Armitage *et al.*, (2002) and it is entirely possible that the country rocks which formed the floor of the relatively thin Platreef also formed its roof.

Our observations outlined above are mutually supporting and strongly suggest that the Platreef was intruded first, and that there was a sufficient break in time to allow almost total crystallization, cooling and local alteration of the Platreef before intrusion of the hangingwall gabbro-norites. If the fine-grained pyroxenite at the top of the Platreef represents the remnants of an upper chill zone, it implies that the Platreef may have originally been a very thin, possibly sill-like, package of pyroxenites without any significant column of magma above it. Intrusion of the magma that formed the hangingwall took place as a separate, later event, and the cold Platreef formed the floor of this larger intrusion.

With such evidence, the model of Platreef intrusion in post lower Main Zone times (Friese, 2004; Friese and Chunnet, 2005) seems untenable. This model is based on several lines of evidence that can be interpreted in more than one way, or is directly contradicted by the new evidence that we present. Friese (2004) considers a thrust zone at the contact between the footwall and the Main Zone, along which the Platreef has later intruded, and states that the Platreef is bounded by major thrust zones at the contacts with the footwall and hangingwall. Whilst there is occasionally sheared pyroxenite below the hangingwall contact, this is by no means widespread, and no evidence of shearing in the hangingwall is seen. We have also found no evidence of the footwall contact being sheared, and Friese (2004) misinterprets the observation by Armitage *et al.* (2002) of lenses of serpentinite following the layering as representing thrust duplexes. These bands are elongate bodies and layers of serpentinite, usually with transitional boundaries, which represent compositional variations in the original bedded sediments, where forsterite has preferentially formed during contact metamorphism and been subsequently serpentinized. Figure 3.2 shows that the bands/lenses of compositional variations in the footwall have a relatively high angle to the footwall contact, and are truncated at the contact, strongly suggesting that they are not tectonic lenses formed by shearing along the contact zone.

3.6.5 Source of PGE in the Platreef

The discovery that there is a magmatic break associated with the base of the hangingwall has profound implications for the genesis of PGE mineralization in the Platreef. Until now, most studies have assumed that there was an extensive column of magma above the Platreef (represented by the hangingwall units) that could have supplied PGE via settling of immiscible sulfides to the reef. If the Platreef was intruded and crystallized before intrusion of the hangingwall magma, this *cannot* be the source of PGE for the Platreef. The mass balance question of how to account for the enormous mass of PGE in the Platreef is unresolved (Cawthorn *et al.*, 2002). If the hangingwall magma is not responsible, another source of and mechanism for concentration of PGE in the Platreef must be considered.

3.7 Conclusions

The evidence we present from mapping observations on a metre scale to mineralogical textures on a millimetre scale support the hypothesis that the Platreef formed prior to intrusion of the hangingwall gabbro-norites. Furthermore, the presence of: (i) PGE mineralization located at the base of the hangingwall where it is in direct contact with mineralized reef; (ii) mineralogical textures at the contact that indicate chilling and erosion; (iii) the truncation of replaced reef and sheared pyroxenite by the hangingwall; and (iv) partially recrystallized reef xenoliths within the hangingwall suggest that the Platreef pyroxenites were cooled and almost completely crystallized before the Main Zone was intruded. The intrusion of the Main Zone magma imparted an unconformable contact on the Platreef, and where the Main Zone magma cut down into mineralized portions of Platreef, PGE and S from the reef were incorporated into the new magma, and localized zones of basal PGE and BMS mineralization were formed in topographic hollows. The incorporation of xenoliths of calc-silicate into the Main Zone magma show that if the Platreef was intruded first, it could not have formed a complete barrier between the footwall and the Main Zone magma. This can be explained by there being an irregular floor topography at the time of Platreef intrusion, possibly caused by syn-emplacement diapirism of the footwall; or by interpreting the xenoliths as derived from the roof of the cold, thin Platreef, rather than from the floor beneath.

3.8 Acknowledgements

The authors would like to thank the management of Anglo Platinum, and in particular Alfred Sarila, for allowing Paul Armitage and David Holwell to undertake fieldwork on the Potgietersrus Platinums Limited lease area. Alan Bye and Richard Montjoie are acknowledged for their useful discussions, and Jay Cockayne is thanked for proof-reading the manuscript. David Holwell's PhD research is funded by the Natural Environment Research Council and supported by Anglo Platinum through Industrial CASE project (NER/S/C/2003/11952). Rais Latypov and Julian Menuge are thanked for their positive reviews and suggestions on improving the manuscript.

Chapter 4

Three-dimensional mapping of the Platreef at the Zwartfontein South mine: implications for the timing of magmatic events in the northern limb of the Bushveld Complex, South Africa

Published as:

D. A. Holwell and A. Jordaan. 2006. Three-dimensional mapping of the Platreef at the Zwartfontein South mine: implications for the timing of magmatic events in the northern limb of the Bushveld Complex, South Africa. *Applied Earth Science (Transactions of the Institute of Mining and Metallurgy B)*, **115**, 41-48

Co-author roles:

A Jordaan mapped the ZSW1 and ZSS2 faces (see Fig. 4.2) in the Zwartfontein pit and was involved with discussion in the field and provided drill chip information in the form of bench composites. All other mapping and interpretation was undertaken by the first author.

4.1 Abstract

The Platreef is a pyroxenitic unit with Ni-Cu-PGE mineralization that forms the base of the layered igneous succession in the northern limb of the Bushveld Complex. It rests upon sediments of the Transvaal Supergroup and Archaean granite/gneiss basement, and is overlain by norites and gabbronorites assigned to the Main Zone of the Complex. Detailed lithological mapping of a series of bench faces on bench 222 of the Zwartfontein South pit was undertaken to define a rectangular block. This information, coupled with drill chip data obtained during the drilling of the blast grids in the enclosing area has allowed us to constrain, with a high degree of confidence, the three-dimensional nature of the lithological relationships on a local scale, not achieved by any previous study. The inter-connectivity of the mapped faces has allowed the first well constrained, three-dimensional representation of the Platreef-hangingwall contact to be generated. It has revealed finger-like intrusions of hangingwall gabbronorite which cut down into the Platreef along zones of low competency such as NE-SW and N-S trending shear zones. This relationship demonstrates that the emplacement of Main Zone-type hangingwall magma occurred after a significant period of time that had allowed both crystallization and deformation of the Platreef to take place.

4.2 Introduction

The Platreef of the northern limb of the Bushveld Complex is one of the world's largest deposits of platinum-group elements (PGE) with associated Ni and Cu, and is currently undergoing an period of intense exploration activity. The advent of mining of the Platreef in 1992 by the opening of Anglo Platinum's Sandsloot mine (Fig. 4.1) paved the way for a new wave of research on the deposit (Bye and Bell, 2001; Armitage *et al.*, 2002; Friese, 2004; Friese and Chunnet, 2004; McDonald *et al.*, 2005; Holwell *et al.*, 2005; Holwell *et al.*, 2006). The success of the operation at Sandsloot led to the opening of Anglo Platinum's Zwartfontein South mine (Fig. 4.1) in 2002 and to a boom in exploration along the entire length of the northern limb by both Anglo Platinum and a host of junior companies. The sheer volume of core drilled during these recent exploration programmes by junior companies has facilitated an expanding number of academic studies to be performed outside of Anglo Platinum's lease area (Hutchinson and Kinnaird, 2005; Kinnaird, 2005; Kinnaird *et al.*, 2005; Naldrett, 2005). The majority of these studies have utilized borehole core samples which have obvious limitations in trying to interpret three- or even two-dimensional geological relationships and structures. Some of the studies undertaken in the open pit mine at Sandsloot

have used the mapping of individual bench faces to illustrate the two dimensional nature of the Platreef (Armitage *et al.*, 2002; McDonald *et al.* 2005; Holwell *et al.*, 2005). We have developed this approach and for the first time, have utilized a series of interconnected face maps and drill chip information to produce a three dimensional representation of a section of the Platreef in the Zwartfontein South mine. The results of this have revealed geological relationships that have important and unambiguous implications for the timing of magmatic and structural events in the northern limb of the complex.

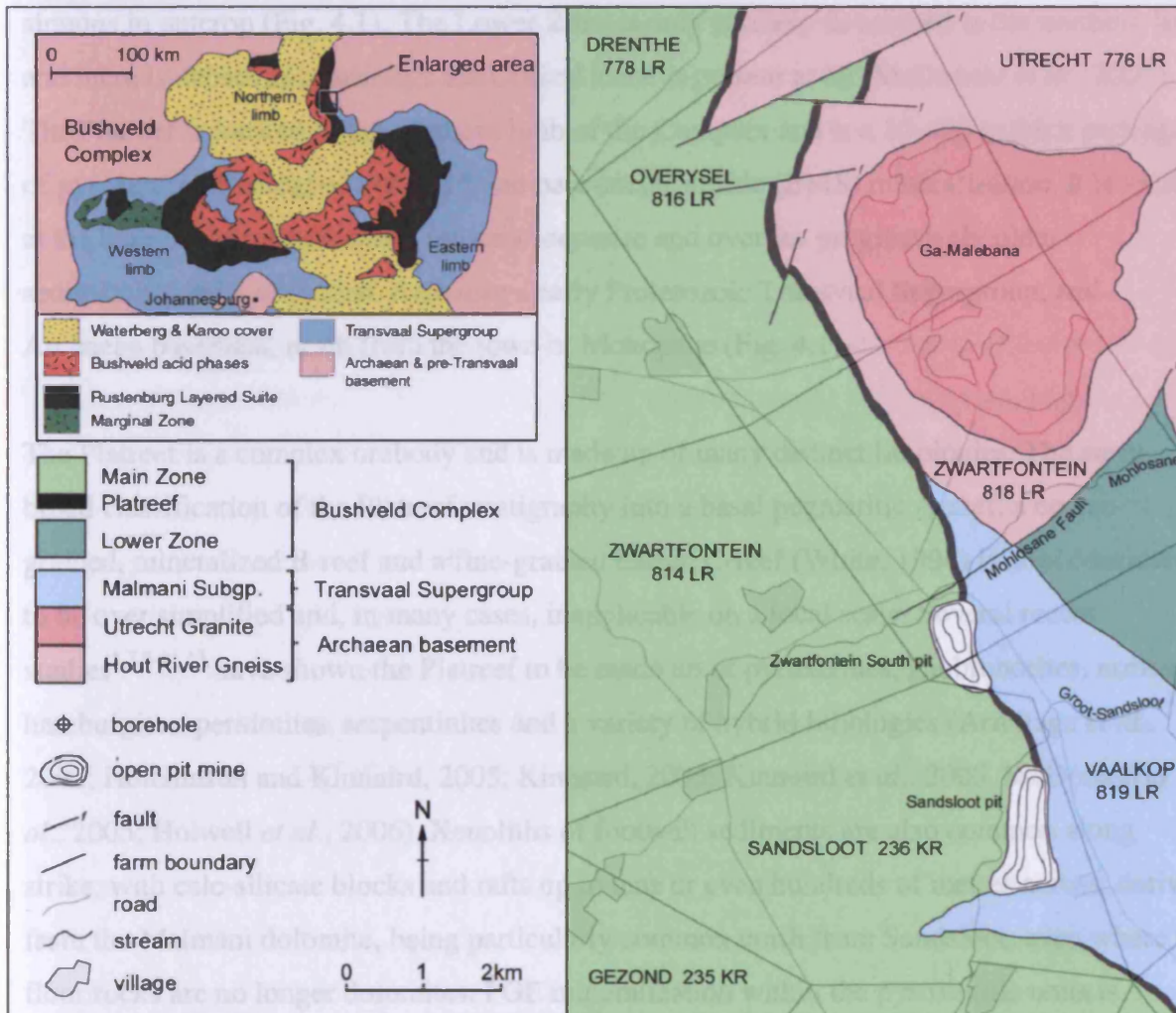


Figure 4.1. Geological map of the central portion of the Platreef showing the location of the Zwartfontein South pit.

4.3 Geological setting of the Platreef

The 2.06 Ga Bushveld Complex is the world's largest layered igneous complex and is located in the north-eastern part of South Africa, north of Johannesburg (Fig. 4.1). The Complex is made up of layered ultramafic and mafic cumulates intruded into Paleaeoproterozoic

sediments of the Transvaal Supergroup and Archaean basement in the northern part of the Kaapvaal Craton. The ultramafic-mafic sequence is divided into five zones (Hall, 1932) comprising a Marginal Zone of norites, Lower Zone pyroxenites and harzburgites, Critical Zone chromitite-pyroxenite-norite cyclic units, Main Zone gabbronorites and Upper Zone anorthosites, gabbronorites and magnetites. The Complex is divided into five limbs: roughly symmetrical eastern and western limbs, a southern (Bethal) limb covered by younger sediments to the south of the eastern limb, a far western limb and a northern limb, which is sinuous in outcrop (Fig. 4.1). The Lower Zone is only partially developed in the northern limb and there is debate as to whether the Critical Zone is present at all (McDonald *et al.*, 2005). The Platreef is located in the northern limb of the Complex and is a 10-400 m thick package of pyroxenitic lithologies with PGE and base-metal sulfide (BMS) mineralization. It is located at the base of the layered mafic igneous sequence and overlies progressively older sedimentary units of the late Archaean - early Proterozoic Transvaal Supergroup, and Archaean basement, north from the town of Mokopane (Fig. 4.1).

The Platreef is a complex orebody and is made up of many distinct lithologies. The early, broad classification of the Platreef stratigraphy into a basal pegmatitic A-reef, a coarse-grained, mineralized B-reef and a fine-grained barren C-reef (White, 1994) is now considered to be over simplified and, in many cases, inapplicable on a local scale. Several recent studies^{1,7,9-11,13} have shown the Platreef to be made up of pyroxenites, gabbronorites, norites, harzburgites, peridotites, serpentinites and a variety of hybrid lithologies (Armitage *et al.*, 2002; Hutchinson and Kinnaird, 2005; Kinnaird, 2005; Kinnaird *et al.*, 2005, McDonald *et al.*, 2005; Holwell *et al.*, 2006). Xenoliths of footwall sediments are also common along strike, with calc-silicate blocks and rafts up to tens or even hundreds of metres across, derived from the Malmani dolomite, being particularly common north from Sandsloot, even where the floor rocks are no longer dolomites. PGE mineralization within the pyroxenitic units is generally associated with BMS, although the distribution is heterogeneous. PGE distribution into the footwall is also sporadic and can attain depths of over 100 m. Hydrothermal redistribution, both within the reef and into the footwall, is common in areas where the floor rocks are particularly reactive, such as at Sandsloot, and this can result in the decoupling of PGE from sulfides (Holwell *et al.*, 2006). In contrast, where the floor rocks are particularly anhydrous, such as the gneisses on the farm Overysel, hydrothermal activity is minimal and PGE and BMS are more intimately associated (Holwell and McDonald, 2005a). The hangingwall rocks are gabbronorites and norites attributed to the Main Zone of the Bushveld

Complex. Until recently, it was assumed that the Platreef was either of Critical Zone affinity (von Gruenewaldt *et al.*, 1989; White, 1994), or that it marked the base of the Main Zone in the northern limb (van der Merwe, 1976; Kruger, 2005a). In both cases it was not assumed that there was a significant time-gap between the intrusions of the magma that formed the Platreef and the magma that formed the hangingwall gabbro-norites. Friese (2004) and Friese and Chunnnett (2004) suggested that the Platreef was a post lower Main Zone intrusion. However, the work of Holwell *et al.* (2005) at Sandsloot and Naldrett (2005) at Drenthe both concluded that the hangingwall magma was intruded post-Platreef, and after a significant time period to allow almost total crystallization of the Platreef magma.

4.4 The Platreef at Zwartfontein South

4.4.1 Footwall lithologies

The footwall rocks on the southern part of the farm Zwartfontein are metasediments derived from the Malmani dolomite (Fig. 4.1). Typically, they are crudely banded calc-silicates with lenses and bands of serpentinite which follow the relict bedding. In places, and especially close to the contact with the Platreef, metamorphic clinopyroxenites, locally known as ‘parapyroxenites’ are developed which can occur as almost pure green diopsidites. Xenoliths of calc-silicate within the Platreef pyroxenites commonly contain such diopside-rich bands and pods, and are also often highly serpentinitized. Mineralization is sporadic in the footwall, but can occur tens of metres into the clinopyroxenites and calc-silicates, and is particularly common in serpentinites. Xenoliths within the Platreef pyroxenites are also sporadically mineralized.

4.4.2 Platreef lithologies

The Platreef itself is made up of feldspathic pyroxenites, which vary in grain size, but are commonly medium-grained with cumulus orthopyroxene, intercumulus plagioclase, oikocrystic clinopyroxene and sporadic BMS. At the top of the reef, a fine-grained feldspathic pyroxenite that is characteristically barren of mineralization (analogous to the ‘C’-reef of White, 1994) is occasionally present. Parts of the pyroxenites appear serpentinitized, exhibiting a much darker colour and amorphous texture, and in thin section can be seen to contain abundant secondary olivine and can be classed petrologically as peridotites or feldspathic peridotites and are variably serpentinitized. These rocks correspond to the ‘olivine-replaced reef’ at Sandsloot (Holwell *et al.*, 2006), however, due to the extent of the serpentinitization, it

is unclear whether any of these are true igneous peridotites occur such as those that at Turfspruit (Kinnaird *et al.*, 2005). The peridotites are usually associated with serpentinized xenoliths and McDonald *et al.* (2005) suggested that the olivine-replaced reef at Sandsloot was formed by the percolation of a late-stage Fe-rich fluid through the Platreef, which may be related to the serpentinization of such xenoliths. Mineralization is common within the olivine bearing rocks. The presence of these xenoliths, rafts and associated peridotites and serpentinites is a common feature at Zwartfontein South and serpentinization is much more extensive than is observed at Sandsloot.

4.4.3 Hangingwall lithologies

The hangingwall is made up of medium-grained gabbro-norites with cumulus plagioclase, cumulus and intercumulus orthopyroxene and oikocrystic clinopyroxene. A thin (<2 m) mottled anorthosite is occasionally present at the base of the hangingwall, comprised of >80% cumulus plagioclase with occasional large oikocrysts of orthopyroxene and clinopyroxene, which give the 'mottled' appearance. Irregularly shaped, intrusive, fine-grained melagabbro-norites are a common feature towards the base of the hangingwall, and very occasionally are also seen to penetrate the Platreef. The intrusions occasionally contain minor PGE and BMS mineralization.

4.5 Mapping

This paper describes the lithological and structural nature of a portion of the Platreef by utilising face mapping together with drill chip information from an area of bench 222 in the northern part of the Zwartfontein South pit (Fig. 4.2) which constitutes a three dimensional, roughly rectangular block. The obvious advantage of working with bench faces in an open pit mine is that three-dimensional field relationships and structures can be identified and visualized to a much greater degree of confidence than is possible with borehole cores or field outcrops. The mapping we have performed has managed to constrain with great confidence, the nature of the lithological relationships on a local scale (100s of metres), and in a three-dimensional manner, not achieved by any previous study. A set of 10 m high bench faces on bench 222 were mapped at 1:100 scale which define a roughly rectangular block, and are shown in Fig. 4.2, with a plan map inferred between the face maps utilising additional information from drill chips generated during development of the blast grid for the bench. The mapping took place in November and December of 2005.

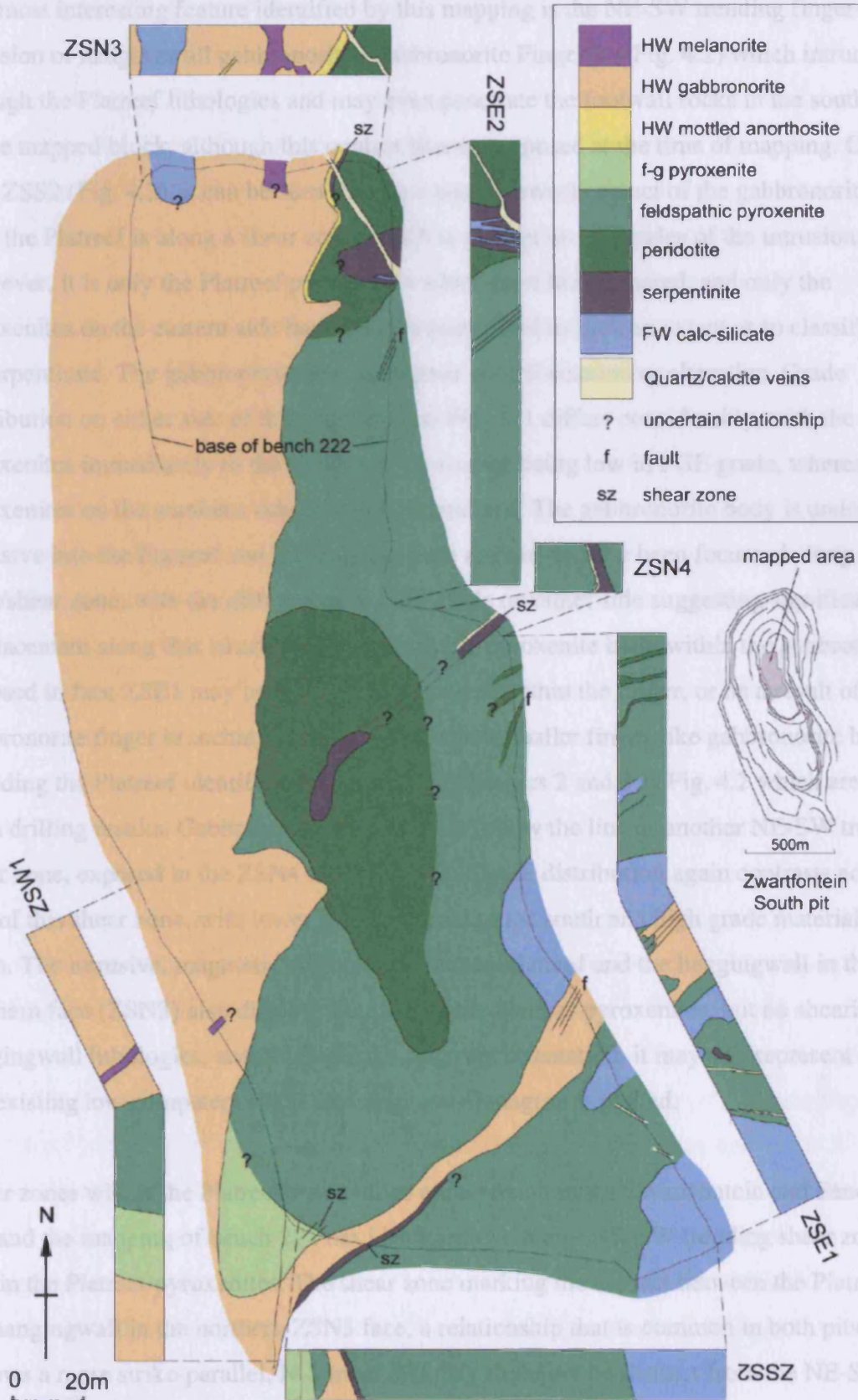


Figure 4.2: Geological face maps and plan map from bench 222 at the Zwartfontein South pit. The plan map is the surface corresponding to the tops of the bench faces mapped.

The most interesting feature identified by this mapping is the NE-SW trending finger-shaped intrusion of hangingwall gabbronorite (Gabbronorite Finger 1 – Fig. 4.2) which intrudes down through the Platreef lithologies and may even penetrate the footwall rocks in the southern part of the mapped block, although this contact was not exposed at the time of mapping. On face map ZSS2 (Fig. 4.2), it can be seen that the eastern (lower) contact of the gabbronorite finger with the Platreef is along a shear zone, which is present on both sides of the intrusion.

However, it is only the Platreef pyroxenites which have been sheared, and only the pyroxenites on the eastern side have been serpentinized to such an extent as to classify them as serpentinite. The gabbronorite has undergone no deformation or alteration. Grade distribution on either side of the Gabbronorite Finger 1 differs considerably, with the pyroxenites immediately to the north of the intrusion being low in PGE grade, whereas the pyroxenites on the southern side are well mineralized. The gabbronorite body is undoubtedly intrusive into the Platreef and this emplacement appears to have been focussed along a fault/shear zone, with the differences in PGE grade on either side suggesting significant displacement along this structure. The feldspathic pyroxenite body within the gabbronorite exposed in face ZSE1 may be a xenolith of Platreef within the finger, or be a result of the gabbronorite finger branching. There are two much smaller finger-like gabbronorite bodies intruding the Platreef identified as Gabbronorite Fingers 2 and 3 in Fig. 4.2 which are inferred from drilling results. Gabbronorite Finger 2 may follow the line of another NE-SW trending shear zone, exposed in the ZSN4 face (Fig. 4.2). Grade distribution again contrasts across the line of this shear zone, with lower grade material to the south and high grade material to the north. The intrusive, magmatic contact between the Platreef and the hangingwall in the northern face (ZSN3) also displays shearing of the Platreef pyroxenites, but no shearing of the hangingwall lithologies, and although of a different orientation, it may still represent a zone of pre-existing low competence that the hangingwall magma exploited.

Shear zones within the Platreef pyroxenites are common in the Zwartfontein and Sandsloot pits and the mapping of bench 222 has identified two major NE-SW trending shear zones within the Platreef pyroxenites. The shear zone marking the contact between the Platreef and the hangingwall in the northern ZSN3 face, a relationship that is common in both pits^{2,3} follows a more strike-parallel, N-S trend and may therefore be distinct from the NE-SW trending shear zones. The shear zone exposed in the ZSN4 face dips steeply to the southwest and is likely to continue across the pit, as serpentinite was encountered along the same strike direction during drilling. The shear zones are up to a few metres wide, are marked by

extensive serpentinization of the pyroxenites, with closely spaced fractures on a centimetre scale displaying serpentine slickenfibres on their surfaces. The presence of serpentine and the alteration of the pyroxenite indicates significant hydrothermal fluid flow along these discontinuities. Some pyrite has been precipitated along the fracture surfaces although the presence of PGE is variable from one shear zone to the next. The shear zones do not penetrate the hangingwall, and are intruded by hangingwall rocks and are therefore pre-gabbro intrusion. The intersection of the shear zones with the footwall calc-silicates was not observed in any of the available faces, and therefore it is unclear to what extent the footwall rocks underwent shearing/faulting as a response to the same deformation.

The large calc-silicate body present in the south-eastern corner of the mapped area is true footwall, which can be seen on adjacent benches in the pit. Calc-silicate xenoliths are present within the Platreef pyroxenites in the ZSE1 and ZSE2 faces. Serpentinites may be derived from either igneous or metasedimentary precursors. The serpentinite body in the northern part of the ZSE2 face is likely to be a serpentinized metasedimentary xenolith as it exhibits bands of diopside. Peridotitic lithologies may also be ambiguous as to whether the olivine is igneous or secondary, but the apparent halo of peridotite around the aforementioned serpentinized xenolith suggests that here the alteration of pyroxenite to olivine-bearing rocks may be related to the alteration of the xenolith. The large zone of peridotite in the centre of the mapped area is likely to be an altered raft of calc-silicate.

The mottled anorthosite, which commonly occurs at the base of the hangingwall is present in the ZSN3 face in the northern part of the pit, but is not present in the ZSW1 face and it is uncertain where it is present or absent in the intervening area as inferred from the drill chip results. There is also a thin band of mottled anorthosite which follows the same orientation as the Platreef-hangingwall contact exposed around 25 m into the hangingwall in the ZSN3 face. Around 40 m into the hangingwall in the ZSN3 face, a calc-silicate xenolith 15 m wide is exposed within the gabbroites. The irregular, apparently intrusive fine-grained melagabbroite bodies are present near the base of the hangingwall in the ZSN3 and ZSW1 faces, and are a common feature of the lower parts of the hangingwall in the pit.

4.6 Discussion

The mapping of bench faces in the open pit mine at Zwartfontein South has allowed us to reveal the form and structure of a section of the Platreef with a greater degree of certainty than has been previously possible. The real advancement of this study is the inter-connectivity of the mapped faces, which has allowed the first well constrained three-dimensional model of the hangingwall contact to be generated.

4.6.1 Timing of magmatic events:

The geological relationships we have identified support the theory that the hangingwall magma intruded after a significant time break following Platreef intrusion (Holwell *et al.*, 2005). The intrusive finger of gabbro-norite clearly post-dates Platreef emplacement. In addition, it appears to have exploited a shear zone, as seen by the sheared and serpentinized pyroxenite at the contact. The frequently observed relationship of the uppermost portion of the Platreef being sheared below the hangingwall gabbro-norite, as is seen for example in the ZSN3 face, may be an illustration of the same tendency for the gabbro-norite magma to exploit less competent zones. It is unclear as to whether the shear zones penetrate the footwall rocks in the area we have mapped. Armitage *et al.* (2002) mapped several faces in the Sandsloot pit, and recognized a series of pegmatoidal gabbro-norite dykes that penetrated the footwall, but were not able to establish whether these cut the Platreef. It is possible that these are hangingwall fingers, analogous to the one we have mapped at Zwartfontein South, that have penetrated the footwall. The lack of shearing in the hangingwall, and the fact that the hangingwall rocks intrude along these shear zones is clear evidence that NE-SW strike-slip shearing of the Platreef pyroxenites occurred before the emplacement of the hangingwall gabbro-norites. The contrasts in grade distribution across the shear zones suggests that there may have been a significant displacement up to tens of metres before intrusion of the hangingwall. Alternatively, these contrasts may be caused by the shear zones and/or gabbro-norite bodies providing barriers to post-emplacement hydrothermal redistribution of PGE.

The earliest work on the Platreef also identified veins of hangingwall norite intruding down into the Platreef (Wagner, 1929). However, the significance of this was not recognized until the work at Sandsloot (Holwell *et al.*, 2005) and this work at Zwartfontein. In addition, the recent work by Naldrett (2005) has also identified hangingwall intrusions in the Platreef, north of Zwartfontein on the farm Drenthe (Fig. 1), similar to the one we have identified in

the Zwartfontein South pit, that also appear to have exploited a less competent layer. In this case however, it is a horizon where altered dolomite is common rather than a shear zone that the gabbro-norite has invaded.

The presence of fine-grained melagabbro-norite intrusions near the base of the hangingwall is common at Zwartfontein. The intrusions are post-Platreef as they do occasionally cut down into the Platreef but these occurrences are much rarer than in the hangingwall. The irregular nature of the intrusions, such as the one exposed in the ZSN3 face, and the fact that they rarely penetrate the Platreef, may suggest they formed when the main body of gabbro-norite was not fully crystallized, whereas the Platreef was. This would explain the preference for the irregular shape of the intrusions in the softer hangingwall. The origin of these intrusions is uncertain, but they may represent a late stage residual melt or a hybrid melt of assimilated Platreef, particularly as they occasionally contain PGE mineralization.

Figure 4.3 shows the schematic magmatic history at Zwartfontein South. Initially, the Platreef magma intruded (Fig. 4.3a) over Malmani dolomite and beneath roof rocks of uncertain affinity either Rooiberg felsites (Kruger, 2005a) or more likely Malmani dolomite. The presence of the xenolith of calc-silicate in the hangingwall in the ZSN3 face suggests this is a distinct possibility. The presence of calc-silicate xenoliths within the hangingwall was discussed by Holwell *et al.* (2005), who concluded that the Platreef either must not have formed a complete barrier between the hangingwall magma and the floor rocks, or that the roof rocks to the Platreef in the area north of Sandsloot were also calc-silicates. For simplicity, Fig. 4.3a shows the Platreef intrusion as a single magma body, but it is possible that emplacement occurred as a series of magma pulses (Kinnaird, 2005). Intrusion of the Platreef magma was subsequently followed by a period of crystallization and shearing (Fig. 4.3b), with associated hydrothermal fluid activity and serpentinization. The hangingwall magma then intruded over the virtually solidified Platreef forming a magmatic unconformity and exploited zones of weakness such as the shear zones to intrude down into the Platreef (Figs 4.3c,d). Tilting then occurred (Fig 4.3e) to attain the presently observed dips; finally erosion and mining exposed the surface shown in Fig. 4.3f, which corresponds with the lower half of the plan map in Fig. 4.2.

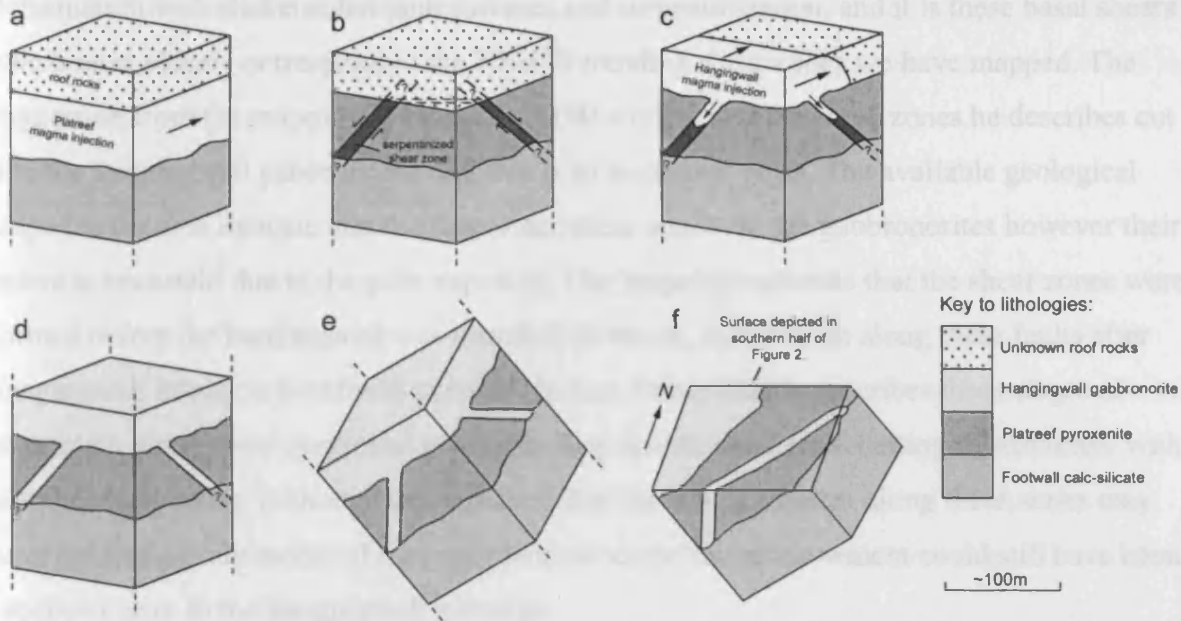


Figure 4.3. Three dimensional schematic representation of the stages involved in the intrusion of the Platreef and hangingwall gabbronorite in the area mapped at Zwartfontein South. All views are facing north-northwest. *a*: intrusion of Platreef magma over dolomite floor rocks and beneath unknown roof rocks. *b*: cooling, crystallization and deformation of the Platreef occurs. *c*: intrusion of hangingwall magma exploits zones of weakness such as shear zones, and intrudes down into the Platreef. *d*: crystallization of hangingwall magma followed by *e*: tilting. *f* shows the planar surface which corresponds to the southern portion of the plan map of the area mapped in Fig. 2.

4.6.2 Timing of deformation events

Our mapping of the intrusive nature of the gabbronorites along shear zones in the Zwartfontein pit, and the discontinuation of the deformation zones into the adjacent hangingwall rocks, together with previous petrological studies (Holwell *et al.*, 2005) clearly indicate that shearing of the Platreef took place before the intrusion of the gabbronoritic magma. Two orientations of such deformation zones which the gabbronoritic magma appears to have exploited have been identified in this study: one set striking roughly NE-SW and dipping steeply, and another, strike parallel, N-S trending set. Extensive structural work by Friese (2004) in the Sandsloot and Zwartfontein South pits also identified similar features and classified the former as strike-slip shear zones, and the latter as Group 1 layer subparallel thrust zones. Friese (2004) describes three orders of NE-SW trending, steep to subvertically dipping strike-slip shear zones. First order shear zones include major structural boundaries such as the Mohlosane fault (Fig. 1), and all others as either second or third order, which interlink between the major first order shear zones. Friese (2004) describes these smaller shear zones as being 10-20m thick and comprising a 50cm thick basal shear of intense

deformation with slickensided fault surfaces and serpentization, and it is these basal shears which most closely correspond to the NE-SW trending shear zones we have mapped. The suggestion from the mapping in Friese's (2004) work is that the shear zones he describes cut into the hangingwall gabbro-norite and this is an important point. The available geological maps for the area indicate that the first-order shear zones cut the gabbro-norites however their extent is uncertain due to the poor exposure. Our mapping indicates that the shear zones were formed before the hangingwall was intruded, however, reactivation along these faults after hangingwall intrusion is entirely possible. In fact, Friese (2004) describes three stages of movement along these zones and notes that they exhibit clear cross cutting relationships with all other fault zones. Although this indicates that the last movement along these zones may have been relatively recent, if they are reactivated, the initial movement could still have been produced prior to the hangingwall intrusion.

Friese (2004) also describes the shear zones that commonly occur immediately below the hangingwall contact (Bye and Bell, 2001; Armitage *et al.*, 2002;), that he interprets to be oblique frontal ramp structures. A particularly contentious conclusion of the study of Friese (2004) is the suggestion that the Platreef was intruded in post-lower Main Zone times, i.e. after the intrusion of the hangingwall magma, however the petrological and lithological relationships described here and in Holwell *et al.* (2005) are entirely conflicting with this theory. Friese (2004) partially based this theory on a limited exposure where a sliver of sheared Platreef pyroxenite is present between two bodies of hangingwall gabbro-norite, and attributed this to Platreef being thrust up into the hangingwall. In the light of our identification of finger like bodies of gabbro-norite that dissect the underlying Platreef, it is possible that this exposure represents a similar intrusive feature. Friese (2004) attributes the timing of the formation of both the NE-SW trending strike-slip shear zones and the N-S trending Group 1 thrusts in the Bushveld rocks to the reactivation of Neoproterozoic (2.78-2.64 Ga) crustal sinistral strike-slip shear zone systems during the Ubendian Orogeny (2.058-1.86 Ga). The fact we have shown evidence of shearing within the Platreef that the hangingwall magma exploited during its intrusion, the evident break in time between intrusion of the Platreef and hangingwall emplacement must have fundamentally seen the initiation of such deformation, with both the NE-SW and N-S trending shear zones produced before the emplacement of the hangingwall magma. Thus, the time-break in between Platreef and hangingwall gabbro-norite intrusion may be a considerable one. It is this early stage of deformation which is not recognized by Friese (2004). Further reactivation, however, along these deformation zones,

particularly the NE-SW trending structures, after emplacement of the hangingwall is likely to have taken place, and produced the offsets observed on the first-order shear zones, such as the Mohlosane fault.

4.7 Conclusions

Detailed mapping on a scale not previously performed has allowed us to generate the first three-dimensional representation of the contact between the Platreef and its hangingwall with a high degree of certainty. This has revealed important and unambiguous lithological relationships in the Platreef at the Zwartfontein South pit that unequivocally show that the hangingwall gabbro-norites cut down into the Platreef along zones of low competency such as NE-SW and N-S trending shear zones. This clearly demonstrates that emplacement of the hangingwall gabbro-norites occurred after crystallization of the Platreef pyroxenites and at least two phases of deformation, and that there must have been a significant time break between the intrusion of the Platreef and gabbro-norite magmas. Further reactivation of these deformation zones took place after the emplacement of the gabbro-norites.

4.8 Acknowledgements

The management of Anglo Platinum are thanked for allowing David Holwell to undertake fieldwork on the Potgietersrust Platinum Limited lease area and for providing permission to publish this paper, and without whom, this study could not have been possible. David Holwell's PhD research is funded by the Natural Environment Research Council and supported by Anglo Platinum through Industrial CASE project (NER/S/C/2003/11952). Thanks to Iain McDonald for his support and comments, and to Cheryl Tippins for assistance drafting Figure 3. The quality of the manuscript benefited from reviews by Paul Nex and Jock Harmer.

Chapter 5

Platinum-group mineral assemblages in the Platreef at the Sandsloot Mine, northern Bushveld Complex, South Africa

Published as:

D. A. Holwell, I. McDonald and P. E. B. Armitage. 2005. Platinum-group mineral assemblages in the Platreef at the Sandsloot Mine, northern Bushveld Complex, South Africa. *Mineralogical Magazine*, **70**, 83-101.

Co-author roles:

Both I. McDonald and P. E. B. Armitage provided discussion during the preparation of the manuscript. P. E. B. Armitage provided around half of the sample suite.

5.1 Abstract

Platinum-group mineral (PGM) assemblages in the Platreef at Sandsloot, northern Bushveld Complex, in a variety of lithologies reveal a complex multi-stage mineralization history. During crystallization of the Platreef pyroxenites, platinum-group elements (PGE) were distributed throughout the interstitial liquid forming a telluride-dominant assemblage, devoid of PGE sulfides. Redistribution of PGE into the metamorphic footwall by hydrothermal fluids has formed arsenide-, alloy- and antimonide-dominant assemblages, indicating a significant volatile influence during crystallization. Serpentinization of the footwall has produced an antimonide-dominant PGM assemblage. Parts of the igneous reef were subjected to alteration by a late-stage, Fe-rich fluid, producing ultramafic zones where the telluride-dominant assemblage has been recrystallized to an alloy-dominant one, particularly rich in Pt-Fe and Pd-Pb alloys. A thin, small-volume zone of PGE-BMS mineralization along the base of the hangingwall contains a primary PGM assemblage that is locally altered to one dominated by Pt/Pd germanides. This is thought to have formed when the new pulse of Main Zone magma entered the chamber, and scavenged PGE by assimilation of the underlying mineralized Platreef pyroxenites. That each major rock type at Sandsloot contains a distinctive PGM assemblage reflects the importance of syn- and post-placement fluid and magmatic processes on the development of Platreef mineralization.

5.2 Introduction

The Bushveld Complex of South Africa is the largest layered igneous intrusion in the world and is the largest single host of platinum-group elements (PGE) yet discovered. The major PGE deposits of the Bushveld Complex are the stratiform Merensky Reef and UG2 chromitite layer, and the stratabound, but not stratiform, Platreef. The complex can be divided into an eastern and western limb of similar size; a southern limb, identified beneath cover rocks by gravity studies; and a smaller northern limb (Cawthorn *et al.*, 2002). The Platreef, located in the northern limb, has an estimated Pt+Pd reserve of 16.3 million ounces (Cawthorn, 1999), and is currently being mined by open-pit methods by Potgietersrus Platinums Ltd., a subsidiary of Anglo Platinum, at the Sandsloot and Zwartfontein South pits ~30km northwest of the town of Mokopane (formerly Potgietersrus; Fig. 5.1).

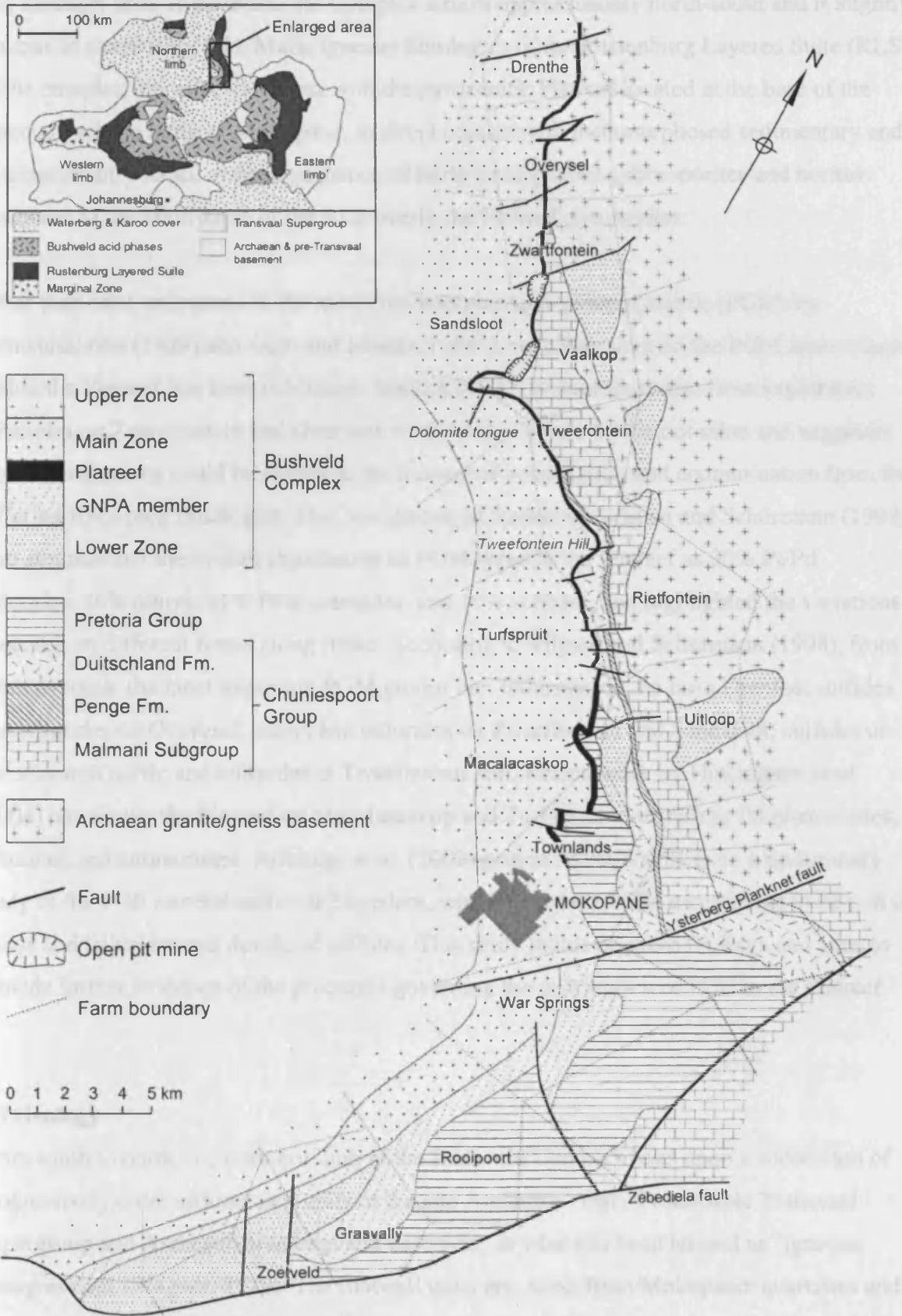


Figure 5.1. Geological map of the central and southern sections of the northern limb of the Bushveld Complex, showing the Platreef and localities and lithologies referred to in the text. After Kinnaird and Nex (2003), von Gruenewaldt *et al.* (1989), Hammerbeck and Schürmann (1998).

The northern limb of the Bushveld Complex strikes approximately north-south and is slightly sinuous in shape (Fig. 5.1). Mafic igneous lithologies of the Rustenburg Layered Suite (RLS) of the complex dip west-southwest with the pyroxenitic Platreef located at the base of the igneous package north of Mokopane, in direct contact with metamorphosed sedimentary and igneous country rocks. A thick sequence of fairly homogenous gabbro-norites and norites attributed to the Main Zone of the RLS overly the Platreef pyroxenites.

Other than brief references to the most common platinum-group minerals (PGM) by Schneiderhöhn (1929) and Gain and Mostert (1982), very little data on the PGM assemblages within the Platreef has been published. Kinloch (1982) summarized data from exploration boreholes on Zwartfontein and Overysel, north of the current Sandsloot mine and suggested regional variations could be related to the amount of assimilation and contamination from the differing floor rock lithologies. This was discussed further by Viljoen and Schürmann (1998), who summarized the overall abundances of PGM types in the Platreef as 30% Pt/Pd tellurides, 26% alloys, 21% PGE arsenides, and 19% sulfides, and highlighted the variations observed on different farms along strike. According to Viljoen and Schürmann (1998), from north to south, the most important PGM groups are: tellurides on the farm Drenthe; sulfides and tellurides on Overysel; alloys and tellurides on Zwartfontein and Sandsloot; sulfides on Tweefontein north; and tellurides at Tweefontein Hill. Recent work by Hutchinson *et al.* (2004) has shown the Platreef on Macalacaskop and Turfspruit to be rich in Pd bismuthides, tellurides and antimonides. Armitage *et al.* (2002) presented the results from a preliminary study of the PGE mineralization at Sandsloot, which found the PGM assemblage to be rich in alloys and tellurides and devoid of sulfides. This study builds on these findings and aims to provide further evidence of the processes governing the distribution of PGE in the Platreef.

5.3 Geology

From south to north, the northern limb of the Bushveld Complex rests upon a succession of progressively older sedimentary units of the late Archaean - early Proterozoic Transvaal Supergroup and Archaean granite/gneiss basement, in what has been termed an 'igneous transgression' (Wagner, 1929). The footwall units are, north from Mokopane: quartzites and shales of the Timeball Hill Formation; shales of the Deutschland Formation; the Penge Banded Iron Formation; dolomite of the Malmani Formation and, north of Zwartfontein, Archaean granite/gneiss basement (Fig. 5.1). Samples used in this study were taken from the

Sandslot mine, where the footwall is Malmani Dolomite. The hangingwall along the entire strike of the reef is composed of gabbronorites and norites ascribed to the Main Zone of the RLS.

The geology of the Platreef at Sandslot Mine has been described by Harris and Chaumba (2001), Armitage *et al.* (2002), McDonald *et al.* (2005), and Holwell *et al.* (2005) and is summarized below, together with the authors' own observations on previously undescribed lithologies. The majority of the Platreef 'package' can be divided into hangingwall lithologies, igneous Platreef lithologies, and a variety of metamorphic footwall lithologies. There are variations in lithology on a metre scale along the length of the Platreef in the Sandslot pit, and the variations are summarized in Fig 5.2.

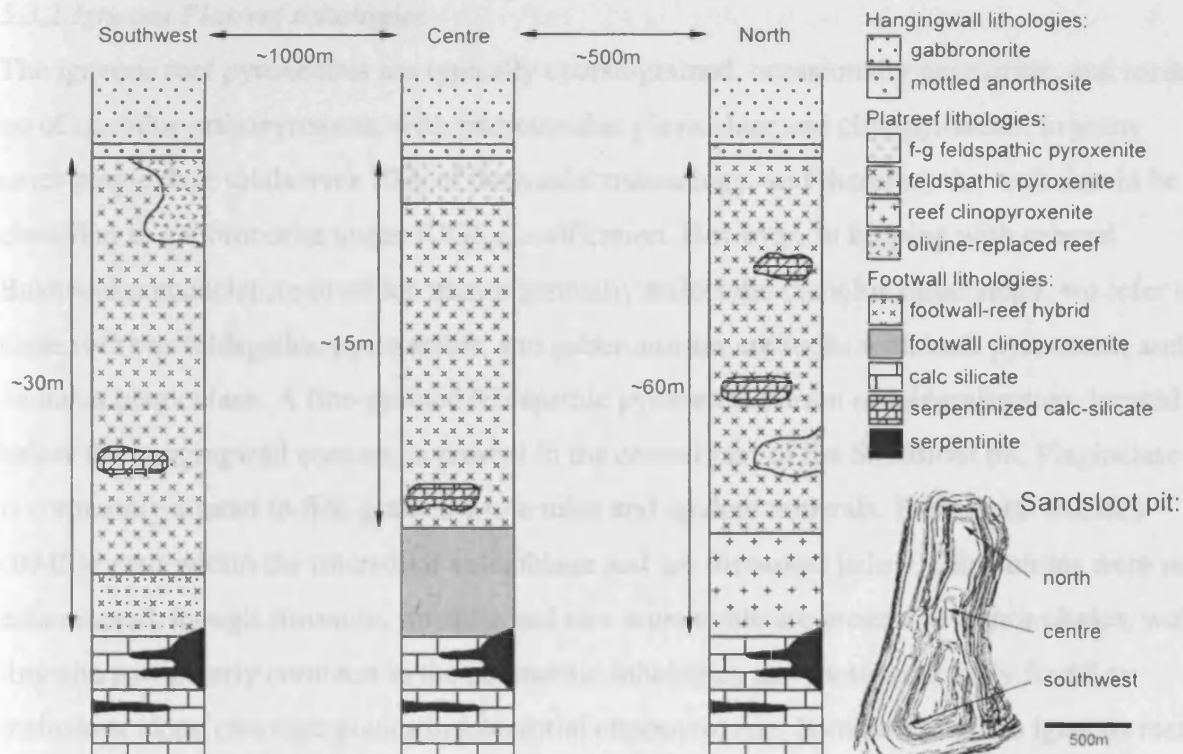


Figure 5.2. Simplified stratigraphic representation showing all major rock units in the southwestern, central and northern parts of the Sandslot pit.

5.3.1 Footwall lithologies

The lowermost footwall lithology exposed in the Sandslot pit are a series of highly altered and variably serpentinized, metamorphosed calc-silicate rocks, derived from the Malmani Dolomite. These generally retain some semblance of the original bedding and are often

interbanded with more massive clinopyroxenites and thin serpentinites. In many places, the immediate footwall to the Platreef pyroxenites, separating the igneous reef and the calc-silicates, and are a series of clinopyroxenites, which are either green, granoblastic diopsidites, often recrystallized with 120° grain boundary triple junctions, or more amorphous purple-grey clinopyroxenites. Olivine is present in variable amounts, and is usually serpentinized, occasionally to a stage where no relict olivine remains. The rocks are of metamorphic origin, as shown by a higher Ca content in the clinopyroxenes compared to those in the igneous pyroxenites, and a whole-rock Cr content much lower than the igneous reef (Harris and Chaumba, 2001). These rocks were termed 'parapyroxenites' by Wagner (1929). Xenoliths of clinopyroxenite and calc-silicate where all original features have been overprinted occur regularly throughout the igneous reef at Sandsloot and are usually serpentinized.

5.3.2 Igneous Platreef lithologies

The igneous reef pyroxenites are typically coarse-grained, occasionally pegmatitic, and made up of cumulus orthopyroxene, with intercumulus plagioclase and clinopyroxene. In many cases plagioclase totals over 10% of the modal mineralogy, and therefore the rock should be classified as gabbronorite under IUGS classification. However, in keeping with general Bushveld nomenclature in which names generally reflect the cumulus mineralogy, we refer to these rocks as feldspathic pyroxenites, and gabbronorites are rocks with both pyroxenes, and cumulus plagioclase. A fine-grained feldspathic pyroxenite barren of mineralization, located below the hangingwall contact, is present in the central part of the Sandsloot pit. Plagioclase is commonly altered to fine grained white mica and epidote minerals. Base metal sulfides (BMS) occur within the interstitial assemblage and are discussed below. Chromitites were not encountered, though chromite, ilmenite and rare armalcolite are present as minor phases, with ilmenite particularly common in the pegmatitic lithologies and most commonly found as inclusions along cleavage planes in interstitial clinopyroxene. Some areas of the igneous reef in the southwestern and northern parts of the pit contain a considerable amount of replacement olivine, which is Fe-rich (Fo₆₂₋₆₇) and overprints orthopyroxene, producing peridotitic zones with up to 60% olivine (Fig. 5.3A). This is thought to have formed from the reaction of a late stage, Fe-rich, SiO₂-poor fluid with the primary Platreef pyroxenites (McDonald *et al.*, 2005), causing desilication of orthopyroxene to form olivine. Parts of the igneous reef are also overprinted with a secondary, low-grade metamorphic assemblage that includes chlorite, sericite, actinolite and sphene highly suggestive of abundant fluid alteration. The basal part of the igneous reef in some sections in the southwest part of the pit is marked

by a wehrlitic rock with igneous, though not cumulus, textures which is often partially serpentinized. This has been interpreted as a footwall-reef hybrid lithology by McDonald *et al.* (2005), on the basis that geochemically, the rocks are intermediate between reef pyroxenite and footwall clinopyroxenite in terms of Ca and Cr content. In the northern part of the pit, the lower part of the igneous Platreef is comprised of clinopyroxenite, with cumulus clinopyroxene, and ~5% highly altered interstitial plagioclase. These rocks contain 1000-2000ppm Cr and the clinopyroxenes have a composition of Wo_{45} which are consistent with the Platreef pyroxenites. In contrast footwall clinopyroxenites contain <100ppm Cr and have clinopyroxene compositions of Wo_{50} .

5.3.3 Hangingwall lithologies

The hangingwall to the Platreef pyroxenites is made up of norites and gabbro-norites, resembling those of the Main Zone elsewhere in the Bushveld Complex. Plagioclase is the cumulus phase and makes up around 50-70% of the modal assemblage, with oikocrystic orthopyroxene and clinopyroxene making up the remainder in a crystallization sequence plagioclase-orthopyroxene-clinopyroxene. Base metal sulfides (pentlandite, pyrrhotite and chalcopyrite) and oxides (almost exclusively ilmenite) are rare. A thin (<1m) mottled anorthosite layer is often present at the base of the hangingwall. The contact with the underlying pyroxenites is sharp and undulatory and is described in detail by Holwell *et al.* (2005).

5.4 Mineralization

Base metal sulfides (primary pyrrhotite, pentlandite, chalcopyrite and minor secondary pyrite and bornite) are common throughout the reef pyroxenites, though heterogeneously distributed, and occur within the interstitial assemblage. However, the sulfides do not occur as well defined euhedral crystal aggregates with sharp linear contacts with surrounding silicates as, for example, they do in the Merensky Reef. They are invariably 'ragged' in morphology due to the common intergrowth with plagioclase and secondary amphiboles, particularly actinolite, epidote and micas (Fig. 5.3B,C,D). In samples where plagioclase has been replaced by white mica, small blebs of sulfide commonly rim the outer edge of the interstitial region (Fig. 5.3B,C), and rarely encroach into orthopyroxene, however, interstitial clinopyroxene often contains blebs of sulfide along cleavage planes. In the footwall, the assemblage is more

diverse and contains the above assemblage along with minor amounts of sphalerite (ZnS), millerite (NiS), galena (PbS), chalcocite (Cu₂S) and alabandite (MnS).

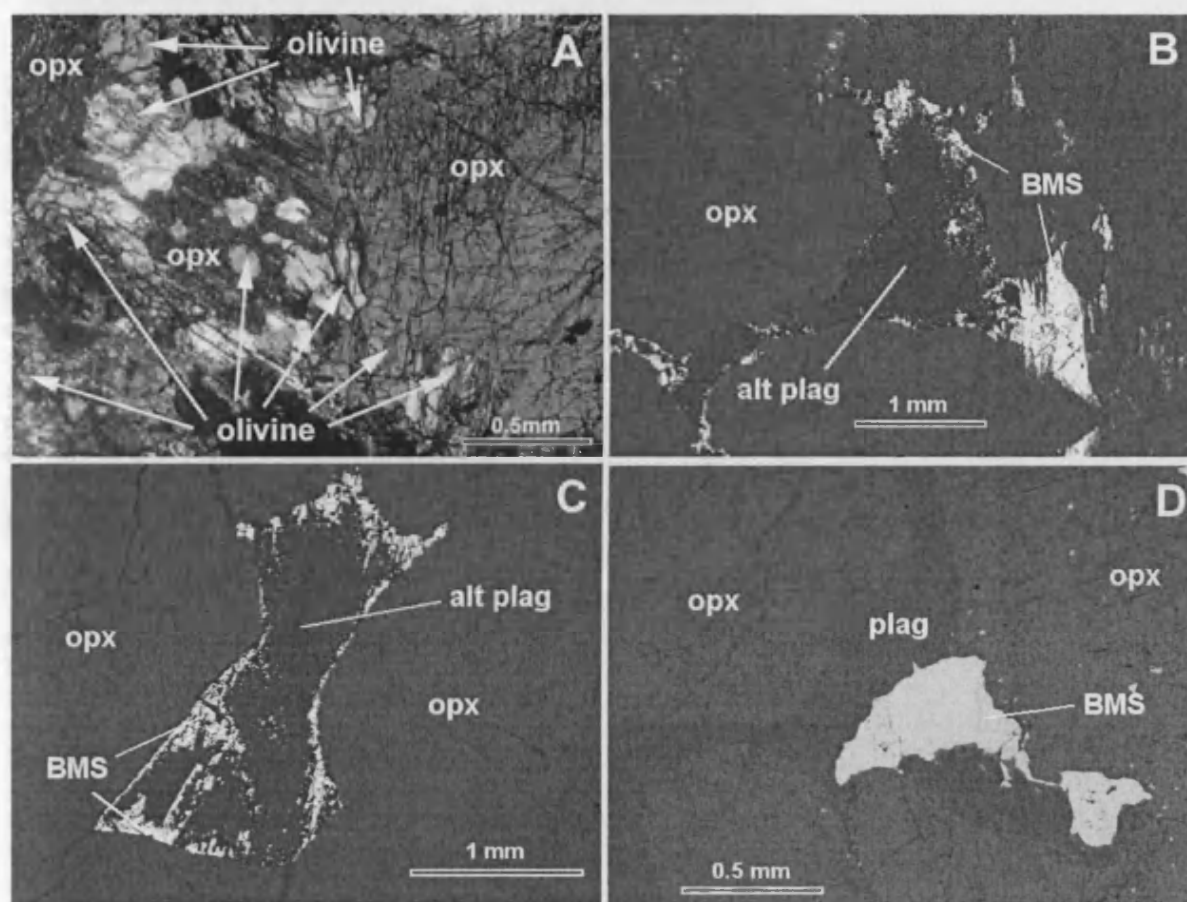


Figure 5.3. A. Thin section of olivine replaced reef showing olivine overprinting orthopyroxene (opx); in cross-polarized transmitted light (sample SW43). B-D: Backscattered electron photomicrographs of: B and C, typical association of base-metal sulfides (BMS) intergrown with altered plagioclase (alt plag) at the edge of the interstitial region enclosing cumulus, sulfide-free orthopyroxene in Platreef pyroxenites at Sandsloot (SNS1-29). D: typical association of discrete BMS grains with unaltered plagioclase (plag) from the Merensky Reef in the eastern Bushveld for comparison.

PGE mineralization occurs throughout the igneous reef, its xenoliths, into the footwall and occasionally at the base of the hangingwall. Grades are variable within the igneous reef, and are more erratic through the footwall, though it is generally lower than in the igneous reef, however some serpentinized units carry very high grades. Table 5.1 shows Pt/Pd ratios for a range of reef, footwall and hangingwall samples together with an indication of grade. Pt/Pd ratios in the igneous reef and hangingwall are around unity, which decrease slightly into the footwall, as would be expected if PGE were transported into the footwall via fluid activity, due to the greater relative mobility of Pd compared to Pt and the other PGE (e.g. Wood,

2002). Conversely, Pt/Pd ratios >1 in some reef samples may indicate removal of greater amounts of Pd during remobilization of PGE into the footwall and therefore it is likely that the original Pt/Pd ratio of the igneous Platreef was probably unity or lower.

Table 5.1. Pt/Pd ratios and relative grade for selected hangingwall (HW), reef and footwall (FW) samples. PGE grade based on Rh+Pt+Pd+Au determined by Ni-S fire assay techniques, described in Chapter 6.3: low = <2.0ppm; intermediate = 2.0-6.0ppm; high = >6.0ppm.

Sample	Lithology	PGE grade	Pt/Pd
PA-N1-31	HW norite	low	1.36
PA-N3X4A	HW gabbronorite	intermediate	0.91
PA-N3X4B	HW mottled anorthosite	low	0.87
PA-SW1-47B	HW gabbronorite chill	low	0.95
PA-SW1-32	Reef feldspathic pyroxenite	intermediate	0.81
PA-SW1-28	Reef feldspathic pyroxenite	high	1.28
PA-SW1-20	Reef feldspathic pyroxenite	intermediate	0.88
PA-N1-30	Reef feldspathic pyroxenite	high	0.93
PA-N1-22	Reef feldspathic pyroxenite	intermediate	1.04
PA-N1-24	Reef feldspathic pyroxenite	intermediate	0.98
PA-N1-26	Reef feldspathic pyroxenite	high	1.94
PA-SW2-49	Reef feldspathic pyroxenite	high	1.48
DH-G	Reef feldspathic pyroxenite	high	1.03
DH-P	Reef pegmatoidal pyroxenite	intermediate	0.79
PA-SW1-40	Olivine-replaced reef	intermediate	0.55
PA-SW1-43	Olivine-replaced reef	high	0.70
SNN1-68	Reef clinopyroxenite	low	0.81
PA-SW1-8	Serpentinized calc-silicate xenolith	high	0.99
PA-SW1-1	FW clinopyroxenite	high	0.86
PA-E55	FW clinopyroxenite	intermediate	0.98
PA-EX6	FW calc-silicate	intermediate	0.84
PA-SW1-4	FW serpentinized calc-silicate	low	0.65
PA-S2-12	FW serpentinized calc-silicate	low	0.55
PA-S0	FW serpentinite	low	0.54

5.5 Platinum-Group Minerals

Fifty-eight polished thin sections and blocks from the hangingwall, igneous reef and metamorphic footwall from the Sandsloot pit were analyzed at Cardiff University using a Cambridge Instruments LEO S360 scanning electron microscope, coupled to an Oxford Instruments INCA energy dispersive X-ray analysis system. Over 1000 individual PGM grains were identified and are listed in Table 5.2. Each individual grain was classified by type and association. The vast majority of PGM were Pt and Pd minerals, while the only major carriers of Ir, Ru and Rh identified were members of the hollingworthite/platarsite/irarsite series. No carriers of Os were found, which may suggest Os may not be present in discrete minerals, but as a trace component in BMS, for example. The PGM identified were grouped

as: (1) Pt/Pd tellurides; (2); Pt/Pd bismuthides (3) Pt/Pd arsenides; (4) Pt/Pd antimonides; (5); Pt/Pd germanides (6); PGE sulfides (7) PGE sulfarsenides; (8) PGE alloys with Fe, Cu, Sn, Pb, Tl; and (9) Au and Ag bearing phases. Each occurrence was also classified by its association: enclosed in sulfide, at sulfide-silicate boundary, or enclosed by silicates, in keeping with other studies of the PGE deposits of the Bushveld Complex.

Table 5.2. Name and ideal formulae of all occurrences of PGM and Au-Ag minerals in the variety of host-rock types. Key to lithology abbreviations: HW: hangingwall gabbronorite; PXT: reef pyroxenite; PEG: reef pegmatoid; ORR: olivine-replaced reef; CPX: reef clinopyroxenite; FRH: footwall-reef hybrid; FWC: footwall clinopyroxenite; CS: calc-silicate; PSP: partially serpentized footwall; TSP: totally serpentized footwall. Unconstrained phases were too small to determine formula

Name	Formula	HW	PXT	PEG	ORR	CPX	FRH	FWC	CS	PSP	TSP	Total
Kotulskite	PdTe	7	53	24	45	1	2	7	8	44	1	192
Sperrylite	PtAs ₂		30	6	6		2	52	18	13	4	131
Moncheite	PtTe ₂	1	50	36	18	6	1	5	1	9	1	128
unnamed	(Pd,Pt) ₂ Ge	65		3								68
Electrum	Au,Ag	1	15	4	9		1	5	1	20	2	58
Hessite	Ag ₂ Te		36					5	1	2		44
Sudburyite	PdSb							5	5	29		39
Zvyagintsevite	Pd ₃ Pb	4		2	21					1		28
Palladoarsenide	Pd ₂ As		2	1	1		18	4		1		27
Paolovite	Pd ₂ Sn	1						20		3		24
Geversite	PtSb ₂			4						5	14	23
unnamed	Pd ₅ Bi ₃ (Te,Sb) ₂							23				23
Pt-Fe alloy	Pt ₂ Fe	10			8					4		22
Froodite	PdBi ₂		1		2				1	16		20
Michenerite	PdBiTe	1	6			3		6				16
Sobolevskite	PdBi		2		3	3		3		5		16
unnamed	Pd ₂ (Sn,Sb)							15				15
Stibiopalladinite	Pd ₅ Sb ₂		2		3	1		4	1	3		14
Mertieite II	Pd ₈ (Sb,As) ₃		7						6			13
Atokite	Pd ₃ Sn				5		1	1	1			8
Native silver	Ag		5		1					2		8
Hollingworthite	RhAsS				1			2			4	7
unnamed	Pd ₃ Tl	7										7
Irarsite	IrAsS		2	1	2							5
Isoferroplatinum	Pt ₃ Fe		2	1				1				4
Merenskyite	PdTe ₂		2		2							4
Tulameenite	Pt ₂ FeCu				4							4
Platarsite	PtAsS		3									3
Rustenburgite	Pt ₃ Sn			3								3
Tetraferroplatinum	PtFe	1		2								3
Stillwaterite	Pd ₈ As ₃	1	1									2
unnamed	Pd ₅ Sb ₃									2		2
Auricupride	Au,Cu			1								1
Insizawite	PtBi ₂			1								1
Laurite	RuS ₂	1										1
Majakite	PdNiAs							1				1
Menshikovite	Pd ₃ Ni ₂ As ₃		1									1
Niggliite	PtSn										1	1
Palarstenide	Pd ₅ SnAs										1	1
Palladian gold	Au,Ag,Pd			1								1
Palladobismutharsenide	Pd ₂ (Bi,As)	1										1
Plumbopalladinite	Pd ₃ Pb ₂							1				1
Stannopalladinite	Pd ₅ Sn ₂ Cu			1								1
unnamed	PtAg ₂		1									1
unnamed	Pt ₂ SbSb										1	1
unnamed	PdTe ₃ Pb ₃							1				1
unnamed	Pd ₂ Bi							1				1
unnamed	Pd ₃ Bi ₂							1				1
unnamed	Pd ₂ (Sb,Bi,Te)							1				1

Table 5.2. (contd.)

Name	Formula	HW	PXT	PEG	ORR	CPX	FRH	FWC	CS	PSP	TSP	Total
Unconstrained phases:												
	Pd-As-Sb			2								2
	Pd-Te-Bi				2							2
	Pt-Cu-Fe-Ag							2				2
	Pt-Pd-Sb-As								1		1	2
	Pt-Pb-Ag		1									1
	Pt-Fe-Te	1										1
	Pt-Au-Cu-Fe				1							1
	Pt-Pd-Pb-Te				1							1
	Pd-Pb-Te				1							1
	Pd-Pb-Pt				1							1
	Pd-Bi-Pb-Pt				1							1
	Pt-Pd-Te-Sb										1	1
	Pt-As-Sn-Sb										1	1
	Pt-Fe-Te-Pb										1	1
Composite polyphase grains, unconstrained compositions:												
	Pd-Sn-As-Te-Pb				1							1
	Au-Cu-Pt-Pd-Ag				1							1
	Pd-Pt-Fe-Cu-Sn-Te				1							1
	Pd-Pb-Te-Pt-Ir				1							1
	Pd-Pt-Te-Bi-Cu-Fe				1							1
	Pd-Bi-Sb-Sn-Te							1				1
	Ni-Bi-Pd-Ag-Au								1			1
	Pt-Sb-Te-Bi-Pb-As										1	1
	Pt-Sb-As-Au-Pb										1	1
	Pd-Sn-Sb-Pt-As										1	1
	Pt-Sb-Te-Bi-As										1	1
Total PGM grains:		102	222	79	156	23	23	163	44	132	64	1008

5.5.1 Grain size and morphology

Each PGM grain's long and short axes were measured in micrometres. Grains smaller than 1 µm were ignored due to their relative volumetric insignificance, and the difficulties in accurately determining their composition. Relative proportions of the various minerals phases and PGM species type are based on an estimation of area (and by inference, volume) of each grain. Using the long and short axes dimensions, the area of each grain was approximated to the area of an ellipse around the two axes. This therefore produces data which accurately reflect the relative proportions of each PGM type within an assemblage. This method of data presentation is preferable to proportions of PGM type by number of grains, which can be biased by a relatively large amount of very small grains, for example. This approach is particularly pertinent when comparing PGM data with Pt/Pd ratios. If, say, the Pt/Pd ratio of the whole-rock sample is around unity, when using the proportion by number of grains method, there may appear to be a deficit of one particular PGE represented by discreet PGM phases, which may be wrongly attributed to its presence in BMS phases or silicates. Therefore we present all the assemblage data in percentage of total area of all PGM.

Grain size data for all PGM grains greater than 1 µm in their longest dimension are shown in Fig. 5.4. From Fig. 5.4, it can be seen that in most rock types, around 80% of grains are less than 10 µm in length, with the exception of pegmatitic reef rocks, which have a higher average grain size with 50% of grains larger than 5 µm. The units with the lowest average PGM grain sizes (>70% of grains under 5 µm) are the footwall calc-silicates, the reef clinopyroxenites and the hangingwall gabbro-norite. No grains of over 100 µm were found.

PGM morphology varies with individual phases and also with association. Where surrounded by sulfides, PGM, and particularly electrum, are commonly present as rounded blebs. Where surrounded by silicates, grains vary from anhedral to euhedral. Moncheite (PtTe₂) is commonly found as laths, Pt₂Fe as cubic crystals, and sperrylite as tetrahedra. Most PGM identified occur as single phase grains, though they may occasionally occur as compositionally zoned (Fig. 5.5a) or polyphase grains (Fig. 5.5b).

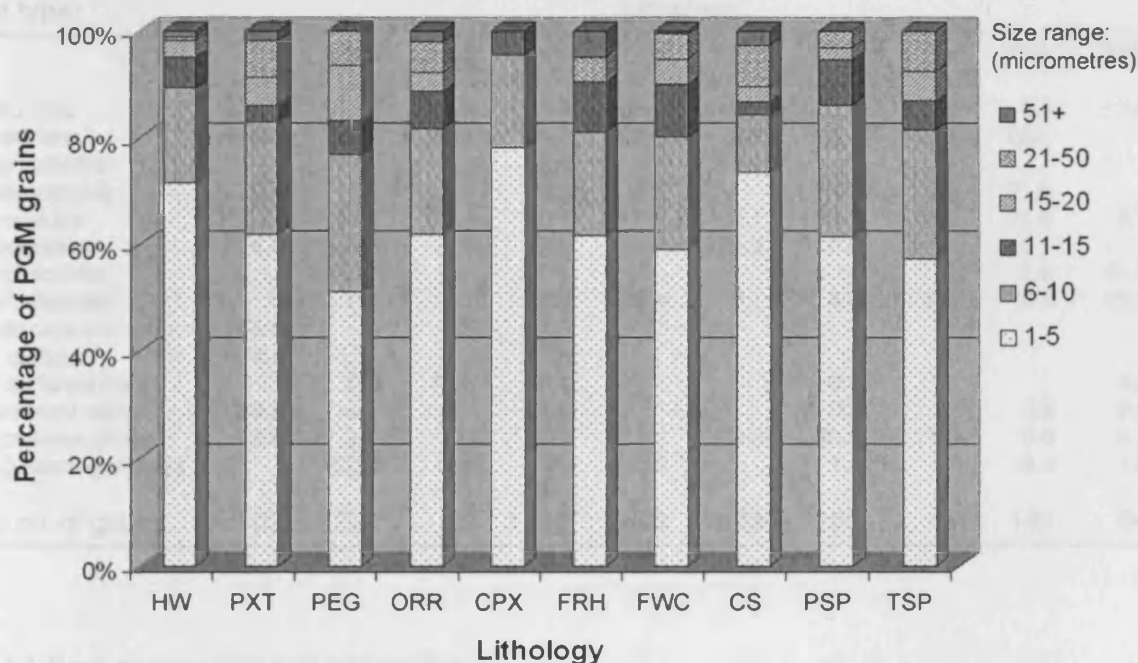


Figure 5.4. Range of PGM grain size (longest axis) in the various host rock lithologies at Sandsloot. See Table 5.2 for lithology abbreviations.

5.5.2 Assemblages

The PGM mineralogy in the variety of host rock lithologies studied are summarized in Table 5.3. The most notable characteristic of the Sandsloot PGM assemblages identified here is the

complete lack of PGE sulfides (also noted by Armitage *et al.*, 2002), with the exception of a single grain of laurite (RuS₂) in the hangingwall gabbro. This is unusual in that throughout the Merensky Reef, the UG2 chromitite and elsewhere in the Platreef, namely Zwartfontein north, Overysel (Kinloch, 1982) and Drenthe (Gain and Mostert, 1982), PGE-sulfides are ubiquitous in the form of cooperite (PtS), braggite [(Pt,Pd)S], laurite and other rarer minerals. The only other PGM found at Sandsloot containing any sulfur are a few occurrences of the sulfarsenide hollingworthite/platarsite/irarsite series. As a whole, the Platreef at Sandsloot can be said to be dominated by Pt/Pd tellurides, alloys, and to a lesser extent, PGE arsenides and antimonides. In detail though, there is a great variation from one host rock type to another, particularly in terms of igneous reef versus metamorphic footwall, and several major trends in the PGM assemblage can be identified.

Table 5.3. Proportions of PGM type within each lithology in percentage of the total area of PGM. See Table 5.2 for key to lithology abbreviations.

PGM type:	Lithology:									
	HW	PXT	PEG	ORR	CPX	FRH	FWP	CS	PSP	TSP
Pt-tellurides	0.6	40.1	38.8	4.9	11.6	0.3	10.3	0.2	6.8	0.2
Pd-tellurides	6.0	19.2	18.2	31.1	26.6	3.6	1.6	6.1	26.4	
Pt-bismuthides				0.1						
Pd-bismuthides	0.4	0.8		3.5	4.0		22.3	0.1	21.8	
Pt-arsenides		10.8	23.4	20.1	8.5	1.1	18.6	79.5	21.6	9.1
Pd-arsenides	0.5	0.5	0.5			89.2	0.2		0.1	
Pt-antimonides									2.6	46.3
Pd-antimonides		0.9		2.7	39.4		4.9	2.8	0.6	35.0
Pd-germanides	55.3		0.5							
PGE sulfides	0.4									
PGE sulfarsenides		0.8	14.5	0.1			0.3			4.4
Pt-dominant alloys	28.2	0.1		25.3			0.3		0.2	3.0
Pd-dominant alloys	8.6	3.8	0.3	9.1		5.8	40.1	11.3	0.6	0.2
Au/Ag bearing phases		23.0	3.8	3.1	9.9		1.4		19.3	1.6
Total no. of grains	102	222	79	156	23	23	163	44	132	64

5.5.2.1 Reef pyroxenites and pegmatites

The igneous reef pyroxenites and pegmatites are dominated by Pt and Pd tellurides, particularly moncheite and kotulskite (PdTe). Hessite (Ag₂Te) and electrum (Au,Ag) are common in the pyroxenites. Arsenides, particularly sperrylite, as throughout the deposit as a whole, are common, particularly in the pegmatites. The immediate associations of the PGM are shown in Table 5.4. Most PGM in the pyroxenites and pegmatites are surrounded by silicates or located at the BMS-silicate boundary. However, even where surrounded by silicates, the PGM retain a strong spatial relationship with the BMS and many are in

association with secondary amphiboles which replace BMS, and very few are found completely isolated from any BMS. The secondary assemblages of tremolite and actinolite around BMS grains in the primary Platreef pyroxenites are similar to those found in the Merensky Reef and UG2 chromitite, described by Li *et al.* (2004). The appearance of PGM as satellite grains around BMS grains may be due to the regression of the BMS boundary, with the PGM (originally at the edge of the sulfide blebs) remaining in their original positions. This association has also been noted in the Platreef at Macalacaskop and Turfspruit (Hutchinson and Kinnaird, 2005). The replacement by amphiboles and epidote appears to be paragenetically late as there is evidence of secondary minerals cross cutting the PGM, such as in Fig 5.5a. Most electrum is found as rounded blebs within BMS grains. PGE antimonides were found to be extremely rare in the Platreef pyroxenites.

Table 5.4. Textural associations of PGM (excluding Au/Ag alloy) in the variety of host-rock types in percentage number of grains. See Table 5.2 for key to lithology abbreviations.

All PGM, Au, Ag phases										
Association:	HW	PXT	PEG	ORR	CPX	FRH	FWP	CS	PSP	TSP
Enclosed in BMS (%)	10.3	12.6	9.1	8.2		77.8	10.4	6.4	21.2	
BMS-silicate contact (%)	29.9	38.1	16.9	49.0	30.4	11.1	27.6	14.9	60.6	11.5
Enclosed in silicate (%)	59.8	49.3	74.0	42.8	69.6	11.1	62.0	78.7	18.2	88.5
Pt-dominant phases										
Association:	HW	PXT	PEG	ORR	CPX	FRH	FWP	CS	PSP	TSP
Enclosed in BMS (%)	23.1	8.4	11.9	6.5			9.8	4.3		
BMS-silicate contact (%)	53.8	37.3	26.2	41.3			14.8	8.7	67.6	7.4
Enclosed in silicate (%)	23.1	54.2	61.9	52.2	100.0	100.0	75.4	87.0	32.4	92.6
Pd-dominant phases										
Association:	HW	PXT	PEG	ORR	CPX	FRH	FWP	CS	PSP	TSP
Enclosed in BMS (%)	8.0	8.5	3.1	6.1		72.2	10.5	8.7	29.2	
BMS-silicate contact (%)	22.7	34.1	3.1	51.0	40.0	16.7	34.7	21.7	55.6	16.1
Enclosed in silicate (%)	69.3	57.3	98.8	42.9	60.0	11.1	54.8	69.6	15.3	83.9

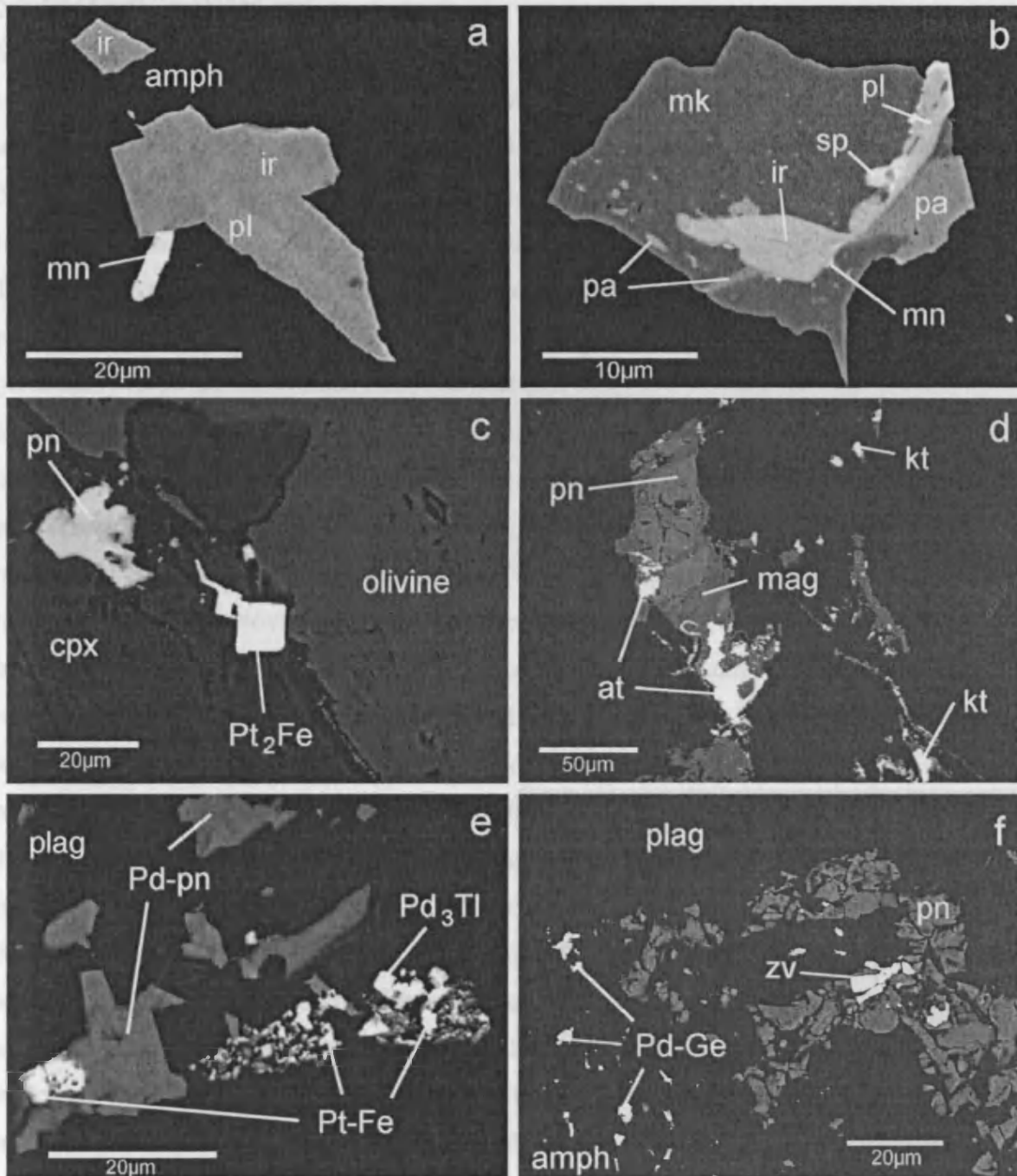


Figure 5.5. Backscattered electron photomicrographs of PGM found in Sandsloot Platreef samples. *a*: zoned grain of irarsite (ir) and platarsite (pl) with moncheite (mn) from pegmatoidal pyroxenite reef sample DH-P. Note how the grain is cut by a secondary amphibole. *b*: polyphase PGM from pyroxenite reef comprised of menshikovite (mk), irarsite (ir), platarsite (pl), palladoarsenide (pa), sperrylite (sp) and moncheite (mn). *c*: typically cubic crystal of Pt_2Fe from olivine-replaced reef (PA-SW1-43). *d*: association of atokite (at) and kotulskite (kt) with pentlandite (pn), oxidized to magnetite (mag) in a partially serpentinized sample of footwall. *e*: typical association of Pt-Fe alloy intergrown with palladian pentlandite (Pd-pn) and Pd_3Ti from hangingwall gabbro. *f*: cluster of Pd germanides surrounded by secondary amphiboles replacing non-Pd-bearing pentlandite with zvgintsevite (zv) in the same hangingwall gabbro as *e*.

antimonides. Table 5.2, however, reveals that this figure comes from a single, relatively large grain of sibiopalladinite, and other than this, the assemblage is similar to the reef pyroxenite.

5.5.2.2 Olivine-replaced reef

Samples of reef pyroxenite which have undergone replacement by Fe-rich olivine have their own distinctive Pd-rich and alloy-dominant PGM assemblage, with abundant Pd tellurides, and Pt-Fe alloys. Table 5.3 indicates that Pt arsenides are also very abundant, however, Table 5.2 shows that only six sperrylites, in a total of 156 grains, were identified, though all were large relative to the other grains, which has caused the high percentage by area in Table 5.3. Table 5.1 shows that the Pt/Pd ratio in these rocks is around 0.6, therefore in this case, the proportion by area data in Table 5.3 appears to have been skewed by a small number of particularly large grains. We therefore consider that the true dominant species in this assemblage are Pd tellurides and alloys. The most common telluride, kotulskite, commonly contains much higher concentrations of Pb (up to 12wt%) than kotulskite in the unaltered pyroxenites, with a representative composition in these rocks of $\text{Pd}_1\text{Te}_{0.74}\text{Bi}_{0.14}\text{Pb}_{0.12}$. The most common Pd-alloy is zvyagintsevite (Pd_3Pb), which is particularly characteristic of this lithology. The Pt-Fe alloys have a typical composition of Pt_2Fe , which is intermediate between isoferroplatinum (Pt_3Fe) and tetraferroplatinum (PtFe), and is therefore referred to under the nomenclature of Cabri and Feather (1975) as Pt-Fe alloy. In these rocks, Pt-Fe alloys occur as discrete cubic crystals (Fig. 5.5c) rather than as intergrowths with BMS or magnetite, which is the more common mode of occurrence in the Merensky Reef (Kinloch, 1982; Kinloch and Peyerl, 1990). The other common Pt-dominant alloy in the olivine-replaced rocks is tulameenite (Pt_2FeCu), which was not found in any of the other lithologies. A few examples of PGE bismuthides and antimonides were also found in the replaced reef, which are absent or extremely rare in the unaltered pyroxenite reef. Arsenides and electrum are also present. Only 8% of PGM are included in BMS (Table 5.4) and many of the 43% which are surrounded by silicates do not show the close spatial relationship to BMS that those in the unaltered reef show, with some often isolated along veins.

5.5.2.3 Reef clinopyroxenites

The reef clinopyroxenites at the base of the Platreef in the northern part of the pit were found to be low grade (Table 5.1). The grade is also known to decrease with depth away from the contact with overlying feldspathic pyroxenites, such that the calc-silicate footwall is not exposed in the northern part of the pit. From Table 5.3 it appears that the 23 PGM grains found differed from the reef pyroxenites in that they contained a high proportion of antimonides. Table 5.2, however, reveals that this figure comes from a single, relatively large grain of stibiopalladinite, and other than this, the assemblage is similar to the reef pyroxenites,

containing mainly tellurides. The small number of grains located requires any trends identified to be taken with caution, however it appears that the assemblage is similar to the reef pyroxenites, with a slight increase in the number of PGM containing Bi and Sb. None of the PGM are included in BMS, and all of the Pt phases and 60% of the Pd phases are located in silicates, which is much higher than in the reef pyroxenites (Table 5.4). Overall grain size was very low (Fig. 5.4), with most grains under 5µm in length, and the largest being only 15µm in its longest dimension.

5.5.2.4 Footwall clinopyroxenites

The footwall clinopyroxenites are dominated by Pd-dominant alloys, particularly paolovite (Pd_2Sn) and the similar, but unnamed phase $\text{Pd}_2(\text{Sn},\text{Sb})$, which contain Sn and Sb in equal proportions. Bismuthides, in particular an unnamed phase with composition close to $\text{Pd}_5\text{Bi}_3(\text{Te},\text{Sb})_2$ are also common. Almost a third of all grains were sperrylite, making it the most abundant phase by occurrence, although sperrylite only made up 19% of the assemblage by area (Tables 5.2, 5.3). Other than sperrylite, very few of the PGM grains were Pt phases. A few tellurides and antimonides make up the remainder of the assemblage. Almost two-thirds of PGM in the footwall clinopyroxenites are surrounded by silicates (Table 5.4). This figure rises to three-quarters when only the Pt dominant phases are considered, which reflects the preference of sperrylite to be isolated in silicate grains away from BMS grains.

5.5.2.5 Footwall calc-silicates

The calc-silicates, like the clinopyroxenites, are telluride-poor, and are rich in arsenides, particularly sperrylite, which makes up nearly 80% of the assemblage (Table 5.3). There are fewer alloys than in the clinopyroxenites, although Pd-dominant alloys are still the second most common PGM type, however, in contrast to the clinopyroxenites, bismuthides are very rare. Table 5.4 shows 79% of all PGM grains being enclosed within silicate minerals, a figure probably enlarged partially by the relative paucity of BMS in the the calc-silicates compared to the igneous reef. As in the clinopyroxenites, the Pt phases (largely sperrylite) show a strong preference to be associated with silicates.

5.5.2.6 Footwall-reef hybrid

A sample of footwall-reef hybrid rock contained a high number of palladoarsenide (Pd_2As) grains, concentrated in and along fractures in BMS grains. Comparatively few PGM were found elsewhere in the sample, which include a few tellurides. The small number of PGM

grains in the sample means any trends must be viewed cautiously, though it does show a marked increase in arsenides and Pd minerals compared to the primary reef pyroxenites, possibly indicating a more volatile influenced environment more akin to the footwall assemblages than the igneous pyroxenites.

5.5.2.7 Footwall serpentinites

Two types of serpentinite were studied: partially and completely serpentized footwall. In the partially serpentized samples, where up to 60% fresh metamorphic olivine (FO_{88}) is still present, the assemblage is dominated by Pd tellurides and lesser amounts of Pd bismuthides and Pt arsenides. As in the olivine-replaced reef, kotulskite contains relatively high concentrations of Pb (often higher than Bi) which substitutes for Te in the ideal formula $PdTe$. Significantly, the PGM in this rock type are very much associated with BMS (Table 5.4), which are variably oxidized to Fe-oxide phases (Fig. 5.5d), an association also noted in serpentized parts of the Platreef on Drenthe by Gain and Mostert (1982). Li *et al.* (2004) describe BMS being replaced by magnetite in areas of serpentization in the Merensky Reef and UG2 in the western Bushveld. Nearly all of the kotulskite and electrum is found in association with these partially oxidized blebs of BMS. PGM in the completely serpentized rocks, however, are almost completely silicate associated (Table 5.4), with completely serpentized footwall containing very few BMS, with most altered to magnetite. This PGM assemblage has the most predominant enrichment in antimony in any of the assemblages and is characterized by the presence of geversite ($PtSb_2$) and sudburyite ($PdSb$). A few arsenides, tellurides and sulfarsenides make up most of the remainder of the assemblage.

5.5.2.8 Hangingwall gabbronorite

Samples from the base of the hangingwall were surprisingly found to contain appreciable occurrences of PGM. Sporadic BMS occur in both the mottled anorthosite and the basal part of the overlying gabbronorite in places where the hangingwall sits on coarse-grained mineralized reef (Holwell *et al.*, 2005). One sample of gabbronorite, taken from just above the basal contact with the thin mottled anorthosite that forms the base of the hangingwall in places, was considerably rich in PGM. Patches of Pt_2Fe intergrown with chalcopyrite and pentlandite are common (Fig. 5.5e), an association which differs from the discreet cubic crystals of Pt_2Fe found in the replaced reef. The only grain of PGE sulfide (laurite) found in the entire suite of samples studied was located in the centre of one of these Pt_2Fe alloy-BMS intergrowths. Also associated with the intergrowths were several grains of the unknown Pd-Tl

alloy, Pd₃Tl (Fig. 5.5e). The only other published occurrences of any Pd-Tl minerals is a very rare, unconstrained Pd-Tl phase from the Platreef on Zwartfontein and the Merensky Reef in the eastern Bushveld (Kinloch, 1982) and a mineral close to the formula Pd₃Tl, with some substitution of Tl by Re, in the Wetlegs deposit of the Duluth Complex, Minnesota (Severson and Hauck, 2003). Significantly, the pentlandite which is intergrown with Pt-Fe and Pd-Tl alloys in Fig. 5.5e also contains up to 6wt% Pd, which is the highest recorded natural concentration of Pd in pentlandite (L. J. Cabri, pers. comm.). Overall, however, the sample was particularly rich in the unnamed Pd germanide phase with composition close to Pd₂Ge. Sixty four individual grains, plus many <1µm, were found, of which 11 contained some Pt in place of Pd, and most contained some As in place of Ge. Typical analyses of this phase are shown in Table 5.5, together with the ideal compositions for Pd₂Ge and Pd₁₁Ge₅, the latter of which the analyses more closely match. Armitage *et al.* (2002) noted a single grain of (Pd,Pt)₂Ge in the Platreef, and the only other recorded occurrences of PGE-germanides anywhere in the world are an unconstrained Pd-Ge phase from the UG-2 chromitite (McLaren and de Villiers, 1982), Pd₂Ge recorded from the Noril'sk Ni-Cu-PGE orebody (Komarova *et al.*, 2002) and (Pd,Pb)₂Ge (Grokhovskaya *et al.*, 2005). The Pd₂Ge grains, and some rarer kotulskite and Pd arsenides are found as satellite grains around larger BMS minerals which are intergrown with secondary amphiboles (Fig. 5.5f). The association of Pd-bearing pentlandite, PGE alloy intergrowths and PGE sulfides with unaltered BMS does not hold any PGE germanides, whereas germanides are present in association with non-PGE-bearing, partially replaced BMS. The remainder of the hangingwall assemblage is made up of zvyagintsevite, kotulskite and a few arsenides.

Table 5.5. Compositions of unnamed Pd-germanide phase from the base of the hangingwall gabbronorite, together with the ideal compositions of Pd₂Ge and Pd₁₁Ge₅.

Grain no:	1	2	3	4	Pd ₂ Ge	Pd ₁₁ Ge ₅
wt% Pd	75.84	76.52	60.00	59.51	74.56	76.32
Pt			18.33	17.23		
Ge	21.80	20.42	21.96	21.44	25.43	23.67
As	2.54	3.53		0.77		
Total	100.18	100.47	100.28	98.95	100.00	100.00

5.6 Discussion

The results from this study show the Platreef to be a very complex PGE orebody both lithologically and mineralogically. The PGM mineralogy at Sandsloot is distinctive within the Platreef compared to other areas. In detail, we have shown that the variety of host rock types in the Platreef contain their own, characteristic PGM assemblages which reflect the processes involved in redistributing the PGE through the reef and into the footwall during the evolution of the Platreef, though the mechanism which led to the initial introduction of PGE into the Platreef has yet to be resolved.

The most characteristic feature of the Sandsloot PGM assemblage, in comparison to most other tabular Bushveld PGE orebodies, is the complete lack of PGE sulfides. Throughout the Merensky Reef, PGE sulfides make up a substantial proportion of the overall PGM assemblage (e.g. Kinloch, 1982; Mostert *et al.*, 1982; Mossom, 1986; Prichard *et al.*, 2004a). In the Platreef, on the farms Drenthe and Overysel, to the north of Sandsloot, these minerals make up greater than or nearly half the volume percentage of the assemblage (Gain and Mostert, 1982; Kinloch, 1982). Kinloch (1982, Table 6) lists PGM from eight borehole cores on Zwartfontein, the first five of which are sulfide-poor, alloy and telluride dominant, the remaining three are sulfide dominant and similar to the Overysel data in the same table. The footwall changes from dolomite in the southern and central part of Zwartfontein (Fig. 5.1) to Archaean basement in the northern part of the farm. The cores listed in Table 6 of Kinloch (1982) are shown in south to north order (P. Hey, pers. comm.) with the change from a dolomite footwall to one composed of granite and gneiss directly corresponding to the change in the PGM assemblage with respect to the presence of PGE sulfides. South of Sandsloot, on Tweefontein where BIF and shales of the Dutchland Formation sediments form the footwall, sulfides are again reported (Viljoen and Schürmann, 1998). Immediately to the south though, on Turfspruit and Macalacaskop where the footwall is Dutchland Formation and Pretoria Group shales and sandstones, Hutchinson *et al.* (2004) describe a number of PGM assemblages with very few PGE sulfides. The lack of sulfides is most likely to be due to low fS_2 which would have prevented any free S being available to combine with PGE. This appears to be directly related to footwall lithology, with low fS_2 conditions characteristic of areas where the Platreef magma has interacted with dolomitic footwall. Elsewhere in the Bushveld Complex, potholed Merensky Reef (Kinloch, 1982) and the platiniferous dunite pipes (Tarkian and Stumpfl, 1975) contain relatively few PGE sulfides and are dominated by alloys, tellurides and sperrylite. Volatile activity is thought to be important in both these

mineralizing environments, which therefore suggests a link between volatile activity and sulfide-poor, alloy-dominated PGM assemblages. The Platreef at Sandsloot is certainly more alloy-rich and sulfide-poor than at Overysel and Drenthe (Gain and Mostert, 1982; Viljoen and Schürmann, 1998) where the footwall is Archaean granite/gneiss basement. This would suggest that greater volatile activity affected the Platreef where it intruded the dolomites than where it intruded the granites and gneisses, which is manifested in distinctively different PGM assemblages.

The pyroxenites and pegmatites of the igneous reef contain a typical PGM assemblage dominated by Pt and Pd tellurides, electrum and some arsenides. Their presence in the interstitial regions, in a proximal association with BMS indicates a spatial relationship with the sulfides. Typically, magmatic PGE associations are of Os, Ir and Ru with chromite (Lee, 1996), and Pt, Pd and Rh concentrated with sulfides (Naldrett and Duke, 1980). In a typical immiscible sulfide separating from a silicate magma and collecting base metals and PGE (e.g. Naldrett *et al.*, 1986), the sulfide liquid collects the PGE, and PGM are commonly found included in, or more commonly, at the margins of BMS grains. In our samples, most PGM are found either at the sulfide-silicate boundary, or are silicate hosted as satellite grains around altered BMS. The intergrowth of BMS with plagioclase and the frequent distribution of small blebs of sulfide and PGM around the edge of interstitial areas, suggests that if PGE were originally held in the sulfide liquid, redistribution of the PGE occurred during fluid fluxing after orthopyroxene crystallization, but before the interstitial silicate melt crystallized. The fact that the pegmatitic rocks show a considerably larger average PGM grain size also suggest that the PGM crystallized at a similar, early stage, though their relative enrichment in Pd tellurides and sperrylite would suggest greater degrees of hydrothermal fluid activity, which would be expected if the pegmatoidal nature of the lithology is due to hydrothermal fluid interaction. The reef clinopyroxenites have a similar PGM assemblage, although do contain a few antimonides and bismuthides, more commonly found in the footwall. Texturally, the PGM in these rocks have less of an association with BMS, which is more characteristic of the footwall lithologies. This evidence, together with the fact that the PGE grade decreases away from the contact with the reef pyroxenites, may suggest the PGE have been transported from the feldspathic pyroxenites by hydrothermal activity.

Base metal sulfides in the igneous reef have been variably altered around their margins and replaced by actinolite, tremolite and epidote. The appearance of PGM as satellite grains

around BMS may be the result of PGM, originally at the edge of the sulfide grains, remaining in situ, as the BMS boundary regressed. A similar association is found in the Merensky Reef and UG2 chromitite (Li *et al.* 2004), who suggest possible reactions for the replacement of BMS by amphiboles and epidote. All of the reactions proposed by Li *et al.* (2004) involve the addition of aqueous Ca, Mg and Si, all of which are readily available from the assimilation of the siliceous Malmani dolomite. However, rather than the BMS being replaced directly by silicates, it is more likely that the fluids reacted with the BMS to form sulfuric acid, dissolving the BMS around its margins and hydrous silicates were able to grow into the voids around the regressed margins. The PGM appear to be paragenetically earlier than the episode of alteration that formed the hydrous silicates, as seen by the cross-cutting of PGM by the secondary minerals (Fig. 5.5a). This observation for the Platreef would appear to contrast with the conclusions of Li *et al.* (2004) who suggested that secondary hydrothermal alteration may have been important in redistributing PGE in the Merensky Reef. In the case of the Platreef at Sandsloot, it seems that fluid fluxing at or close to the time of crystallization, and not later hydrothermal alteration, was the most important factor in redistributing PGE through the primary reef.

The presence of Pt-Fe alloy in crystal form (rather than as intergrowths), Pd alloys and Pd tellurides in olivine-replaced portions of reef is analogous to the volatile-influenced ultramafic platiniferous pipes of the eastern Bushveld and pegmatoid-replaced Merensky Reef potholes (Kinloch and Peyerl, 1990). McDonald *et al.* (2005) suggested that the olivine-replaced lithologies formed in a similar way, from a late-stage Fe-rich, Si-poor fluid that percolated through parts of the pyroxenite, replacing orthopyroxene with olivine (Fig. 5.3A). At present, the origin of this fluid remains unclear, although it may have been derived from serpentinization of the olivine-bearing footwall lithologies. The fluid also appears to have been Pb-rich as seen by the formation of abundant zvyagintsevite (Pd_3Pb), and the replacement of some Te by Pb in kotulskite. If PGM were present in the protolith (most likely reef pyroxenite), the Fe-rich fluid seems likely to have recrystallized Pt into Pt-Fe alloys, and the assemblage therefore post-dates the main episode of mineralization.

The difference in the nature of the PGM between the igneous reef and metamorphic footwall units that contain PGE mineralization is striking. The dominance of tellurides, alloys and electrum with a complete lack of antimony observed in the igneous reef, is reversed in the footwall, with arsenides, bismuthides and antimonides dominating. The dominance of PGM

containing elements such as As and Sb in the footwall lithologies suggests a significant amount of volatile activity involved in the redistribution of PGE into the footwall. However, the role of elements such as As, Sb, Se and Te is believed to be to immobilize the PGE, rather than be transported with them, as reduced forms of these elements cannot be transported with Pt and Pd (Wood, 2002). The almost total absence of antimonides in the igneous reef is analogous to normal Merensky Reef, where PGE antimonides are very rare (Kinloch, 1982), whereas in areas where fluid activity has been prevalent, antimonides are common. For example, the type localities for the PGE antimonides genkinite, geversite, stibiopalladinite, stumpflite, sudburyite and naldrettite and ungavaite are, respectively: the Onvervacht pipe (Bushveld Complex, RSA); the Driekop pipe (Bushveld Complex, RSA); Tweefontein Hill (Bushveld Complex, RSA); the Driekop pipe; Copper Cliff (Sudbury, Canada), and the Mesamax Northwest deposit (Québec, Canada) (Cabri, 2002; Cabri *et al.*, 2005; A. McDonald *et al.*, 2005), all of which have been fluid affected. This would imply that PGE antimonides are indicative of fluid transport of PGE, and are present in secondary assemblages. The fluid activity that redistributed the PGE would be expected to have preferentially transported the more mobile Pd into the footwall over Pt, therefore producing low Pt/Pd ratios in the footwall, and raising the Pt/Pd slightly in the igneous reef. Table 5.1 shows Pt/Pd ratios for reef sample in the range 0.79-1.94, whereas in footwall samples the ratio is 0.54-0.98, and in the replaced reef it is around 0.6, showing a relative enrichment in Pd over Pt in the areas where the greatest fluid activity appears to have taken place, indicating the PGE were introduced by fluid activity.

Partial serpentinization of footwall olivine desulfurizes BMS to form magnetite, a feature also seen in the Merensky Reef and UG2 (Li *et al.*, 2004) and in its early stages appears to form a telluride dominant PGM assemblage (often Pb-bearing) which is not dissimilar to that found in the olivine-replaced reef. If there is a link between the two assemblages, it may be that the Fe-rich fluids that altered the reef originated from serpentinization of the footwall. Further degrees of serpentinization are associated with a generally fine-grained, disseminated, low-temperature PGM assemblage rich in volatile elements such as Sb and As. The antimonide dominant assemblage formed is likely to represent recrystallization of the telluride dominant assemblage.

The PGM assemblage at the base of the hangingwall is of particular interest, as until very recently (Holwell *et al.*, 2005), the hangingwall was not thought to contain any PGE

mineralization, except around calc-silicate rafts (Kinnaird *et al.*, 2005). Holwell *et al.* (2005), conclude that the Platreef was almost completely crystallized when the hangingwall gabbro-norites were intruded. Localized assimilation of mineralized reef into the new magma incorporated PGE-rich sulfide into the hangingwall magma. The observed high Pd content in pentlandite requires rapid cooling (Makovicky, 2002), which would be likely if the hangingwall magma chilled against a crystallized and relatively cooled Platreef. The PGE-rich sulfide liquid cooled rapidly to form, first monosulfide solid solution (*mss*), then the 'primary' assemblage of Pd-pentlandite, Pt-Fe alloy-BMS intergrowths and laurite. In particular, the presence of Pt-Fe alloy-BMS intergrowths is a characteristic texture associated with primary BMS, present in Merensky Reef that has not undergone significant volatile interaction (Kinloch, 1982) and in other layered intrusions (Cabri, 2002). Here we refer to 'primary' magmatic sulfides as pyrrhotite and pentlandite derived from the recrystallization of *mss* on cooling from magmatic temperatures. The PGE mineralization seems to exhibit a two stage crystallization history. The primary assemblage appears to have been locally altered on a centimetre-scale, with Pd apparently exsolved from pentlandite, BMS surrounded by secondary amphiboles, and the PGM assemblage altered to one rich in germanides.

Holwell *et al.* (2005) suggest that the PGE in the basal portion of the hangingwall originated in the Platreef, and was assimilated into the magma that formed the hangingwall gabbro-norites, forming an unusual, 'primary' assemblage of PGM, which formed as a result of the in situ cooling and fractional crystallization of a PGE-rich sulfide liquid, at the base of the hangingwall which is distinct from, and post-dates, the main episode of mineralization in the Platreef.

5.7 Conclusions

The variety of characteristic PGM assemblages in the host of rock types of the Platreef at Sandsloot reflects the fluid and magmatic processes which affected the Platreef during and after emplacement. The method of initial introduction of PGE is still to be resolved; however, from the data presented here, it is possible to describe a sequence of events which redistributed PGE and/or recrystallized PGM through the reef and its footwall and hangingwall, each of which producing a characteristic assemblage in distinct lithologies.

1. During crystallization of the igneous reef, PGM crystallized around the margins of BMS within the interstitial liquid forming a telluride-dominant assemblage, in close

spatial association with BMS. Fluids, originating from assimilation and metamorphism of the dolomitic floor, are likely to have circulated within the interstitial liquid during crystallization. The lack of PGE-sulfides suggests conditions during this time were characterized by low fS_2 .

2. During emplacement of the reef, fluid activity was very significant in redistributing PGE into the footwall. The footwall contains characteristic arsenide,- alloy- and antimonide-dominant PGM assemblages, showing a significant volatile influence during crystallization of this secondary assemblage.
3. Serpentinization of footwall olivine also appears to convert earlier BMS to oxides, with PGE-tellurides remaining in association with the remnant sulfides. Further degrees of serpentinization, where all olivine is replaced, produces a more volatile-enriched antimonide-dominant PGM assemblage, without the association with BMS.
4. Late-stage, Fe-rich fluids percolating through certain parts of the igneous reef desilicated orthopyroxene to form olivine, producing peridotitic zones. PGM were also recrystallized by this fluid, to form an alloy-dominant PGM assemblage of Pt-Fe and Pd-Pb alloys, together with possibly pre-formed tellurides.
5. After a period of cooling and almost total crystallization of the pyroxenitic reef, the hangingwall magma was intruded, locally assimilating PGE-rich pyroxenite reef and cooling quickly to form a separate, primary PGM-BMS assemblage of Pd-bearing pentlandite, Pt-Fe alloy-BMS intergrowths and laurite. Later, localized alteration has recrystallized PGM, producing a germanide-dominant PGM assemblage of satellite grains around altered BMS.

This paper summarizes the assemblages present in various rock types at Sandsloot. Elsewhere along the Platreef the rock types and PGM assemblages are known to be different (e.g. Kinloch, 1982; Viljoen and Schürmann, 1998; Hutchinson and Kinnaird, 2005) and the Platreef is obviously a highly complex orebody with a varied and complex magmatic and fluid history determined by several factors, most importantly, the interaction of the Platreef magma with the varying floor rocks. The results of this study reveal the importance of syn- and post-emplacement fluid activity on the mineralogy and distribution of PGE in the Platreef on a metre scale at this locality, with the presence of dolomite as the footwall rock producing a distinctively PGE sulfide-poor PGM assemblage. Further work is planned to attempt to constrain this footwall control by investigation into the PGM mineralogy in other sections along strike where the footwall is different.

5.8 Acknowledgements

The authors would like to thank the management of Anglo Platinum for allowing access to Sandsloot mine for Paul Armitage and David Holwell to collect samples and their permission for publication of this work. David Holwell's PhD research is funded by the Natural Environment Research Council and supported by Anglo Platinum through Industrial CASE project (NER/S/C/2003/11952). Pete Fisher is thanked for his assistance in the SEM analytical work at Cardiff University. Louis Cabri, Chris Ballhaus and Grant Cawthorn are thanked for their reviews and suggestions which have helped to improve the quality of the manuscript.

Chapter 6

Petrology, geochemistry and the mechanisms determining the distribution of Platinum-Group Element and Base Metal Sulfide mineralization in the Platreef at Overysel, northern Bushveld Complex, South Africa

Published as:

D. A. Holwell and I. McDonald. 2006. Petrology, geochemistry and the mechanisms determining the distribution of Platinum-Group Element and Base Metal Sulfide mineralization in the Platreef at Overysel, northern Bushveld Complex, South Africa. *Mineralium Deposita*, **41**, 575-598.

Co-author roles:

I. McDonald was involved in discussion during the preparation of the manuscript.

6.1 Abstract

Platinum-group element (PGE) mineralization within the Platreef at Overysel is controlled by the presence of base-metal sulfides (BMS). The floor rocks at Overysel are Archaean basement gneisses and unlike other localities along the strike of the Platreef, where the floor is comprised of Transvaal Supergroup sediments, the intimate PGE-BMS relationship holds strong into the footwall rocks. Decoupling of PGE from BMS is rare and the BMS and platinum-group mineral assemblages in the Platreef and the footwall are almost identical. There is minimal overprinting by hydrothermal fluids and therefore the mineralization style present at Overysel may represent the most 'primary' style of Platreef mineralization preserved anywhere along strike.

Chondrite-normalized PGE profiles reveal a progressive fractionation of the PGE with depth into the footwall, with Ir, Ru and Rh dramatically depleted with depth compared to Pt, Pd and Au. This feature is not observed at Sandsloot and Zwartfontein, to the south of Overysel, where the footwall rocks are carbonates. There is evidence from rare earth element (REE) abundances and the amount of interstitial quartz towards the base of the Platreef pyroxenites that contamination by a felsic melt derived from partial melting of the gneissic footwall has taken place. Textural evidence in the gneisses suggests that a sulfide liquid percolated down into the footwall through a permeable, inter-granular network that was produced by partial melting around grain boundaries in the gneisses that was induced by the intrusion of the Platreef magma. PGE were originally concentrated within a sulfide liquid in the Platreef magma, and the crystallization of monosulfide solid solution (*mss*) from the sulfide liquid removed the majority of the IPGE and Rh from it whilst still within the mafic Platreef. Transport of PGE into the gneisses, via downward migration of the residual sulfide liquid, fractionated out the remaining IPGE and Rh in the upper parts of the gneisses leaving a 'slick' of disseminated sulfides in the gneiss, with the residual liquid becoming progressively more depleted in these elements relative to Pt, Pd and Au. Highly sulfide-rich zones with massive sulfides formed where ponding of the sulfide liquid occurred due to permeability contrasts in the footwall.

This study highlights the fact that there is a fundamental floor rock control on the mechanism of distribution of PGE from the Platreef into the footwall rocks. Where the floor rocks are sediments, fluid activity related to metamorphism, assimilation and later serpentinization has in places decoupled PGE from BMS, and transport of PGE into the footwall is via

hydrothermal fluids. In contrast, where the floor is comprised of anhydrous gneiss, such as at Overysel, there is limited fluid activity and PGE behaviour is controlled by the behaviour of sulfide liquids, producing an intimate PGE-BMS association.

Xenoliths and irregular bands of chromitite within the Platreef are described in detail for the first time. These are rich in the IPGE and Rh, and evidence from laurite inclusions indicate they must have crystallized from a PGE-saturated magma. The disturbed and xenolithic nature of the chromitites would suggest they are rip-up clasts, either disturbed by later pulses of Platreef magma in a multi-phase emplacement, or transported into the Platreef from a pre-existing source in a deeper staging chamber or conduit.

6.2 Introduction

The Platreef is located in the northern limb of the Bushveld Complex, South Africa. It is one of the world's largest deposits of platinum-group elements (PGE) and currently the most extensively explored PGE deposit in the world. The Platreef is comprised of a 10-400m thick package of pyroxenitic lithologies with PGE and base-metal sulfide (BMS) mineralization, and is located at the base of the igneous sequence, overlain by norites and gabbronorites generally assigned to the Main Zone of the Complex (e.g. van der Merwe, 1976). From south to north, the northern limb of the Bushveld Complex rests upon a succession of progressively older sedimentary units of the late Archaean - early Proterozoic Transvaal Supergroup, and Archaean basement, in what has been termed an 'igneous transgression' (Wagner, 1929). The footwall units are, north from Mokopane: quartzites and shales of the Timeball Hill Formation; shales of the Deutschland Formation; the Penge banded iron formation; the Malmani dolomite and, north from the farm Zwartfontein, Archaean basement granites and gneisses, which form the footwall on the farm Overysel (Fig. 6.1).

The only mining of the Platreef currently being undertaken is by Anglo Platinum at the Sandsloot open pit mine, opened in 1992, and at Zwartfontein South pit, opened in 2002. The studies of Harris and Chaumba (2001), Armitage *et al.* (2002), Friese (2004), McDonald *et al.* (2005) and Holwell *et al.* (2006) have all utilized data from the Sandsloot mine in their respective studies of Platreef contamination, mineralization, structure, geochemistry and mineralogy. The success of the operations at Sandsloot and Zwartfontein have led to a boom in exploration activity since the turn of the millennium and the quantity and availability of

exploration drill core has facilitated an expanding number of studies to be undertaken on other sections of the Platreef (Kinnaird and McDonald, 2005). Kinnaird *et al.* (2005), Kinnaird (2005) and Hutchinson and Kinnaird (2005) have recently presented Platreef studies from the area currently licenced by Ivanhoe Nickel and Platinum on the farms Turfspruit and Macalacaskop, and Manyeruke *et al.* (2005) from the farm Piet Potgietersrust Town and Townlands (Townlands, Fig. 6.1).

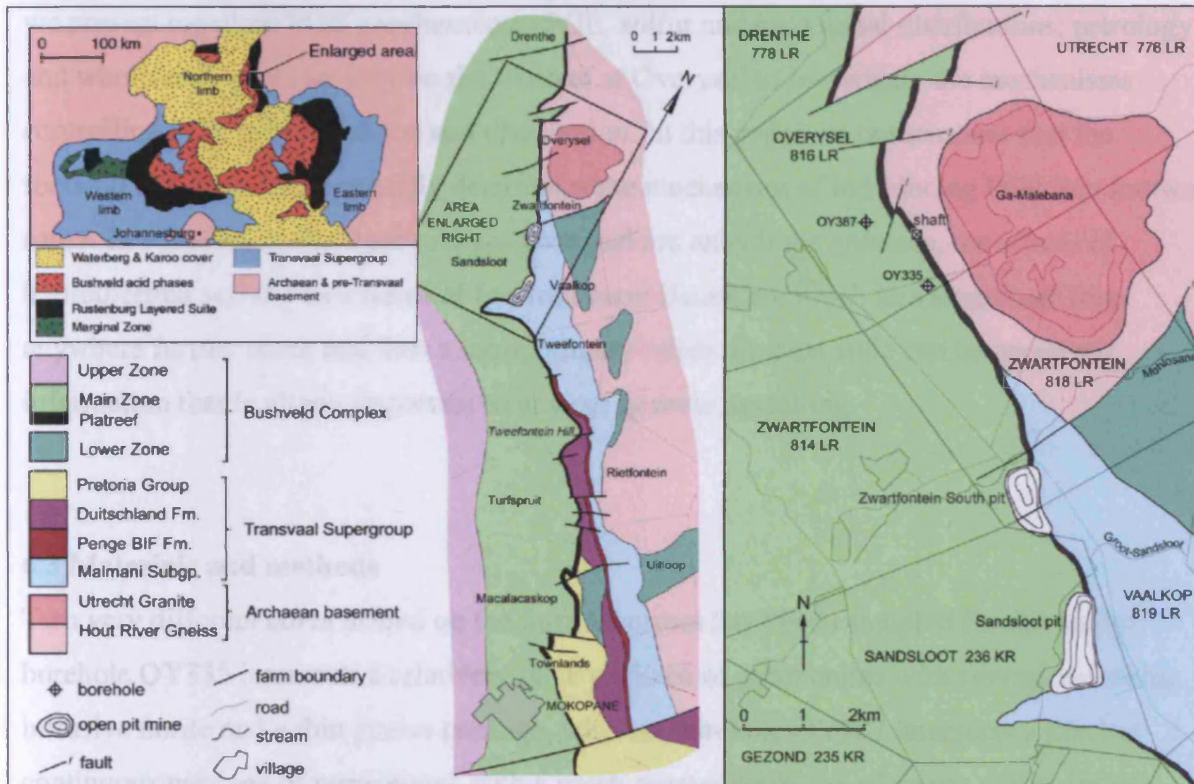


Figure 6.1. Geological map of the Platreef, showing farms referred to in the text, together with a detailed map of the Sandsloot-Overysel area showing the locality of boreholes OY335 and OY387 and the 1980 shaft, based on field mapping and published maps of the Geological Survey of South Africa.

As more information becomes available from different localities along strike, it is becoming clear that the Platreef is a highly complex orebody, whose lateral variations are at least in part directly related to the assimilation of, and contamination by, differing floor rocks. The interaction of the Platreef magma with the immediate floor rocks, and in particular the amount of associated fluid activity, appears to have had a profound effect on the platinum-group mineralogy and PGE distribution (Hutchinson and Kinnaird, 2005; Holwell *et al.*, 2006). In addition, where the floor rocks are sediments of the Transvaal Supergroup, hydrothermal

overprinting may have significantly altered the original mineralization style, which leads to limitations in attempting to understand the underlying mineralization mechanisms.

This study presents the first new data on the Platreef at Overysel since the brief accounts in White (1994) and is also the first detailed investigation since the petrographic and isotopic studies of Cawthorn *et al.* (1985) and Barton *et al.* (1986). However, the latter papers addressed the issue of floor rock contamination, rather than mineralization. For the first time, we present together: PGE geochemistry; PGE, sulfur and base metal distributions; petrology and whole-rock geochemistry on the Platreef at Overysel to investigate the mechanisms controlling PGE mineralization and distribution. In this paper we demonstrate that the footwall lithology fundamentally determines the mechanism of introducing PGE into footwall rocks. In addition, as the floor rocks at Overysel are anhydrous gneisses, the effects of hydrothermal activity as a result of footwall assimilation are much less significant than anywhere further south and thus a more primary mineralization style can be preserved, information that is vitally important to any ore genesis modelling.

6.3 Materials and methods

Two very different cores drilled on the farm Overysel have been sampled for this study: borehole OY335 intersects a relatively thick package of pyroxenites with several xenoliths, intrusive norite and a thin gneiss package, whereas borehole OY387 intersects a thin but continuous package of pyroxenites with a much greater thickness of gneiss and zones of mineralization that extend well into the footwall. The locations of the boreholes are shown in Fig. 6.1. Samples were taken at regular intervals down the hole and particularly where a change in lithology or zone of mineralization was encountered. Samples comprized between 15 and 25cm of quarter-core, depending on thickness of lithology. It should be pointed out that as the samples were collected primarily to study the mineralization, the proportion of mineralized samples is not representative of the core as a whole, as more samples were taken in mineralized sections. Stratigraphic logs of the two cores are shown in Fig. 6.2, together with the position of the samples and zones of mineralization based on visible BMS. Sample numbers refer to depth in metres, but do not reflect true thickness, with normal dips around 45°. A thin section was cut from each sample, with the remainder crushed and powdered for geochemical analysis. Additional samples (OY08, OY16) were obtained from the dumps at the disused exploration shaft, sunk in 1980, near the village of Ga-Melebana (Fig. 6.1).

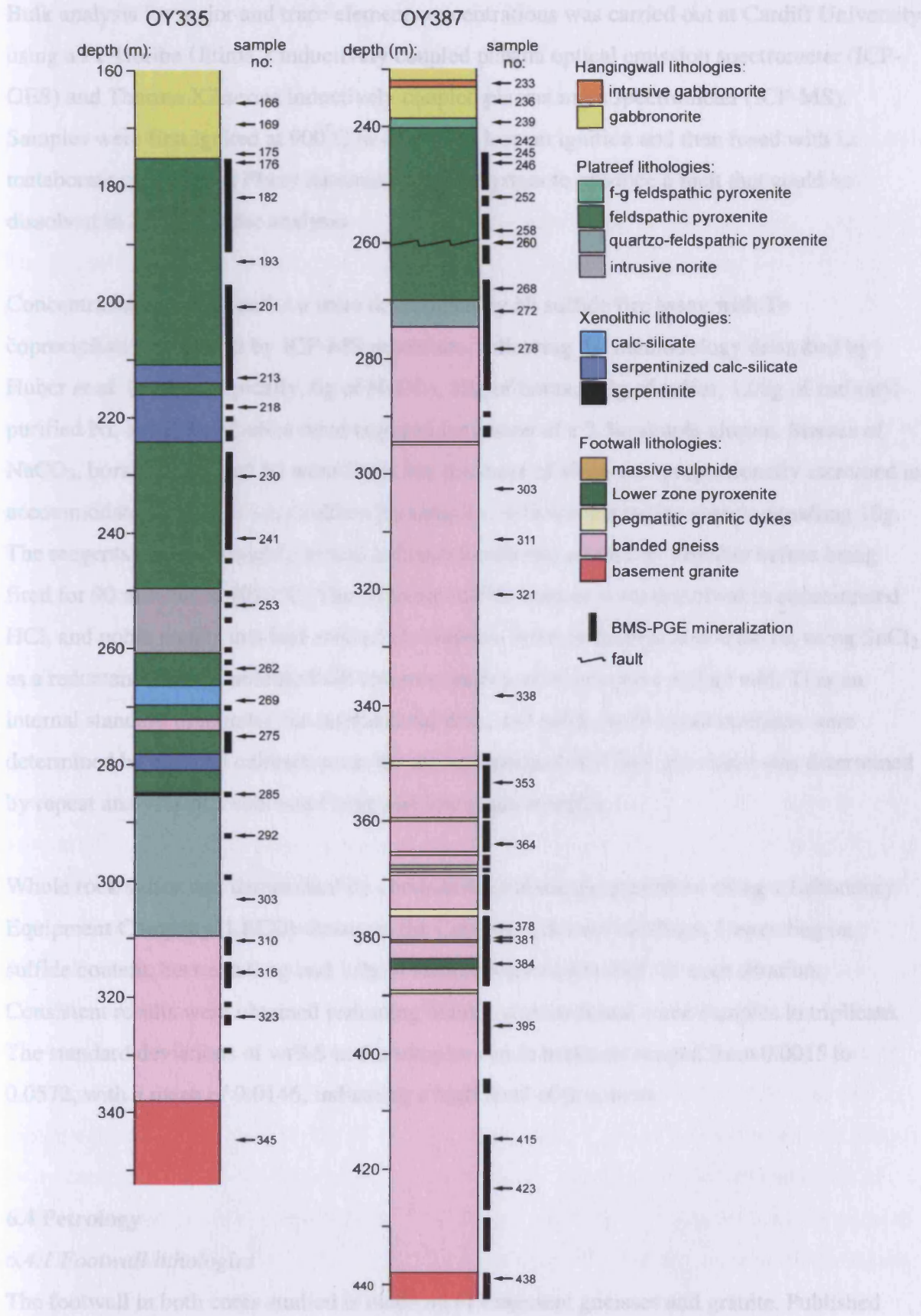


Figure 6.2. Stratigraphic logs of borehole cores OY335 and OY387 showing the positions of the samples and zones of visible BMS-PGE mineralization.

Bulk analysis for major and trace element concentrations was carried out at Cardiff University using a JY Horiba Ultima 2 inductively coupled plasma optical emission spectrometer (ICP-OES) and Thermo X7 series inductively coupled plasma mass spectrometer (ICP-MS). Samples were first ignited at 900°C to determine loss on ignition and then fused with Li metaborate on a Claisse Fluxy automated fusion system to produce a melt that could be dissolved in 2% HNO₃ for analysis.

Concentrations of PGE and Au were determined by Ni sulfide fire assay with Te coprecipitation followed by ICP-MS procedure, following the methodology described by Huber *et al.* (2001). Typically, 6g of NaCO₃, 12g of borax, 0.9g of sulfur, 1.08g of carbonyl-purified Ni, and 2.5g of silica were required for fusion of a 7.5g sample aliquot. Masses of NaCO₃, borax, sulfur and Ni were fixed, but the mass of silica was proportionally increased to accommodate smaller or very sulfur-rich samples, with sample+silica always equalling 10g. The reagents were thoroughly mixed and transferred into a fire-clay crucible before being fired for 90 minutes at 1050°C. The resultant sulfide buttons were dissolved in concentrated HCl, and noble metals that had entered the solution were co-precipitated with Te, using SnCl₂ as a reductant. Finally, soluble PGE chloro-complex solutions were spiked with Tl as an internal standard to monitor for instrumental drift, and noble metal concentrations were determined by external calibration on the aforementioned ICP-MS. Precision was determined by repeat analyses of a sub-set of high and low grade samples.

Whole rock sulfur was determined by combustion iodometric procedure using a Laboratory Equipment Company (LECO) titrator at the Camborne School of Mines. Depending on sulfide content, between 0.1g and 1.0g of sample were combusted for each titration. Consistent results were obtained rerunning blanks, standards and some samples in triplicate. The standard deviations of wt%S in the samples run in triplicate ranged from 0.0015 to 0.0572, with a mean of 0.0146, indicating a high level of precision.

6.4 Petrology

6.4.1 Footwall lithologies

The footwall in both cores studied is made up of basement gneisses and granite. Published mapping by the Geological Survey of South Africa identifies the granite in the Overysel area as Utrecht Granite, and the gneisses as Hout River Gneiss. The true thickness of the gneiss

varies, being 20m thick in OY335 and 117m in OY387. The outcrop of Utrecht granite forms a prominent, roughly circular group of hills, and it is likely that the granite is a domal body intruded into the gneisses. This would explain why borehole OY387 intersects a greater thickness of gneiss before intersecting granite, as it was drilled further away from the surface outcrop of the dome of granite (Fig. 6.1). Both cores intersect pink granite at the base and conventionally this is the point at which drilling was terminated during the drilling campaign. The gneisses, which have traditionally been termed 'granofels' by exploration and mining geologists on the Platreef, are a set of banded gneisses comprising pale, quartzo-feldspathic bands and darker, more mafic orthopyroxene-rich bands. Cawthorn *et al.* (1985) referred to the rocks as banded tonalitic gneisses and stated that on mineralogical and textural grounds, they could be termed enderbites. The rocks contain a very restricted, anhydrous mineralogy of quartz, Na-rich plagioclase, orthopyroxene (En_{70-75}) and occasionally garnet and microcline indicative of granulite facies metamorphic conditions. Biotite is occasionally present as a retrograde phase. Texturally, orthopyroxene occurs in bands which can be medium-grained (Fig. 6.3a) or made up of fine-grained aggregates (Fig. 6.3b) that appear to be the product of deformation-induced grain-size reduction before or during high-grade metamorphism prior to Bushveld intrusion.

Base metal sulfides are present sporadically in the gneisses. They typically occur as small blebs along grain boundaries with concave edges against the silicates and have no preferred association with either the pyroxenitic or felsic bands. In places, the sulfide content of the rock can become very high, with both net-textured and massive sulfides present in the OY387 core at around 380m depth. Massive sulfides are also known to be common at the Platreef-footwall contact in the Overysel area (R. Montjoie, pers. comm. 2004). Sulfide blebs are typically made up of pyrrhotite, with pentlandite around the margins and chalcopyrite either at the margins or as laths within pyrrhotite. Platinum-group minerals (PGM), mostly Pt and Pd tellurides with some Pt sulfides, sperrylite ($PtAs_2$) and Pd bismuthides, are located at the margins of the sulfide blebs (Holwell and McDonald, 2005b). The BMS grains are not altered as is commonly the case in the Platreef pyroxenites. The massive sulfide contains bands of chalcopyrite and pyrrhotite separated by thin bands of pentlandite. The margin of the massive sulfide is gradational, and does not appear to be a fracture fill. The net textured sulfide shows a very unusual texture, where the blebs occur not just at grain boundaries, but also within grains. In both cases, the BMS exhibit concave boundaries against the silicates (Fig. 6.4).

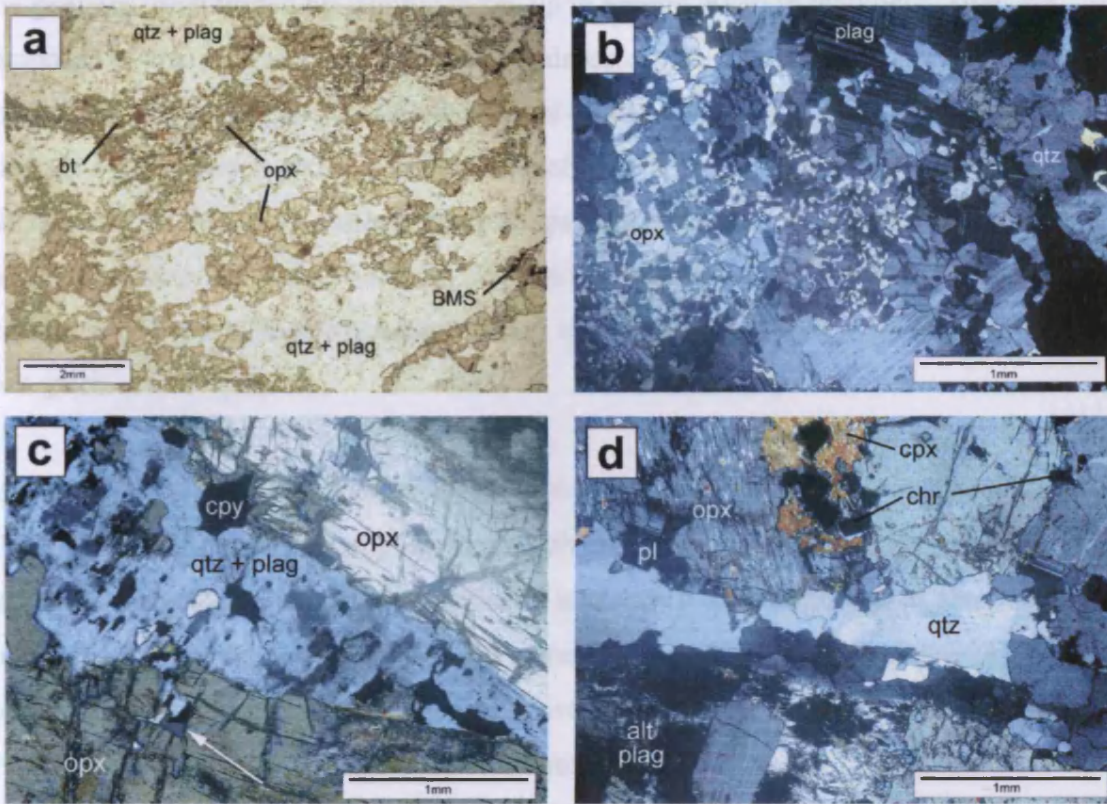


Figure 6.3. Thin section photographs of some of the lithologies present at Overysel. *a* is taken in plane polarized light; all others are in cross-polarized light. *a*: banded footwall gneiss (OY387-321) showing wispy bands of quartz and plagioclase (qtz + plag) and bands of both medium- and fine-grained orthopyroxene (opx). *b*: footwall gneiss (OY335-323) showing fine-grained recrystallized orthopyroxene in optical continuity set within medium-grained quartz and plagioclase. *c*: Lower Zone-like pyroxenite (OY387-384) showing lath-shaped orthopyroxene crystals being invaded (arrowed) by graphically intergrown quartz and feldspar and sulfides (opaque), mostly chalcopyrite (cpy). *d*: chromitiferous quartzo-feldspathic pyroxenite (OY335-303), with cumulus chromite (chr). A vein of quartz and some plagioclase cuts across the centre of the section.

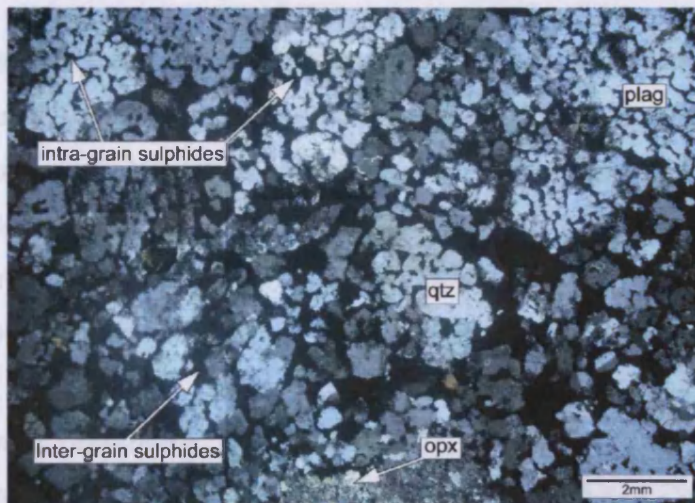


Figure 6.4. Net-textured sulfides within the gneisses (sample OY387-378) showing concave boundaries of interconnected BMS blebs both at quartz and plagioclase grain boundaries (lower part of image), and within silicates (upper part of image).

The gneisses are intruded by granitic dykes up to around 30cm in thickness. They are composed of coarse-grained quartz and K-feldspar, which commonly display a myrmekitic intergrowth. They may also contain needles of biotite several cm long, and some accessory minerals such as zircon and xenotime. Some of the dykes are characteristically pink, whilst others are white. No cross-cutting relationships between the two dyke types were observed to constrain relative age relationships. Where the dykes have intruded, the adjacent gneisses are pervasively altered by hydrous minerals such as amphiboles and chlorite which produces a dark green colouration.

Borehole OY387 intersects a 3m thick zone of pyroxenite deep into the gneisses (sample OY387-384). This rock contains abundant, lath-shaped cumulus orthopyroxene (En₈₈). The interstitial assemblage comprises graphically intergrown quartz and plagioclase, together with abundant BMS (mostly chalcopyrite) and some chromite (Cr₂O₃ content: 55wt%). The quartz and plagioclase appear to corrode the orthopyroxene as if a quartzo-feldspathic melt has invaded the rock (Fig. 6.3c). The pyroxenite resembles samples of Lower Zone-type pyroxenite taken from the satellite body exposed along the Mohlosane stream bed on the farm Zwartfontein (Fig. 6.1). These rocks contain lath-shaped orthopyroxene with a composition of En₈₆ and have whole-rock Cr₂O₃ contents (0.5wt%) identical to the footwall pyroxenite in OY387-384. The lath-like nature of the orthopyroxenes, together with their high Mg content, which is considerably higher than both the Platreef and gneiss orthopyroxenes, makes it likely that this pyroxenite represents a small body of Lower Zone material similar to that developed on Zwartfontein.

The Utrecht granite is a pink, fine- to medium-grained granite consisting of mesoperthitic alkali feldspar, quartz, minor muscovite and accessory monazite and kobeite. The presence of K-feldspar and absence of plagioclase distinguish the granite from the quartzo-feldspathic regions of the gneisses. Where mineralized, the rock has a bleached appearance and contains some secondary amphiboles and micas. Chalcopyrite and millerite are the most common sulfides, with no pentlandite present.

6.4.2 Igneous Platreef lithologies

The igneous reef pyroxenites have thicknesses of 95m in OY335 and 25m in OY387. The relatively thin reef in OY387 may be due to an irregular floor topography, or as a result of faulting, which may be indicated by an infilled fracture zone in the core at 260m (Fig. 6.2).

The pyroxenites are typically coarse-grained and made up of cumulus orthopyroxene (En₇₅₋₈₀), with 5-20% intercumulus plagioclase (variably altered to sericite), up to 5% clinopyroxene and a little quartz, with some accessory phlogopite, chromite and ilmenite. In many cases plagioclase totals over 10% of the modal mineralogy, and therefore the rock should be classified as norite under IUGS classification. However, in keeping with general Bushveld nomenclature in which names reflect the cumulus mineralogy, we refer to these rocks as feldspathic pyroxenites to avoid confusion with hangingwall norites and gabbro-norites, which contain cumulus plagioclase. A fine-grained feldspathic pyroxenite barren of mineralization, located below the hangingwall contact, is present in borehole OY387 and this probably correlates to the 'C'-reef of White (1994), although the observed clinopyroxene content of generally around 10% is much less than that suggested by White. Alteration by micas and carbonates occurs sporadically, where the interstitial minerals can almost be completely altered, and the cumulus orthopyroxenes may be shot through with veinlets of the alteration minerals. Such alteration gives the rocks a dark green colouration.

At Sandsloot and Zwartfontein, quartz is very rare in the feldspathic pyroxenites. In contrast, towards the base of the reef at Overysel, quartz becomes common in the interstitial assemblage as the footwall contact is approached. One such quartzo-feldspathic pyroxenite sample (OY335-303) from just above the footwall contact contains abundant, disseminated chromite and veinlets of quartzo-feldspathic material and is shown in Fig. 6.3d.

Base metal sulfides occur within the interstitial assemblage as blebs that can range up to a few centimetres in diameter, but are more commonly <10mm. Typically, they comprise a pyrrhotite core, with pentlandite and chalcopyrite margins. Minor pyrite is also present. The most common PGM are Pt and Pd tellurides, with some Pt sulfides and sperrylite (Holwell and McDonald, 2005b). The PGM are commonly located towards the margins of the BMS blebs, which are commonly altered so that the BMS margin appears to have regressed, leaving satellite PGM grains within secondary silicates as described by Hutchinson and Kinnaird (2005) and Holwell *et al.* (2006).

Chromitites were observed in the cores as small, angular xenoliths within the feldspathic pyroxenites in the central portion of the Platereef pyroxenites in both cores, but not as layers or stringers. Chromitite bodies at Overysel are common in places, and the exploration mining at Overysel (described by White, 1994) encountered some large bodies of chromitite. Samples

taken from the dumps at the disused shaft show some massive chromitites up to 30cm in thickness, and bifurcating chromitites interbanded with lenses of feldspathic pyroxenite (Fig. 6.5a) and some thin layers of chromitite are also present within feldspathic pyroxenites (Fig. 6.5b). The underground workings showed these bodies to be lensoidal and not to be laterally persistent (J. White, pers. comm., 2005). The chromitite layers are made up of up to 50modal% cumulus chromite grains within oikocrystic plagioclase and rarer orthopyroxene, variably altered to sericite and with some phlogopite present (Fig. 6.5c). The density of chromite grains is less where orthopyroxene is the oikocrystic phase (Fig. 6.5c). The interbanded feldspathic pyroxenites show evidence of a high degree of hydrothermal alteration, with the development of large amphiboles and fine-grained masses of sericite (Fig. 6.5d). Chromite grains are occasionally euhedral (Fig. 6.5e) or more commonly subhedral with irregular margins, which appear to be corroded and infilled by silicates (Fig. 6.5f). Some BMS are present within the chromitites and are mostly pentlandite (Figs. 6.5e, f), with rarer chalcopyrite.

Table 6.1 shows the compositions of chromite grains from chromitite layers and xenoliths and disseminated grains within Platreef feldspathic pyroxenite and in the Lower Zone-type pyroxenite in the footwall of OY387. Compositions of grains within individual samples were very consistent, and two representative analyses from each sample are shown in Table 6.1. Although within each sample there is relatively little compositional variability, between samples there appears to be less consistency, with both FeO and Al₂O₃ contents varying considerably. However, the Cr₂O₃ contents of chromites in all the chromitite layers and xenoliths fall within the range 41-46wt%, with the disseminated chromite within pyroxenites having a greater compositional range of 42-49wt% Cr₂O₃, which may be due to exchange reactions with the surrounding silicates. A common feature of all the Platreef chromites is a relatively high TiO₂ content that is generally >1wt% and may exceed 2wt% in some disseminated chromites, plus detectable levels of V₂O₅ (0.3-1.2wt%). The chromites from the Lower Zone-type pyroxenite are very different, with systematically higher Cr₂O₃ contents (around 55wt%) coupled with very low TiO₂ (<0.5wt%) and no detectable V₂O₅ content. The compositions are consistent with chromites in the Lower Zone of the northern Bushveld Complex at Grasvally in terms of Cr₂O₃ and TiO₂ contents (van der Merwe, 1976; Hulbert and von Gruenewaldt, 1982; Hulbert and von Gruenewaldt, 1986).

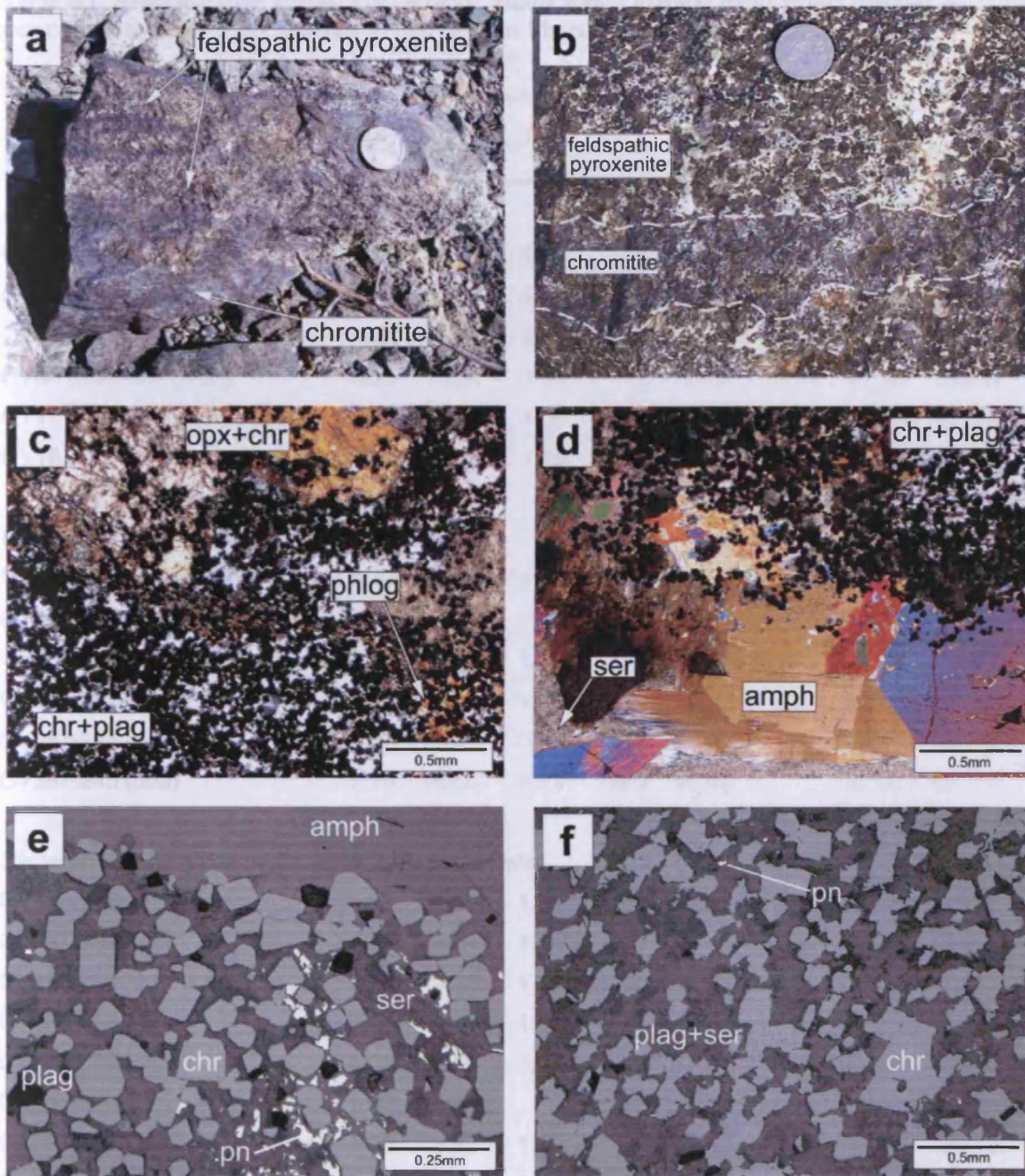


Figure 6.5. Chromitites obtained from the underground workings on Overysel: *a*: sample OY08, of feldspathic pyroxenite with irregular bands of chromitite; *b*: highly feldspathic pyroxenite with a 3cm thick chromitite layer. Way up uncertain; *c*: thin section of one of the chromitite bands shown in *a*, showing cumulus chromite (chr) with oikocrystic plagioclase (plag) and orthopyroxene (opx) and accessory phlogopite (phlog) in cross-polarized light (xpl); *d*: thin section showing the margin of a chromitite band from sample OY08 with secondary amphiboles (amph) and sericite (ser) after pyroxene and plagioclase, shown in xpl; *e*: euhedral chromite grains in sample OY08 with pentlandite (pn) in plagioclase and sericite, at the margin of a chromitite band in contact with secondary amphiboles, shown in reflected light; *f*: subhedral chromitite grains within a chromitite band from sample OY08 in reflected light.

Table 6.1. Representative analyses of chromite grains within Platreef rocks from Overysel, as determined by SEM-EDA analysis as described in Chapter 5.5. Total Fe expressed as FeO.

Sample	Lithology	MgO	Al ₂ O ₃	TiO ₂	V ₂ O ₅	Cr ₂ O ₃	MnO	FeO	Total
<i>Chromitite layers</i>									
OY08 (euhedral grain)		3.43	10.48	1.33	0.31	41.81	0.69	42.81	100.86
OY08 (euhedral grain)		1.37	9.25	1.00		41.74	0.56	46.88	100.81
OY08 (anhedral grain)		4.84	11.22	0.90	0.31	44.75	0.54	38.27	100.38
OY08 (anhedral grain)		4.20	10.64	1.31		44.05	0.87	38.95	100.01
OY16 (feldspathic chromitite)		5.98	14.07	1.39	0.27	42.40	0.49	36.29	100.89
OY16 (feldspathic chromitite)		6.04	13.70	1.79	0.35	42.25		37.02	101.14
<i>Chromitite pods/xenoliths</i>									
OY335-241 (xenolith)		6.62	14.85	1.05	0.41	42.10		34.89	99.92
OY335-241 (xenolith)		6.70	14.80	1.04	0.55	42.06		34.68	99.83
OY335-262 (xenolith)		7.88	16.08	1.20	0.38	42.37		32.38	100.28
OY335-262 (xenolith)		7.68	15.99	1.26		42.20	0.53	32.40	100.06
OY387-245 (pod)		7.53	16.69	0.58	0.61	46.39		28.92	100.72
OY387-245 (pod)		7.18	15.50	0.89	0.69	46.49		30.00	100.74
<i>Disseminated chromite within feldspathic pyroxenite</i>									
OY387-246		4.93	11.06	1.74	0.71	47.88	0.57	33.46	100.35
OY387-246		4.79	9.64	1.51	0.77	49.40	0.61	33.87	100.59
OY387-258		3.98	9.83	1.27	0.58	45.86	0.76	38.55	100.81
OY387-258		3.72	9.83	1.08	0.45	46.54		38.58	100.21
OY387-268		1.05	3.53	1.74	1.18	42.66	0.65	48.53	99.34
OY387-268		1.02	5.93		0.73	46.02	0.76	45.28	99.73
OY335-303		4.30	8.62	1.69		42.51		42.05	99.18
OY335-303		3.17	6.31	2.18	0.68	42.97		44.10	99.42
<i>Lower Zone pyroxenite</i>									
OY387-384		4.01	8.29	0.48		55.29		32.60	100.67
OY387-384		4.90	8.56			55.59	0.65	30.23	99.93

The reef in the OY335 core is intersected by an intrusive norite, locally referred to as 'hybrid norite.' It is a fine-grained rock containing around 55% plagioclase, 30% orthopyroxene, often altered by radiating amphiboles, 10% clinopyroxene and 5% quartz. There are coarse-grained regions with a similar mineralogy, although these areas contain more quartz and also abundant blebs of BMS, whereas the fine-grained areas are barren of mineralization.

Serpentinization, which is very common in the Platreef further south (Armitage *et al.*, 2002; Kinnaird, 2004; Holwell *et al.*, 2006; Holwell and Jordaan, 2006), is present only as thin bands, a few centimetres thick in the cores studied. These bands contain olivine, which is almost completely converted to serpentine, magnetite, and BMS, mostly pyrrhotite. Xenoliths of calc-silicate up to 10m thick are also present in the OY335 core, three of which are serpentinized (Fig. 6.2) and contain abundant olivine and clinopyroxene, with some orthopyroxene and amphibole. This is distinguished as an olivine-bearing metasedimentary rock, rather than an olivine-bearing igneous lithology of Platreef affinity, by its Cr content (c.f. McDonald *et al.*, 2005; Kinnaird, 2005). The rock contains 50ppm Cr, whereas Platreef pyroxenites contain around 2000ppm Cr (Table 6.2). The margins of the serpentinized xenolith are gradational with the surrounding feldspathic pyroxenite. Another xenolith, at 269m, is not serpentinized and contains a typical calc-silicate assemblage of diopside, wollastonite, calcite and andradite garnet.

6.4.3 Hangingwall lithologies

The hangingwall is made up of gabbro-norites comprising 40-80% cumulus plagioclase, with cumulus and intercumulus orthopyroxene and oikocrystic clinopyroxene. The orthopyroxenes contain inclusions of small plagioclase crystals at their margins only, suggesting that plagioclase and orthopyroxene crystallized coevally. Some samples show textures of inverted pigeonite within the pyroxenes. Ilmenite and BMS are small, accessory phases. The hangingwall in OY387 is intruded by a fine-grained melanorite such as those described from Zwartfontein South pit by Holwell and Jordaan (2006) that are made up of around 50% plagioclase, 35% orthopyroxene and 15% clinopyroxene.

6.5 Rare earth element geochemistry

Whole-rock REE and Eu/Eu* values are shown in Table 6.2 and chondrite-normalized REE patterns for Platreef, hangingwall and footwall rocks from the two borehole cores are shown

in Figs. 6.6a-d. The chondrite-normalized fields for the Platreef pyroxenites in both cores are relatively fractionated, with enrichment in the light rare earth elements (LREE). In most cases, the profiles are trough-shaped and show a gently positive gradient in the heavy rare earth elements (HREE) from Ho to Lu. The field for pyroxenites in the OY335 core, in which a much thicker sequence of pyroxenites is intersected, is more extensive than that of the OY387 pyroxenites, and exhibits a higher upper limit of absolute REE concentrations. Of particular note is that the individual profiles of the samples from the OY335 core become progressively more enriched with depth and proximity to the footwall. A moderately positive Eu anomaly (average $\text{Eu}/\text{Eu}^* = 1.35$) is exhibited by most of the pyroxenites in the OY387 core, although it is not as well developed in the samples from OY335 (average $\text{Eu}/\text{Eu}^* = 1.03$). One sample of reef pyroxenite from OY387 (sample OY387-268) shows a very enriched pattern with a positive Eu anomaly. This sample is highly altered by sericite but contains around 10% quartz in its modal mineralogy, which is reflected by its whole rock SiO_2 content, which is around 57wt%, whereas all other pyroxenites from both cores typically contain 51-54wt% SiO_2 (Table 6.2). The intrusive norite (OY335-253) shows a similar profile to the pyroxenites, with the exception that it has a large positive Eu anomaly that is likely to reflect its high plagioclase content.

The chondrite-normalized REE fields for the gneisses in both sample suites exhibit highly fractionated patterns that are much more enriched than those of the Platreef pyroxenites. The granite in the OY335 core shows a very strongly fractionated pattern and the greatest depletion in the HREE of any of the samples. The altered granite in the OY387 core differs from the relatively fresh granite in the OY335 core by having a large positive Eu anomaly. The Lower Zone-like pyroxenite has a profile not dissimilar to the Platreef pyroxenites, except that it exhibits a slight negative Eu anomaly ($\text{Eu}/\text{Eu}^* = 0.73$) and is more noticeably trough-shaped. The profiles of hangingwall rocks are similar from both cores and show a more fractionated pattern than the pyroxenites, with a greater enrichment in the LREE.

For comparison, Figs. 6.6e-f show the chondrite-normalized REE fields for the Platreef rocks at Sandsloot from McDonald *et al.* (2005) and the data of Manyeruke *et al.* (2005) for Platreef rocks at Townlands. The pyroxenites at Sandsloot show very similar REE patterns to those at Overysel, with the exception that they have a negative Eu anomaly, which is also seen in the footwall sediments. The patterns from Townlands are interesting, in that they show three distinct profiles in three portions of the Platreef, which Manyeruke *et al.* (2005) suggest

formed from three separate intrusive events, with the REE becoming less enriched from the Lower to the Upper Platreef. When compared to the data for Overysel and Sandsloot, it is the Upper Platreef at Townlands which shows the closest appearance in terms of REE patterns. The Lower Platreef at Townlands is much more REE enriched than any of the Platreef rocks from Overysel or Sandsloot.

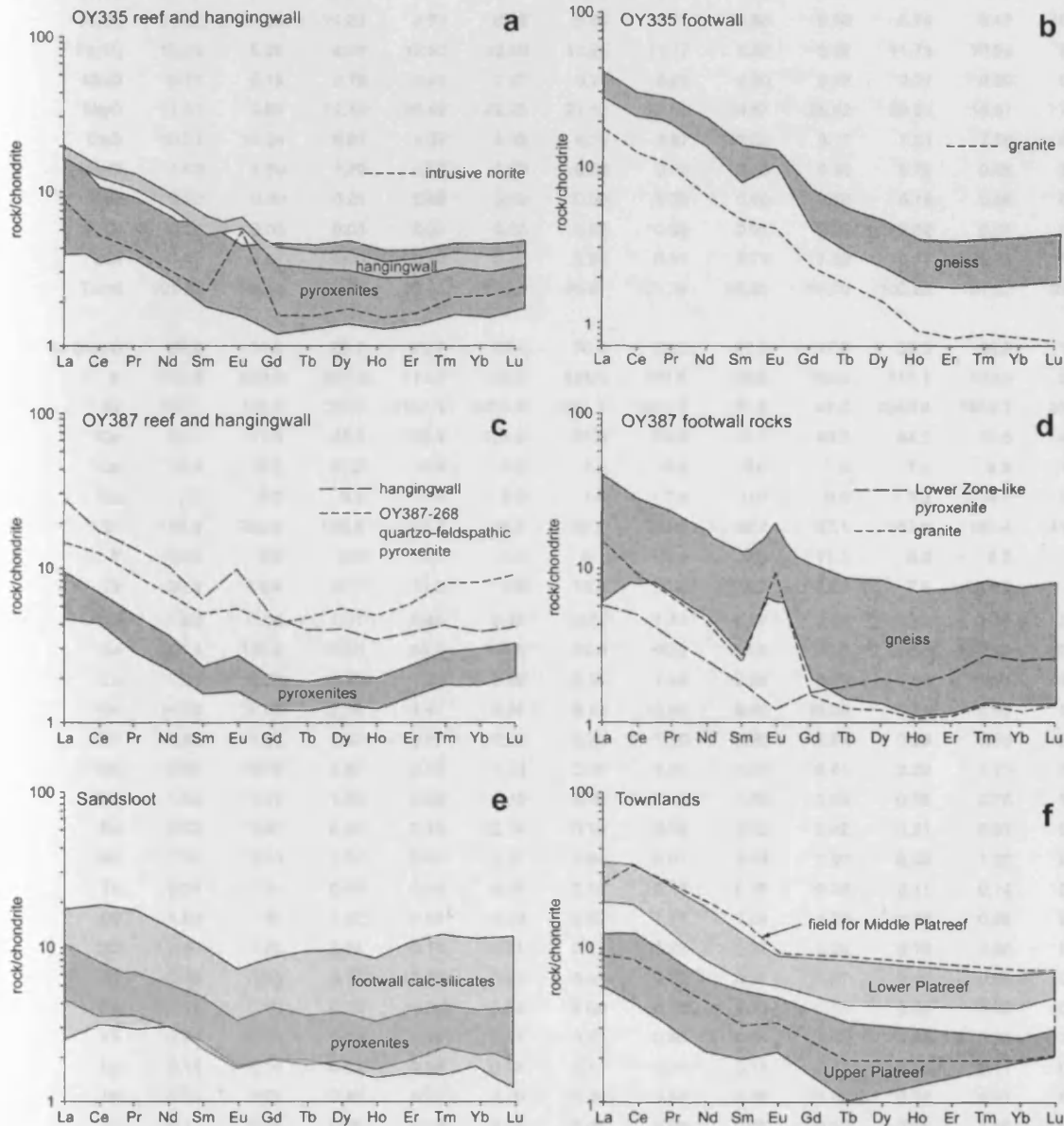


Figure 6.6. Chondrite-normalized REE plots for *a*: Platreef and hangingwall rocks from the OY335 core; *b*: footwall rocks from the OY335 core; *c*: Platreef and hangingwall rocks from the OY387 core; *d*: footwall rocks from the OY387 core; *e*: Platreef pyroxenites and footwall calc-silicates from Sandsloot (from McDonald *et al.* 2005); *f*: Upper, Middle and Lower Platreef rocks from Townlands (from Manyeruke *et al.* 2005). Normalising factors are from Taylor and McLennan (1985).

Table 6.2. Geochemical data for all samples from the OY335 and OY387 cores and chromitite samples from the underground workings on Overysel. Lithological units: HWG – hangingwall gabbro-norite; HWI – hangingwall intrusive gabbro-norite; FPX – feldspathic pyroxenite; SX – serpentinized xenolith; IN – intrusive norite; SPT – serpentinite; QFPX – quartzo-feldspathic pyroxenite; GN – gneiss; LZZP – Lower Zone-like pyroxenite; GT – granite.

Borehole	OY335	OY335	OY335	OY335	OY335	OY335	OY335	OY335	OY335	OY335	OY335	OY335
Sample	166	169	175	176	182	193	201	213	218	230	241	253
Lithology	HWG	HWG	HWG	FPX	FPX	FPX	FPX	SX	SX	FPX	FPX	IN
SiO ₂ (wt%)	52.72	51.08	52.49	51.74	52.05	51.66	54.47	42.21	41.23	51.94	53.47	54.67
TiO ₂	0.32	0.23	0.26	0.14	0.14	0.18	0.26	0.26	0.36	0.15	0.18	0.10
Al ₂ O ₃	14.22	16.68	14.20	5.78	6.03	5.94	8.67	6.80	5.60	6.74	8.49	18.18
Fe ₂ O ₃	10.00	8.29	9.08	12.53	13.50	12.25	11.17	8.32	8.92	11.75	10.59	5.94
MnO	0.18	0.15	0.16	0.20	0.23	0.19	0.22	0.20	0.22	0.21	0.20	0.12
MgO	11.53	8.87	12.10	23.42	22.85	21.12	18.58	24.67	26.82	20.57	18.61	7.13
CaO	10.21	10.54	9.01	4.27	4.42	4.70	6.57	12.22	9.17	7.21	7.56	8.34
Na ₂ O	1.63	1.80	1.70	0.58	0.49	0.58	0.82	0.10	0.23	0.72	0.98	3.05
K ₂ O	0.22	0.30	0.21	0.08	0.05	0.06	0.05	0.00	0.03	0.19	0.25	0.74
P ₂ O ₅	0.04	0.03	0.03	0.02	0.02	0.02	0.03	0.01	0.02	0.02	0.01	0.01
LOI	0.47	0.62	0.50	0.90	0.76	3.26	0.51	3.79	7.09	0.77	0.72	1.22
Total	101.53	98.58	99.75	99.65	100.53	99.97	101.34	98.60	99.70	100.28	101.07	99.51
Sc (ppm)	30.2	24.9	25.7	26.7	28.4	30.6	29.5	27.2	17.0	30.3	28.6	11.6
V	155.9	128.9	127.3	113.7	116.5	124.4	137.5	89.6	65.9	117.1	122.0	62.0
Cr	725.1	460.2	777.3	2161.4	2334.6	1981.1	1612.7	50.9	47.0	2043.4	1959.7	379.0
Co	50.3	41.0	48.3	128.4	126.9	87.0	69.9	46.1	40.2	84.5	75.6	45.6
Ga	12.4	14.2	12.2	5.9	6.3	7.4	9.4	8.0	7.5	7.2	8.8	18.3
Rb	3.2	5.3	3.3	1.4	2.2	1.0	1.5	0.0	0.9	3.3	4.9	15.6
Sr	186.8	225.8	188.6	64.7	66.2	66.2	102.0	56.7	37.1	167.8	193.4	414.6
Y	10.5	9.3	8.0	4.1	3.8	6.1	8.0	7.6	11.1	5.3	6.3	4.7
Zr	30.1	19.4	17.1	11.5	7.6	13.7	36.4	25.7	51.0	7.8	11.9	6.6
Nb	1.86	1.16	1.31	0.44	0.47	0.71	1.74	0.57	1.82	0.73	1.34	2.51
Ba	104.4	146.0	112.0	55.5	54.5	48.6	60.5	35.6	40.8	149.5	105.9	229.8
La	7.31	6.30	6.85	1.93	1.46	2.15	7.55	2.88	4.05	1.88	1.94	3.32
Ce	14.33	12.42	12.08	4.47	3.96	6.16	10.46	6.40	10.65	3.44	4.66	5.11
Pr	1.80	1.54	1.47	0.57	0.52	0.79	1.30	0.96	1.54	0.56	0.63	0.60
Nd	6.95	6.09	5.67	2.18	1.93	3.05	4.93	4.27	6.41	2.29	2.73	2.27
Sm	1.64	1.41	1.26	0.52	0.43	0.75	1.14	1.23	1.69	0.58	0.76	0.54
Eu	0.52	0.61	0.52	0.16	0.14	0.19	0.33	0.33	0.42	0.21	0.31	0.49
Gd	1.37	1.23	1.06	0.45	0.37	0.64	0.97	1.09	1.50	0.55	1.22	0.50
Tb	0.24	0.21	0.19	0.08	0.07	0.12	0.17	0.19	0.26	0.11	0.14	0.09
Dy	1.59	1.42	1.22	0.56	0.53	0.88	1.17	1.24	1.70	0.79	0.95	0.68
Ho	0.31	0.28	0.24	0.11	0.11	0.17	0.23	0.23	0.34	0.16	0.20	0.13
Er	0.95	0.85	0.73	0.35	0.35	0.54	0.73	0.67	0.97	0.48	0.58	0.41
Tm	0.15	0.13	0.12	0.06	0.06	0.09	0.12	0.10	0.15	0.08	0.09	0.08
Yb	0.99	0.93	0.79	0.44	0.44	0.67	0.80	0.64	1.05	0.60	0.66	0.54
Lu	0.16	0.14	0.13	0.08	0.08	0.11	0.14	0.11	0.17	0.10	0.11	0.10
Hf	0.74	0.52	0.46	0.27	0.20	0.35	0.84	0.98	1.55	0.22	0.31	0.23
Ta	0.11	0.06	0.08	0.03	0.05	0.06	0.09	0.03	0.10	0.06	0.08	0.24
Th	1.38	0.82	0.97	0.44	0.52	0.59	1.22	0.35	0.67	0.22	0.30	0.47
U	0.43	0.31	0.34	0.23	0.28	0.35	0.47	0.25	0.53	0.31	0.29	0.75
Eu/Eu*	1.03	1.39	1.33	0.98	1.03	0.80	0.94	0.85	0.79	1.12	0.98	2.87

Table 6.2 (cont.)

Borehole	OY335	OY335	OY335	OY335	OY335	OY335	OY335	OY335	OY335	OY335	OY387
Sample	262	269	275	285	292	303	310	316	323	345	233
Lithology	FPX	CSX	FPX	SPT	QFPX	QFPX	GN	GN	GN	GT	HWI
SiO₂ (wt%)	51.43	43.85	48.06	36.53	56.01	51.11	61.45	67.23	59.07	76.72	50.36
TiO ₂	0.23	0.08	0.18	0.24	0.08	0.18	0.26	0.22	0.31	0.02	0.62
Al ₂ O ₃	6.53	1.09	3.92	4.45	10.09	10.59	16.97	16.40	19.65	14.50	11.52
Fe ₂ O ₃	10.60	2.28	12.97	14.00	7.77	9.89	6.07	4.49	5.48	0.36	14.72
MnO	0.23	0.35	0.23	0.09	0.18	0.18	0.18	0.07	0.18	0.02	0.25
MgO	17.62	16.42	22.41	33.20	15.84	17.36	4.92	2.09	4.09	0.17	10.90
CaO	12.99	29.70	10.33	1.37	7.15	6.43	5.55	4.33	6.33	1.08	9.23
Na ₂ O	0.72	0.01	0.35	0.08	1.70	1.13	4.48	4.60	4.52	4.70	1.34
K ₂ O	0.08	-0.01	0.06	0.03	0.18	0.50	0.47	0.49	0.24	1.67	0.01
P ₂ O ₅	0.02	0.00	0.03	0.02	0.01	0.02	0.24	0.12	0.29	0.04	0.01
LOI	0.55	7.60	0.84	8.68	1.71	0.76	0.39	0.66	0.13	0.29	0.39
Total	101.00	101.39	99.37	98.68	100.73	98.14	100.98	100.70	100.30	99.55	99.36
Sc (ppm)	36.7	1.5	29.6	12.5	21.5	25.1	15.0	5.9	13.2	0.9	40.5
V	159.5	13.9	206.4	63.8	73.8	185.6	69.2	39.6	63.9	4.5	327.6
Cr	1428.4	18.6	2134.3	776.0	1072.5	17578.2	186.7	107.8	193.7	69.7	1213.0
Co	62.7	4.4	100.9	115.3	61.4	70.8	29.8	42.0	21.2	2.5	72.6
Ga	8.2	1.7	5.9	6.9	10.9	12.3	25.4	18.5	29.4	19.4	13.4
Rb	0.9	0.0	1.2	0.8	2.1	11.8	5.6	3.7	1.7	20.3	0.7
Sr	120.0	32.6	89.8	20.3	191.2	249.3	534.4	690.3	610.7	287.4	157.1
Y	11.6	3.0	7.6	2.9	4.1	4.2	9.4	5.7	10.7	2.9	17.6
Zr	11.4	16.9	11.7	10.1	8.6	12.5	47.9	41.8	28.9	19.6	20.8
Nb	1.13	0.59	0.36	0.25	3.63	1.74	7.74	2.21	5.56	1.06	1.05
Ba	48.5	0.6	110.8	19.8	165.6	219.6	342.8	667.6	485.9	631.0	80.0
La	2.30	3.32	2.73	0.94	2.19	2.21	10.82	14.10	16.18	6.98	5.68
Ce	6.33	8.10	6.92	2.89	4.94	4.77	21.20	22.66	29.71	12.31	12.19
Pr	1.00	0.98	0.97	0.36	0.66	0.59	2.74	2.66	3.87	1.41	1.62
Nd	4.65	3.63	4.15	1.38	2.62	2.23	10.77	9.80	15.14	4.65	7.68
Sm	1.49	0.70	1.15	0.31	0.66	0.52	2.50	1.83	3.23	1.07	2.07
Eu	0.40	0.16	0.33	0.07	0.25	0.24	0.89	0.92	1.13	0.35	0.63
Gd	1.45	0.53	1.06	0.27	0.57	0.46	1.83	1.22	2.25	0.69	2.32
Tb	0.27	0.08	0.20	0.05	0.10	0.09	0.27	0.16	0.31	0.10	0.41
Dy	1.86	0.51	1.26	0.37	0.64	0.61	1.48	0.87	1.75	0.51	2.75
Ho	0.36	0.09	0.23	0.08	0.12	0.12	0.25	0.15	0.29	0.08	0.54
Er	1.08	0.26	0.66	0.31	0.36	0.39	0.72	0.41	0.83	0.20	1.76
Tm	0.17	0.04	0.09	0.06	0.06	0.06	0.11	0.06	0.12	0.03	0.27
Yb	1.15	0.22	0.62	0.54	0.39	0.44	0.80	0.43	0.88	0.21	1.76
Lu	0.19	0.03	0.10	0.11	0.07	0.07	0.12	0.07	0.14	0.03	0.29
Hf	0.36	0.31	0.29	0.28	0.24	0.33	1.22	0.83	0.62	0.62	0.64
Ta	0.11	0.05	0.14	0.03	0.54	0.21	0.86	0.14	0.44	0.13	0.08
Th	0.31	0.94	0.42	0.30	0.34	0.45	0.43	0.37	0.22	0.31	0.19
U	0.47	0.43	0.37	0.18	0.92	0.35	1.02	0.33	0.40	0.72	0.09
Eu/Eu*	0.83	0.76	0.90	0.77	1.22	1.47	1.22	1.77	1.22	1.17	0.87

Table 6.2 (cont.)

Borehole	OY387	OY387	OY387	OY387	OY387	OY387	OY387	OY387	OY387	OY387	OY387	OY387
Sample	236	239	242	246	252	258	268	272	278	296	311	321
Lithology	HWG	FPX	FPX	FPX	FPX	FPX	QFPX	QFPX	GN	GN	GN	GN
SiO₂ (wt%)	51.13	54.11	54.10	51.80	53.74	52.40	56.98	52.60	56.55	60.79	59.66	57.30
TiO₂	0.21	0.23	0.14	0.15	0.12	0.12	0.16	0.11	0.11	0.16	0.18	0.37
Al₂O₃	18.94	8.39	9.16	5.92	6.92	10.08	6.17	13.70	21.34	21.84	18.78	4.92
Fe₂O₃	7.17	12.49	10.28	12.56	12.57	9.74	10.20	10.10	3.90	1.94	3.53	12.91
MnO	0.13	0.23	0.21	0.24	0.21	0.20	0.18	0.14	0.08	0.05	0.09	0.26
MgO	7.77	19.69	20.37	22.81	19.88	18.67	16.21	12.05	5.57	2.87	6.35	19.54
CaO	10.40	5.01	5.06	3.25	4.08	6.43	4.46	6.81	8.12	6.32	5.00	2.50
Na₂O	2.13	0.75	0.74	0.25	0.69	0.63	0.56	1.69	3.66	5.04	4.03	0.86
K₂O	0.02	0.03	0.00	0.04	0.03	0.05	0.04	0.05	0.04	0.02	0.06	0.19
P₂O₅	0.05	0.02	0.00	0.00	0.01	0.00	0.01	0.02	0.02	0.04	0.06	0.12
LOI	0.70	0.24	1.19	1.77	0.99	1.59	3.62	2.11	0.49	1.04	0.96	0.46
Total	98.65	101.19	101.25	98.78	99.23	99.91	98.58	99.38	99.87	100.10	98.69	99.44
Sc (ppm)	19.0	28.2	25.3	29.0	25.5	25.3	26.7	18.1	9.4	5.7	13.4	30.1
V	100.0	145.8	112.7	149.7	114.2	93.2	102.9	77.8	26.0	17.5	48.4	107.0
Cr	588.6	1965.5	2160.4	8185.2	2566.9	2644.3	2118.6	1193.4	435.9	156.5	585.4	1565.3
Co	36.8	77.9	77.4	106.2	142.6	87.1	106.0	123.0	31.4	9.5	20.5	75.1
Ga	17.1	8.9	8.1	6.7	7.6	8.6	10.5	13.1	22.9	23.2	24.1	10.1
Rb	4.0	1.2	1.7	1.1	1.3	3.5	7.7	7.4	1.2	2.2	2.1	2.7
Sr	274.1	102.6	110.2	55.6	83.7	128.8	51.5	161.1	806.1	909.8	837.8	80.6
Y	10.0	5.8	5.1	3.8	4.6	4.0	15.4	4.6	3.3	5.1	4.8	11.2
Zr	19.5	7.9	12.4	9.2	9.5	9.1	125.0	16.8	13.6	31.3	36.5	62.4
Nb	1.07	1.17	1.33	0.87	2.67	1.23	8.52	2.97	0.75	2.18	2.01	4.97
Ba	154.0	56.1	60.1	24.2	41.4	83.5	67.9	88.3	296.3	655.4	1295.8	256.1
La	10.03	3.14	3.42	1.72	2.06	2.26	5.34	2.38	5.94	9.92	7.25	4.43
Ce	16.42	5.72	6.57	4.22	4.69	4.42	11.77	5.00	9.08	16.86	12.77	12.08
Pr	1.83	0.58	0.67	0.39	0.47	0.41	1.24	0.49	0.92	1.81	1.27	1.59
Nd	7.32	2.34	2.60	1.57	1.76	1.60	4.82	1.91	3.44	6.69	4.61	7.24
Sm	1.46	0.53	0.53	0.36	0.39	0.36	1.15	0.45	0.63	1.15	0.84	1.75
Eu	0.85	0.23	0.23	0.14	0.18	0.24	0.47	0.24	0.72	1.23	1.19	0.52
Gd	1.50	0.59	0.56	0.37	0.45	0.41	1.31	0.49	0.58	0.97	0.78	1.77
Tb	0.23	0.11	0.10	0.07	0.08	0.07	0.27	0.08	0.08	0.14	0.10	0.27
Dy	1.53	0.78	0.70	0.51	0.60	0.56	2.06	0.62	0.51	0.79	0.67	1.70
Ho	0.30	0.17	0.14	0.10	0.13	0.12	0.42	0.13	0.09	0.14	0.13	0.32
Er	0.95	0.59	0.49	0.37	0.44	0.40	1.47	0.41	0.28	0.45	0.44	1.03
Tm	0.15	0.10	0.09	0.06	0.08	0.07	0.28	0.07	0.05	0.07	0.07	0.17
Yb	0.96	0.75	0.58	0.44	0.56	0.47	1.98	0.49	0.32	0.47	0.49	1.11
Lu	0.16	0.13	0.10	0.08	0.10	0.09	0.34	0.08	0.05	0.07	0.09	0.19
Hf	0.53	0.24	0.31	0.22	0.26	0.26	3.38	0.44	0.33	0.75	0.93	1.43
Ta	0.08	0.10	0.10	0.11	0.28	0.12	0.88	0.37	0.11	0.39	0.35	0.97
Th	0.88	0.31	0.59	0.35	0.57	0.58	3.97	1.06	0.30	0.18	0.38	0.76
U	0.31	0.30	0.33	0.38	1.03	1.52	9.16	2.84	0.26	0.26	0.39	2.24
Eu/Eu*	1.73	1.28	1.29	1.17	1.31	1.87	1.17	1.59	3.60	3.47	4.42	0.89

Table 6.2 (cont.)

Borehole	OY387	OY387	OY387	OY387	OY387	OY387	OY387	OY387	OY387	OY387	OY08	OY16
Sample	338	353	364	378	381	384	395	415	423	438	CHR	CHR
Lithology	GN	GN	GN	GN	GN	LZP	GN	GN	GN	GT	CHR	CHR
SiO₂												
(wt%)	59.64	47.99	49.83	50.62	56.48	60.05	64.20	57.69	67.56	73.28	41.04	39.69
TiO₂	0.30	1.53	1.18	0.17	1.39	0.08	0.16	0.45	0.04	0.03	0.44	0.55
Al₂O₃	22.25	14.05	12.75	13.97	14.36	3.80	18.57	21.79	19.33	16.06	10.94	11.80
Fe₂O₃	2.74	16.29	15.92	18.68	13.87	9.53	3.09	3.81	1.86	0.38	16.09	15.75
MnO	0.05	0.25	0.24	0.15	0.20	0.11	0.09	0.13	0.02	0.01	0.26	0.22
MgO	2.28	8.00	8.43	5.74	6.91	25.30	3.24	4.64	1.10	0.07	15.09	13.77
CaO	7.29	11.80	11.20	3.81	4.39	0.85	3.22	4.85	0.63	1.11	6.07	6.25
Na₂O	4.51	1.05	1.32	3.78	3.20	0.64	4.85	4.42	5.21	5.54	0.88	1.10
K₂O	0.25	0.11	0.17	0.33	0.32	0.16	0.39	0.80	2.42	1.50	0.51	0.20
P₂O₅	0.14	0.08	0.05	0.03	0.31	0.01	0.03	0.26	0.03	0.02	0.05	0.03
LOI	0.18	-0.16	-0.16	2.65	0.16	0.19	1.84	1.59	1.32	0.47	1.44	0.60
Total	99.62	100.98	100.92	99.93	101.58	100.72	99.68	100.43	99.52	98.45	92.82	89.96
Sc (ppm)	7.4	42.5	43.0	12.6	24.6	12.7	7.4	11.0	4.2	0.2	23.5	22.6
V	55.8	340.1	353.9	67.6	214.6	19.6	27.3	31.4	0.6	0.8	390.6	512.0
Cr	179.1	208.9	256.3	743.6	1704.2	4995.2	74.9	174.0	49.3	59.5	52764.3	71800.4
Co	10.6	72.1	81.7	310.1	89.4	135.5	19.0	18.0	29.1	2.5	134.9	118.5
Ga	21.7	18.9	17.6	18.4	21.9	8.7	27.5	32.5	22.8	17.0	20.1	22.8
Rb	0.7	0.3	1.7	2.0	1.9	2.3	5.1	13.0	14.9	8.9	12.7	5.2
Sr	898.5	254.3	215.6	506.2	294.1	19.4	422.0	596.5	252.7	414.3	139.3	216.0
Y	8.4	17.3	15.2	5.5	20.0	6.2	14.3	18.2	6.2	3.3	10.1	6.4
Zr	53.6	20.5	18.2	19.5	86.8	10.7	28.0	98.4	16.2	14.5	55.0	11.8
Nb	1.92	1.42	2.50	1.49	6.24	3.93	17.92	22.94	5.10	1.59	3.416	0.913
Ba	417.7	45.0	103.1	479.9	395.0	84.6	1201.1	2049.0	1415.8	2082.3	113.0	199.4
La	14.22	2.20	3.13	6.36	9.83	2.05	7.94	7.75	7.24	5.09	5.503	3.011
Ce	26.35	8.38	7.54	11.45	18.19	4.81	13.74	17.59	11.25	9.46	11.752	6.307
Pr	3.07	1.33	1.11	1.14	2.42	0.47	1.43	2.45	1.07	0.90	1.557	0.832
Nd	12.13	7.30	5.77	4.16	11.33	1.79	5.29	10.79	3.75	3.06	6.159	3.468
Sm	2.12	2.31	1.89	0.69	2.88	0.42	1.18	2.72	0.81	0.56	1.409	0.837
Eu	1.68	1.16	0.85	0.78	1.13	0.11	1.13	1.51	1.24	0.93	0.403	0.315
Gd	1.93	2.82	2.36	0.66	3.22	0.49	1.37	2.65	0.72	0.48	1.320	0.847
Tb	0.25	0.47	0.40	0.11	0.49	0.10	0.25	0.42	0.12	0.07	0.231	0.154
Dy	1.40	3.02	2.59	0.73	3.17	0.76	1.78	2.80	0.80	0.46	1.519	0.984
Ho	0.26	0.57	0.48	0.14	0.60	0.15	0.35	0.52	0.15	0.09	0.289	0.195
Er	0.76	1.67	1.44	0.51	1.81	0.54	1.24	1.60	0.52	0.28	0.889	0.584
Tm	0.10	0.24	0.21	0.10	0.29	0.10	0.23	0.27	0.10	0.05	0.150	0.101
Yb	0.66	1.45	1.27	0.70	1.82	0.60	1.60	1.73	0.83	0.28	1.022	0.662
Lu	0.11	0.23	0.21	0.12	0.30	0.10	0.28	0.26	0.16	0.05	0.164	0.107
Hf	1.15	0.67	0.58	0.50	1.86	0.30	0.89	2.49	0.63	0.45	0.994	0.050
Ta	0.12	0.10	0.32	0.22	0.74	0.85	2.31	3.31	0.97	0.62	0.310	0.195
Th	0.11	0.02	0.16	0.10	0.53	0.83	3.44	0.78	0.78	0.28	1.811	0.506
U	0.10	0.03	0.41	0.33	1.33	2.58	5.55	2.21	4.52	0.48	0.889	0.598
Eu/Eu*	2.50	1.39	1.23	3.46	1.13	0.73	2.71	1.70	4.86	5.32	0.89	1.13

6.6 PGE and BMS mineralization

At Overysel, there appears to be a well-constrained PGE-BMS relationship both in the Platreef and into the footwall. Table 6.3 shows S contents, together with an indication of PGE grade and selected Ni, Cu and S ratios of samples from the two Overysel cores. Figures 6.7a and c show the abundances of Pt, Pd, Rh and S with depth for the two cores. There is an excellent correlation between S and the PGE, with the exception of a notable few samples in the OY335 core. Sample OY335-230, an altered feldspathic pyroxenite, contains very high PGE and only moderate S. This may be due to the hydrothermal processes that altered the rock upgrading the PGE content and/or removing sulfide. OY335-285 is a sample of serpentinite that contains abundant pyrrhotite, but a very low PGE grade, which is consistent with the observations from Sandsloot and Zwartfontein where BMS and PGE appear to be decoupled in serpentinites (Holwell *et al.*, 2006). Sample OY335-303 has moderate grades of PGE but low sulfur. This is a sample of chromiferous quartzo-feldspathic pyroxenite, and may indicate that PGE in this sample are controlled by chromite rather than sulfides. Samples in the OY387 core are very consistent with PGE being controlled by the presence of sulfides. In particular, the section of feldspathic pyroxenites, which are largely unaltered, show distinctly parallel PGE and S patterns. With depth into the footwall, the S/PGE ratios are more variable, as seen by the less parallel nature of the trends in Fig. 6.7, though there is still an undoubted correlation between S and PGE.

Figures 6.7b and d show the correlation between Cu, Ni and S in the two cores. There is a consistent correlation in the distribution of the three elements with $S > Ni > Cu$, with the exception of some very low sulfide samples, the significance of which should be taken with caution as small analytical errors may become significant at such low concentrations. Furthermore, as some Ni will be present in orthopyroxene, in very sulfide-poor samples, the contribution by orthopyroxene to the whole-rock Ni content will become more significant. This is not true for Cu, which will only be present in sulfide. The feldspathic pyroxenites exhibit near-parallel distribution trends, indicating a consistent BMS assemblage. The sample of serpentinite (OY335-285) shows high S but relatively moderate Cu and Ni contents, which reflects its pyrrhotite-dominant BMS content. As with the S/PGE ratios, the Ni/Cu, Ni/S and Cu/S ratios appear to be slightly less consistent with depth. For example in Table 6.3, it can be seen that the Ni/Cu ratio in the section of mineralized pyroxenites in the OY387 core is consistently around 4-6, with the exception of OY387-239 which has a very low sulfide content and thus the high Ni/Cu ratio is dominated by Ni in orthopyroxene with very little

accompanying Cu. With depth into the footwall, Ni/Cu varies between 0.2 and 11.8 (in samples with BMS) with no apparent systematic increase or decrease with depth.

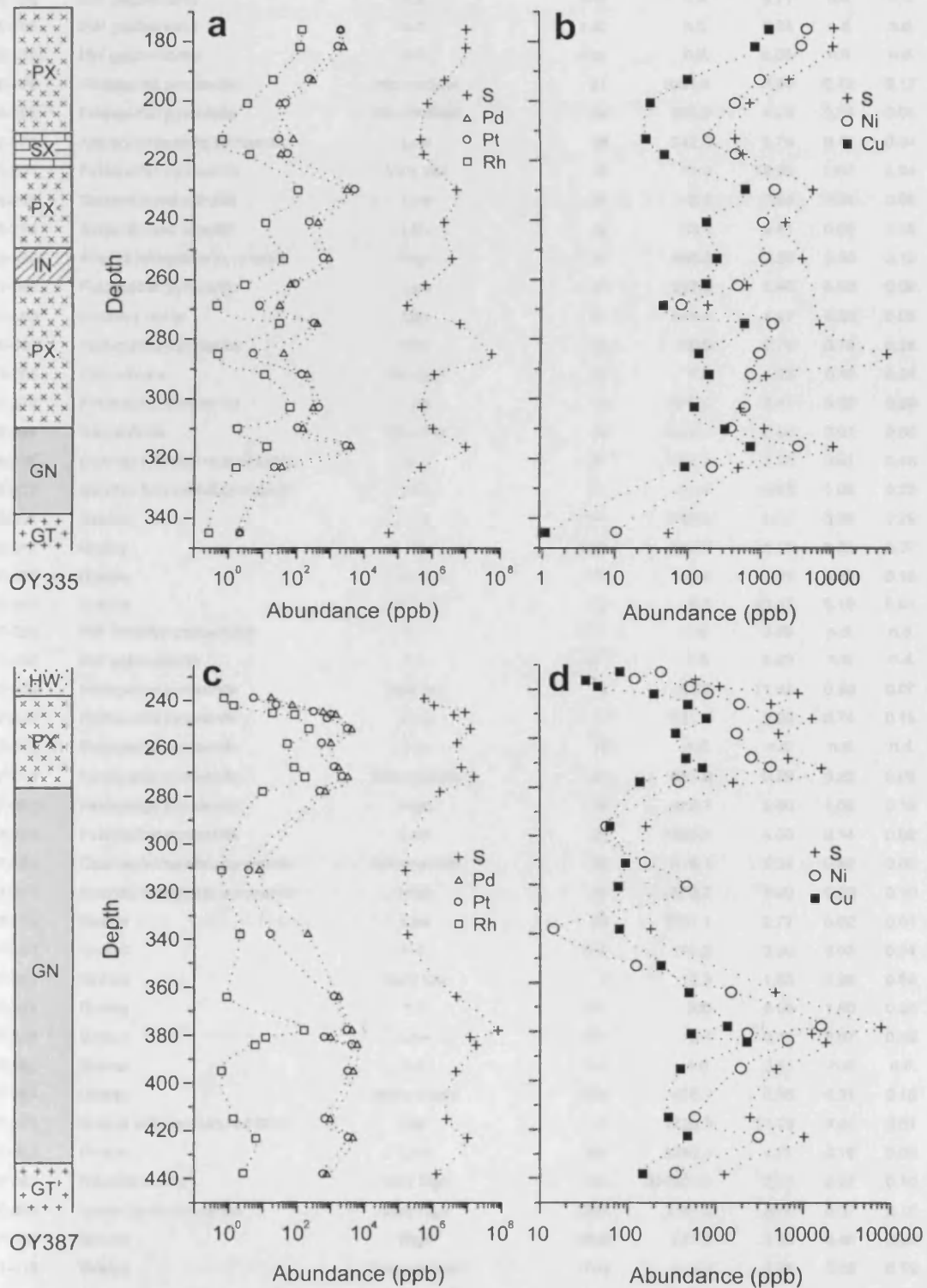


Figure 6.7. Distribution profiles with depth for *a*: S, Pd, Pt and Rh for the OY335 core; *b*: S, Cu and Ni for the OY335 core; *c*: S, Pd, Pt and Rh for the OY387 core; and *d*: S, Ni and Cu for the OY387 core. Key to stratigraphic column: HW: hangingwall gabbronorite; PX: Platreef pyroxenite; SX: serpentinized calc-silicate xenolith; IN: intrusive norite; GN: gneiss; GT: granite.

Table 6.3. Indications of PGE grade, PGE sloping profiles (Pt+Pd)/(Ir+Ru) and S contents of samples from the Overysel cores and chromitite grab samples, together with Ni/Cu, Ni/S and Cu/S ratios. n.d. – not determined

Sample	Lithology	PGE grade	Sloping profile	S (ppm)	Ni/Cu	Ni/S	Cu/S
OY335-166	HW gabbro	n.d.	n.d.	n.d.	5.71	n.d.	n.d.
OY335-169	HW gabbro	n.d.	n.d.	n.d.	6.23	n.d.	n.d.
OY335-175	HW gabbro	n.d.	n.d.	n.d.	8.05	n.d.	n.d.
OY335-176	Feldspathic pyroxenite	Intermediate	21	1021.8	3.34	0.42	0.12
OY335-182	Feldspathic pyroxenite	Intermediate	24	980.9	4.29	0.36	0.08
OY335-193	Altered feldspathic pyroxenite	Low	18	242.2	9.79	0.41	0.04
OY335-201	Feldspathic pyroxenite	Very low	10	71.0	14.68	0.63	0.04
OY335-213	Serpentinized xenolith	Low	79	42.9	7.53	0.46	0.06
OY335-218	Serpentinized xenolith	Low	12	53.8	9.81	0.86	0.08
OY335-230	Altered feldspathic pyroxenite	High	57	500.2	2.55	0.30	0.12
OY335-241	Feldspathic pyroxenite	Low	51	207.3	5.96	0.50	0.08
OY335-253	Intrusive norite	Low	31	356.4	4.47	0.30	0.06
OY335-262	Feldspathic pyroxenite	Low	32	60.9	2.70	0.76	0.28
OY335-269	Calc-silicate	Very low	84	17.8	1.73	0.43	0.24
OY335-275	Feldspathic pyroxenite	Low	15	623.0	2.41	0.22	0.09
OY335-285	Serpentine	Very low	48	5256.0	6.68	0.01	0.00
OY335-292	Quartzo-feldspathic pyroxenite	Low	37	114.0	3.73	0.61	0.16
OY335-303	Quartzo-feldspathic pyroxenite	Low	11	51.4	4.63	1.08	0.23
OY335-310	Gneiss	Low	291	106.8	1.18	0.35	0.29
OY335-316	Gneiss	High	2838	966.0	4.41	0.33	0.07
OY335-323	Gneiss	Very low	78	48.4	2.29	0.43	0.18
OY335-245	Granite	Very low	12	5.5	10.47	0.19	0.01
OY387-233	HW intrusive gabbro	n.d.	n.d.	n.d.	2.86	n.d.	n.d.
OY387-236	HW gabbro	n.d.	n.d.	n.d.	3.63	n.d.	n.d.
OY387-239	Feldspathic pyroxenite	Very low	8	58.9	11.42	0.90	0.07
OY387-242	Feldspathic pyroxenite	Low	17	111.8	3.94	0.74	0.18
OY387-245	Feldspathic pyroxenite	Low	19	n.d.	n.d.	n.d.	n.d.
OY387-246	Feldspathic pyroxenite	Intermediate	26	867.9	3.89	0.22	0.05
OY387-252	Feldspathic pyroxenite	High	26	422.7	5.60	1.09	0.19
OY387-258	Feldspathic pyroxenite	Low	25	1265.3	5.00	0.14	0.02
OY387-268	Quartzo-feldspathic pyroxenite	Intermediate	28	518.7	5.34	0.49	0.09
OY387-272	Quartzo-feldspathic pyroxenite	High	27	673.2	6.00	0.63	0.10
OY387-278	Gneiss	Low	88	1591.1	2.77	0.02	0.01
OY387-303	Gneiss	n.d.	n.d.	159.2	0.90	0.03	0.04
OY387-311	Gneiss	Very low	5	16.3	1.63	0.98	0.60
OY387-321	Gneiss	n.d.	n.d.	300	6.06	1.60	0.20
OY387-338	Gneiss	Low	297	18.4	0.17	0.07	0.45
OY387-353	Gneiss	n.d.	n.d.	n.d.	0.51	n.d.	n.d.
OY387-364	Gneiss	Intermediate	1864	478.7	2.96	0.31	0.10
OY387-378	Gneiss with net-textured BMS	High	78	7726.3	11.79	0.21	0.01
OY387-381	Gneiss	Low	365	1250.1	4.27	0.18	0.04
OY387-381	Massive sulfide	Very high	545	387500.0	2.73	0.28	0.10
OY387-384	Lower-Zone pyroxenite	Very high	1797	1787.5	2.95	0.37	0.12
OY387-395	Gneiss	High	7000	481.2	4.85	0.40	0.08
OY387-415	Gneiss	Intermediate	1790	247.0	1.98	0.23	0.12
OY387-423	Gneiss	High	4893	1002.7	6.44	0.31	0.04
OY387-438	Granite	Low	1942	125.8	2.37	0.28	0.11
OY08C	Chromitite layer	Intermediate	4	2000	n.d.	n.d.	n.d.
OY08A	Feldspathic pyroxenite + chromitite	Intermediate	8	5200	7.60	0.48	0.06
OY16	Feldspathic chromitite	Low	9	2400	3.14	0.52	0.16

6.7 PGE geochemistry

Figure 6.8 shows a selection of PGE ratios with depth from mineralized portions through the OY387 core, in which mineralization penetrates particularly deeply into the footwall gneisses and granite. We also consider the feldspathic pyroxenite in this core to be a fresh, unaltered section, devoid of xenoliths or any significant alteration or secondary overprints. Pt/Pd and Pt/Au ratios are consistently around 0.7-0.8 and 5-8, respectively, through the whole section, with no suggestion of any systematic variation with depth. The only sample that strays significantly from these values is the massive sulfide sample at 381m, which has relatively high Pd and low Au values in relation to Pt.

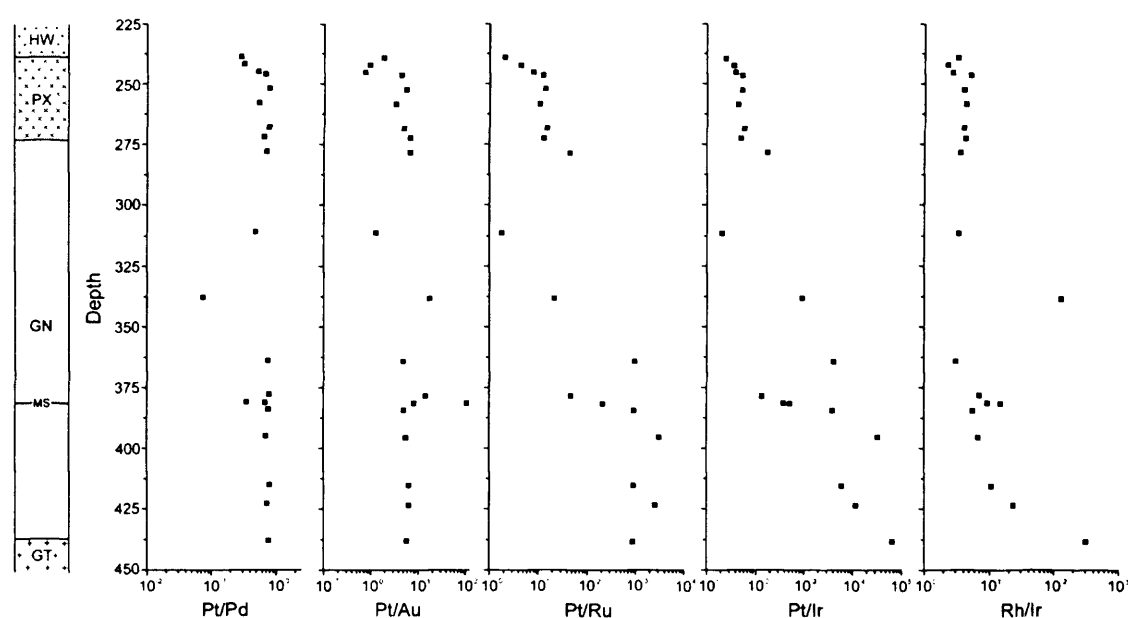


Figure 6.8. Selected PGE ratios with depth through core OY387. Note the different logarithmic horizontal scales. Key to stratigraphic column: HW: hangingwall gabbro; PX: Platreef pyroxenite; GN: gneiss; MS: massive sulfide; GT: granite.

As Pt/Pd and Pt/Au are relatively constant throughout the section, Pt/IPGE Pd/IPGE and Au/IPGE show almost identical trends. Therefore, here we only use Pt to compare the abundance of these elements with that of Ru and Ir. The Pt/Ru and Pt/Ir ratios show very different patterns to the Pt/Pd and Pt/Au ratios, with a pronounced increase in both Pt/Ru and Pt/Ir with depth (note the log scales in Fig. 6.8). There is little divergence of Rh abundance away from Pt and Pd in the reef and the upper section of the gneisses in OY387, but this becomes pronounced below 340m depth (Fig. 6.7c). Although Rh is fractionated with depth relative to Pt, Pd and Au, it is not as fractionated as Ir, as seen by the increasing Rh/Ir values with depth in Fig. 6.8). This apparent fractionation of PGE with depth into the footwall seems

to increase almost exponentially. It is only in the footwall that these trends are seen however, with no systematic variation with depth within the pyroxenite reef. So, relative amounts of Pt, Pd and Au stay reasonably constant with depth into the footwall, whereas the ratios of these elements over Rh, Ru and Ir increase dramatically with depth.

These relationships can be readily identified in chondrite-normalized plots of whole-rock PGE and Au (Fig. 6.9a). All reef pyroxenite samples show a moderately positive slope, which peaks at Pd and is typical of the Platreef (Barnes and Maier, 2002a; Armitage *et al.*, 2002). Figure 6.9b shows data we have collected from Sandsloot and Zwartfontein South for comparison. The upper gneiss samples fall into a similar envelope as the pyroxenites, with a little steepening in some profiles that reveal a relative depletion of Ir and Ru. The lower gneiss and granite show a considerably steeper profile with pronounced depletion in the IPGEs, though an almost identical range in Pt, Pd and Au values. The depletion of Rh, Ru and Ir relative to Pt, Pd and Au increases from Rh, through Ru to Ir. The decrease in the relative depletion from Ir through Ru to Rh can also be seen in the increase in sloping profile (Table 6.3). The sloping profile, defined as $(Pt+Pd)/(Ir+Ru)$, for average pyroxenite reef is around 23, for upper gneiss ~104, and ~2252 for lower gneiss and granite. Though much thinner, the gneisses in borehole OY335 show a similar pattern, which can be seen in the increase in sloping profile of samples OY335-310 and 316 in Table 6.3. The two samples below are not mineralized. The apparently fresh, unaltered nature of the mineralization in the pyroxenites in the OY387 core is shown by the consistent sloping profile of around 25, showing little decoupling between PGE with depth, or due to any alteration.

The profiles for the small number of chromitiferous rocks analyzed show a very different pattern in Fig. 6.9, with an apparent negative Pt anomaly and a lower overall gradient of the profile as seen by the sloping profiles of <12 in samples OY335-303, OY08A, OY08C and OY16, which all contain appreciable chromite and are low in sulfide. The chromitites and the chromitiferous quartzo-feldspathic pyroxenite (sample OY335-303) all show this pattern, however, the apparent depletion in Pt is misleading, and the anomaly is caused by a relative enrichment in Rh, Ru and Ir, rather than a depletion in Pt. The relative proportions of Pt and Pd ($Pt/Pd=0.76$) in the chromitite are comparable to the reef pyroxenites, however, the concentrations of Rh, Ru and Ir are highly enriched in these samples (Fig. 6.9a) and are almost an order of magnitude higher than most reef samples with similar Pt and Pd contents. A curious feature is the low Au abundance in both the samples OY08 and OY335-303.

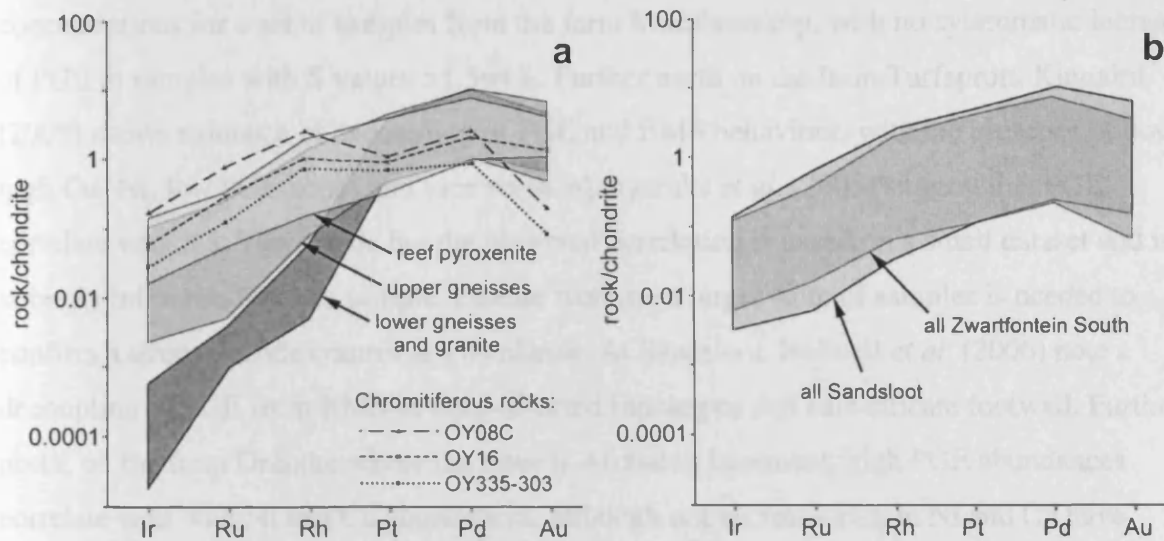


Figure 6.9. Chondrite-normalized PGE profile ranges of *a*: Overysel reef pyroxenite, upper gneisses, and lower gneisses and granite with individual profiles for the chromitiferous samples OY08C (chromitite band), OY16 (feldspathic chromitite) and OY335-303 (chromitiferous quartzo-feldspathic pyroxenite); and *b*: all reef, footwall and hangingwall at Sandsloot and Zwartfontein South.

6.8 Discussion

Firstly, it is important to note that the Platreef at Overysel and elsewhere is a highly complex orebody and is extremely variable along strike on both a kilometre and metre scale. As this study is based on two cores, it is important to acknowledge that what those cores show may not be totally representative of the orebody as a whole. Nevertheless, the results of this study have revealed a number of distinctive features present at Overysel which contrast with mineralization styles observed further south. The major features identified are: 1, the strong correlation between PGE and sulfides through both the reef *and* its footwall; 2, fractionation of the PGE with depth into the footwall; 3, development of layered and disseminated chromitites, along with chromitite xenoliths. These features have genetic implications for, and provide an insight into, the mechanisms involved in Platreef mineralization.

6.8.1 The PGE-S correlation

In the samples we have studied from Overysel, it is clear that PGE mineralization is controlled by the presence and abundance of base metal sulfides. Wherever BMS occur in the cores we have studied, PGE mineralization is also present, and in largely proportional amounts, with high BMS content corresponding to high PGE grades with only a few rare exceptions. Such a consistent BMS-PGE correlation is unusual in the Platreef. Kinnaird *et al.* (2005) note a correlation between PGE and S at low but not necessarily at high PGE

concentrations for a set of samples from the farm Macalacaskop, with no systematic increase of PGE in samples with S values >1.5wt%. Further north on the farm Turfspruit, Kinnaird (2005) shows evidence of decoupling of PGE and BMS behaviour, with the presence of both high Cu+Ni, low PGE zones and vice versa. Manyeruke *et al.* (2005) suggest that PGE correlate with S at Townlands but the observed correlation is based on a small dataset and is strongly influenced by one sample. Further work on a larger suite of samples is needed to confirm a strong sulfide control at Townlands. At Sandsloot, Holwell *et al.* (2006) note a decoupling of PGE from BMS in fluid-affected lithologies and calc-silicate footwall. Further north, on the farm Drenthe where the floor is Archaean basement, high PGE abundances correlate well with Ni and Cu abundances, although not all zones rich in Ni and Cu have corresponding high PGE grades (Gain and Mostert, 1982). Nevertheless, where PGE are present, there is always a corresponding BMS presence. It appears therefore, that where sediments form the floor, decoupling of PGE from sulfide is common, whereas in localities where the floor is Archaean basement, PGE are more commonly associated with sulfides. This is also reflected in an important first order control on PGE mineralogy. Platinum and Pd sulfide minerals are restricted to the area where Archaean basement forms the floor to the Platreef (Kinloch, 1982; Gain and Mostert, 1982; Holwell *et al.*, 2006). Where the floor rocks are dolomite, ironstones or shales, PGE sulfides are generally absent from the assemblage.

The observed mineralization style in the Platreef at Overysel is most consistent with an orthomagmatic PGE-BMS association, with PGE originally present within an immiscible sulfide liquid within the Platreef magma. Whether the PGE were scavenged from the Platreef magma by the sulfide liquid, or whether an already PGE-rich sulfide liquid was entrained within the Platreef magma before it was intruded, however, is thus far unclear. The common association of PGM around the margins of BMS blebs is common in many sulfide-associated PGE deposits and it is thought that during lattice reorganization during exsolution of pyrrhotite and pentlandite from *mss*, PGE diffuse to grain boundaries to form discreet PGM phases (e.g. Tredoux *et al.*, 1995; Barnes *et al.*, 2005). As this association is present well into the footwall gneisses, it is likely that the PGE-rich sulfide liquid that was present within the Platreef magma also percolated into the floor rocks.

6.8.2 Distribution and fractionation of PGE into footwall

At Sandsloot, the transport of PGE mineralization into the footwall is thought to have been facilitated by hydrothermal fluid fluxing, which, as outlined above, frequently decouples PGE

and BMS. In contrast, the intimate association of PGE and BMS mineralization well into the footwall at Overysel is more consistent with transport within a sulfide liquid. The similarity of the PGM assemblages and associations in the Platreef and the footwall gneisses also indicates a common mineralization mechanism. This requires a mechanism by which such a sulfide liquid could penetrate the footwall rocks.

The gneisses display evidence of shearing to produce grain-size reduction of orthopyroxene which is likely to have been a result of pre-Bushveld deformation of the basement. However, none of the grains of any phase appears strained, although they appear to have been subjected to very high strain rates. The eradication of such intra-grain deformation is probably a result of thermal overprinting, most likely from the intrusion of the Platreef and the other mafic units of the Bushveld Complex. The intrusion of a magma at 1100-1200°C into crustal rocks at ~5km depth is likely to have heated the surrounding rocks to over 800°C, i.e. to at least pyroxene-hornfels facies, and is likely to have induced partial melting.

Evidence of partial melting of the gneisses is shown by the increased degree of contamination by quartz, a phase which is rare at Sandsloot, in the interstitial assemblage in the basal parts of the Platreef pyroxenite, which gives rise to higher than usual whole-rock SiO₂ contents. The presence of veinlets of quartzo-feldspathic material (e.g. Fig. 6.3d) also indicates that a partial melt from the footwall gneisses has contaminated the lower parts of the Platreef. The REE data also provides further evidence of the role of footwall contamination at Overysel. The gneisses in both sample suites exhibit highly fractionated patterns that are much more enriched than those of the Platreef pyroxenites. The progressive enrichment in the REE with depth in the OY335 pyroxenites may be a result of increasing contamination derived from partial melting of the floor rocks, and in the OY387 core, one particularly quartz-rich sample of pyroxenite contained very high REE concentrations which is likely to be due to a high degree of contamination from the footwall gneisses.

Partial melting at grain boundaries within the granulitic gneisses could have produced an interconnected network of felsic melt surrounding unmelted solid material. A schematic representation of this model is illustrated in Fig. 6.10, where initial intrusion of Platreef magma heats the footwall gneisses (Fig. 6.10a) and induces partial melting along grain boundaries. The interconnectivity of the liquid derived from this melting may have formed a sufficiently permeable network to allow the downward percolation of a much denser sulfide

liquid through the footwall, with some felsic melt correspondingly displaced upwards, to account for the felsic contamination at the base of the Platreef (Fig. 6.10b).

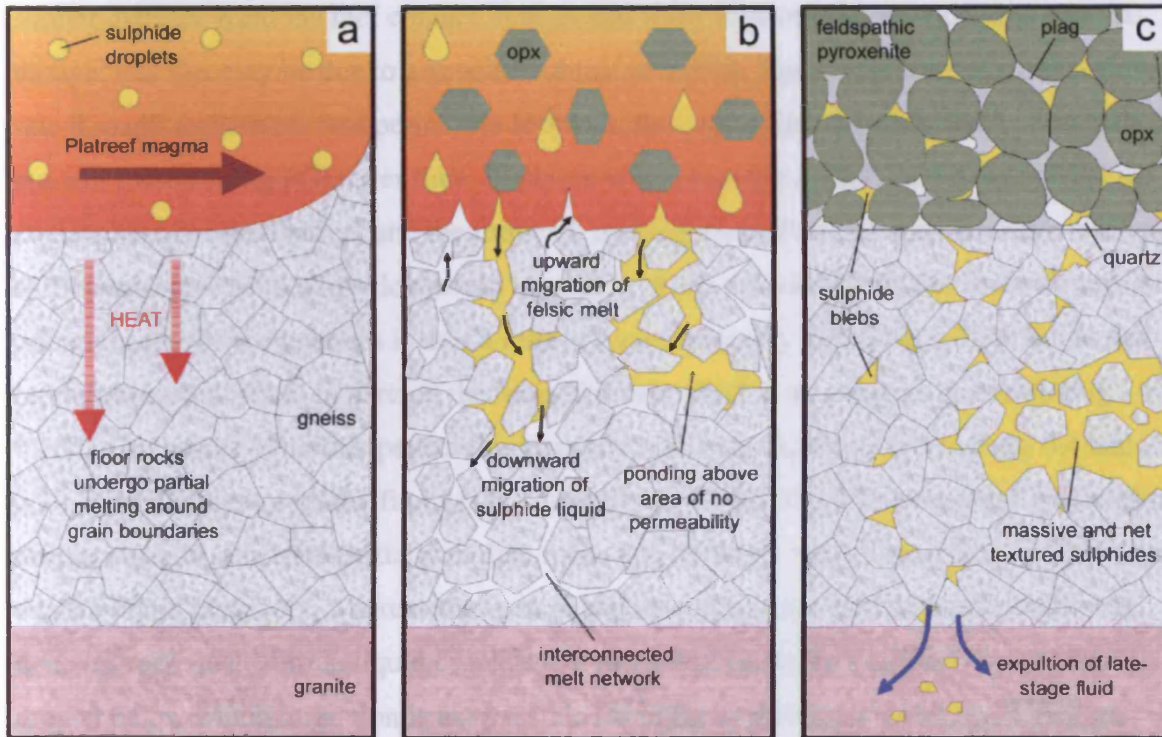


Figure 6.10. Schematic model for the distribution of PGE-rich sulfides into the footwall at Overysel. *a*: Intrusion of the Platreef magma heats the basement gneisses and induces partial melting around grain boundaries. *b*: Partial melting produces an interconnected network of felsic melt, down through which sulfide liquid can migrate, with subsequent upward displacement of felsic melt into the base of the crystallising Platreef magma. Ponding of sulfide occurs over areas of low permeability. *c*: late stage fluids are expelled from the sulfide liquid producing a low-temperature assemblage in the granite. A 'slick' of sulfides is left behind in the footwall by the migrating sulfide liquid, with high sulfide zones present above areas which have not melted. The Platreef pyroxenites crystallize with increasing amounts of quartz towards the base. Approximate vertical scale is 150m.

The nature of the interconnected network is illustrated in one sample from 378m down core OY387, shown in Fig. 6.4 where sulfide has completely penetrated the former melt network to form a remarkable net-textured sulfide, with sulfide surrounding rounded grains that have been melted around their grain boundaries, and in the case of this sample, also within the grains themselves. The amount of sulfide mineralization present within the rock is likely to be a function of permeability, i.e. the amount of partial melt, with ponding of sulfide possible above areas of low permeability (Fig 6.10c), which is likely to be related to heterogeneity in the gneisses. This can explain the presence of massive sulfides at any level within the footwall. In the case of the massive sulfide at 381m depth in the OY387 core, the Lower Zone

pyroxenite developed immediately below it may be responsible for such a permeability contrast. This process can also explain why mineralization penetrates the footwall erratically, such as in the OY335 core, where mineralization in the footwall is developed over a much shorter distance from the reef contact. It does still show similar PGE fractionation patterns though, and this may be due to a smaller volume of sulfide liquid migrating at a much slower rate through a relatively less permeable footwall, thus not achieving such depth penetration, but still fractionating PGE over time. In places where massive sulfides are developed at the contact between the Platreef and the footwall, melting of the footwall may not have reached a sufficient degree as to allow downward migration of the sulfide liquid. The footwall sulfide mineralization in the gneisses is thus a result of a downwardly migrating sulfide liquid that has left behind a 'slick' in parts of the rocks through which it was able to penetrate (Fig. 6.10c). Our model of sulfide penetrating partially molten rock, illustrated in Figs. 6.4 and 6.10, is inconsistent with the findings of Mungall and Su (2005), who concluded that sulfide droplets cannot penetrate partially molten rocks due to the interfacial tension of sulfide-silicate liquid interfaces, whereas they can penetrate solid rocks. However, this work was done on very small sulfide liquid droplets and there is likely to be a critical size of sulfide droplet below which migration is not possible (as in the experiments of Mungall and Su, 2005), and above which, droplets will be able to migrate freely due to density contrasts. The latter is likely to be the case for the volumes of sulfide that have been transported into the footwall of the Platreef (J. Mungall pers. comm., 2006).

The increasing steepness of the chondrite-normalized PGE profiles with depth is consistent with fractionation of PGE within a crystallising sulfide liquid that is migrating downwards, which, by definition, would also imply that the PGE were present in a sulfide liquid. Experimental studies on the partitioning of PGE within the Fe-Ni-Cu-S system (Fleet *et al.*, 1993; Barnes *et al.*, 1997) have shown that Os, Ir, Ru and Rh partition into early crystallizing monosulfide solid solution (*mss*), while Pt, Pd and Au are concentrated in the residual Cu-rich sulfide liquid. The sulfide liquid present within the Platreef magma is proposed to have started to crystallize out *mss*, and with it, the IPGE and Rh, as it sank through the magma leaving a 'slick' of blebs of *mss*. The residual liquid continued to migrate downwards and into the footwall when the melt network became permeable. Ponding may have occurred at the contact if the footwall never became permeable and massive sulfides are sometimes found at this boundary. Where the footwall became permeable due to the formation of the melt network, the migration of the (possibly ponded) sulfide liquid down through the footwall also

left a 'slick' of sulfide blebs through the gneisses, which fractionated out any remaining IPGE and Rh in the upper parts of the gneiss. Although the steepening PGE patterns are consistent with this process, one would also expect an increase in the relative Cu content of the sulfide liquid. Therefore a decrease in Ni/Cu ratio together with increased PGE fractionation patterns with depth would be expected, as has been identified, for example, into the footwall ores at the Strathcona mine, at Sudbury (Naldrett *et al.*, 1982). This, however, is not observed in the Overysel footwall ores and there appears to be no convincing systematic decrease in Ni/Cu ratio in samples with a high sloping profile (Table 6.3, Fig. 6.7).

This does not necessarily invalidate the fractionating sulfide liquid theory however, and the reasons for this lie in the variability in the behaviour of Ni within sulfide liquids. Whilst the experimental data suggests that Os, Ir, Ru and Rh are all highly compatible with *mss* and that Cu, Pt and Pd are all highly incompatible, the behaviour of Ni is much less predictable. Barnes *et al.* (1997) demonstrated that the partition coefficient of Ni between *mss* and sulfide liquid (D_{Ni}) varies both with S content and temperature. In S-poor systems and at high temperatures, Ni is incompatible and behaves in a manner similar to the IPGE and Rh, but in very S-rich systems at lower temperatures (900°C) Ni becomes compatible. Until recently however, virtually all of the experimental work was performed in O-free systems, which is not directly analogous to natural sulfide systems, where O is a major element. However, recent work by Mungall *et al.* (2005) defined partition coefficients for the PGE, Au, Cu and Ni at a variety of fO_2 , fS_2 and temperature conditions spanning the range of T and fO_2 for natural sulfide magmas, and demonstrated that under all conditions Ni was found to be incompatible, and at low fO_2 and fS_2 was even as incompatible as Cu. Therefore under certain conditions, it is entirely possible for Ni to behave in the same way as Cu, and therefore no systematic variation in Ni/Cu would be observed with fractionation. The unpredictability of Ni due to its dependence on so many factors means that it is not as reliable an indicator of the extent of sulfide liquid fractionation, as for example Ir, Ru, Pt and Cu are, and thus our data are still consistent with the fractionation of a sulfide liquid.

6.8.3 Hydrothermal redistribution

An alternative explanation for the distribution of mineralization and the fractionation of PGE into the footwall is via a volatile phase, such as that proposed by Iljina *et al.* (1992) for the Konttijärvi intrusion in Finland. This deposit includes a marginal series of pyroxenitic rocks which host disseminated PGE-bearing sulfide mineralization that is intruded into Archaean

granitoids, and thus is analogous to the Platreef in the Overysel area. Disseminated PGE mineralization in the basement rocks is attributed to a volatile phase that carried the components of sulfides and PGM rather than the percolation a migrating sulfide liquid, on the basis that the ores contain abundant galena. In contrast, at Overysel, the footwall gneisses contain a sulfide assemblage of pyrrhotite, pentlandite and chalcopyrite, almost identical to that in the Platreef itself. This, together with the lack of any accompanying hydrous mineral phases associated with the footwall mineralization, would imply that it is unlikely that the PGE and sulfides were transported in a hydrothermal fluid. Although a hydrothermal fluid may be responsible for fractionating the PGE to produce the observed trends, there is no lowering of Pt/Pd ratio with depth, which would be expected if this were the case, due to the increased mobility of Pd over Pt in hydrothermal fluids (e.g. Wood, 2002). This is in contrast to observations at Sandsloot where Pt/Pd ratios are lower, and there are changes in PGM, in the most fluid affected footwall units compared with the Platreef and hydrothermal processes are believed to be involved (Holwell *et al.*, 2006).

To initiate partial melting of the gneissic footwall, the intrusion of the Platreef magma must have heated the surrounding country rocks to temperatures of over 800°C. The downward percolation of the sulfide liquid would presumably have undergone cooling with time. However, temperatures must have remained above ~800°C throughout a sufficient volume of rock away from the igneous contact for the observed melt network to be present. The low temperature Ni sulfide, millerite, is present towards the very bottom of the sections, particularly in the granite at the bottom of the OY387 core. As millerite is stable at temperatures below 300°C it is unlikely that this phase formed during percolation through a melt network, as the partial melt would have already crystallized by this temperature. It is therefore more likely that the millerite is either a hydrothermal alteration product of pentlandite or the sulfides at the base of the core may be akin to similar assemblages found in alteration zones around the Cu-rich veins at the deepest extremities of the mineralized zones at Sudbury (Li and Naldrett, 1993). They suggest that the hydrothermal assemblages are a result of a hydrothermal liquid separating from the final stages of the crystallization of the sulfide liquid. Given the bleached nature of the granite in the core from borehole OY387 and the presence of hydrous minerals, it is possible that the assemblage of chalcopyrite and millerite formed from the expulsion of a hydrothermal fluid from the final stages in the evolution of the migrating sulfide liquid (Fig. 6.10c).

6.8.4 Chromitites

As a general rule, chromitites are unusual within the Platreef and very little work has thusfar been undertaken on them. Their presence is erratic, but they have been recorded on Tweefontein North, where a thin chromitite resembling one of the two developed in the Merensky Reef can be consistently correlated between boreholes close to the top contact of the Platreef (White 1994). Erratic and relatively thick chromitites were also apparently encountered in the south pit at Sandsloot, however mining operations moved too quickly to allow detailed study of them (R. Hieber pers. comm., 2006). The presence of these bodies, including those at Overysel is potentially an important insight into the mineralising events that formed the Platreef. The morphology of the chromitites at Overysel is discontinuous and although some thin layers reminiscent of the chromitite stringers in the Merensky Reef are present (e.g. Fig. 6.6b), they were not found to be laterally continuous in the underground workings. Several small xenoliths of chromitite are found within the pyroxenites, whose compositions are comparable to those in the more defined layers (see Table 6.1). We have also observed angular clasts of chromitite up to 30cm across within Platreef pyroxenite in the Zwartfontein South pit. The presence of xenoliths (possibly rip-up clasts), together with the discontinuity of layers, suggests a highly turbulent and most likely a multi-phase emplacement environment. This also leads to a potential complication in interpreting geochemical trends within the Platreef. Although it is easy to identify chromitite xenoliths within a pyroxenite, presumably any magma injection that ripped up earlier generation(s) of chromitites would have also ripped up early-formed pyroxenite cumulates, which visually would be almost impossible to identify within later pyroxenite. Therefore there is a possibility that xenoliths composed of early generations of pyroxenite may also be present, along with the chromite xenoliths, in later pyroxenites.

It has been proposed by Kruger (2005b) that the Platreef is the product of Main Zone magma which has ripped up and assimilated previously solidified Lower Zone rocks and as such, the chromitites within the Platreef are Lower Zone chromitite xenoliths. The difference between the compositions of the chromites within the layers and xenoliths in the Platreef and those in the Lower Zone type pyroxenite in the footwall in the OY387 core (Table 6.1) and in the Lower Zone rocks of the northern limb reported by van der Merwe (1976), Hulbert and von Gruenewaldt (1982) and Hulbert and von Gruenewaldt (1986) does not, however, support the notion that the xenoliths are rip-up clasts of Lower Zone material.

The chromitites contain the highest levels of Ir, Ru and Rh in Platreef rocks, as seen in Fig. 6.9. The association of the IPGE and Rh with chromitites is well known and the discovery that laurite is stable at chromite-based liquidus temperatures, together with its common inclusion within chromite grains, indicates this can be treated as a primary magmatic texture (Brenan and Andrews, 2001). Preliminary PGM studies we have performed on these rocks have revealed very few occurrences of laurite, and no occurrences of Os-Ir alloy included within chromite grains in the chromitites from Overysel. The presence of laurite and Os-Ir alloy as inclusions is taken to indicate conditions of base metal sulfide undersaturation (Brenan and Andrews, 2001). As they are not present, it would suggest that at the time of chromite precipitation, base metal sulfide saturation is likely to have already occurred. The fact that Pt/Pd ratios within the chromitites are comparable to the pyroxenites would also imply that during chromitite formation, the PGE-rich magma was also sulfur-saturated. This is because if chromite precipitated significantly before sulfur-saturation it would be expected to fractionate Pt over Pd, leading to higher Pt/Pd ratios within the chromitites (e.g. Barnes and Maier 2002b), which is not observed in the Platreef chromitites. It is likely that chromite precipitation occurred at a similar time, or slightly after sulfur saturation, with some IPGE and Rh fractionating with the chromite, although due to their relatively small volume, there were sufficient amounts of these elements available to also be concentrated within the sulfide liquid.

If the chromitite lenses and blocks represent rip-up clasts, they must have formed (together with sulfur saturation and PGE scavenging) prior to emplacement of the Platreef, possibly in an external staging chamber or conduit and this would support the theory of Barton *et al.* (1986) and Lee (1996) that the PGE-rich sulfides in the Platreef formed before emplacement. Conversely, if the chromitites formed virtually in situ in the Platreef magma, they must have been affected by further turbulent pulses of magma that disturbed them and entrained xenoliths of them.

6.8.5 Comparison with other Platreef localities

The mineralization style at Overysel contrasts with that found in the existing mines at Zwartfontein South and Sandsloot, as well as further south at Turfspruit. Work by Armitage *et al.* (2002) and Holwell *et al.* (2006) have shown that fluid activity has exercised a considerable influence on the distribution and mineralogy of PGE at Sandsloot, a feature that is minimal at Overysel, except within xenolithic material. This is likely to be related to a

fundamental footwall control, with the dolomites at Sandsloot and Zwartfontein releasing large volumes of fluids during assimilation and metamorphism and subsequent serpentinization, whereas the gneissic footwall at Overysel produced a felsic partial melt and very few volatiles. The mechanism of distribution of PGE into the footwall differs with footwall lithology. At Overysel, the distribution into the footwall appears to be via a downwardly migrating sulfide liquid, with little fluid influence, whereas at Sandsloot, fluid activity is largely responsible for the transportation of PGE into the calc-silicate footwall and has resulted in some decoupling of PGE from BMS (Holwell *et al.* 2006). Further south, on the farms Tweefontein and Turfspruit, where the footwall is comprised of Penge Formation ironstones and hornfelsed shales of the Duitschland Formation, PGE have not been significantly transported into the footwall (Hutchinson and Kinnaird, 2005; Nex, 2005). The large crystals of sperrylite that are developed in the footwall on Tweefontein Hill (e.g. Wagner, 1929) represent PGE that have been remobilized during post-Platreef faulting (Nex, 2005). Instead, at Tweefontein and Turfspruit, significant amounts of PGE are associated with sulfide-rich zones perched above competent, refractory footwall or above rafts of cordierite-spinel hornfels (Kinnaird, 2005; Sharman-Harris *et al.*, 2005). While it is clear that many of these high-grade contact metamorphic rocks have not developed a partial melt network comparable to that found at Overysel, melting and devolatilization of sedimentary rafts have released volatiles (notably S, Sb and As) into the Platreef magma that have had an influence on mineralogy (Hutchinson and Kinnaird, 2005).

The lack of hydrothermal interaction and overprinting in the area of the Platreef that overlies Archaean basement as opposed to Transvaal sediments raises the possibility that the mineralization style present at localities such as Overysel may represent the closest manifestation of what may be described as the 'primary' style of mineralization in the Platreef which we suggest is an orthomagmatic BMS-PGM assemblage such as that preserved in the pyroxenites at Overysel.

In terms of REE geochemistry, the pyroxenites at Sandsloot show very similar REE patterns to those at Overysel, with the exception that they have a negative Eu anomaly, which is thought to be a consequence of contamination from footwall sediments of the Malmani Formation, which show a pronounced negative Eu anomaly (McDonald *et al.*, 2005). The patterns from Townlands are interesting, in that they show three distinct profiles in three portions of the Platreef, with the REE becoming less enriched from the Lower to the Upper

Platreef (Fig. 6.6). Given the overlap of the field of Middle Platreef samples, this may represent a mixing of the two magmas, however the difference between the Upper and Lower packages is striking. There appear to be similarities between the Platreef pyroxenites at Overysel and Sandsloot with the 'Upper' and possibly 'Middle Platreef' at Townlands. However, the highly enriched REE profiles for the 'Lower Platreef' at Townlands seem to represent a magma pulse that has not occurred further north. Manyeruke *et al.* (2005) suggest that the three geochemically distinct pyroxenites at Townlands represent separate sill-like intrusions.

The notion of the Platreef being the result of a number of magmatic pulses of different compositions has also been advocated recently by Kinnaird (2005), whose geochemical data indicate breaks and trends that appear to be inconsistent with a single magma. Whilst our sampling may not be of a fine enough scale to distinguish any distinct magmatic pulses, it does reveal the absence of magmatic events and magma compositions which are evident elsewhere in the Platreef, such as the highly REE-enriched 'Lower Platreef' developed on Townlands. Also, the thick zones of high-Cr serpentinites found within the reef at Turfspruit interpreted as serpentinitized harzburgites by Kinnaird *et al.* (2005) are not present in our suite of samples at Overysel. There is a huge variation in thickness of the Platreef, for example at Sandsloot the reef can be as little as 10m thick, whereas it can be up to 400m thick further south at Turfspruit (Kinnaird *et al.*, 2005). The variation in thickness of the reef is likely to be, at least in part, due to topographic irregularities or diapirism in the footwall as discussed by Holwell *et al.* (2005) and Nex (2005). The most obvious of these features is the antiformal "tongue" of Malmani dolomite developed immediately south of the Sandsloot mine. If these structures acted as temporary barriers to the passage of magma, it is possible that some magmatic pulses or sill emplacement events may be missing from the flanks or basins between such footwall topographic highs. This may explain the absence at the base of the Overysel section of a REE-enriched pyroxenite unit corresponding to that observed at Townlands.

6.9 Conclusions

Platreef mineralization at Overysel, both in the reef pyroxenites and in the gneissic footwall, is controlled by the presence of base metal sulfides. Platinum-group elements were concentrated within a sulfide liquid in the Platreef magma. Crystallization of *mss* from the

sulfide liquid within the Platreef removed the majority of the IPGE and Rh from the residual sulfide liquid. Intrusion of the Platreef magma induced partial melting of the footwall gneisses, which formed an interconnected network of inter-granular melt. Transport of PGE into the gneisses was via the downward migration of the sulfide liquid, depleted of much of its original IPGE and Rh, but still rich in Pt, Pd and Au, through this permeable network. As the sulfide liquid migrated, it fractionated out the remaining IPGE and Rh in the upper parts of the gneisses leaving behind a 'slick' of disseminated sulfides, with the residual liquid becoming progressively more depleted in these elements relative to Pt, Pd and Au.

Permeability contrasts in the partially melted gneiss may have induced ponding of the sulfide liquid, locally producing massive sulfides. Hydrothermal activity, unlike at Sandsloot and Zwartfontein, is minimal due to the anhydrous nature of the footwall and is only significantly present in and around serpentinitized xenoliths, and at the very base of the cores where low-temperature sulfide assemblages may have been formed from the expulsion of a late stage fluid from the sulfide liquid.

The question of whether the PGE in the Platreef were scavenged from the magma itself by the sulfide liquid, or whether the magma brought in an already PGE-rich sulfide remains to be fully resolved. However, the presence of xenoliths of chromitite with PGM inclusions within the chromites and associated sulfides suggest that the chromitites formed from a PGE-enriched magma. Their occurrence as xenoliths suggests a turbulent environment during emplacement of the Platreef and it is possible that they were transported into the Platreef as xenoliths in the Platreef magma. These findings increase the likelihood that the magma also contained a pre-formed PGE-enriched sulfide liquid as suggested by Barton *et al.* (1986).

The results of this study, together with previous work from the Sandsloot (Armitage *et al.*, 2002; Holwell *et al.*, 2006) and Turfspruit (Hutchinson and Kinnaird, 2005) area indicate that there is a fundamental footwall control on the amount of distribution and the mechanism of distribution of PGE within the Platreef, and in particular its footwall. A separate study is underway to expand these contrasts by investigating the PGM mineralogy at Overysel. Where the floor rocks are carbonates, fluid activity related to metamorphism, assimilation and later serpentinitization have in places decoupled PGE from BMS. In contrast, where the floor is anhydrous gneiss, there is limited fluid activity and PGE behaviour is controlled by the behaviour of sulfide liquids.

6.10 Acknowledgements

The authors would like to thank the management of Anglo Platinum for giving permission to publish this work and for allowing access to the Sandsloot and Zwartfontein South mines and core from Overysel. David Holwell's PhD research is funded by the Natural Environment Research Council and supported by Anglo Platinum through Industrial CASE project (NER/S/C/2003/11952). Whole-rock sulfur analysis was performed at the Camborne School of Mines, UK, and funded by the Society of Economic Geologists' Hugh Exton McKinstry Fund. Professor Tony Harris is acknowledged for his insightful discussions on the metamorphic petrology of the footwall and Jeff White, Jim Mungall, and Tony Naldrett are also thanked for their comments. Constructive reviews by Steve Prevec and an anonymous referee helped improve the quality of the manuscript. Thanks also to Cheryl Tippins for her assistance drafting some of the figures and to Jay Cockayne for her support and for proof reading the manuscript.

Chapter 7

Distribution of platinum-group elements in the Platreef at Overysel, northern Bushveld Complex: a combined PGM and LA ICP-MS study

Submitted as:

D. A. Holwell and I. McDonald. 2007. Distribution of platinum-group elements in the Platreef at Overysel, northern Bushveld Complex: a combined PGM and LA ICP-MS study.

Contributions to Mineralogy and Petrology, (in review)

Co-author roles:

I. McDonald was involved in discussion during the preparation of the manuscript, and processed the LA-ICP-MS data.

7.1 Abstract

Detailed mineralogical and laser ablation-inductively coupled plasma-mass spectrometry (LA-ICP-MS) studies have revealed the physical manifestation of the platinum-group elements (PGE) within the Platreef at Overysel, in the northern limb of the Bushveld Complex, South Africa. In addition, these natural samples corroborate experimental studies on the partitioning behaviour of PGE within a fractionating sulfide liquid. The PGE in the Platreef were originally concentrated in an immiscible sulfide liquid along with certain semi-metals such as Bi and Te. As the sulfide liquid began to crystallize, virtually all the Os, Ir, Ru and Rh partitioned into monosulfide solid solution (mss), which on further cooling, exsolved to form pyrrhotite and pentlandite with Os, Ir and Ru remaining in solid solution in both phases. Rhodium preferentially partitioned into pentlandite during the exsolution process. Platinum, some Pd and Au were concentrated in the residual sulfide liquid after mss crystallization, and were then concentrated in a late stage melt along with Te and Bi, which was expelled to the grain boundaries during crystallization of intermediate solid solution (iss) to form Pt and Pd tellurides and electrum around the margins of the sulfide grains. Tiny droplets of this melt trapped in the crystallizing mss and iss cooled to form Pt-Bi-Te microinclusions in all sulfide phases, whilst the excess Pd was accommodated in solid solution in pentlandite. The sulfide liquid also penetrated the gneissic floor rocks and produced similar PGM assemblages in the footwall. Minor redistribution and recrystallization by hydrothermal fluids occurred around xenoliths and at the very base of the mineralized zone within the footwall. The role of a sulfide liquid in the collection of PGE to form the Platreef is unquestionable. The overall lack of secondary alteration coupled with the volatile-poor nature of the footwall have allowed the preservation of what may be the most 'primary' style of Platreef mineralization, with IPGE, Rh and some Pd, being present in solid solution within sulfide minerals and Pt, Au and some Pd present as PGM around the margins of the blebs. The lack of PGM inclusions within early liquidus phases suggests very early sulfur saturation in the Platreef, which lends support to theories involving S saturation occurring prior to intrusion of the Platreef, possibly within a staging chamber.

7.2 Introduction

The Bushveld Complex in South Africa is the world's largest layered igneous intrusion, made up of a 7-8km thick sequence of mafic and ultramafic lithologies covering an area of 65,000km² (Eales and Cawthorn, 1996). It is the largest repository of magmatic ore deposits on Earth and contains around 75% of the world's resources of platinum-group elements in three main deposits: the UG2 chromitite, the Merensky Reef and the Platreef (Kendall, 2006). The Platreef is a 10-400m thick unit of pyroxenitic lithologies with platinum-group element (PGE) and base-metal sulfide (BMS) mineralization located in the northern limb of the Complex (Kinnaird and McDonald, 2005). North from the town of Mokopane, the Platreef forms the base of the Bushveld layered igneous sequence and rests unconformably upon a succession of progressively older sedimentary units of the late Archaean - early Proterozoic Transvaal Supergroup, and Archaean basement (Fig. 7.1). Northwards from Mokopane, these footwall units are comprised of: quartzites and shales of the Timeball Hill Formation; shales of the Deutschland Formation; the Penge banded iron formation; the Malmani Subgroup dolomites and, north from the farm Zwartfontein, Archaean basement granites and gneisses, which form the footwall on the farm Overysel. The Platreef is overlain by norites and gabbro-norites generally assigned to the Main Zone of the Complex (Fig. 7.1).

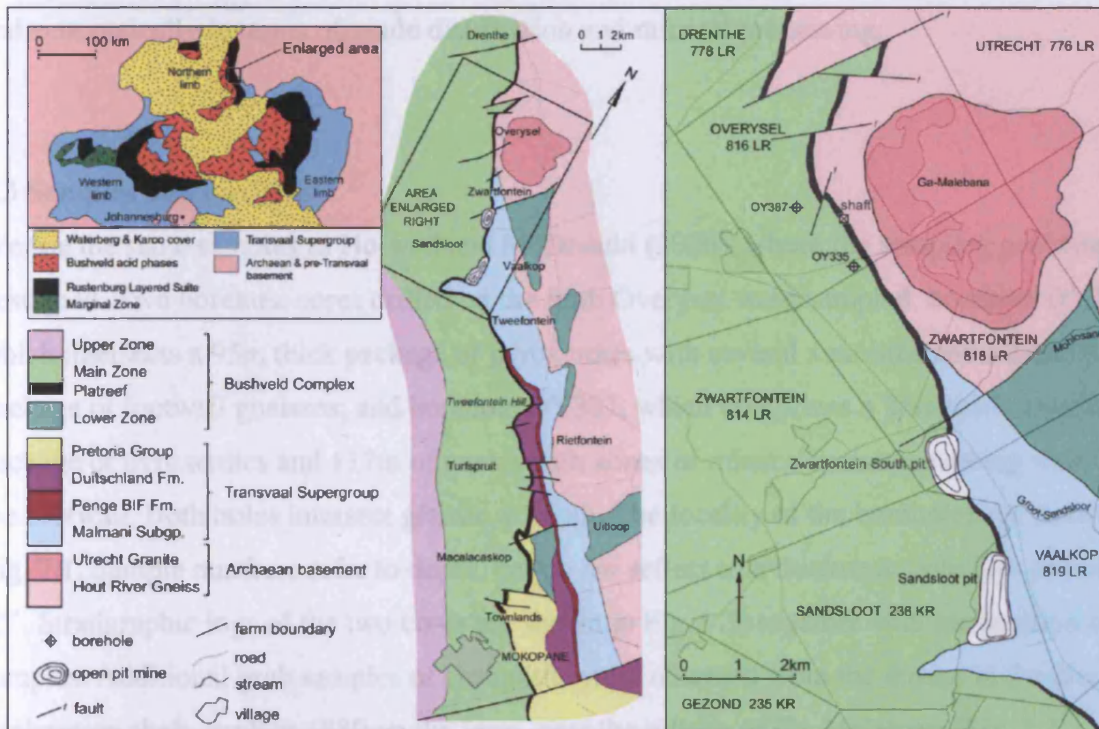


Figure 7.1. Geological map of the Platreef, showing the locality of boreholes OY335 and OY387, the 1980 shaft and farms referred to in the text. Based on field mapping and published maps of the Geological Survey of South Africa.

The increase in exploration and mining activity in recent years has facilitated an expanding number of studies to be undertaken on the Platreef, including detailed mineralogical studies of the platinum-group minerals (PGM) by Armitage *et al.* (2002) and Holwell *et al.* (2006) at Sandsloot, where the footwall is Malmani Subgroup, and by Hutchinson and Kinnaird (2005) at Macalacaskop and Turfspruit, where the floor rocks are Duitschland Formation. These studies have highlighted the differences in PGM mineralogy at localities along strike where the interaction of the Platreef magma with different floor rock lithologies appears to have had an important influence on the resulting PGM mineralogy. This study provides the first detailed investigation into the PGM at a locality where Archaean granites and gneisses form the floor and follows up the petrological and geochemical investigation into the Platreef at Overysel by Holwell and McDonald (2006).

This study is also the first laser ablation-inductively coupled plasma-mass spectrometry (LA-ICP-MS) study into the PGE contents of the BMS within the Platreef to be combined with PGM studies in order to investigate the physical manifestation of the PGE. The purpose of this is to constrain where each of the PGE reside in relation to sulfide minerals, data which is important both scientifically, as it reveals important information regarding the processes involved in noble metal enrichment and sulfide liquid fractionation in Ni-Cu-PGE deposits, and economically in terms of grade distribution and mineral processing.

7.3 Samples and methods

We use the same samples as Holwell and McDonald (2006), where the sampling procedure is described. Two borehole cores drilled on the farm Overysel were sampled: borehole OY335 which intersects a 95m thick package of pyroxenites with several xenoliths and a 20m thick package of footwall gneisses; and borehole OY387, which comprizes a 25m thick, continuous package of pyroxenites and 117m of gneiss with zones of mineralization extending well into the footwall. Both holes intersect granite at depth. The locality of the boreholes are shown in Fig. 7.1. Sample numbers refer to depth, but do not reflect true thickness, with dips around 45°. Stratigraphic logs of the two cores are shown in Fig. 7.2, together with the position of the samples. Additional grab samples of chromitite were obtained from the dumps at the disused exploration shaft, sunk in 1980 on the farm, near the village of Ga-Melebana (Fig. 7.1).

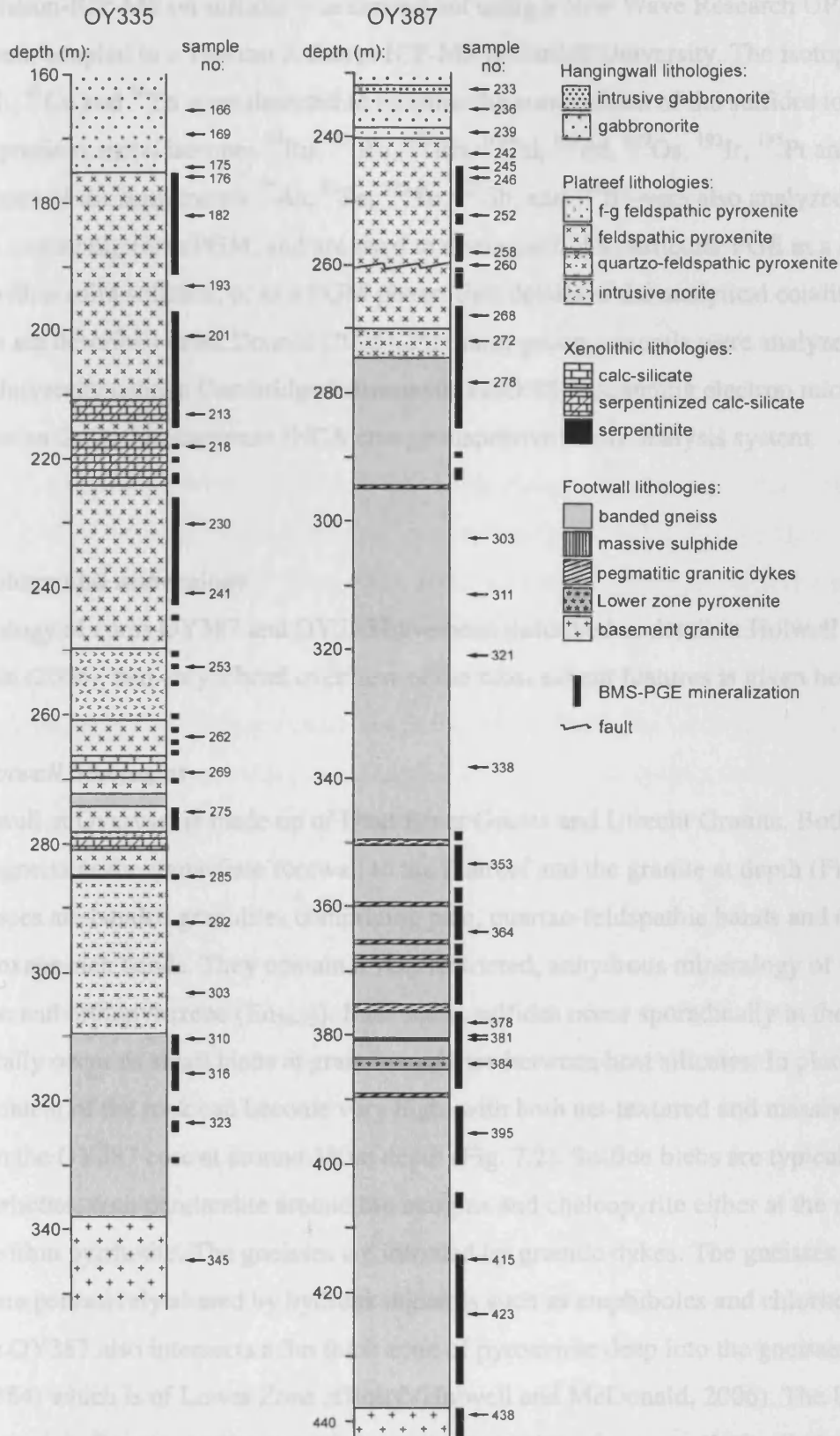


Figure 7.2. Stratigraphic logs of borehole cores OY335 and OY387 showing the positions of the samples and zones of visible BMS-PGE mineralization.

Laser-ablation-ICP-MS on sulfides was carried out using a New Wave Research UP213 UV laser system coupled to a Thermo X Series ICP-MS at Cardiff University. The isotopes ^{33}S , ^{59}Co , ^{61}Ni , ^{65}Cu and ^{66}Zn were detected to monitor the composition of the sulfides together with the precious metal isotopes ^{99}Ru , ^{101}Ru , ^{103}Rh , ^{105}Pd , ^{106}Pd , ^{189}Os , ^{193}Ir , ^{195}Pt and ^{197}Au . The isotopes of the semi metals ^{75}As , ^{82}Se , ^{125}Te , ^{121}Sb , and ^{209}Bi were also analyzed as these elements commonly form PGM, and are used to distinguish if a particular PGE in a sulfide is present within solid solution, or as a PGM phase. Full details of the analytical conditions and standards are described in McDonald (2005). Platinum-group minerals were analyzed at Cardiff University using a Cambridge Instruments LEO S360 scanning electron microscope, coupled to an Oxford Instruments INCA energy dispersive X-ray analysis system.

7.4 Petrology and mineralogy

The petrology of cores OY387 and OY335 have been described in detail in Holwell and McDonald (2006), and only a brief overview of the most salient features is given here.

7.4.1 Footwall lithologies

The footwall at Overysel is made up of Hout River Gneiss and Utrecht Granite. Both cores intersect gneiss as the immediate footwall to the Platreef and the granite at depth (Fig. 7.2). The gneisses are banded granulites comprising pale, quartzo-feldspathic bands and darker, orthopyroxene-rich bands. They contain a very restricted, anhydrous mineralogy of quartz, oligoclase and orthopyroxene (En_{70-75}). Base metal sulfides occur sporadically in the gneisses and typically occur as small blebs at grain boundaries between host silicates. In places, the sulfide content of the rock can become very high, with both net-textured and massive sulfides present in the OY387 core at around 380m depth (Fig. 7.2). Sulfide blebs are typically made up of pyrrhotite, with pentlandite around the margins and chalcopyrite either at the margins or as laths within pyrrhotite. The gneisses are intruded by granitic dykes. The gneisses adjacent to these are pervasively altered by hydrous minerals such as amphiboles and chlorite.

Borehole OY387 also intersects a 3m thick zone of pyroxenite deep into the gneisses (sample OY387-384) which is of Lower Zone affinity (Holwell and McDonald, 2006). The Utrecht granite is a pink, fine- to medium-grained granite consisting of mesoperthitic alkali feldspar, quartz and minor muscovite. Where mineralized, the rock has a bleached appearance and contains some secondary amphiboles and micas, with chalcopyrite and millerite the most common sulfides.

7.4.2 Igneous Platreef lithologies

The pyroxenites are typically medium- to coarse-grained and made up of cumulus orthopyroxene (En₇₅₋₈₀), 5-20% intercumulus plagioclase, up to 5% clinopyroxene and a little quartz, with some accessory phlogopite, chromite and ilmenite. Quartz becomes more common with depth, and is indicative of an increasing amount of contamination from a felsic melt derived from partial melting of the footwall gneisses. Alteration by micas and carbonates occurs sporadically. Sulfides occur within the interstitial assemblage as blebs, made up of a pyrrhotite core, with pentlandite and chalcopyrite margins, and are commonly <10mm and make up <3% of the total modal assemblage. Chromitites are present in both cores as small, angular xenoliths within the feldspathic pyroxenites. Chromitite bodies also occur, and the exploration mining (described by White 1994), encountered some large but discontinuous chromitite bodies. Samples of chromitite taken from the dumps at the disused shaft are irregular and discontinuous, up to 30cm thick and contain some pentlandite, with rarer chalcopyrite. Xenoliths of calc-silicate up to 10m thick are also present in the OY335 core, some of which are serpentinized (Fig. 7.2), and containing abundant metamorphic olivine and clinopyroxene, with some orthopyroxene, amphibole and BMS. The overlying hangingwall rocks are made up of gabbro-norites comprising 40-80% cumulus plagioclase, with cumulus and intercumulus orthopyroxene and oikocrystic clinopyroxene.

7.5 PGE mineralization

Holwell and McDonald (2006) identified a number of features of the PGE mineralization at Overysel, many of which were unique to the locality and can be summarized as follows:

1. PGE mineralization within the two cores mirrors the presence and abundance of BMS.
2. Pt/Pd ratios are consistently around 0.7-0.8 and Pt/Au ratios are around 7-8 throughout both the Platreef and the footwall.
3. With depth into the footwall, progressive fractionation of the PGE is observed. This is seen in the sloping profile (Pt+Pd)/(Ir+Ru), which increases by several orders of magnitude with depth into the footwall, with strong depletions in Ir, Ru and Rh observed on normalized plots.
4. PGE were transported into the footwall gneisses within a fractionating sulfide liquid that percolated down through an interconnected, inter-granular melt network. This is in contrast to the calc-silicate floor at Sandsloot, where the main mechanism for transport of PGE the footwall is believed to be within a hydrothermal fluid.

5. The millerite and chalcopyrite-rich assemblage in the bleached granite at the base of the gneisses in core OY387 is a hydrothermal assemblage, possibly formed by the expulsion of a fluid from the final stages of the evolving sulfide liquid.

In light of these discoveries, particularly the strong PGE-BMS relationships, this study builds upon them by investigating the way in which the PGE mineralization has manifested itself in terms of the platinum-group mineralogy and the role of BMS as hosts for PGE.

7.6 Platinum Group Mineralogy

Forty three polished thin sections and blocks from the Platreef, xenoliths therein and the footwall from the two borehole cores, along with underground chromitite samples obtained from the dumps were examined for PGM on the SEM. More than 750 individual PGM grains were identified and are listed in Table 7.1. The PGM identified were grouped as: (1) Pt/Pd sulfides; (2) other PGE sulfides; (3) Pt/Pd tellurides; (4) Pt/Pd arsenides; (5) Pt/Pd antimonides; (6) Pt/Pd bismuthides; (7) PGE sulfarsenides; (8) Pt/Pd alloys with Fe, Cu, Sn, Pb; and (9) Au- and Ag-bearing minerals. Each occurrence was also classified by its textural association and by its size.

7.6.1 Grain size and relative grain area

Each PGM grain's long and short axes were measured in micrometres. Relative proportions of the various mineral phases and PGM species type are based on an estimation of area (and by inference, volume) of each grain. Using the long and short axis dimensions, the area of each grain was approximated to the area of an ellipse around the two axes, in the manner described in Holwell *et al.* (2006) for PGM at Sandsloot. This produces data that accurately reflect the relative proportions of each PGM type within an assemblage, and is directly comparable to the Sandsloot database in Holwell *et al.* (2006). This method of data presentation is preferable to proportions of PGM type by number of grains, which can give erroneous significance to large numbers of very small grains.

7.6.2 Assemblages

The PGM assemblage in each lithology is shown in Table 7.2, together with an overall total in percentage of the total area in 100% PGM. The textural associations of the PGM within each lithology are shown in Table 7.3. The vast majority are Pt and Pd phases and the most common types of PGM are Pt and Pd tellurides, which make up 46% of all PGM identified. Platinum arsenides, exclusively in the form of sperrylite (PtAs₂), and Pt sulfides (mostly cooperite, PtS) are common and Pt and Pd bismuthides are also important. Alloys, antimonides and sulfarsenides are minor phases. In detail, PGM assemblages vary with host rock lithology.

Table 7.1. List of all PGM identified, together with ideal formulae, and number of occurrences within the lithologies in the Overysel cores. RFP = reef feldspathic pyroxenite; ARP = altered reef feldspathic pyroxenite; CHR = chromitite; CSX = calc-silicate xenoliths; CQP = chromitiferous quartzofeldspathic pyroxenite; GS = gneiss; AGS = amphibolitic gneiss; NTS = net-textured sulfides; MS = massive sulfides; LZP = gneiss-hosted Lower Zone pyroxenite; BGT = basement granite.

Name	Ideal formula	RFP	ARP	CHR	CQP	CSX	GS	AGS	NTS	MS	LZP	BGT	Total
Moncheite	PtTe ₂	50	21				47	9	38	101	2	4	272
Kotulskite	PdTe	10	16	7		1	39	5		3			81
Sobolevskite	PdBi	1	11	14	1	5	14				1	14	61
Electrum	Au-Ag	15	9			1	16	2		2		4	49
Sperrylite	PtAs ₂	5	11	7		9	4	3		2	1	4	46
Cooperite	PtS	4	16	8	4		8	4		1			45
Michenerite	PdTeBi	2	7	8			10	1		3	1	2	34
Froodite	PdBi ₂	2	1				13	2			5	5	28
Merenskyite	PdTe ₂	5	3			5	7	1	4				25
Hollingworthite	RhAs ₂			10		6							16
unnamed	Pd(Bi,Sb)					13							13
Laurite	RuS ₂			11									11
Maslovite	PtTeBi							2		6	1		9
Platarsite	PtAsS			7		1							8
Insizawaite	PtBi ₂		1	1			2	1			2	1	8
Hessite	Ag ₂ Te	2				1	1					3	7
Stibiopalladinite	Pd ₅ Sb ₂					1	3	1					5
unnamed	PtCuBiS ₃						1					4	5
Paolovite	Pd ₂ Sn		4				1						5
Atokite	Pd ₃ Sn	1	1				2						4
Crerarite	(Pt,Pb)Bi ₃ S ₄						4						4
unconstrained	Pt-Pd-Te-Bi	2						1					3
Palarstenide	Pd ₅ (Sn,As) ₂		3										3
Rustenburgite	Pt ₃ Sn	2			1								3
unconstrained	Pd-Pt-Te						2						2
unconstrained	Bi-Pb-Pt-Cu-Bi-S										1	1	2
Pd-melonite	(Ni,Pd)Te ₂	1											1
unconstrained	Pt-As-Te-Bi		1										1
unconstrained	Pd-Pt-Te-Bi-As		1										1
Native silver	Ag						1						1
unconstrained	Pt-Cu-Bi-Te						1						1
Palladian gold	Au-Pd						1						1
Braggite	(Pt,Pd)S						1						1
Argentite	Ag ₂ S						1						1
unconstrained	Pt-Pd-Cu-Bi-S							1					1
unnamed	(Pt,Cu,Rh,Ir) ₂ S ₃			1									1
unnamed	PdPtBi			1									1
unnamed	Ag ₄ S										1		1

Table 7.2. Proportions of PGM type within each lithology in the Overysel cores, in percentage of the total area of 100% PGM. For lithology abbreviations, see Table 7.1 ALL = all PGM in all lithologies.

PGM type	RFP	ARP	CHR	CQP	CSX	GS	AGS	NTS	MS	LZP	BGT	ALL
Pt sulfides	4.3	64.9	8.4	92.2		18.7	17.9		2.5		5.4	13.4
Other PGE sulfides			30.8									0.6
Pt tellurides	51.3	8.1				17.5	29.2	97.3	88.5	1.3	12.9	25.5
Pd tellurides	13.2	18.5	19.1		10.4	49.2	4.0	2.7	3.3	1.0	0.5	20.8
Pt arsenides	1.1	2.5	7.9		86.2	5.7	3.8		5.0	0.1	1.6	16.7
Pd antimonides					0.5	0.4	0.4					0.2
Pt bismuthides		0.2	0.5			0.1	0.1			82.7	2.9	5.9
Pd bismuthides	0.4	1.7	9.1	3.9	2.1	4.7	0.7			14.9	30.9	5.9
PGE sulfarsenides			24.2		0.7							0.6
Pt dominant alloys	0.3			3.9								<0.1
Pd dominant alloys	7.5	1.8				0.8						0.9
Au/Ag minerals	21.9	2.3			0.1	2.9	43.9		0.7		45.8	9.5

Table 7.3. Associations of all PGM and Au, Ag phases, Pt dominant phases only, and Pd dominant phases only within each lithology in the Overysel cores in percentage of the number of grains. For lithology abbreviations, see Table 7.1.

All PGM, Au, Ag phases											
Association	RFP	ARP	CHR	CQP	CSX	GS	AGS	NTS	MS	LZP	BGT
Sulfide	2.6	8.6	4.0			6.2	15.6	9.5	83.1	21.4	4.8
Sulfide/silicate	28.1	37.1	20.0	66.6	59.5	48.0	50.0	81.0	11.0	42.9	21.4
Primary silicate	45.6	28.6	36.0	16.7	16.7	32.8	21.9	9.5	5.9	14.3	73.8
Secondary silicate oxide	23.7	25.7	21.3		23.8	13.0	12.5			21.4	
			18.7	16.7							
Pt-dominant:											
Association	RFP	ARP	CHR	CQP	CSX	GS	AGS	NTS	MS	LZP	BGT
Sulfide	4.0	11.9	4.2			6.8	23.8	10.5	87.3	14.3	
Sulfide/silicate	29.0	35.7	20.8	60.0		60.3	38.1	81.6	10.9	28.6	14.3
Primary silicate	46.0	38.1	41.7	20.0	55.6	27.4	28.6	7.9	1.8	14.3	85.7
Secondary silicate oxide	21.0	14.3	16.6		44.4	5.5	9.5			42.8	
			16.6	20.0							
Pd-dominant:											
Association	RFP	ARP	CHR	CQP	CSX	GS	AGS	NTS	MS	LZP	BGT
Sulfide	8.7	5.4	3.5			3.6				28.6	
Sulfide/silicate	39.1	38.2	27.6	100.0	61.3	39.5	80.0	75.0	16.7	57.1	20.0
Primary silicate	34.8	21.8	24.1		3.2	39.5	10.0	25.0	83.3	14.3	80.0
Secondary silicate oxide	17.4	34.6	31.0		35.5	17.4	10.0				
			13.8								

The PGM assemblage within the reef feldspathic pyroxenites is overwhelmingly dominated by Pt tellurides, most of which also contain some Bi in place of Te, for example, most moncheites have the formula $Pt(Te,Bi)_2$. Ni tellurides are absent from the assemblage and no Ni is present in solid solution within the Pt/Pd telluride phases. Sulfides and alloys are present, but rare. Although 7.46% of the assemblage by area is comprised of Pd alloys (Table 7.2), it can be seen from Table 7.1 that this contribution is skewed by a single, though large,

grain of atokite (Pd_3Sn). Electrum (Au,Ag) is common and makes up 22% of the whole assemblage. Most PGM grains are associated with BMS, although very few are actually included within BMS grains, and most occur either as grains at the contact between BMS and silicate phases or within silicate phases as satellite grains around BMS (Figs. 7.3a, b, Table 7.3). Where alteration of the reef pyroxenite by sericite and carbonates has taken place, there is a decrease in the proportion of telluride PGM phases, and a corresponding relative increase in sulfides. Sobolevskite (PdBi) is very common, although the grains are very small and the proportion by area is minimal. Some Pd-Sn alloys such as paolovite (Pd_2Sn) are present and sperrylite is more common than in unaltered reef. The spatial associations are highly comparable to those in the unaltered reef.

The chromitites contain a very distinctive PGM assemblage, dominated by laurite and the sulfarsenides hollingworthite (RhAsS) and platarsite (PtAsS). The major carrier of Pd is sobolevskite-kotulskite solid solution, $\text{Pd}(\text{Bi},\text{Te})$, which contains almost equal atomic proportions of Bi and Te. This is the only lithology which contains any significant discrete Rh phases and is the sole lithology to contain any Ru- or Ir-bearing PGM. Laurite is occasionally Ir-bearing, hollingworthite and platarsite are usually Ir- and Ru-bearing and Rh-bearing sperrylite is also common. Most of the PGM, particularly the Pd-bearing phases, are silicate-hosted, with 20% of all grains being located at the boundary between silicates and small sulfide (almost exclusively pentlandite) grains within the silicate matrix. In Table 7.3, the 'oxide' associations refer to PGM in contact with chromite grains, which was the most common occurrence for laurite. Two PGM grains, one laurite and one cooperite, were found as inclusions within chromites. In the chromitiferous quartzo-feldspathic pyroxenite, only six PGM were found, which were dominated the sulfide cooperite rather than laurite. No PGM were found as inclusions in the chromites in this lithology.

The PGM assemblage in the serpentinized calc-silicate xenoliths is the most arsenide dominant in the whole sample suite, with 82% sperrylite by area. Palladium tellurides are the next most common PGM type. There are also several smaller grains of the Pd bismuthides sobolevskite and an unnamed phase $\text{Pd}(\text{Bi},\text{Sb})$. This is the only rock type, other than the chromitites, in which sulfarsenides are present, mainly hollingworthite (RhAsS). The associations of the PGM within this assemblage differ from all the others in that it is the Pd phases which show a distinct association with BMS over Pt phases, with all the Pt minerals enclosed within silicates.

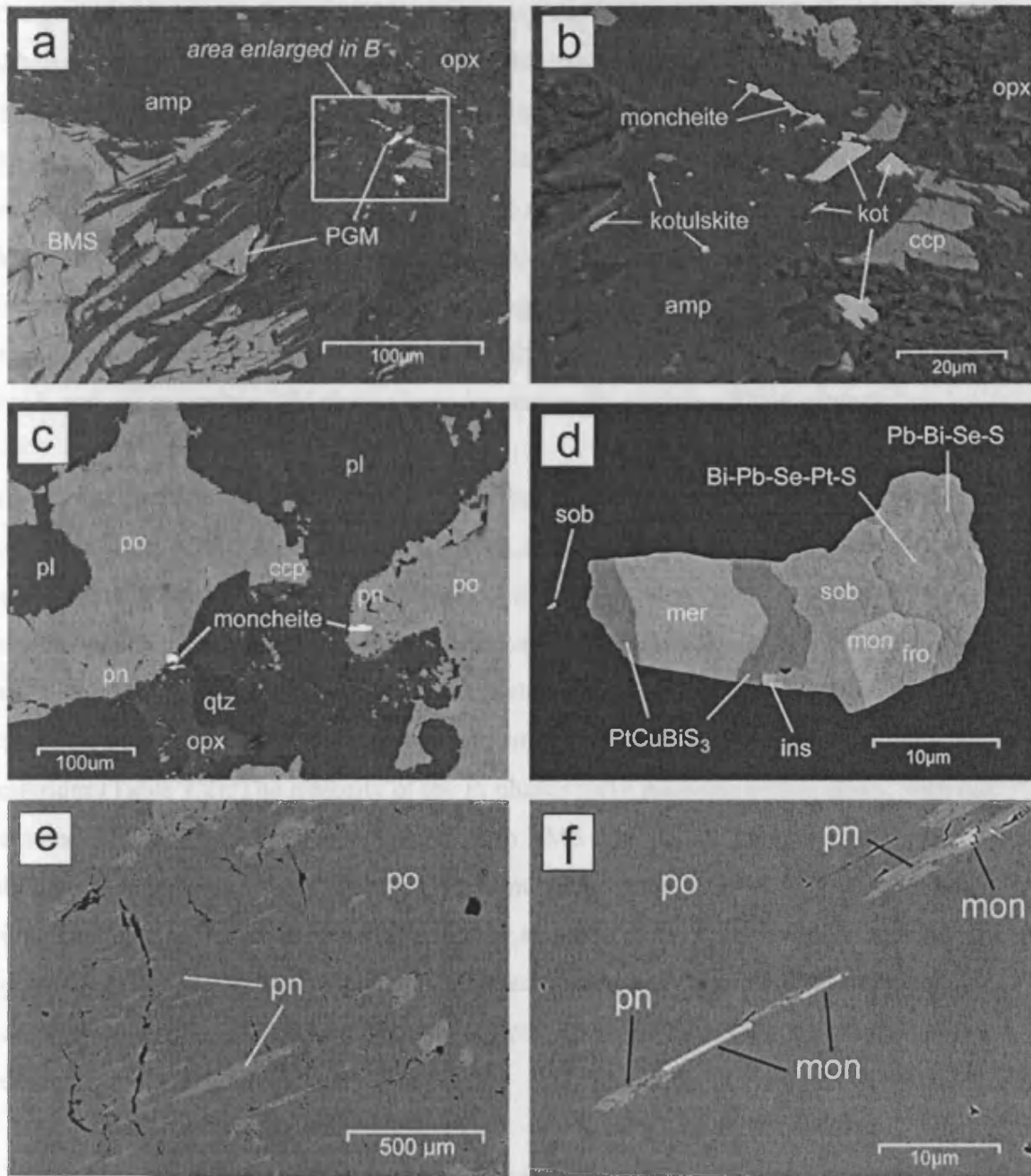


Figure 7.3. Backscattered scanning electron micrographs of:

(a): typical association of PGM at the contact between BMS and silicates, and as satellite grains in close proximity to the BMS grain, enclosed within secondary amphiboles (amp) between the BMS and primary silicates such as orthopyroxene (opx) from sample OY335-176. (b): Enlarged area from A, showing grains of moncheite (mon) and kotulskite (kot) and remnant chalcopyrite (ccp) enclosed in secondary amphibole. (c): typical association of PGM (moncheite) located at the edge of BMS grains made up of pyrrhotite (po), pentlandite (pn) and chalcopyrite (ccp) within footwall gneiss (OY335-316) composed of quartz (qtz), plagioclase (plag) and orthopyroxene (opx). (d): polyphase PGM enclosed within quartz in a sample of mineralized basement granite (OY387-438), containing sobolevskite (sob), the unnamed phase PtCuBiS_3 , merenskyite (mer), insizawite (ins), moncheite (mon), froodite (fro), and two intergrown, unconstrained Pb-Bi-Se-S phases, one of which is Pt-bearing. (e): exsolution lamellae of pentlandite within pyrrhotite in a sample of massive sulfide OY387-381. (f): enlarged view of massive sulfide showing the association of moncheite with exsolved pentlandite within pyrrhotite.

The gneisses have a similar assemblage to that of the reef pyroxenites. Tellurides dominate, although unlike in the pyroxenites, Pd phases are more common than moncheite. Sulfides (cooperite, crerarite: $(\text{Pt,Pb})\text{Bi}_3\text{S}_4$, and a single grain of braggite $(\text{Pt,Pd})\text{S}$) make up 18.7% of the assemblage. All PGM were spatially associated with BMS and most grains were found at the sulfide-silicate contact (Fig. 7.3c, Table 7.3). Altered, or amphibolitic, gneisses are dominated by a few large grains of electrum. Aside from the Au and Ag minerals, the overall assemblage has a more Pt-dominated assemblage than the rest of the gneiss. The associations were similar to the unaltered gneiss, though only Pt phases were observed as inclusions within BMS, and the majority of Pd phases were located at the sulfide-silicate contact.

The net-textured and massive sulfides within the gneisses are overwhelmingly dominated by tellurides, most of which also contain some Bi. Indeed, the net-textured sulfide sample contained no other type of PGM, with 97% of the grains being moncheite, and the remainder merenskyite. Virtually all grains were located around the sulfide margins in the net-textured sulfide, and only Pt minerals were found as inclusions in the sulfides. The massive sulfide contained a few sulfides, arsenides and electrum, although was still made up of 88% Pt tellurides (Table 7.2). The majority of the Pt phases were included within BMS, with the remainder being located at the contact between BMS and silicate phases. The Pd phases were almost all concentrated along the edge of the massive sulfide zone and included within silicates. Many of the moncheite grains appear to be exsolved, along with pentlandite, out of pyrrhotite. Figures 7.3e and f show the preferred orientation of pentlandite and moncheite exsolved from pyrrhotite, with moncheite typically rimmed by pentlandite in such textural relationships.

The mafic Lower Zone-like pyroxenite intersected within the lower gneiss in borehole OY387 has an assemblage dominated by bismuthides, particularly insizawite (PtBi_2) and froodite (PdBi_2) . No Au minerals were found. The BMS in this lithology were dominated by chalcopyrite.

Some BMS and PGE mineralization was identified in the sample of altered basement granite. The assemblage in the altered and mineralized basement granite contained 46% Au and Ag minerals by area, with the true PGM assemblage being dominated by the Pd bismuthides sobolevskite and froodite. This is the most bismuthide-dominant assemblage observed in any of the lithologies. Moncheite and the unnamed bismutho-sulfide PtCuBiS_3 were also

common. A complex polyphase grain of bismuthides, tellurides and PtCuBiS₃ from a sample of granite is shown in Fig. 7.3d. The majority of PGM found were included in primary silicates, with only electrum occurring as inclusions in BMS. The BMS phases in this lithology are dominated by chalcopyrite and millerite (NiS).

7.7 LA-ICP-MS analysis

A prominent finding of this and other recent investigations into the PGE mineralogy within the Platreef (e.g. Armitage *et al.*, 2002; Hutchinson and Kinnaird, 2005; Holwell *et al.*, 2006) is that the vast majority of PGM, excluding those in the chromitites, are Pt and Pd phases. The failure to locate enough PGM to account for the observed whole rock contents of Rh, Ru, Ir and Os, particularly in the Platreef pyroxenites, indicates that these elements are likely to be present in trace concentrations in other minerals; most likely in solid solution within BMS, which typically make up around 2-3% of the modal assemblage in the pyroxenites. Ore microscopy studies and SEM-based analyses are not sufficient for detecting trace levels of PGE within sulfide minerals. Laser-ablation ICP-MS (LA-ICP-MS) techniques are the most precise way of achieving detection to such low levels as tens of parts per billion, which is one to three orders of magnitude greater than can be achieved by other in situ techniques such as micro-Proton Induced X-ray Emission (micro-PIXE) and Secondary Ion Mass Spectrometry (SIMS) (Cabri *et al.*, 2003). We performed a series of LA-ICP-MS analyses on a number of sulfide phases from the Platreef feldspathic pyroxenites, chromitites and the basement gneisses at Overysel, together with a few samples of Platreef feldspathic pyroxenite from Sandsloot for an along-strike comparison. Full analyses are given in Appendix 3, and a summary of the results of the analyses are shown in Table 7.4. The results from the Platreef pyroxenites are plotted in Fig. 7.4 and a selection of time resolved analysis (TRA) spectra are shown in Fig. 7.5 to illustrate the most important features.

Table 7.4. Compositions of base metal sulfides from the Platreef at Overysel and Sandsloot as determined by LA-ICP-MS analysis.

Overysel Reef pyroxenites:

Pyrrhotite	S	Co	Ni	Cu	Os	Ir	Ru	Rh	Pt	Pd	Au	Te	Bi
<i>n</i> =8	wt%	ppm	wt%	wt%	ppm								
Mean	38.7	22.8	0.51	0.00	0.93	1.80	7.81	0.45	0.61	0.06	0.00	1.64	0.92
σ	1.7	12.1	0.13	0.00	0.11	0.34	2.31	0.55	0.59	0.04	0.00	0.87	0.64
Max	40.1	41.7	0.71	0.01	1.05	2.32	11.6	1.59	1.74	0.11	0.01	2.60	1.52
Min	34.6	9.0	0.34	bdl	0.76	1.29	4.17	0.01	0.01	bdl	bdl	bdl	bdl
Pentlandite	S	Co	Ni	Cu	Os	Ir	Ru	Rh	Pt	Pd	Au	Te	Bi
<i>n</i> =8	wt%	ppm	wt%	wt%	ppm								
Mean	33.7	2969	34.4	0.02	0.59	1.20	5.16	15.0	0.45	119	0.00	1.49	0.85
σ	0.4	1653	5.6	0.05	0.22	0.57	1.80	17.3	0.29	43.4	0.00	1.41	0.88
Max	34.1	5514	48.1	0.15	0.88	2.26	7.07	58.1	0.88	183	0.01	3.61	2.56
Min	33.0	714	29.9	0.00	0.15	0.61	1.43	0.04	0.02	68.6	bdl	bdl	bdl
Chalcopyrite	S	Co	Ni	Cu	Os	Ir	Ru	Rh	Pt	Pd	Au	Te	Bi
<i>n</i> =6	wt%	ppm	wt%	wt%	ppm								
Mean	35.1	3.1	0.06	28.2	0.00	0.00			1.31	0.54	0.01	1.54	1.67
σ	0.6	6.4	0.11	4.3	0.00	0.00			2.06	0.59	0.01	1.51	1.14
Max	35.6	16.1	0.26	34.1	0.01	0.01	bdl	bdl	2.29	1.73	0.02	3.03	3.03
Min	33.9	0.1	0.00	23.8	bdl	bdl	bdl	bdl	0.01	0.21	bdl	bdl	bdl

Sandsloot Reef pyroxenites

Pyrrhotite	S	Co	Ni	Cu	Os	Ir	Ru	Rh	Pt	Pd	Au	Te	Bi
<i>n</i> =5	wt%	ppm	wt%	wt%	ppm								
Mean	38.4	6.47	0.15		1.83	2.87	13.9	0.18	1.32	0.07		1.34	0.48
σ	0.67	2.57	0.02		0.72	0.68	4.43	0.10	1.05	0.07		1.24	0.37
Max	38.8	10.4	0.18	bdl	2.86	3.85	17.3	0.29	2.70	0.16	bdl	3.29	0.92
Min	37.3	3.57	0.12	bdl	1.06	2.22	8.06	0.06	0.09	bdl	bdl	0.15	bdl
Pentlandite	S	Co	Ni	Cu	Os	Ir	Ru	Rh	Pt	Pd	Au	Te	Bi
<i>n</i> =7	wt%	ppm	wt%	wt%	ppm								
Mean	35.6	4398	31.0	0.02	2.02	3.60	15.1	25.1	0.96	102		1.99	0.87
σ	0.22	1171	2.44	0.02	1.28	1.99	8.94	16.1	0.81	31.1		2.07	0.88
Max	35.2	5586	32.8	0.04	4.21	5.02	29.3	45.5	2.07	143	bdl	6.14	2.52
Min	35.8	3068	26.7	bdl	0.64	1.36	4.64	8.20	0.07	67.7	bdl	bdl	bdl
Chalcopyrite	S	Co	Ni	Cu	Os	Ir	Ru	Rh	Pt	Pd	Au	Te	Bi
<i>n</i> =3	wt%	ppm	wt%	wt%	ppm								
Mean	34.7	78.6	0.53	30.4	0.03	0.09		0.61	0.12	1.73	0.01	0.22	0.10
σ	0.24	135	0.90	1.42	0.04	0.16		0.62	0.14	2.62	0.01	0.31	0.16
Max	34.8	235	1.57	32.0	0.06	0.27	bdl	1.05	0.28	4.76	0.01	0.44	0.28
Min	34.4	0.07	0.01	29.4	bdl	bdl	bdl	bdl	0.02	0.11	bdl	bdl	bdl

Table 7.4 (cont.)

Overysel chromitites

Pyrrhotite <i>n</i> =1	S wt%	Co ppm	Ni wt%	Cu wt%	Os ppm	Ir ppm	Ru ppm	Rh ppm	Pt ppm	Pd ppm	Au ppm	Te ppm	Bi ppm
	38.8	62.7	0.03	bdl	bdl	bdl	bdl	bdl	bdl	0.03	0.07	0.01	19.7
Pentlandite <i>n</i> =1	S wt%	Co ppm	Ni wt%	Cu wt%	Os ppm	Ir ppm	Ru ppm	Rh ppm	Pt ppm	Pd ppm	Au ppm	Te ppm	Bi ppm
	35.8	5079	33.7	bdl	0.49	bdl	6.87	Bdl	bdl	72.4	bdl	0.81	0.59
Pyrite <i>n</i> =2	S wt%	Co ppm	Ni wt%	Cu wt%	Os ppm	Ir ppm	Ru ppm	Rh ppm	Pt ppm	Pd ppm	Au ppm	Te ppm	Bi ppm
Mean	54.0	127	0.23					0.02		0.19	0.08	1.16	64.9
<i>σ</i>	<i>0.00</i>	<i>122</i>	<i>0.21</i>					<i>0.01</i>		<i>0.08</i>	<i>0.02</i>	<i>1.20</i>	<i>60.8</i>
Max	54.0	213	0.37	bdl	bdl	bdl	bdl	0.02	bdl	0.25	0.09	2.00	108
Min	54.0	40.3	0.08	bdl	bdl	bdl	bdl	0.01	bdl	0.13	0.06	0.31	21.9

Overysel Footwall rocks:

Pyrrhotite <i>n</i> =6	S wt%	Co ppm	Ni wt%	Cu wt%	Os ppm	Ir ppm	Ru ppm	Rh ppm	Pt ppm	Pd ppm	Au ppm	Te ppm	Bi ppm
Mean	39.0	57.1	0.70		0.06	0.11	0.35	0.85	3.34	0.02		1.75	3.97
<i>σ</i>	<i>1.11</i>	<i>23.7</i>	<i>0.21</i>		<i>0.05</i>	<i>0.07</i>	<i>0.33</i>	<i>1.50</i>	<i>4.10</i>	<i>0.03</i>		<i>1.62</i>	<i>4.84</i>
Max	40.0	86.4	1.09	bdl	0.13	0.23	0.82	3.10	9.77	0.08	bdl	2.97	11.1
Min	37.2	39.5	0.47	bdl	0.02	0.04	0.50	bdl	0.01	bdl	bdl	bdl	bdl
Pentlandite <i>n</i> =10	S wt%	Co ppm	Ni wt%	Cu wt%	Os ppm	Ir ppm	Ru ppm	Rh ppm	Pt ppm	Pd ppm	Au ppm	Te ppm	Bi ppm
Mean	33.5	3144	31.6	0.06	0.03	0.03		0.59	0.45	78.0	0.05	2.81	8.08
<i>σ</i>	<i>1.06</i>	<i>1239</i>	<i>6.62</i>	<i>0.11</i>	<i>0.03</i>	<i>0.03</i>		<i>0.78</i>	<i>0.63</i>	<i>44.5</i>	<i>0.09</i>	<i>6.20</i>	<i>22.1</i>
Max	36.1	5184	43.6	0.29	0.07	0.08	bdl	2.04	1.73	170	0.28	18.1	71.0
Min	32.2	788	17.7	bdl	bdl	bdl	bdl	bdl	bdl	28.6	bdl	bdl	0.20
Chalcopyrite <i>n</i> =10	S wt%	Co ppm	Ni wt%	Cu wt%	Os ppm	Ir ppm	Ru ppm	Rh ppm	Pt ppm	Pd ppm	Au ppm	Te ppm	Bi ppm
Mean	34.6	22.7	0.33	27.4	0.00			0.28	0.06	1.71	0.04	0.17	1.13
<i>σ</i>	<i>0.94</i>	<i>52.2</i>	<i>0.67</i>	<i>5.09</i>	<i>0.01</i>			<i>0.22</i>	<i>0.12</i>	<i>1.83</i>	<i>0.05</i>	<i>0.06</i>	<i>1.15</i>
Max	35.4	159	1.84	34.8	0.02	bdl	bdl	0.48	0.32	5.75	0.18	0.25	2.85
Min	32.1	0.10	bdl	19.3	bdl	bdl	bdl	bdl	bdl	0.18	bdl	bdl	bdl
Pyrite <i>n</i> =3	S wt%	Co ppm	Ni wt%	Cu wt%	Os ppm	Ir ppm	Ru ppm	Rh ppm	Pt ppm	Pd ppm	Au ppm	Te ppm	Bi ppm
Mean	53.5	20.9	0.01	0.02					0.03	0.04	0.01	0.43	12.5
<i>σ</i>	<i>0.20</i>	<i>4.31</i>	<i>0.01</i>	<i>0.03</i>					<i>0.05</i>	<i>0.02</i>	<i>0.02</i>	<i>0.27</i>	<i>15.6</i>
Max	53.7	25.0	0.02	0.05	bdl	bdl	bdl	bdl	0.09	0.06	0.03	0.62	23.5
Min	53.3	16.4	bdl	0.03	bdl	bdl	bdl						
<u>Limits of detection</u>	S wt%	Co ppm	Ni wt%	Cu wt%	Os ppm	Ir ppm	Ru ppm	Rh ppm	Pt ppm	Pd ppm	Au ppm	Te ppm	Bi ppm
	0.31	0.74	<0.01	<0.01	0.015	0.005	0.067	0.011	0.017	0.034	0.006	0.35	0.84

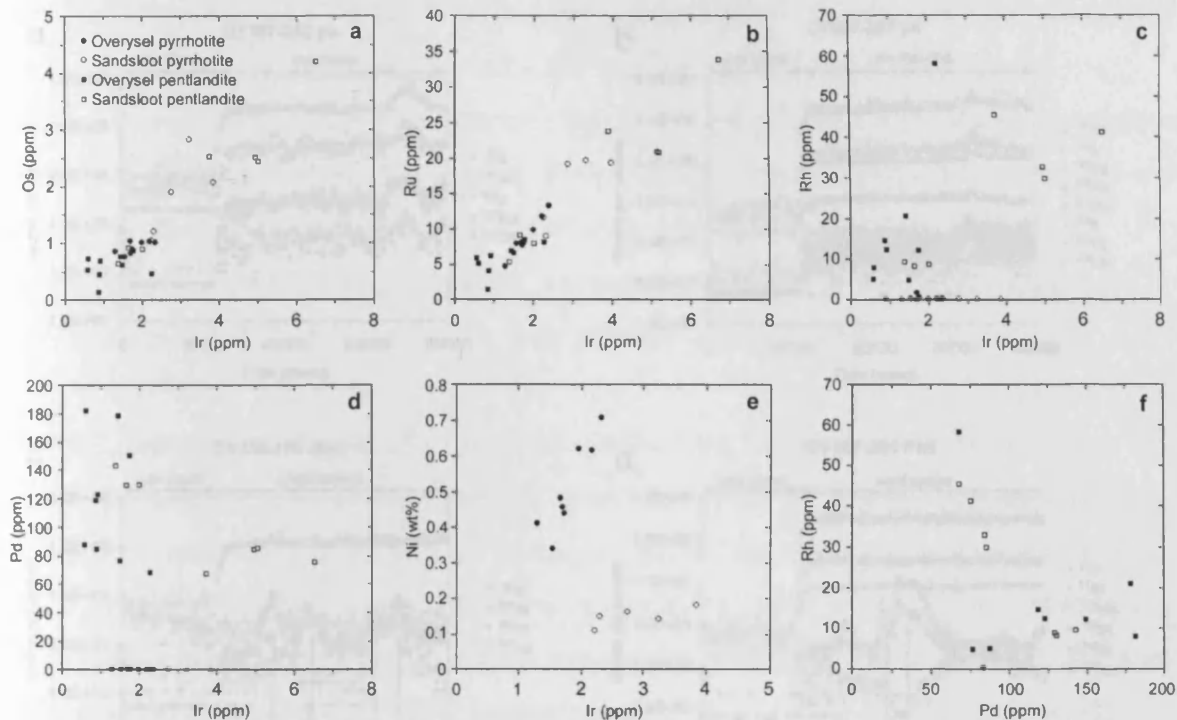


Figure 7.4. PGE contents of pyrrhotite and pentlandite grains plotted as: (a) Ir vs Os, (b) Ir vs Ru, (c) Ir vs Rh, (d) Ir vs Pd; (e) Ir vs Ni for pyrrhotite and (f) Pd vs Rh for pentlandite.

7.8 PGE contents of BMS and other phases

7.8.1 Platreef feldspathic pyroxenites

Pyrrhotite, pentlandite and chalcopyrite were analyzed in the Platreef pyroxenites. From Table 7.4 it can be seen that pyrrhotite is the major carrier of Os, Ir and Ru, holding on average 1ppm Os, 2ppm Ir and 8ppm Ru, and the standard deviations show that the values are highly consistent both within and between samples. Figures 7.4a and b show a high degree of correlation between these elements in pyrrhotites. Some grains held minor amounts of Rh, but no appreciable Pd was present in any of the pyrrhotites (Fig. 7.4d). There is a positive correlation between the IPGE and Ni contents in pyrrhotite which is illustrated in Fig. 7.4e. However, different slopes are evident at different locations, with the Sandsloot samples showing greater PGE and lower Ni contents than those found at Overysel. Fig. 7.5a shows a TRA spectrum for a pyrrhotite grain from the Platreef pyroxenites. This shows the smooth, parallel patterns of Ru, Ir and Os with S, indicating that the IPGE are present in solid solution in the pyrrhotite.

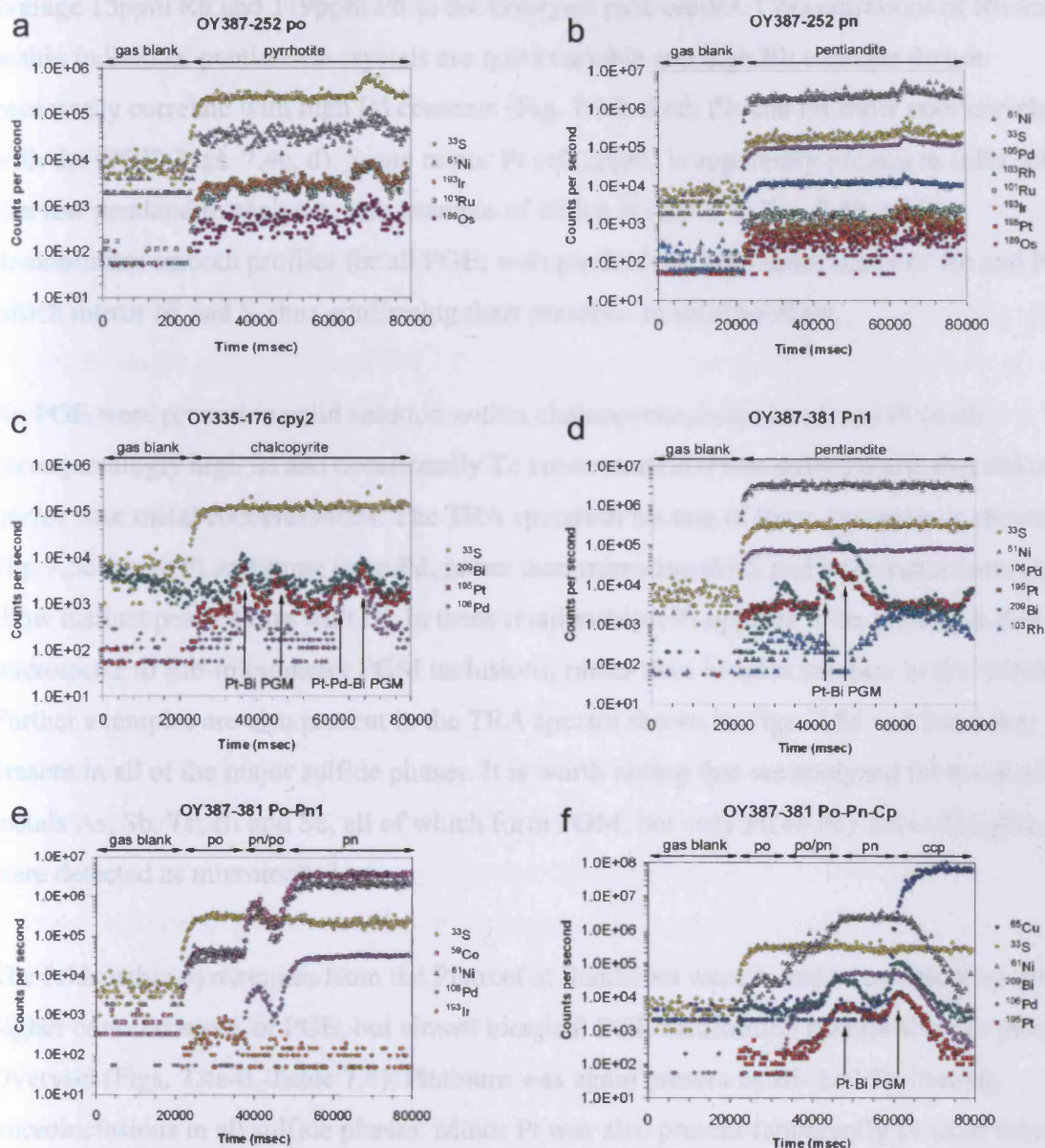


Figure 7.5. Selected TRA spectra for: (a) pyrrhotite, (b) pentlandite and (c) chalcopyrite with PGM from the Platreef pyroxenites; (d) pentlandite with PGM, (e) composite pyrrhotite-pentlandite, (f) composite pyrrhotite-pentlandite-chalcopyrite with PGM.

Pentlandite was also found to contain concentrations of the IPGE with similarly high degrees of correlation between these elements (Figs. 7.4a, b). Their concentrations, however, are consistently lower than those in pyrrhotite (Table 7.4, Figs. 7.4a, b), with pyrrhotite, on average, hosting 1.5 times as much Os, Ir and Ru than pentlandite in the Overysel samples. This is not a consistent relationship however, with the two samples from Sandsloot showing opposite trends (Table 7.4). Pentlandite is the major carrier of Rh and Pd, containing on

average 15ppm Rh and 119ppm Pd in the Overysel pyroxenites. Concentrations of Rh and Pd within individual pentlandite crystals are quite variable and high Rh contents do not necessarily correlate with high Pd contents (Fig. 7.4f). Both Rh and Pd show poor correlations with the IPGE (Figs. 7.4c, d). Some minor Pt (<0.2ppm) is apparently present in solid solution in a few pentlandite analyses, one example of which is shown in Fig. 7.5b, which demonstrates smooth profiles for all PGE, with particularly high abundances of Rh and Pd which mirror Ni and S, thus confirming their presence in solid solution.

No PGE were present in solid solution within chalcopyrite, however, some Pt (with correspondingly high Bi and occasionally Te concentrations) was detected and that did not mirror base metal concentrations. The TRA spectrum for one of these examples is shown in Fig. 7.5c where Pt and some trace Pd, rather than mirroring the S and base metal contents, show distinct peaks along with Bi. In these relationships, Pt appears to be present as discrete, micrometer to sub-micrometer PGM inclusions, rather than in solid solution in the sulfide. Further examples are also present in the TRA spectra shown in Figs. 7.5d and f and they are present in all of the major sulfide phases. It is worth noting that we analyzed for the semi-metals As, Sb, Te, Bi and Se, all of which form PGM, but only Pt(+/-Pd)-Bi(+/-Te) phases were detected as microinclusions.

The feldspathic pyroxenites from the Platreef at Sandsloot were found to contain consistently higher concentrations of PGE, but almost identical PGE distribution relationships to those at Overysel (Figs. 7.4a-d, Table 7.4). Platinum was again present as Bi- and Te-bearing microinclusions in all sulfide phases. Minor Pt was also present (apparently in solid solution) in pyrrhotite and pentlandite in one sample from Sandsloot at concentrations of around 2ppm (Table 7.4).

7.8.2 Chromitites

The majority of the IPGE and Rh in the pyroxenitic rocks appear to be present in solid solution within pyrrhotite and pentlandite rather than as PGM. The chromitites, in contrast, contain abundant Rh-, Ru- and Ir-bearing PGM (Table 7.2), and have elevated concentrations of these elements relative to Pt and Pd (Holwell and McDonald, 2006). A few sulfide grains were sufficiently large to analyze effectively by laser ablation. One grain of pentlandite, was found to contain no Ir or Rh (Table 7.4). It did, however, contain some Os and Ru in comparable concentrations to the pyroxenite-hosted sulfides, implying that all the Ir and Rh

within the chromitites may be present as PGM. A grain of pyrrhotite was also analyzed and found to contain no PGE in solid solution, and was also very low in Ni content.

7.8.3 Footwall gneisses

Holwell and McDonald (2006) showed that there is fractionation of PGE with depth into the gneissic footwall at Overysel. Whole-rock values of Ir, Ru and Rh drop off dramatically relative to Pt, Pd and Au with increasing depth into the footwall, and this is also reflected in the PGE content of the sulfides. From Table 7.4 it can be seen that the IPGE content of footwall pyrrhotite and pentlandite is very low, compared to their reef equivalents. Rhodium is present within the pentlandite in variable, but always low (<2ppm), concentrations. Whole-rock concentrations of Pt and Pd remain comparable to the reef in mineralized footwall samples. Pentlandite still hosts appreciable amounts of Pd, although to a lesser degree than in the reef, and this is reflected in the greater proportions of Pd-bearing PGM within the footwall rocks compared with the reef pyroxenites (Table 7.3).

The Pt/Pd ratio for the massive sulfide sample is 0.35, however, virtually all of the PGM found in this sample were Pt phases (Table 7.2) and there is therefore a case of apparently 'missing' Pd, not represented by any discrete PGM phases. Figure 7.5d shows a particularly smooth TRA spectrum for a pentlandite from the massive sulfide sample in the footwall (OY387-381), and demonstrates clearly that Pd is present in solid solution, with the Pd signal mirroring perfectly the profiles of Ni and S. It appears that some Pt is also present in solid solution in low concentrations, but occasional peaks with corresponding Bi peaks indicate the presence of very small Pt-Bi PGM microinclusions as well. The spectrum also shows low concentrations of Rh within the pentlandite, and that a sharp decrease in the Rh signal occurs as the Pt-rich PGM is sampled, indicating a lack of Rh in the PGM phase. Figure 7.5e illustrates a case where the laser path has passed over pyrrhotite and into pentlandite. The transition can easily be seen by the increase in Ni, as pentlandite is sampled by the laser. This also illustrates the presence of Pd in homogeneous solid solution in pentlandite, and also shows no variation towards the margin of the pentlandite grain. Another polyphase TRA spectrum is shown in Fig. 7.5f where the laser has sampled firstly pyrrhotite before passing into pentlandite, as seen by the increase in Ni and Pd, and finally chalcopyrite which is shown by the drop in Ni and Pd and the increase in Cu. Two Pt-Bi PGM were sampled, which are labelled on Fig. 7.5f, the first, at around 50 seconds, is close to the pyrrhotite-pentlandite contact, and the second, at around 63 seconds, appears to be at the boundary between the

pentlandite and the chalcopyrite. Laser analysis of the exsolution flames of pentlandite in pyrrhotite such as those in Figs. 7.3e and f shows that the pentlandite flames also contain Pd in solid solution. Chalcopyrite in the footwall rocks did not contain any appreciable PGE. Three examples of pyrite within the footwall were analyzed and were not found to contain any PGE in solid solution or as microinclusions.

An important relationship in determining the timing of PGE and S saturation in the magma are inclusion relationships in high-temperature cumulus phases. The earliest crystallizing phases in the Platreef at Overysel are chromite, then orthopyroxene. We performed a number of LA-ICP-MS analyses on chromite grains from the chromitite layers, xenoliths and feldspathic pyroxenites, together with several analyses of cumulus orthopyroxenes from the feldspathic pyroxenites. None of the analyses revealed the presence of any PGE, either in solid solution, or as microinclusions, within chromite or orthopyroxene.

7.9 Mass balance

For a semi-quantitative indication of the proportions of the PGE present within sulfide minerals and as discrete PGM phases, we adopted a similar approach to the technique used by Ballhaus and Sylvester (2000), in which we recalculate the whole-rock PGE contents to the equivalent in 100% sulfide, and plot the values on a chondrite normalized diagram along with the PGE concentrations of the BMS. As chalcopyrite contains virtually no PGE in solid solution, we recalculate the whole rock PGE contents to 100% pyrrhotite and pentlandite, as these are the two phases which contain PGE. Including chalcopyrite in the calculations would effectively 'dilute' the PGE content of the calculated sulfide fraction. To improve the technique of Ballhaus and Sylvester (2000), we take into account the different proportions of the sulfide phases present. To calculate this, we adapted the technique described in Huminicki *et al.* (2005), where all the whole-rock Cu and a corresponding amount of S are used to calculate the proportion of chalcopyrite. To improve this further, we used Cu and Ni concentrations obtained by acid leach, which extracts base metals only from the sulfide phase and thus no correction is needed to allow for Ni within silicates, which is necessary if using conventional whole-rock data. The amount of S used in these calculations is based on SEM-EDA analyses of sulfide phases. All whole-rock Ni and a corresponding amount of S are allocated to pentlandite, with the remaining S used to calculate the amount to pyrrhotite. A small correction is made to allow for trace amounts of Ni in pyrrhotite as determined by

SEM-EDA analysis. This method does not take into account minor pyrite, however this phase is relatively insignificant volumetrically.

For the pyroxenite samples we analyzed by LA-ICP-MS, we calculated the mean pyrrhotite, pentlandite and chalcopyrite fractions, and then re-calculated the whole-rock concentrations of the PGE and Au to those in 100% sulfide, containing pyrrhotite and pentlandite only. The chondrite normalized values for average PGE contents of pyrrhotite and pentlandite as determined by LA-ICP-MS are plotted with the average whole-rock concentrations for the same samples in Figs. 7.6a and b together with those calculated for sulfides of the Merensky Reef by Ballhaus and Sylvester (2000), and these are shown in Fig. 7.6c and d for comparison. The rationale for this method is that an element whose concentration within a sulfide is as high or higher than the bulk value indicates its presence in solid solution, whereas if it falls below, some of that element must be present as discrete phases. It can be seen that the IPGE are comfortably held in solid solution within both pyrrhotite and pentlandite, and Rh and Pd in pentlandite. The slightly higher abundances of Rh and Pd in pentlandite compared to the bulk composition is due to their presence primarily in pentlandite, and thus the bulk rock value is 'diluted' by pyrrhotite that is relatively barren of Rh and Pd (a similar effect on all elements would occur if chalcopyrite were included in the calculations). For this reason we have also plotted the whole-rock values recalculated to 100% pentlandite on Fig. 7.6b (c.f Fig. 7.6d, where Ballhaus and Sylvester (2000) did not make this correction). Our results show that whole-rock Rh is almost exactly the same as Rh in pentlandite, whereas Pd in pentlandite falls below the whole-rock if recalculated to 100% pentlandite, indicating some Pd-bearing PGM. The large negative anomalies in both Pt and Au show that these are not significantly present in solid solution and must reside in discrete Pt- and Au-bearing phases. These results are entirely consistent with the LA-ICP-MS data which show the all the IPGE in solid solution in pyrrhotite and pentlandite, all Rh and some Pd in pentlandite, and corroborate the PGM studies, which identified 57% of all PGM in the pyroxenites to be Pt phases, 22% electrum and 21% Pd phases (Table 7.2). From Fig. 7.6 it can be seen that our data from the Platreef show remarkable similarities to that for the Merensky Reef sulfides, which would suggest that the sulfides in both deposits were enriched in PGE at an early stage and underwent a similar cooling history.

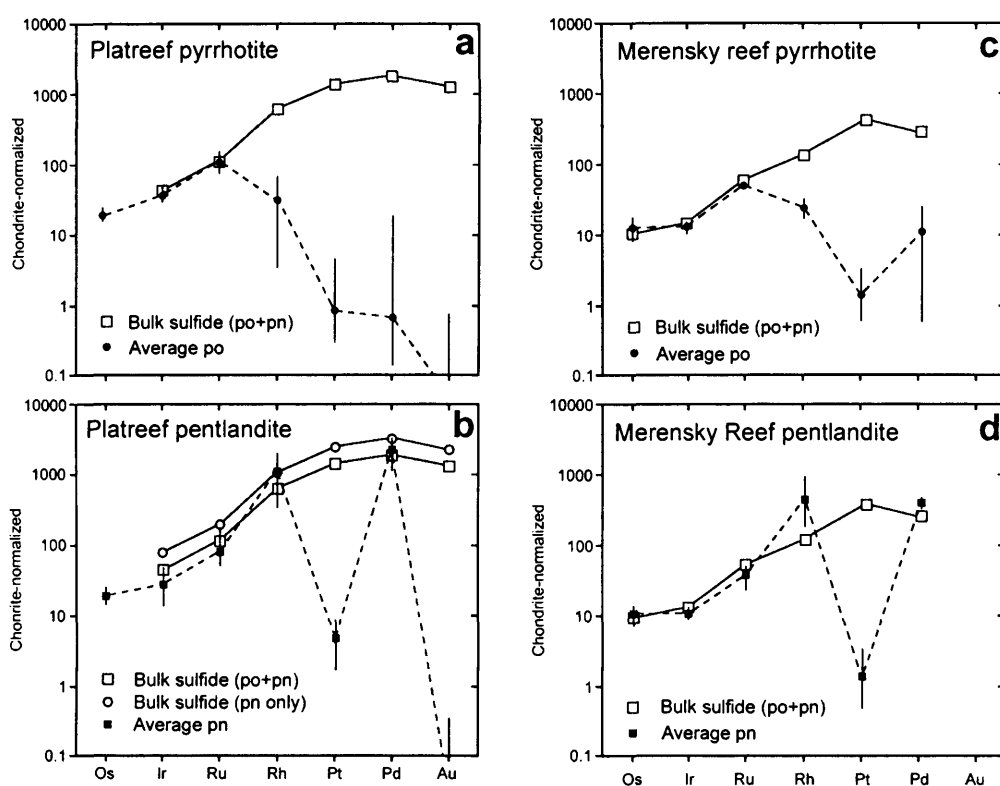


Figure 7.6. Chondrite normalized diagrams of average PGE in (a) pyrrhotite and bulk sulfide recalculated to 100% sulfide (po+pn) for Overysel Platreef pyroxenites, and (b) pentlandite and bulk sulfide recalculated to 100% sulfide (po+pn and pn only) for Overysel Platreef pyroxenites, (c) pyrrhotite and bulk sulfide recalculated to 100% sulfide (po+pn) for the Merensky Reef (d) pentlandite and bulk sulfide recalculated to 100% sulfide (po+pn) for the Merensky Reef. Merensky Reef data from Ballhaus and Sylvester (2000).

7.10 Discussion

This study into the PGM mineralogy of the Platreef at Overysel has revealed characteristic PGM assemblages and associations in different lithologies which are dominated by Pt and Pd phases. The LA-ICP-MS study has not only identified the major carriers of the IPGE and Rh in the Platreef to be pyrrhotite and pentlandite, but also provides an insight into the partitioning behaviour of the individual PGE during crystallization of a sulfide liquid and also reveals the processes involved in the enrichment in noble metals in the Platreef.

7.10.1 The role of a sulfide liquid in Platreef PGE mineralization

The chalcophile nature of the PGE is well known and, in the presence of a sulfide liquid, the high distribution coefficients (D) of the PGE between sulfide and silicate melts imply that they will be effectively collected by any sulfide liquid separating from a silicate magma. There have been several studies into the Fe-Ni-Cu-S system which have been used to assess

the partitioning of PGE during the crystallization of monosulfide solid solution (mss) from a sulfide liquid (e.g. Fleet *et al.*, 1993; Li *et al.*, 1996; Barnes *et al.*, 1997; Ballhaus *et al.*, 2001; Mungall *et al.*, 2005). Their data are summarized in Table 7.5 and show that D_{Pt} , D_{Pd} and D_{Au} are all <1 and these elements are therefore concentrated in the residual liquid during mss crystallization. D_{Os} , D_{Ir} , D_{Ru} and D_{Rh} are all much >1 in S-rich systems and partition into mss. However, the partitioning is particularly affected by varying fS_2 conditions and the compatibility in mss of these elements decreases as the S-content of the liquid decreases, so that in very S-poor, alloy-dominant systems, only Ru remains compatible in mss. As the Platreef is relatively S-rich, the PGE in a sulfide liquid within the Platreef should behave in the manner expected from the experimental results during the crystallization of mss. The work of Holwell and McDonald (2006) demonstrated that, originally, PGE were present in a sulfide liquid within the Platreef magma, which cooled to form the observed pyrrhotite-pentlandite-chalcopyrite-PGM assemblage. Therefore, our LA-ICP-MS analyses of the sulfide phases and the complementary PGM studies can be used to compare the natural partitioning behaviour in the Platreef with that expected from the experimental results.

Table 7.5. Experimentally derived partition coefficients for the noble metals between monosulfide solid solution and sulfide liquid (900-1200°C).

Os	Ir	Ru	Rh	Pt	Pd	Au	Reference
4.3	3.6	4.2	3.0	0.2	0.2	0.09	Fleet <i>et al.</i> (1993)
	1.1-13		0.047-8.3	0.05-0.16	0.08-0.27		Li <i>et al.</i> (1996)
	0.43-17		0.045-7.43	0.013-0.46	0.005-0.44		Barnes <i>et al.</i> (1997)
5	3.1-11.8	3-19	1.5-3.5	0.017-0.13	0.058-0.19		Ballhaus <i>et al.</i> (2001)
	4.55-7.68	8.71-13.5	3.45-5.66	0.035-0.052	0.072-0.12	0.006-0.013	Mungall <i>et al.</i> (2005)

Using the partitioning data obtained during the experimental studies, one would expect the IPGE and Rh to be enriched in mss, and to be present in solid solution within its cooling products: pyrrhotite and pentlandite, which is precisely what is observed in our LA-ICP-MS analyses. The IPGE should concentrate in early crystallizing mss, which on cooling exsolves to Fe-mss and Ni-mss then to pyrrhotite and pentlandite with the IPGE remaining in solid solution (Barnes *et al.*, 2006). The enrichment of the IPGE in pyrrhotite compared to pentlandite (1.5 times) may indicate a slight preference for these elements to partition into pyrrhotite during the exsolution process. A similar relationship was also found to be present in the sulfides of the Merensky Reef, where Ballhaus and Sylvester (2000) noted the IPGE to

be about 1.2 times more enriched in pyrrhotite than pentlandite, although this is not necessarily a consistent relationship, as seen by the contrasting concentrations in the Sandsloot samples and Barnes *et al.* (2006) found broadly similar IPGE concentrations in pyrrhotite and pentlandite in their LA-ICP-MS study on samples from Noril'sk. Rhodium is also compatible in mss, however it is present only in pentlandite in our samples, and therefore during the exsolution process it appears that Rh preferentially partitions into the Ni-rich mss which forms pentlandite on cooling.

According to the experimental studies, after crystallization of mss, Pt, Pd and Au should be concentrated in the residual sulfide liquid which will crystallise intermediate solid solution (iss), which on cooling exsolves to chalcopyrite plus pentlandite. Peregoedova (1998) showed experimentally that Pt and Pd (and by implication, Au) are also incompatible in iss. However, some Pd is present in solid solution in pentlandite in significant amounts (up to 180ppm, Table 7.4) and the presence of Pd within the pentlandite exsolution flames in pyrrhotite such as those shown in Figs. 7.3e and f implies that some Pd is likely to have been present in mss.

Fleet *et al.* (1993) included minor amounts of As, Bi and Te, which are also highly chalcophile at magmatic temperatures and are among the most common elements to form PGM with Pt and Pd. They found that during quenching, Bi, Te and As segregate as a late residual liquid which scavenges Pt preferentially over Pd. Helmy *et al.* (2006) performed experiments in sulfide-telluride systems and found that telluride (and bismuthide and antimonide) melt is immiscible in sulfide melt below temperatures of 1000°C. Furthermore, telluride melt remains liquid after the sulfide solidus and that Pt and Pd strongly partition into this melt. They also noted that Pt and Pd are more strongly complexed with Te and Bi than S, and Pd will only enter mss when the Pd/semi metal ratio is sufficiently high to have an excess of Pd that cannot be accommodated by the telluride/bismuthide melt. Therefore a high Pd/semi metal ratio can explain the presence of Pd in pentlandite in our samples. These observations by Helmy *et al.* (2006) seem to substantiate the theories of Cabri and Laflamme (1976), Prichard *et al.* (2004b) and Barnes *et al.* (2006) who all suggested that Pt, Pd and Au along with semi metals such as Bi, Te, As and Sb are concentrated in a late-stage residual melt after the crystallization of iss. Subsequent crystallization of this liquid then forms PGM around the margins of the sulfide blebs and in small veinlets injected into the surrounding silicates, which explains the tendency for PGM to be present around the margins of sulfide blebs. Over half of the PGM in the reef pyroxenites are hosted by primary silicates around the

margins of the BMS grains and this may support the theory of late-stage injection of this PGE-semi metal rich liquid into surrounding silicates. Later alteration of the sulfide blebs, with replacement by secondary amphiboles around the margins of BMS blebs, appears not to affect the early formed PGM, which are then isolated as satellite grains within secondary silicates around the BMS blebs as is shown in Fig. 7.3a.

The case of the Pt-Bi-Te microinclusions within all sulfides is interesting as it infers that Pt and Bi were present in both mss and iss. It is unlikely that they exsolved from the sulfide liquid as exsolution tellurides/bismuthides have characteristically high Ni contents, which our tellurides/bismuthides do not. Platinum is also incompatible in both mss and iss, however it is highly compatible in telluride and bismuthide melt, which is immiscible in sulfide melt below 1000°C (Helmy *et al.*, 2006). The microinclusions are suggested to represent minute droplets of this immiscible melt that remained trapped within crystallising mss and iss, and failed to be expelled to the grain boundaries to form the satellite PGM grains as described above. This also implies Bi and Te were present within the initial sulfide liquid. The footwall gneisses also display a similar BMS-Pt/Pd telluride assemblage and it is assumed that these assemblages formed directly from the crystallization of a sulfide melt in a similar manner to that described for the pyroxenites, a process which is summarized in Fig. 7.7.

Hutchinson and McDonald (2005) presented some initial results for Pt and Pd in sulfides from a LA-ICP-MS study on the Platreef at Turfspruit (Fig. 7.1). They also found that Pt was not present in solid solution in any of the sulfide phases, but was present as Pt-Pd-Bi microinclusions within all phases. Palladium was found to be present erratically in pentlandite, but more commonly as PGM inclusions, and the overall abundances of the IPGE within the sulfides was much lower than at Overysel (Hutchinson and McDonald, 2006). Hutchinson and McDonald (2005) attributed the absence of PGE within sulfides to the degree of contamination from assimilated footwall rocks (e.g. Sharman-Harris *et al.*, 2005), which also introduced elements such as As, Sb, Bi and Te. As a consequence, the PGE (particularly Pt and Pd) effectively formed PGM with these elements which were either not collected by the sulfide liquid, or were expelled from them during crystallization. The partial melting of the floor on Overysel is thought to post-date the mineralization (Barton *et al.* 1986) and is unlikely to have released similar concentrations of volatile elements as the sedimentary floor at Turfspruit. Our data implies that that Bi and Te were present within the mineralizing sulfide liquid, and that local contamination at Turfspruit served to increase the amounts of semi

metals, particularly Sb and As, in that area which resulted in a higher volume of immiscible semi metal rich melt, restricting the amount of PGE that partitioned into the sulfides.

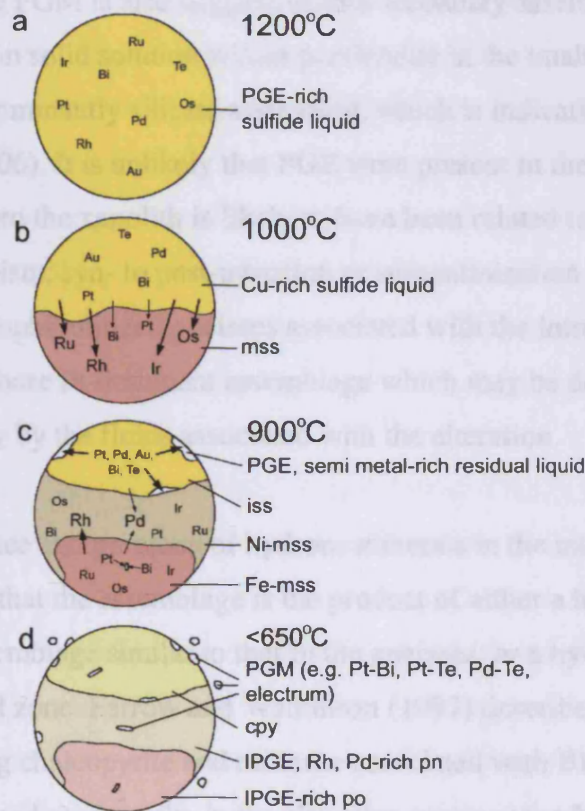


Figure 7.7. Schematic representation of the partitioning behaviour of the PGE within cooling droplets of sulfide within the Platreef magma. *a*: PGE and semi metals are concentrated within droplets of sulfide liquid at magmatic temperature. *b*: at around 1000°C, mss crystallizes, into which the IPGE and Rh are strongly partitioned. Some small amounts of Pt, Pd and semi metals are trapped in mss. *c*: on further cooling to 900°C, iss crystallizes, at which point the semi metals and most of the Pt, Pd and Au form an immiscible liquid which is expelled to grain boundaries. Any Pt and semi metals present within mss and iss form very small droplets of this liquid and are trapped within the sulfide. Ni-rich and Fe-rich mss separate, with Rh and some Pd partitioning into the Ni-rich portion. *d*: Below 650°C, IPGE-rich pyrrhotite exsolves from Fe-mss, IPGE, Rh and Pd rich pentlandite exsolves from Ni-mss and iss recrystallises to chalcopyrite. The Pt, Pd, Au and semi metal rich liquid crystallises PGM around the margins of the sulfide blebs, and as tiny microinclusions where trapped within sulfide.

7.10.2 Hydrothermal effects on PGM mineralogy

The most unaltered PGM assemblages in the Platreef appear to be the sulfide-associated telluride and chromite-associated laurite dominant assemblages. All others are likely to be secondary: either modified from the original telluride-dominant one, or ones related to transport by a hydrothermal fluid. The serpentinized calc-silicate xenoliths show a distinctive assemblage, dominated by sperrylite, with some bismuthides, hollingworthite and Pd

tellurides. The presence of sperrylite in calc-silicate footwall rocks at Sandsloot is common, as is the presence of Pd tellurides in serpentinized footwall rocks, and these associations are thought to be characteristic of hydrothermal transport of PGE (Holwell *et al.*, 2006). The presence of Rh-bearing PGM is also suggestive of a secondary assemblage as all Rh appears to be sufficiently held in solid solution within pentlandite in the unaltered assemblages. The associations are also dominantly silicate associated, which is indicative of volatile activity (e.g. Holwell *et al.*, 2006). It is unlikely that PGE were present in the original protolith, so introduction of PGE into the xenolith is likely to have been related to fluid activity associated with either metamorphism, syn- to post-intrusion or serpentinization after intrusion and xenolithization. The amphibolitized gneisses associated with the intrusion of late-stage granitic dykes have a more Pt-dominant assemblage which may be due to the more mobile Pd being transported away by the fluids associated with the alteration.

The bleached appearance and presence of hydrous minerals in the mineralized basement granite would suggest that the assemblage is the product of either a hydrothermal modification of an assemblage similar to that in the gneisses, or a hydrothermal halo at the base of the mineralized zone. Farrow and Watkinson (1997) describe almost identical sulfide assemblages containing chalcopyrite and millerite associated with Bi-bearing PGM such as sobolevskite, froodite and michenerite in the alteration zones around the Cu-rich veins at the deepest extremities of the mineralized zones at Sudbury which they estimate to have formed at around 200-300°C. Holwell and McDonald (2006) suggested that the strikingly similar assemblage in the granite in borehole OY387 was formed by the expulsion of a hydrothermal fluid from the final stages in the evolution of the migrating sulfide liquid, analogous to that postulated for Sudbury by Li and Naldrett (1993). The assemblage in the thin Lower Zone-like pyroxenite may be of similar origin as it contains abundant bismuthides, associated with a chalcopyrite-dominant BMS assemblage. This contrasts with the Ni-rich magmatic sulfides that might be expected in such rocks if the sulfide were of a magmatic origin (c.f. the Lower Zone-hosted Volspruit deposit, Hulbert and von Gruenewaldt, 1982; Harmer, 2004).

7.10.3 Chromitites and the timing of S saturation

Inclusion relationships, and in particular the presence of PGM microinclusions, have been used as an important indicator of the processes involved in noble metal enrichment in magmatic PGE deposits. Ballhaus and Sylvester (2000) identified PGM microinclusions within chromite and olivine in the Merensky Reef and suggested that they formed from the

development of PGE clusters (as proposed by Tredoux *et al.*, 1995) in the magma, prior to collection by early crystallizing phases in the magma. The lack of such PGM microinclusions in high-temperature cumulus phases in the Platreef may imply that sulfur saturation and collection of PGE and semi metals by the resultant sulfide droplets occurred prior to the crystallization of any cumulus phases. If so, it is possible that when the Platreef magma was intruded it already contained pre-formed sulfide droplets, such as in the model of Lee (1996), who suggested the PGE-rich sulfides were pre-concentrated in a deep staging chamber. In such a case, the mass balance problem of the large volume of magma needed to be processed to extract the volumes of PGE present in the Platreef (e.g. Cawthorn *et al.*, 1985; Cawthorn *et al.*, 2002), which is imposed by the late intrusion of Main Zone rocks (Holwell *et al.*, 2005; Holwell and Jordaan, 2006) can be resolved.

In our chromitite samples, the PGM assemblage is dominated by minerals containing the IPGE and Rh, such as laurite and hollingworthite, which are typical of chromite-associated PGE deposits. The presence of laurite with chromite, especially as inclusions, is considered to be of magmatic origin in chromite ores (Bockrath *et al.*, 2004) and the behaviour of Ru is an important indicator of fS_2 conditions within a silicate magma. Laurite and Ru-Os-Ir alloy form under conditions of sulfur-undersaturation (Brenan and Andrews, 2001), and therefore the presence of inclusions of these phases within primary liquidus phases such as chromite would suggest that early crystallization took place in sulfide-undersaturated conditions. Additionally, Bockrath *et al.* (2004) showed experimentally that, although thermodynamically, laurite can be a liquidus phase that crystallizes directly from a sulfide-undersaturated magma, many grains of laurite may be 'secondary', although still magmatic. Their experiments showed that Ru metal nucleates on the surfaces of chromite grains, and that later reaction between Ru and S following an increase in fS_2 forms laurite. In either of the above cases, the presence of laurite is indicative of sulfur-undersaturated conditions at the time of chromite precipitation. This common association in the Overysel chromitites of laurite on the surfaces of chromite grains may imply that the chromitites crystallized under conditions of S undersaturation, however very few were found as inclusions and no Ru-Os-Ir alloy was found.

If sulfur-saturation occurs concurrently with, or prior to, the earliest crystallizing phases, laurite and Ru-Ir-Os alloy will not form and the IPGE will partition into mss (Brenan and Andrews, 2001). There are no records of Ru-Ir-Os alloy in the Platreef and, with the exception of the chromitites described here laurite is also very rare (Kinloch, 1982; Armitage

et al., 2002; Hutchinson and Kinnaird, 2005; Holwell *et al.*, 2006). The fact that the chromitites contain appreciable amounts of Rh- and Ir-bearing PGM, particularly hollingworthite which is a relatively high temperature phase stable to at least 850°C (Makovicky, 2002), would suggest that the PGM formed at a similar, or earlier, time to the sulfides, with Rh and Ir forming discrete sulfarsenide PGM associated with chromite grains. These factors, together with the high concentrations of the IPGE within the cooling products of mss would strongly support a theory of sulfur saturation, and concentration of PGE within the sulfide liquid, occurring concurrently with or prior to chromite precipitation. Given the relatively small volumetric proportions of chromite in the Platreef, it is likely that chromite precipitation occurred at a similar time to S saturation with laurite and hollingworthite forming with chromite, but still allowing for appreciable amounts of the IPGE and Rh to be scavenged by the sulfide liquid.

7.10.4 Comparison with other Platreef localities and economic implications

The dominance of Pt and Pd tellurides and bismuthotellurides in the Platreef pyroxenites is common throughout the Platreef (Viljoen and Schürmann, 1998; Hutchinson and Kinnaird, 2005; Holwell *et al.*, 2006). Hutchinson and Kinnaird (2005) attributed the mineralogy of the PGM at Turfspruit, which is dominated by tellurides, antimonides and bismuthides, to be a result of the incorporation of S, As, Te, Bi and Sb into the Platreef magma from devolatilization of Dutchland Formation floor rocks. However, whilst this may be the case with Sb and As (antimonides and arsenides are very rare at Overysel), the ubiquity of Te and Bi along strike may suggest its presence in the Platreef magma was derived before emplacement, rather than as a local addition from floor rocks.

Away from the ubiquitous tellurides, the PGM mineralogy at Overysel contrasts sharply with that found further south where sediments form the floor. The major contrasts between Overysel and Sandsloot are the presence of PGE sulfides and paucity of antimonides and alloys at Overysel. Work by Armitage *et al.* (2002) and Holwell *et al.* (2006) have shown that fluid activity has exercised a considerable influence on the resulting mineralogy, distribution and BMS association of the PGE, particularly into the footwall at Sandsloot, with all of the antimonide and alloy dominated assemblages at Sandsloot occurring within rocks that have been subjected to significant fluid activity related. Such volatile activity is more uncommon at Overysel, except within and around calc-silicate xenoliths, and the extent of hydrothermal activity is governed by a fundamental footwall control. The dolomite floor at Sandsloot

released large volumes of fluids during assimilation and metamorphism, and subsequent serpentinization, whereas the largely anhydrous gneissic footwall at Overysel produced few volatiles. As a result of the lack of hydrothermal redistribution at Overysel, the PGE telluride-BMS association observed in the pyroxenites at this locality appear to be the most 'primary' mineralization style preserved, in terms of it being unaltered by fluids, and being a direct result of the fractional crystallization of a sulfide liquid. The ubiquity of this assemblage to varying degrees all along strike indicates a common initial mineralization style, but also that hydrothermal redistribution is highly variable along strike.

This study has revealed that the Platreef at Overysel preserves a mineralization style that is the product of the fractional crystallization of a sulfide liquid within the Platreef magma. Pyrrhotite and pentlandite host virtually all of the bulk Os, Ir and Ru. Virtually all the bulk Rh and some Pd is hosted by pentlandite, whereas virtually all Pt and Au, and some Pd form discrete PGM that are in close spatial association with BMS. This knowledge has obvious implications for exploration and mineral processing. More important, is the identification that extensive hydrothermal activity disrupts this assemblage by redistributing the PGE, changing the mineralogy, and often decoupling the PGE-BMS association. The amount of hydrothermal activity is fundamentally controlled by footwall lithology and for this reason, in different areas of the Platreef (and by implication other basal PGE-BMS deposits, where the assimilation of reactive footwall rocks has been extensive) the 'classic' primary associations are less likely to hold true throughout the reef. As a result, exploration for, and recovery of, the ore in such areas may suffer without detailed mineralogical investigations.

7.11 Conclusions

This combined PGM and LA-ICP-MS study has revealed the complex behaviour of the PGE during Platreef mineralization. A sulfide liquid originally concentrated PGE and semi metals such as Bi and Te in the Platreef magma at an early stage, before the crystallization of cumulus orthopyroxene, but concurrently with chromite. This possibly occurred in a deep staging chamber or conduit prior to intrusion. During post-intrusion crystallization of the sulfide, IPGE and Rh partition into early crystallizing mss, which on further cooling exsolved to pyrrhotite and pentlandite, with the IPGE remaining in solid solution within both phases and Rh partitioning preferentially into pentlandite. Virtually all Pt, Au and some Pd was concentrated with semi metals such as Bi and Te in a late stage melt with some excess Pd

partitioning into Ni-rich mss. This immiscible semi metal rich melt cooled to form PGM around the margins of the sulfide blebs. Tiny droplets trapped in the crystallized mss and formed PGM microinclusions. Some secondary redistribution by minor hydrothermal activity has occurred in and around xenoliths, and in the deepest zones of footwall mineralization, which typically form more bismuthide-dominated PGM assemblages and have led to the decoupling of PGM from sulfide minerals. Overall, however, the lack of hydrothermal interaction and overprinting compared to that observed in areas where sediments form the immediate footwall, raises the possibility that the Platreef at Overysel represents the most 'primary' style of Platreef mineralization. As such, the Platreef can be considered to be primarily an orthomagmatic PGE-Cu-Ni sulfide deposit.

7.12 Acknowledgements

The authors would like to thank the management of Anglo Platinum for giving permission to publish this work, and for allowing access to core from Overysel and to the Sandsloot mine. David Holwell's PhD research is funded by the Natural Environment Research Council and supported by Anglo Platinum through Industrial CASE project (NER/S/C/2003/11952). Pete Fisher is thanked for his assistance in the SEM analytical work at Cardiff University and Jay Cockayne for proof reading the manuscript. Constructive reviews by Chris Ballhaus and an anonymous referee are greatly acknowledged in improving the quality and focus of the manuscript.

Chapter 8

Sulfur isotope variations within the Platreef: genetic implications for the origin of sulfide mineralization

Submitted as:

D. A. Holwell, A. J. Boyce and I. McDonald. 2007. Sulfur isotope variations within the Platreef: genetic implications for the origin of sulfide mineralization. *Economic Geology*, (submitted, in review)

Co-author roles:

A. J. Boyce was involved in discussion on aspects involving the isotopic analyses and interpretation. I. McDonald was involved in discussion on the implications of the data in the regional context of the Platreef.

8.1 Abstract

The Platreef, the world's third largest platinum-group element (PGE) deposit, is a 10-400m pyroxenitic unit at the base of the northern limb of the mafic Bushveld Complex, hosting PGE mineralization in association with base metal sulfides. The sulfide mineralization is thought to have been either (i) largely magmatic in origin, with contamination by assimilation of local floor rocks considered an ore-modifying process, or (ii) that assimilation of country rock S and silicic contamination caused S saturation in the magma with contamination being fundamental to the ore-forming process. We have performed an extensive and detailed sulfur isotope study of the Platreef which indicates that magmatic signatures ($\delta^{34}\text{S} = 0$ to $+2\%$) are preserved in early formed sulfide droplets within the Platreef pyroxenites in the area from Sandsloot to Witrivier. These values are comparable to sulfide inclusions in diamonds in the nearby Klipspringer kimberlite and are considered to have a primary mantle origin. There is no indication of any significant external S in any of the primary sulfides in the Sandsloot-Witrivier area, however, later sulfides found in calc-silicate floor rocks at Sandsloot and Zwartfontein and in xenoliths of calc-silicate throughout the section indicate an input of country rock S. Anhydrite bearing horizons in the Malmani dolomites may have exchanged S with sulfide magmatic Platreef sulfide during extensive hydrothermal activity following Platreef intrusion, giving sulfides in the fluid affected rocks a heavier S isotope signature than the early formed sulfides. The Archaean basement, although it does contain minor amounts of sulfide, is not a significant contributor to the S budget of the Platreef. Previous studies have indicated that in areas where the sedimentary floor rocks contain appreciable sulfides, rather than sulfates, such as at Turfspruit, the Platreef sulfides are extensively contaminated with country rock S. Assimilation of pyrite-bearing shales in the Turfspruit area has locally upgraded the S content of the Platreef and given the basal Platreef sulfides a heavier isotopic signature.

Sulfur saturation in the Platreef magma took place before contamination, probably in a staging chamber prior to intrusion. A major pulse of magma entrained the pre-formed PGE-rich sulfides and was injected to form the Platreef, where assimilation of country rock sulfides upgraded the S content on a strictly local scale, and hydrothermal leaching introduced S from country rock sulfates into later stage sulfides, again on a local scale. South of Zwartfontein, it is proposed that the Platreef was intruded into sediments of the Transvaal Supergroup, which formed the floor and the roof of the Platreef. North of Zwartfontein, the Platreef intruded the boundary between the Malmani Supergroup sediments and the Archaean basement. This

could have potentially mineralized the roof calc-silicates north of Zwartfontein in a similar manner to the floor in the Sandsloot area. The later intrusion of the Main Zone magma formed a magmatic unconformity on top of the cold Platreef, and entrained large rafts of mineralized calc-silicate for tens of kilometres north of the last footwall outcrop of calc-silicate.

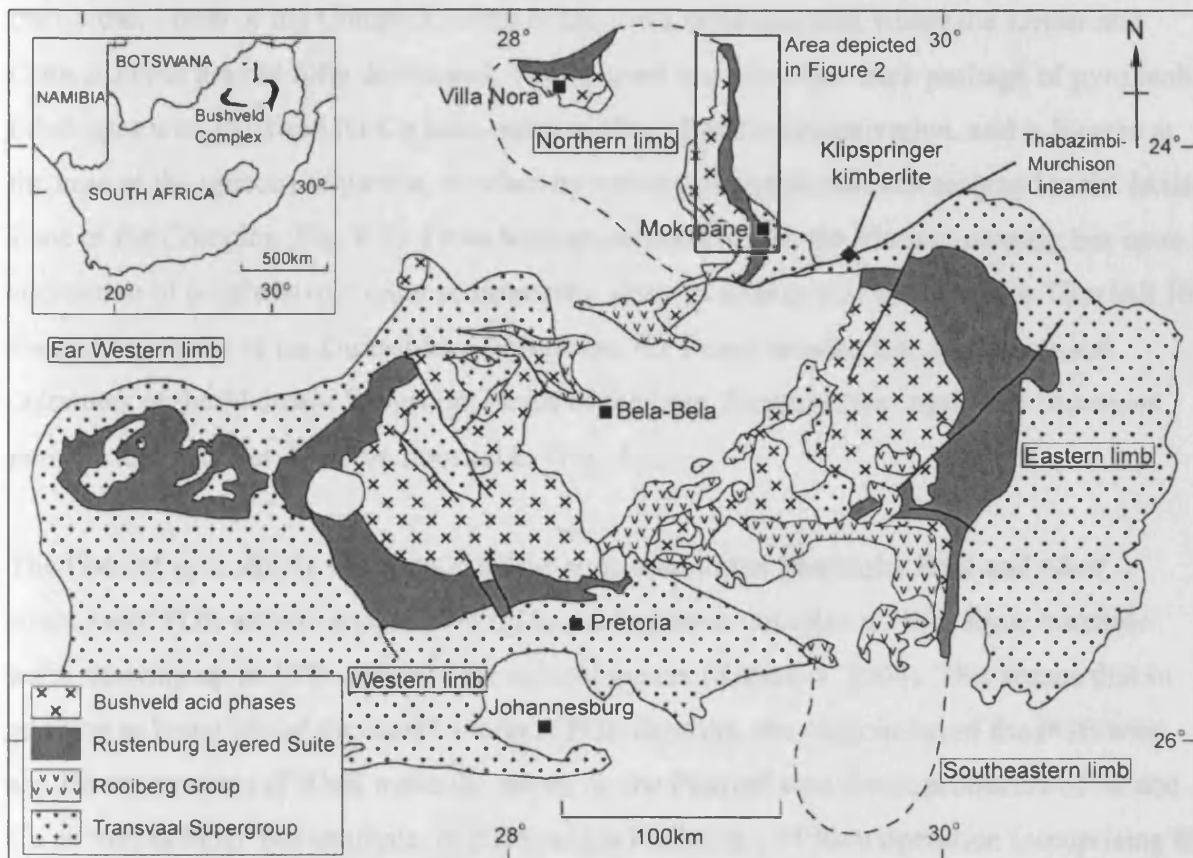


Figure 8.1. Geological map of the Bushveld Complex showing the location of the northern limb and the Klipspringer kimberlite (after Kinnaird *et al.*, 2005).

8.2 Introduction

The 2.06Ga Bushveld Complex is the world's largest layered igneous complex and is located in the north-eastern part of South Africa (Fig. 8.1). The Complex holds around 75% of the world's known resources of platinum-group elements (PGE), including the three largest deposits on earth: the UG2 chromitite, the Merensky Reef and the Platreef (Cawthorn, 1999). The Complex is made up of layered ultramafic and mafic cumulates intruded into Palaeoproterozoic sediments of the Transvaal Supergroup and Archaean granite/gneiss basement. The ultramafic-mafic sequence, known as the Rustenburg Layered Suite (Fig. 8.1),

is divided into five zones (Hall, 1932) comprising a Marginal Zone of norites, Lower Zone pyroxenites and harzburgites, Critical Zone chromitite-pyroxenite-norite cyclic units, Main Zone gabbro-norites and Upper Zone anorthosites, ferrogabbros and magnetites. The Complex is divided into five limbs: roughly symmetrical Eastern and Western limbs, a smaller Northern limb, plus a Southern limb covered by younger rocks and an extension of the Western limb to the west known as the Far Western limb (Fig. 8.1). The Platreef is located in the northern limb of the Complex, north of the town of Mokopane, where the Lower and Critical Zones are not fully developed. The Platreef is a 10-400m thick package of pyroxenitic lithologies with PGE and Ni-Cu base-metal sulfide (BMS) mineralization, and is located at the base of the igneous sequence, overlain by norites and gabbro-norites assigned to the Main Zone of the Complex (Fig. 8.2). From Mokopane northwards, the Platreef directly lies upon a succession of progressively older sedimentary units: quartzites and shales of the Timeball Hill Formation, shales of the Duitschland Formation, the Penge banded iron formation and dolomites of the Malmani Subgroup. North of the farm Zwartfontein, Archaean basement granites and gneisses form the floor rocks (Fig. 8.2).

The Platreef is relatively enriched in sulfur compared to the Merensky Reef and other stratabound PGE-sulfide deposits within layered igneous complexes, with some borehole cores showing up to 30% sulfides over several metres (Kinnaird, 2004). This means that in addition to being one of the world's largest PGE deposits, the association of the PGE with significant amounts of BMS make the mines on the Platreef significant producers of Ni and Cu as well as PGE. For example, in 2005 Anglo Platinum's PPRust operation (comprising the Sandsloot and Zwartfontein South mines) produced over 400,000 ounces of refined PGE along with 4600 tons of Ni and 2700 tons of Cu (Anglo Platinum Annual Report, 2005). Despite its major economic significance, the processes governing the formation of the mineralization are contentious, with the origin of sulfur key to the debate. Buchanan *et al.* (1981) concluded that the Platreef mineralization was the result of an initially sulfur-rich magma incorporating additional sulfur from the assimilation of sulfur bearing footwall rocks. Buchanan and Rouse (1984) agreed with this and added that silicic contamination from dolomite and granite triggered the precipitation of immiscible sulfides. Kruger (2005a) also advocated the assimilation of S from country rocks in the formation of the Platreef and Merensky Reef. In contrast, Barton *et al.* (1986) and Lee (1996) concluded that the sulfide mineralization was of primary magmatic origin, with pre-formed PGE-enriched sulfides introduced from a staging chamber and settling out along the base of the intrusion to form the

proto-Platreef. In these models, immiscible sulfide liquid precipitation and PGE enrichment predated interaction with the country rocks, and was not a consequence thereof. This study uses conventional and *in situ* laser sulfur isotope analyses of carefully paragenetically defined sulfides within the Platreef to test these competing theories and assess the role of contamination in triggering sulfur saturation in the Platreef.

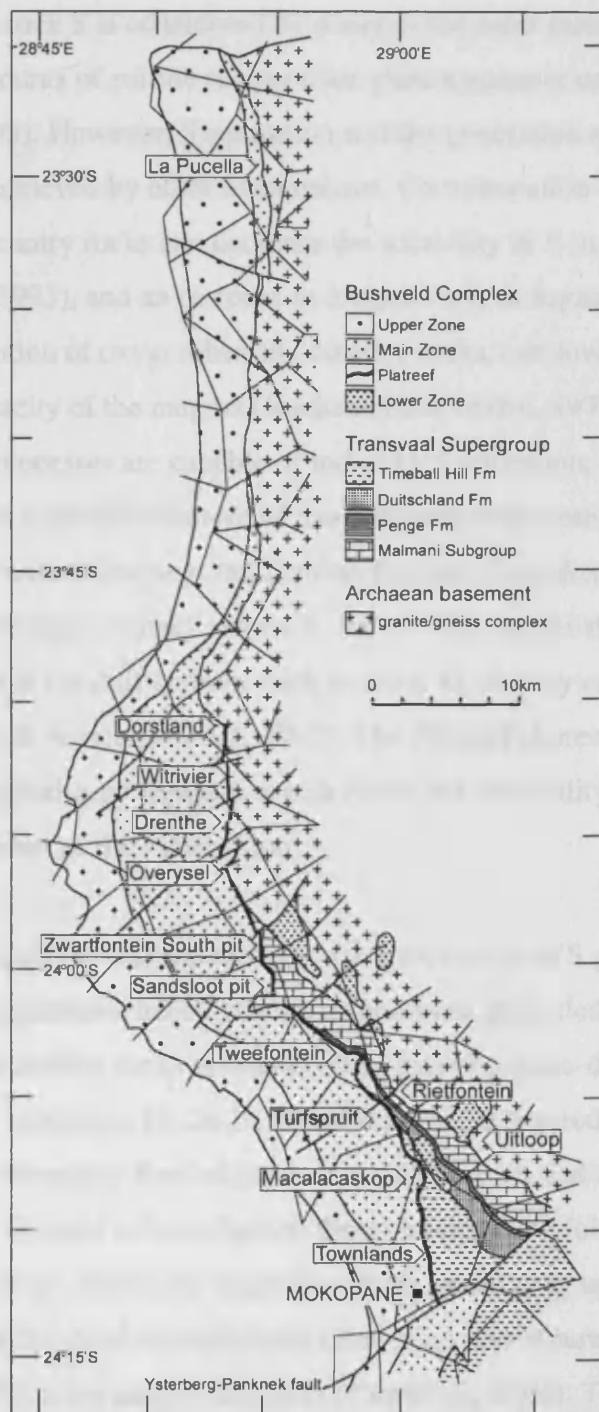


Figure 8.2. Geological map of the northern limb of the Bushveld Complex showing the localities referred to in the text (after van der Merwe, 1978).

8.3 Sulfur Saturation and the use of Sulfur Isotopes

The role of externally derived S is considered by many workers to be a critical factor in the development of magmatic Ni-Cu-PGE deposits. Assimilation of country rock S is considered essential in producing S saturation in high-degree mantle melts such as komatiites (e.g. Keays, 1995; Lambert *et al.*, 1998). In basaltic melts, such as those that formed the Bushveld Complex, although S saturation can be attained during low pressure fractionation, assimilation of country rock S is considered by many as the most reasonable mechanism for producing the large amounts of sulfide required for giant magmatic ore deposits (e.g. Li *et al.*, 2002; Ripley *et al.*, 2003). However, S saturation and the generation of economic sulfide mineralization can be achieved by other mechanisms. Contamination by silica due to the assimilation of felsic country rocks can decrease the solubility of S in a mafic magma (Irvine, 1975; Li and Naldrett, 1993), and an increase in magma oxygen fugacity, for example in response to the assimilation of oxygen-bearing country rocks, can lower the FeO content and thus the S-carrying capacity of the magma (Buchanan and Nolan, 1979). As a variety of contamination-related processes are capable of inducing S saturation, basal and marginal sulfide mineralization is a common feature of many layered intrusions. Examples include the Basal Series of the Stillwater Complex; the Penikat-Portimo Complex, Finland; the MuskoX intrusion, Canada; the Federov-Pansky intrusion, Russia (see compilation by Lee, 1996, and references therein); and in conduit systems such as Noril'sk (Ripley *et al.*, 2003) and the Uitkomst Complex, South Africa (Li *et al.*, 2002). The Platreef shares many characteristics with these basal or marginal-type deposits, which raises the possibility that contamination was a factor in the development of the Platreef too.

Sulfur isotopes can uniquely assess the role that externally derived S plays in mafic magmatic systems, providing a quantitative indicator of S assimilation, provided that the isotopic composition of S in the country rocks is distinct from that of mantle-derived S ($\delta^{34}\text{S}$ 0 \pm 2‰). Relatively sulfide-poor stratiform Ni-Cu-PGE reef deposits in layered mafic-ultramafic complexes such as the Merensky Reef of the Bushveld Complex and the J-M reef of the Stillwater Complex are thought to have formed through one of the following ways: magma mixing (e.g. Campbell *et al.*, 1983), by magmatic fluids percolating upwards through a crystal pile to be deposited at a chemical reaction front (Boudreau and Meurer, 1999), or due to pressure fluctuations within the magma chamber (Cawthorn, 2005). They are not considered to be the result of assimilation of external S, and S isotope studies of these S-poor deposits indicate little or no contribution from country rocks to the S budget, and all have isotopic

ratios indicative of mantle-derived S only (see compilation by Ripley and Li (2003), and references therein). In contrast, S-rich deposits such as Noril'sk, the Duluth Complex, Voisey's Bay (Ripley and Li, 2003) and the Uitkomst Complex (Li *et al.*, 2002) commonly display a wide range of $\delta^{34}\text{S}$ values indicating addition of crustally-derived S with variable $\delta^{34}\text{S}$ compositions.

In the primary magmatic scenario for the Platreef sulfide mineralization proposed by Barton *et al.* (1986) and Lee (1996), the S isotope signature of early-formed sulfides should be consistent with mantle values, although secondary sulfides and sulfides near the basal contact may show evidence of the addition of country-rock S. In the contamination-driven hypothesis advocated by Buchanan *et al.* (1981) and Buchanan and Rouse (1984), significant addition of S from contamination to produce S saturation in the Platreef would be reflected by a component of crustal S derived from the country rocks, and this should be present in sulfides throughout the Platreef succession. If silicic contamination occurred from S-poor country rocks, such as basement granites as suggested by Barton *et al.* (1986), then the S isotope ratio should retain a dominant mantle signature. If changes in $f\text{O}_2$ caused by assimilating country rock sediments triggered S saturation, the S isotope signature would be expected to show evidence of floor rock S input.

8.4 Previous Platreef S Isotope Work

A compilation of the Platreef S isotope data available in the literature is shown in Fig. 8.3. Until very recently, the only S isotope work that had been performed on the Platreef was by Buchanan *et al.* (1981) and Buchanan and Rouse (1984), who presented limited data for various sulfides from the farms Tweefontein and Turfspruit, including a $\delta^{34}\text{S}$ value of +7.1‰ in a sample of sulfate from the evaporite-bearing Malmani Subgroup. Their pyroxenite values between +2.7 and +6.3‰ for Tweefontein were considered to be magmatic signatures, with the elevated values attributed to contamination by anhydrite from the Malmani Subgroup. Additional data from the farm Turfspruit (Fig. 8.2) was presented by Buchanan and Rouse (1984), including anhydrite associated with the Deutschland Formation with a $\delta^{34}\text{S}$ value of +17‰. The data of these two studies are, however, very limited and an effort to assess the least contaminated, most magmatic sulfides was not made, and therefore the interpretations should be viewed with caution.

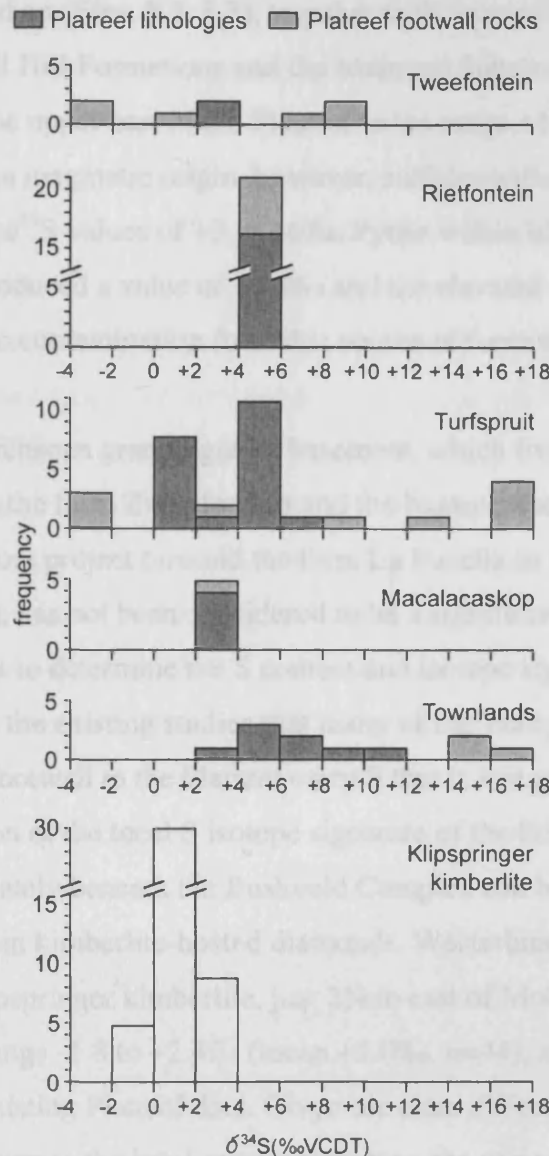


Figure 8.3. Summary of previous S isotope data on the Platreef and sulfide inclusions in diamonds from the nearby Klipspringer kimberlite. Tweefontein data from Buchanan *et al.* (1981) and Buchanan and Rouse (1984), Rietfontein data from Sharman-Harris *et al.* (2005), Turfspruit data from Buchanan and Rouse (1984) and Sharman-Harris *et al.* (2005), Macalacaskop data from Sharman-Harris *et al.* (2005), Townlands data from Manyeruke *et al.* (2005) and Klipspringer kimberlite data from Westerlund *et al.* (2004).

It was over twenty years before any further work on Platreef S isotopes was produced.

Manyeruke *et al.* (2005) published data for sulfides in the Platreef on the farm Townlands (Fig. 8.2) that displayed $\delta^{34}\text{S}$ values ranging from +2.6 to +10.1‰ (Fig. 8.3), indicating an element of isotopically heavy external S contamination, with footwall rocks of the Timeball Hill Formation displaying $\delta^{34}\text{S}$ values in the range +14 to +17‰. A more detailed study by Sharman-Harris *et al.* (2005) presented data for the Platreef on the farms Rietfontein,

Turfspruit and Macalacaskop (Figs. 8.2, 8.3), together with footwall lithologies from the Duitschland and Timeball Hill Formations and the Malmani Subgroup. They reported $\delta^{34}\text{S}$ values of sulfides from the upper part of the Platreef in the range +1.1 to +1.8‰, which the authors consider to be of a magmatic origin, however, sulfides within the lower 180m of the Platreef package showed $\delta^{34}\text{S}$ values of +3 to +6‰. Pyrite within black shales of the Duitschland Formation produced a value of +8.2‰ and the elevated values in the lower Platreef were attributed to contamination from this source of footwall sulfide.

Prior to this study, the Archaean granite/gneiss basement, which forms the floor to the Platreef northwards from the farm Zwartfontein and the basement to the Main Zone-hosted PGE deposits on the Aurora project (around the farm La Pucella in the far north of the Northern limb – Fig. 8.2), has not been considered to be a significant source of S, and no work has been carried out to determine the S content and isotope signatures of these rocks. However, it is clear from the existing studies that many of the Transvaal Supergroup sediments that form the footwall to the Platreef carry S that is isotopically heavier than magmatic S. An indication of the local S isotope signature of the lithospheric mantle of the Kaapvaal Craton immediately beneath the Bushveld Complex can be estimated from a suite of sulfide inclusions within kimberlite-hosted diamonds. Westerlund *et al.* (2004) analyzed such a suite from the Klipspringer kimberlite, just 25km east of Mokopane (Fig. 8.1), which gave $\delta^{34}\text{S}$ values in the range -1.8 to +2.4‰ (mean +1.0‰, $n=44$), and these are plotted on Fig. 8.3 along with the existing Platreef data. Given the clear difference in S isotope signature of the Transvaal Supergroup to the local mantle signature, the use of S isotopes to assess the role of contamination in the Platreef is clearly vindicated.

This study aims to use S isotopes to examine the origin(s) of S in the Platreef, and quantitatively assess the role of contamination in the development of the mineralization, with consequent genetic implications for the origin of the deposit. In addition, we investigate the S isotope signature of the Archaean basement rocks in the vicinity of the northern limb of the Bushveld Complex.

8.5 Samples and Methods

Samples for this study were collected from Anglo Platinum's open pit mines at Sandsloot and Zwartfontein South, and from two borehole cores drilled on the farm Overysel (Fig. 8.2). One borehole core drilled through the Platreef and additional samples of Archaean basement on the farm Witrivier were sampled from drillcore archived by Anooraq Resources. Samples of Archaean basement were also collected from several boreholes on Pan Palladium's Aurora Project, on the farm La Pucella (Fig. 8.2). The sample suite covers a full range of Platreef lithologies, as well as mineralization at the base of the hangingwall and mineralized rocks from a variety of footwall lithologies and xenoliths. This is by far the largest, most geographically extensive and texturally diverse suite of Platreef samples that has ever been analyzed for S isotopes. A schematic representation of the lithologies present along the strike section we have sampled is shown in Fig. 8.4. Detailed maps of the rock relationships at Sandsloot are given in Armitage *et al.* (2002) and McDonald *et al.* (2005), and at Zwartfontein South by Holwell and Jordaan (2006). Detailed lithological logs of the borehole cores from Overysel are given in Holwell and McDonald (2006).

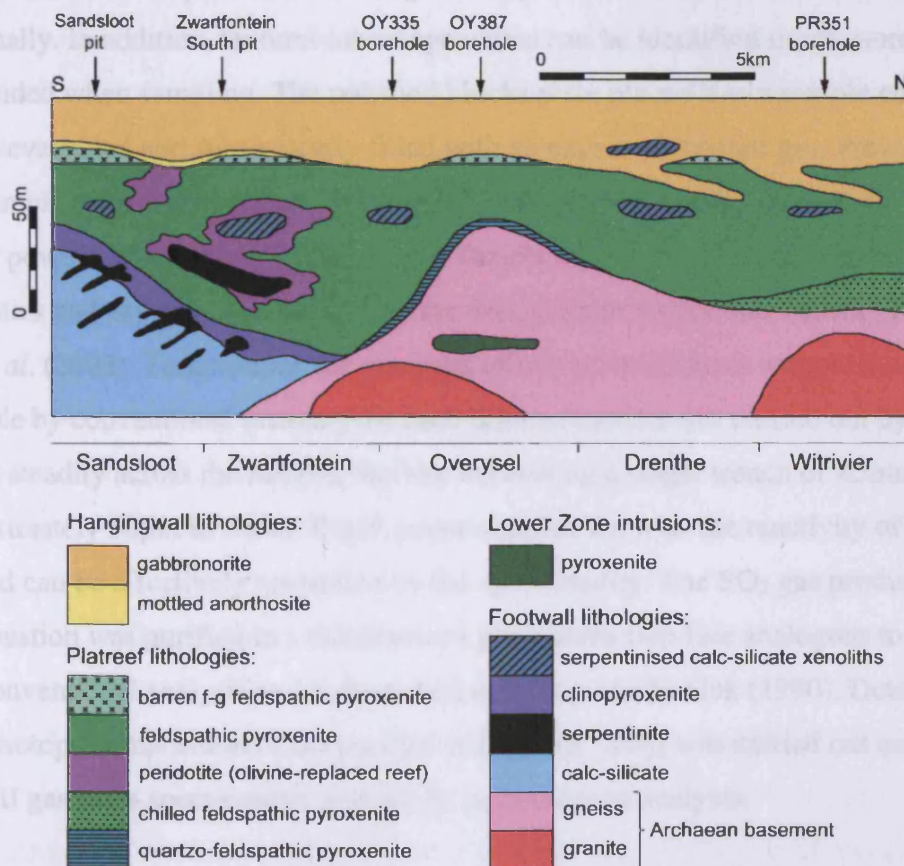


Figure 8.4. Schematic cross section showing the major lithologies encountered along strike of the Platreef and the corresponding positions of the sample localities.

Sulfide samples for conventional analysis were selected on the basis of textural and compositional homogeneity by reflected-light microscopy. Sulfides were micro-drilled from polished slabs and subsequently converted to SO₂ for mass spectrometric analysis by combustion with cuprous oxide, following the procedure of Robinson and Kusakabe (1975). Samples were combusted under vacuum at 1070°C for 25 minutes, and the SO₂ gas produced was cryogenically purified using a CO₂/acetone slush trap to remove water and a standard n-pentane trap to separate SO₂ and trace CO₂, prior to analysis on a VG SIRA II gas mass spectrometer. Raw machine $\delta^{66}\text{SO}_2$ data were converted to $\delta^{34}\text{S}$ values by calibration with international standards NBS-123 (+17.1‰) and IAEA-S-3 (-31‰), as well as SUERC's internal lab standard CP-1 (-4.6‰). Reproducibility of the analytical results was controlled through replicate measurements of these standards. All sulfur isotope compositions were calculated relative to Vienna Canon Diablo Troilite (V-CDT), and are reported in standard notation.

A series of *in situ* laser combustion analyses were performed on polished slabs of 48 samples. The laser ablation technique allows analysis of samples that would be too small to analyze conventionally. In addition, textural inhomogeneities can be identified much more efficiently and be avoided when sampling. The polished blocks were placed into a sample chamber, which was evacuated and subsequently filled with an excess of oxygen gas. Previously selected sample areas were combusted using a SPECTRON LASERS 902Q CW Nd-YAG laser (1-W power), operating in TEM₀₀ mode. Details of the system design, laser characteristics and experimental conditions are described in Kelley and Fallick (1990) and Wagner *et al.* (2002). To minimize the potential effects of small-scale sample heterogeneity undetectable by conventional preanalysis, each laser extraction was carried out by moving the laser beam steadily across the sample, thereby excavating a single trench of <3mm in length and approximately 50µm in width. Depth penetration varies with the reactivity of each mineral and can be effectively controlled by the spot velocity. The SO₂ gas produced by each laser combustion was purified in a miniaturized glass extraction line analogous to the one used for conventional analysis and is described in Kelley and Fallick (1990). Determination of the sulfur isotope composition of the purified SO₂ gas ($\delta^{66}\text{SO}_2$) was carried out on-line by the VG SIRA II gas mass spectrometer as used for conventional analysis.

During the laser ablation technique, there is a systematic fractionation of $\delta^{34}\text{S}$ values of the resulting SO₂ gas compared to the mineral $\delta^{34}\text{S}$, and small correction factors are required to

allow for this (Wagner *et al.*, 2002). We calculated the fractionation factors based on repeated laser and conventional analyses of individual sulfide phases during this study. Table 8.1 lists the corrected laser data and the fractionation factors.

Whole rock sulfur concentrations were determined by standard combustion iodometric procedures using a Laboratory Equipment Company (LECO) titrator at the Camborne School of Mines, UK. Depending on sulfide content, between 0.1g and 1.0g of sample were combusted for each titration. Consistent results were obtained re-running blanks, standards and selected samples in triplicate. The standard deviations of the weight percentage of S in the samples run in triplicate ranged from 0.0015 to 0.0572, with a mean of 0.0146.

8.6 Petrology and Mineralization

The petrology of the reef and its footwall at Sandsloot are described in detail by Armitage *et al.* (2002), McDonald *et al.* (2005) and Holwell *et al.* (2006), at Zwartfontein by Holwell and Jordaan (2006) and at Overysel by Holwell and McDonald (2006) and are summarized here. Fig. 8.4 shows a generalized section through the lithologies present along the strike of the Platreef, which were sampled for this study. The footwall at Sandsloot and Zwartfontein is made up of variably serpentinized calc-silicates derived from metamorphism of the Malmani Subgroup, and a unit of metamorphic clinopyroxenite at the contact with the overlying feldspathic pyroxenites of the Platreef. The feldspathic pyroxenites contain >70% cumulus orthopyroxene with intercumulus plagioclase and clinopyroxene. At the top of the Platreef succession, a fine-grained feldspathic pyroxenite barren of mineralization is often present. The pyroxenites are occasionally altered to olivine-bearing lithologies and contain abundant xenoliths of variably serpentinized calc-silicate. Veins of quartz-feldspar-calcite cross-cut all lithologies and are most common at Sandsloot and Zwartfontein. The footwall north of Zwartfontein, including Overysel, Drenthe, Witrivier and La Pucella, comprises Archaean basement made up of banded gneisses containing quartz, Na-rich plagioclase and orthopyroxene, and granites. The gneisses at Overysel have undergone partial melting during the intrusion of the Platreef (Cawthorn *et al.*, 1985; Holwell and McDonald, 2006). As a result, the lowermost Platreef pyroxenites contain abundant quartz. At Drenthe and Witrivier, the uppermost part of the Platreef pyroxenites is intruded by a body of gabbroites thought to be of hangingwall affinity (Naldrett, 2005). The base of the pyroxenites at Witrivier is very fine-grained and appears chilled against the footwall gneisses and granites. The hangingwall

along the entire strike length is made up of gabbro-norites and norites, with a thin (<1m) mottled anorthosite often present at the very base of the hangingwall that is particularly common at Sandsloot, Zwartfontein and Turfspruit.

8.6.1 Sulfide mineralization

Stratigraphically, PGE and BMS mineralization is heterogeneously distributed throughout the pyroxenitic Platreef lithologies. The richest mineralization is usually hosted by medium- or coarse-grained feldspathic pyroxenites and typically makes up around 2-3% of the modal mineralogy, although the stratigraphic position of the most mineralized portions can vary on a scale of tens of metres. There are sporadic, thin zones of mineralization at the very base of the hangingwall that are almost always in contact with underlying mineralized Platreef pyroxenite (Holwell *et al.*, 2005). The mineralization can also extend to some considerable depths into both the metasedimentary and gneissic footwall, the extent and volume of which also varies considerably on a local scale.

Texturally, PGE mineralization is usually associated with BMS in unaltered reef sections. The most primary sulfide texture is illustrated in Figs. 8.5a and b, and is of fractionated blebs of sulfide comprising a core of pyrrhotite, with pentlandite and chalcopyrite around the margins residing as interstitial phases between cumulus orthopyroxene grains within the feldspathic pyroxenites. Pentlandite also occurs as exsolution flames within pyrrhotite (Figs. 8.5a, c). Pyrrhotite and pentlandite are the cooling products of monosulfide solid solution which is the first phase to crystallize from a sulfide liquid, with the residual sulfide liquid forming intermediate solid solution, which on cooling forms chalcopyrite and some pentlandite (e.g. Barnes *et al.*, 2006). Whilst all these sulfides are actually low temperature phases, we refer to this textural association in the feldspathic pyroxenites as the most 'primary' in that they are unaltered, and are the direct cooling product of a fractionating sulfide liquid within the Platreef magma.

In the footwall gneisses at Overysel, the sulfide assemblage is similar to the reef pyroxenites and texturally, the sulfides occur around rounded silicate grains (Fig. 8.5d) that Holwell and McDonald (2006) have interpreted to be the product of the percolation of a sulfide liquid through a network of inter-granular pore-space, formed during partial melting of the footwall gneisses. Massive sulfides (Fig. 8.5c) occur close to the Platreef contact and at depth within the gneissic footwall, and Holwell and McDonald (2006) have suggested that these were

likely to occur above zones of low permeability where the downward migration of the sulfide liquid was restricted or not possible. The assemblages deeper into the footwall can become more chalcopyrite dominated (Fig. 8.5d). In all the above assemblages, platinum-group minerals (PGM) are commonly located around the margins of the sulfide blebs.

In parts of the reef that have undergone significant fluid interaction, such as in serpentinites and calc-silicates, PGE and BMS are often decoupled, and the sulfide textures are less consistent. Although pyrrhotite, pentlandite and chalcopyrite remain the major phases, they are joined by pyrite, bornite, galena, chalcocite and a host of minor sulfide phases. Fig. 8.5e illustrates the more disseminated nature of sulfide mineralization within a sample of calc-silicate, and the lack of the well defined phase zonation that is seen in the 'primary' blebs. In serpentinitized footwall rocks, chalcopyrite is rare, and granular pyrrhotite and pentlandite are often altered to magnetite (Fig. 8.5f). All of these assemblages within metasedimentary rocks, or hydrothermally altered rocks, that lack the zoned, fractionated textures of the blebs within the reef, we have termed 'secondary', in that they are not the direct *in situ* cooling product of a sulfide within the Platreef magma, having undergone significant hydrothermal redistribution. However, they are directly related to the Platreef sulfides in that they have associated PGE mineralization.

The Archaean basement rocks north of Zwartfontein contain some sulfide mineralization. This relatively low-volume mineralization consists of disseminated pyrite, millerite and chalcopyrite within basement gneisses, granites and amphibolites (Fig. 8.5g). This is unrelated to the main Platreef mineralizing event due to the lack of associated PGE mineralization and distinct sulfide assemblages. We have termed these 'basement' sulfides to distinguish that they are not Platreef related.

Late-stage veins containing calcite, quartz and feldspar, locally referred to as quartzo-feldspathic, or QF, veins contain sporadic sulfide mineralization. The sulfide assemblage is very different to that in the Platreef, and is made up of large blebs and veins of most commonly chalcopyrite (Fig. 8.5h), with some galena, sphalerite, bornite, pyrrhotite and pentlandite. Due to the cross-cutting nature of these veins and their clearly post-Platreef and lower Main Zone age, we have distinguished these as 'late stage' sulfides.

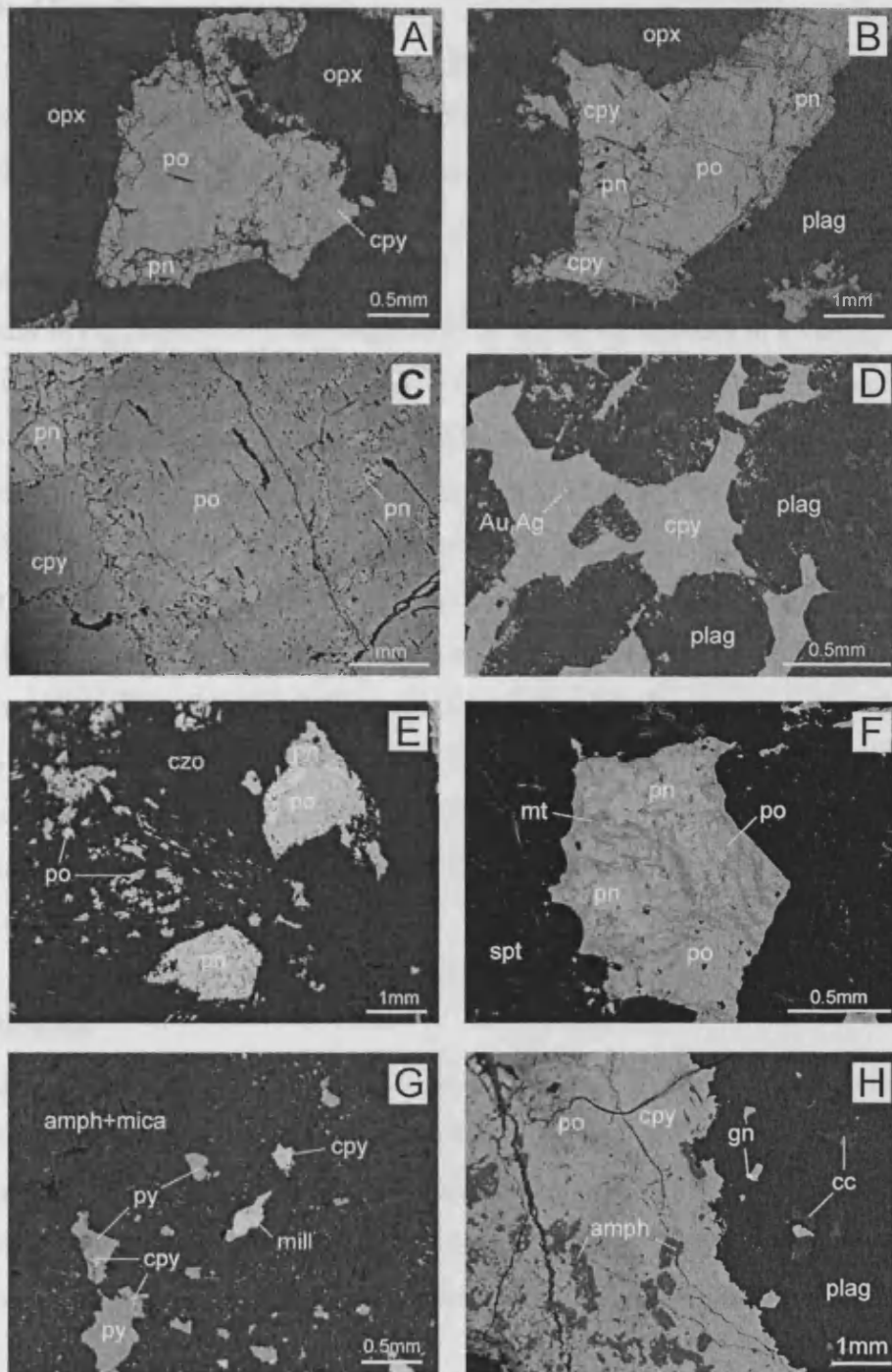


Figure 8.5. Backscattered electron photomicrographs of sulfides from the Platreef. (A – SNN1-8) and (B – DH-P): interstitial fractionated sulfide blebs made up of pyrrhotite (po) with pentlandite (pn) and chalcopyrite (cpy) rims surrounded by cumulus orthopyroxene (opx) and intercumulus plagioclase (plag); (C): massive sulfide from the footwall at Overysel (sample OY387-381); (D): chalcopyrite dominated assemblage with electrum (Au,Ag) in gneiss (OY335-316) from the base of the OY387 core; (E): disseminated sulfide within clinzoisite (czo) from within calc-silicate footwall rock at Sandsloot (SNS1-40); (F): altered sulfide assemblage of pyrrhotite and pentlandite from within a serpentinized footwall calc-silicate from Sandsloot (SNS1-39). Magnetite (mt) replaces the sulfides that are surrounded by serpentinite (spt). (G): disseminated assemblage of pyrite (py), millerite (mill) and chalcopyrite within amphibolite xenolith in Archaean basement granite at Witrivier (PR369-44). (H): vein of chalcopyrite and pyrrhotite with galena (gn) in a late stage cross cutting vein from Sandsloot (SNN1-65) containing plagioclase and calcite (cc).

8.7 Analytical Results

The results of over 120 analyses of sulfides from the Platreef and associated country rocks on the farms Sandsloot, Zwartfontein, Overysel, Witrivier and La Pucella are listed in Table 8.1. Where available, corresponding whole-rock S concentrations are also given.

8.7.1 Sandsloot

The histogram in Fig. 8.6a shows the range of $\delta^{34}\text{S}$ values for sulfides in a variety of rock types from the Sandsloot pit. The range in $\delta^{34}\text{S}$ for primary sulfides in the Platreef feldspathic pyroxenites is 0 to +2.6‰, with a mean of +1.8‰. Footwall calc silicates and xenoliths of serpentized calc-silicate contain sulfides with slightly heavier $\delta^{34}\text{S}$ values in the range +2.5 to +6‰, although not all footwall rocks display heavy signatures. A large bleb of sulfide in a footwall serpentinite (SNS1-39) had some of the lightest $\delta^{34}\text{S}$ values of all the Sandsloot samples at +0.3‰. The analysis from a sample of hangingwall mottled anorthosite (SNN1-7a – Table 8.1) gave a $\delta^{34}\text{S}$ value of +2.2‰, which is almost identical to the feldspathic pyroxenites that it rests upon (+1.8 to +2.6‰; SNN1-8, 18a, 37 - Table 8.1). The analyses from olivine-replaced reef gave variable $\delta^{34}\text{S}$ values of +1.4 and +3.1‰. Chalcopyrite, pyrrhotite and sphalerite in late-stage quartz-feldspar-calcite veins gave consistently heavy signatures of around +8‰.

8.7.2 Zwartfontein

Data from the Zwartfontein South pit are shown in Fig. 8.6b. Primary sulfide in the Platreef pyroxenites gave $\delta^{34}\text{S}$ values between -0.6 and +1.9‰ (mean +0.7‰). Olivine-replaced reef samples produced similar values, as did some chalcopyrite within a calc-silicate xenolith. Veins of pyrite within a sample of sheared serpentinite, which formed the upper contact of the Platreef against hangingwall mottled anorthosite, gave a slightly heavier $\delta^{34}\text{S}$ value of +3.2‰.

8.7.3 Overysel

The histogram in Fig. 8.6c displays the range in $\delta^{34}\text{S}$ of sulfides in a variety of rock types from the two cores drilled on the farm Overysel. In addition, the data from cores OY335 and OY387 are plotted with depth in Figs. 8.7a and b. Virtually all the analyses from the Platreef pyroxenites have $\delta^{34}\text{S}$ values of around +2‰ (mean +1.8‰), comparable to that at Sandsloot. No analyses gave results heavier than +2.1‰. One sample of quartzo-feldspathic pyroxenite, which is at the base of the pyroxenite package in core OY387, produced a slightly heavier $\delta^{34}\text{S}$ signature of +2.4‰.

Table 8.1. Results of all conventional (c) and laser (l) S isotope analyses for Platreef sulfides together with whole rock S concentrations where available from Sandsloot, Zwartfontein, Overysel and Witrivier, and Archaean basement rocks from Witrivier and La Pucella. Abbreviations of sulfide phases: po – pyrrhotite; pn – pentlandite; cpy – chalcopyrite; sph – sphalerite; py – pyrite; mill – millerite. Fractionation factors used to correct laser data: po -1.0, pn -1.6, cpy -1.5, py -1.3.

Sample	Lithology	Sulfide	texture	$\delta^{34}\text{S}(\text{‰VCDT})$	wt%S	c/l
Sandsloot central						
DH-P2	Pegmatitic feldspathic pyroxenite	po	primary	+1.9		c
SNS1-29	Feldspathic pyroxenite	cpy	primary	+0.3	0.696	l
SNS1-31a	Pegmatitic feldspathic pyroxenite	po	primary	+1.3	0.506	l
SNS1-35	Footwall clinopyroxenite	po	secondary	+4.1	1.384	c
SNS1-35	Footwall clinopyroxenite	po	secondary	+5.0	1.384	l
SNS1-39	Serpentinized footwall	pn	secondary	+1.4	10.391	l
SNS1-39	Serpentinized footwall	pn	secondary	+0.3	10.391	l
SNS1-40	Calc-silicate	po(+pn)	secondary	+2.7	0.486	c
Sandsloot north						
SNN1-7a	Mottled anorthosite	po	primary	+2.2	0.039	l
SNN1-8	Feldspathic pyroxenite	po(+pn)	primary	+1.8	0.785	c
SNN1-8	Feldspathic pyroxenite	pn	primary	+2.2	0.785	l
SNN1-18a	Feldspathic pyroxenite	po(+pn)	primary	+2.3	0.494	c
SNN1-18a	Feldspathic pyroxenite	po(+pn)	primary	+2.6	0.494	c
SNN1-37	Pegmatitic feldspathic pyroxenite	po(+pn)	primary	+2.1	0.320	c
SNN1-40	Serpentinized calc-silicate xenolith	po	secondary	+4.2	2.628	c
SNN1-40	Serpentinized calc-silicate xenolith	po	secondary	+4.8	2.628	c
SNN1-40	Serpentinized calc-silicate xenolith	po	secondary	+5.8	2.628	l
SNN1-43	Peridotite (olivine replaced reef)	po(+pn)	secondary	+3.1	2.298	c
SNN1-43	Peridotite (olivine-replaced reef)	cpy	secondary	+1.4	2.298	l
SNN1-65	Quartzo-feldspathic vein	cpy	secondary	+8.6	0.683	c
SNN1-65	Quartzo-feldspathic vein	cpy	secondary	+8.5	0.683	c
SNN1-65	Quartzo-feldspathic vein	cpy	secondary	+8.1	0.683	c
SNN1-65	Quartzo-feldspathic vein	cpy	secondary	+8.1	0.683	c
SNN1-65	Quartzo-feldspathic vein	cpy	secondary	+8.2	0.683	l
SNN1-65	Quartzo-feldspathic vein	po	secondary	+8.0	0.683	l
SS-05	Quartzo-feldspathic vein	cpy	secondary	+11.1		c
SS-07	Quartzo-feldspathic vein	sph	secondary	+7.6		c
Zwartfontein South						
ZSS1-98	Feldspathic pyroxenite	po	primary	+0.9	0.201	l
ZSS1-98	Feldspathic pyroxenite	cpy	primary	+1.9	0.201	l
ZSE1-20	Feldspathic pyroxenite	pn	primary	-0.6		l
ZSE2-70	Feldspathic pyroxenite	po	primary	+0.8		l
ZSE2-70	Feldspathic pyroxenite	cpy	primary	+0.7		l
ZSN3-52	Serpentinized pyroxenite	pn	secondary	+1.8		c
ZSN3-52	Serpentinized pyroxenite	cpy	secondary	+0.9		c
ZSN3-14	Serpentinized pyroxenite	po	secondary	+1.9		c
ZSN3-47	Serpentinite	py	secondary	+3.2		l
ZSE2-20	Calc-silicate	cpy	secondary	+1.9		l
Overysel OY335						
OY335-176	Feldspathic pyroxenite	po	primary	+1.5	1.022	c
OY335-182	Feldspathic pyroxenite	po+pn	primary	+1.7	0.981	c
OY335-193	Altered feldspathic pyroxenite	po(+pn)	primary	+2.0	0.242	c
OY335-193	Altered feldspathic pyroxenite	pn	primary	+2.1	0.242	l
OY335-218	Serpentinized xenolith	po	secondary	+2.5	0.054	l
OY335-230	Altered feldspathic pyroxenite	pn	late stage	+1.8	0.500	c
OY335-230	Altered feldspathic pyroxenite	pn	late stage	+2.0	0.500	l
OY335-230	Altered feldspathic pyroxenite	pn	late stage	+1.9	0.500	l
OY335-253	Intrusive norite	pn	primary	+2.5	0.356	l
OY335-275	Altered feldspathic pyroxenite	pn	primary	+2.0	0.621	l
OY335-275	Altered feldspathic pyroxenite	cpy	primary	+1.4	0.621	l
OY335-310	Gneiss	po(+pn)	secondary	+3.1	0.107	c
OY335-310	Gneiss	pn	secondary	+3.1	0.107	c
OY335-310	Gneiss	po	secondary	+2.1	0.107	l
OY335-323	Gneiss	pn	secondary	+1.6	0.048	l
Overysel OY387						
OY387-246	Feldspathic pyroxenite	py	primary	+2.0	0.423	l
OY387-252	Feldspathic pyroxenite	cpy	primary	+2.0	1.265	l
OY387-252	Feldspathic pyroxenite	pn	primary	+0.4	1.265	l

Table 8.1 (cont.).

Sample	Lithology	Sulfide	texture	$\delta^{34}\text{S}(\text{‰VCDT})$	wt%S	c/l
OY387-252	Feldspathic pyroxenite	pn	primary	+2.0	1.265	l
OY387-258	Feldspathic pyroxenite	po(+pn)	primary	+2.0	0.519	c
OY387-258	Feldspathic pyroxenite	po	primary	+1.7	0.519	l
OY387-260	Quartz vein	py	secondary	+4.0		c
OY387-260	Quartz vein	py	secondary	+3.6		c
OY387-260	Quartz vein	py	secondary	+3.8		l
OY387-260	Quartz vein	py	secondary	+3.7		l
OY387-272	Quartzo-feldspathic pyroxenite	po	primary	+2.3	1.591	l
OY387-272	Quartzo-feldspathic pyroxenite	pn	primary	+2.4	1.591	l
OY387-364	Amphibolitic gneiss	po	secondary	+3.5	0.479	l
OY387-378	Net-textured sulfide in gneiss	po	secondary	+4.9	7.726	c
OY387-378	Net textured sulfide in gneiss	po	secondary	+4.6	7.726	l
OY387-380	Gneiss	cpy	secondary	+4.7	1.253	c
OY387-381	Massive sulfide	cpy	secondary	+3.2	38.750	c
OY387-381	Massive sulfide	po	secondary	+4.3	38.750	c
OY387-381	Massive sulfide	po	secondary	+5.1	38.750	c
OY387-381	Massive sulfide	cpy2	secondary	+4.8	38.750	c
OY387-381	Massive sulfide	cpy1	secondary	+5.0	38.750	c
OY387-381	Massive sulfide	cpy	secondary	+3.8	38.750	l
OY387-381	Massive sulfide	cpy	secondary	+4.5	38.750	l
OY387-381	Massive sulfide	po	secondary	+5.3	38.750	l
OY387-381	Massive sulfide	cpy1	secondary	+2.1	38.750	l
OY387-381	Massive sulfide	pn	secondary	+4.5	38.750	l
OY387-384	Lower Zone pyroxenite	cpy	secondary	+4.8	1.788	c
OY387-384	Lower Zone pyroxenite	cpy	secondary	+5.1	1.788	l
OY387-395	Gneiss	cpy	secondary	+3.4	0.481	l
OY387-415	Gneiss	cpy	secondary	+2.1	0.247	l
OY387-423	Gneiss	pn(+cp)	secondary	+4.6	1.003	c
OY387-438	Granite	cpy	secondary	+4.9	0.126	l
Witrivier						
PR351-44	Gabbroonrite	pn(+po)	secondary	+4.1		c
PR351-44	Gabbroonrite	po	secondary	+3.0		l
PR351-44	Gabbroonrite	pn	secondary	+2.0		l
PR351-44	Gabbroonrite	cpy	secondary	+2.9		l
PR351-51	Feldspathic pyroxenite	po	primary	+0.9		l
PR351-51	Feldspathic pyroxenite	pn	primary	+0.2		l
PR351-59	Massive sulfide bleb in serpentinite	po2	secondary	+3.7		c
PR351-59	Massive sulfide bleb in serpentinite	po1	secondary	+4.2		c
PR351-59	Massive sulfide bleb in serpentinite	cpy	secondary	+1.4		c
PR351-59	Massive sulfide bleb in serpentinite	po2	secondary	+0.8		c
PR351-59	Massive sulfide bleb in serpentinite	po1	secondary	+1.6		l
PR351-59	Massive sulfide bleb in serpentinite	po2	secondary	+3.7		l
PR351-59	Massive sulfide bleb in serpentinite	po2	secondary	+2.5		l
PR351-59	Massive sulfide bleb in serpentinite	cpy	secondary	+1.2		l
PR351-65	Feldspathic pyroxenite	po	primary	+1.8		l
PR351-75	Feldspathic pyroxenite	po	primary	+2.0		c
PR351-75	Feldspathic pyroxenite	po	primary	+2.0		l
PR351-88	Feldspathic pyroxenite	py	primary	+0.9		c
PR351-88	Feldspathic pyroxenite	py	primary	-0.4		l
PR351-88	Feldspathic pyroxenite	cpy	primary	-0.7		l
PR351-94	Feldspathic pyroxenite	pn	primary	+1.7		c
PR351-94	Feldspathic pyroxenite	pn	primary	+1.1		l
PR351-107	Chilled feldspathic pyroxenite	po	primary	+2.2		c
PR351-107	Chilled feldspathic pyroxenite	po	primary	+0.5		l
PR351-107	Chilled feldspathic pyroxenite	py	primary	+0.3		l
PR351-112	Granite	cpy	secondary	+2.1		c
PR351-112	Granite	cpy	secondary	+2.1		c
PR351-115	Granite	cpy	basement	-1.7		l
PR351-115	Granite	mill	basement	-1.9		l
PR369-44	Amphibolite xenolith in granite	py	basement	-1.2		l
La Pucella						
DH20 (LAP29)	Granite	py	basement	-1.5		l
DH21 (LAP26)	Granite	py	basement	+0.1		l
DH22 (LAP31)	Granite	cpy	basement	+0.5		l
DH23 (LAP47)	Granite	py	basement	+1.3		c
DH23 (LAP47)	Granite	cpy	basement	-0.9		l
DH24 (LAP47)	Granite	py	basement	+0.2		l
DH25 (LAP52)	Granite	py	basement	+0.8		l

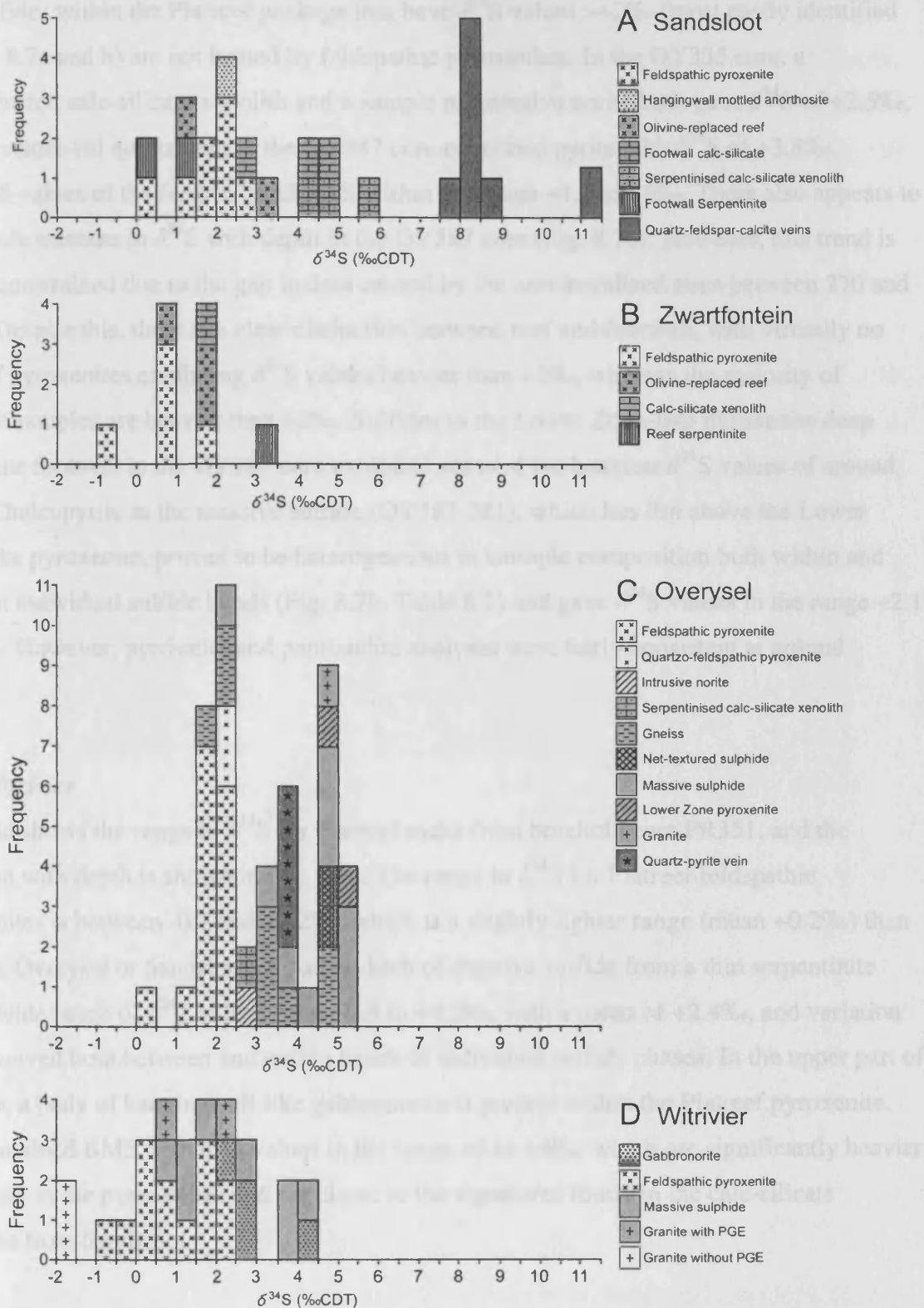


Figure 8.6. Range in $\delta^{34}\text{S}$ values for sulfides within each rock type and an indication on their paragenesis based on textural evidence and host rock lithology from (A): the Sandsloot pit; (B): the Zwartfontein South pit; (C): borehole cores OY335 and OY387 from Overysel; and (D): borehole core PR351 from Witrivier.

The sulfides within the Platreef package that have $\delta^{34}\text{S}$ values $>+2\text{‰}$ (most easily identified in Figs. 8.7a and b) are not hosted by feldspathic pyroxenites. In the OY335 core, a serpentinized calc-silicate xenolith and a sample of intrusive norite both gave $\delta^{34}\text{S}$ of $+2.5\text{‰}$, and a fracture-fill quartz vein in the OY387 core contained pyrite with $\delta^{34}\text{S}$ of $+3.8\text{‰}$. The $\delta^{34}\text{S}$ values of the footwall rocks fall within the range $+1.5$ to $+5\text{‰}$. There also appears to be a crude increase in $\delta^{34}\text{S}$ with depth in the OY387 core (Fig. 8.7b). However, this trend is poorly constrained due to the gap in data caused by the unmineralized zone between 270 and 360m. Despite this, there is a clear distinction between reef and footwall, with virtually no Platreef pyroxenites exhibiting $\delta^{34}\text{S}$ values heavier than $+2\text{‰}$, whereas the majority of footwall samples are heavier than $+2\text{‰}$. Sulfides in the Lower Zone-like pyroxenite deep within the footwall in the OY387 core exhibited some of the heaviest $\delta^{34}\text{S}$ values of around $+5\text{‰}$. Chalcopyrite in the massive sulfide (OY387-381), which lies 3m above the Lower Zone-like pyroxenite, proved to be heterogeneous in isotopic composition both within and between individual sulfide bands (Fig. 8.7b, Table 8.1) and gave $\delta^{34}\text{S}$ values in the range $+2.1$ to $+5\text{‰}$. However, pyrrhotite and pentlandite analyses were fairly consistent at around $+4.5\text{‰}$.

8.7.4 Witrivier

Fig. 8.6d shows the range in $\delta^{34}\text{S}$ for Platreef rocks from borehole core PR351, and the variation with depth is shown in Fig. 8.7c. The range in $\delta^{34}\text{S}$ for Platreef feldspathic pyroxenites is between -0.7 and $+2.2\text{‰}$, which is a slightly lighter range (mean $+0.2\text{‰}$) than found at Overysel or Sandsloot. A 4x2cm bleb of massive sulfide from a thin serpentinite gave a wide range of $\delta^{34}\text{S}$ values from $+0.8$ to $+4.2\text{‰}$, with a mean of $+2.4\text{‰}$, and variation was observed both between and within bands of individual sulfide phases. In the upper part of the core, a body of hangingwall-like gabbronorite is present within the Platreef pyroxenite. This contained BMS with $\delta^{34}\text{S}$ values in the range $+2$ to $+4\text{‰}$, which are significantly heavier than those in the pyroxenites and are closer to the signatures found in the calc-silicate xenoliths from Sandsloot.

The increase in $\delta^{34}\text{S}$ into the footwall at Overysel suggests there is possibly a source of isotopically heavy S in the Archaean basement. To investigate this, samples of Archaean basement that contain sulfides that are not related to the Platreef mineralization were required. Samples that contain BMS with no associated PGE may possibly be of non-Platreef origin. Unfortunately, all the samples of footwall sulfides in the Overysel samples had PGE

associated with them and were therefore all probably Platreef affected. The footwall in the PR351 core is made up of gneisses, granites and granite mylonites. Sulfides were present in two associations: (1) chalcopyrite-rich veins with PGM, assumed to be related to the Platreef mineralization on the basis of the presence of PGE; and (2) disseminated pyrite, chalcopyrite and millerite with no associated PGM. The latter are interpreted to be basement mineralization, not associated with the Platreef mineralizing event, and possibly pre-Bushveld. The sulfides with associated PGE have $\delta^{34}\text{S}$ values comparable to the Platreef pyroxenites, confirming their likely Platreef association. However, the basement mineralization produced the lightest $\delta^{34}\text{S}$ signature seen in all the rock types of around -1.5‰ (Table 8.1, Fig. 8.6d). A sample of amphibolite within granite in another core from Witrivier (PR369) that contained disseminated pyrite and millerite was also analyzed, and that too was found to have a similarly light $\delta^{34}\text{S}$ signature of -1.2‰ .

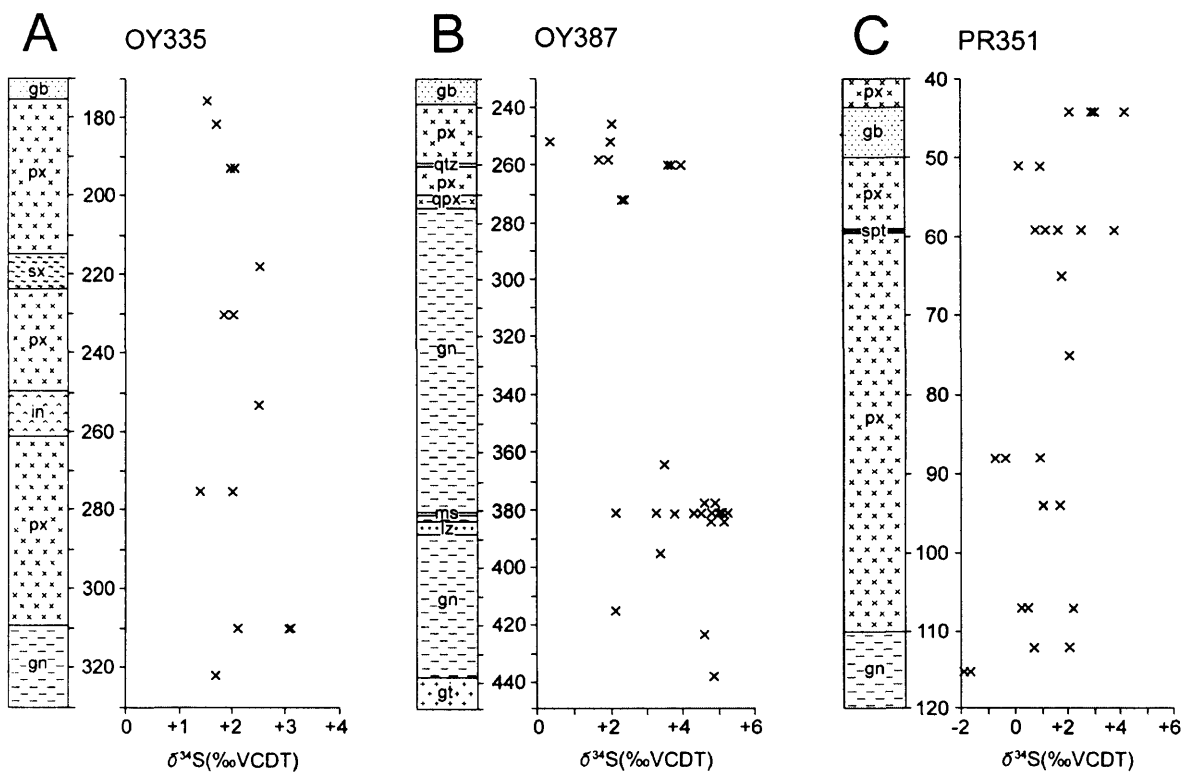


Figure 8.7. Variations in $\delta^{34}\text{S}$ for sulfides with depth in metres in the boreholes cores (A): OY335 from Overysel; (B): OY387 from Overysel; and (C): PR351 from Witrivier. Simplified stratigraphic logs each core are shown on the left hand side of each plot. Key to lithologies: gb: gabbronorite; px: Platreef feldspathic pyroxenite; sx: serpentized calc-silicate xenolith; in: intrusive norite; gn: gneiss; qtz: quartz vein; qpx: quartzo-feldspathic pyroxenite; ms: massive sulfide; lz: Lower Zone-like pyroxenite; gt: granite; spt: serpentinite.

8.7.5 *La Pucella*

To supplement the 'basement' sulfide analyses at Witrivier, a suite of samples of Archaean basement obtained from cores drilled on La Pucella was also analyzed to identify whether there was any indication of isotopically heavy S in the Archaean basement further north. All these samples contained fine-grained, disseminated pyrite, chalcopyrite and/or millerite with no associated PGE mineralization. The results are shown in Table 8.1 and fall in the range -0.9 to +1.3‰, which are lighter than any expected heavy component at Overysel, are well within the range for magmatic sulfides and are similar to the 'basement' sulfides at Witrivier.

8.8 Discussion

The results of this investigation provide the most comprehensive S isotope study of the Platreef thus far undertaken, and for the first time cover areas with dramatically different footwall lithologies. These data, along with the data from previous studies, now allow a thorough assessment of the contribution of magmatic and country rock S to the S budget of the Platreef, and provide an insight into the mechanisms controlling S saturation, and thus present major constraints on any genetic model for the origin of Platreef mineralization.

8.8.1 *Magmatic S isotope signatures*

The range in $\delta^{34}\text{S}$ values indicative of primary, normal mantle derived S associated with mafic and ultramafic rocks is around $0\pm 2\text{‰}$ (Omhoto and Rye, 1979). More specifically, using the sulfide inclusions within diamonds of the Klipspringer kimberlite (Westerlund *et al.* 2004) as a sample of the local mantle, the S isotope signature of the lithospheric mantle beneath the Kaapvaal Craton appears to be in the range -1.8 to +2.4‰ (mean +1.0‰). The most 'primary' sulfide assemblage in the Platreef is the unaltered, fractionated polyphase blebs of pyrrhotite, pentlandite, chalcopyrite within the main Platreef feldspathic pyroxenites (Figs. 8.5a, b). No samples of this type in our study area from Sandsloot to Witrivier produced $\delta^{34}\text{S}$ values heavier than +2.6‰, with a mean $\delta^{34}\text{S}$ value of +1.4‰, which is identical to the mean value reported by Sharman-Harris *et al.* (2005) further south at Turfspruit for what they considered to be 'magmatic' sulfides in the Platreef. All these values are within error of the magmatic range indicated from the Klipspringer kimberlites, and thus strongly imply that magmatic S dominates in the earliest, uncontaminated 'primary' sulfides in the Platreef.

The sample of mineralized hangingwall mottled anorthosite from Sandsloot has an almost identical $\delta^{34}\text{S}$ signature to the pyroxenites that it rests upon. This is consistent with the theory described by Holwell *et al.* (2005), suggesting that the PGE and sulfide in zones at the base of the hangingwall were scavenged from the cool, crystallized Platreef by the magma that formed the hangingwall, rather than being introduced within the new magma.

Samples of altered, olivine-bearing reef from Sandsloot and Zwartfontein, with the exception of one sample at Sandsloot, all have magmatic signatures (mean +1.8‰, $n=5$). The process that altered these rocks is thought to have been percolation of a late-stage Fe-rich melt or fluid through the pyroxenites (McDonald *et al.*, 2005). If so, the sulfide in these rocks was either present in the pyroxenite protolith (and the alteration process did not upgrade the sulfide content significantly) or, if the alteration process added sulfide, it was similarly dominated by primary mantle S. What is clear is that if redistribution of the sulfide occurred during the alteration process, it took place with minimal interaction with footwall-derived S (which would lead to more positive $\delta^{34}\text{S}$, see below).

About 20% of the footwall calc-silicate samples and xenoliths have $\delta^{34}\text{S}$ signatures consistent with magmatic values. These analyses came from a sample that was very S rich (SNS1-39, Table 8.1) and was in very close proximity to the Platreef pyroxenites. It is therefore possible that these sulfides were swamped by S from the magmatic sulfide of the Platreef, which invaded the rocks, with only a relatively small volume of country rock S restricting the amount of country rock S available for it to react with.

8.8.2 Non-magmatic S isotope signatures

Although the 'primary' sulfides show magmatic S isotope values, around 70% of sulfide analyses in the other lithologies show consistently heavier signatures. The previously published data for the Malmani Subgroup in this area indicate that S in this formation has a heavy $\delta^{34}\text{S}$ signature of around +7‰ (Buchanan *et al.*, 1981). Sulfides in the footwall calc-silicates and xenoliths at Sandsloot exhibit $\delta^{34}\text{S}$ values consistently a few per mil heavier than the magmatic range, with a mean of +4.4‰. It is likely that hydrothermal distribution of sulfide and PGE into the footwall, as a result of assimilation and metamorphism of the footwall rocks, led to interaction between magmatically derived S and S released from the floor to produce the intermediate $\delta^{34}\text{S}$ ratios observed in the immediate floor rocks and xenoliths.

The sample of serpentinite from the reef at Zwartfontein contains a similar S isotope signature to the calc-silicates at Sandsloot. The fact that the sulfides in this sample were present as small veins would suggest they are 'secondary', and that these sulfides probably formed during hydrothermal activity either during serpentinization or along the serpentinized zones which acted as fluid conduits. Their elevated S isotope signatures, coupled with the association of serpentinites with altered calc-silicate xenolith material at Zwartfontein (Holwell and Jordaan, 2006), would imply that serpentinite hosted sulfides are of a similar nature to those in the calc-silicate footwall and have undergone hydrothermal exchange of S.

If the assimilation of footwall sediments by melting is invoked as the mechanism for S addition, then a magma at up to 1200°C should melt any sedimentary sulfides present and incorporate them into any entrained sulfide liquid. Pyrite, for example in the footwall sediments at Turfspruit, should break down at around 810°C, releasing sulfur into such a magma. However, the source of S in the Malmani Subgroup is generally assumed to be an evaporitic sulfate, such as anhydrite or gypsum, which have melting points of 1450-1460°C. Ripley *et al.* (2003) discussed this problem and suggested that the most likely transfer mechanism of S from evaporites to a magma is through the leaching of sulfate by hydrothermal fluids, with diffusive transfer of S via the fluid phase. The fluid fluxing involved during and after emplacement of the Platreef in the Sandsloot-Zwartfontein area, particularly in the footwall and in the xenoliths, is likely to have involved such processes.

The extent of assimilation of crustal S by mafic magmas can be modelled using a simple two-component mixing model (Ripley and Li, 2003):

$$\delta^{34}\text{S}(\text{sulfide mixture}) = \frac{\delta^{34}\text{S}_c f_c C_c^s + \delta^{34}\text{S}_m f_m C_m^s}{f_c C_c^s + f_m C_m^s} \quad (1)$$

where f_c and f_m are the fractional abundances of the contaminant and the magma, respectively, and C^s is the S concentration. Such calculations are of necessity generalized as a result of extrapolating from single specimens to bulk rock packages in terms of isotope ratio and S concentration. In the case of heterogeneously bedded sediments such as the Malmani Subgroup, these are particularly difficult to estimate. In addition, if a S-bearing fluid phase has been involved as is likely in the Sandsloot area, significantly less volumes of contaminant

would be needed to cause the same shift in isotope composition (Li *et al.*, 2002).

Nevertheless, a semi-quantitative estimate on the amount of contamination can be calculated.

If we assume an isotope composition in a mantle-derived Platreef magma of $\delta^{34}\text{S} = +1.0\text{‰}$ (the mean of the Klipspringer Kimberlite sulfide inclusions) and a S concentration of 1000ppm, and take the Malmani sulfate value of $+7.1\text{‰}$ from Buchanan *et al.* (1981), and assume a concentration of 2wt% S in the Malmani (as Li *et al.*, 2002, estimated for the Malmani in contact with the Uitkomst Complex), it requires around 6% assimilation of the Malmani to produce sulfides with the mean calc-silicate and xenolith $\delta^{34}\text{S}$ value of $+4.4\text{‰}$. This is somewhat less than the 18% contamination suggested by Harris and Chaumba (2001) on the basis of oxygen isotope studies of silicate minerals, however the discrepancy could easily be understood through the inherent uncertainties of the calculation. For example, if the Malmani contained just 0.58wt% S, the observed $\delta^{34}\text{S}$ values of $+4.4\text{‰}$ would be produced with 18% contamination. CaO/Al₂O₃ ratios can also be used to assess the degree of contamination. A rock containing orthopyroxene and plagioclase should have a 'magmatic' CaO/Al₂O₃ ratio of around 0.6. Using the data of McDonald *et al.* (2005) for Sandsloot, footwall calc-silicate rocks have a CaO/Al₂O₃ ratio in the region of 2.8, and the Platreef feldspathic pyroxenites have a ratio of around 0.9, indicating contamination from a Ca-rich end member (most likely the Malmani dolomites). To shift the ratio in the pyroxenite from 0.6 to 0.9, it would require approximately 15% contamination by a rock with a CaO/Al₂O₃ ratio of 2.8, which is similar to the value calculated by Harris and Chaumba (2001). So if around 15% contamination is assumed, it is likely that the S content of the Malmani was less than 0.6wt%, and given the likelihood of a fluid being involved, probably even lower.

Unfortunately, no whole-rock S data for the Malmani is available to test this, however, some work has been done on the lateral relative of the Malmani - the Campbellrand Subgroup in the Griqualand West area, near Kimberley - by the Agouon-Griqualand Palaeoproterozoic Drilling Project. No anhydrite or gypsum was found in these sediments and the carbonates hold 0.15-0.18wt% S (S. Schroeder, pers. commun., 2006). There is, however, evidence of the former presence of evaporites in these rocks (Gandin *et al.*, 2005). If the Malmani contained such a low S concentration, it would require over 40-45% assimilation to produce $\delta^{34}\text{S}$ values of $+4.4\text{‰}$. Such an amount of contamination seems unlikely as it would be manifested in the petrology of the reef, for example with increased clinopyroxene contents, but this is not observed, and it is likely that preservation of sulfates in the Malmani was greater than in the

Campbellrand Subgroup. The inherent uncertainties in the calculations are compounded at Sandsloot by the fact that S from sulfate in the floor is more likely transferred by hydrothermal mechanisms rather than assimilation, and therefore a much smaller amount of the contaminant could produce the observed values. As such, calculations such as these for areas where the contaminant is sulfate rather than sulfide may not be valid.

As mentioned above, it is much more likely that country rock sulfides can be assimilated by melting compared to country rock sulfates. For this reason, the two-component mixing model may be more reliable for assessing sulfide contamination in the Turfspruit area. Using the same magmatic composition as before, but using the $\delta^{34}\text{S}$ value of +8‰ for pyrite in Duitschland Formation shales from Sharman-Harris *et al.* (2005), and a 2wt% S concentration in the shales, it would take around 8% assimilation to produce the sulfides with a $\delta^{34}\text{S}$ value of the sort reported by Sharman-Harris *et al.* (2005) for ‘contaminated’ Platreef of around +5‰. Alternatively, if the shales contained just 1wt% S, it would take around 12% assimilation of shales to produce the observed ratios. For the Townlands area, if we take the hornfels values from Manyeruke *et al.* (2005) of around +15‰ to represent the $\delta^{34}\text{S}$ signature of the local Timeball Hill sediments, and again assume a concentration of 2wt% S, only 5% assimilation would be required to produce the observed Platreef ratios of around +8‰. Despite the limitations of this method, it does show that contamination of the Platreef by country rock sediments was most likely less than 20% assimilation, and in many cases, maybe less than 10%, and this seems to be corroborated by the calculations of Harris and Chaumba (2001) based on O isotopes, the CaO/Al₂O₃ ratios, and the lack of petrological evidence of major contamination in the Platreef pyroxenites.

The late stage veins that cross-cut all lithologies in the Sandsloot and Zwartfontein pits contain sulfides with the heaviest isotopic signature in our dataset of around +8‰, similar to that published for sulfate in the Malmani Subgroup (Buchanan *et al.*, 1981). The veins carry a distinct sulfide assemblage that includes chalcopyrite, sphalerite, galena and pyrrhotite (Fig. 8.5h). Observations to date indicate that the veins are not common elsewhere along strike, being rare or absent in the Platreef on Townlands (Manyeruke *et al.*, 2005), Turfspruit (Hutchinson and Kinnaird, 2005) and Overysel (Holwell and McDonald, 2006). Many veins contain a very high calcite content and it is likely that the fluids that formed them originated in the carbonate country rocks. Sulfate in the Malmani Subgroup may have been the sole contributor to the S in the resultant sulfides, given that they exhibit almost identical S isotope

signatures to the published data from sulfate in the Malmani. This is assuming that the Malmani itself does not contain significant sulfides in addition to sulfates. Diagenetic sulfides in the Malmani have never been referred to in Platreef literature. However, there is at least one known occurrence of Pb-Zn mineralization in the Malmani on the farm Uitloop (Fig. 8.2), and numerous other Pb-Zn MVT deposits occur in the Malmani from elsewhere in the Transvaal basin that encircles the Bushveld Complex (Martini *et al.*, 1995), the source of S in which is thought to be sourced from the leaching of Malmani sulfates (Clay, 1986). Unfortunately, no S isotope information is available on these MVT sulfides in the vicinity of the northern limb of the Bushveld, however, remobilization of such mineralization could provide a source of the Pb and Zn for the galena and sphalerite in the late stage veins.

A curious feature is the apparent increase in $\delta^{34}\text{S}$ values with depth into the footwall at Overysel (Fig. 8.7b). The lowermost samples from the OY387 core exhibit $\delta^{34}\text{S}$ values of around +5‰. At Sandsloot, mineralization is distributed into the footwall by hydrothermal processes related to skarn formation. At Overysel, mineralization appears to have penetrated the footwall gneisses through an interconnected melt network produced by partial melting of the gneiss around grain boundaries (Holwell and McDonald, 2006). The increase in $\delta^{34}\text{S}$ values would suggest that the downwardly migrating liquid may have incorporated a pre-existing, isotopically heavy sulfide within the footwall. The Archaean basement has not been previously implicated as a source of S to the Platreef, in part presumably due to the lack of studies conducted in the area. In the samples from Witrivier, 'basement' sulfides had slightly negative $\delta^{34}\text{S}$. Similarly, the 'basement' sulfides from La Pucella showed a very limited, mantle range of around 0‰. The existing data suggest, therefore, that pre-existing sulfides in the Archaean basement have a mantle isotopic signature within error of, but around 1 per mil lighter on average than the Platreef magmatic $\delta^{34}\text{S}$ signature, and therefore could not have caused the increase in $\delta^{34}\text{S}$ with depth into the footwall at Overysel.

Whilst Archaean basement-hosted sulfides typically have a limited signature, around 0‰ or lower (e.g. Grassineau *et al.*, 2005, and our Witrivier and La Pucella data), our Overysel data suggest that local gneisses may have heterogeneous S isotope compositions, and there may be a distinct source of isotopically heavy sulfides in the Hout River Gneisses in the Overysel area. An important point to consider if this is the case, is that there has been little contribution from such a source of isotopically heavy footwall S to the Platreef itself, which is consistent with the theory that the sulfide liquid percolated down into the footwall, with no significant

upward movement of S out of the footwall rocks. It also implies that any assimilation of rafts of Archaean basement into the Platreef magma was not a major factor in upgrading the Platreef S content.

Another potential source of the elevated $\delta^{34}\text{S}$ values in the Overysel footwall may be the Lower Zone-like pyroxenite located at around 385m depth in the OY387 core. Lower Zone rocks in the northern limb of the Bushveld Complex south of Mokopane are known to contain occasional concentrations of sulfides, such as the PGE-BMS reefs of the Volspruit subzone (Hulbert and von Gruenewaldt, 1982), which intriguingly have a similar S isotope signature of around +4‰ (Hulbert, 1983). Such mineralized layers have not been identified in any of the satellite bodies of Lower Zone rocks north of Mokopane, which the pyroxenite in the OY387 footwall is thought to be similar to. This is not to say that it did not originally contain some sulfide, however, sulfide mineralization within the Lower Zone pyroxenite in the OY387 core is thought to be related to the downward percolation of sulfide liquid from the Platreef (Holwell and McDonald, 2006). It is difficult to explain how interaction of the Platreef magmatic sulfide liquid with sulfide in the Lower Zone body can have caused elevated $\delta^{34}\text{S}$ values in the gneisses above it, given its proposed downward migration.

An interesting feature of the two massive sulfide samples studied: one in the gneissic footwall at Overysel and the other in a serpentinite (most likely an altered calc-silicate xenolith) in the Witrivier Platreef pyroxenites, is that they display considerable variation in $\delta^{34}\text{S}$ values, both between and within sulfide phases. The massive sulfide in the serpentinite at Witrivier shows a range of 3‰ in the analyses, which indicates that these textures are disequilibrium textures and are not magmatic. The variation is likely to be related to hydrothermal activity, possibly related to the serpentinization.

Another rock type which proved to have a non-magmatic S isotope signature was the gabbronorite in the upper part of the core from Witrivier. This is considered to be a body of hangingwall gabbronorite intruded down into the Platreef, a feature also identified at Drenthe (Naldrett, 2005) and Zwartfontein (Holwell and Jordaan, 2006). At Drenthe (Fig. 8.2), Naldrett notes that the gabbronorite contains sulfides, and suggests they have been cannibalized from the Platreef pyroxenites in a manner analogous to that proposed by Holwell *et al.* (2005) to explain the occasional presence of PGE-BMS mineralization at the base of the hangingwall. The contrasting isotopic signatures between the gabbronorite and the enclosing

pyroxenites at Witrivier, however, does not support the simple incorporation of pre-existing sulfide, unless, of course, the gabbro-noritic magma assimilated a significant amount of mineralized calc-silicate xenoliths during intrusion with $\delta^{34}\text{S}$ signatures around +4‰. This is possible, as Naldrett (2005) notes that at Drenthe gabbro-norite bodies may have preferentially intruded along horizons where altered calc-silicate is particularly common.

An alternative explanation could be that the roof rocks to the Platreef were calc-silicates. The fact that calc-silicate xenoliths are present within the Platreef several kilometres further north of the last footwall outcrop of the Malmani Subgroup, together with the presence of large rafts (up to 2km in length) of calc-silicate at the base of the Main Zone in the Drenthe-Dorstland area (Fig. 8.2) (van der Merwe, 1978), makes this a distinct possibility. The presence of Transvaal sediments as the roof rocks would explain this relationship, and further south on Turfspruit Kinnaird (2005) also notes xenoliths of hornfels at the base of the hangingwall. The calc-silicate rafts within the Main Zone have associated PGE and BMS mineralization (Kinnaird *et al.*, 2005). The fluids released during assimilation and metamorphism appear to have been responsible for the distribution of PGE mineralization into the calc-silicate footwall at Sandsloot (Holwell *et al.*, 2006). If the roof rocks were also calc-silicates (i.e. the Platreef intruded as a sill-like body), then by the same process they could also have become mineralized and picked up similar $\delta^{34}\text{S}$ signatures to the footwall calc-silicates, which at Sandsloot are around +4‰. There are no significant concentrations of sulfides in the Main Zone in the vicinity of the Platreef, and as such, it can be assumed that the Main Zone magma was relatively S poor, and therefore the amount of magmatic S in the Main Zone magma was very low. Thus, any assimilation of mineralized calc-silicates could have induced the precipitation of sulfides with an almost identical isotopic signature to that of the assimilated material. The Witrivier gabbro-norite data are tantalizingly close to this. In either of the above cases, the elevated $\delta^{34}\text{S}$ signature of the gabbro-norite intrusions is attributed to the assimilation of mineralized calc-silicates, as either xenoliths or roof rocks to the Platreef.

8.8.3 S isotope variations along strike

This study, together with that of Sharman-Harris *et al.* (2005) and Manyeruke *et al.* (2005), demonstrates the variation in S isotope composition along the strike of the Platreef. It is now becoming clear that the interaction of the Platreef magma with the variety of differing floor rock lithologies is a critical factor determining the mineralogy, distribution and style of the mineralization on a local (km) scale (Nex, 2005; Kinnaird *et al.*, 2005; Hutchinson and

Kinnaird, 2005; Holwell *et al.*, 2006), and we can now add the $\delta^{34}\text{S}$ signature to that list. The work of Sharman-Harris *et al.* (2005) on Rietfontein, Turfspruit and Macalacaskop showed that in the lower 180m of a 400m thick Platreef succession, the sulfides contain a significant S contribution from the assimilation of pyrite in shales of the Duitschland Formation. At Townlands, all the pyroxenitic Platreef samples that Manyeruke *et al.* (2005) analyzed showed a significant external contribution to the $\delta^{34}\text{S}$ signature (+2.6 to +10.1‰), and they attributed this to assimilation of footwall sediments, which have $\delta^{34}\text{S}$ values of around +15‰. At Sandsloot and Zwartfontein, we have shown that although the footwall rocks do appear to have elevated $\delta^{34}\text{S}$ signatures, ‘primary’ sulfides in the Platreef have a magmatic signature and do not show a significant external contribution to their S budget. Similarly at Overysel and Witrivier, the Platreef pyroxenites have magmatic isotope signatures, and the contribution of S from the Archaean footwall is minimal.

8.8.4 The sources of S in the Platreef

This investigation has proven that the ‘primary’ sulfides in the pyroxenites that constitute the Platreef in the strike section from Sandsloot to Witrivier (including Zwartfontein and Overysel; Fig. 8.2) have a homogeneous magmatic signature, and show little evidence of contamination from footwall S, even in localities where there is evidence of a source of footwall S, such as Sandsloot. This is in contrast to the findings of Sharman-Harris *et al.* (2005) in localities further to the south, where assimilation of footwall S has apparently contaminated the lower portions of the Platreef. Upgrading of the S budget is also likely to have occurred and the abundance of sulfides in the Platreef around Tweefontein, Turfspruit and Macalacaskop (Fig. 8.2) is higher than in the Sandsloot-Overysel area, and often includes net textured and massive sulfides (Nex, 2005; Hutchinson and Kinnard, 2005). However, our data indicate that this process was strictly localized and insignificant in the area where the Malmani Subgroup forms the footwall. The reason for this may be related to the chemical manifestation of the S in the footwall sediments with sulfides assimilated and sulfates transferring S through leaching by hydrothermal fluids (Ripley *et al.*, 2003). By this mechanism, transfer of S from the Malmani could not have taken place until sufficient fluids had been liberated by intrusion and assimilation. This process produced the mixed isotopic signatures in the ‘secondary’ sulfides present in and around calc-silicate xenoliths and footwall, but left the early-crystallized primary sulfides unaffected. This also shows a fundamental difference in the contamination mechanism between Turfspruit and Sandsloot. Footwall sulfides at Turfspruit contaminate the Platreef by being assimilated, whereas

footwall sulfates at Sandsloot only contaminate Platreef-sourced sulfides within and around calc-silicate xenoliths and footwall through hydrothermal leaching.

8.8.5 Mechanisms of S saturation in the Platreef

The issue of how the Platreef magma attained S saturation has not yet been resolved. Theories include the addition of sedimentary S (Buchanan *et al.*, 1981; Buchanan and Rouse, 1986; Sharman-Harris *et al.*, 2005), silicic contamination from the assimilation of country rocks (Buchanan and Rouse, 1986) and an increase in oxygen fugacity in the magma as a response to devolatilization of assimilated dolomite (Buchanan *et al.*, 1981). Barton *et al.* (1986) concluded that S saturation was attained prior to any contamination, and Lee (1996) developed this by proposing that S saturation occurred pre-emplacment in a staging chamber, and that base metals and PGE were concentrated in this sulfide before emplacement. For the first time, detailed S isotope information from localities along the Platreef that cover virtually the entire range of footwall lithologies is available so that these theories can be tested.

A fundamentally important observation is that significant sulfide mineralization is present along the entire strike length of the Platreef from Townlands in the south to Dorstland in the north, regardless of footwall lithology. Some areas have footwall rocks that are known to contain S either predominantly as sulfide (e.g. Townlands, Macalacaskop and Turfspruit) or predominantly as sulfate (e.g. Tweefontein, Sandsloot, Zwartfontein). In the areas with sulfides in the floor rocks, the isotopic evidence is that some of this has been incorporated into the Platreef magma by assimilation (Manyeruke *et al.*, 2005; Sharman-Harris *et al.*, 2005). However, the isotopic evidence from the upper Platreef in the study of Sharman-Harris *et al.* (2005) shows a clear magmatic signature, thus S saturation was achieved by the magma at least in this later/upper package of magma without any apparent addition of country rock S. This relationship demonstrates that although in such localities significant upgrading of the Platreef S budget may have occurred through the addition of country rock S, this did not exclusively trigger S saturation.

It has long been thought that contamination from sulfate in the Malmani Subgroup contributed S to the Platreef S budget, triggering S saturation (Buchanan *et al.*, 1981), and although there is evidence of interaction with sedimentary S in the 'secondary' sulfides of the footwall rocks and xenoliths, primary sulfide mineralization at Sandsloot and Zwartfontein

shows no significant addition of external S. Sulfur saturation, however, may have been initiated by an increase in fO_2 . The devolatilization of somewhere in the region of 18% dolomite (Harris and Chaumba, 2001) would have produced a considerable amount of CO_2 , which could have increased the fO_2 , lowering the FeO content of the magma and thus the S-carrying capacity, inducing S saturation as suggested by Buchanan *et al.* (1981). Although such degassing may be partly responsible for initiating S saturation, it is not believed to be capable of significantly altering the S isotope ratios (Ripley *et al.*, 2003). Silicic contamination (as described by Irvine, 1975) may also be a factor, due to the siliceous nature of the dolomites of the Malmani Subgroup (Armitage *et al.*, 2002).

Where the floor rocks are Archaean basement, addition of S from the floor has never been considered a factor. Although we have shown there are sulfides in the basement, the isotope data does not provide sufficient evidence, nor are they present in sufficiently voluminous amounts, to indicate that they had a major role in the main Platreef mineralization event. A change in fO_2 in the manner described above for the Malmani is highly unlikely due to the lack of volatiles that would be released by assimilating an essentially anhydrous gneiss. Silicic contamination by partial melting of the gneisses may, however, have been responsible for triggering the precipitation of a sulfide liquid in the area.

The timing of the mineralization in relation to any contamination is critical in constraining the role contamination may or may not have had in the mineralization. As mentioned above, the silicic contamination from the Archaean basement is thought to post-date the mineralization. This implies that the sulfide was present within the magma during emplacement, and was not precipitated as a result of contamination. At Sandsloot, Harris and Chaumba (2001) noted that pyroxenes within the Platreef showed evidence of contamination in their oxygen isotope ratios that could be explained by the assimilation of up to 18% dolomite. Therefore the dolomite contamination must have occurred at a very early stage in the emplacement history to affect the earliest crystallizing silicate: orthopyroxene. The fact we have shown that primary sulfides in the reef at Sandsloot are relatively unaffected by contamination from the dolomite would strongly imply that the sulfides were entrained within a Platreef magma that had already reached S saturation before intrusion, but that orthopyroxene crystallization took place *in situ*.

Two important over-arching observations emerge from this study. Firstly, economic sulfide mineralization is present along the entire strike length of the Platreef regardless of footwall lithology. Secondly, for each locality, it is possible to attribute at least one contamination-related process directly related to the footwall lithology in that area as a possible cause of S saturation in the Platreef magma. Until now, all of the previous studies have considered the problem by focussing on one area, and thus the mechanisms suggested, whilst they may be applicable to the area in question, cannot necessarily be applied to the Platreef as a whole. Whilst it may be possible that, at Turfspruit, addition of S from pyrite in the shales triggered S saturation, at Tweefontein and Sandsloot devolatilization of dolomite was responsible, and at Overysel silicic contamination caused the precipitation of an immiscible sulfide liquid, the likelihood of all these processes occurring contemporaneously and to sufficiently effective degrees is doubtful.

What seems more likely, and is supported by the isotope data, is a situation similar to that invoked by Lee (1996) who suggested that sulfides were formed in a staging chamber prior to emplacement, and that the formation of this Ni-Cu-PGE-rich immiscible sulfide predated local contamination, and was not a consequence of it. Given the total dominance of magmatic S in the Platreef feldspathic pyroxenites unaffected by contamination, the Platreef can be considered to be primarily an orthomagmatic sulfide deposit, and the magma from which it formed had most likely attained S saturation before its emplacement. Contamination by floor rocks, particularly the Deutschland shales, locally upgraded the S content and subsequent hydrothermal activity derived from the assimilation and metamorphism of footwall rocks, particularly dolomites, locally mobilized PGE and S. The mobilized Platreef PGE and S then interacted with hydrothermally leached footwall S, and precipitated secondary sulfides in the footwall, in xenoliths and in other fluid-affected parts of the reef.

8.8.6 A genetic model for Platreef mineralization

Using the isotope data from this study and the investigations of other workers discussed above, it is now possible to define several fundamental features that any genetic model for Platreef mineralization must be able to account for:

1. The most primary sulfide mineralization in the Platreef is magmatic in origin and magmatic S dominates the 'primary' sulfides within the Platreef pyroxenites.
2. Sulfur saturation occurred before intrusion.

3. Contamination is a localized process and is directly related to the immediate footwall rocks.
4. Mechanisms of S contamination are different according to whether the external source of S is present as sulfide or sulfate.
5. Contaminant signatures from footwall rocks are only present where those particular rocks are in contact with the Platreef, with the exception of Malmani-derived calc-silicates.

In order to account for the above, we follow the suggestion first made by Lee (1996) and propose that the source magma of the Platreef attained S saturation before emplacement, most likely in a deep, intermediate chamber that fed the northern limb, such as that proposed to have fed the Uitkomst Complex to the east of the eastern Bushveld by de Waal and Gauert (1997). This is represented in Fig. 8.8a, where sulfide droplets collect at the base of the intermediate chamber. Flow of an earlier generation of magma (possibly that which developed the Lower Zone) over these sulfides may have contributed to the high metal tenors of these sulfides. This can explain the mass balance problem of how such a small volume package of magma such as the Platreef could have attained such a high concentration of PGE in the absence of an overlying magma column from which to draw PGE (c.f. Cawthorn *et al.*, 1985; Cawthorn *et al.*, 2002; Holwell *et al.*, 2005). The body of Main Zone magma has been suggested as the source of PGE to the Merensky Reef (e.g. Maier and Barnes, 1999), however, the intrusion of the Main Zone significantly after the Platreef in the northern limb (Holwell *et al.*, 2005; Holwell and Jordaan, 2006) rules out the possibility that this mechanism enriched the Platreef with PGE.

Evidence that it may have been the northern limb Lower Zone magma that provided the PGE for the Platreef sulfides lies in the composition of olivines within the Lower Zone cumulates in the Grasvally area to the southwest of Mokopane. Fig. 8.9 shows a Ni vs Fo plot for olivine compositions within the Lower Zone succession described by Hulbert (1983), together with data for the eastern limb. It is clear that the majority of the northern limb compositions below the chromitite layers (i.e. within the lower >1000m of strata), have compositions which fall significantly outside the field for layered intrusions, showing considerable depletions in Ni. If the magma that formed these olivines came into contact with immiscible sulfide before emplacement, such as in a staging chamber as suggested, it would become depleted in chalcophile elements such as Ni and the PGE, and subsequent olivines would contain abnormally low Ni contents.

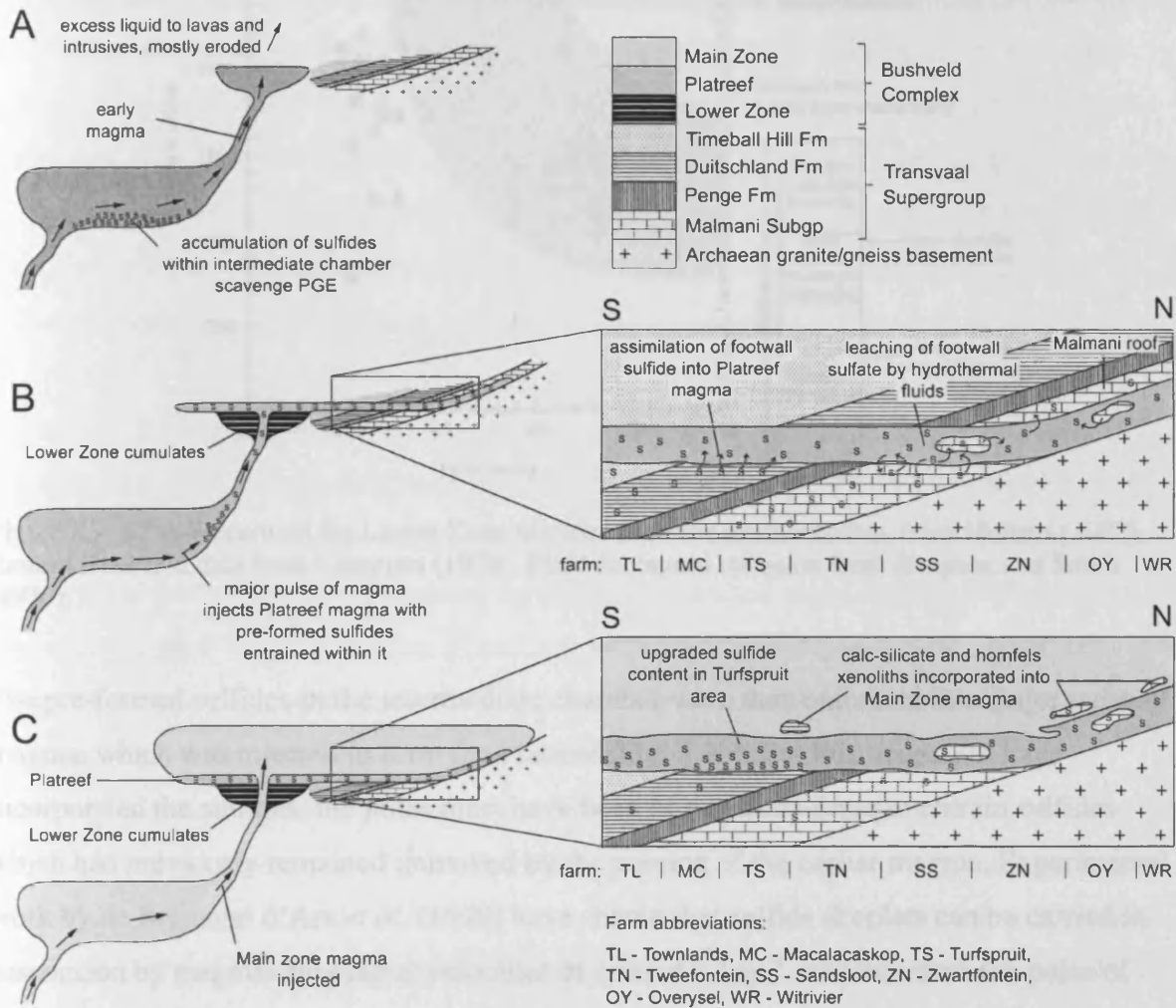


Figure 8.8. Genetic model for the intrusion and mineralization in the Platreef, with the presence of a deep, intermediate magma chamber. *a*: S saturation is attained in the intermediate chamber and sulfides accumulate at the base of the chamber. The passage of Lower Zone magma over these sulfides may have contributed significantly to their metal tenors. *b*: A major pulse of magma entrains the magmatic sulfides and is emplaced by spreading out from a central feeder pipe/dyke to form the Platreef. North of Zwartfontein, Malmani rocks form the roof. Footwall sulfides are locally assimilated, whereas footwall sulfate reacts with magmatic sulfides via hydrothermal leaching (inset). *c*: Injection of Main Zone magma spreads out over the Platreef forming a magmatic unconformity and incorporating xenoliths of Malmani rocks north of Zwartfontein (inset).

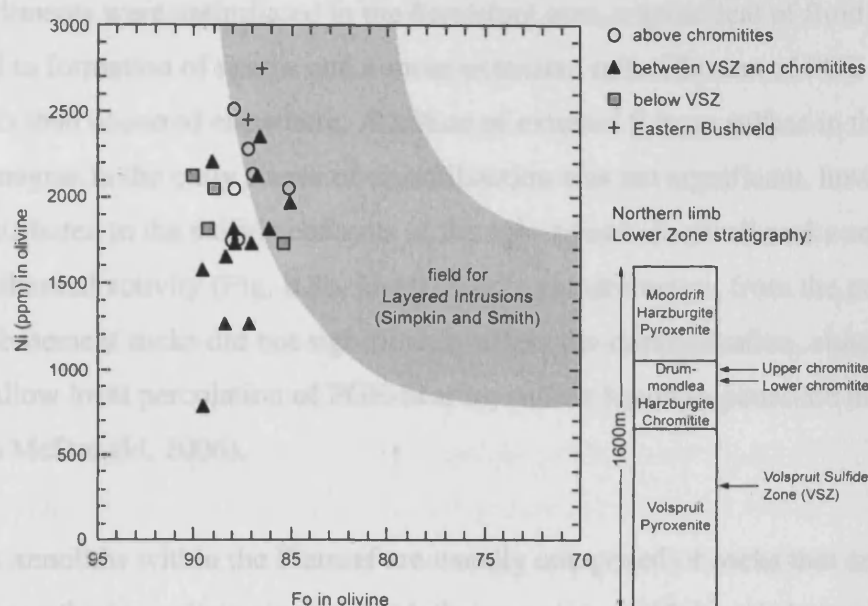


Figure 8.9. Ni vs Fo content for Lower Zone olivines from the northern limb, from Hulbert (1983). Eastern Bushveld data from Cameron (1978). Field for layered intrusion from Simpkin and Smith (1970).

The pre-formed sulfides in the intermediate chamber were then entrained in a major pulse of magma, which was injected to form the Platreef (Fig. 8.8b). For this magma to have incorporated the sulfides, the pulse must have been of sufficient force to entrain sulfides which had previously remained unmoved by the passing of the earlier magma. Experimental work by de Bremond d'Arès *et al.* (1999) have shown that sulfide droplets can be carried in suspension by magmas flowing at velocities of around 0.1ms^{-1} , and therefore the pulse of magma that formed the Platreef must have equalled or exceeded a critical velocity in the same manner to incorporate the sulfides. The actual position of the feeder is unknown, but is likely to have been to the west or south west, down dip of the current outcrop of the northern limb, and may correspond with the massive gravity anomaly that can be seen in Fig. 3 of Cawthorn and Webb (2001), which was suggested as a feeder by van der Merwe (1976). This anomaly is by far the greatest in the whole complex, and does not correspond to a zone of thickest mafic lithology, to which other, lesser anomalies in the rest of the complex have been attributed (du Plessis and Kleywegt, 1987).

Sulfur isotope data indicate that the sulfur mineralization in the Platreef is dominantly... The Platreef magma intruded into a variety of country rock lithologies, the composition and reactivity of which had varying effects on the distribution and mineralogy of the mineralization (Fig. 8.8b, inset). Where pyrite-bearing Duitschland Formation shales were assimilated, local upgrading of the S budget took place (Figs. 8.8b, c, insets). Where Malmani

Subgroup sediments were assimilated in the Sandsloot area, a great deal of fluid fluxing took place that led to formation of skarns and a more extensive redistribution of PGE into the footwall rocks than occurred elsewhere. Addition of external S from sulfate in the Malmani to the Platreef magma in the early stages of crystallization was not significant, however, this probably contributed to the sulfide contents of the calc-silicate footwall rocks and xenoliths during hydrothermal activity (Fig. 8.8b, inset). Silicic contamination from the partial melting of Archaean basement rocks did not significantly affect the mineralization, although partial melting did allow local percolation of PGE-bearing sulfide liquid to penetrate the footwall (Holwell and McDonald, 2006).

Country rock xenoliths within the Platreef are usually composed of rocks that are present as footwall rocks in the immediate vicinity, with the exception of Malmani-derived calc-silicates. The presence of calc-silicate xenoliths in the Platreef for many kilometres further north of their last occurrence as footwall rocks has been used as evidence that the Platreef was intruded in a northwardly direction (Cawthorn *et al.*, 1985; Friese, 2004). However, the lack of any other type of xenolith north of their footwall outcrop and the discontinuation of the apparent S contamination of the Platreef north of Turfspruit do not support this, and an easterly or northeasterly emplacement direction appears more likely, particularly if fed by the proposed feeder to the west of Mokopane. The presence of mineralized calc-silicates in the Main Zone in the Drenthe-Witrivier area can be explained if the roof rocks to the Platreef were Malmani dolomites (Fig. 8.8b, inset). This implies that north of Zwartfontein, rather than the Platreef continuing to cut down through the country rock stratigraphy, it exploited the boundary between the Malmani and the Archaean basement. This also explains the relative dearth of granite and gneiss xenoliths in the Platreef (Cawthorn *et al.*, 1985). When the Main Zone magma was intruded (Fig. 8.8c), it formed a magmatic unconformity over the Platreef and incorporated calc-silicate xenoliths north of Zwartfontein (Fig. 8.8c, inset).

8.9 Conclusions

Sulfur isotope data indicate that the sulfide mineralization in the Platreef is dominantly magmatic in origin, and magmatic signatures are preserved in early formed sulfide droplets within the Platreef pyroxenites in the area of the Platreef from Sandsloot to Witrivier. Sulfur saturation is likely to have taken place prior to intrusion, and was not caused by contamination-related effects such as the addition of country rock S, silicic contamination, or

devolatilization of the magma following assimilation of country rocks. Therefore we favour models for Platreef mineralization that involve early S saturation, most likely in a deep staging chamber or conduit followed by a pulse or pulses of magma that transported these sulfides into the Platreef. In areas where the floor rocks contain appreciable sulfides, such as at Turfspruit, the Platreef sulfides are contaminated with assimilated country rock S. Assimilation of around 5-12% country rocks in the Turfspruit area has locally upgraded the S content of the Platreef and given the Platreef sulfides a heavier isotopic signature. Where the floor rocks contain sulfate such as at Sandsloot, contamination by country rock S is by hydrothermal leaching and is restricted to 'secondary' sulfide assemblages in footwall rocks and xenoliths. The Archaean basement is not a significant contributor to the S budget of the Platreef. Whilst contamination has clearly affected the distribution and style of sulfide mineralization in the Platreef, this is strictly on a local scale and is post-magmatic. Significant PGE-rich sulfide mineralization occurs throughout the entire strike length of the Platreef, regardless of footwall lithology, with localized contamination acting purely as an ore-modifying, rather than ore-forming, process.

8.10 Acknowledgements

This work was undertaken as part of DAH's PhD research which is funded by a Natural Environment Research Council (NERC) Industrial CASE studentship (NER/S/C/2003/11952), supported by Anglo Platinum. The S isotope work was carried out via a NERC Facilities grant (IP/839/1104) awarded to IMcD at the Isotope Community Support Facility at SUERC. SUERC is supported by NERC and the Scottish Universities consortium. AJB is funded by NERC support of the Isotope Communities Support Facility at SUERC. The authors would like to thank the management of Anglo Platinum for giving permission to publish this work and for allowing access to Sandsloot and Zwartfontein mines and core from Overysel. Gernot Wober at Anoroaq Resources and Nevan Pillay at Pan Palladium are thanked for their permission to sample cores drilled on Witrivier and La Pucella, respectively. Alison McDonald is thanked for her invaluable assistance with the analytical work at SUERC. Stefan Schroeder and the Agouron-Griqualand Palaeoproterozoic Drilling Project, funded by the Agouron Institute, are acknowledged for supplying data from the Cambellrand Subgroup. Thanks also to Jay Cockayne for proof reading the manuscript.

Chapter 9

Discussion and conclusions

9.1 Introduction

The aim of this chapter is to synthesize the findings of the preceding chapters and relate them to the initial aims of the project. It is clear that magmatism, contamination and hydrothermal activity have all had important roles in the development of the Platreef and its mineralization, and there is a complex interplay between some or all of these on both a metre and kilometre scale along strike. This interaction between the Platreef magma and the variety of country rock lithologies fundamentally controls many aspects of the style and distribution of the mineralization, and has led to the development of a highly complex and laterally variable orebody.

9.2 Magmatic emplacement

As yet, there is no consensus on the positive identification of feeders to the Bushveld Complex, although Friese (2004) considered the Thabazimbi-Murchison Lineament to be a likely linear feeder, and point feeders have also been suggested by a number of workers (e.g. van der Merwe, 1976; Kinloch and Peyerl, 1990; Kruger, 2005a). The most convincing of these is possibly the site of an enormous gravity anomaly a few kilometres to the west of Mokopane, located close to the Ysterberg-Planknet fault (see Fig. 2.3) that van der Merwe (1976) interpreted as the feeder to the northern limb. This theory has received little attention since (c.f. Cawthorn and Webb, 2001), which is surprising given the fact that it represents the second largest gravity anomaly in South Africa after the Trompsburg anomaly in Orange Free State. Nevertheless, given the anomaly's magnitude, it remains the most likely location for a feeder, certainly for the northern limb, if not necessarily the entire complex.

Numerous apparent differences in the stratigraphy between the northern limb and the rest of the Complex were outlined by McDonald *et al.* (2005, Appendix 5). These differences, coupled with the fact that the northern limb resides in a fundamentally different block of crust to the rest of the Complex (the Pietersburg Block as opposed to the Kaapvaal Shield), and that it is separated from the rest of the Complex by the deep crustal Thabazimbi-Murchison Lineament, means that direct comparisons with the rest of the Complex are difficult, and may even be invalid if the northern limb constitutes a separate intrusion. For this reason, it is important to consider the northern limb in an unbiased way, and not attempt to fit its lithologies and mineralized zones strictly into the stratigraphic zones and reefs defined for the rest of the Complex on the basis of very few sympathetic characteristics.

Stratigraphically, the Platreef lies directly beneath the gabbro-norites assigned to the Main Zone of the northern limb, however, the Platreef should not be considered as the base of this Main Zone unit as it has been previously by van der Merwe (1976) and Kruger (2005a). One of the major findings of this study has been the identification of a significant time-break between the intrusion of the Platreef and the Main Zone magma that formed the hangingwall gabbro-norites. This demonstrates that the Platreef is not part of the gabbro-noritic Main Zone, but rather a separate and older phase of intrusion.

This relationship also has significant implications for the source of PGE to the Platreef in relation to the mass balance problem posed by a relatively thin volume of magma carrying such a large volume of PGE. It would require a volume of mafic magma much, much greater than that represented by the Platreef to be processed in order to extract the observed concentrations of PGE (Cawthorn *et al.*, 2002). In the eastern and western Bushveld Complex, the magma that formed the Main Zone magma has been considered as the source of PGE to the Merensky Reef (Page *et al.*, 1982; Maier *et al.*, 1996; Maier and Barnes, 1999), and the Main Zone in the eastern and western limbs appears to be PGE-depleted (e.g. Maier and Barnes, 1999). This, however, cannot be the case in the northern limb. The findings presented in Chapters 3 and 4 clearly show that the Platreef was almost completely (if not totally) crystallized, and even deformed, prior to the intrusion of the hangingwall magma, and thus this magma could not have provided an *in situ* source of PGE to the Platreef. In addition, this work has also, for the first time, identified zones of PGE mineralization at the base of the hangingwall unit, a lithology previously regarded as barren, which have formed by the cannibalization of mineralized reef into localized zones at the base of the hangingwall.

The roof rocks to the Rustenburg Layered Suite are often thought to be felsites of the Rooiberg Formation (e.g. Cheney and Twist 1991; Kruger 2005a). This may not necessarily be true for the northern limb. Metasedimentary rocks that conventionally form the footwall for the Platreef are present as xenoliths within the base of the Main Zone, particularly to the north of Zwartfontein (van der Merwe, 1978). This can be explained if Transvaal sediments formed not just the floor to the Platreef during its intrusion, but also its roof. The presence of PGE-mineralized Malmani-derived calc-silicate xenoliths within the Main Zone rocks many kilometres north of the last footwall outcrop can be explained if the Platreef magma, during intrusion, exploited the Malmani-Archaeon basement boundary. Therefore, north of

Zwartfontein, the floor rocks to the Platreef were gneisses and the roof rocks calc-silicates. These roof rocks would have had the potential to be mineralized by hydrothermal activity in a similar manner to the floor rocks at Sandsloot. The later intrusion of the Main Zone could then have entrained some of these mineralized rocks, and preserved some as xenoliths such as those observed at Drenthe described by Kinnaid *et al.*, 2005.

9.3 Source of sulfide

The fundamental observation that the rocks representing the Main Zone in the northern limb cannot be a possible *in situ* source of PGE to the Platreef lends considerable support to the theories that suggest that the PGE were pre-concentrated before intrusion of the Platreef in, for example, a staging chamber or conduit system (Lee, 1996). If this were the case, then the mass balance problem can be overcome, as there is the potential for a large volume of magma to come into contact with, and lose PGE to, an immiscible sulfide present in such an intermediate chamber. For example, if sulfide saturation occurred at an early stage, then the passage of a magma, such as that which formed the Lower Zone in the northern limb, over immiscible sulfide droplets at the base of the staging chamber/walls of the conduit could have potentially contributed a large volume of PGE to the sulfide. The Lower Zone cumulates above the Volspruit Subzone in the Grasvally area to the south of Mokopane are notably poor in PGE and sulfide (even in chromitite layers, which typically contain <1000ppb total PGE; Hulbert, 1983) and olivine in this part of the sequence contains lower concentrations of Ni than might be expected given the high Fo content of the olivine. These features could be explained by the extraction of the PGE from the source magma prior to its emplacement in the Grasvally chamber. A later pulse of mafic magma then entrained the sulfides in the intermediate chamber and emplaced them as the Platreef.

Evidence of such a deep magmatic source to the mineralization is found in the isotope signature and geochemistry of the sulfides. The isotope signature of the earliest formed, and least altered or mobilized sulfides, in areas of the Platreef that are relatively uncontaminated, consistently have $\delta^{34}\text{S}$ values of around 0 to +2‰, which are entirely consistent with a mantle source and are identical to the signatures of sulfide inclusions in diamonds within the nearby Klipspringer kimberlite (Westerlund *et al.*, 2004), which can be assumed to have sampled the local mantle sulfur source and to be representative of the local mantle signature. The presence of a mantle signature in the widespread early sulfides in the Platreef pyroxenites strongly

indicates an initial magmatic source for the sulfide mineralization. In addition, in the same areas, the fractionated nature of sulfide blebs, the solid solution behaviour of PGE in some sulfide minerals, and the presence of Pt and Pd tellurides and bismuthotellurides around the margins of the sulfide blebs are all entirely consistent with the PGE initially being concentrated within a sulfide liquid. The presence of Pt-Bi(-Te) microinclusions within these very early sulfide phases also indicates that the semi metals Bi and Te were also present within the sulfide liquid and were pre-concentrated along with the PGE.

9.4 'Primary' Platreef mineralization

The most 'primary' style of mineralization in the Platreef is preserved in the feldspathic pyroxenites that have experienced minimal input from contamination by reactive footwall rocks, such as at calc-silicate xenolith-free sections at Overysel. The presence of a virtually anhydrous footwall north of the farm Zwartfontein has severely limited contamination and particularly hydrothermal activity, and consequently it is here that the most primary assemblages are preserved. Although the sulfides pyrrhotite, pentlandite and chalcopyrite are all low temperature phases, we term them 'primary', as texturally and mineralogically, they are the direct cooling products of the *in situ* fractional crystallization of sulfide liquid droplets. The 'primary' Platreef mineralization style has the following characteristics:

- Sulfides are present as fractionated blebs within the interstitial regions in feldspathic pyroxenites between cumulus orthopyroxene grains,
- Sulfide blebs are made up of pyrrhotite, pentlandite and chalcopyrite, which show an Fe-Ni-Cu zonation towards the margin,
- The IPGE are concentrated in solid solution in pyrrhotite and pentlandite,
- Rh and some Pd are present in solid solution in pentlandite,
- Some Pd and all the Pt and Au are present as discrete PGM located around the margins of the sulfide blebs. The PGM occur as Pt and Pd tellurides and bismuthotellurides, Pt sulfides, Pt arsenides and Au is present as electrum.

As such, the Platreef can be considered to be, in genetic terms, an orthomagmatic sulfide deposit, with the PGE and some semi metals such as Te and Bi collected by immiscible sulfide droplets.

The association of tellurides and bismuthotellurides around the margins of sulfide grains is a common texture in many disseminated PGE-sulfide deposits, including the Merensky Reef (e.g. Prichard *et al.*, 2004a), the Great Dyke of Zimbabwe (e.g. Oberthür *et al.*, 2003), the Federov Pansky Intrusion, Kola Peninsula (e.g. Schissel *et al.*, 2002) and the Suhanko-Konttijärvi intrusion, Finland (e.g. Iljina *et al.*, 1992). The association of the PGM with, and particularly as inclusions within, magmatic sulfide droplets in these examples implies a magmatic origin. However, Pt and Pd tellurides are often considered to be characteristic of low-temperature, hydrothermal environments (e.g. Augé *et al.*, 2002). Whilst they are undoubtedly formed at relatively low-temperature, their presence in these types of deposit is almost certainly as a result of cooling and fractionation from a magmatic sulfide liquid.

9.5 Contamination

The extensive sulfur isotope work in this study has revealed the role of contamination on Platreef mineralization on a scale that has never previously been possible. Where previous studies have concentrated on individual localities along the Platreef, this study has been able to bring existing data together with an extensive set of new data from more localities along strike than ever before. In doing so, it has produced the first truly regional assessment of the role of contamination along the strike of the Platreef. The S isotope signature of the early formed sulfides in parts of the Platreef that have been subjected to relatively small amounts of contamination has shown that there is very little input of country rock S to the original Platreef sulfides. However, in places where the footwall contains sulfides, such as at Turfspruit where pyrite is present in the Deutschland Formation (Sharman-Harris *et al.*, 2005), there is evidence that the country rock S has been incorporated into the early Platreef sulfides, particularly towards the basal contact. Where the floor rocks contain sulfates, rather than sulfides, such as at Sandsloot where the Malmani rocks contain anhydrite, the early formed sulfides appear to be unaffected by contamination. Previous oxygen isotope studies at Sandsloot have shown that a considerable amount of contamination has taken place, with the assimilation of up to 18% dolomite (Harris and Chaumba, 2001). This contamination has not affected the early formed magmatic sulfides, however, later sulfides in fluid affected lithologies such as serpentinites and footwall calc-silicates show evidence of some input of country rock S in their isotope signatures. The absence of a contaminant signature in the early sulfides at Sandsloot compared to Turfspruit is likely to be a function of the manifestation of the S in the footwall: at Sandsloot it is present as sulfate, and at Turfspruit, sulfide. Sulfide

will be assimilated by the magma at magmatic temperatures, however sulfate will not and is much more likely to interact with any magmatic sulfide by hydrothermal leaching. Thus, S exchange where the country rocks contain S as sulfide is by assimilation at an early stage and where it is present as sulfate, S exchange takes place at a later stage, and is controlled by fluid activity.

The nature and extent of contamination by country rock S is therefore a very localized process and serves primarily to upgrade the S content in places. It is not, however, a significant trigger to sulfide saturation and collection of PGE as suggested by Buchanan *et al.* (1981), Buchanan and Rouse (1984) and Sharman-Harris *et al.* (2005). Contamination by localized processes such as silicic contamination, an increase in fO_2 conditions, or the addition of country rock S may appear to be plausible as triggers for S saturation when considering individual areas, as all previous studies prior to this one have done. However, as significant sulfide mineralization is present along the entire strike length of the Platreef regardless of footwall lithology, these individual explanations cannot be applied to the Platreef as a whole, without the unlikely scenario of a variety of individual, localized processes occurring concurrently. What is more likely is that sulfide saturation took place prior to intrusion, and contamination acted as an ore-modifying rather than an ore-forming process.

Whilst contamination may not have triggered sulfide saturation, it undoubtedly did affect the petrology of parts of the Platreef, although this, like upgrading of the S budget, was also on a local scale. Lithologies such the olivine-replaced reef at Sandsloot and the extensive serpentized pyroxenites and peridotites at Zwartfontein South appear to be related to fluids released from the metamorphism, assimilation or serpentization of footwall calc-silicates. At Overysel, the basal section of the Platreef contains abundant quartz, which is related to the incorporation of a felsic melt derived from the partial melting of the footwall gneisses in the area. All these variations along strike are directly related to the nature of the local floor rock lithology.

9.6 Hydrothermal activity and redistribution of PGE into footwall rocks

The assimilation of the variety of footwall sediments in the area to the south of Overysel released significant volumes of fluids into the Platreef magma, and the area around Sandsloot and Zwartfontein South appears to have been particularly affected by such volatile activity,

with significant redistribution of PGE and sulfide mineralization into both the calc-silicate footwall rocks and xenoliths. The study of the PGM mineralogy at Sandsloot (Chapter 5) has revealed that hydrothermal activity plays a significant role in the distribution and mineralogy of the PGE, and that, importantly, PGE mineralogy is a particularly useful tool in identifying hydrothermal processes. The presence of distinct PGM assemblages in individual rock types is directly related to the fluids (or lack thereof) that have passed through the rock which, in turn, affect the nature of the lithology. For example, in the feldspathic pyroxenites at Overysel, where fluid activity has been relatively limited, a 'primary' assemblage of Pt and Pd tellurides associated with the sulfide blebs is preserved. At Sandsloot, in the olivine-replaced reef at Sandsloot, a lithology that is thought to have undergone significant hydrothermal overprinting by an Fe-rich fluid to produce the observed silicate mineralogy (McDonald *et al.*, 2005), the PGE mineralogy has been altered, with Pt present as Pt-Fe alloys rather than tellurides, and a much poorer association of the PGM with BMS has been produced. The decoupling of PGE from BMS appears to be a prevalent feature of fluid-affected lithologies, with calc-silicates and footwall serpentinites often containing high PGE and low BMS concentrations, or vice versa. In such cases, the use of the visual identification of sulfide minerals as an exploration tool to indicate the presence of PGE becomes much less robust.

This decoupling of PGE from BMS, particularly in the footwall, is much rarer at Overysel, where the gneissic footwall contains a BMS and PGM assemblage very similar to that in the feldspathic pyroxenites. This is due to a similar mineralization mechanism and is directly related to the nature of the floor rocks. The Archaean gneisses are relatively anhydrous and therefore would have released very few fluids during metamorphism and assimilation. Instead, partial melting around grain boundaries produced an interconnected melt network down through which, the PGE-rich sulfide liquid from the Platreef was able to percolate, producing similar sulfide and PGM assemblages and associations as it cooled to those in the reef, but also caused fractionation of PGE with depth. The mechanism of distribution of PGE into the footwall, like many other aspects of the Platreef mineralization, is therefore fundamentally determined by the nature of the floor rocks.

The PGM mineralogy is also apparently controlled by the nature of the floor rocks. Whilst the assemblages in individual rock types at a given locality reflect the nature of individual fluid events on a local scale, on a kilometre scale, the footwall control is evident in the presence

and absence of certain PGM types. Some PGM such as Pt and Pd tellurides and sperrylite are common throughout the Platreef and occur at most localities along strike, and are the preserved remnants of the 'primary' mineralization style. PGE sulfides such as cooperite, however, appear to only be present where the floor is Archaean basement, and a high proportion of alloys and antimonides are characteristic of the area where dolomites form the floor. The localized study at Sandsloot found that the lithologies containing the majority of these locality-characteristic phases are metasedimentary footwall rocks or rocks that have experienced hydrothermal activity related to the alteration of the local floor rocks.

9.7 Conclusions

The many findings of this study can be used to generate an outline model for the formation of the Platreef and the northern limb of the Bushveld Complex as a whole. The proposed model is illustrated in Fig. 9.1 and can be summarized in the following stages:

1. Lower Zone magma is intruded. This may have been from a feeder to the west of Mokopane, possibly on the Ysterberg-Planknet fault, as suggested by van der Merwe (1976). This intrusive event formed a magma chamber and cumulates in the area south of the fault, represented by the Grasvally-Volspruit body, and finger-like satellite intrusions into the country rocks to the north (Fig. 9.1a).
2. Sulfide saturation was achieved by the magma in a deep staging chamber and the sulfide droplets scavenged PGE and base metals, together with semi-metals such as Bi and Te from the magma that passed over them (Fig. 9.1a). This may have occurred during the passage of the magma that formed the Lower Zone.
3. A large pulse of magma entrained the now PGE-rich sulfides and was intruded into the Transvaal Supergroup country rocks to form the Platreef. The magma intruded across dipping strata, entraining xenoliths of local floor rocks. Where it met the Transvaal-Archaean basement boundary, it exploited this boundary, and incorporated xenoliths of Malmani dolomites from the roof for several kilometres north of the last footwall outcrop (Fig. 9.1b).
4. Assimilation of footwall sulfides in some areas, e.g. Turfspruit, locally upgraded the S content of the Platreef sulfide fraction (Fig. 9.1b, inset).
5. The PGE-rich sulfide liquid in the Platreef fractionated as it cooled, with the IPGE and Rh being concentrated into early crystallising mss, with Pt, Pd, Au and some semi metals being concentrated into a late-stage residual liquid. During exsolution of

- pyrrhotite and pentlandite from mss, and chalcopyrite from iss, the IPGE remained in solid solution in pyrrhotite and pentlandite. All the Rh and some Pd remained in solid solution in pentlandite. The remainder of the Pd, plus virtually all the Pt and Au and semi metals are present as discrete PGM around the margins of the BMS blebs.
6. Assimilation of footwall sediments, particularly carbonates, released large volumes of volatiles into the Platreef magma. The interaction of a variety of fluids released from the various footwall lithologies were responsible for redistributing and recrystallising PGE in the Platreef, and in particular for redistributing PGE and sulfides into the footwall rocks, xenoliths and Malmani roof (Fig 9.1b, inset). In places where the footwall contained sulfate, S exchange of country rock S with the magmatic sulfide occurred during hydrothermal leaching, and affected late-stage sulfides.

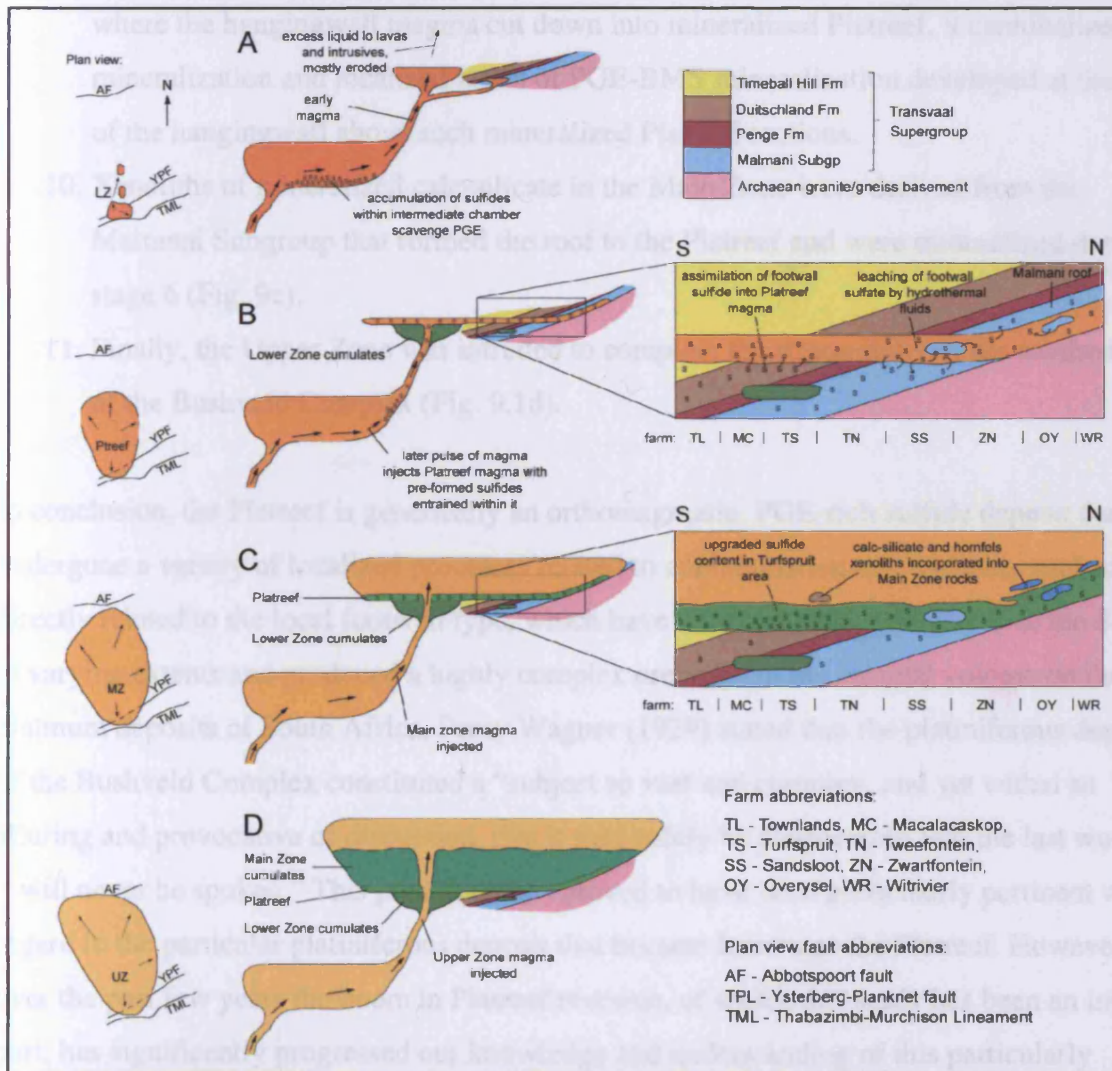


Figure 9.1. Model for the formation of the northern limb of the Bushveld Complex.

7. Where the floor rocks were anhydrous gneisses, partial melting of the footwall occurred around grain boundaries; with some of the felsic melt produced contaminating the basal part of the Platreef pyroxenites. Development of an interconnected melt network allowed the downward percolation of sulfide from the Platreef into the gneisses. This process fractionated the PGE, with the assemblages becoming more IPGE-poor with depth.
8. A significant period of crystallization and cooling occurred, during which some shearing of the Platreef pyroxenites occurred, producing steeply dipping NE-SW and strike parallel, westerly dipping N-S shear zones in the Platreef.
9. The gabbro-noritic Main Zone magma was then intruded and exploited some of these shear zones to occasionally produce finger-like intrusions down into the Platreef (Fig. 9.1c). The Platreef-hangingwall contact is therefore a magmatic unconformity, and where the hangingwall magma cut down into mineralized Platreef, it cannibalized the mineralization and localized zones of PGE-BMS mineralization developed at the base of the hangingwall above such mineralized Platreef sections.
10. Xenoliths of mineralized calc-silicate in the Main Zone were derived from the Malmani Subgroup that formed the roof to the Platreef and were mineralized during stage 6 (Fig. 9c).
11. Finally, the Upper Zone was intruded to complete the stratigraphy of the northern limb of the Bushveld Complex (Fig. 9.1d).

In conclusion, the Platreef is genetically an orthomagmatic, PGE-rich sulfide deposit that has undergone a variety of localized processes related to contamination and hydrothermal activity directly related to the local footwall type, which have altered the original nature of the deposit to varying extents and produced a highly complex orebody. In his seminal volume on the platinum deposits of South Africa, Percy Wagner (1929) stated that the platiniferous deposits of the Bushveld Complex constituted a “subject so vast and complex, and yet withal so alluring and provocative of discussion, that it may safely be prophesied that the last word on it will never be spoken.” This prediction has proved to have been particularly pertinent with regard to the particular platiniferous deposit that became known as the Platreef. However, over the past few years the boom in Platreef research, of which this study has been an integral part, has significantly progressed our knowledge and understanding of this particularly enigmatic deposit.

References

-
- AIM Resources, 2004, Independent Valuation of the Mokopane Platreef Project. 18 p.
- Alapieti, T.T. and Lahtinen, J.J., 2002, Platinum-Group element mineralization in layered intrusions of northern Finland and the Kola Peninsula, Russia: *in* Cabri, L.J., ed., The geology, geochemistry, mineralogy and mineral beneficiation of platinum-group elements. Canadian Institute of Mining, Metallurgy and Petroleum, Special Volume 54, p. 507-546.
- Armitage, P.E.B., McDonald, I., Edwards, S.J. and Manby, G.M., 2002, Platinum-group element mineralization in the Platreef and calc-silicate footwall at Sandsloot, Potgietersrus District, South Africa: Applied Earth Science (Transactions of the Institute of Mining and Metallurgy B), v. 111, p. B36-45.
- Ashwal, L.D., Webb, S.J. and Knoper, M.W., 2004, Magmatic stratigraphy in the Bushveld Northern Lobe: continuous geophysical and mineralogical data from the 2950m Bellevue drillcore: South African Journal of Geology, v. 108, p. 199-232.
- Augé, T., Salpeteur, I., Bailey, L., Mukherjee, M. M. and Patra, R. N., 2002, Magmatic and hydrothermal platinum-group minerals and base-metal sulfides in the Baula Complex, India: Canadian Mineralogist, v. 40, p. 277-309.
- Ballhaus, C. and Sylvester, P.J., 2000, Noble metal enrichment processes in the Merensky Reef, Bushveld Complex: Journal of Petrology, v. 41, p.545-561.
- Ballhaus, C., Tredoux, M. and Späth, A., 2001, Phase relations in the Fe-Ni-Cu-PGE-S system at magmatic temperature and application to Massive Sulphide Ores of the Sudbury Igneous Complex: Journal of Petrology, v. 42, p.1911-1926.
- Barnes, S-J., and Maier, W.D., 2002a, Platinum-group element distributions in the Rustenburg Layered Suite of the Bushveld Complex, South Africa: *in* Cabri, L.J., ed., The geology, geochemistry, mineralogy and mineral beneficiation of platinum-group elements. Canadian Institute of Mining, Metallurgy and Petroleum, Special Volume 54, p. 553-580.
- Barnes, S-J., and Maier, W.D., 2002b, Platinum-group elements and microstructures of normal Merensky Reef from Impala Platinum Mines, Bushveld Complex: Journal of Petrology, v. 43, p. 103-128.
- Barnes, S-J., Makovicky, E., Makovicky, M., Rose Hansen, J. and Karup Moller, S., 1997, Partition coefficients for Ni, Cu, Pd, Pt, Rh and Ir between monosulphide solid solution and sulphide liquid and the formation of compositionally zoned Ni-Cu sulphide bodies by fractional crystallization of a sulphide liquid: Canadian Journal of Earth Sciences, v. 34, p. 366-374.
- Barnes, S-J., Cox, R.A. and Zientek, M.L., 2005, Cobalt, gold and platinum-group element distribution in compositionally zoned sulphide droplets from the Medvezhy Creek Mine, Noril'sk, Russia: *in* Törmänen, T.O. and Alapieti, T.T., eds., 10th International Platinum Symposium, 2005, Extended Abstracts, p. 43-46.
- Barnes, S-J., Cox, R.A. and Zientek, M.L., 2006, Platinum-group element, gold, silver and base metal distribution in compositionally zoned sulfide droplets from the Medvezky Creek Mine, Noril'sk, Russia: Contributions to Mineralogy and Petrology, v. 152, p. 187-200.
- Barton Jr, J.M., Cawthorn, R.G. and White, J., 1986, The role of contamination in the evolution of the Platreef of the Bushveld Complex: Economic Geology, v. 81, p. 1096-1104.
-

- Bockrath, C., Ballhaus, C. and Holzheid, A., 2004, Stabilities of laurite RuS₂ and monosulfide liquid solution at magmatic temperature: *Chemical Geology*, v. 208, p. 265-271.
- Boudreau, A.E. and Meurer, W.P., 1999, Chromatographic separation of the platinum-group elements, gold, base metals, and S during degassing of a compacting and solidifying crystal pile: *Contributions to Mineralogy and Petrology*, v. 134, p. 174-185.
- Brenan, J.M. and Andrews, D., 2001, High-temperature stability of laurite and Ru-Os-Ir alloy and their role in PGE fractionation in mafic magmas: *Canadian Mineralogist*, v. 39, p. 341-360.
- Buchanan, D.L. and Nolan, J., 1979, Solubility of S and sulfide immiscibility in synthetic thoeilitic melts and their relevance to the Bushveld Complex: *Canadian Mineralogist*, v. 17, p. 483-494.
- Buchanan, D.L. and Rouse, J.E., 1984, Role of contamination in the precipitation of sulphides in the Platreef of the Bushveld Complex: *in* Buchanan D.L. and Jones M.J., eds., *Sulphide deposits in mafic and ultramafic rocks*, London, IMM, p. 141-146.
- Buchanan, D.L., Nolan, J., Suddaby, P., Rouse, J.E., Viljoen, M.J., Davenport, J.W.J., 1981, The genesis of sulphide mineralisation in a portion of the Potgietersrus Limb of the Bushveld Complex: *Economic Geology*, v. 76, p. 568-579.
- Buick, I.S., Maas, R. and Gibson, R., 2001, Precise U-Pb titanite age constraints on the emplacement of the Bushveld Complex, South Africa: *Journal of the Geological Society*, London, v. 158, p. 3-6.
- Bye, A.R., 2001, Mining the Platreef: *Applied Earth Science (Transactions of the Institute of Mining and Metallurgy B)*, v. 110, p. B209-210.
- Bye A.R. and Bell F.G., 2001, Stability and slope design at Sandsloot open pit, South Africa. *International Journal of Rock Mechanics and Mining Sciences*: v. 38, p. 449-466.
- Cabri, L.J., 2002, The platinum-group minerals: *in* Cabri, L.J., ed., *The geology, geochemistry, mineralogy and mineral beneficiation of platinum-group elements*, Canadian institute of Mining, Metallurgy and Petroleum, Special Volume 54, p. 13-129.
- Cabri, L.J. and Feather, C.E., 1975, Platinum-iron alloys: a nomenclature based on a study of natural and synthetic alloys: *Canadian Mineralogist*, v. 13, p. 117-126.
- Cabri, L.J. and Laflamme, J.H.G., 1976, The mineralogy of the platinum-group elements from some copper-nickel deposits of the Sudbury area, Ontario: *Economic Geology*, v. 71, p. 1159-1195.
- Cabri, L.J., McDonald, A.M., Stanley, C.J., Rudashevsky, N.S., Poirier, G., Durham, B.R., Mungall, J.E. and Rudashevsky, V.N., 2005, Naldrettite, Pd₂Sb, a new intermetallic mineral from the Mesamax Northwest deposit, Ungava region, Quebec, Canada: *Mineralogical Magazine*, v. 69, p. 89-97.
- Cabri, L.J., Sylvester, P.J., Tubrett, M.N., Peregoedova, A. and Laflamme, J.H.G., 2003, Comparison of LAM-ICP-MS and Micro-PIXE results for palladium and rhodium in selected samples of Noril'sk and Talnakh sulfides: *Canadian Mineralogist*, v. 41, p. 321-329.
- Cameron, E.N., 1978, The Lower Zone of the Eastern Bushveld Complex in the Olifants River Trough: *Journal of Petrology*, v. 19, p. 437-462.
- Campbell, I.H., Naldrett, A.J. and Barnes, S-J., 1993, A model for the origin of platinum-rich sulfide horizons in the Bushveld and Stillwater Complexes: *Journal of Petrology*, v. 24, p. 133-165.

-
- Carlson, R.W., Pearson, D.G., Boyd, S.B., Shirey, S.B., Irvine, G., Menzies, A.H. and Gurney, J.J., 1999, Re-Os systematics of lithospheric peridotites: implications for lithosphere formation and preservation: *in* Gurney, J.J., Gurney, J.L., Pascoe, M.D. and Richardson, S.H., eds., Proceedings of the seventh International Kimberlite Conference. Red Roof Design, Cape Town, South Africa, p. 99-108.
- Cawthorn, R.G., 1999, The platinum and palladium resources of the Bushveld Complex: *South African Journal of Science*, v. 95, p. 481-489.
- Cawthorn, R.G., 2005, Pressure fluctuations and the formation of the PGE-rich Merensky and chromitite reefs, Bushveld Complex: *Mineralium Deposita*, v. 40, p. 231-235.
- Cawthorn, R.G., and Webb, S.J., 2001, Connectivity between the western and eastern limbs of the Bushveld Complex: *Tectonophysics*, v. 330, p. 195-209.
- Cawthorn, R.G., Barton Jr, J.M. and Viljoen, M.J., 1985, Interaction of floor rocks with the Platreef on Overysel, Potgietersrus, Northern Transvaal: *Economic Geology*, v. 80, p. 988-1006.
- Cawthorn, R.G., Merkle, R.K.W. and Viljoen, M.J., 2002, Platinum-Group elements in the Bushveld Complex: *in* Cabri, L.J., ed., The geology, geochemistry, mineralogy and mineral beneficiation of platinum-group elements, Canadian institute of Mining, Metallurgy and Petroleum, Special Volume 54, p. 389-430.
- Cheney, E. S. and Twist, D., 1991, The conformable emplacement of the Bushveld mafic rocks along a regional unconformity in the Transvaal succession of South Africa: *Precambrian Research*, v. 52, p. 115-132.
- Clay, A.N., 1986, The stratigraphy of the Malmani dolomite Subgroup in the Carletonville area, Transvaal: genetic implications for lead-zinc mineralisation, *in* Anhaeusser, C.R. and Maske, S., eds., Mineral Deposits of Southern Africa, Geological Society of Southern Africa, Johannesburg, p. 853-860.
- de Bremond d'Ars, J., Arndt, N.T. and Hallot, E., 1999, Analog experimental investigation of the formation of magmatic sulfide deposits, *in* Stanley, C.J., *et al.*, eds., Mineral Deposits: Processes to Processing, Balkema, Rotterdam, p. 705-708.
- de Waal, S.A. and Gauert, C.D.K., 1997, The Basal Gabbro Unit and the identity of the parental magma of the Uitkomst Complex, Badplaas, South Africa: *South African Journal of Geology*, v. 100, p. 349-361.
- de Wit, M.J., Roering, C., Armstrong, R.A., Tredoux, M., de Ronde, C.E.J., Hart, R.J., Green, R., Peberdy, E. and Hart, R.A., 1992, Formation of an Archaean continent: *Nature*, v. 357, p. 553-562.
- du Plessis, A. and Kleywegt, R.J., 1987, A dipping sheet model for the mafic lobes of the Bushveld Complex: *South African Journal of Geology*, v. 90, p. 1-6.
- du Pleiss, C.P. and Walraven, F., 1990, The tectonic setting of the Bushveld Complex in southern Africa, Part 1: Structural deformation and distribution: *Tectonophysics*, v. 179, p. 305-319.
- Eales, H.V. and Cawthorn, R.G., 1996, The Bushveld Complex: *in* Cawthorn, R.G., ed., Layered Intrusions, Elsevier Science, p. 181-230.
- Farrow, C.E.G. and Watkinson, D.H., 1997, Diversity of precious-metal mineralization in footwall Cu-Ni-PGE deposits, Sudbury, Ontario: implications for hydrothermal models of formation: *Canadian Mineralogist*, v. 35, p. 817-839.
-

-
- Fleet, M.E., Chryssoulis, S.L., Stone, W.E. and Weisener, C.G., 1993, Partitioning of platinum-group elements and Au in the Fe-Ni-Cu-S system: experiments on the fractional crystallization of sulfide melt: *Contributions to Mineralogy and Petrology*, v. 115, p. 36-44.
- Friese, A.E.W., 2004, Geology and tectono-magmatic evolution of the PPL concession area, Villa Nora-Potgietersrus Limb, Bushveld Complex: Geological Visitor Guide, Potgietersrus Platinums Limited, 57 p.
- Friese, A.E.W. and Chunnett, G.K., 2004, Tectono-magmatic development of the northern limb of the Bushveld Igneous Complex, with special reference to the mining area of Potgietersrus Platinums Limited: *Geoscience Africa 2004, Abstract Volume, July 2004*, University of the Witwatersrand, Johannesburg, South Africa, p. 209-210.
- Gain, S.B. and Mostert, A.B., 1982, The geological setting of the platinoïd and base metal sulphide mineralization in the Platreef of the Bushveld Complex in Drenthe, north of Potgietersrus: *Economic Geology*, v. 77, p. 1395-1404.
- Gandin, A., Wright, D.T. and Melezhik, V., 2005, Vanished evaporites and carbonate formation in the Neoproterozoic Kogelbeen and Gamohaam formations of the Campbellrand Subgroup, South Africa: *Journal of African Earth Sciences*, v. 41, p. 1-23.
- Gauert, D.D.K., de Waal, S.A. and Wallmach, T., 1995, Geology of the ultrabasic to basic Uitkomst complex, eastern Transvaal, South Africa: an overview: *Journal of African Earth Sciences*, v. 21, p. 553-570.
- Good, N., and de Wit, M., 1997, The Thabazimbi-Murchison Lineament of the Kaapvaal Craton, South Africa: 2700 Ma of episodic deformation: *Journal of the Geological Society, London*, v. 154, p. 93-97.
- Grassineau, N.V., Appel, P.W.U., Fowler, C.M.R. and Nisbet, E.G., 2005, Distinguishing biological from hydrothermal signatures via sulfur and carbon isotopes in Archaean mineralizations at 3.8 to 2.7Ga: *in* McDonald, I., Boyce, A.J., Butler, I.B., Herrington, R.J. and Polya, D.A., eds., *Mineral Deposits and Earth Evolution: Geological Society, Special Publications*, 248, Geological Society of London, p. 195-212.
- Grobler, N.J. and Whitfield, G.G., 1970, The olivine-apatite magnetites and related rocks in the Villa Nora occurrence of the Bushveld Igneous Complex: *Geological Society of South Africa, Special Publication*, 1, p. 1161-1177.
- Grokhovskaya, T.L., Lapina, M.I., Ganin, V.A. and Grinevich, N.G., 2005, PGE mineralization in the Burakovsk Layered Complex, Southern Karelia, Russia: *Geology of Ore Deposits*, v. 47, p. 283-308.
- Hall A.L., 1932, *The Bushveld Igneous Complex in the central Transvaal: Geological Society, South Africa, Memoir*, 28, 544 p.
- Hammerbeck, E.C.I. and Schürmann, L.W., 1998, Nickel: *in* Wilson, M.G.C. and Anhaeusser, C.R., eds., *The mineral resources of Southern Africa*, Council for Geoscience, p. 471-482.
- Harmer, R.E., 2004, The Volspruit PGE-Ni reef: platinum mineralization in the Lower Zone south of Mokopane: *Geoscience Africa 2004, Abstract Volume*, University of the Witwatersrand, Johannesburg, South Africa, p. 256-257.
- Harmer, R.E., Pillay, N. and Davis, P.G., 2004, The Aurora project - Main Zone hosted PGE-base metal mineralization at the northern outcrop limit of the Bushveld northern limb, north of Mokopane:
-

-
- Platreef Workshop field guide, Mokopane 16-19 July, 2004, Geoscience Africa, University of the Witwatersrand.
- Harris, C. and Chaumba, J.B., 2001, Crustal contamination and fluid-rock interaction during the formation of the Platreef, Northern Limb of the Bushveld Complex, South Africa: *Journal of Petrology*, v. 42, p. 1321-1347.
- Hattingh, P.J., 1995, Palaeomagnetic constraints on the emplacement of the Bushveld Complex: *Journal of African Earth Sciences*, v. 21, p. 549-551.
- Hattingh, P.J. and Pauls, N.D., 1994, New palaeomagnetic results from the northern Bushveld Complex of South Africa: *Precambrian Research*, v. 69, p. 229-240.
- Hatton, C.J., 1995, Mantle plume origin for the Bushveld and Ventersdorp provinces: *Journal of African Earth Sciences*, v. 21, p. 571-577.
- Hatton, C.J. and von Gruenewaldt, G., 1987, The geological setting and the petrogenesis of the Bushveld chromitite layers: *in* Stowe, C.W., ed., *Evolution of the chromium orefields*, Van Nostrand Reinhold, New York, p. 109-143.
- Helmy, H.M., Ballhaus, C., Berndt, J., Bockrath, C. and Wohlgemuth-Ueberwasser, C., 2006, Formation of Pt, Pd and Ni tellurides: experiments in sulfide-telluride systems: *Contributions to Mineralogy and Petrology* (in press).
- Hoatson, D.M. and Keays, R.R., 1989, Formation of platiniferous sulfide horizons by crystal fractionation and magma mixing in the Munni Munni layered intrusion, west Pilbara block, Western Australia: *Economic Geology*, v. 84, p. 1775-1804.
- Holwell, D.A. and Jordaan, A., 2006, Three-dimensional mapping of the Platreef at the Zwartfontein South mine: implications for the timing of magmatic events in the northern limb of the Bushveld Complex, South Africa: *Applied Earth Science (Transactions of the Institute of Mining and Metallurgy B)*, v. 115, p. 41-48.
- Holwell, D.A. and McDonald, I., 2005a, Variations in platinum group element mineralization within the Platreef, northern Bushveld Complex, South Africa: *in* Törmänen, T.O. and Alapieti, T.T., eds., 10th International Platinum Symposium, University of Oulu, Extended Abstracts, p. 110-113.
- Holwell, D.A. and McDonald, I., 2005b, Platinum-group mineral assemblages within the Platreef, northern Bushveld Complex, South Africa: *in* Törmänen, T.O. and Alapieti, T.T., eds., 10th International Platinum Symposium, 2005, Extended Abstracts, p. 373-376.
- Holwell, D.A. and McDonald, I., 2006, Petrology, geochemistry and the mechanisms determining the distribution of Platinum-Group Element and Base Metal Sulfide mineralization in the Platreef at Overysel, northern Bushveld Complex, South Africa: *Mineralium Deposita*, v. 41, p. 575-598.
- Holwell, D.A., McDonald, I. and Armitage, P.E.B., 2004, Platinum-group mineral assemblages in the Platreef at Sandsloot mine, Limpopo Province, South Africa: *Geoscience Africa 2004, Abstract Volume*, July 2004. University of the Witwatersrand, Johannesburg, South Africa, p. 282-283.
- Holwell, D.A., Armitage, P.E.B. and McDonald, I., 2005, Observations on the relationship between the Platreef and its hangingwall. *Applied Earth Science (Transactions of the Institute of Mining and Metallurgy B)*, v. 114, p. B199-207.
-

-
- Holwell, D.A., McDonald, I and Armitage, P.E.B., 2006, Platinum-group mineral assemblages in the Platreef at the South Central Pit, Sandsloot Mine, northern Bushveld Complex, South Africa: *Mineralogical Magazine*, v. 70, p. 83-101.
- Huber, H., Koeberl, C., McDonald, I. and Reimold, W.U., 2001, Geochemistry and petrology of Witwatersrand and Dwyka diamictites from South Africa: Search for an extraterrestrial component: *Geochimica et Cosmochimica Acta*, v. 65, p.2007-2016.
- Hulbert, L.J., 1983, A petrographical investigation of the Rustenburg Layered Suite and associated mineralization south of Potgietersrus: Unpublished DSc dissertation, University of Pretoria, 511 p.
- Hulbert, L.J. and von Gruenewaldt, G., 1982, Nickel, copper and platinum mineralisation in the Lower Zone of the Bushveld Complex, south of Potgietersrus: *Economic Geology*, v. 77, p. 1296-1306.
- Hulbert, L.J. and von Gruenewaldt, G., 1986, The structure of the upper and lower chromitite layers on the farms Grasvally and Zoetveld, south of Potgietersrus: *in* Anhausser, C.R. and Maske, S., eds., *Mineral Deposits of Southern Africa*. Volume 2, Geological Society of Southern Africa, Johannesburg, p. 1237-1249
- Huminicki, M.A.E., Sylvester, P.J., Cabri, L.J., Leshner, C.M. and Tubrett, M., 2005, Quantitative mass balance of platinum group elements in the Kelly Lake Ni-Cu-PGE deposit, Copper Cliff Offset, Sudbury: *Economic Geology*, v. 100, p. 1631-1646.
- Hutchinson, D. and Kinnaird, J.A., 2005, Complex multi-stage genesis for the Ni-Cu-PGE mineralisation in the southern region of the Platreef, Bushveld Complex, South Africa: *Applied Earth Science (Transactions of the Institute of Mining and Metallurgy B)*, v. 114, p. B208-224.
- Hutchinson, D. and McDonald, I., 2005, Breaking the rules. Divergent behaviour of platinum and palladium in the northern limb of Bushveld Complex, RSA: *in* Törmänen, T.O. and Alapieti, T.T., eds., 10th International Platinum Symposium, 2005, Extended Abstracts, p. 118-121.
- Hutchinson, D. and McDonald, I., 2006, Formation of high-temperature Pt-arsenides and antimonides and their subsequent expulsion from sulphide liquids. A case study by laser ablation ICP-MS from the Northern Limb of the Bushveld Complex, RSA: *Mineralium Deposita* (submitted)
- Hutchinson, D., Kinnaird, J.A. and Schurmann, L.W., 2004, Complex, multi-stage mineralization history in the southern sector of the Platreef, Bushveld Complex, RSA: *Geoscience Africa 2004, Abstract Volume*, July 2004. University of the Witwatersrand, Johannesburg, South Africa, p. 293-294.
- Iljina, M.J., Alapieti, T.T. and McElduff, B.M., 1992, Platinum-group element mineralisation in the Suhanko-Konttijärvi intrusion, Finland: *Australian Journal of Earth Science*, v. 39, p. 303-313.
- Irvine, T.N., 1975, Crystallization sequences in the Muskox intrusion and other layered intrusions – II. Origin of chromitite layers and similar deposits of other magmatic ores: *Geochimica et Cosmochimica Acta*, v. 39, p. 991-1020.
- Irvine, T.N., 1988, Muskox Intrusion, Northwest Territories: *in* Hulbert, L.J., Duke, J.M., Eckstrand, O.R., Lydon, J.W., Scoates, R.F.J. and Cabri, L.J., eds., *Geological environments of the platinum-group elements*, Geological Survey of Canada, Open File 1440, p. 25-39.
- Keys, R.R., 1995, The role of komatiitic and picritic magmatism and S-saturation in the formation of ore deposits: *Lithos*, v. 34, p. 1-18.
- Kendall, T., 2006, *Platinum 2006: Johnson Matthey, Royston, UK*, 52 p.
-

-
- Kelley, S.P. and Fallick, A.E., 1990, High precision spatially resolved analysis of $\delta^{34}\text{S}$ in sulfides using a laser extraction system: *Geochimica et Cosmochimica Acta*, v. 54, p. 883-888.
- Kendall, T., 2006, *Platinum 2006*: Johnson Matthey, Royston, UK, 52p.
- Kinloch, E.D., 1982, Regional trends in the platinum-group mineralogy of the Critical Zone of the Bushveld Complex, South Africa: *Economic Geology*, v. 77, p. 1328-1347.
- Kinloch, E.D. and Peyerl, W., 1990, Platinum-group minerals in various rock types of the Merensky Reef: genetic implications: *Economic Geology*, v. 85, p. 537-555.
- Kinnaid, J.A., 2004, What are the questions we need to ask about the Platreef?: Platreef Workshop field guide, Mokopane 16-19 July, 2004, Geoscience Africa, University of the Witwatersrand.
- Kinnaid, J.A., 2005, Geochemical evidence of multiphase emplacement in the southern Platreef: *Applied Earth Science (Transactions of the Institute of Mining and Metallurgy B)*, v. 114, p. B225-242.
- Kinnaid, J.A. and Nex P.A.M., 2003, Mechanisms of marginal mineralization in the Bushveld Complex: *Applied Earth Science (Transactions of the Institute of Mining and Metallurgy B)*, v. 112, p. B206-208.
- Kinnaid, J.A. and McDonald, I., 2005, An introduction to the mineralisation in the northern limb of the Bushveld Complex: *Applied Earth Science (Transactions of the Institute of Mining and Metallurgy B)* v. 114, p. B194-198.
- Kinnaid, J.A., Hutchinson, D., Schürmann, L., Nex, P.A.M. and de Lange, R., 2005, Petrology and mineralization of the southern Platreef: northern limb of the Bushveld Complex, South Africa: *Mineralium Deposita*, v. 40, p. 576-597.
- Komarova, M.Z., Kozyrev, S.M., Simonov, O.N. and Lulko, V.A., 2002, The PGE mineralization of disseminated sulphide ores of the Noril'sk-Taimyr region: *in* Cabri, L.J., ed., *The geology, geochemistry, mineralogy and mineral beneficiation of platinum-group elements*, Canadian institute of Mining, Metallurgy and Petroleum, Special Volume, p. 547-567.
- Kruger, F.J., 2005a, Filling the Bushveld Complex magma chamber: lateral expansion, floor interaction, magmatic unconformities and giant chromitite and PGE deposits: *Mineralium Deposita*, v. 40, p. 451-472.
- Kruger, F.J., 2005b, Thoughts on the Platreef - a Critical Zone or Main Zone phenomenon?: 2nd Platreef Workshop, Abstract Volume, Geological Society of South Africa.
- Lambert, D.D., Foster, J.G., Frick, L.R., Ripley, E.M. and Zientek, M.L., 1998, Geodynamics of magmatic Cu-Ni-PGE sulfide deposits: New insights from the Re-Os isotopic system: *Economic Geology*, v. 93, p. 121-138.
- Lee, C.A., 1996, A review of mineralization in the Bushveld Complex and some other layered mafic intrusions, *in* Cawthorn, R.G., ed., *Layered Intrusions*, Elsevier Science, 103-146.
- Li, C. and Naldrett, A.J., 1993, Platinum-group minerals from the Deep Copper Zone of the Strathcona deposit, Sudbury, Ontario: *Canadian Mineralogist*, v. 31, p. 31-44.
- Li, C., Barnes, S-J., Makovicky, E., Rose-Hansen, J., Makovicky, M., 1996, Partitioning of nickel, copper, iridium, rhenium, platinum and palladium between monosulfide solid solution and sulfide
-

liquid: effects of composition and temperature: *Geochimica et Cosmochimica Acta*, v. 60, p. 1231-1238.

Li, C., Ripley, E.M., Maier, W.D. and Gomwe, T.E.S., 2002, Olivine and S isotopic compositions of the Uitkomst Ni-Cu sulfide ore-bearing complex, South Africa: evidence for S contamination and multiple magma emplacements: *Chemical Geology*, v. 188, p. 149-159.

Li, C., Ripley, E.M., Merino, E. and Maier, W.D., 2004, Replacement of base metal sulphides by actinolite, epidote, calcite and magnetite in the UG2 and Merensky Reef of the Bushveld Complex, South Africa: *Economic Geology*, v. 99, p. 173-184.

Makovicky, E., 2002, Ternary and quaternary phase systems with PGE: *in* Cabri, L.J., ed., The geology, geochemistry, mineralogy and mineral beneficiation of platinum-group elements, Canadian institute of Mining, Metallurgy and Petroleum, Special Volume 54, p. 131-175.

Maier, W. D., 2002, Pt, Pd, Cu and sulfur contents of the Platreef on the farm Townlands, northern Bushveld Complex: *in* Boudreau, A., ed., 9th International Platinum Symposium, extended abstracts, 21-25 July 2002, Billings, Montana, USA.

Maier, W.D., and Barnes, S.J., 1999, Platinum-group elements in silicate rocks of the Lower, Critical and Main Zones at union section, western Bushveld Complex: *Journal of Petrology*, v. 40, p. 1647-1671.

Maier, W.D., Barnes, S-J., Teigler, B., de Klerk, W.J., Mitchell, A.A., 1996, Cu/Pd and Cu/Pt of silicate rocks in the Bushveld Complex: implications for platinum-group element exploration: *Economic Geology*, v. 91, p. 1151-1159.

Maier, W.D., Barnes, S-J., and van der Merwe, M.J., 2001, Platinum-group elements in the Pyroxenite Marker, Bushveld Complex: implications for formation of the Main Zone: *South African Journal of Geology*, v. 104, p. 301-308.

Manyeruke, T.D., Maier, W.D. and Barnes, S-J., 2005, Major and trace element geochemistry of the Platreef on the farm Townlands, northern Bushveld Complex: *South African Journal of Geology*, v. 108, p. 381-396.

Martini, J.E.J., Eriksson, P.G. and Snyman, C.P., 1995, The early Proterozoic Mississippi Valley-type Pb-Zn-F deposits of the Cambellrand and Malmani Subgroups, South Africa: *Mineralium Deposita*, v. 30, p. 135-145.

McCourt, S. and Vearncombe, J., 1987, Shear zones bounding the Central Zone of the Limpopo Mobile Belt, southern Africa: *Journal of Structural Geology*, v. 9, p. 127-137.

McDonald, I., 2005, Development of sulfide standards for the in-situ analysis of platinum-group elements by laser ablation inductively coupled plasma-mass spectrometry (LA-ICP-MS): *in* Törmänen, T.O. and Alapieti, T.T., eds., 10th International Platinum Symposium, 2005, Extended Abstracts, p 468-471.

McDonald, I., Vaughan, D.J. and Tredoux, M., 1995, Platinum mineralization in quartz veins near Naboomspruit, central Transvaal: *South African Journal of Geology*, v. 98, p. 168-175.

McDonald, A.M., Cabri, L.J., Stanley, C.J., Rudashevsky, N.S., Poirier, G., Durham, B.R., Mungall, J.E. and Rudashevsky, V.N, 2005, Ungavaite, Pd₄Sb₃, a new intermetallic mineral from the Mesamax Northwest deposit, Ungava region, Quebec, Canada: Description and genetic implications: *Canadian Mineralogist*, v. 43, p. 1735-1744.

-
- McDonald, I., Holwell, D.A. and Armitage, P.E.B., 2005, Geochemistry and mineralogy of the Platreef and "Critical Zone" cumulates of the Northern limb of the Bushveld Complex, South Africa: implications for Bushveld stratigraphy and the development of PGE mineralization: *Mineralium Deposita*, v. 40, p. 526-549.
- McLaren, C.H. and de Villiers, J.P.R., 1982, The platinum-group chemistry and mineralogy of the UG-2 chromitite layer of the Bushveld Complex: *Economic Geology*, v. 77, p. 1348-1366.
- Merensky, H., 1925, Report on the platinum occurrence on the properties of Potgietersrust Platinums, Limited: Report to Shareholders, London and Rhodesia Mining and Land Company Ltd, Johannesburg, South Africa. 6 p.
- Meyer, R. and de Beer, H., 1987, Structure of the Bushveld Complex from resistivity measurements: *Nature*, v. 325, p. 610-612.
- Miller Jr., J.D. and Ripley, E.M., 1996, Layered intrusions of the Duluth Complex, Minnesota, USA: *in* Cawthorn, R.G., ed., *Layered Intrusions*, Elsevier Science, p. 257-301.
- Mills Davies, J.E., 1925, The geology of the Transvaal platinum deposits: *The South African Mining and Engineering Journal*, v. 36, p. 63-66.
- Mossom, R.J., 1986, The Atok Platinum Mine: *in* Anhaeusser, C.R., and Maske, S., eds., *Mineral Deposits of Southern Africa*, vols I and II, Geological Society of South Africa, Johannesburg, p. 1143-1154.
- Mostert, A.B., Hofmeyr, P.K. and Potgieter, G.A., 1982, The platinum-group mineralogy of the Merensky Reef at the Impala Platinum Mines, Bophuthatswana: *Economic Geology*, v. 77, p. 1385-1394.
- Mostert, A.B., 1982, The mineralogy, petrology and sulfide mineralization of the Platreef north-west of Potgietersrus, Transvaal, Republic of South Africa: *South Africa Geological Survey, Bulletin*, 72, 48 p.
- Mothetha, M.V. and Kinnaird, J.A., 2005, Mineral chemistry for the southern sector of the Platreef: 2nd Platreef Workshop, Abstract Volume, Geological Society of South Africa.
- Mungall, J.E. and Su, S., 2005, Interfacial tension between magmatic sulfide and silicate liquids: constraints on kinetics of sulfide liquation and sulfide migration through silicate rocks: *Earth and Planetary Science Letters*, v. 234, p. 135-149.
- Mungall, J.E., Andrews, D.R.A., Cabri, L.J., Sylvester, P.J. and Tubrett, M., 2005, Partitioning of Cu, Ni, Au, and platinum-group elements between monosulfide solid solution and sulfide melt under oxygen and sulfur fugacities: *Geochimica et Cosmochimica Acta*, v. 69, p. 4349-4360.
- Naldrett A.J., 2005, The Platreef: death at Drenthe; resurrection at Aurora: 2nd Platreef Workshop, Mokopane, Abstract Volume, Geological Society of South Africa, 2005.
- Naldrett, A.J. and Duke, J.M., 1980, Platinum metals in magmatic sulphide ores: *Science*, v. 208, p. 1417-1424.
- Naldrett, A.J., Innes, D.G., Sowa, J. and Gorton, M.P., 1982, Compositional variations within and between five Sudbury ore deposits: *Economic Geology*, v. 77, p. 1519-1534.
-

-
- Naldrett, A.J., Gasparini, E.C., Barnes, S.J., von Gruenewaldt, G. and Sharpe, M.R., 1986, The Upper Critical Zone of the Bushveld Complex and the origin of Merensky-type ores: *Economic Geology*, v. 81, p. 1105-1117.
- Nell, J., 1985, The Bushveld metamorphic aureole in the Potgietersrus Area: evidence for a two-stage metamorphic event: *Economic Geology*, v. 80, p. 1129-1152.
- Nex, P.A.M., 2005, The structural setting of mineralisation on Tweefontein Hill, northern limb of the Bushveld Complex, South Africa: *Applied Earth Science (Transactions of the Institute of Mining and Metallurgy B)*, v. 114, p. B243-291.
- Nyama, N., Nex, P.A.M. and Yao, Y., 2005, Preliminary petrological studies of the Platreef on Tweefontein Hill, Bushveld Igneous Complex, South Africa: *in* Törmänen, T.O. and Alapieti, T.T., eds., 10th Intl. Platinum Symposium, University of Oulu, Ext. Abstracts, 505-508.
- Oberthur, T., Weiser, T.W., Gast, L. and Kojonen, K., 2003, Geochemistry and mineralogy of platinum-group elements at Hartley Platinum Mine, Zimbabwe: *Mineralium Deposita*, v. 38, p. 312-326.
- Ohmoto, H. and Rye, R.O., 1979, Isotopes of sulfur and carbon: *in* Barnes, H.L., ed., *Geochemistry of Hydrothermal Ore Deposits*, 2nd ed: Wiley and Sons, London, p. 509–567.
- Page, N.J., von Gruenewaldt, G., Haffty, J. and Aruscavage, P.J., 1982, Comparisons of platinum, palladium and rhodium distributions in some layered intrusions with specific relation to the late differentiates (Upper Zone) of the Bushveld Complex, South Africa: *Economic Geology*, v. 77, p. 1405-1418.
- Papunen, H., Distler, V. and Sokolov, A., 1992, PGE in the upper Proterozoic Dovirensky layered Complex, north Baikal area, Siberia: *Australian Journal of Earth Sciences*, v. 39, p. 327-334.
- Peck, D.C., Keays, R.R., James, R.S., Chubb, P.T. and Reeves, S.J., 2001, Controls on the formation of contact-type platinum-group element mineralization in the East Bull Lake intrusion: *Economic Geology*, v. 96, p. 559-581.
- Peregoedova, A.V., 1998, The experimental study of the Pt-Pd-partitioning between monosulfide solid solution and Cu-Ni-sulfide melt at 900-840°C: *in* 8th International. Platinum Symposium abstracts, Geological Society of South Africa and the South African Institute of Mining and Metallurgy, Symposium Series, S18, p. 325-373.
- Prichard, H.M., Barnes, S.-J., Maier, W.D. and Fisher, P.C., 2004a, Variations in the nature of the platinum-group minerals in a cross-section through the Merensky Reef at Impala Platinum: implications for the mode of formation of the reef: *Canadian Mineralogist*, v. 42, p. 423-437.
- Prichard, H.M., Hutchinson, D. and Fisher, P.C., 2004b, Petrology and crystallization history of multiphase sulfide droplets in a mafic dike from Uruguay: implications for the origin of Cu-Ni-PGE sulfide deposits: *Economic Geology*, v. 99, p. 365-376.
- Ripley, E.M. and Li, C., 2003, S isotope exchange and metal enrichment in the formation of magmatic Cu-Ni-(PGE) deposits: *Economic Geology*, v. 98, p. 635-641.
- Ripley, E.M., Li, C. and Shin, D., 2002, Paragneiss assimilation in the genesis of magmatic Ni-Cu-Co sulfide mineralization at Voizey's Bay, Labrador: $\delta^{34}\text{S}$, $\delta^{13}\text{C}$ and Se/S evidence: *Economic Geology*, v. 97, p. 1307-1318.
-

-
- Ripley, E.M., Lightfoot, P.C., Li, C. and Elswick, E.R., 2003, S isotopic studies of continental flood basalts in the Noril'sk region: Implications for the association between lavas and ore-bearing intrusions: *Geochimica et Cosmochimica Acta*, v. 67, p. 2805-2817.
- Robinson, B.W. and Kusakabe, M., 1975, Quantitative preparation of sulfur dioxide for $^{34}\text{S}/^{32}\text{S}$ analyses from sulfides by combustion with cuprous oxide: *Analytical Chemistry*, v. 47, p. 1179-1181.
- Ruiz, J., Barra, F., Ashwal, L.D. and LeGrange, M., 2004, Re-Os systematics on sulfides of the Platreef, Bushveld Complex, South Africa: *Geoscience Africa 2004, Abstract Volume*, University of the Witwatersrand, Johannesburg, South Africa, p. 564.
- Schissel, D., Tsvetkov, A.A., Mitrofanov, F.P. and Korchagin, A.U., 2002, Basal platinum-group element mineralization in the Federov Pansky layered mafic intrusion, Kola Peninsula, Russia: *Economic Geology*, v. 97, p. 1657-1677.
- Schneiderhöhn, H., 1929, The mineragraphy, spectrography and genesis of the platinum-bearing nickel-pyrrhotite ores of the Bushveld Complex: *in* Wagner, P.A., *The platinum deposits and mines of South Africa*, Oliver and Boyd, Edinburgh, p. 206-246.
- Seversen, M.J. and Hauck, S.A., 2003, Platinum group elements (PGEs) and platinum group minerals (PGMs) in the Duluth Complex: Technical Report NRRI/TR-2003/37, Natural Resources Research Unit, University of Minnesota, Duluth, 296 p.
- Sharman-Harris, E., Kinnaird, J.A., Harris, C., Horstmann, U.E. and Wing, B., 2005, A new look at sulphide mineralisation of the northern limb, Bushveld Complex: a stable isotope study: *Applied Earth Science (Transactions of the Institute of Mining and Metallurgy B)*, v. 114, p. 252-263.
- Silver, P.G., Fouch, M.J., Gao, S.S., Schmitz, M. and Kaapvaal Seismic Group, 2004, Seismic anisotropy, mantle fabric, and the magmatic evolution of Precambrian southern Africa: *South African Journal of Geology*, v. 107, p. 45-58.
- Simpkin, T. and Smith, J.V., 1970, Minor element distribution in olivine: *Journal of Geology*, v. 78, p. 304-325.
- Spies, L., 2005, The Akanani Platinum Project: 2nd Platreef Workshop, Abstract Volume, Geological Society of South Africa.
- Tarkian, M. and Stumpfl, E.F., 1975, Platinum mineralogy of the Driekop Mine, South Africa: *Mineralium Deposita*, v. 10, p. 71-85.
- Taylor, S.R. and McLennan, S.M., 1985, *The Continental Crust: its composition and evolution*: Blackwell Scientific, UK, 312 p.
- Tommasi, A. and Vauchez, A., 2001, Continental rifting parallel to ancient collisional belts: an effect of the mechanical anisotropy of the lithospheric mantle: *Earth and Planetary Science Letters*, v. 185, p. 199-210.
- Tredoux, M., Lindsay, N.M., Davies, G. and McDonald, I., 1995, The fractionation of platinum-group elements in magmatic systems, with the suggestion of a novel causal mechanism: *South African Journal of Geology*, v. 98, p. 157-167.
- Uken, R. and Watkeys, M. K., 1997, Diapirism initiated by the Bushveld Complex, South Africa: *Geology*, v. 25, p. 723-726.
-

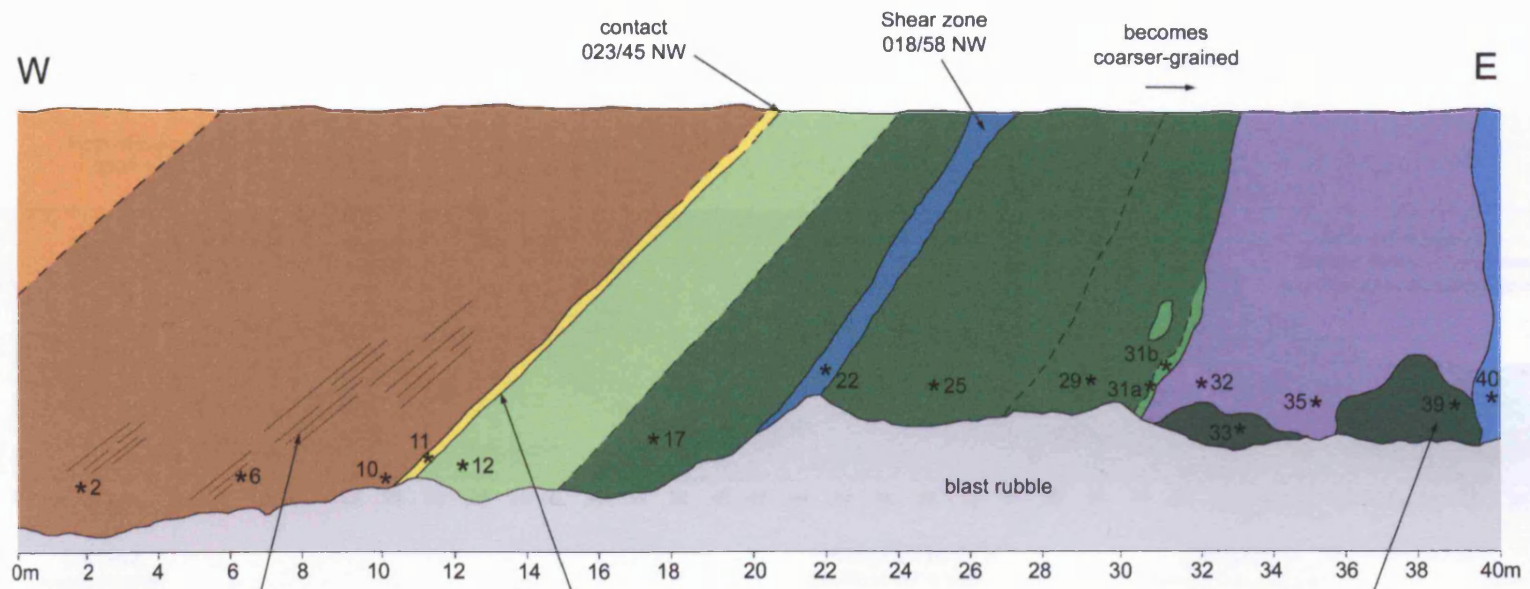
-
- van der Merwe, M.J., 1976, The Layered Sequence of the Potgietersrus Limb of the Bushveld Complex: *Economic Geology*, v. 71, p. 1337-1351.
- van der Merwe, M.J., 1978, The geology of the basic and ultramafic rocks of the Potgietersrus Limb of the Bushveld Complex: Unpublished PhD thesis, University of the Witwatersrand, 176 p.
- Viljoen, M.J. and Schürmann, L.W., 1998, Platinum group metals: *in* Wilson, M.G.C. and Anhaeusser, C.R., eds., *The mineral resources of Southern Africa*, Council for Geoscience, p. 532-568.
- Viljoen, M.J. and Scoon, R.N., 1985, The distribution and main geologic features of discordant bodies of iron-rich ultramafic pegmatite in the Bushveld Complex: *Economic Geology*, v. 80, p. 1109-1128.
- von Gruenewaldt, G., Hulbert, L.J. and Naldrett, A.J., 1989, Contrasting platinum-group element concentration patterns in cumulates of the Bushveld Complex: *Mineralium Deposita*, v. 24, p. 219-229.
- Wagner, P.A., 1929, *The platinum deposits and mines of South Africa*: Oliver and Boyd, Edinburgh, 326 p.
- Wagner, T., Boyce, A.J. and Fallick, A.E., 2002, Laser combustion analysis of $\delta^{34}\text{S}$ of sulfosalt minerals: Determination of the fractionation systematics and some crystal-chemical considerations: *Geochimica et Cosmochimica Acta*, v. 66, p. 2855-2863.
- Walraven, F., Armstrong, R.A. and Kruger, F.J., 1990, A chronostratigraphic framework for the north-central Kaapvaal Craton, the Bushveld Complex and Vredefort structure: *Tectonophysics*, v. 171, p. 23-48.
- Westerlund, K.J., Gurney, J.J., Carlson, R.W., Shirey, S.B., Hauri, E.H. and Richardson, S.H., 2004, A metasomatic origin for late Archean eclogitic diamonds: Implications from internal morphology of diamonds and Re-Os and S isotope characteristics of their sulfide inclusions from the late Jurassic Klipspringer kimberlites: *South African Journal of Geology*, v. 107, p. 119-130.
- Westland, A.D., 1981, Inorganic chemistry of the platinum-group elements: *in* Cabri, L.J., ed., *Platinum-group elements: mineralogy, geology, recovery*, Canadian Institute of Mining and Metallurgy, Special Volume, 23, p. 5-18.
- White, J.A., 1994, The Potgietersrus Prospect - Geology and exploration history: XVth CMMI Congress, Johannesburg, SAIMM, v. 3, p. 173-181.
- Wood, S.A., 2002, The aqueous geochemistry of the platinum-group elements with applications to ore deposits: *in* Cabri, L.J., ed., *The geology, geochemistry, mineralogy and mineral beneficiation of platinum-group elements*, Canadian Institute of Mining, Metallurgy and Petroleum, Special Volume 54, p. 211-249.

Appendix 1

Geological face maps from the Sandsloot and Zwartfontein South pits.

Contents:

This appendix contains the geological face maps generated from field mapping in the pits during the field seasons.



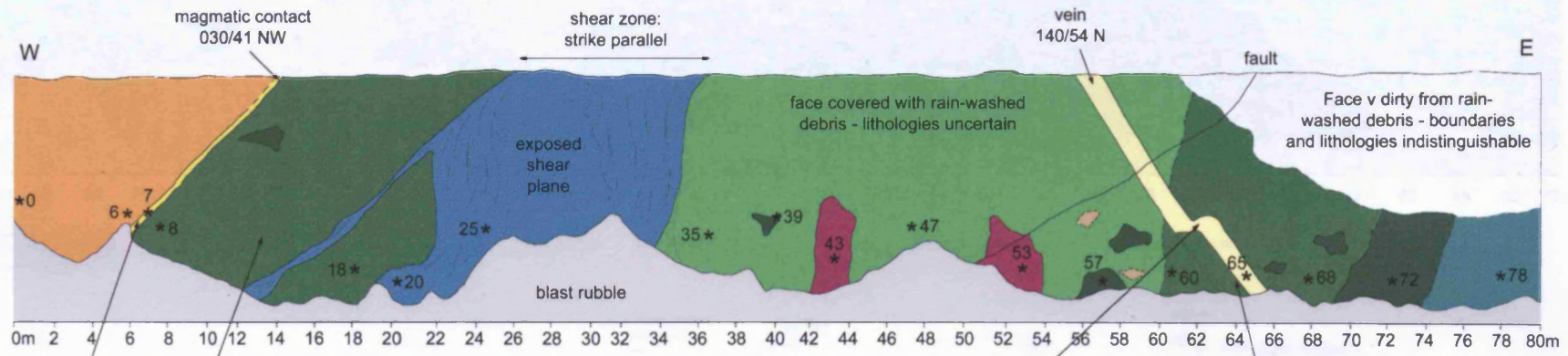
Modal layering in HW melanorite defined by proportions of plag/opx

Magmatic contact with mottled anorthosite at base

Massive sulphide blebs in serpentinite

KEY:

 HW gabbronorite	 Pyroxenite	 FW clinopyroxenite
 HW melanorite	 Feldspathic pyroxenite	 FW serpentinite
 HW mottled anorthosite	 Sheared pyroxenite	 FW calc-silicate
	 Pegmatitic pyroxenite	 * sample location



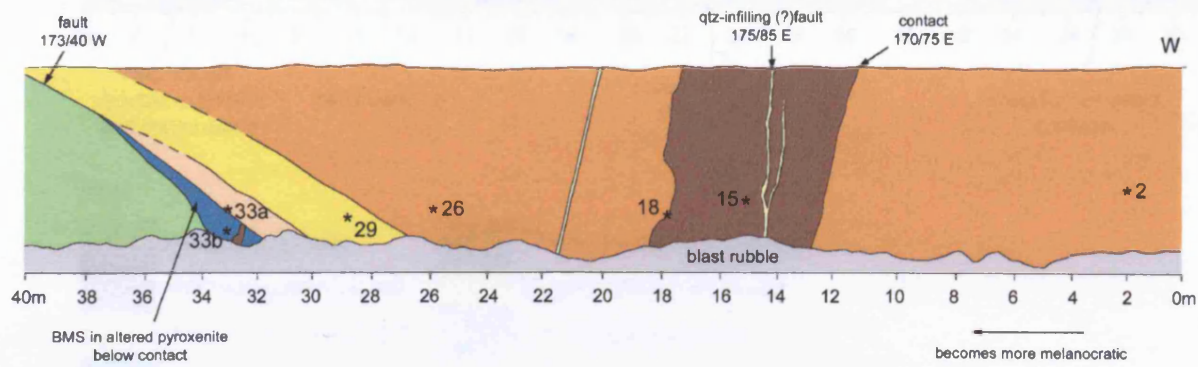
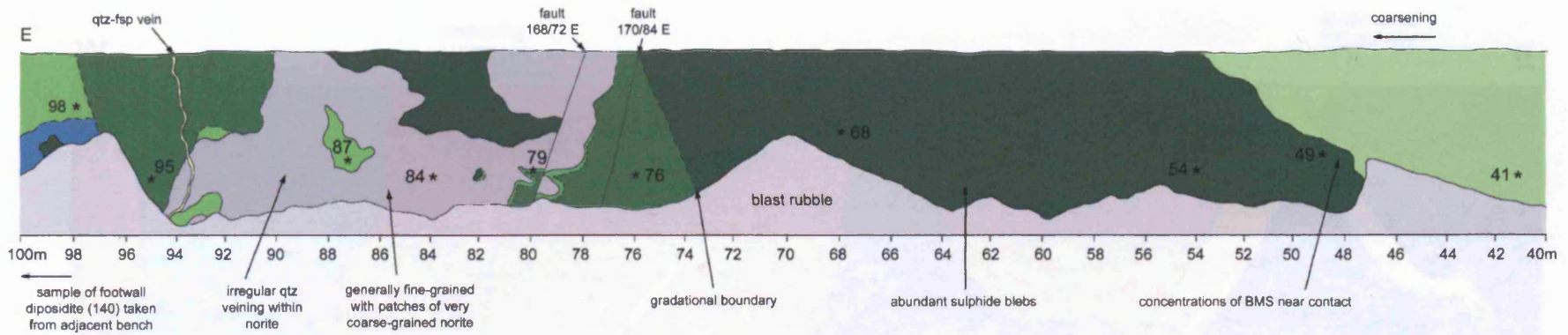
some BMS in mottled anorthosite
grain size highly variable

no apparent fault causing offset in vein

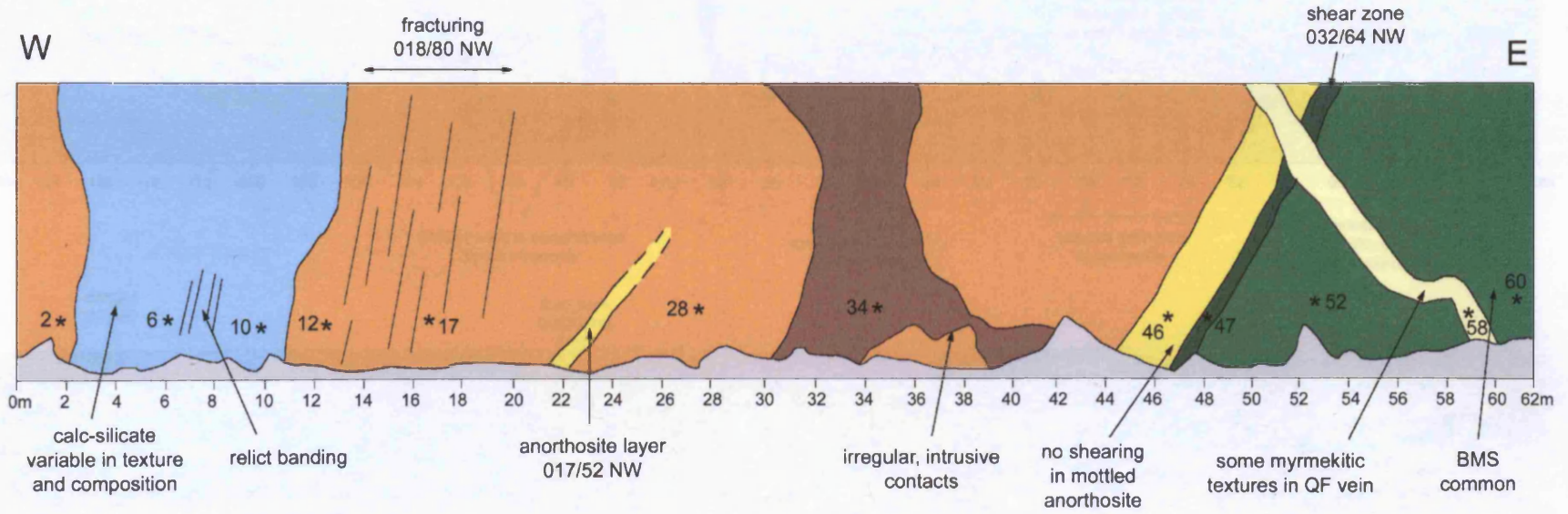
vein intruded along shear surface

KEY:

 HW gabbro	 Feldspathic pyroxenite	 Peridotite	 Serpentinite
 HW mottled anorthosite	 Sheared pyroxenite	 Felsic pegmatite	 Quartz-feldspar vein
	 Pegmatitic pyroxenite	 Clinopyroxenite	 * sample location

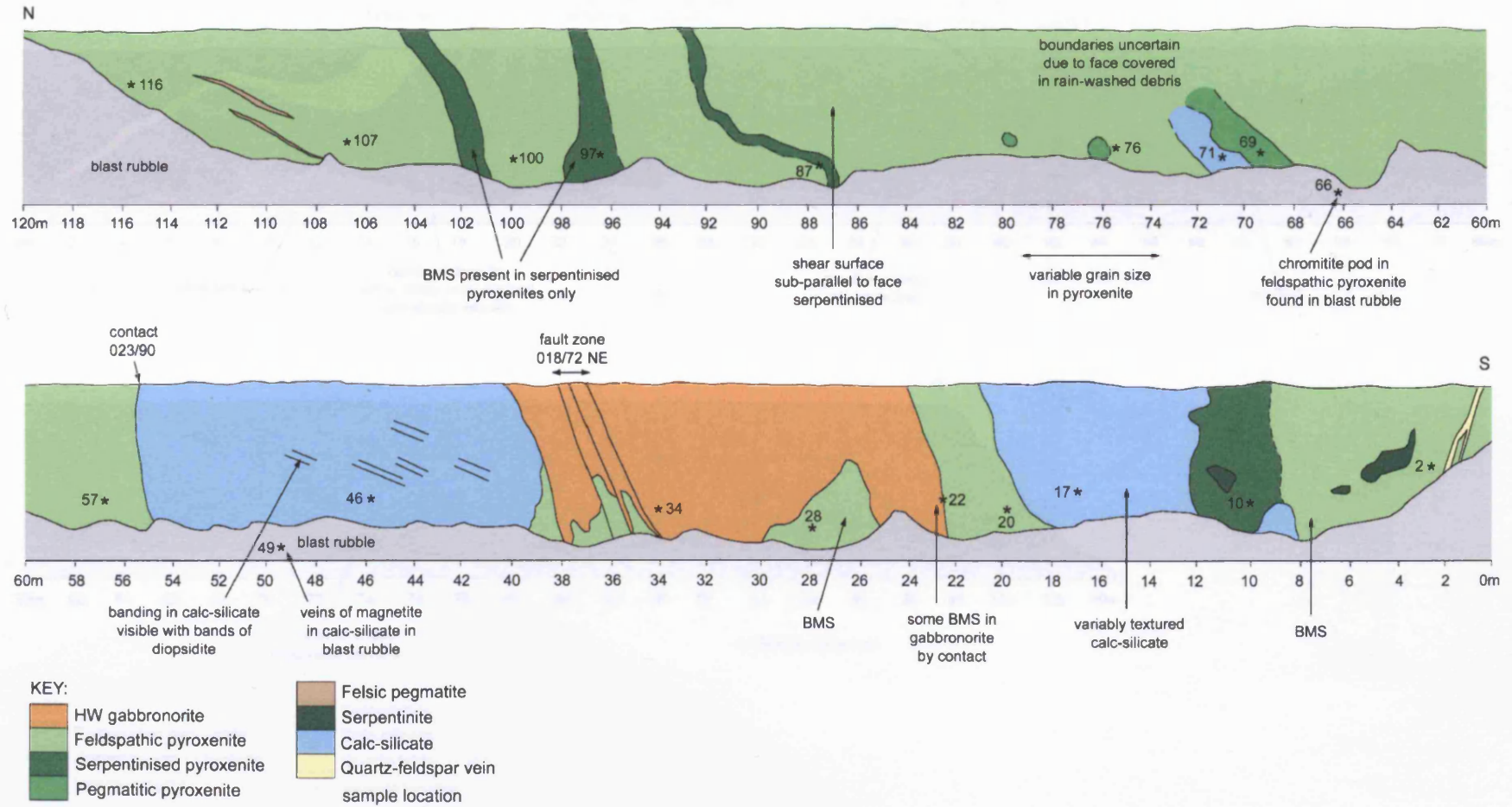


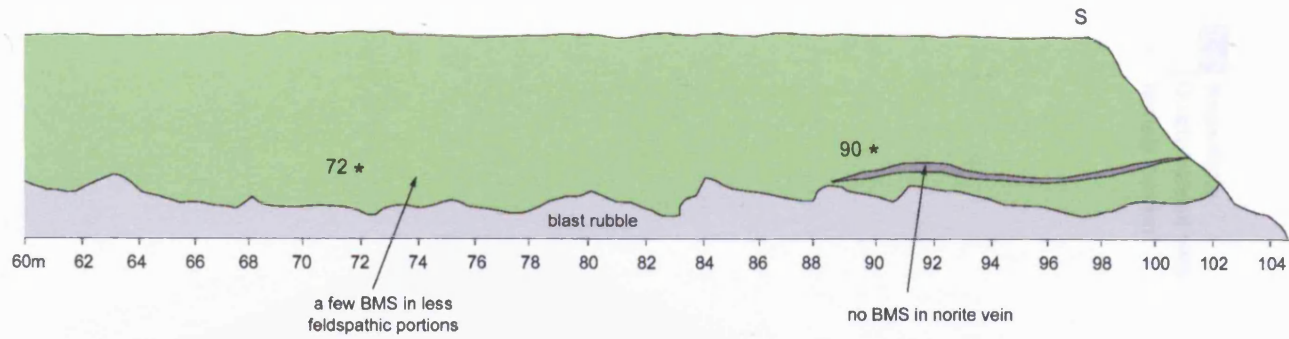
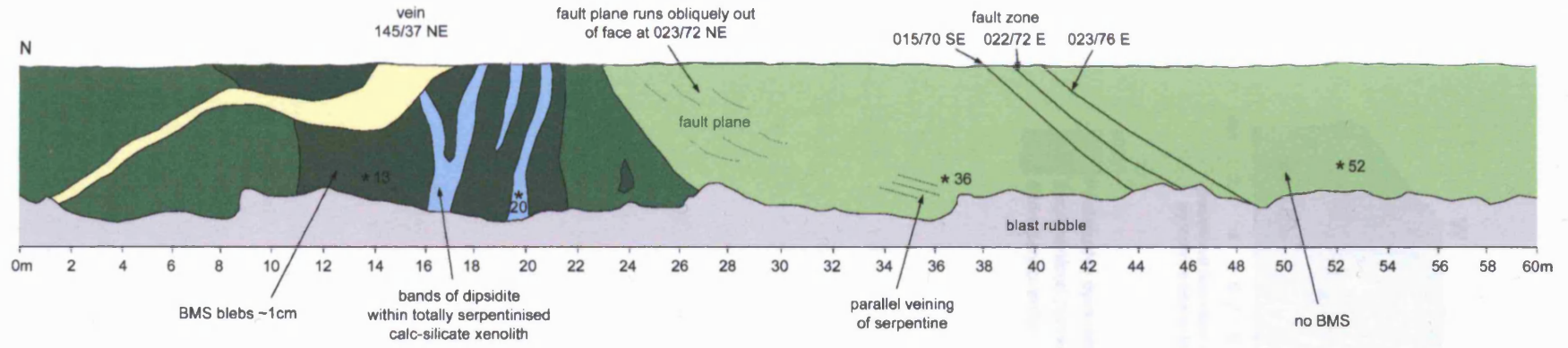
- KEY:
- HW gabbronorite
 - HW melagabbronorite
 - HW mottled anorthosite
 - HW spotted norite
 - Altered pyroxenite
 - Fine-grained feldspathic pyroxenite
 - Serpentinite
 - Serpentinised pyroxenite
 - Pegmatitic pyroxenite
 - Feldspathic pyroxenite
 - Intrusive norite
 - Quartz-feldspar vein
 - * sample location



KEY:

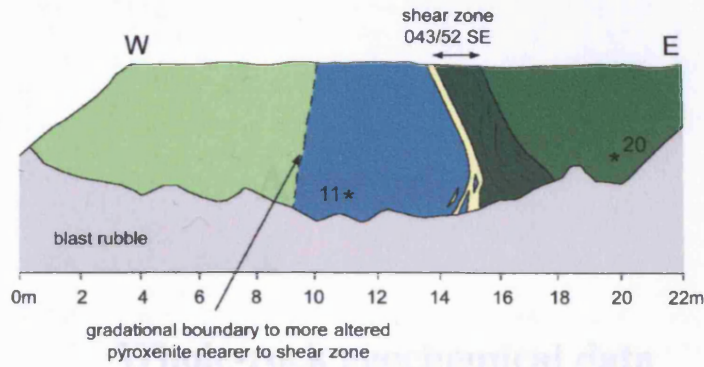
- | | |
|--|---|
|  HW gabbronorite |  Serpentinised pyroxenite |
|  HW melagabbronorite |  Quartzo-feldspathic vein |
|  HW mottled anorthosite |  Calc-silicate xenolith |
|  Serpentinite | * sample location |





- KEY:
- Feldspathic pyroxenite
 - Serpentinised pyroxenite
 - Intrusive norite
 - Calc-silicate
 - Quartz-feldspar vein
 - * sample location

Zwartfontein, ZSN4 face:



- KEY:
- Feldspathic pyroxenite
 - Serpentinised pyroxenite
 - Altered pyroxenite
 - Quartz-feldspar vein
 - * sample location

...also comprise all whole-rock geochemical data. Major and trace elements were analysed by inductively coupled plasma optical emission spectrometry (ICP-OES) and by inductively coupled plasma-mass spectrometry (ICP-MS). Sulphur was determined by a wet-oxidation procedure using a Leco analyser (equipment: LECO, USA). Carbon and oxygen values were determined by wet-oxidation with TGA, and nitrogen followed by a similar procedure. Methodware described in Chapter 6, section 6.1.1. For the samples from the Zwartfontein face, the analytical data can be found in the Appendix 1, Table 1.

Legend of abbreviations of the following tables:

FP	Feldspathic pyroxenite	SP	Serpentine
SPX	Serpentinised pyroxenite	QFV	Quartz-feldspar vein
APX	Altered pyroxenite	SR	Serpentine
QFV	Quartz-feldspar vein		
SR	Serpentine		

Appendix 2

Whole-rock geochemical data

Contents:

This appendix contains all whole-rock geochemical data. Major and trace elements were determined by inductively coupled plasma-optical emission spectrometry (ICP-OES) and by inductively coupled plasma-mass spectrometry (ICP-MS). Sulphur was determined by combustion iodometric procedure using a Laboratory Equipment Company (LECO) titrator. PGE and Au values were determined Ni sulphide fire assay with Te coprecipitation followed by ICP-MS procedure. Methods are described in Chapter 6, section 6.3. Data for the samples collected by Paul Armitage for the Sandsloot pit can be found in McDonald et al. (Appendix 5).

Key to lithology abbreviations in the following tables:

AFPX	Altered Platreef feldspathic pyroxenite	IN	Intrusive norite
CPX	Platreef clinopyroxenite	LZP	Lower Zone pyroxenite
CSX	Calc-silicate xenolith	MS	Massive sulphide
FCPX	Footwall clinopyroxenite	PEGP	Pegmatitic Platreef feldspathic pyroxenite
FPX	Platreef feldspathic pyroxenite	PDT	Peridotite (olivine-replaced reef)
GN	Gneiss	QF	Quartzo-feldspathic vein
GT	Granite	QFPX	Quartzo-feldspathic pyroxenite
HWA	Hangingwall mottled anorthosite	SCSX	Serpentinised calc-silicate xenolith
HWGN	Hangingwall gabbro-norite	SPT	Serpentinite
HWMN	Hangingwall fine-grained melanorite		
intrusive			

Sandsloot, SNS1 face samples:

Sam- ple Lith:	SNS1 2	SNS1 6	SNS1 10	SNS1 11	SNS1 12	SNS1 17	SNS1 22	SNS1 25	SNS1 29	SNS1 31a	SNS1 32	SNS1 33	SNS1 35	SNS1 39	SNS1 40
	HWGN	HWGN	HWGN	HWA	FPX	FPX	AFPX	FPX	FPX	PEGP	FCPX	SPT	FCPX	MS	FCPX
SiO ₂ (wt%)	52.15	50.99	51.28	51.19	50.89	52.52	49.88	51.58	47.60	49.91	43.55	39.60	42.79	34.86	45.10
TiO ₂	0.15	0.20	0.17	0.05	0.19	0.15	0.18	0.21	0.20	0.20	0.38	0.22	0.37	0.30	0.35
Al ₂ O ₃	17.61	10.51	17.66	27.95	5.92	6.56	6.13	6.66	6.62	8.98	6.94	4.09	7.10	5.75	5.41
Fe ₂ O ₃	7.31	11.34	7.57	1.77	12.10	11.92	12.16	11.53	13.19	10.69	9.89	8.30	10.39	22.00	5.92
MnO	0.13	0.20	0.13	0.04	0.21	0.22	0.20	0.21	0.21	0.19	0.24	0.35	0.30	0.36	0.29
MgO	10.67	18.25	10.95	1.64	23.90	23.40	21.99	22.42	21.72	17.57	13.73	32.27	15.25	14.48	15.39
CaO	10.35	7.08	9.29	12.90	4.72	4.76	5.02	5.31	8.74	11.02	24.82	10.13	21.76	17.31	25.55
Na ₂ O	1.55	0.92	1.69	2.25	0.52	0.57	0.80	0.71	0.18	0.77	0.04	0.06	0.06	0.05	0.02
K ₂ O	0.28	0.17	0.24	0.75	0.11	0.21	0.17	0.25	0.02	0.13	0.04	0.03	0.05	0.04	0.03
P ₂ O ₅	0.02	0.01	0.05	0.01	0.04	0.02	0.01	0.03	0.02	0.02	0.01	0.00	0.01	0.01	0.00
LOI	0.39	0.15	0.71	1.52	0.91	0.51	2.82	0.59	1.64	0.82	1.30	5.24	1.47	4.19	1.19
Total	100.61	99.81	99.72	100.06	99.51	100.83	99.37	99.49	100.12	100.28	100.93	100.28	99.55	99.35	99.24
Sc (ppm)	21.00	28.23	19.22	4.74	29.75	29.89	32.33	29.59	28.32	32.22	17.10	7.74	12.15	9.39	12.64
V	103.97	145.10	101.95	27.17	153.02	149.56	153.46	153.23	147.57	173.68	77.12	32.10	57.57	37.50	51.87
Cr	782.7	1288.3	879.5	98.0	2071.2	2061.8	1875.9	1841.5	1693.6	1251.0	71.9	30.7	48.3	41.1	83.04
Co	40.71	62.95	42.68	7.51	76.85	76.23	79.53	71.10	108.23	85.94	69.53	46.57	70.06	508.87	31.11
Ni	202.0	333.0	228.1	44.2	526.7	532.7	870.7	525.4	3073.0	2322.5	3955.8	1904.5	3906.6	48276.6	1942.7
Cu	167.2	41.9	33.0	9.9	116.6	39.7	337.3	64.4	724.2	277.3	679.7	299.3	791.1	5079.4	617.1
Zn	48.95	202.35	43.12	8.31	129.14	78.97	79.76	82.65	104.91	67.33	121.38	51.50	94.80	480.57	31.62
Sr	217.73	128.92	244.14	367.34	59.97	109.27	59.97	134.91	42.60	129.13	4.37	8.35	13.01	10.57	5.45
Ba	91.81	53.15	102.92	268.65	40.66	90.53	67.24	116.71	41.25	132.56	2.63	2.39	166.16	5.11	2.05
Ga	13.59	9.78	14.78	18.20	6.79	7.01	5.54	7.15	6.31	8.56	7.47	4.97	8.13	5.70	5.92
Rb	3.27	2.71	3.40	9.64	2.62	2.91	2.11	4.26	1.19	1.73	0.20	0.48	4.32	0.69	0.16
Y	5.93	7.65	6.30	2.02	6.71	5.35	6.59	7.52	6.80	9.02	10.02	6.10	10.58	7.33	8.60
Zr	9.84	11.71	7.08	1.57	8.44	10.41	11.15	14.07	16.46	14.14	20.31	26.42	35.47	35.22	29.95
Nb	0.39	0.49	0.25	0.03	0.28	0.40	0.12	0.39	0.50	0.43	0.19	0.08	0.59	0.30	0.07
Cs	0.08	0.15	0.25	0.43	0.25	0.13	0.35	0.18	0.31	0.34	0.02	0.16	0.03	0.09	0.03
La	4.04	3.63	5.12	3.27	2.52	2.37	1.85	3.67	3.28	3.45	5.48	1.39	7.10	2.12	2.34
Ce	7.80	6.47	9.44	6.34	5.60	4.35	4.45	6.89	6.80	7.68	10.42	3.47	14.33	5.45	5.99
Pr	0.93	0.80	1.14	0.69	0.72	0.54	0.59	0.85	0.84	1.10	1.40	0.56	1.83	0.80	0.98
Nd	3.60	3.11	4.07	2.42	2.89	2.14	2.45	3.30	3.29	4.72	5.91	2.85	7.28	3.47	4.64
Sm	0.77	0.76	0.84	0.45	0.77	0.53	0.68	0.85	0.83	1.23	1.60	0.82	1.73	1.01	1.32
Eu	0.47	0.33	0.52	0.59	0.23	0.22	0.20	0.30	0.23	0.39	0.51	0.22	0.49	0.27	0.33
Gd	0.83	0.87	0.86	0.40	0.84	0.63	0.78	0.89	0.86	1.35	1.66	0.93	1.81	1.08	1.40
Tb	0.14	0.16	0.15	0.06	0.15	0.11	0.14	0.16	0.15	0.23	0.27	0.16	0.30	0.19	0.24
Dy	0.90	1.10	0.94	0.33	0.99	0.78	0.96	1.12	1.02	1.50	1.70	1.01	1.82	1.19	1.43
Ho	0.18	0.23	0.20	0.06	0.20	0.17	0.20	0.23	0.21	0.29	0.32	0.19	0.34	0.22	0.27
Er	0.58	0.77	0.61	0.18	0.66	0.57	0.69	0.75	0.70	0.90	0.96	0.57	1.03	0.67	0.78
Tm	0.09	0.13	0.10	0.03	0.11	0.09	0.11	0.12	0.11	0.14	0.14	0.09	0.15	0.10	0.12
Yb	0.63	0.89	0.67	0.16	0.76	0.68	0.77	0.84	0.81	0.92	0.92	0.58	1.03	0.62	0.77
Lu	0.10	0.16	0.11	0.03	0.13	0.11	0.13	0.13	0.13	0.14	0.14	0.09	0.16	0.10	0.13
Hf	0.26	0.34	0.18	0.06	0.29	0.31	0.31	0.38	0.45	0.51	0.99	1.24	1.61	1.45	1.30
Ta	0.03	0.03	0.03	0.00	0.02	0.03	0.01	0.03	0.05	0.03	0.05	0.02	0.05	0.02	0.03
Th	0.29	0.45	0.32	0.03	0.25	0.40	0.20	0.48	0.82	0.46	0.75	0.15	0.40	0.19	0.26
U	0.08	0.12	0.08	0.01	0.05	0.13	0.05	0.17	0.27	0.12	0.47	0.03	0.26	0.06	0.13
S (wt%)	0.021	0.027	0.015	0.006	0.054	0.008	0.086	0.020	0.696	0.505	1.603	0.416	1.384	10.391	0.485
Os (ppb)	2.7	1.4	0.8	0.5	0.3	0.2	2.2	8.7	18.6	12.7	26.5	9.1	20.2	406.5	23.7
Ir	0.7	0.4	0.4	0.8	0.1	0.2	1.1	1.0	45.6	22.9	48.3	20.1	40.5	485.2	37.8
Ru	1.9	0.6	0.8	3.0	0.4	0.7	4.5	1.1	202.3	88.2	181.3	78.7	153.3	1843.5	133.3
Rh	0.7	1.2	0.6	0.7	0.6	0.5	6.6	1.4	184.90	97.4	218.6	81.0	175.1	2168.0	173.1
Pt	4.8	4.9	3.9	8.2	8.2	6.8	510.8	8.2	2564.0	1552.0	3742.5	1310.0	2466.5	33285.0	3782.5
Pd	3.3	6.1	4.0	11.4	6.4	6.0	392.0	10.4	1623.0	1579.0	3154.0	1058.0	2603.0	62930.0	3236.0
Au	4.5	3.3	3.0	3.2	5.1	2.8	90.7	6.0	533.7	259.8	702.8	132.4	199.9	1897.0	1611.0

Sandsloot, SNN1 face samples:

Sample	SNN1 0	SNN1 7a	SNN1 7b	SNN1 8	SNN1 18a	SNN1 20	SNN1 25	SNN1 37	SNN1 40	SNN1 43	SNN1 47	SNN1 53	SNN1 57	SNN1 60
Lithology	HWGN	HWA	FPX	AFPX	FPX	AFPX	AFPX	PEGP	SPT	PDT	PEGP	PDT	SPT	AFPX
SiO ₂ (wt%)	50.32	49.81	52.14	51.41	51.88	47.83	52.26	51.45	36.35	46.73	50.10	45.27	35.66	47.17
TiO ₂	0.20	0.51	0.21	0.21	0.14	0.16	0.24	0.24	0.20	0.16	0.16	0.21	0.07	0.13
Al ₂ O ₃	20.74	24.37	5.25	4.83	8.52	5.93	6.10	11.60	6.36	4.19	8.65	4.05	7.48	3.17
Fe ₂ O ₃	5.38	3.00	14.91	13.72	10.62	12.89	10.93	9.09	15.92	12.27	11.05	10.94	8.98	12.59
MnO	0.10	0.08	0.23	0.23	0.20	0.21	0.20	0.17	0.29	0.17	0.17	0.31	0.11	0.15
MgO	5.76	2.62	20.35	21.02	21.33	24.15	21.17	15.95	23.99	23.24	18.05	20.83	33.50	17.93
CaO	11.54	12.68	5.24	5.11	4.81	3.70	4.82	7.45	10.40	9.45	8.12	14.19	0.49	13.71
Na ₂ O	2.19	2.90	0.67	0.64	0.74	0.67	1.15	1.48	0.08	0.16	0.82	0.31	0.03	0.22
K ₂ O	0.57	1.13	0.17	0.11	0.27	0.11	0.15	0.34	0.02	0.02	0.08	0.07	0.01	0.04
P ₂ O ₅	0.02	0.04	0.03	0.02	0.02	0.02	0.02	0.04	0.02	0.02	0.02	0.02	0.02	0.01
LOI	2.13	2.21	1.14	0.93	1.20	4.49	3.22	1.50	5.82	3.91	1.59	2.85	12.19	3.20
Total	98.95	99.36	100.33	98.23	99.74	100.16	100.26	99.30	99.44	100.33	98.80	99.05	98.55	98.33
Sc (ppm)	17.98	13.97	31.19	31.88	23.27	23.26	28.98	21.69	0.59	27.57	23.35	22.11	5.00	26.79
V	98.68	101.47	153.62	154.85	117.35	116.23	152.56	118.28	68.80	104.27	106.84	82.72	25.20	99.27
Cr	399.4	203.8	1929.0	1790.0	2135.9	1846.1	2035.1	1387.7	58.1	1248.9	1651.2	1695.1	132.4	1156.4
Co	32.4	18.1	158.3	122.7	102.2	104.9	80.8	78.7	140.5	156.8	126.3	99.7	75.1	173.4
Ni	190.2	223.9	7988.2	4678.1	3160.7	2693.3	585.4	1803.2	2209.7	5351.8	3918.7	2459.0	645.5	3891.7
Cu	15.4	19.5	2151.1	1099.4	494.1	809.3	14.9	491.2	1422.1	1571.1	977.7	1163.6	564.9	2056.1
Zn	42.50	17.62	139.55	115.46	99.82	156.99	125.37	77.77	185.83	95.47	92.21	65.13	90.57	90.94
Sr	320.53	423.11	65.64	59.40	177.59	35.86	60.24	267.35	30.80	29.36	169.83	31.11	7.19	14.84
Ba	206.49	347.33	49.30	48.85	197.87	38.71	63.04	160.05	14.94	30.81	50.63	33.50	7.10	18.42
Ga	15.79	17.84	5.98	5.70	7.29	5.98	6.92	10.39	8.89	4.56	7.87	5.13	9.62	5.34
Y	7.31	7.63	7.41	7.39	4.09	5.84	8.19	7.07	9.84	5.89	5.23	7.29	1.94	5.88
Zr	15.22	16.26	28.01	18.87	11.27	17.00	20.57	62.48	30.85	10.20	15.45	21.31	9.52	8.45
Nb	0.63	2.47	1.19	0.79	0.50	0.71	0.81	1.57	1.64	0.40	0.64	0.75	0.76	0.38
Cs	203.30	321.80	47.78	47.02	187.56	39.18	64.41	155.68	15.41	32.48	51.07	36.99	8.82	22.02
La	5.53	7.34	2.93	2.71	3.02	4.69	3.66	6.87	7.05	3.05	3.13	2.82	2.82	2.52
Ce	10.98	13.96	6.28	5.87	5.17	8.43	7.76	13.35	15.60	5.79	6.15	6.70	6.14	5.37
Pr	1.34	1.69	0.81	0.77	0.59	0.93	1.00	1.58	1.95	0.75	0.75	0.95	0.74	0.72
Nd	5.13	6.50	3.25	3.17	2.07	3.25	3.88	5.65	7.14	2.98	2.81	4.16	2.57	2.93
Sm	1.16	1.40	0.81	0.81	0.44	0.66	0.90	1.11	1.44	0.75	0.61	1.10	0.39	0.72
Eu	0.58	0.74	0.20	0.19	0.28	0.15	0.25	0.47	0.37	0.20	0.26	0.31	0.10	0.33
Gd	1.13	1.42	0.90	0.91	0.49	0.72	1.00	1.09	1.40	0.83	0.66	1.15	0.34	0.84
Tb	0.19	0.23	0.16	0.16	0.09	0.13	0.18	0.18	0.23	0.14	0.12	0.19	0.05	0.15
Dy	1.23	1.33	1.09	1.12	0.58	0.87	1.24	1.13	1.45	0.97	0.80	1.24	0.29	0.97
Ho	0.24	0.26	0.23	0.24	0.12	0.19	0.26	0.23	0.30	0.19	0.17	0.24	0.06	0.20
Er	0.70	0.70	0.73	0.75	0.40	0.58	0.81	0.68	0.92	0.59	0.52	0.67	0.22	0.57
Tm	0.11	0.10	0.12	0.12	0.07	0.09	0.13	0.11	0.15	0.09	0.08	0.10	0.04	0.09
Yb	0.69	0.60	0.85	0.86	0.48	0.67	0.93	0.71	1.02	0.59	0.62	0.65	0.38	0.56
Lu	0.10	0.08	0.14	0.14	0.07	0.09	0.16	0.10	0.17	0.09	0.09	0.09	0.07	0.09
Hf	0.40	0.49	0.81	0.53	0.29	0.46	0.54	1.37	0.76	0.28	0.39	0.71	0.25	0.27
Ta	0.05	0.16	0.06	0.05	0.04	0.07	0.07	0.11	0.15	0.05	0.05	0.05	0.08	0.03
Th	0.52	0.23	0.71	0.72	0.55	1.01	0.92	1.60	1.84	0.68	0.51	0.59	1.39	0.42
U	0.12	0.07	0.20	0.18	0.18	0.52	0.26	0.78	0.31	0.20	0.19	0.20	0.51	0.15
S (wt%)	0.011	0.039	1.447	0.785	0.494	0.438	0.021	0.321	2.628	2.298	1.123	0.976	0.779	2.171
Os (ppb)	1.0	1.0	39.5	23.6	17.0	9.1	0.2	1.6	0.7	18.5	11.9	4.2	1.3	7.6
Ir	0.7	2.0	91.8	54.1	38.9	17.9	0.2	3.0	1.5	40.5	26.7	9.9	2.9	15.8
Ru	5.7	5.6	378.7	214.3	156.9	76.5	1.6	11.2	4.2	144.6	98.7	32.9	10.5	50.8
Rh	0.6	4.5	346.9	205.8	159.3	69.0	0.4	14.7	7.0	154.5	111.5	41.2	11.8	65.7
Pt	11.6	106.1	4085.3	2266.3	2596.3	612.6	1.9	465.0	97.7	2244.0	1725.0	912.7	82.8	979.5
Pd	10.1	128.1	4322.8	2620.8	2277.8	727.9	3.9	461.1	167.4	2251.2	1735.0	961.3	206.3	1296.8
Au	2.8	25.6	758.6	1581.2	174.5	118.2	2.3	197.1	28.1	402.4	433.1	188.2	17.5	155.8

Sandsloot, SNN1 face samples (cont.):

Sample	SNN1 65	SNN1 68	SNN1 72	SNN1 78
Lithology	QF	CPX	SPT	CPX
SiO ₂ (wt%)	74.59	50.87	36.72	49.39
TiO ₂	0.08	0.23	0.23	0.20
Al ₂ O ₃	10.63	4.13	8.28	4.31
Fe ₂ O ₃	1.89	8.94	9.45	7.62
MnO	0.03	0.20	0.09	0.19
MgO	0.19	16.89	33.04	16.51
CaO	4.08	18.23	1.32	19.28
Na ₂ O	6.08	0.41	0.05	0.25
K ₂ O	0.03	0.04	0.00	0.03
P ₂ O ₅	0.00	0.01	0.01	0.01
LOI	0.99	1.32	11.98	1.65
Total	98.60	101.26	101.18	99.45
Sc (ppm)	0.89	44.20	8.17	43.68
V	7.82	161.83	51.47	154.14
Cr	89.5	2074.0	83.7	1185.8
Co	25.7	96.1	66.5	75.0
Ni	243.3	2361.2	444.9	1338.7
Cu	2645.5	980.1	321.9	676.9
Zn	66.03	58.71	97.99	86.46
Sr	22.05	41.93	5.40	14.10
Ba	10.19	25.38	4.77	8.45
Ga	16.55	5.42	11.34	5.13
Y	27.11	10.47	10.79	9.14
Zr	24.87	17.40	53.87	11.74
Nb	12.31	0.76	1.03	0.47
Cs	16.45	27.80	5.90	10.12
La	13.67	3.57	4.52	2.44
Ce	27.87	8.31	20.01	5.83
Pr	3.37	1.17	3.62	0.89
Nd	11.92	5.08	15.54	4.07
Sm	3.12	1.38	3.38	1.18
Eu	0.25	0.37	0.24	0.33
Gd	3.29	1.54	2.50	1.35
Tb	0.63	0.27	0.37	0.23
Dy	4.23	1.75	2.06	1.54
Ho	0.84	0.35	0.37	0.31
Er	2.48	1.00	1.04	0.86
Tm	0.40	0.15	0.16	0.13
Yb	2.70	0.96	1.08	0.83
Lu	0.42	0.14	0.16	0.14
Hf	1.04	0.51	1.76	0.35
Ta	1.86	0.06	0.21	0.03
Th	10.94	0.73	2.02	0.41
U	6.28	0.24	0.31	0.16
S (wt%)	0.683	0.673	0.733	0.361
Os (ppb)	0.0	5.1	0.2	2.2
Ir	0.1	10.7	0.3	5.0
Ru	0.2	37.8	1.1	18.8
Rh	0.6	42.8	1.0	19.9
Pt	5.4	547.6	16.3	275.9
Pd	8.2	679.6	23.5	324.6
Au	4.1	84.6	4.2	38.9

Zwartfontein, ZSS1 face samples:

Sample	ZSS1	ZSS1	ZSS1	ZSS1	ZSS1	ZSS1	ZSS1	ZSS1	ZSS1	ZSS1	ZSS1	ZSS1	ZSS1
Lithology	2	15	26	29	33a	33b	41	54	68	84	87	98	140
	HWGN	HWMN	HWGN	HWA	HWN	AFPX	FPX	SPT	SPT	IN	FPX	FPX	FCPX
SiO ₂ (wt%)	51.26	52.22	51.35	51.79	50.78	50.11	53.98	39.74	38.00	51.20	52.24	49.43	49.21
TiO ₂	0.17	0.24	0.15	0.10	0.12	0.23	0.20	0.14	0.14	0.26	0.35	0.24	0.13
Al ₂ O ₃	22.80	16.40	22.18	27.09	22.13	6.51	6.53	2.61	2.45	16.45	8.01	13.16	1.01
Fe ₂ O ₃	4.54	8.34	4.92	2.24	4.59	12.52	11.45	9.26	12.24	8.44	15.14	10.03	1.81
MnO	0.09	0.16	0.10	0.06	0.11	0.24	0.23	0.49	0.40	0.18	0.30	0.32	0.21
MgO	5.25	8.72	6.33	2.48	7.31	16.33	20.40	36.40	34.31	8.67	14.43	12.81	15.97
CaO	12.18	13.40	11.26	13.13	10.03	9.16	5.91	0.25	2.29	12.00	7.81	10.51	28.52
Na ₂ O	1.94	1.66	1.77	2.14	1.79	0.84	0.59	0.11	0.11	2.27	1.46	1.29	0.00
K ₂ O	0.18	0.20	0.26	0.32	0.43	0.07	0.04	0.02	0.02	0.19	0.25	0.13	0.00
P ₂ O ₅	0.00	0.00	0.00	0.00	0.01	0.01	0.01	0.01	0.01	0.00	0.02	0.01	0.00
LOI	1.19	0.34	1.54	1.12	1.50	5.12	0.86	12.07	10.65	1.56	0.33	2.21	3.35
Total	99.60	101.69	99.86	100.47	98.79	101.14	100.19	101.11	100.62	101.21	100.32	100.16	100.13
Sc (ppm)	16.0	39.9	17.3	8.6	10.6	35.9	32.4	18.3	12.5	33.5	37.0	35.7	2.9
V	93.7	183.3	89.8	65.2	70.4	174.4	151.3	58.3	46.4	151.7	168.2	167.3	64.6
Cr	271.5	320.4	491.9	206.9	751.4	1773.3	2217.6	334.0	751.5	522.4	579.3	483.8	32.3
Co	25.4	53.5	29.8	11.7	30.4	86.4	82.9	157.8	104.2	51.6	92.3	68.7	9.7
Ni	115.2	206.5	157.8	75.0	172.9	505.0	546.2	2273.8	771.3	303.8	823.3	835.4	33.6
Cu	23.6	80.0	19.1	50.1	16.0	65.9	68.6	122.0	65.4	56.9	140.1	170.8	27.5
Zn	35.9	44.6	36.9	22.1	29.4	56.6	47.9	32.7	32.4	52.0	73.9	44.6	8.3
Sr	315.1	195.0	307.2	367.3	346.1	18.5	95.6	2.3	3.5	395.2	235.4	347.2	33.6
Ba	116.9	63.7	208.9	166.5	278.7	4.5	33.4	2.7	3.7	389.6	189.9	232.8	17.4
Ga	17.6	16.2	16.4	19.4	16.0	7.1	6.8	4.5	4.7	15.5	10.4	12.7	1.7
Rb	1.4	0.4	2.8	2.1	5.4	0.2	0.4	0.3	0.1	2.3	2.5	1.2	0.0
Y	321.0	198.2	310.6	368.8	348.9	18.1	95.5	1.9	3.2	406.9	232.7	358.4	34.0
Zr	5.5	12.0	4.1	2.2	2.3	6.5	5.1	4.9	3.3	10.8	13.1	10.3	2.6
Nb	10.5	10.7	12.7	3.8	4.8	14.5	9.6	18.6	12.3	10.5	24.6	9.8	13.5
Cs	0.47	0.17	0.12	0.11	0.10	0.43	0.23	0.33	0.11	0.26	2.07	0.26	0.06
La	4.61	3.71	2.62	2.79	2.79	2.43	2.34	2.53	1.90	4.05	6.68	2.52	2.14
Ce	8.59	7.39	6.20	4.94	4.92	5.22	4.39	6.28	3.31	8.36	12.58	6.92	4.88
Pr	0.93	0.96	0.64	0.46	0.44	0.58	0.44	0.72	0.36	1.12	1.49	0.94	0.57
Nd	3.73	4.68	2.56	1.77	1.68	2.57	1.87	2.86	1.59	5.13	6.04	4.31	2.25
Sm	0.81	1.36	0.53	0.34	0.30	0.65	0.47	0.59	0.41	1.29	1.43	1.19	0.47
Eu	0.62	0.63	0.51	0.62	0.59	0.17	0.21	0.10	0.11	0.64	0.40	0.52	0.12
Gd	0.79	1.54	0.57	0.34	0.29	0.78	0.54	0.65	0.44	1.44	1.52	1.33	0.44
Tb	0.13	0.27	0.09	0.05	0.05	0.13	0.10	0.11	0.08	0.24	0.27	0.23	0.07
Dy	0.85	1.87	0.61	0.34	0.32	0.95	0.72	0.73	0.52	1.73	1.89	1.57	0.41
Ho	0.16	0.37	0.12	0.07	0.06	0.19	0.15	0.15	0.10	0.33	0.38	0.31	0.08
Er	0.51	1.16	0.38	0.20	0.22	0.63	0.52	0.49	0.31	1.07	1.28	1.02	0.24
Tm	0.08	0.19	0.06	0.03	0.04	0.10	0.09	0.08	0.05	0.16	0.21	0.15	0.04
Yb	0.53	1.17	0.39	0.20	0.27	0.64	0.61	0.50	0.32	1.07	1.45	1.04	0.28
Lu	0.12	0.23	0.07	0.04	0.04	0.14	0.09	0.09	0.06	0.21	0.23	0.20	0.04
Hf	0.28	0.38	0.31	0.09	0.11	0.38	0.24	0.47	0.40	0.34	0.73	0.29	0.25
Ta	0.03	0.02	0.01	0.01	0.01	0.04	0.02	0.05	0.02	0.02	0.22	0.02	0.01
Th	0.33	0.16	0.11	0.05	0.11	0.39	0.28	0.79	0.15	0.16	2.77	0.33	0.12
U	0.15	0.13	0.08	0.06	0.08	0.17	0.12	0.15	0.10	0.13	1.93	0.20	0.13
S (wt%)	0.015	0.044	nd	nd	0.001	0.083	0.009	0.292	0.057	0.016	0.323	0.201	0.001
Ir (ppb)	0.5	0.0	nd	nd	0.7	0.0	0.0	2.8	40.2	0.0	5.4	8.7	0.0
Ru	5.2	0.1	nd	nd	5.3	0.4	0.7	11.1	146.6	0.2	20.6	33.6	0.5
Rh	0.2	0.0	nd	nd	1.3	0.1	0.2	11.8	173.6	0.3	23.2	35.7	0.2
Pt	13.5	14.7	nd	nd	3.8	7.1	7.7	148.2	2065.8	4.9	259.2	363.5	1.2
Pd	3.2	6.5	nd	nd	5.0	3.8	6.4	180.5	2652.3	10.3	353.0	579.8	2.4
Au	0.9	1.4	nd	nd	0.0	3.4	3.1	10.5	163.6	1.4	54.4	67.3	0.1

Overysel, OY335 core samples:

	OY335	OY335	OY335	OY335	OY335	OY335	OY335	OY335	OY335	OY335	OY335	OY335
Sample	166	169	175	176	182	193	201	213	218	230	241	253
Lithology	HWGN	HWGN	HWMN	FPX	FPX	AFPX	FPX	SCSX	SCSX	AFPX	FPX	IN
SiO ₂ (wt%)	52.72	51.08	52.49	51.74	52.05	51.66	54.47	42.21	41.23	51.94	53.47	54.67
TiO ₂	0.32	0.23	0.26	0.14	0.14	0.18	0.26	0.26	0.36	0.15	0.18	0.10
Al ₂ O ₃	14.22	16.68	14.20	5.78	6.03	5.94	8.67	6.80	5.60	6.74	8.49	18.18
Fe ₂ O ₃	10.00	8.29	9.08	12.53	13.50	12.25	11.17	8.32	8.92	11.75	10.59	5.94
MnO	0.18	0.15	0.16	0.20	0.23	0.19	0.22	0.20	0.22	0.21	0.20	0.12
MgO	11.53	8.87	12.10	23.42	22.85	21.12	18.58	24.67	26.82	20.57	18.61	7.13
CaO	10.21	10.54	9.01	4.27	4.42	4.70	6.57	12.22	9.17	7.21	7.56	8.34
Na ₂ O	1.63	1.80	1.70	0.58	0.49	0.58	0.82	0.10	0.23	0.72	0.98	3.05
K ₂ O	0.22	0.30	0.21	0.08	0.05	0.06	0.05	0.00	0.03	0.19	0.25	0.74
P ₂ O ₅	0.04	0.03	0.03	0.02	0.02	0.02	0.03	0.01	0.02	0.02	0.01	0.01
LOI	0.47	0.62	0.50	0.90	0.76	3.26	0.51	3.79	7.09	0.77	0.72	1.22
Total	101.53	98.58	99.75	99.65	100.53	99.97	101.34	98.60	99.70	100.28	101.07	99.51
Sc (ppm)	30.2	24.9	25.7	26.7	28.4	30.6	29.5	27.2	17.0	30.3	28.6	11.6
V	155.9	128.9	127.3	113.7	116.5	124.4	137.5	89.6	65.9	117.1	122.0	62.0
Cr	725.1	460.2	777.3	2161.4	2334.6	1981.1	1612.7	50.9	47.0	2043.4	1959.7	379.0
Co	50.3	41.0	48.3	128.4	126.9	87.0	69.9	46.1	40.2	84.5	75.6	45.6
Ni	248.1	186.3	457.3	4342.8	3597.0	996.6	447.4	197.2	464.0	1540.6	1050.5	1094.3
Cu	43.5	29.9	56.7	1301.2	839.4	101.8	30.5	26.2	47.3	605.0	176.3	245.0
Zn	116.0	76.3	75.5	127.1	92.0	79.1	68.3	58.9	86.7	125.0	158.0	60.1
Sr	186.8	225.8	188.6	64.7	66.2	66.2	102.0	56.7	37.1	167.8	193.4	414.6
Ba	104.4	146.0	112.0	55.5	54.5	48.6	60.5	35.6	40.8	149.5	105.9	229.8
Ga	12.4	14.2	12.2	5.9	6.3	7.4	9.4	8.0	7.5	7.2	8.8	18.3
Rb	3.2	5.3	3.3	1.4	2.2	1.0	1.5	0.0	0.9	3.3	4.9	15.6
Y	10.5	9.3	8.0	4.1	3.8	6.1	8.0	7.6	11.1	5.3	6.3	4.7
Zr	30.1	19.4	17.1	11.5	7.6	13.7	36.4	25.7	51.0	7.8	11.9	6.6
Nb	1.86	1.16	1.31	0.44	0.47	0.71	1.74	0.57	1.82	0.73	1.34	2.51
La	7.31	6.30	6.85	1.93	1.46	2.15	7.55	2.88	4.05	1.88	1.94	3.32
Ce	14.33	12.42	12.08	4.47	3.96	6.16	10.46	6.40	10.65	3.44	4.66	5.11
Pr	1.80	1.54	1.47	0.57	0.52	0.79	1.30	0.96	1.54	0.56	0.63	0.60
Nd	6.95	6.09	5.67	2.18	1.93	3.05	4.93	4.27	6.41	2.29	2.73	2.27
Sm	1.64	1.41	1.26	0.52	0.43	0.75	1.14	1.23	1.69	0.58	0.76	0.54
Eu	0.52	0.61	0.52	0.16	0.14	0.19	0.33	0.33	0.42	0.21	0.31	0.49
Gd	1.37	1.23	1.06	0.45	0.37	0.64	0.97	1.09	1.50	0.55	1.22	0.50
Tb	0.24	0.21	0.19	0.08	0.07	0.12	0.17	0.19	0.26	0.11	0.14	0.09
Dy	1.59	1.42	1.22	0.56	0.53	0.88	1.17	1.24	1.70	0.79	0.95	0.68
Ho	0.31	0.28	0.24	0.11	0.11	0.17	0.23	0.23	0.34	0.16	0.20	0.13
Er	0.95	0.85	0.73	0.35	0.35	0.54	0.73	0.67	0.97	0.48	0.58	0.41
Tm	0.15	0.13	0.12	0.06	0.06	0.09	0.12	0.10	0.15	0.08	0.09	0.08
Yb	0.99	0.93	0.79	0.44	0.44	0.67	0.80	0.64	1.05	0.60	0.66	0.54
Lu	0.16	0.14	0.13	0.08	0.08	0.11	0.14	0.11	0.17	0.10	0.11	0.10
Hf	0.74	0.52	0.46	0.27	0.20	0.35	0.84	0.98	1.55	0.22	0.31	0.23
Ta	0.11	0.06	0.08	0.03	0.05	0.06	0.09	0.03	0.10	0.06	0.08	0.24
Th	1.38	0.82	0.97	0.44	0.52	0.59	1.22	0.35	0.67	0.22	0.30	0.47
U	0.43	0.31	0.34	0.23	0.28	0.35	0.47	0.25	0.53	0.31	0.29	0.75
S (wt%)	nd	nd	nd	1.022	0.981	0.242	0.071	0.043	0.054	0.500	0.207	0.356
Ir (ppb)	nd	nd	nd	46.5	37.3	8.0	1.9	0.1	1.1	48.0	3.4	10.4
Ru	nd	nd	nd	149.3	132.6	22.2	5.7	1.3	6.3	91.5	9.2	39.2
Rh	nd	nd	nd	149.3	136.0	21.8	3.9	0.7	4.4	111.2	12.5	39.5
Pt	nd	nd	nd	2106.5	1727.5	256.6	46.4	32.6	51.7	4880.5	232.8	670.5
Pd	nd	nd	nd	2004.5	2433.5	301.6	33.4	82.8	35.7	3069.5	422.4	847.6
Au	nd	nd	nd	390.6	207.2	245.7	7.2	17.1	6.0	220.5	58.0	123.8

Overysel, OY335 core samples (cont.):

Sample	OY335	OY335	OY335	OY335	OY335	OY335	OY335	OY335	OY335	OY335
Lithology	262	269	275	285	292	303	310	316	323	345
	FPX	CSX	FPX	SPT	QFPX	QFPX	GN	GN	GN	GT
SiO ₂ (wt%)	51.43	43.85	48.06	36.53	56.01	51.11	61.45	67.23	59.07	76.72
TiO ₂	0.23	0.08	0.18	0.24	0.08	0.18	0.26	0.22	0.31	0.02
Al ₂ O ₃	6.53	1.09	3.92	4.45	10.09	10.59	16.97	16.40	19.65	14.50
Fe ₂ O ₃	10.60	2.28	12.97	14.00	7.77	9.89	6.07	4.49	5.48	0.36
MnO	0.23	0.35	0.23	0.09	0.18	0.18	0.18	0.07	0.18	0.02
MgO	17.62	16.42	22.41	33.20	15.84	17.36	4.92	2.09	4.09	0.17
CaO	12.99	29.70	10.33	1.37	7.15	6.43	5.55	4.33	6.33	1.08
Na ₂ O	0.72	0.01	0.35	0.08	1.70	1.13	4.48	4.60	4.52	4.70
K ₂ O	0.08	0.00	0.06	0.03	0.18	0.50	0.47	0.49	0.24	1.67
P ₂ O ₅	0.02	0.00	0.03	0.02	0.01	0.02	0.24	0.12	0.29	0.04
LOI	0.55	7.60	0.84	8.68	1.71	0.76	0.39	0.66	0.13	0.29
Total	101.00	101.40	99.37	98.68	100.73	98.14	100.98	100.70	100.30	99.55
Sc (ppm)	36.7	1.5	29.6	12.5	21.5	25.1	15.0	5.9	13.2	0.9
V	159.5	13.9	206.4	63.8	73.8	185.6	69.2	39.6	63.9	4.5
Cr	1428.4	18.6	2134.3	776.0	1072.5	17578.2	186.7	107.8	193.7	69.7
Co	62.7	4.4	100.9	115.3	61.4	70.8	29.8	42.0	21.2	2.5
Ni	463.0	77.3	1392.3	918.6	703.7	559.6	375.8	3185.0	209.8	10.5
Cu	171.2	44.5	577.7	137.5	188.6	120.9	317.3	722.7	91.7	1.0
Zn	85.8	45.6	95.0	695.2	54.7	114.8	91.6	83.1	96.8	19.3
Sr	120.0	32.6	89.8	20.3	191.2	249.3	534.4	690.3	610.7	287.4
Ba	48.5	0.6	110.8	19.8	165.6	219.6	342.8	667.6	485.9	631.0
Ga	8.2	1.7	5.9	6.9	10.9	12.3	25.4	18.5	29.4	19.4
Rb	0.9	0.0	1.2	0.8	2.1	11.8	5.6	3.7	1.7	20.3
Y	11.6	3.0	7.6	2.9	4.1	4.2	9.4	5.7	10.7	2.9
Zr	11.4	16.9	11.7	10.1	8.6	12.5	47.9	41.8	28.9	19.6
Nb	1.13	0.59	0.36	0.25	3.63	1.74	7.74	2.21	5.56	1.06
La	2.30	3.32	2.73	0.94	2.19	2.21	10.82	14.10	16.18	6.98
Ce	6.33	8.10	6.92	2.89	4.94	4.77	21.20	22.66	29.71	12.31
Pr	1.00	0.98	0.97	0.36	0.66	0.59	2.74	2.66	3.87	1.41
Nd	4.65	3.63	4.15	1.38	2.62	2.23	10.77	9.80	15.14	4.65
Sm	1.49	0.70	1.15	0.31	0.66	0.52	2.50	1.83	3.23	1.07
Eu	0.40	0.16	0.33	0.07	0.25	0.24	0.89	0.92	1.13	0.35
Gd	1.45	0.53	1.06	0.27	0.57	0.46	1.83	1.22	2.25	0.69
Tb	0.27	0.08	0.20	0.05	0.10	0.09	0.27	0.16	0.31	0.10
Dy	1.86	0.51	1.26	0.37	0.64	0.61	1.48	0.87	1.75	0.51
Ho	0.36	0.09	0.23	0.08	0.12	0.12	0.25	0.15	0.29	0.08
Er	1.08	0.26	0.66	0.31	0.36	0.39	0.72	0.41	0.83	0.20
Tm	0.17	0.04	0.09	0.06	0.06	0.06	0.11	0.06	0.12	0.03
Yb	1.15	0.22	0.62	0.54	0.39	0.44	0.80	0.43	0.88	0.21
Lu	0.19	0.03	0.10	0.11	0.07	0.07	0.12	0.07	0.14	0.03
Hf	0.36	0.31	0.29	0.28	0.24	0.33	1.22	0.83	0.62	0.62
Ta	0.11	0.05	0.14	0.03	0.54	0.21	0.86	0.14	0.44	0.13
Th	0.31	0.94	0.42	0.30	0.34	0.45	0.43	0.37	0.22	0.31
U	0.47	0.43	0.37	0.18	0.92	0.35	1.02	0.33	0.40	0.72
S (wt%)	0.061	0.018	0.623	5.256	0.114	0.051	0.107	0.966	0.048	0.005
Ir (ppb)	1.1	0.1	9.7	0.1	2.0	15.1	0.4	0.7	0.2	0.0
Ru	3.4	0.3	35.5	0.8	7.0	49.9	0.5	1.7	0.6	0.3
Rh	2.9	0.4	30.4	0.5	10.9	62.1	1.8	13.3	1.7	0.3
Pt	81.0	7.5	322.1	4.9	140.8	424.1	106.9	2837.1	22.7	2.2
Pd	62.7	30.0	371.9	39.1	193.7	299.7	155.0	3978.2	37.6	2.2
Au	10.4	5.5	45.6	15.3	31.2	9.7	18.9	618.1	16.4	1.4

Overysel, OY387 core samples:

Sample	OY387 233	OY387 236	OY387 239	OY387 242	OY387 246	OY387 252	OY387 258	OY387 268	OY387 272	OY387 278	OY387 296	OY387 311	OY387 321
Lithology	HWMN	HWGN	FPX	FPX	FPX	FPX	FPX	QFPX	QFPX	GN	GN	GN	GN
SiO ₂ (wt%)	50.36	51.13	54.11	54.10	51.80	53.74	52.40	56.98	52.60	56.55	60.79	59.66	57.30
TiO ₂	0.62	0.21	0.23	0.14	0.15	0.12	0.12	0.16	0.11	0.11	0.16	0.18	0.37
Al ₂ O ₃	11.52	18.94	8.39	9.16	5.92	6.92	10.08	6.17	13.70	21.34	21.84	18.78	4.92
Fe ₂ O ₃	14.72	7.17	12.49	10.28	12.56	12.57	9.74	10.20	10.10	3.90	1.94	3.53	12.91
MnO	0.25	0.13	0.23	0.21	0.24	0.21	0.20	0.18	0.14	0.08	0.05	0.09	0.26
MgO	10.90	7.77	19.69	20.37	22.81	19.88	18.67	16.21	12.05	5.57	2.87	6.35	19.54
CaO	9.23	10.40	5.01	5.06	3.25	4.08	6.43	4.46	6.81	8.12	6.32	5.00	2.50
Na ₂ O	1.34	2.13	0.75	0.74	0.25	0.69	0.63	0.56	1.69	3.66	5.04	4.03	0.86
K ₂ O	0.01	0.02	0.03	0.00	0.04	0.03	0.05	0.04	0.05	0.04	0.02	0.06	0.19
P ₂ O ₅	0.01	0.05	0.02	0.00	0.00	0.01	0.00	0.01	0.02	0.02	0.04	0.06	0.12
LOI	0.39	0.70	0.24	1.19	1.77	0.99	1.59	3.62	2.11	0.49	1.04	0.96	0.46
Total	99.36	98.65	101.19	101.25	98.78	99.23	99.91	98.58	99.38	99.87	100.10	98.69	99.44
Sc (ppm)	40.5	19.0	28.2	25.3	29.0	25.5	25.3	26.7	18.1	9.4	5.7	13.4	30.1
V	327.6	100.0	145.8	112.7	149.7	114.2	93.2	102.9	77.8	26.0	17.5	48.4	107.0
Cr	1213.0	588.6	1965.5	2160.4	8185.2	2566.9	2644.3	2118.6	1193.4	435.9	156.5	585.4	1565.3
Co	72.6	36.8	77.9	77.4	106.2	142.6	87.1	106.0	123.0	31.4	9.5	20.5	75.1
Ni	248.06	124.72	531.19	827.75	1926.64	4636.93	1801.42	2568.68	4303.20	398.67	58.64	160.87	482.27
Cu	86.68	34.40	46.49	209.94	495.23	828.21	361.03	480.62	718.31	143.96	65.29	98.54	79.54
Zn	70.7	61.9	51.7	51.0	58.0	58.7	49.4	62.3	44.3	40.1	36.7	45.4	70.8
Sr	157.1	274.1	102.6	110.2	55.6	83.7	128.8	51.5	161.1	806.1	909.8	837.8	80.6
Ba	80.0	154.0	56.1	60.1	24.2	41.4	83.5	67.9	88.3	296.3	655.4	1295.8	256.1
Ga	13.4	17.1	8.9	8.1	6.7	7.6	8.6	10.5	13.1	22.9	23.2	24.1	10.1
Rb	0.7	4.0	1.2	1.7	1.1	1.3	3.5	7.7	7.4	1.2	2.2	2.1	2.7
Y	17.6	10.0	5.8	5.1	3.8	4.6	4.0	15.4	4.6	3.3	5.1	4.8	11.2
Zr	20.8	19.5	7.9	12.4	9.2	9.5	9.1	125.0	16.8	13.6	31.3	36.5	62.4
Nb	1.05	1.07	1.17	1.33	0.87	2.67	1.23	8.52	2.97	0.75	2.18	2.01	4.97
Cs	82.3	159.5	58.3	63.5	27.3	44.3	87.7	74.2	95.8	299.8	670.5	1321.3	260.6
La	5.68	10.03	3.14	3.42	1.72	2.06	2.26	5.34	2.38	5.94	9.92	7.25	4.43
Ce	12.19	16.42	5.72	6.57	4.22	4.69	4.42	11.77	5.00	9.08	16.86	12.77	12.08
Pr	1.62	1.83	0.58	0.67	0.39	0.47	0.41	1.24	0.49	0.92	1.81	1.27	1.59
Nd	7.68	7.32	2.34	2.60	1.57	1.76	1.60	4.82	1.91	3.44	6.69	4.61	7.24
Sm	2.07	1.46	0.53	0.53	0.36	0.39	0.36	1.15	0.45	0.63	1.15	0.84	1.75
Eu	0.63	0.85	0.23	0.23	0.14	0.18	0.24	0.47	0.24	0.72	1.23	1.19	0.52
Gd	2.32	1.50	0.59	0.56	0.37	0.45	0.41	1.31	0.49	0.58	0.97	0.78	1.77
Tb	0.41	0.23	0.11	0.10	0.07	0.08	0.07	0.27	0.08	0.08	0.14	0.10	0.27
Dy	2.75	1.53	0.78	0.70	0.51	0.60	0.56	2.06	0.62	0.51	0.79	0.67	1.70
Ho	0.54	0.30	0.17	0.14	0.10	0.13	0.12	0.42	0.13	0.09	0.14	0.13	0.32
Er	1.76	0.95	0.59	0.49	0.37	0.44	0.40	1.47	0.41	0.28	0.45	0.44	1.03
Tm	0.27	0.15	0.10	0.09	0.06	0.08	0.07	0.28	0.07	0.05	0.07	0.07	0.17
Yb	1.76	0.96	0.75	0.58	0.44	0.56	0.47	1.98	0.49	0.32	0.47	0.49	1.11
Lu	0.29	0.16	0.13	0.10	0.08	0.10	0.09	0.34	0.08	0.05	0.07	0.09	0.19
Hf	0.64	0.53	0.24	0.31	0.22	0.26	0.26	3.38	0.44	0.33	0.75	0.93	1.43
Ta	0.08	0.08	0.10	0.10	0.11	0.28	0.12	0.88	0.37	0.11	0.39	0.35	0.97
Th	0.19	0.88	0.31	0.59	0.35	0.57	0.58	3.97	1.06	0.30	0.18	0.38	0.76
U	0.09	0.31	0.30	0.33	0.38	1.03	1.52	9.16	2.84	0.26	0.26	0.39	2.24
S (wt%)	nd	nd	0.059	0.112	0.868	0.423	1.265	0.519	0.673	1.591	0.159	0.016	nd
Ir (ppb)	nd	nd	0.2	0.7	8.1	18.7	61.5	13.1	22.6	44.3	2.8	0.2	nd
Ru	nd	nd	2.7	5.6	42.1	75.6	228.5	51.4	86.0	162.6	11.3	2.3	nd
Rh	nd	nd	0.8	1.6	21.9	94.6	246.7	57.2	91.6	194.4	10.4	0.7	nd
Pt	nd	nd	5.6	25.0	335.5	972.3	3215.0	562.9	1336.5	2212.5	520.4	4.1	nd
Pd	nd	nd	19.4	80.7	632.2	1434.5	4186.8	1044.4	1722.9	3366.5	725.0	8.4	nd
Au	nd	nd	3.0	26.2	446.4	213.0	567.5	161.4	260.7	321.6	75.5	3.1	nd

Overysel, OY387 core samples (cont.):

Sample	OY387 338	OY387 353	OY387 364	OY387 378	OY387 381	OY387 381	OY387 384	OY387 395	OY387 415	OY387 423	OY387 438
Lithology	GN	GN	GN	GN	GN	MS	LZP	GN	GN	GN	GT
SiO ₂ (wt%)	59.64	47.99	49.83	50.62	56.48	nd	60.05	64.20	57.69	67.56	73.28
TiO ₂	0.30	1.53	1.18	0.17	1.39	nd	0.08	0.16	0.45	0.04	0.03
Al ₂ O ₃	22.25	14.05	12.75	13.97	14.36	nd	3.80	18.57	21.79	19.33	16.06
Fe ₂ O ₃	2.74	16.29	15.92	18.68	13.87	nd	9.53	3.09	3.81	1.86	0.38
MnO	0.05	0.25	0.24	0.15	0.20	nd	0.11	0.09	0.13	0.02	0.01
MgO	2.28	8.00	8.43	5.74	6.91	nd	25.30	3.24	4.64	1.10	0.07
CaO	7.29	11.80	11.20	3.81	4.39	nd	0.85	3.22	4.85	0.63	1.11
Na ₂ O	4.51	1.05	1.32	3.78	3.20	nd	0.64	4.85	4.42	5.21	5.54
K ₂ O	0.25	0.11	0.17	0.33	0.32	nd	0.16	0.39	0.80	2.42	1.50
P ₂ O ₅	0.14	0.08	0.05	0.03	0.31	nd	0.01	0.03	0.26	0.03	0.02
LOI	0.18	-0.16	-0.16	2.65	0.16	nd	0.19	1.84	1.59	1.32	0.47
Total	99.62	100.98	100.92	99.93	101.58	nd	100.72	99.68	100.43	99.52	98.45
Sc (ppm)	7.4	42.5	43.0	12.6	24.6	nd	12.7	7.4	11.0	4.2	0.2
V	55.8	340.1	353.9	67.6	214.6	nd	19.6	27.3	31.4	0.6	0.8
Cr	179.1	208.9	256.3	743.6	1704.2	nd	4995.2	74.9	174.0	49.3	59.5
Co	10.6	72.1	81.7	310.1	89.4	nd	135.5	19.0	18.0	29.1	2.5
Ni	14.23	125.91	1520.97	16348.85	2317.91	109220.09	6767.66	1947.12	586.22	3124.35	356.30
Cu	83.37	245.68	513.62	1387.08	542.65	39930.73	2291.26	401.86	295.47	484.66	150.15
Zn	43.5	58.3	55.6	62.3	68.3	nd	62.0	41.2	50.1	31.0	30.6
Sr	898.5	254.3	215.6	506.2	294.1	nd	19.4	422.0	596.5	252.7	414.3
Ba	417.7	45.0	103.1	479.9	395.0	nd	84.6	1201.1	2049.0	1415.8	2082.3
Ga	21.7	18.9	17.6	18.4	21.9	nd	8.7	27.5	32.5	22.8	17.0
Rb	0.7	0.3	1.7	2.0	1.9	nd	2.3	5.1	13.0	14.9	8.9
Y	8.4	17.3	15.2	5.5	20.0	nd	6.2	14.3	18.2	6.2	3.3
Zr	53.6	20.5	18.2	19.5	86.8	nd	10.7	28.0	98.4	16.2	14.5
Nb	1.92	1.42	2.50	1.49	6.24	nd	3.93	17.92	22.94	5.10	1.59
Cs	414.6	46.7	108.5	482.9	400.3	nd	86.4	1203.2	2055.4	1428.4	2068.6
La	14.22	2.20	3.13	6.36	9.83	nd	2.05	7.94	7.75	7.24	5.09
Ce	26.35	8.38	7.54	11.45	18.19	nd	4.81	13.74	17.59	11.25	9.46
Pr	3.07	1.33	1.11	1.14	2.42	nd	0.47	1.43	2.45	1.07	0.90
Nd	12.13	7.30	5.77	4.16	11.33	nd	1.79	5.29	10.79	3.75	3.06
Sm	2.12	2.31	1.89	0.69	2.88	nd	0.42	1.18	2.72	0.81	0.56
Eu	1.68	1.16	0.85	0.78	1.13	nd	0.11	1.13	1.51	1.24	0.93
Gd	1.93	2.82	2.36	0.66	3.22	nd	0.49	1.37	2.65	0.72	0.48
Tb	0.25	0.47	0.40	0.11	0.49	nd	0.10	0.25	0.42	0.12	0.07
Dy	1.40	3.02	2.59	0.73	3.17	nd	0.76	1.78	2.80	0.80	0.46
Ho	0.26	0.57	0.48	0.14	0.60	nd	0.15	0.35	0.52	0.15	0.09
Er	0.76	1.67	1.44	0.51	1.81	nd	0.54	1.24	1.60	0.52	0.28
Tm	0.10	0.24	0.21	0.10	0.29	nd	0.10	0.23	0.27	0.10	0.05
Yb	0.66	1.45	1.27	0.70	1.82	nd	0.60	1.60	1.73	0.83	0.28
Lu	0.11	0.23	0.21	0.12	0.30	nd	0.10	0.28	0.26	0.16	0.05
Hf	1.15	0.67	0.58	0.50	1.86	nd	0.30	0.89	2.49	0.63	0.45
Ta	0.12	0.10	0.32	0.22	0.74	nd	0.85	2.31	3.31	0.97	0.62
Th	0.11	0.02	0.16	0.10	0.53	nd	0.83	3.44	0.78	0.78	0.28
U	0.10	0.03	0.41	0.33	1.33	nd	2.58	5.55	2.21	4.52	0.48
S (wt%)	0.018	nd	0.479	7.726	1.250	38.750	1.787	0.481	0.247	1.003	0.126
Ir (ppb)	0.0	nd	0.3	24.7	1.3	31.4	1.1	0.1	0.1	0.3	0.0
Ru	0.8	nd	1.3	73.5	3.4	58.8	4.8	1.1	0.9	1.3	0.7
Rh	2.3	nd	0.9	173.5	12.5	488.2	6.4	0.7	1.5	6.8	2.8
Pt	16.9	nd	1313.8	3396.7	708.4	12820.3	4606.8	3364.2	834.7	3363.2	613.4
Pd	224.2	nd	1737.7	4293.5	1030.3	36283.2	5948.5	4746.3	1032.7	4599.5	779.4
Au	1.0	nd	268.0	228.9	85.2	113.7	913.6	593.7	127.9	521.9	102.6

Appendix 3

LA-ICP-MS analyses of sulphides

Contents:

This appendix contains the LA-ICP-MS data performed on sulphide minerals, which are summarized in Table 7.4 in Chapter 7.

Overysel Reef pyroxenites

	S	Co	Ni	Cu	Os	Ir	Ru	Rh	Pd	Pt	Au	Te	Bi
Pyrrhotite	wt%	ppm	wt%	wt%	ppm								
OY387-252-Po1	39.43	21.1	0.62	bdl	1.02	1.97	4.46	0.22	bdl	0.01	bdl	bdl	bdl
OY387-252-Po2	34.64	10.7	0.41	bdl	0.85	1.29	2.03	0.05	0.03	0.18	bdl	bdl	bdl
OY387-252-Po-Pn1	38.81	22.8	0.48	bdl	1.05	1.68	3.55	0.01	bdl	0.15	bdl	bdl	bdl
OY335-193 Po1	38.60	41.7	0.46	0.01	0.84	1.70	4.20	1.59	0.09	1.03	0.01	1.90	1.34
OY335-193 Po2	39.82	31.3	0.44	bdl	0.89	1.73	3.83	0.91	0.08	1.74	bdl	2.60	1.52
OY335-193 Po-Pn-Cp	40.07	33.9	0.34	0.01	0.76	1.54	3.85	0.47	0.11	0.83	bdl	1.55	bdl
OY387-258 Po1	39.50	11.6	0.71	bdl	1.02	2.32	5.91	0.27	0.06	0.69	bdl	0.52	bdl
OY387-258 Po-Pn	39.01	9.0	0.62	bdl	1.03	2.18	5.25	0.04	bdl	0.23	bdl	bdl	bdl
Pentlandite	wt%	ppm	wt%	wt%	ppm								
OY387-252-Pn1	33.44	2676.3	33.44	bdl	0.88	1.75	9.59	11.99	150.42	0.19	bdl	bdl	2.56
OY387-252-Pn2	32.97	1682.1	38.16	bdl	0.72	0.61	6.28	7.87	182.58	0.73	bdl	bdl	bdl
OY387-176 Pn1	33.69	5514.3	48.12	bdl	0.77	1.43	13.27	20.58	178.98	0.79	0.01	2.49	1.39
OY387-176 Pn2	33.81	3517.7	31.26	bdl	0.69	0.92	8.78	12.28	123.38	0.49	bdl	3.61	bdl
OY387-176 Cp-Pn1	33.63	3413.3	33.07	0.15	0.15	0.87	7.91	14.44	119.28	0.88	0.01	bdl	bdl
OY335-193 Pn1	34.06	4074.3	32.34	0.01	0.61	1.49	5.28	4.72	76.86	0.33	bdl	0.93	0.92
OY335-193 Po-Pn-Cp	34.12	4370.1	29.86	bdl	0.47	2.26	32.56	58.14	68.64	0.25	bdl	2.61	1.29
OY387-258 Pn1	33.65	760.3	32.36	bdl	0.45	0.90	1.94	0.04	84.76	0.38	bdl	0.68	bdl
OY387-258 Po-Pn	33.89	713.9	31.24	bdl	0.53	0.57	5.07	5.10	87.95	0.02	bdl	bdl	bdl
Chalcopyrite	wt%	ppm	wt%	wt%	ppm								
OY387-176 Cp1	35.41	bdl	bdl	24.41	bdl	bdl	bdl	bdl	0.40	2.29	bdl	2.63	3.03
OY387-176 Cp2	35.64	16.1	0.26	30.35	bdl	bdl	bdl	bdl	1.73	5.10	bdl	3.03	2.16
OY387-176 Cp-Pn1	35.35	bdl	0.01	25.43	bdl	bdl	bdl	bdl	0.29	0.44	bdl	0.48	0.97
OY387-193 Cp1	33.89	1.7	bdl	23.80	bdl	0.01	bdl	bdl	0.23	0.01	bdl	bdl	bdl
OY387-252 Cp1	35.29	bdl	0.01	34.05	0.01	bdl	0.07	bdl	0.21	0.02	bdl	bdl	bdl
OY387-258 Cp1	35.15	bdl	bdl	31.39	bdl	bdl	bdl	bdl	0.38	0.01	0.02	bdl	bdl

Sandsloot Reef pyroxenites

	S	Co	Ni	Cu	Os	Ir	Ru	Rh	Pd	Pt	Au	Te	Bi
Pyrrhotite	wt%	ppm	wt%	wt%	ppm								
SNN1-8 Po1	38.82	5.33	0.12	bdl	1.06	2.22	5.35	0.18	0.02	1.79	bdl	0.88	0.64
SNN1-8 Po-Pn1 (Po)	38.18	3.57	0.15	bdl	1.24	2.29	4.27	0.12	0.08	1.58	bdl	1.76	0.92
SNN1-29 Po1	38.83	10.44	0.18	bdl	2.07	3.85	8.59	0.29	bdl	0.46	bdl	0.63	bdl
SNN1-29 Po-Pn-Cp	38.71	5.86	0.14	bdl	2.86	3.23	8.83	0.26	0.16	2.70	bdl	3.29	bdl
SNN1-29 Po-Pn1 (Po)	37.25	7.17	0.17	bdl	1.93	2.75	8.42	0.06	0.02	0.09	bdl	bdl	bdl
Pentlandite	wt%	ppm	wt%	wt%	ppm								
SNN1-8 Pn1 (Pt-Bi)	35.42	3068.9	30.18	bdl	0.64	1.36	7.01	9.44	143.42	2.07	bdl	1.64	2.52
SNN1-8 Pn2	35.23	3262.7	31.84	bdl	0.90	1.98	7.73	8.63	129.94	1.52	bdl	1.00	bdl
SNN1-8 Po-Pn1	35.61	3284.1	29.21	bdl	0.90	1.64	8.06	8.20	130.32	1.75	bdl	1.54	1.01
SNN1-29 Pn1 (Pt-Bi)	35.80	5574.6	32.82	0.04	2.45	5.02	23.91	29.65	84.80	0.59	bdl	0.99	bdl
SNN1-29 Pn1	35.81	5586.8	32.65	0.04	2.51	4.96	25.34	32.90	84.26	0.07	bdl	0.60	bdl
SNN1-29 Po-Pn-Cp-X	35.70	5456.3	33.53	0.03	4.21	6.50	35.44	41.27	75.52	0.58	bdl	bdl	bdl
SNN1-29 Po-Pn1	35.79	4559.0	26.69	bdl	2.53	3.73	33.00	45.48	67.71	0.11	bdl	6.14	bdl
Chalcopyrite	wt%	ppm	wt%	wt%	ppm								
SNN1-8 Cp1b	34.37	bdl	0.01	29.42	bdl	0.00	0.14	0.17	0.33	0.05	0.00	0.44	bdl
SNN1-29 Cp-Po	34.79	bdl	0.02	32.02	0.00	0.00	0.01	bdl	0.11	0.02	0.01	bdl	bdl
SNN1-29 Po-Pn-Cp	34.78	235.57	1.57	29.71	0.06	0.27	0.68	1.05	4.76	0.28	0.01	bdl	bdl

Overysel chromitites

	S	Co	Ni	Cu	Os	Ir	Ru	Rh	Pd	Pt	Au	Te	Bi
Pyrrhotite	wt%	ppm	wt%	wt%	ppm								
OY16 Po1	38.82	62.67	0.03	bdl	bdl	bdl	bdl	bdl	0.03	bdl	0.07	bdl	19.74
Pentlandite													
OY-08B Pn1	35.80	5079.3	33.72	bdl	0.49	bdl	3.16	bdl	72.40	bdl	0.00	0.81	bdl
Pyrite													
OY-08B Py1 (As rich)	53.95	213.80	0.08	bdl	bdl	bdl	0.03	0.02	0.25	bdl	0.09	2.00	107.9
OY-08B Py1 (As poor)	53.95	40.25	0.37	bdl	bdl	bdl	0.02	0.01	0.13	bdl	0.06	bdl	21.87

Appendix 3. LA-ICP-MS of sulphides

Overysel Footwall rocks													
	S	Co	Ni	Cu	Os	Ir	Ru	Rh	Pd	Pt	Au	Te	Bi
	wt%	ppm	wt%	wt%	ppm								
Pyrrhotite													
OY387-378 Po1	39.84	57.9	1.09	bdl	0.13	0.23	0.40	bdl	bdl	0.02	bdl	bdl	bdl
OY387-378 Po2	39.79	42.8	0.71	bdl	0.08	0.15	0.26	bdl	bdl	0.01	bdl	bdl	bdl
OY387-378 Po-Pn-Cp	39.95	31.2	0.57	bdl	0.08	0.12	0.36	0.02	bdl	0.02	bdl	bdl	bdl
OY387-381 Po2	38.72	39.5	0.47	bdl	0.02	0.10	0.07	3.10	9.77	0.01	bdl	2.97	3.60
OY387-381 Po-Pn2	37.15	84.6	0.68	bdl	0.02	0.04	0.07	0.12	3.84	0.01	bdl	3.60	2.00
Pentlandite													
OY335-316 Py-Pn	33.26	788.9	30.32	0.01	bdl	bdl	0.07	bdl	110.90	0.03	0.02	bdl	2.20
OY335-316 Pn1 (+Po)	36.07	3104.8	17.72	0.29	0.01	0.03	0.18	0.39	55.35	0.15	0.28	18.08	70.95
OY387-378 Pn1	33.81	4312.0	31.10	0.01	0.01	0.04	bdl	0.03	40.54	1.11	0.12	bdl	2.48
OY387-378 Po-Pn-Cp	33.89	2768.1	25.72	bdl	0.04	0.08	0.95	1.84	29.63	0.15	bdl	bdl	bdl
OY387-381 Pn2	32.94	5184.9	34.32	bdl	0.04	0.06	bdl	2.04	1.73	78.21	bdl	bdl	bdl
OY387-381 Po-Pn1	32.79	4451.0	34.61	bdl	bdl	0.02	bdl	0.39	0.85	61.37	bdl	bdl	bdl
OY387-384 Pn1	33.19	2887.6	33.84	bdl	0.07	0.04	0.21	0.26	103.54	0.02	bdl	1.54	bdl
OY387-384 Pn2	33.95	2775.1	32.84	bdl	0.01	0.01	0.10	0.08	28.60	bdl	0.05	1.05	0.86
OY387-384 Cp-Pn	32.16	2786.7	31.83	0.05	0.06	0.04	0.07	0.31	101.59	bdl	bdl	1.37	bdl
OY387-395 Cp-Pn	32.96	2388.6	43.55	0.26	0.01	bdl	0.03	0.01	170.66	bdl	0.02	bdl	3.50
Chalcopyrite													
OY335-316 Cp1	34.69	bdl	0.01	19.30	bdl	bdl	0.32	0.19	0.29	bdl	0.03	bdl	bdl
OY335-316 Cp2	35.43	bdl	0.01	27.06	bdl	bdl	bdl	bdl	0.36	bdl	0.05	bdl	bdl
OY387-378 Cp1	32.12	bdl	bdl	28.95	bdl	bdl	bdl	bdl	0.18	bdl	bdl	bdl	bdl
OY387-378 Po-Pn-Cp	35.29	159.6	1.84	31.82	bdl	bdl	bdl	bdl	5.75	0.03	0.01	bdl	bdl
OY387-384 Cp1	34.46	bdl	bdl	26.46	bdl	bdl	0.40	0.42	0.73	bdl	0.04	bdl	0.08
OY387-384 Cp2	34.63	bdl	bdl	23.07	bdl	bdl	bdl	bdl	3.29	0.01	0.04	bdl	0.09
OY387-384 Cp-Pn	35.24	65.4	0.80	22.47	bdl	bdl	0.38	0.48	2.79	0.06	0.18	bdl	1.57
OY387-395 Cp1	34.55	bdl	bdl	34.11	bdl	bdl	bdl	bdl	0.84	bdl	0.02	bdl	0.96
OY387-395 Cp-Pn	35.05	bdl	0.01	34.80	0.02	bdl	bdl	bdl	2.44	0.01	0.06	bdl	2.31
Pyrite													
OY335-316 Py1	53.67	16.4	bdl	bdl	bdl	bdl	0.03	bdl	0.04	0.01	0.00	bdl	bdl
OY335-316 Py	53.27	21.3	0.02	bdl	bdl	bdl	bdl	bdl	0.06	0.09	0.03	bdl	23.50
OY335-316 Py-Pn	53.42	25.0	0.01	0.05	bdl	bdl	bdl	bdl	0.03	0.00	0.01	0.62	1.44
Millerite													
OY387-395 Mill1	35.08	2053.6	66.90	0.01	bdl	bdl	0.11	0.03	44.11	bdl	0.01	0.78	54.37
Limit of detection													
	0.31	0.74	<0.01	<0.01	0.015	0.005	0.067	0.011	0.026	0.017	0.006	0.35	0.84

Appendix 4

Mineral chemistry

Contents:

This appendix contains the SEM EDA data from the analysis of silicate and oxide phases in the Platreef.

Key to lithology abbreviations in the following tables:

AFPX	Altered Platreef feldspathic pyroxenite	HWGN	Hangingwall gabbronorite
AGN	Amphibolitised gneiss	HWMN	Hangingwall fine-grained melanorite
CHR	Chromitite		intrusive
CHRX	Chromitite xenolith	HWSA	Hangingwall spotted anorthosite
CPX	Platreef clinopyroxenite	IN	Intrusive norite
CSX	Calc-silicate xenolith	LZP	Lower Zone pyroxenite
FCHR	Feldspathic chromitite	PEGP	Pegmatitic Platreef feldspathic pyroxenite
FCPX	Footwall clinopyroxenite	PDT	Peridotite (olivine-replaced reef)
FPX	Platreef feldspathic pyroxenite	QFPX	Quartzo-feldspathic pyroxenite
GN	Gneiss	SCSX	Serpentinised calc-silicate xenolith
HWA	Hangingwall mottled anorthosite	SPT	Serpentinite

Sandsloot, SNN1 sample suite, orthopyroxene

Sample	SNN1 0	SNN1 0	SNN1 0	SNN1 0	SNN1 0	SNN1 7a	SNN1 7a	SNN1 7a	SNN1 7a	SNN1 7b	SNN1 7b	SNN1 7b	SNN1 7b	SNN1 7b	SNN1 7b
Lithology	HWGN	HWGN	HWGN	HWGN	HWGN	HWGN	HWGN	HWGN	HWGN	HWA	FPX	FPX	FPX	FPX	FPX
MgO	23.17	23.93	23.87	23.49	23.62	23.02	22.95	23.18	23.45	22.97	27.12	27.31	26.85	26.34	27.38
Al ₂ O ₃	0.66	0.85	0.62	1.18	0.72	0.99	0.69	0.81	0.46	0.85	1.18	0.73	0.76	0.67	0.81
SiO ₂	53.30	52.83	52.98	52.58	53.26	53.49	53.72	53.13	53.13	53.28	54.41	54.68	54.68	54.50	54.43
CaO	2.44	1.22	0.92	0.99	1.45	2.81	2.63	2.72	0.89	4.52	0.75	0.62	1.02	1.11	1.03
TiO ₂					0.28	0.26	0.28	0.31	0.27	0.27					0.26
Cr ₂ O ₃	0.26	0.40		0.31		0.28		0.29		0.38	0.37	0.27			
MnO	0.32	0.35	0.56	0.42	0.43	0.32	0.42	0.43	0.51	0.34	0.37	0.33	0.31		0.32
FeO	20.06	20.96	21.47	20.71	20.75	19.82	19.43	19.71	21.88	18.18	17.08	16.94	17.79	17.76	16.97
Total	100.20	100.54	100.41	99.67	100.53	100.99	100.11	100.57	100.59	100.79	101.27	100.88	101.41	100.64	100.9
En	64.04	65.44	65.25	65.57	65.06	63.66	64.21	64.04	64.48	63.07	72.82	73.29	71.47	70.99	72.73
Wo	4.85	2.40	1.81	1.99	2.87	5.59	5.29	5.40	1.76	8.92	1.45	1.20	1.95	2.15	1.97
Fs	31.11	32.16	32.94	32.44	32.07	30.76	30.50	30.56	33.76	28.01	25.74	25.51	26.57	26.86	25.30
Mg#	67.30	67.05	66.46	66.90	66.98	67.42	67.79	67.70	65.63	69.25	73.89	74.18	72.90	72.55	74.19
Sample	SNN1 8	SNN1 8	SNN1 8	SNN1 8	SNN1 8	SNN1 18a	SNN1 18a	SNN1 18a	SNN1 18a	SNN1 18a	SNN1 25	SNN1 25	SNN1 25	SNN1 25	SNN1 25
Lithology	FPX	FPX	FPX	FPX	FPX	FPX	FPX	FPX	FPX	FPX	AFPX	AFPX	AFPX	AFPX	AFPX
MgO	26.76	27.09	26.60	27.65	26.55	29.44	29.62	28.83	29.19	28.39	29.15	28.19	28.33	28.80	28.78
Al ₂ O ₃	1.06	1.04	1.36	1.40	1.04	0.86	0.93	1.26	1.49	1.30	0.96	0.72	0.91	0.66	0.80
SiO ₂	54.43	54.63	54.56	54.56	54.62	54.69	54.74	54.63	54.80	53.52	54.70	54.26	54.73	54.49	54.29
CaO	1.57	1.87	1.79	1.36	2.18	1.46	0.86	1.17	0.84	1.97	1.14	1.64	1.42	0.91	1.27
TiO ₂	0.28			0.24		0.26						0.31		0.29	0.32
Cr ₂ O ₃	0.37	0.50	0.48	0.57		0.51	0.51	0.50	0.43	0.54	0.42	0.27	0.37	0.46	0.38
MnO	0.37	0.29	0.32	0.31	0.31		0.44		0.29	0.28	0.36	0.48	0.33	0.30	0.41
FeO	16.07	15.80	15.96	15.16	16.00	13.92	13.99	13.19	14.05	12.87	13.95	14.38	14.53	14.93	14.67
Total	100.91	101.23	101.08	101.27	100.69	101.15	101.09	99.58	101.09	98.85	100.68	100.25	100.62	100.84	100.91
En	72.51	72.63	72.20	74.46	71.57	76.86	77.77	77.77	77.47	76.67	77.12	75.30	75.54	76.12	75.89
Wo	3.06	3.60	3.49	2.63	4.23	2.74	1.62	2.27	1.60	3.83	2.17	3.15	2.72	1.73	2.41
Fs	24.43	23.77	24.31	22.91	24.20	20.39	20.61	19.97	20.93	19.50	20.71	21.55	21.74	22.15	21.71
Mg#	74.79	75.34	74.81	76.47	74.73	79.03	79.05	79.57	78.73	79.72	78.83	77.74	77.65	77.46	77.76
Sample	SNN1 37	SNN1 37	SNN1 37	SNN1 37	SNN1 37	SNN1 43	SNN1 43	SNN1 43	SNN1 43	SNN1 43	SNN1 48	SNN1 48	SNN1 48	SNN1 48	SNN1 48
Lithology	FPX	FPX	FPX	FPX	FPX	PDT	PDT	PDT	PDT	PDT	PEGP	PEGP	PEGP	PEGP	PEGP
MgO	1	1	1	1	1	1	1	1	1	1	1	1	1	1	1
Al ₂ O ₃	27.77	29.19	26.88	29.04	28.89	29.81	30.25	31.20	29.74	29.31	27.84	25.71	29.49	26.58	28.02
SiO ₂	1.14	1.35	0.47	1.23	1.24	1.40	1.06	0.51	1.10	1.45	1.41	1.18	1.30	1.40	1.14
CaO	54.03	54.46	53.97	54.85	54.46	54.11	54.48	54.93	54.63	54.20	53.91	52.94	54.43	53.47	54.10
TiO ₂	0.66	1.39	0.83	2.24	0.94	2.30	1.58	0.43	1.83	3.54	3.44	4.92	1.23	2.21	1.25
Cr ₂ O ₃	0.25														
MnO	0.34	0.44		0.40	0.42	0.28	0.28				0.61	0.52	0.42	0.50	0.45
FeO		0.26	0.31			0.27		0.36	0.27		0.31	0.30	0.29		0.31
Total	16.10	13.65	17.35	13.13	14.42	11.58	11.89	12.21	12.28	10.53	12.41	13.05	12.34	15.37	14.74
Sample	100.29	100.73	99.80	100.88	100.39	99.76	99.55	99.66	99.85	99.04	99.93	98.62	99.51	99.52	100.00
En	74.49	77.12	72.23	76.38	76.72	78.53	79.48	81.33	78.37	77.61	74.68	70.30	79.06	72.24	75.34
Wo	1.27	2.64	1.60	4.24	1.79	4.36	2.98	0.81	3.47	6.74	6.63	9.67	2.37	4.32	2.42
Fs	24.24	20.24	26.16	19.38	21.49	17.12	17.53	17.86	18.16	15.65	18.68	20.02	18.57	23.44	22.24
Mg#	75.45	79.21	73.41	79.76	78.12	82.10	81.93	81.99	81.19	83.22	79.99	77.83	80.98	75.50	77.21

Sandsloot, SNN1 sample suite, clinopyroxene

Sample	SNN1	SNN1	SNN1	SNN1	SNN1	SNN1	SNN1	SNN1	SNN1	SNN1	SNN1	SNN1	SNN1	SNN1
Lithology	HWGN	HWGN	HWGN	HWGN	HWGN	HWGN	HWGN	HWGN	HWGN	HWA	HWA	HWA	FPX	FPX
MgO	14.64	14.60	14.65	14.42	14.77	15.17	15.27	14.02	14.65	14.21	14.58	15.18	15.73	16.12
Al ₂ O ₃	1.09	1.38	1.61	1.58	1.38	1.24	1.40	2.34	1.10	1.78	1.56	1.58	1.80	1.74
SiO ₂	52.30	52.03	51.86	51.95	52.25	52.32	52.37	48.94	52.74	51.75	52.72	52.62	52.98	51.25
CaO	21.91	21.86	22.53	21.65	22.55	20.91	19.60	20.40	22.29	22.65	22.40	21.19	22.63	22.45
TiO ₂	0.38	0.43	0.35	0.56	0.49	0.59	0.48	6.20		0.79	0.62	0.47	0.34	0.82
Cr ₂ O ₃				0.28									0.30	0.70
MnO	0.31					0.29	0.25			0.32				
FeO	9.11	8.93	8.35	9.27	8.45	10.24	11.04	9.09	9.21	9.11	9.31	10.32	6.74	5.44
Total	99.74	99.23	99.36	99.71	99.89	100.75	100.40	100.98	99.99	100.61	101.19	101.36	100.52	98.54
En	41.23	41.32	41.22	40.98	41.34	42.19	42.94	41.49	40.87	39.90	40.60	41.92	43.96	45.64
Wo	44.36	44.48	45.58	44.23	45.38	41.81	39.63	43.40	44.71	45.73	44.84	42.07	45.47	45.70
Fs	14.39	14.18	13.18	14.78	13.27	15.98	17.42	15.09	14.41	14.35	14.54	15.99	10.57	8.64
Mg#	74.12	74.45	75.77	73.49	75.70	72.53	71.14	73.32	73.92	73.54	73.62	72.38	80.62	84.08

Sample	SNN1	SNN1	SNN1	SNN1	SNN1	SNN1	SNN1	SNN1	SNN1	SNN1	SNN1	SNN1	SNN1	SNN1
Lithology	FPX	SCSX	SCSX	SCSX	PDT	PDT	PDT	PDT	PDT	PDT	PDT	PDT	PDT	CPX
MgO	16.28	12.68	13.15	12.37	16.64	15.84	16.42	15.98	16.33	16.29	16.20	17.92	17.34	16.61
Al ₂ O ₃	0.42	8.22	7.58	8.39	1.98	1.99	1.24	1.93	2.43	2.04	1.81	1.87	2.13	2.14
SiO ₂	53.14	45.82	46.33	45.56	52.27	51.81	52.75	52.01	51.67	51.83	52.02	52.09	51.95	52.36
CaO	22.91	25.28	25.42	24.78	22.76	22.08	22.63	22.10	21.29	22.48	22.64	18.59	20.50	22.66
TiO ₂		0.40	0.30	0.45	0.37	0.33	0.57		0.48	0.67	0.36	0.42	0.41	
Cr ₂ O ₃					0.61	0.50	0.43	0.79	0.36	0.55	0.41	0.37	0.41	0.48
MnO						0.28						0.26	0.26	
FeO	6.18	7.60	6.91	7.85	5.14	5.97	6.19	6.24	5.99	5.58	5.46	7.33	6.36	5.44
Total	98.92	100.00	99.69	99.40	99.79	98.81	100.23	99.05	98.55	99.43	98.91	98.85	99.35	99.68
En	44.94	36.10	37.24	35.76	46.36	45.17	45.40	45.17	46.65	45.77	45.58	50.62	48.64	46.19
Wo	45.47	51.75	51.76	51.50	45.59	45.27	44.99	44.92	43.73	45.42	45.79	37.75	41.34	45.31
Fs	9.57	12.14	10.98	12.73	8.03	9.55	9.60	9.90	9.60	8.80	8.62	11.62	10.01	8.49
Mg#	82.44	74.83	77.23	73.74	85.23	82.54	82.54	82.03	82.93	83.88	84.09	81.33	82.93	84.47

Sample	SNN1	SNN1	SNN1	SNN1	SNN1	SNN1	SNN1	SNN1	SNN1	SNN1	SNN1	SNN1	SNN1	SNN1
Lithology	CPX	CPX	CPX	CPX	CPX	CPX	CPX	CPX	CPX	CPX	CPX	CPX	CPX	CPX
MgO	16.56	16.42	16.91	16.69	16.49	17.63	16.94	18.22	17.13	16.78	16.84	16.90	16.46	16.78
Al ₂ O ₃	2.08	2.21	2.22	1.93	1.95	2.25	1.97	1.84	2.04	2.08	1.23	2.36	1.71	1.18
SiO ₂	52.40	52.04	52.68	52.42	52.83	52.59	52.26	53.03	52.77	53.33	53.02	52.36	52.88	53.06
CaO	23.11	22.78	23.35	23.13	22.57	19.78	22.15	19.22	22.18	22.94	22.80	22.71	22.63	22.90
TiO ₂	0.37	0.34	0.30	0.36	0.46	0.31	0.37	0.30	0.29	0.28			0.32	
Cr ₂ O ₃	0.38	0.46	0.60	0.45	0.50	0.55	0.51	0.48	0.41	0.43	0.36	0.35		0.38
MnO								0.27				0.30		
FeO	4.76	5.43	5.42	5.23	6.19	7.11	6.04	7.37	5.63	5.60	5.24	5.39	5.83	5.72
Total	99.65	99.68	101.48	100.21	100.99	100.22	100.23	100.46	100.70	101.45	99.49	100.36	99.84	100.02
En	46.19	45.80	46.02	46.03	45.56	49.18	46.72	50.36	47.27	46.07	46.55	46.61	45.72	46.03
Wo	46.35	45.69	45.69	45.86	44.83	39.67	43.92	38.20	44.00	45.29	45.31	45.03	45.19	45.16
Fs	7.45	8.50	8.27	8.09	9.59	11.13	9.34	11.43	8.71	8.63	8.12	8.34	9.08	8.80
Mg#	86.11	84.35	84.76	85.04	82.60	81.55	83.33	81.50	84.43	84.23	85.13	84.82	83.42	83.94

Sandsloot, SNN1 sample suite, plagioclase

Sample	SNN1	SNN1	SNN1	SNN1	SNN1	SNN1	SNN1	SNN1	SNN1	SNN1	SNN1	SNN1	SNN1	SNN1
	0	0	0	0	0	7a	7a	7a	7a	7a	7a	7a	7a	7b
Lithology	HWGN	HWGN	HWGN	HWGN	HWGN	HWGN	HWGN	HWGN	HWGN	HWA	HWA	HWA	HWA	HWA
Na ₂ O	3.28	3.87	3.97	2.73	4.08	3.38	4.82	3.71	4.33	3.89	4.29	3.43	4.53	4.50
Al ₂ O ₃	31.62	31.06	30.89	32.47	30.18	31.40	28.87	31.29	29.88	30.68	30.02	31.22	29.91	30.17
SiO ₂	49.78	50.93	50.90	48.44	51.53	50.40	52.47	50.92	51.96	50.73	52.63	50.31	53.75	52.79
K ₂ O		0.00			0.19		0.27		0.23				0.32	
CaO	14.99	14.04	13.90	15.88	13.68	15.05	12.00	14.07	13.32	14.17	13.23	14.82	12.88	13.31
Total	99.66	99.91	99.65	99.52	99.65	100.22	98.43	100.00	99.72	99.48	100.17	99.77	101.39	100.77
An#	83.47	80.04	79.46	86.54	78.75	83.11	73.34	80.74	77.27	80.10	77.32	82.68	75.86	76.58

Sample	SNN1	SNN1	SNN1	SNN1	SNN1	SNN1	SNN1	SNN1	SNN1	SNN1	SNN1	SNN1	SNN1	SNN1
	7b	7b	7b	7b	7b	7b	8	8	8	8	8	18a	18a	18a
Lithology	HWA	HWA	FPX	FPX	FPX	FPX	FPX	FPX	FPX	FPX	FPX	FPX	FPX	FPX
Na ₂ O	4.17	4.34	4.89	4.38	4.90	4.31	5.12	4.06	3.91	3.43	4.21	3.84	4.97	4.07
Al ₂ O ₃	30.71	30.03	30.02	30.54	29.28	30.34	29.43	30.44	30.73	31.46	30.09	30.30	28.60	30.47
SiO ₂	52.23	52.12	53.59	52.49	53.79	52.15	54.12	52.00	51.31	50.51	52.33	50.88	52.45	51.91
K ₂ O	0.30	0.18	0.21	0.31	0.24	0.26	0.41	0.24	0.28	0.22	0.28	0.25	0.29	0.29
CaO	13.71	13.32	12.78	13.48	12.23	13.25	11.88	13.39	13.64	14.92	13.24	13.73	11.59	13.59
Total	101.12	99.99	101.49	101.21	100.44	100.31	100.97	100.14	99.87	100.54	100.15	99.00	97.61	100.34
An#	78.42	77.23	74.28	77.28	73.39	77.26	71.94	78.47	79.40	82.78	77.66	79.80	72.05	78.68

Sample	SNN1	SNN1	SNN1	SNN1	SNN1	SNN1
	18a	18a	37	37	37	53
Lithology	FPX	FPX	FPX	FPX	FPX	PDT
Na ₂ O	4.57	4.41	5.48	5.44	3.84	5.43
Al ₂ O ₃	29.91	30.75	28.69	28.22	31.28	28.41
SiO ₂	52.59	52.54	53.94	54.31	50.01	53.74
K ₂ O	0.31	0.21	0.17	0.28		0.41
CaO	12.61	13.60	11.45	11.05	14.32	11.00
Total	100.00	101.51	99.74	99.29	99.46	98.97
An#	75.31	77.32	69.78	69.18	80.47	69.13

Sandsloot, SNN1 sample suite, olivine

Sample	SNN1	SNN1	SNN1	SNN1	SNN1	SNN1	SNN1	SNN1
	40	40	40	40	53	53	53	53
Lithology	SCSX	SCSX	SCSX	SCSX	PDT	PDT	PDT	PDT
MgO	47.62	48.76	48.53	48.41	40.42	39.94	40.14	39.53
SiO ₂	39.90	40.21	40.26	39.77	37.92	38.25	38.05	38.05
CaO		0.20	0.25					
MnO	0.89	1.16	1.10	1.03	0.41	0.46	0.55	0.47
FeO	11.02	10.57	11.08	11.16	21.80	21.61	22.03	21.54
Total	99.43	100.91	101.21	100.37	100.55	100.27	100.77	99.60
Mg#	88.51	89.15	88.64	88.55	76.77	76.71	76.45	76.58

Sandsloot, SNS1 sample suite, orthopyroxene

	SNS1													
Sample	2	2	2	2	6	6	6	6	10	10	10	10	11	11
Lithology	HWGN													
MgO	26.32	26.31	26.28	26.36	27.44	25.51	26.62	27.04	26.78	26.29	26.63	26.08	27.40	27.57
Al ₂ O ₃	1.37	0.94	0.83	0.83	0.81	1.31	0.75	0.86	0.83	0.60	0.75	0.77	0.88	0.64
SiO ₂	54.23	54.07	53.66	54.30	54.30	53.72	54.19	53.96	53.28	53.45	53.26	53.03	54.19	54.45
CaO	1.55	2.62	2.17	2.32	0.89	4.14	2.23	0.99	0.94	1.89	1.05	1.99	1.35	0.89
TiO ₂					0.30						0.31			0.28
Cr ₂ O ₃	0.48	0.26		0.46		0.43	0.44		0.37	0.29	0.40	0.29	0.34	0.33
MnO		0.34	0.36	0.36	0.37	0.35		0.37	0.34	0.32	0.34	0.30	0.41	0.31
FeO	17.23	16.56	16.73	16.69	17.01	15.38	16.65	17.13	17.70	16.81	17.50	16.94	16.87	16.95
Total	101.18	101.09	100.03	101.33	101.11	100.84	100.88	100.36	100.24	99.65	100.25	99.40	101.45	101.42
En	70.94	70.18	70.59	70.49	72.93	68.73	70.86	72.37	71.63	70.90	71.58	70.45	72.41	73.09
Wo	3.00	5.03	4.19	4.46	1.70	8.02	4.27	1.90	1.81	3.66	2.03	3.87	2.57	1.70
Fs	26.06	24.79	25.22	25.05	25.37	23.25	24.87	25.73	26.57	25.44	26.40	25.68	25.02	25.22
Mg#	73.13	73.90	73.68	73.78	74.19	74.72	74.02	73.77	72.94	73.59	73.06	73.29	74.32	74.35
	SNS1													
Sample	11	11	11	12	12	12	12	17	17	17	17	17	22	22
Lithology	HWGN	HWGN	HWA	FPX										
MgO	26.76	27.19	25.57	26.95	29.05	28.39	27.78	28.79	28.02	27.87	28.04	28.60	27.79	26.43
Al ₂ O ₃	1.03	0.89	0.97	0.95	0.39	0.91	1.01	1.10	0.93	1.04	0.90	0.75	0.75	0.78
SiO ₂	54.01	54.11	54.09	54.20	54.87	54.14	54.30	54.06	53.82	54.01	54.25	54.05	53.79	53.32
CaO	1.81	1.42	3.02	3.95	0.82	1.41	2.14	0.80	1.98	1.62	2.03	1.10	1.14	3.24
TiO ₂				0.26	0.30									0.28
Cr ₂ O ₃		0.38	0.50	0.52		0.50	0.52	0.40	0.55	0.40	0.48	0.31	0.26	0.44
MnO		0.33	0.31	0.32	0.31			0.41	0.43		0.38	0.36		0.33
FeO	16.59	16.90	15.96	13.65	15.33	15.13	14.59	15.02	14.56	14.37	14.12	14.97	15.69	14.59
Total	100.20	101.23	100.41	100.79	101.08	100.48	100.34	100.58	100.29	99.30	100.19	100.14	99.42	99.41
En	71.61	72.13	69.68	71.96	75.96	74.92	74.07	76.18	74.49	75.12	74.93	75.68	74.28	71.54
Wo	3.48	2.71	5.92	7.58	1.54	2.68	4.10	1.52	3.78	3.14	3.90	2.09	2.19	6.30
Fs	24.91	25.16	24.41	20.45	22.50	22.41	21.83	22.30	21.72	21.74	21.17	22.23	23.53	22.16
Mg#	74.19	74.14	74.06	77.87	77.15	76.98	77.24	77.35	77.42	77.56	77.97	77.30	75.94	76.35
	SNS1													
Sample	22	22	22	25	25	25	25	29	29	29	31a	31a	31a	31a
Lithology	FPX													
MgO	27.89	27.54	27.79	28.51	28.27	28.20	28.77	28.22	27.12	28.24	27.18	27.25	26.80	25.95
Al ₂ O ₃	0.83	1.12	0.95	0.90	1.30	0.99	0.77	1.23	1.07	0.94	1.19	1.35	1.07	0.82
SiO ₂	53.85	53.52	53.56	54.53	54.45	54.11	54.20	54.15	54.12	54.14	53.96	53.67	53.64	53.13
CaO	1.18	2.15	1.02	0.95	1.27	1.62	1.14	2.58	1.74	1.20	2.44	1.71	2.81	1.92
TiO ₂			0.30	0.29			0.33			0.26				
Cr ₂ O ₃	0.36	0.50	0.44	0.27	0.34	0.38	0.38	0.43	0.39	0.33	0.28	0.37	0.37	0.27
MnO	0.33		0.28	0.35	0.30	0.36	0.40		0.27	0.37	0.33	0.35		0.30
FeO	15.41	14.91	15.54	15.25	14.95	14.73	15.22	13.56	15.57	15.35	15.08	15.52	15.36	16.83
Total	99.85	99.74	99.89	101.05	100.88	100.39	101.22	100.17	100.29	100.85	100.47	100.22	100.05	99.22
En	74.60	73.53	74.62	75.52	75.24	74.94	75.45	74.89	73.08	74.87	72.68	73.27	71.58	70.56
Wo	2.27	4.13	1.97	1.81	2.43	3.10	2.15	4.92	3.37	2.29	4.69	3.31	5.40	3.75
Fs	23.13	22.34	23.41	22.67	22.33	21.97	22.40	20.19	23.55	22.84	22.63	23.42	23.02	25.68
Mg#	76.33	76.70	76.11	76.91	77.12	77.33	77.11	78.76	75.63	76.63	76.26	75.78	75.66	73.32

Sandsloot, SNS1 sample suite, clinopyroxene

Sample	SNS1	SNS1	SNS1	SNS1										
	2	2	2	2	6	6	6	6	10	10	10	11	11	11
Lithology	HWGN	HWA	HWA	HWA										
MgO	15.68	15.65	15.51	15.96	15.73	15.70	15.71	15.83	15.69	15.38	15.47	14.88	14.84	14.61
Al ₂ O ₃	1.39	1.40	1.42	1.40	1.48	1.89	1.86	1.61	1.24	1.24	1.72	1.41	1.63	1.56
SiO ₂	51.87	52.21	52.42	52.43	52.27	51.72	52.58	51.96	52.01	51.53	51.75	51.84	51.53	51.11
CaO	22.33	22.55	22.78	22.29	22.94	22.64	22.82	22.40	22.44	22.71	23.17	22.23	22.31	23.01
TiO ₂	0.58	0.54	0.56	0.65	0.57	0.38	0.42	0.66	0.52	0.52	0.79	0.69	0.70	0.71
Cr ₂ O ₃	0.48	0.41	0.47	0.43	0.53	0.75	0.57	0.65	0.64	0.56	0.60		0.32	
MnO			0.28											
FeO	7.46	7.18	7.22	7.42	7.16	6.66	6.97	7.25	6.80	6.60	7.25	8.91	9.07	8.45
Total	99.80	99.94	100.66	100.59	100.67	99.74	100.92	100.36	99.35	98.53	100.75	99.96	100.41	99.44
En	43.65	43.60	43.15	44.15	43.40	43.95	43.60	43.96	44.02	43.43	42.73	41.49	41.25	40.70
Wo	44.69	45.17	45.57	44.33	45.51	45.57	45.53	44.73	45.26	46.10	46.02	44.56	44.59	46.08
Fs	11.65	11.22	11.27	11.51	11.08	10.46	10.85	11.30	10.70	10.45	11.24	13.94	14.15	13.21
Mg#	78.93	79.53	79.29	79.31	79.65	80.77	80.07	79.55	80.44	80.59	79.18	74.85	74.46	75.50
Sample	SNS1	SNS1	SNS1	SNS1										
	12	12	17	17	17	22	22	25	25	29	31a	31a	31a	31a
Lithology	FPX	FPX	FPX	FPX										
MgO	16.27	16.55	15.85	16.86	15.77	16.01	16.05	17.71	16.43	16.03	16.03	16.10	16.44	16.70
Al ₂ O ₃	1.27	1.48	1.68	1.86	1.88	1.04	1.37	1.97	2.03	1.63	2.09	2.04	1.73	2.09
SiO ₂	53.39	52.48	52.02	51.67	51.49	52.29	51.82	53.03	52.42	52.14	52.00	51.92	52.30	52.89
CaO	23.80	23.04	22.76	20.80	23.24	22.80	22.69	20.39	22.40	21.97	21.68	21.92	21.81	20.62
TiO ₂	0.35	0.61	0.61	0.37	0.45	0.40	0.57	0.27		0.69	0.33	0.34	0.51	0.32
Cr ₂ O ₃	0.57	0.61	0.78	0.70	0.70	0.55	0.64	0.73	0.77	0.56	0.61	0.50	0.55	0.54
MnO														0.31
FeO	5.63	5.67	5.83	6.67	5.96	5.91	5.82	7.62	6.35	6.89	7.04	6.75	6.65	7.91
Total	101.28	100.43	99.53	98.93	99.47	98.99	98.96	101.71	100.40	99.91	99.78	99.57	99.99	101.38
En	44.52	45.59	44.66	47.41	44.02	44.82	45.04	48.32	45.51	44.91	45.06	45.16	45.85	46.43
Wo	46.82	45.63	46.11	42.05	46.64	45.89	45.78	40.00	44.61	44.25	43.82	44.21	43.73	41.22
Fs	8.64	8.76	9.22	10.52	9.33	9.28	9.16	11.66	9.87	10.83	11.10	10.62	10.40	12.34
Mg#	83.74	83.87	82.89	81.83	82.50	82.84	83.09	80.55	82.18	80.57	80.23	80.95	81.50	79.00
Sample	SNS1	SNS1	SNS1	SNS1										
	31b	31b	31b	32	32	32	32	33	33	33	33	35	35	35
Lithology	FCPX	SPT	SPT	SPT	SPT	FCPX	FCPX	FCPX						
MgO	15.99	15.66	15.36	15.80	16.00	15.21	15.90	13.86	14.04	14.07	14.27	13.89	11.45	13.88
Al ₂ O ₃	1.80	2.12	1.35	1.08	0.76			9.18	8.96	9.31	9.19	7.30		7.52
SiO ₂	51.66	51.39	52.33	53.05	53.58	53.45	54.32	48.26	48.16	47.86	48.47	47.61	52.48	47.67
CaO	22.46	21.87	22.47	25.77	25.91	25.63	26.07	25.11	25.15	25.13	24.92	25.73	25.48	24.99
TiO ₂		0.34	0.31					0.62	0.63	0.66	0.66	0.58		0.36
Cr ₂ O ₃	0.46	0.57	0.42											
MnO	0.28					0.29	0.49			0.26	0.28		0.72	0.31
FeO	6.22	7.03	6.43	4.80	4.85	5.46	4.56	3.67	3.64	3.59	3.54	4.68	11.09	4.22
Total	98.87	98.97	98.67	100.49	101.09	100.04	101.35	100.70	100.58	100.88	101.33	99.80	101.21	98.95
En	44.88	44.32	43.73	42.67	42.83	41.44	42.73	40.79	41.09	41.19	41.75	39.66	31.81	40.56
Wo	45.32	44.50	45.99	50.04	49.87	50.20	50.38	53.14	52.92	52.90	52.42	52.83	50.89	52.51
Fs	9.79	11.16	10.27	7.27	7.28	8.34	6.87	6.06	5.97	5.89	5.81	7.50	17.29	6.92
Mg#	82.08	79.88	80.98	85.43	85.46	83.23	86.14	87.06	87.30	87.47	87.78	84.10	64.79	85.43

	SNS1	SNS1	SNS1	SNS1	SNS1	SNS1	SNS1
Sample	35	39	39	40	40	40	40
Lithology	FCPX	SPT	SPT	FCPX	FCPX	FCPX	FCPX
MgO	16.46	13.72	15.70	15.42	15.62	16.17	16.90
Al ₂ O ₃	1.99	8.88	2.60	2.93	1.24		0.42
SiO ₂	52.50	47.48	51.64	51.79	53.06	53.79	53.93
CaO	26.26	25.10	25.90	25.73	25.66	26.21	25.93
TiO ₂	0.47	0.48	0.38	0.41			
Cr ₂ O ₃							
MnO						0.27	0.35
FeO	3.58	3.58	4.20	3.90	5.02	4.00	3.59
Total	101.26	99.23	100.43	100.17	100.60	100.44	101.12
En	44.07	40.62	42.80	42.70	42.34	43.39	44.99
Wo	50.55	53.43	50.77	51.23	50.01	50.57	49.63
Fs	5.37	5.94	6.42	6.06	7.63	6.02	5.36
Mg#	89.12	87.23	86.95	87.57	84.72	87.81	89.35

Sandsloot, SNS1 sample suite, plagioclase

	SNS1	SNS1	SNS1	SNS1	SNS1	SNS1	SNS1	SNS1	SNS1	SNS1	SNS1	SNS1	SNS1	SNS1
Sample	2	2	2	2	2	6	6	6	6	6	10	10	10	10
Lithology	HWGN	HWGN	HWGN	HWGN	HWGN	HWGN	HWGN	HWGN	HWGN	HWGN	HWGN	HWGN	HWGN	HWGN
Na ₂ O	3	3	3	3	3	3	3	3	3	3	3	3	3	3
Al ₂ O ₃	4.12	3.50	3.83	2.95	3.88	3.54	3.94	3.23	2.97	4.45	3.68	4.13	3.96	3.87
SiO ₂	30.40	31.56	30.76	32.06	30.89	31.12	30.58	31.47	31.67	30.26	31.43	30.28	30.46	30.50
K ₂ O	51.48	50.18	51.25	48.82	50.68	49.94	51.03	49.42	48.75	51.80	50.94	51.44	51.78	51.48
CaO	0.16	0.17	0.22		0.18	0.20	0.21			0.20	0.14	0.30	0.30	0.24
Total	13.91	14.71	13.94	15.48	14.26	14.48	14.04	14.88	15.44	13.37	14.51	13.53	13.92	13.90
	100.07	100.12	100.00	99.30	99.89	99.28	99.79	99.00	98.83	100.09	100.69	99.67	100.41	100.00
An#	78.86	82.29	80.09	85.29	80.24	81.89	79.75	83.58	85.18	76.86	81.34	78.36	79.53	79.88

	SNS1	SNS1	SNS1	SNS1	SNS1	SNS1	SNS1	SNS1	SNS1	SNS1	SNS1	SNS1	SNS1	SNS1
Sample	11	11	11	11	11	11	11	11	12	12	12	12	12	17
Lithology	HWGN	HWGN	HWGN	HWGN	HWA	HWA	HWA	HWA	FPX	FPX	FPX	FPX	FPX	FPX
Na ₂ O	3	3	3	3	3	3	3	3	3	3	3	3	3	3
Al ₂ O ₃	4.61	4.78	4.45	3.93	3.49	3.45	3.47	3.28	3.20	3.66	5.09	3.31	3.64	4.34
SiO ₂	29.80	29.32	29.81	30.25	31.26	31.18	31.09	31.08	31.68	31.26	29.49	31.80	31.51	30.15
K ₂ O	52.41	52.62	52.65	51.43	50.60	50.00	50.73	50.27	49.56	50.39	53.28	49.15	50.24	51.97
CaO	0.33	0.27	0.27	0.20	0.19	0.23	0.20							0.16
Total	12.41	12.63	13.05	13.53	14.38	14.88	14.22	14.84	15.18	14.27	12.14	15.23	14.70	12.96
	99.56	99.61	100.23	99.34	99.92	99.75	99.72	99.47	99.62	99.58	99.99	99.49	100.10	99.58
An#	74.84	74.49	76.42	79.19	81.99	82.66	81.91	83.33	83.98	81.16	72.50	83.57	81.70	76.75

	SNS1	SNS1	SNS1	SNS1	SNS1	SNS1	SNS1	SNS1	SNS1	SNS1	SNS1	SNS1	SNS1	SNS1
Sample	17	17	17	17	22	22	22	22	22	25	25	25	25	25
Lithology	FPX	FPX	FPX	FPX	FPX	FPX	FPX	FPX	FPX	FPX	FPX	FPX	FPX	FPX
Na ₂ O	3	3	3	3	3	3	3	3	3	3	3	3	3	3
Al ₂ O ₃	3.73	4.82	3.42	4.04	4.31	4.82	4.25	4.51	4.40	4.80	4.87	4.87	4.85	4.98
SiO ₂	30.86	29.26	31.68	30.28	30.20	29.73	30.45	30.66	30.46	29.52	29.67	29.27	29.12	29.09
K ₂ O	50.28	52.33	49.40	50.87	50.64	52.68	52.29	52.79	52.22	53.01	53.28	53.60	53.32	53.35
CaO	0.18	0.19	0.19	0.31			0.22	0.24	0.18		0.27	0.30	0.35	0.28
Total	13.81	12.48	14.97	13.61	13.61	12.71	13.42	12.88	13.22	12.48	12.51	12.01	12.31	12.06
	98.85	99.08	99.65	99.12	98.76	100.17	100.65	101.02	100.31	100.07	100.64	100.09	99.88	99.87
An#	80.36	74.10	82.87	78.83	77.73	74.45	77.73	75.94	76.86	74.18	73.95	73.16	73.72	72.80

	SNS1	SNS1	SNS1	SNS1	SNS1	SNS1	SNS1	SNS1	SNS1
Sample	29	29	29	29	31a	31a	31a	31a	31a
Lithology	FPX	FPX	FPX	FPX	FPX	FPX	FPX	FPX	FPX
Na ₂ O	3	3	3	3	3	3	3	3	3
Al ₂ O ₃	5.04	5.28	4.70	4.26	2.89	5.72	4.52	4.28	4.51
SiO ₂	29.45	28.76	29.23	30.20	32.44	27.87	29.39	29.94	29.71
K ₂ O	53.17	54.39	53.18	51.26	48.57	55.50	52.22	51.91	51.84
CaO	0.37	0.31	0.29	0.25		0.58	0.38	0.18	0.29
Total	12.19	11.35	12.55	13.36	15.90	10.66	12.82	13.04	12.98
	100.22	100.08	99.95	99.33	99.81	100.33	99.32	99.35	99.34
An#									
	72.78	70.38	74.69	77.61	85.88	67.32	75.81	77.10	76.08

Sandsloot, SNS1 sample suite, olivine

	SNS1	SNS1	SNS1	SNS1	SNS1
Sample	33	33	33	33	33
Lithology	SPT	SPT	SPT	SPT	SPT
MgO	48.14	48.08	48.05	48.04	48.05
SiO ₂	39.82	40.11	40.04	40.03	40.21
CaO	0.18				0.23
MnO	1.06	1.15	1.06	1.05	1.03
FeO	11.58	11.71	11.52	11.74	11.8
Total	100.78	101.05	100.66	100.86	101.32
Mg#	88.11	87.98	88.14	87.94	87.89

Zwartfontein, ZSS1 sample suite, orthopyroxene

	ZSS1	ZSS1	ZSS1	ZSS1	ZSS1	ZSS1	ZSS1	ZSS1	ZSS1	ZSS1	ZSS1	ZSS1	ZSS1
Sample	2	2	2	2	2	18n	18n	18n	18n	18n	18m	18m	18m
Lithology	HWGN	HWGN	HWGN	HWGN	HWGN	HWGN	HWGN	HWGN	HWGN	HWGN	HWMN	HWMN	HWMN
MgO	24.12	24.36	24.83	24.04	24.31	23.24	25.64	23.04	23.32	22.52	23.07	22.90	22.76
Al ₂ O ₃	1.01	0.80	1.00	0.93	1.17	0.83	1.40	0.83	0.74	0.46	0.57	0.55	0.66
SiO ₂	52.57	52.53	53.04	52.41	52.56	52.23	53.35	52.40	53.13	52.06	52.59	52.50	52.89
CaO	2.20	1.14	1.52	0.98	1.44	1.87	0.97	3.40	0.89	1.64	1.06	1.09	0.99
TiO ₂		0.34								0.31	0.35		
Cr ₂ O ₃		0.27	0.32		0.26	0.29	0.37	0.25					
MnO	0.39		0.37	0.35	0.32	0.47	0.37	0.41	0.43	0.49	0.43	0.43	0.44
FeO	18.77	20.66	20.02	21.01	19.41	21.55	19.36	20.60	22.02	22.27	23.05	22.78	22.99
Total	99.06	100.10	101.11	99.72	99.47	100.47	101.47	100.93	100.54	99.74	101.11	100.25	100.73
En	66.57	66.24	66.82	65.80	67.08	63.36	68.92	62.20	64.21	62.22	62.75	62.80	62.57
Wo	4.37	2.23	2.94	1.93	2.86	3.67	1.87	6.60	1.76	3.26	2.07	2.15	1.96
Fs	29.07	31.53	30.24	32.27	30.06	32.97	29.20	31.21	34.03	34.53	35.18	35.05	35.47
Mg#	69.60	67.75	68.85	67.09	69.06	65.77	70.24	66.59	65.36	64.31	64.07	64.18	63.82

Appendix 4. Mineral chemistry

	ZSS1													
Sample	18m	18m	29	29	29	29	33a	33a	33a	33a	33a	41	41	41
Lithology	HWMN	HWMN	HWA	HWA	HWA	HWA	HWSA	HWSA	HWSA	HWSA	HWSA	FPX	FPX	FPX
MgO	1	1	1	1	1	1	1	1	1	1	1	1	1	1
Al ₂ O ₃	23.24	22.66	27.16	25.56	26.53	26.00	26.77	26.63	26.49	26.76	26.63	27.47	28.21	27.94
SiO ₂	0.68	1.19	1.00	0.70	0.97	0.58	0.81	0.81	1.24	0.81	0.60	0.95	0.90	0.78
CaO	52.39	52.36	53.54	53.28	53.70	53.49	53.22	52.89	52.87	53.19	53.71	54.42	54.22	53.74
TiO ₂	1.20	1.21	1.05	1.76	2.04	0.77	0.95	1.46	1.50	0.96	1.28	2.04	0.76	1.26
Cr ₂ O ₃	0.27	0.26	0.28			0.30	0.26							
MnO		0.28			0.35		0.36	0.54	0.35	0.35	0.25	0.35	0.41	0.38
FeO	0.36	0.43	0.40	0.51	0.39	0.39	0.40	0.37	0.30	0.26	0.31	0.35	0.43	0.28
Total	22.41	22.22	16.98	17.98	17.28	19.21	17.18	15.94	16.14	16.61	17.45	15.43	15.96	15.43
	100.56	100.60	100.42	99.79	101.26	100.75	99.96	98.63	98.90	98.95	100.23	101.01	100.90	99.81
En														
Wo	63.36	62.95	72.54	69.24	70.38	69.64	72.17	72.71	72.33	72.77	71.31	73.07	74.80	74.50
Fs	2.35	2.42	2.02	3.43	3.89	1.48	1.84	2.87	2.94	1.88	2.46	3.90	1.45	2.42
	34.29	34.64	25.45	27.33	25.73	28.87	25.99	24.42	24.73	25.35	26.22	23.03	23.75	23.09
Mg#														
	64.89	64.50	74.03	71.70	73.23	70.69	73.52	74.86	74.52	74.17	73.11	76.03	75.90	76.34
Sample	ZSS1													
	41	41	79	79	79	79	79	79	79	79	84	84	84	87
Lithology	FPX	FPX	FPX	FPX	FPX	IN	FPX							
MgO	1	1	1	1	1	1	1	1	1	1	1	1	1	1
Al ₂ O ₃	27.92	27.73	23.22	23.29	23.17	22.43	23.37	22.68	22.91	22.50	21.92	22.63	22.23	22.78
SiO ₂	0.92	1.10	0.32	0.41	0.55	0.49	0.47	0.45	0.83	0.55	0.79	0.78	0.66	
CaO	53.95	54.24	52.60	52.94	52.18	52.00	52.62	52.76	52.40	52.35	51.67	51.79	51.72	52.69
TiO ₂	1.03	1.40	0.90	0.76	0.77	1.32	0.81	1.31	0.98	1.26	1.05	0.87	1.17	1.12
Cr ₂ O ₃						0.31		0.38		0.36	0.24	0.26	0.21	
MnO	0.55	0.35												
FeO		0.39	0.51	0.38	0.59	0.52	0.64	0.50	0.52	0.49	0.45	0.52	0.45	0.49
Total	15.81	15.64	22.23	22.43	22.91	22.66	22.62	22.52	22.92	23.44	22.89	22.93	22.92	22.30
	100.19	100.84	99.78	100.21	100.17	99.74	100.06	100.61	100.19	101.23	98.78	99.79	99.48	100.04
En														
Wo	74.39	73.92	63.89	63.94	63.34	62.14	63.77	62.55	62.81	61.54	61.71	62.65	61.86	63.10
Fs	1.97	2.68	1.78	1.50	1.51	2.63	1.59	2.60	1.93	2.48	2.13	1.73	2.34	2.23
	23.64	23.40	34.33	34.56	35.15	35.23	34.64	34.85	35.26	35.98	36.16	35.62	35.79	34.67
Mg#														
	75.89	75.96	65.05	64.92	64.31	63.82	64.80	64.22	64.04	63.11	63.05	63.75	63.35	64.54
Sample	ZSS1													
	87	87	87	87	98	98	98	98	98					
Lithology	FPX													
MgO	1	1	1	1	1	1	1	1	1					
Al ₂ O ₃	22.84	22.89	23.39	22.98	24.20	23.16	23.44	23.27	23.35					
SiO ₂	0.81	0.88	0.70	0.39	0.73	1	0.74	0.84	0.77					
CaO	51.75	52.25	52.23	52.75	52.98	51.85	51.95	52.13	52.09					
TiO ₂	0.89	0.96	0.66	1.01	1.24	1.08	1.03	1.09	1.17					
Cr ₂ O ₃					0.32	0.3		0.35						
MnO														
FeO	0.49	0.48	0.39	0.62	0.54	0.47	0.45	0.33	0.4					
Total	22.98	22.42	22.06	22.78	21.18	21.01	21.41	21.32	21.51					
	99.75	99.89	99.43	100.52	101.19	98.87	99	99.33	99.29					
En														
Wo	62.79	63.30	64.53	62.98	65.45	64.83	64.76	64.61	64.39					
Fs	1.76	1.91	1.31	1.99	2.41	2.17	2.05	2.18	2.32					
	35.45	34.79	34.16	35.03	32.14	33.00	33.19	33.22	33.29					
Mg#														
	63.91	64.53	65.39	64.26	67.06	66.27	66.11	66.04	65.92					

Zwartfontein, ZSS1 sample suite, clinopyroxene

Sample	ZSS1 2	ZSS1 2	ZSS1 2	ZSS1 18n	ZSS1 18n	ZSS1 18n	ZSS1 18n	ZSS1 18n	ZSS1 18n	ZSS1 18m	ZSS1 18m	ZSS1 18m	ZSS1 18m	ZSS1 18m	ZSS1 29
Lithology	HWGN	HWGN	HWGN	HWGN	HWGN	HWGN	HWGN	HWGN	HWGN	HWMN	HWMN	HWMN	HWMN	HWMN	HWA
MgO	14.50	14.75	14.24	14.39	14.48	14.16	14.99	14.27	14.20	14.18	14.56	14.15	14.38	15.16	
Al ₂ O ₃	1.71	1.55	1.84	1.51	1.50	1.53	1.26	1.29	1.87	1.76	1.36	1.73	1.62	1.28	
SiO ₂	51.11	51.14	51.05	51.97	51.96	51.44	52.29	51.45	51.34	51.64	51.56	51.38	51.84	51.91	
CaO	22.05	21.96	22.53	22.84	22.47	22.86	22.58	22.23	22.01	22.66	22.90	22.55	22.08	22.82	
TiO ₂	0.63	0.54	0.71	0.69	0.60	0.58	0.52	0.58	0.59	0.49	0.50	0.56	0.71	0.50	
Cr ₂ O ₃						0.39				0.36	0.29	0.35			
MnO				0.39										0.30	
FeO	9.06	9.24	8.85	9.56	9.53	9.86	8.57	9.88	9.87	9.43	9.04	9.10	9.94	8.44	
Total	99.06	99.18	99.21	101.36	100.54	100.81	100.22	99.70	99.87	100.52	100.21	99.83	100.56	100.41	
En	40.91	41.28	40.22	39.77	40.24	39.19	41.60	39.86	39.92	39.64	40.33	39.89	40.13	41.75	
Wo	44.73	44.19	45.75	45.39	44.89	45.49	45.05	44.64	44.49	45.55	45.61	45.70	44.30	45.19	
Fs	14.34	14.51	14.02	14.83	14.86	15.31	13.34	15.48	15.57	14.79	14.05	14.39	15.56	13.04	
Mg#	74.04	73.99	74.14	72.84	73.03	71.90	75.71	72.02	71.94	72.82	74.16	73.48	72.05	76.20	
Sample	ZSS1 29	ZSS1 29	ZSS1 29	ZSS1 33a	ZSS1 33a	ZSS1 33a	ZSS1 41	ZSS1 41	ZSS1 41	ZSS1 41	ZSS1 68	ZSS1 68	ZSS1 68	ZSS1 68	
Lithology	HWA	HWA	HWA	HWSA	HWSA	HWSA	FPX	FPX	FPX	FPX	SPT	SPT	SPT	SPT	
MgO	15.12	15.61	15.49	15.27	15.36	15.66	15.69	15.82	15.99	16.92	15.02	15.16	14.89	15.72	
Al ₂ O ₃	1.09	1.68	1.28	1.91	1.72	1.17	1.63	1.87	1.45	1.42	4.85	4.77	4.93	3.81	
SiO ₂	52.65	52.11	52.32	51.68	51.61	52.11	52.47	52.58	52.44	52.41	49.57	49.49	49.39	50.47	
CaO	21.99	22.77	21.91	23.36	23.10	23.39	23.29	23.01	23.47	20.71	24.27	24.48	24.63	24.54	
TiO ₂	0.59		0.47	0.29		0.38	0.40	0.48	0.34	0.48	0.80	0.93	0.90	0.82	
Cr ₂ O ₃		0.53		0.53	0.46	0.69	0.75	0.55	0.69	0.62	0.59	0.76	0.81	0.67	
MnO													0.31		
FeO	9.00	7.57	9.07	7.02	6.48	5.86	6.00	6.52	5.78	7.19	4.58	3.98	4.37	4.12	
Total	100.43	100.26	100.54	100.06	98.72	99.26	100.23	100.82	100.16	99.75	99.68	99.56	100.23	100.15	
En	42.02	43.08	42.63	42.41	43.14	43.78	43.82	43.91	44.28	47.20	42.86	43.32	42.48	44.06	
Wo	43.94	45.18	43.35	46.64	46.64	47.02	46.77	45.92	46.73	41.54	49.79	50.29	50.52	49.45	
Fs	14.03	11.72	14.00	10.94	10.21	9.19	9.40	10.15	8.98	11.25	7.33	6.38	6.99	6.48	
Mg#	74.96	78.61	75.27	79.49	80.86	82.65	82.33	81.22	83.14	80.75	85.39	87.16	85.86	87.18	
Sample	ZSS1 68	ZSS1 76	ZSS1 76	ZSS1 76	ZSS1 84	ZSS1 84	ZSS1 84	ZSS1 84	ZSS1 87	ZSS1 87	ZSS1 98	ZSS1 98	ZSS1 98	ZSS1 98	
Lithology	SPT	PDT	PDT	PDT	IN	IN	IN	IN	FPX	FPX	FPX	FPX	FPX	FPX	
MgO	15.28	21.36	16.46	17.65	13.98	14.01	14.13	14.34	13.92	14.57	15.11	14.74	14.14	14.64	
Al ₂ O ₃	4.51	2.99	2.47		1.68	1.54	1.56	1.50	1.67	1.35	1.59	1.73	1.68	1.19	
SiO ₂	49.81	55.10	52.38	54.60	50.78	50.70	50.79	51.36	51.39	52.12	51.93	52.46	50.90	51.90	
CaO	24.55	13.46	25.44	26.05	21.60	20.88	22.23	22.54	21.65	22.02	22.14	22.25	21.94	22.33	
TiO ₂	0.67	0.29	0.61		0.67	0.66	0.56	0.67	0.47		0.63	0.55	0.54	0.31	
Cr ₂ O ₃	0.77				0.28	0.25									
MnO		0.37			0.28	0.24	0.32			0.29					
FeO	4.32	5.52	4.01	2.39	10.02	10.17	9.81	9.46	10.02	8.87	9.57	9.57	9.36	9.06	
Total	99.92	99.09	101.36	100.69	99.28	98.45	99.40	99.87	99.12	99.21	100.98	101.30	98.55	99.43	
En	43.21	62.57	44.48	46.79	39.79	40.34	39.67	39.99	39.64	41.18	41.51	40.82	40.20	40.91	
Wo	49.92	28.35	49.43	49.65	44.20	43.22	44.87	45.19	44.33	44.74	43.73	44.30	44.85	44.87	
Fs	6.85	9.07	6.08	3.55	16.00	16.43	15.45	14.80	16.01	14.06	14.75	14.87	14.93	14.21	
Mg#	86.31	87.33	87.97	92.94	71.32	71.06	71.96	72.98	71.23	74.54	73.78	73.30	72.91	74.22	

Zwartfontein, ZSS1 sample suite, clinopyroxene

Sample	ZSS1 2	ZSS1 2	ZSS1 2	ZSS1 2	ZSS1 18n	ZSS1 18n	ZSS1 18n	ZSS1 18n	ZSS1 18m	ZSS1 18m	ZSS1 18m	ZSS1 18m	ZSS1 29	ZSS1 29
Lithology	HWGN	HWGN	HWGN	HWGN	HWGN	HWGN	HWGN	HWGN	HWMN	HWMN	HWMN	HWMN	HWA	HWA
Na ₂ O	4.15	3.93	3.89	3.48	4.11	3.92	4.27	3.97	4.36	4.33	4.68	4.91	3.36	3.54
Al ₂ O ₃	29.95	30.20	30.38	30.68	30.00	30.29	29.88	30.70	29.89	29.99	29.73	29.26	31.20	30.78
SiO ₂	51.25	50.39	51.19	49.82	51.07	51.46	52.42	51.15	52.13	52.11	52.16	53.25	50.05	50.17
K ₂ O	0.21	0.27	0.21		0.21	0.21	0.22		0.28		0.25		0.18	0.23
CaO	13.75	14.05	14.21	14.71	13.42	13.93	13.40	14.15	13.25	13.21	13.02	12.52	15.02	14.58
Total	99.31	98.84	99.88	98.69	98.81	99.82	100.19	99.97	99.91	99.64	99.84	99.94	99.81	99.30
An#	78.55	79.80	80.15	82.37	78.30	79.71	77.62	79.75	77.06	77.13	75.46	73.81	83.17	81.99
Sample	ZSS1 29	ZSS1 29	ZSS1 33a	ZSS1 33a	ZSS1 33a	ZSS1 33a	ZSS1 41	ZSS1 41	ZSS1 41	ZSS1 79	ZSS1 79	ZSS1 79	ZSS1 79	ZSS1 79
Lithology	HWA	HWA	HWSA	HWSA	HWSA	HWSA	FPX	FPX	FPX	FPX	FPX	FPX	IN	IN
Na ₂ O	3.53	3.32	3.59	3.42	2.83	3.99	4.22	4.26	4.29	7.37	7.46	6.82	5.49	6.89
Al ₂ O ₃	31.21	31.35	30.67	31.20	31.94	29.82	30.15	30.26	30.57	25.85	26.03	27.13	28.00	26.13
SiO ₂	50.10	49.70	50.09	49.61	47.89	51.12	51.46	51.84	51.90	58.14	57.95	56.96	53.77	56.74
K ₂ O		0.21	0.16		0.16	0.23		0.19	0.19	0.19	0.18	0.30	0.20	0.37
CaO	14.77	14.84	14.50	15.05	16.03	13.75	13.61	13.48	13.89	8.30	8.20	9.49	11.23	8.82
Total	99.61	99.42	99.00	99.28	98.85	98.91	99.44	100.03	100.84	99.86	99.82	100.70	98.68	98.96
An#	82.22	83.17	81.70	82.95	86.23	79.20	78.09	77.76	78.16	55.45	54.85	60.60	69.33	58.59
Sample	ZSS1 79	ZSS1 79	ZSS1 84	ZSS1 84	ZSS1 84	ZSS1 98	ZSS1 98	ZSS1 98	ZSS1 98					
Lithology	IN	IN	IN	IN	IN	FPX	FPX	FPX	FPX					
Na ₂ O	5.92	5.81	4.39	4.60	4.64	4.70	4.64	4.49	4.25					
Al ₂ O ₃	27.94	27.66	29.05	29.03	29.00	30.23	30.04	30.30	30.15					
SiO ₂	54.94	54.98	52.07	52.06	51.86	52.97	52.64	52.46	51.85					
K ₂ O	0.26	0.56	0.28	0.26	0.27	0.35	0.30	0.36	0.23					
CaO	10.91	10.34	12.88	12.55	12.48	13.11	13.34	13.43	13.53					
Total	99.97	99.35	98.67	98.49	98.25	101.37	100.96	101.04	100.01					
An#	67.07	66.30	76.43	75.10	74.83	75.51	76.06	76.78	77.87					

Zwartfontein, ZSS1 sample suite, olivine

Sample	ZSS1 76	ZSS1 76	ZSS1 76	ZSS1 76	ZSS1 76	ZSS1 76
Lithology	PDT	PDT	PDT	PDT	PDT	PDT
MgO	45.14	44.69	44.26	44.30	44.49	44.49
SiO ₂	39.38	38.83	38.80	38.55	38.46	38.59
MnO	0.77	0.82	0.74	0.70	0.84	0.59
FeO	16.73	16.77	16.48	16.39	16.34	16.37
Total	102.02	101.11	100.28	99.94	100.15	100.04
Mg#	82.78	82.61	82.72	82.81	82.91	82.89

Overysel, OY335 sample suite, orthopyroxene

	OY335	OY335	OY335	OY335	OY335	OY335	OY335	OY335	OY335	OY335	OY335	OY335	OY335	OY335
Sample	166	166	166	166	166	169	169	169	169	169	175	175	175	175
Lithology	HWGN	HWGN	HWGN	HWGN	HWGN	HWGN	HWGN	HWGN	HWGN	HWGN	HWGN	HWGN	HWGN	HWGN
MgO	23.19	23.51	23.72	23.72	23.80	24.03	24.45	24.65	24.44	24.53	24.38	25.16	24.89	24.69
Al ₂ O ₃	0.66	0.97	0.63	0.83	0.75	0.91	0.84	0.94	0.80	0.65	1.39	1.30	0.77	0.97
SiO ₂	51.90	52.13	52.55	52.33	52.57	52.84	53.10	52.92	52.71	53.14	53.08	53.12	53.14	52.90
CaO	0.75	1.57	0.69	0.73	1.61	2.03	1.78	1.57	0.74	2.46	2.97	2.04	1.44	2.19
TiO ₂												0.34	0.26	
Cr ₂ O ₃		0.40					0.28		0.37		0.29	0.44	0.45	0.30
MnO	0.55	0.32	0.50	0.49	0.49	0.47	0.40	0.50	0.47	0.39	0.35	0.33		0.38
FeO	21.68	20.25	21.81	21.41	20.19	19.70	20.02	20.42	21.98	18.04	18.01	18.43	19.38	18.90
Total	98.72	99.16	99.90	99.51	99.40	100.25	100.59	101.35	101.14	99.50	100.61	101.17	99.88	100.33
En	64.60	65.30	65.07	65.42	65.59	65.76	66.14	66.20	65.51	67.35	66.57	68.06	67.63	66.96
Wo	1.50	3.14	1.36	1.45	3.19	3.99	3.46	3.03	1.43	4.86	5.83	3.97	2.81	4.27
Fs	33.89	31.56	33.57	33.14	31.22	30.25	30.39	30.77	33.06	27.79	27.60	27.98	29.55	28.77
Mg#	65.59	67.41	65.96	66.38	67.75	68.49	68.52	68.27	66.46	70.79	70.69	70.87	69.59	69.95
	OY335	OY335	OY335	OY335	OY335	OY335	OY335	OY335	OY335	OY335	OY335	OY335	OY335	OY335
Sample	176	176	176	176	176	182	182	182	182	182	193	193	193	
Lithology	FPX	FPX	FPX	FPX	FPX	FPX	FPX	FPX	FPX	FPX	AFPX	AFPX	AFPX	
MgO	26.01	29.10	26.60	30.22	29.07	28.22	28.57	27.76	26.56	28.59	27.58	27.93	26.94	
Al ₂ O ₃	1.26	1.34	1.46	1.29	1.40	1.63	1.21	1.28	1.08	1.36	1.33	1.23	1.87	
SiO ₂	52.94	53.69	53.25	54.41	53.92	54.01	54.36	53.96	53.66	53.93	54.01	54.07	53.17	
CaO	2.95	2.52	2.20	1.88	2.02	3.76	0.89	2.39	3.25	3.28	2.03	1.43	1.32	
TiO ₂						0.28								
Cr ₂ O ₃	0.42	0.43	0.47	0.45	0.56	0.35		0.36	0.41	0.49	0.30	0.28	0.59	
MnO	0.36	0.32	0.28	0.32		0.34	0.33		0.29			0.32	0.35	
FeO	14.99	11.59	15.85	11.00	12.22	11.92	15.01	13.70	14.67	12.21	14.15	14.79	16.26	
Total	98.95	98.99	100.10	99.57	99.19	100.50	100.36	99.45	99.92	99.87	99.40	100.04	100.51	
En	71.18	77.77	71.74	80.06	77.77	75.03	75.92	74.69	71.53	75.63	74.58	74.96	72.78	
Wo	5.80	4.84	4.27	3.58	3.89	7.19	1.70	4.62	6.29	6.24	3.95	2.76	2.56	
Fs	23.02	17.38	23.99	16.35	18.35	17.78	22.38	20.69	22.17	18.13	21.47	22.28	24.65	
Mg#	75.56	81.73	74.94	83.04	80.91	80.84	77.23	78.31	76.34	80.67	77.65	77.09	74.70	
	OY335	OY335	OY335	OY335	OY335	OY335	OY335	OY335	OY335	OY335	OY335	OY335	OY335	
Sample	193	193	201	201	201	201	213	213	213	213	230	230	230	
Lithology	AFPX	AFPX	FPX	FPX	FPX	FPX	SCSX	SCSX	SCSX	SCSX	AFPX	AFPX	AFPX	
MgO	29.30	28.20	29.54	29.09	28.46	26.91	30.88	29.84	30.22	30.29	28.12	27.17	28.46	
Al ₂ O ₃	1.48	0.84	1.71	1.46	1.48	1.05	0.95	1.01	1.07	0.98	0.82	1.27	1.35	
SiO ₂	54.02	54.40	54.51	54.16	54.13	53.64	54.90	54.97	55.01	54.83	53.50	53.05	53.63	
CaO	1.46	0.96	1.98	1.30	1.75	1.82	0.61	2.09	2.00	2.17	1.80	2.94	2.11	
TiO ₂							0.34	0.33	0.38	0.33				
Cr ₂ O ₃	0.43	0.31	0.72	0.59	0.47	0.32					0.32	0.33	0.65	
MnO		0.28				0.42			0.40	0.36		0.44	0.33	
FeO	13.32	15.00	11.73	13.23	13.33	15.73	12.02	12.14	11.69	11.71	14.06	14.28	13.60	
Total	100.01	99.98	100.18	99.84	99.62	99.88	99.70	100.39	100.77	100.66	98.62	99.47	99.81	
En	77.46	75.59	78.68	77.68	76.51	72.64	81.13	78.21	79.07	78.84	75.38	72.85	75.67	
Wo	2.78	1.85	3.79	2.50	3.38	3.53	1.15	3.94	3.76	4.06	3.47	5.67	4.03	
Fs	19.76	22.56	17.53	19.83	20.11	23.83	17.72	17.85	17.16	17.10	21.15	21.49	20.29	
Mg#	79.67	77.01	81.78	79.67	79.19	75.30	82.07	81.41	82.16	82.17	78.09	77.22	78.85	

Appendix 4. Mineral chemistry

	OY335													
Sample	241	241	241	241	241	253	253	253	253	262	262	262	262	292
Lithology	FPX	FPX	CHR	CHR	CHR	IN	IN	IN	IN	FPX	FPX	FPX	FPX	FPX
MgO	28.19	27.77	30.79	31.11	31.47	26.21	26.36	25.82	25.88	27.25	27.92	27.36	29.24	29.91
Al ₂ O ₃	1.66	1.06	1.24	1.2	1.02	0.93		0.62	1.01	0.49		0.97	1.28	1.24
SiO ₂	54.18	53.74	55.24	54.5	55.18	53.34	53.59	53.56	53.65	54.15	54.55	53.31	54.11	54.81
CaO	2.26	2.06	1.2	0.66	0.57	0.96	1.62	2.73	2.41	1.61	1.48	0.90	1.47	0.58
TiO ₂								0.31		0.31				
Cr ₂ O ₃	0.47	0.3	0.57	0.54	0.53			0.26		0.25	0.29	0.29	0.39	
MnO		0.5				0.52	0.63	0.51	0.43	0.35	0.32	0.30	0.40	0.44
FeO	13.54	14.82	11.48	10.83	11.83	17.95	17.81	16.36	16.29	16.69	16.38	16.17	13.36	13.34
Total	100.3	100.2	100.5	98.84	100.6	99.90	100.00	100.17	99.67	101.10	100.94	99.31	100.25	100.33
En	75.35	73.92	80.82	82.60	81.70	70.89	70.26	69.85	70.41	72.141	73.135	73.784	77.367	79.100
Wo	4.34	3.94	2.26	1.26	1.06	1.87	3.10	5.31	4.71	3.064	2.787	1.745	2.796	1.103
Fs	20.31	22.14	16.91	16.14	17.23	27.24	26.64	24.84	24.87	24.795	24.078	24.471	19.837	19.797
Mg#	78.77	76.95	82.70	83.66	82.58	72.24	72.51	73.77	73.90	74.42	75.23	75.09	79.59	79.98
	OY335													
Sample	292	292	292	292	292	303	303	303	303	316	316	316	316	
Lithology	FPX	FPX	FPX	FPX	FPX	QFPX	QFPX	QFPX	QFPX	GN	GN	GN	GN	
MgO	30.31	30.35	30.06	30.34	29.59	29.51	30.20	28.99	30.05	24.42	25.06	24.34	24.19	
Al ₂ O ₃			0.91		1.09	1.79	1.79	1.57	1.50	0.57	0.55	0.46	0.63	
SiO ₂	55.53	55.00	54.88	55.36	55.32	53.68	54.21	53.80	54.61	53.01	53.87	53.18	53.48	
CaO	0.95	0.79	0.58	0.42	2.62	1.66	0.64	2.01	1.97	0.61	0.43	0.55	0.55	
TiO ₂													0.35	
Cr ₂ O ₃			0.33		0.58	0.79	0.61	0.66	0.56					
MnO	0.43	0.36	0.32	0.37		0.27	0.29	0.35	0.76	0.66	0.82	0.86		
FeO	13.33	12.83	13.32	13.51	12.00	12.44	12.53	12.24	11.89	21.38	20.71	21.26	20.91	
Total	100.54	99.32	100.40	100.00	101.20	99.87	100.24	99.54	100.93	100.75	101.29	100.62	100.98	
En	78.782	79.622	79.206	79.376	77.445	78.308	80.124	77.713	78.791	66.257	67.746	66.383	66.603	
Wo	1.775	1.490	1.099	0.790	4.930	3.167	1.221	3.874	3.714	1.190	0.836	1.078	1.089	
Fs	19.443	18.888	19.695	19.834	17.625	18.525	18.655	18.413	17.495	32.553	31.418	32.538	32.308	
Mg#	80.21	80.83	80.09	80.01	81.46	80.87	81.11	80.85	81.83	67.06	68.32	67.11	67.34	

Overysel, OY335 sample suite, clinopyroxene

	OY335	OY335	OY335	OY335	OY335	OY335	OY335	OY335						
Sample	166	166	166	166	166	166	169	169	169	169	175	175	175	175
Lithology	HWGN	HWGN	HWGN	HWGN	HWGN	HWGN	HWGN	HWGN						
MgO	14.71	15.01	14.76	14.94	14.61	14.78	14.92	15.77	14.58	14.64	15.60	15.42	16.24	15.47
Al ₂ O ₃	1.49	1.12	1.73	1.23	1.83	1.09	1.54	0.87	1.49	1.20	1.15	1.13		1.83
SiO ₂	51.46	51.92	51.20	51.86	51.15	51.94	51.91	53.44	52.57	52.45	51.77	52.78	53.22	52.24
CaO	22.44	22.72	22.50	22.39	23.01	21.95	22.71	23.69	22.72	23.04	23.33	23.64	23.21	22.72
TiO ₂	0.56	0.39	0.62	0.45	0.60	0.33	0.58		0.42	0.41	0.45	0.43	0.31	0.41
Cr ₂ O ₃	0.32			0.33	0.32		0.38	0.38	0.60	0.28	0.36			0.57
MnO	0.27									0.26				
FeO	8.49	8.41	8.29	8.78	7.65	8.60	8.77	7.21	9.14	8.50	6.78	6.72	6.91	6.94
Total	99.75	99.57	99.11	99.97	99.17	98.69	100.80	101.35	101.53	100.77	100.02	100.82	99.88	100.18
En	41.31	41.62	41.47	41.54	41.22	41.77	41.25	42.80	40.45	40.69	43.12	42.61	44.12	43.33
Wo	45.31	45.29	45.45	44.76	46.67	44.60	45.14	46.22	45.32	46.05	46.36	46.97	45.34	45.76
Fs	13.38	13.09	13.07	13.70	12.11	13.64	13.61	10.98	14.23	13.26	10.52	10.42	10.54	10.91
Mg#	75.54	76.08	76.04	75.20	77.29	75.38	75.20	79.58	73.98	75.43	80.39	80.35	80.73	79.89

Appendix 4. Mineral chemistry

	OY335	OY335	OY335	OY335	OY335	OY335	OY335	OY335	OY335	OY335	OY333	OY334	OY335	OY335
Sample	175	175	176	176	182	193	193	193	193	193	201	201	213	213
Lithology	HWGN	HWGN	FPX	FPX	FPX	FPX	FPX	FPX	FPX	FPX	FPX	FPX	SCSX	SCSX
MgO	16.12	15.30	15.83	16.12	19.61	15.66	15.59	17.13	16.26	15.77	19.55	16.91	17.19	16.72
Al ₂ O ₃		1.89	1.95		1.75	1.34	2.03	1.51	0.96	1.89	1.58	1.81	0.45	2.21
SiO ₂	52.91	51.99	52	53.27	52.4	51.92	51.79	51.89	53.01	51.68	53.73	52.68	54.16	51.82
CaO	22.88	22.98	23.28	24.02	15.7	22.99	22.71	19.97	23.44	22.97	14.77	20.17	25.46	22.91
TiO ₂		0.46	0.43		0.28	0.33	0.39	0.38	0.32			0.32		0.73
Cr ₂ O ₃		0.39	0.62	0.29	0.73	0.56	0.68	0.62	0.66	0.73	0.53	0.82		
MnO							0.28	0.28						
FeO	7.16	7.05	5.99	6.48	9.61	5.7	6.32	7.47	5.78	5.63	9.97	6.76	3.08	5.04
Total	99.06	100.65	100.1	100.2	100.1	99.27	99.79	99.25	100.4	98.67	100.14	99.48	101	100.1
En	44.06	42.76	44.06	43.54	54.04	44.25	43.96	48.01	44.72	44.49	54.66	48.03	46.18	46.42
Wo	44.96	46.18	46.59	46.64	31.10	46.71	46.04	40.24	46.35	46.59	29.69	41.19	49.18	45.73
Fs	10.98	11.06	9.36	9.82	14.86	9.04	10.00	11.75	8.92	8.91	15.64	10.78	4.64	7.85
Mg#	80.05	79.45	82.48	81.59	78.43	83.04	81.47	80.34	83.37	83.31	77.75	81.68	90.86	85.53
	OY335	OY335	OY335	OY335	OY335	OY335	OY335	OY335	OY335	OY335	OY335	OY335	OY335	OY335
Sample	213	213	218	218	218	218	218	230	230	241	241	241	241	241
Lithology	SCSX	SCSX	SCSX	SCSX	SCSX	SCSX	SCSX	AFPX	AFPX	FPX	FPX	FPX	FPX	FPX
MgO	16.97	16.93	16.09	15.82	13.45	14.66	16.38	16.10	15.87	15.40	17.37	16.21	15.81	15.98
Al ₂ O ₃	2.19	1.73	6.03	6.14	10.2	9.21	3.62	0.41	2.29	1.91	2.10	1.20	1.59	2.37
SiO ₂	52.24	53.02	49.21	49.12	46.37	46.64	49.91	53.50	51.98	51.59	52.82	53.25	52.09	51.56
CaO	22.2	23.25	25.69	25.39	25.44	24.84	25.9	24.16	21.91	23.08	19.18	23.83	22.61	20.49
TiO ₂	0.5	0.45	0.8	0.94	0.88	1.1	1.27		0.45	0.75	0.39		0.64	0.37
Cr ₂ O ₃								0.47	0.50	0.62	0.59	0.44	0.57	1.20
MnO								0.28						
FeO	5.4	4.59	2.21	2.62	2.49	2.55	2.57	5.83	7.11	6.52	8.05	5.04	6.60	7.01
Total	99.5	100.7	100.9	100.6	99.43	98.99	100.3	100.77	100.11	100.57	100.49	100.61	99.91	99.77
En	47.19	46.74	44.94	44.51	40.59	43.18	44.95	43.82	44.56	43.19	48.69	44.81	44.20	46.12
Wo	44.38	46.15	51.59	51.36	55.20	52.60	51.10	47.28	44.23	46.54	38.65	47.37	45.45	42.52
Fs	8.43	7.11	3.46	4.14	4.22	4.21	3.96	8.90	11.20	10.26	12.66	7.82	10.35	11.35
Mg#	84.85	86.79	92.84	91.50	90.59	91.11	91.91	83.11	79.91	80.80	79.36	85.14	81.02	80.25
	OY335	OY335	OY335	OY335	OY335	OY335	OY335	OY335	OY335	OY335	OY335	OY335	OY335	OY335
Sample	241	253	253	253	262	262	262	262	262	269	269	269	275	292
Lithology	FPX	IN	IN	IN	FPX	FPX	FPX	FPX	FPX	CSX	CSX	CSX	FPX	FPX
MgO	15.79	15.13	15.35	15.58	17.14	16.02	16.32	15.91	16.01	18.66	18.53	18.32	15.72	17.00
Al ₂ O ₃	2.10	0.99	1.43	1.01	1.87	0.92	0.63	0.71	0.79				0.37	0.80
SiO ₂	51.59	52.06	51.94	52.49	51.68	53.03	52.85	52.72	52.42	54.42	54.78	54.45	52.53	54.09
CaO	21.24	22.76	21.68	22.49	19.51	22.45	23.50	23.12	22.27	26.38	26.62	26.58	24.20	23.77
TiO ₂	0.59	0.45	0.55	0.47	0.61	0.28	0.34		0.31					0.30
Cr ₂ O ₃	0.74	0.40	0.28	0.45	0.43	0.49	0.34	0.49	0.33					0.60
MnO									0.29				0.32	
FeO	7.14	7.19	7.79	7.36	7.64	6.85	5.81	5.89	6.18	0.39	0.46	0.53	5.54	4.59
Total	99.18	99.67	99.66	100.47	98.88	100.69	99.79	98.84	98.61	99.84	100.38	99.88	98.68	101.16
En	45.03	42.59	43.47	43.42	48.34	44.49	44.74	44.39	45.11	49.31	48.86	48.56	43.39	46.36
Wo	43.55	46.06	44.15	45.07	39.56	44.83	46.32	46.38	45.12	50.12	50.46	50.65	48.03	46.61
Fs	11.43	11.36	12.38	11.51	12.09	10.68	8.94	9.22	9.77	0.58	0.68	0.79	8.58	7.02
Mg#	79.76	78.95	77.83	79.05	79.99	80.65	83.35	82.80	82.20	98.84	98.63	98.40	83.49	86.84

Overysel, OY335 sample suite, olivine

	OY335	OY335	OY335	OY335	OY335		OY335	OY335	OY335	OY335	OY335
Sample	292	303	303	303	303	Sample	213	213	213	213	213
Lithology	FPX	QFPX	QFPX	QFPX	QFPX	Lithology	PDT	PDT	PDT	PDT	PDT
MgO	16.94	15.66	15.83	15.95	15.69	MgO	42.57	42.82	42.46	42.09	42.05
Al ₂ O ₃	0.56	2.50	2.84	2.96	3.00	SiO ₂	38.15	38.11	38.17	38.37	37.93
SiO ₂	53.40	51.41	52.33	52.13	52.09	MnO	0.28	0.35	0.26		0.33
CaO	23.44	22.73	23.11	23.31	23.61	FeO	18.98	18.79	18.91	19.07	19.34
TiO ₂			0.37		0.30	Total	99.99	100.1	99.81	99.53	99.66
Cr ₂ O ₃	0.65	1.08	1.25	1.11	1.30						
MnO						Mg#	79.99	80.24	80.00	79.73	79.49
FeO	4.71	5.04	4.94	4.85	4.80						
Total	99.70	98.99	101.36	100.99	100.79						
En	46.49	44.96	44.95	45.02	44.37						
Wo	46.25	46.92	47.18	47.30	48.01						
Fs	7.25	8.12	7.87	7.68	7.62						
Mg#	86.50	84.70	85.10	85.42	85.35						

Overysel, OY387 sample suite, plagioclase

	OY335	OY335	OY335	OY335	OY335	OY335	OY335	OY335	OY335	OY335	OY335	OY335	OY335	OY335
Sample	166	166	166	169	169	169	169	176	176	176	176	182	182	182
Lithology	HWGN	HWGN	HWGN	HWGN	HWGN	HWGN	HWGN	FPX						
Na ₂ O	4.59	5.37	4.79	3.97	3.81	3.54	4.34	3.15	3.67	3.68	4.08	3.53	3.11	3.4
Al ₂ O ₃	29.54	28.45	29.1	31.01	30.96	31.30	30.15	31.52	30.72	30.41	30.29	31.58	31.66	31.76
SiO ₂	51.42	53.61	52.5	50.70	50.85	50.34	51.82	48.61	50.55	50.26	50.84	50.28	49.48	49.54
K ₂ O	0.16	0.18	0.24	0.19	0.20		0.20		0.25	0.32	0.36	0.15		
CoO	12.63	11.58	12.28	14.39	14.63	14.73	13.62	15.47	14.29	14.19	13.72	14.85	15.68	15.66
Total	98.75	99.19	99.25	100.26	100.46	99.92	100.13	98.75	99.48	99.15	99.57	100.4	99.94	100.4
An#	75.25	70.44	73.91	80.02	80.93	82.14	77.62	84.44	81.14	80.99	78.80	82.30	84.78	83.58

	OY335	OY335	OY335	OY335	OY335	OY335								
Sample	193	193	193	201	201	201	230	230	241	241	241	253	253	253
Lithology	AFPX	AFPX	AFPX	FPX	FPX	FPX	FPX	FPX	FPX	FPX	FPX	IN	IN	IN
Na ₂ O	4.15	4.14	4.84	4.78	4.21	4.57	4.67	4.75	5.13	4.50	3.64	5.96	4.67	4.83
Al ₂ O ₃	29.87	29.68	28.61	29.60	30.44	29.69	29	29.67	29.03	29.87	31.52	27.75	29.34	28.69
SiO ₂	51.22	51.31	52.78	52.19	51.24	52.08	52.51	51.91	53.77	52.83	50.41	54.89	52.24	53
K ₂ O	0.2	0.25	0.41	0.78			0.35	0.19	0.27	0.18		0.35	0.17	0.22
CoO	13.36	13.46	11.95	11.70	13.69	12.82	12.18	12.63	11.84	13.11	14.75	10.48	12.63	11.96
Total	98.81	99.18	98.59	99.04	99.59	99.16	98.72	99.15	100.05	100.49	100.32	99.43	99.06	98.7
An#	78.06	78.23	73.18	73.01	78.23	75.61	74.24	74.61	71.84	76.30	81.75	66.03	74.93	73.24

	OY335	OY335	OY335	OY335	OY335	OY335	OY335	OY335	OY335	OY335	OY335	OY335	OY335	OY335
Sample	253	262	262	262	262	292	292	292	303	303	303	316	316	316
Lithology	IN	FPX	FPX	FPX	FPX	FPX	FPX	FPX	QFPX	QFPX	QFPX	GN	GN	GN
Na ₂ O	7.78	4.83	5.78	4.62	4.85	7.83	7.22	6.82	3.40	3.53	2.90	8.29	8.43	8.34
Al ₂ O ₃	25.23	30.14	28.12	29.73	29.36	25.00	25.24	26.15	32.17	31.73	32.56	24.20	24.07	23.97
SiO ₂	58.28	52.85	54.31	51.85	52.71	59.71	58.43	56.85	49.32	50.04	48.55	61.46	60.79	60.88
K ₂ O	0.32			0.24	0.17	0.55	0.68	0.48				0.62	0.47	0.59
CoO	7.29	12.67	11.00	12.95	12.24	7.31	7.59	8.61	15.23	15.02	15.63	5.96	5.85	6.00
Total	98.91	100.50	99.20	99.39	99.33	100.72	99.16	98.91	100.12	100.31	99.91	100.53	99.61	99.77
An#	50.87	74.35	67.78	75.60	73.61	50.78	53.74	58.25	83.20	82.46	85.63	44.28	43.41	44.29

Overysel, OY387 sample suite, orthopyroxene

	OY387	OY387	OY387	OY387	OY387	OY387	OY387	OY387	OY387	OY387	OY387	OY387	OY387	OY387
Sample	233	233	233	233	233	233	233	233	239	239	239	239	245	245
Lithology	HWGN	HWGN	HWGN	HWGN	HWMN	HWMN	HWMN	HWMN	FPX	FPX	FPX	FPX	FPX	FPX
MgO	23.03	23.54	21.89	21.89	20.73	20.61	20.22	20.60	29.15	28.72	29.84	29.31	29.28	29.37
Al ₂ O ₃	1.36	0.89	0.44	0.50	0.49	0.63	0.60	0.67	0.89	0.91	0.61	1.15	1.22	1.49
SiO ₂	51.49	52.30	51.68	51.66	51.24	51.03	50.71	50.67	55.50	54.85	54.92	54.52	54.58	54.44
CaO	0.85	0.83	1.05	1.11	1.53	1.10	0.91	1.16	2.53	2.25	0.67	0.83	1.88	1.90
TiO ₂		0.34	0.28		0.29		0.28	0.36						
Cr ₂ O ₃	0.39								0.43	0.40	0.38	0.37	0.62	0.60
MnO	0.44	0.33	0.44	0.48	0.56	0.33	0.50	0.45			0.40	0.37	0.29	
FeO	21.55	21.88	23.63	23.31	24.80	25.42	25.34	25.02	13.01	13.36	13.96	14.18	12.61	12.22
Total	99.13	100.41	99.72	98.95	99.64	99.12	98.57	98.93	101.51	100.49	100.78	100.72	100.47	100.02
En	64.45	64.64	60.97	61.20	57.99	57.79	57.62	58.07	76.17	75.91	78.21	77.41	77.65	78.13
Wo	1.71	1.64	2.10	2.23	3.08	2.22	1.86	2.35	4.75	4.28	1.26	1.58	3.58	3.63
Fs	33.84	33.72	36.93	36.57	38.93	40.00	40.52	39.58	19.08	19.82	20.53	21.02	18.77	18.24
Mg#	65.57	65.72	62.28	62.59	59.83	59.10	58.71	59.47	79.97	79.30	79.21	78.65	80.54	81.07
	OY387	OY387	OY387	OY387	OY387	OY387	OY387	OY387	OY387	OY387	OY387	OY387	OY387	OY387
Sample	245	246	246	246	246	252	252	252	252	252	258	258	258	258
Lithology	FPX	FPX	FPX	FPX	FPX	FPX	FPX	FPX	FPX	FPX	FPX	FPX	FPX	FPX
MgO	29.79	27.77	29.52	28.28	28.10	28.83	27.88	28.82	28.64	28.39	28.97	29.56	29.14	29.43
Al ₂ O ₃	1.64	1.37	1.75	1.65	1.50	0.75	0.87	0.94	0.83	0.77	1.52	0.96	1.43	1.32
SiO ₂	54.68	53.54	53.72	53.32	53.52	53.77	53.65	53.85	54.15	53.97	53.65	53.99	53.39	54.29
CaO	2.09	3.11	0.57	1.95	2.64	0.7	2.11	0.95	0.73	0.86	0.57	0.73	1.55	1.11
TiO ₂			0.25											
Cr ₂ O ₃	0.66	0.56	0.52	0.56	0.61	0.43	0.39	0.5	0.47	0.39	0.58	0.34	0.55	0.56
MnO			0.30		0.31	0.38	0.35	0.32	0.39	0.26	0.32	0.32	0.3	0.39
FeO	11.87	12.28	13.20	12.82	12.05	14.2	13.6	13.95	14.74	14.41	13.61	13.21	12.72	13.4
Total	100.73	98.62	99.83	98.59	98.73	99.05	98.86	99.33	99.95	99.05	99.23	99.11	99.07	100.5
En	78.49	75.26	79.06	76.69	76.44	77.29	75.29	77.20	76.50	76.53	78.26	78.83	77.93	77.96
Wo	3.96	6.06	1.10	3.80	5.16	1.35	4.10	1.83	1.40	1.67	1.11	1.40	2.98	2.11
Fs	17.55	18.68	19.84	19.51	18.40	21.36	20.61	20.97	22.10	21.80	20.63	19.77	19.09	19.92
Mg#	81.73	80.12	79.94	79.72	80.60	78.35	78.51	78.64	77.59	77.83	79.14	79.95	80.32	79.65
	OY387	OY389	OY390	OY391	OY387									
Sample	272	272	272	272	278	278	278	278	278	278	311	311	311	311
Lithology	QFPX	QFPX	QFPX	QFPX	GN									
MgO	26.94	27.00	27.60	25.31	28.71	28.28	28.11	27.91	27.54	27.54	27.16	27.07	24.76	25.74
Al ₂ O ₃	0.67	0.94	0.99	0.86	0.48	0.66	0.65	0.69	0.50	0.63	1.09	1.23	0.97	0.87
SiO ₂	54.46	53.95	54.21	53.60	54.82	55.04	54.62	54.25	54.66	54.64	53.68	53.68	53.09	53.58
CaO	2.31	2.17	1.16	4.82	0.60	0.72	0.66	0.73	0.80	0.77	0.35	0.39	0.33	0.42
TiO ₂												0.32		
Cr ₂ O ₃	0.42	0.40	0.50	0.45	0.30		0.28							
MnO	0.34	0.33	0.37	0.41	0.39	0.39	0.30	0.35	0.49	0.34	0.58	0.48	0.86	0.68
FeO	15.28	15.34	16.14	14.54	15.88	16.20	16.30	16.76	17.25	17.11	17.55	17.81	20.16	19.04
Total	100.42	100.13	100.98	99.99	101.18	101.28	100.92	100.70	101.24	101.03	100.41	100.98	100.17	100.32
En	72.47	72.64	73.62	68.53	75.45	74.64	74.50	73.76	72.87	73.06	72.89	72.49	68.19	70.09
Wo	4.47	4.20	2.22	9.38	1.13	1.37	1.26	1.39	1.52	1.47	0.68	0.75	0.65	0.82
Fs	23.07	23.16	24.16	22.09	23.42	23.99	24.24	24.86	25.61	25.47	26.43	26.76	31.16	29.09
Mg#	75.86	75.82	75.29	75.62	76.31	75.67	75.45	74.80	73.99	74.15	73.39	73.03	68.64	70.67

Appendix 4. Mineral chemistry

	OY387	OY387	OY387	OY387	OY387	OY387	OY387	OY387	OY387	OY387	OY387	OY387	OY387	OY387
Sample	364	364	364	364	378	378	378	384	384	384	384	415	415	415
Lithology	AGN	AGN	AGN	AGN	GN	GN	GN	LZP	LZP	LZP	LZP	GN	GN	GN
MgO	16.91	17.61	17.64	17.97	22.39	22.28	21.48	34.65	35.11	34.59	34.85	27.91	27.64	28.82
Al ₂ O ₃	0.46		0.42	0.53	0.77	0.87	0.76	0.75	0.77	0.68	0.55	1.14	1.15	1.34
SiO ₂	50.27	50.82	50.33	50.24	52.19	51.63	51.61	56.84	56.92	56.96	56.82	54.11	53.95	54.32
CaO	1.22	0.90	1.22	1.08	0.36	0.40	0.39	0.50	0.28	0.35	0.40	0.00	0.21	0.18
TiO ₂	0.28			0.28										
Cr ₂ O ₃								0.28	0.54	0.42	0.27			
MnO	0.57	0.75	0.65	0.48	0.60	0.80	0.76				0.26	0.65	0.66	0.70
FeO	30.00	30.14	29.25	29.17	22.80	23.91	24.67	8.07	7.81	8.02	7.83	16.15	16.90	15.36
Total	99.71	100.22	99.52	99.75	99.11	99.90	99.66	101.10	101.41	101.02	100.98	99.96	100.52	100.73
En	48.84	50.07	50.50	51.17	63.17	61.91	60.33	87.64	88.45	87.92	88.16	75.49	74.15	76.71
Wo	2.53	1.84	2.51	2.21	0.73	0.80	0.79	0.91	0.51	0.64	0.73	0.00	0.41	0.34
Fs	48.63	48.09	46.99	46.62	36.10	37.29	38.88	11.45	11.04	11.44	11.12	24.51	25.44	22.94
Mg#	50.11	51.01	51.80	52.33	63.64	62.41	60.81	88.44	88.90	88.49	88.80	75.49	74.45	76.98

Overysel, OY387 sample suite, clinopyroxene

	OY387	OY387	OY387	OY387	OY387	OY387	OY387	OY387						
Sample	233	233	233	233	233	233	239	239	239	239	246	246	258	258
Lithology	HWGN	HWGN	HWGN	HWMN	HWMN	HWMN	FPX	FPX	FPX	FPX	FPX	FPX	FPX	FPX
MgO	13.79	14.37	14.34	13.36	13.30	14.07	17.60	17.43	17.99	16.62	16.00	16.62	20.85	19.35
Al ₂ O ₃	1.35	1.46	1.72	1.45	1.34	0.93	1.58	1.18	1.27	1.78	2.03	1.34	2.39	2.54
SiO ₂	51.18	51.34	50.88	50.88	51.30	51.87	53.63	53.86	53.61	53.03	51.54	52.12	52.54	51.84
CaO	22.21	22.36	21.36	22.08	22.03	21.94	21.79	21.82	20.35	22.91	23.01	22.36	15.14	17.81
TiO ₂	0.53		0.58	0.39	0.41	0.30	0.29	0.40	0.43	0.32	0.37			
Cr ₂ O ₃				0.37	0.35	0.29	0.60	0.83	0.67	0.80	1.32	0.83	0.90	1.04
MnO	0.27												0.36	
FeO	9.85	9.33	10.43	10.71	9.92	10.55	5.39	5.49	6.68	5.37	4.64	5.29	8.52	7.42
Total	99.17	98.86	99.31	99.24	98.65	99.96	100.89	101.02	100.99	100.83	98.92	98.57	100.71	100.00
En	39.08	40.27	40.33	37.90	38.32	39.34	48.49	48.15	49.46	46.03	45.52	46.60	57.09	53.27
Wo	45.25	45.05	43.19	45.04	45.63	44.10	43.16	43.33	40.22	45.62	47.06	45.07	29.80	35.25
Fs	6.47	6.09	6.85	7.07	6.58	6.88	3.36	3.43	4.19	3.36	2.95	3.37	5.41	4.71
Mg#	71.39	73.29	71.01	68.97	70.49	70.38	85.33	84.98	82.76	84.65	86.00	84.85	81.35	82.29

	OY387	OY387	OY387	OY387	OY387	OY387	OY387	OY387
Sample	258	258	272	272	364	364	364	364
Lithology	FPX	FPX	GN	GN	AGN	AGN	AGN	AGN
MgO	15.36	16.15	16.00	15.86	12.32	12.36	12.45	11.81
Al ₂ O ₃	2.54	2.61	1.38	1.26	1.34	1.06	1.14	1.34
SiO ₂	51.15	51.41	52.85	52.78	50.79	51.88	50.76	50.61
CaO	22.94	21.43	23.04	22.86	21.22	22.20	21.53	22.39
TiO ₂	0.34	0.19		0.32	0.38	0.28	0.42	0.37
Cr ₂ O ₃	1.07	0.96	0.72	0.48				
MnO					0.37	0.30	0.34	
FeO	5.20	5.50	6.27	6.26	13.99	12.24	13.14	13.17
Total	99.60	98.50	100.61	100.15	100.41	100.32	99.78	99.68
En	44.17	46.61	44.34	44.29	34.77	35.12	35.26	33.45
Wo	47.43	44.47	45.90	45.89	43.06	45.35	43.84	45.60
Fs	3.32	3.55	3.95	3.97	9.35	8.11	8.78	8.81
Mg#	84.04	83.96	81.97	81.87	61.08	64.28	62.80	61.51

Overysel, OY387 sample suite, plagioclase

	OY387													
Sample	233	233	233	233	233	233	233	239	239	246	252	258	258	258
Lithology	HWGN	HWGN	HWMN	HWMN	HWMN	HWMN	HWMN	FPX						
Na ₂ O	4.60	3.73	2.90	4.81	4.99	4.42	4.54	6.14	6.21	3.49	3.54	3.39	3.12	2.34
Al ₂ O ₃	28.85	30.56	31.47	28.55	29.04	29.56	28.94	28.22	28.4	30.72	30.85	31.17	31.97	32.73
SiO ₂	52.17	49.52	48.50	52.62	53.00	51.99	52.22	56.11	55.82	49.64	49.56	49.67	48.91	46.89
K ₂ O	0.23			0.31	0.20	0.25	0.22	0.31	0.27	0.15				
CaO	12.32	14.50	15.96	12.10	12.31	12.71	12.47	10.68	10.52	14.62	14.8	14.77	15.66	16.96
Total	98.44	98.61	99.27	98.73	99.82	99.21	98.77	101.5	101.2	98.63	98.76	99	99.97	98.92
An#	74.75	81.12	85.88	73.55	73.16	76.07	75.22	65.78	65.18	82.24	82.21	82.80	84.73	88.90
	OY387													
Sample	272	272	272	272	278	278	278	278	278	278	278	278	311	311
Lithology	GN													
Na ₂ O	5.16	4.25	4.78	4.10	5.91	6.01	5.85	5.87	6.41	5.87	6.48	6.68	7.91	7.53
Al ₂ O ₃	28.58	29.83	29.37	30.57	28.07	28.17	28.23	28.51	27.29	28.01	27.21	26.96	24.67	25.51
SiO ₂	54.07	51.75	52.77	51.68	55.20	56.04	55.77	55.49	56.55	55.61	56.93	56.94	60.12	58.76
K ₂ O	0.27	0.27	0.26	0.30	0.25	0.23	0.29	0.26	0.36	0.25	0.29	0.18	0.39	0.40
CaO	11.51	13.38	12.35	13.72	10.63	10.27	10.59	10.70	9.83	10.56	9.84	9.32	6.44	7.64
Total	99.59	99.49	99.53	100.37	100.06	100.72	101.03	101.13	100.43	100.67	100.75	100.36	99.53	99.83
An#	71.14	77.68	74.06	78.72	66.53	65.38	66.67	66.83	62.89	66.54	62.66	60.66	47.36	52.86
	OY387													
Sample	311	311	364	364	364	378	378	378	378	384	384	384	384	395
Lithology	GN	GN	AGN	AGN	AGN	GN	GN	GN	GN	LZP	LZP	LZP	LZP	GN
Na ₂ O	7.58	7.84	6.27	6.69	6.59	7.94	8.19	6.53	7.33	9.50	9.69	9.40	9.17	9.88
Al ₂ O ₃	25.20	24.70	27.61	26.42	27.05	24.75	23.85	26.86	25.20	23.09	22.72	23.12	22.98	23.42
SiO ₂	59.19	60.54	55.50	56.39	55.86	59.66	60.64	56.07	58.75	62.85	63.72	63.09	63.49	62.95
K ₂ O	0.31	0.45		0.22	0.33	0.61	0.71	0.28	0.45	0.49	0.50	0.58	0.37	
CaO	7.07	6.72	9.95	9.25	9.32	6.52	5.88	9.19	7.60	4.52	4.37	4.60	4.42	4.61
Total	99.35	100.25	99.33	99.31	99.15	99.48	99.27	98.95	99.60	100.45	101.01	100.79	100.44	100.86
An#	50.76	48.65	63.69	60.45	60.98	47.58	44.24	60.87	53.40	34.46	33.26	35.10	34.76	34.02
	OY387													
Sample	395	395	395	415	415	415	415							
Lithology	GN													
Na ₂ O	9.46	10.34	9.12	8.79	9.10	9.06	8.91							
Al ₂ O ₃	23.35	23.00	24.07	23.44	23.48	23.67	23.45							
SiO ₂	63.17	64.05	62.54	61.91	61.79	61.73	62.03							
K ₂ O				0.60	0.41	0.25	0.50							
CaO	4.79	3.80	5.59	4.96	5.09	5.47	5.13							
Total	100.77	101.19	101.33	99.71	99.86	100.18	100.02							
An#	35.88	28.88	40.38	38.41	38.20	40.02	38.89							

All Overysel samples, chromite

	OY335	OY335	OY335	OY335	OY335	OY335	OY335	OY335	OY335	OY335	OY335	OY335	OY335	OY335
Sample	241	241	241	241	241	241	262	262	262	262	262	262	303	303
Lithology	CHRX	CHRX	CHRX	CHRX	CHRX	CHRX	CHRX	CHRX	CHRX	CHRX	CHRX	CHRX	QFPX	QFPX
MgO	6.16	6.62	6.63	6.67	6.70	6.52	7.68	7.55	7.88	7.68	7.49	7.59	4.30	4.53
Al ₂ O ₃	14.97	14.85	15.09	14.42	14.80	15.31	15.52	16.09	16.08	15.99	16.10	15.47	8.62	8.77
TiO ₂	1.00	1.05	1.16	1.29	1.04	1.12	1.09	1.02	1.20	1.26	1.23	1.34	1.69	1.62
V ₂ O ₅		0.41			0.55		0.37	0.40	0.38					0.40
Cr ₂ O ₃	42.48	42.10	43.14	42.82	42.06	42.32	42.02	41.70	42.37	42.20	42.71	43.11	42.51	41.62
MnO						0.59				0.53	0.53			
FeO	34.81	34.89	34.72	34.57	34.68	34.54	31.85	31.75	32.38	32.40	32.52	33.20	42.05	42.03
Total	99.41	99.92	100.74	99.76	99.83	100.41	98.54	98.50	100.28	100.06	100.59	100.71	99.18	98.97

	OY335	OY335	OY335	OY387										
Sample	303	303	303	245	245	245	245	245	246	246	246	246	246	258
Lithology	QFPX	QFPX	QFPX	CHRX	CHRX	CHRX	CHRX	CHRX	FPX	FPX	FPX	FPX	FPX	FPX
MgO	2.82	4.85	3.17	7.53	7.18	7.17	7.32	7.33	4.93	5.07	2.93	4.79	5.16	3.98
Al ₂ O ₃	6.70	9.49	6.31	16.69	15.50	15.37	15.89	16.66	11.06	10.26	9.16	9.64	10.17	9.83
TiO ₂	0.89	1.22	2.18	0.58	0.89	0.90	0.85	0.95	1.74	1.69	1.13	1.51	1.50	1.27
V ₂ O ₅	0.50		0.68	0.61	0.69	0.71	0.56	0.66	0.71	0.78	0.98	0.77	0.59	0.58
Cr ₂ O ₃	46.26	43.31	42.97	46.39	46.49	46.19	45.83	45.76	47.88	48.68	48.90	49.40	50.09	45.86
MnO		0.60				0.57	0.56		0.57		0.55	0.61	0.53	0.74
FeO	41.66	39.64	44.10	28.92	30.00	30.33	30.21	29.44	33.46	34.77	36.99	33.87	33.01	38.55
Total	98.84	99.10	99.42	100.72	100.74	101.25	101.23	100.79	100.35	101.25	100.66	100.59	101.06	100.81

	OY387	OY387	OY387	OY387	OY387	OY387	OY387	OY387	OY387	OY387	OY387	OY387	OY387	OY387
Sample	258	258	258	268	268	268	268	268	268	384	384	384	384	384
Lithology	FPX	FPX	FPX	AFPX	AFPX	AFPX	AFPX	AFPX	AFPX	LZP	LZP	LZP	LZP	LZP
MgO	2.85	4.86	3.72	0.98	1.05	1.69	1.28	1.02	1.54	7.46	4.47	4.01	8.00	4.90
Al ₂ O ₃	9.96	16.12	9.83	3.68	3.53	6.11	4.13	5.93	5.49	10.02	8.96	8.29	10.05	8.56
TiO ₂	0.95	0.59	1.08	1.80	1.74		1.31			0.85	0.61	0.48	0.66	
V ₂ O ₅	0.65		0.45	1.41	1.18		0.98	0.73	1.03					
Cr ₂ O ₃	46.38	41.38	46.54	42.73	42.66	45.69	44.27	46.02	45.95	56.53	55.20	55.29	56.83	55.59
MnO	0.53			0.75	0.65	0.75	0.79	0.76	0.78					0.65
FeO	39.64	36.52	38.58	47.76	48.53	44.48	45.85	45.28	43.95	26.42	32.03	32.60	25.99	30.23
Total	100.97	99.47	100.21	99.11	99.34	98.73	98.61	99.73	98.75	101.28	101.27	100.67	101.54	99.93

	OY08	OY08									
Sample	OY08	OY08									
Lithology	CHR	CHR									
MgO	3.43	2.85	1.37	1.21	2.4	3.83	4.84	4.81	4.2	1.1	0.7
Al ₂ O ₃	10.48	10.08	9.25	8.58	7.15	8.43	11.22	11.6	10.64	7.45	7.45
TiO ₂	1.33	1.16	1	0.96	1.56	1.64	0.9	1.25	1.31	1.49	1.1
V ₂ O ₅	0.31					0.35	0.31	0.28		0.33	0.32
Cr ₂ O ₃	41.81	43.39	41.74	44	42.79	45.15	44.75	44.01	44.05	42.51	42.47
MnO	0.69	0.75	0.56	0.75	1.06	0.58	0.54	0.67	0.87	0.77	0.94
FeO	42.81	42.98	46.88	45.98	46.26	40.52	38.27	38.66	38.95	46.92	46.74
Total	100.86	101.22	100.81	101.47	101.22	100.49	100.83	101.27	100.01	100.57	99.71

	OY16	OY17	OY18	OY19	OY20
Sample	OY16	OY17	OY18	OY19	OY20
Lithology	FCHR	FCHR	FCHR	FCHR	FCHR
MgO	5.6	4.46	5.98	6.04	5.78
Al ₂ O ₃	12.86	10.98	14.07	13.7	12.26
TiO ₂	2.02	1.49	1.39	1.79	1.94
V ₂ O ₅	0.38		0.27	0.35	0.29
Cr ₂ O ₃	41.65	44.35	42.4	42.25	41.43
MnO		0.54	0.49		0.55
FeO	38.87	39.39	36.29	37.02	37.83
Total	101.38	101.21	100.89	101.14	100.24

Appendix 5

Geochemistry and mineralogy of the Platreef and “Critical Zone” of the northern lobe of the Bushveld Complex, South Africa: implications for Bushveld stratigraphy and the development of PGE mineralisation

Published as:

I. McDonald, D. A. Holwell and P. E. B. Armitage. 2005. Geochemistry and mineralogy of the Platreef and “Critical Zone” of the northern lobe of the Bushveld Complex, South Africa: implications for Bushveld stratigraphy and the development of PGE mineralisation.

Mineralium Deposita, **40**, 526-549.

Personal contribution:

I was involved in discussion of the ideas presented by this paper, in particular the ‘Mineralogy of the Platreef’ section. I generated all the whole-rock data and mineral chemistry data, which are shown in Tables 1 and 2 and Fig. 10. As such, this paper contains around half the raw whole-rock geochemical data for the Sandsloot pit undertaken during this project. Figures 1 and 10 were drafted by myself.

Mineralium Deposita (2005)
DOI 10.1007/s00126-005-0018-6

ARTICLE

Iain McDonald · David A. Holwell
Paul E. B. Armitage

Geochemistry and mineralogy of the Platreef and "Critical Zone" of the northern lobe of the Bushveld Complex, South Africa: implications for Bushveld stratigraphy and the development of PGE mineralisation

Received: 14 February 2004 / Accepted: 27 July 2005
© Springer-Verlag 2005

Abstract The northern lobe of the Bushveld Complex is currently a highly active area for platinum-group element (PGE) exploration. This lobe hosts the Platreef, a 10–300-m thick package of PGE-rich pyroxenites and gabbros, that crops out along the base of the lobe to the north of Mokopane (formerly Potgietersrus) and is amenable to large-scale open pit mining along some portions of its strike. An early account of the geology of the deposit was produced by Percy Wagner where he suggested that the Platreef was an equivalent PGE-rich layer to the Merensky Reef that had already been traced throughout the eastern and western lobes of the Bushveld Complex. Wagner's opinion remains widely held and is central to current orthodoxy on the stratigraphy of the northern lobe. This correlates the Platreef and an associated cumulate sequence that includes a chromitite layer known as the Grasvally norite-pyroxenite-anorthosite (GNPA) member directly with the sequence between the UG2 chromitite and the Merensky Reef as it is developed in the Upper Critical Zone of the eastern and western Bushveld. Implicit in this view of the magmatic stratigraphy is that similar Critical Zone magma was present in all three lobes prior to the development of the Merensky Reef and the Platreef. However, when this assumed correlation is examined in detail, it is obvious that there are significant differences

in lithologies, mineral textures and chemistries (Mg# of orthopyroxene and olivine) and the geochemistry of both rare earth elements (REE) and PGE between the two sequences. This suggests that the prevailing interpretation of the stratigraphy of the northern lobe is not correct. The "Critical Zone" of the northern lobe cannot be correlated with the Critical Zone in the rest of the complex and the simplest explanation is that the GNPA-Platreef sequence formed from a separate magma, or mixture of magmas. Chilled margins of the GNPA member match the estimated initial composition of tholeiitic (Main Zone-type) magma rather than a Critical Zone magma composition. Where the GNPA member is developed over the ultramafic Lower Zone, hybrid rocks preserve evidence for mixing between new tholeiitic magma and existing ultramafic liquid. This style of interaction and the resulting rock sequences are unique to the northern lobe. The GNPA member contains at least seven sulphide-rich horizons with elevated PGE concentrations. Some of these are hosted by pyroxenites with similar mineralogy, crystallisation sequences and Pd-rich PGE signatures to the Platreef. Chill zones are preserved in the lowest Main Zone rocks above the GNPA member and the Platreef and this suggests that both units were terminated by a new influx of Main Zone magma. This opens the possibility that the Platreef and GNPA member merge laterally into one another and that both formed in a series of mixing/quenching events involving tholeiitic and ultramafic magmas, prior to the main influx of tholeiitic magma that formed the Main Zone.

Editorial handling: A. Boyce

I. McDonald (✉) · D. A. Holwell
Department of Earth, Ocean and Planetary Sciences,
Cardiff University, P.O. Box 914, Cardiff,
CF10 3YE, UK
E-mail: iain@earth.cf.ac.uk
E-mail: holwellda@Cardiff.ac.uk

P. E. B. Armitage
Department of Earth and Environmental Sciences,
University of Greenwich, Chatham Maritime,
Kent, ME4 4TB, UK

Keywords Bushveld Complex · Platreef · Merensky Reef · Stratigraphy · Platinum-group elements

Introduction

The Bushveld Complex of South Africa is the largest repository of platinum-group elements (PGE) in the

world (Lee 1996; Cawthorn 1999a). All PGE mining activities in the eastern and western lobes of the Bushveld Complex currently take place from tabular horizons within the layered sequence associated with sulphides or chromitite where the PGE are concentrated. The most important of these are the Merensky Reef and the UG2 chromitite layer. The stratigraphy and the positions of the PGE horizons in the eastern and western lobes of the complex are broadly the same (Lee 1996; Cawthorn and Lee 1998; Barnes and Maier 2002a). This, as well as other geophysical evidence, led Cawthorn and Webb (2001) to infer that the eastern and western lobes were connected throughout much of the evolution of the Bushveld Complex, that similar magmas were present in both lobes and that mineralisation processes operated concurrently in both lobes to produce stratiform PGE deposits such as the Merensky Reef and the UG2 chromitite.

While PGE mining and exploration in the eastern and western lobes of the Bushveld Complex to date have produced sufficient data to bring genetic understanding of the Merensky Reef and UG2 chromitite mineralisation to a mature stage, the same cannot be said of the PGE mineralisation in the northern (Potgietersrus) lobe of the complex. In this sector, PGE are associated with a basal unit called the Platreef that rests directly on the early Proterozoic sediments and Archaean granite that form the floor of the complex (Fig. 1). The Platreef is a contaminated, frequently xenolith-rich, unit that is geologically more complex than any of the PGE reefs in the eastern and western lobes, but which is also thicker and carries sufficiently consistent grade to allow large-scale open pit mining along some areas of its strike (Viljoen and Schürmann 1998; Bye 2001; Kinnaird and Nex 2003). Anglo Platinum, currently operates one open pit mine on the farm Sandsloot 236KR, is developing a second on the farm Zwartfontein 818LR, and has plans for others at staged intervals over the next 30 years (Bye 2001). The potential for more high-tonnage and low-cost open pits in this sector have led other companies to explore on the Platreef adjacent to Anglo Platinum's licence area and the northern lobe is currently the most active exploration centre on the Bushveld Complex.

The Platreef was discovered not long after the discovery of the Merensky Reef in the eastern Bushveld in 1924 and was systematically explored and mined until 1930, when the platinum price collapsed during the Great Depression (Buchanan et al. 1981). The most comprehensive early account of the geology of the deposit is given by Wagner (1929) who recognised and documented key features of the Platreef, most notably: (a) the great thickness of the mineralised layer(s); (b) the position of the mineralised pyroxenite ("bronzitite") at the base of the igneous sequence in contact with the metamorphosed sediments and granite; (c) the ratio of Pt:Pd at unity or lower; and (d) the presence of PGE mineralisation in metamorphosed and metasomatised footwall, often at considerable distance from the igneous rocks.

Wagner (1929) observed a "feldspathic bronzitite" and a "pseudoporphyrific poikilitic diallage norite" at many sites along the Platreef and termed these as "Merensky Reef" because of a similar appearance to the rocks of Merensky Reef that were already known in the eastern and western lobes of the Bushveld Complex. Wagner (1929) took this further and evidently believed that not only were the Platreef and the Merensky Reef similar, but that they represented the same layer:

"The Main Potgietersrust or Merensky Platinum Horizon...is the main platinum horizon of the Potgietersrust fields. This is taken to be the equivalent of the Merensky Horizon of the Lydenburg and Rustenburg districts." (p.167).

In discussing the wider genetic aspects of the mineralisation, Wagner (1929)

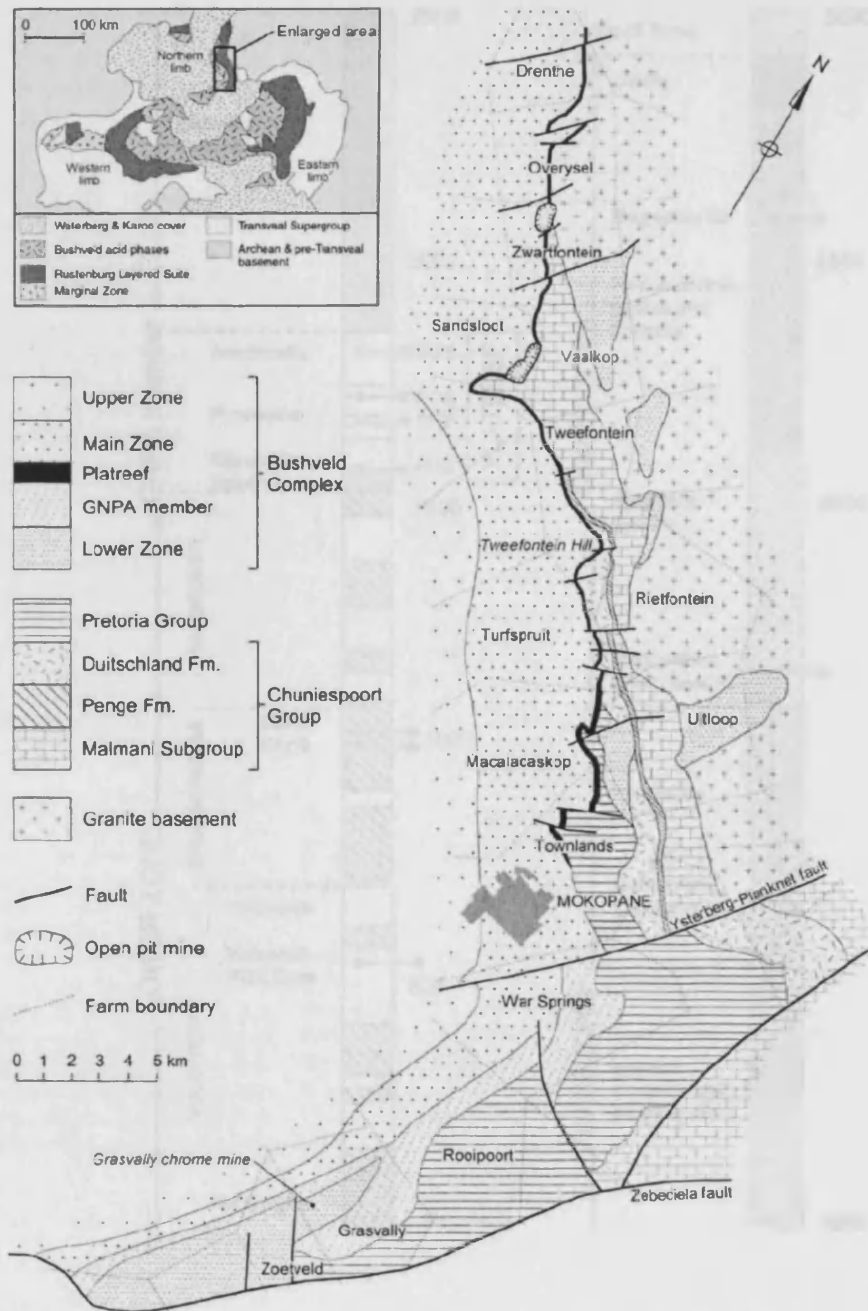
"...maintains that in endeavouring to arrive at the correct solution of the problem, the platinum deposits of the Potgietersrust district must be viewed in their entirety. In other words, the Zwartfontein deposits must be viewed in their relation to the Merensky Horizon as developed to the north and south of them and in the Rustenburg and Lydenburg districts." (p.182).

Wagner's suggestion that there was a direct correlation between the Platreef of the northern lobe and the Merensky Reef elsewhere in the Bushveld Complex is of great importance because it has been accepted uncritically in most subsequent work on the Platreef (e.g. Buchanan et al. 1981; Kinloch 1982; Buchanan and Rouse 1984; White 1994; Vermaak 1995; Viljoen and Schürmann 1998). More fundamentally, the assumed link between the two units is one of the foundations of the prevailing view of the stratigraphy of the northern lobe and its relationship with the rest of the complex.

The northern lobe

The stratigraphy of the northern lobe and the widely accepted view of its relationship with the rest of the Bushveld Complex are summarised in Figs. 2, 3. The northern lobe is divided into four principal zones but detailed elements of the stratigraphy are different from the eastern and western lobes. Lower Zone (LZ) rocks comprise > 1,600 m of pyroxenites and harzburgites with chromitite layers, consisting of at least 37 different cyclic units (Hulbert 1983; Hulbert and Von Gruenewaldt 1985). The LZ is best developed to the south of Mokopane on the farms Grasvally 293KR and Zoetveld 294KR (Hulbert and Von Gruenewaldt 1986) but also occurs as small satellite bodies north of the town (Fig. 1). The mafic rocks

Fig. 1 Geological map of the lower portion of the northern limb of the Bushveld Complex showing the localities described in the text

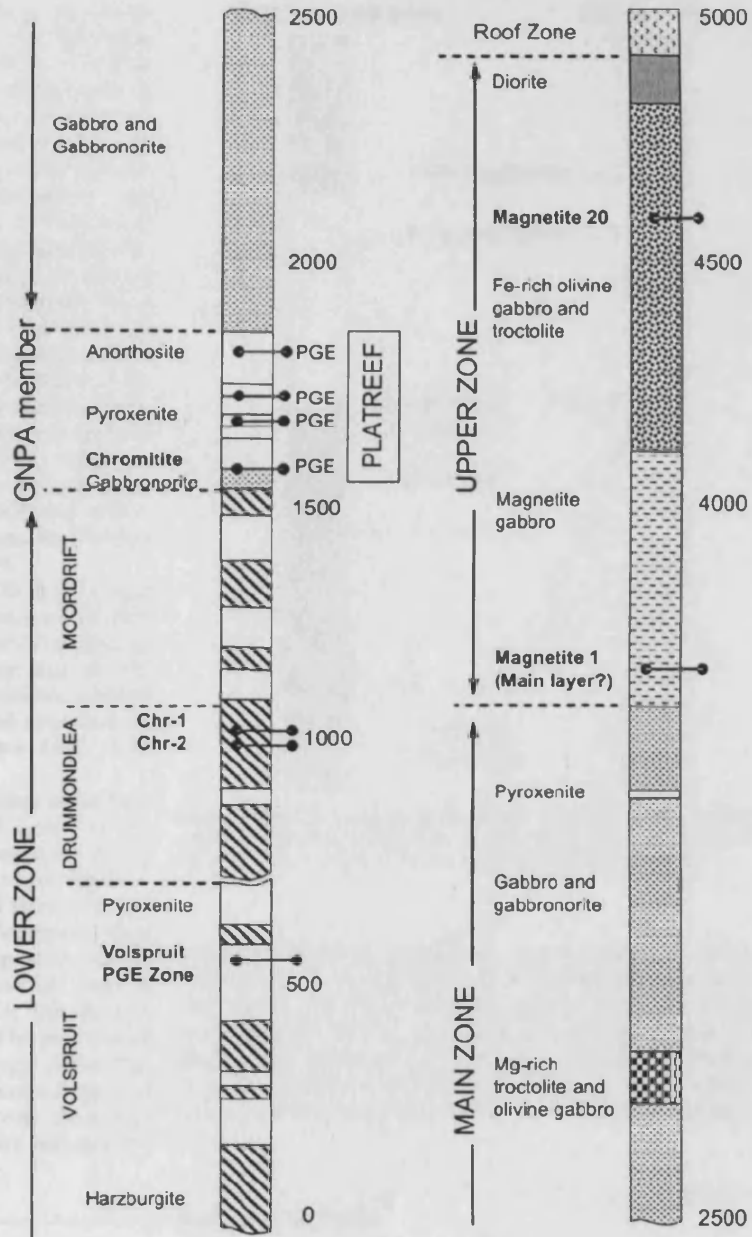


of the LZ here have higher $Mg\#$ ($(Mg/(Mg + Fe))$) values in olivine and orthopyroxene and contain chromitites with higher Cr_2O_3 than similar LZ-type rocks in the rest of the Bushveld Complex. In addition, a sulphide horizon with PGE occurs in the Volspruit Subzone (Fig. 2), whereas the LZ in the rest of the complex contains no

stratiform PGE mineralisation (Hulbert and Von Gruenewaldt 1982; Hulbert 1983). Van der Merwe (1976, 1998) considers these as unique features of the northern lobe, distinctive from the rest of the complex.

A thin sequence of rocks known as the Grasvalley norite-pyroxenite-anorthosite (GNPA) member is

Fig. 2 Stratigraphy of the northern lobe showing the major chromitite, magnetite and Ni-Cu-PGE deposits (after Von Gruenewaldt et al. 1989)



developed over LZ rocks and sediments of the Pretoria Group south of Mokopane (Hulbert 1983; Hulbert and Von Gruenewaldt 1985, 1986; Fig. 1). This sequence contains layered norites, gabbronorites and anorthosites along with a chromitite layer and is termed as the "Critical Zone" in all the current literature on the northern lobe. Hulbert (1983) termed the chromitite layer in the GNPA member the "UG2-like" chromitite and it has been correlated directly with the UG2

chromitite by some authors (e.g. Van der Merwe 1998). The top of the GNPA member is xenolith-rich and hosts PGE mineralisation. The occurrence of both xenoliths and PGE has led to suggestions that the upper part of the GNPA member may correlate with the Platreef north of Mokopane (Von Gruenewaldt et al. 1989).

Van der Merwe (1976) placed the Platreef ('Platinum Horizon' of Wagner 1929 and Willemse 1969) at the base of the Main Zone (MZ). This correlation is not

universally accepted and other authors (e.g. Von Gruenewaldt et al. 1989; White 1994) believe the Platreef to be a part of the Upper Critical Zone (UCZ). The Platreef can be traced for over 30 km along strike north of Mokopane and is generally developed between norites and gabbro-norites ascribed to the MZ and the floor of the complex. As the Platreef strikes north, it transgresses sedimentary rocks of the Transvaal Sequence, and eventually rests on Archaean granite (Fig. 1). The rest of the MZ comprises 2,200 m of gabbros and gabbro-norites. The only reliable markers in this part of the sequence are four prominent pyroxenites developed 300 m above the Platreef and a 100–200-m thick troctolite that is found 1,100 m above the Platreef. These layers have no equivalents in the rest of the Bushveld Complex. Van der Merwe (1976) suggested that a pyroxenite corresponding to the Pyroxenite Marker is developed 2,000 m above the Platreef, but Harris et al. (2004) have discounted this correlation. The pyroxenite unit also appears to be absent in the south of Mokopane and is missing from the stratigraphic compilations by Hulbert (1983) and Von Gruenewaldt et al. (1989).

The Upper Zone is approximately 1,400 m thick and comprises a sequence of magnetite gabbros, anorthosites and olivine diorites, along with a number of magnetite layers. As indicated in Fig. 3, one of these may be correlated on the basis of thickness and vanadium content with the Main Magnetite layer developed elsewhere in the Bushveld Complex (Van der Merwe 1976; Von Gruenewaldt et al. 1989).

The question of how the Platreef and other cumulates that have been ascribed to the "Critical Zone" in the northern lobe actually relate to the stratigraphy of the rest of the Bushveld Complex has important implications for the timing and genesis of the Platreef mineralisation. If it is not equivalent to the Merensky Reef and formed in a separate event, then genetic models constructed for the Platreef on the basis of what is known about the Merensky Reef or which link the two horizons in time may be inappropriate. The purpose of this paper is to critically review the geology of the Platreef and Merensky Reef, using existing knowledge and new geochemical and mineralogical data, with the aim of establishing the validity of the assumed link between the two units.

Samples

Samples of Platreef used in this study were collected from faces 135/014 and 138/014 in the southwest corner (SW1 and SW2 series) and faces 132/038 and 141/011 along the north wall (N1 and N3 series) of the southern central pit at Anglo Platinum's Sandsloot open pit mine (Fig. 4). The footwall is composed primarily of siliceous dolomite and calc-silicate. Close to the contact, these rocks are transformed into a mixture of massive diopside clinopyroxenites, locally rich in metamorphic olivine (commonly referred to as "parapyroxenites"), that have

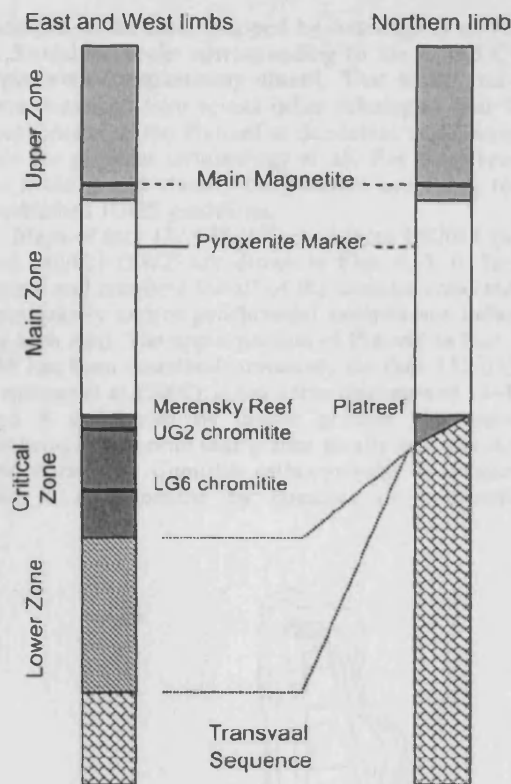


Fig. 3 Currently accepted stratigraphic relationships between the eastern and western limbs and the northern limb of the Bushveld Complex (after White 1994; and Cawthorn and Lee 1998)

suffered variable serpentinisation (Armitage et al. 2002). Additional samples of footwall were collected from faces that connect to the three reef sections along the south and east walls of the pit. These samples are labelled as the S series and the E series, respectively. Sample DH-G is a grab sample collected from the same area as Face 132/038 and is included with the N1 series for comparison.

Analytical methods

The initial preparation of samples was as described by Armitage et al. (2002). Detailed mineralogical examinations and the analysis of silicates were carried out at Cardiff University using a Cambridge Instruments LEO S360 scanning electron microscope coupled to an Oxford Instruments INCA energy dispersive X-ray analysis system. Additional analyses were also carried out at the Natural History Museum using a JEOL 5900LV (SEM) with attached Oxford instruments EDX INCA system. Typical analytical conditions and procedures are described in Hutchinson (2001). Bulk analysis for major

element and trace elements was carried out using a JY Horiba Ultima 2 inductively coupled plasma optical emission spectrometer (ICP-OES) and Thermo X7 series inductively coupled plasma mass spectrometer (ICP-MS). Samples were first ignited at 900°C to determine loss on ignition and then fused with Li metaborate on a Claisse Fluxy automated fusion system to produce a melt that could be dissolved in 2% HNO₃ for analysis. Full details of the ICP analysis procedures and the instrumental parameters are given in McDonald et al. (2005). Geochemical data for Platreef, hanging wall and footwall samples are given in Tables 1, 2, 3. A complete set of silicate mineral data, comprising over 200 analyses, is available from the first author on request.

Petrography of the Platreef at Sandsloot

White (1994) recognised three principal rock types within the Platreef that he termed as A reef, B reef and C reef. The A reef is a pegmatoidal feldspathic pyroxenite at the base of the sequence that carries sporadic base metal sulphide mineralisation. Above this is the B reef, the principal PGE carrier, which is a coarse grained pyroxenite with 50–90% orthopyroxene, common base metal sulphides and very sporadic chromitite. At the top of the sequence is the C reef, which is a fine-grained feldspathic pyroxenite that may contain up to 70% clinopyroxene. Despite the fact that they are essentially mining terms designed to categorise Platreef facies on a broad scale, these have become entrenched in the recent literature (Lee 1996; Viljoen and Schürmann 1998; Cawthorn and Lee 1998; Barnes and Maier 2002a; Cawthorn et al. 2002a) leading to the dangerous misconception that the A–B–C sequence represents "typical" Platreef.

Sections of the Platreef have been described in several papers prior to the A–B–C terminology being introduced, and reveal how, without any preconceived subdivisions, the terminology is simply not applicable in many parts of the Platreef. On the farm Drenthe 788LR, Gain and Mostert (1982) describe a basal feldspathic pyroxenite overlain by norites and melanorites, capped by a feldspathic pyroxenite. This sequence of pyroxenite-norite-pyroxenite is inconsistent with the A, B and C-reefs, as the inferred 'B-reef' is noritic and contains cumulus plagioclase. In the adjacent farm to the south, Overysel 815LR, Cawthorn et al. (1985) describe the Platreef as often having a thin medium-grained norite at the base which grades upwards into a coarse pyroxenite with inhomogenous mineralogy, overlain by gabbro and norite.

More recent work has also revealed limitations with the "A–B–C" terminology (Armitage et al. 2002; Kinnaid et al. 2005). The definitions of the reef types do not conform to the recognised IUGS classifications, are not sufficient to allow unambiguous distinctions between different units, and encourage pigeonholing rather than proper description of potentially new rock types. For

example, in the faces mapped by Armitage et al. (2002) at Sandsloot, rocks corresponding to the A and C reef types were conspicuously absent. That study and new data presented here reveal other lithologies that form components of the Platreef at Sandsloot and do not fit into the previous terminology at all. For these reasons we avoid it and classify our samples according to the established IUGS guidelines.

Maps of face 132/038 (N1), and faces 138/014 (SW1) and 141/021 (SW2) are shown in Figs. 4, 5, 6. Sample points and numbers for all of the samples collected for petrography and/or geochemical analysis are indicated on each map. The upper portion of Platreef in face 132/038 has been described previously (as face 132/035) in Armitage et al. (2002); it has a true thickness of 12–15 m and is dominated by coarse grained pyroxene-rich gabbro-gabbro-norite that grades locally into pyroxenite and websterite. Cumulus orthopyroxene is ubiquitous and is accompanied by cumulus or intercumulus

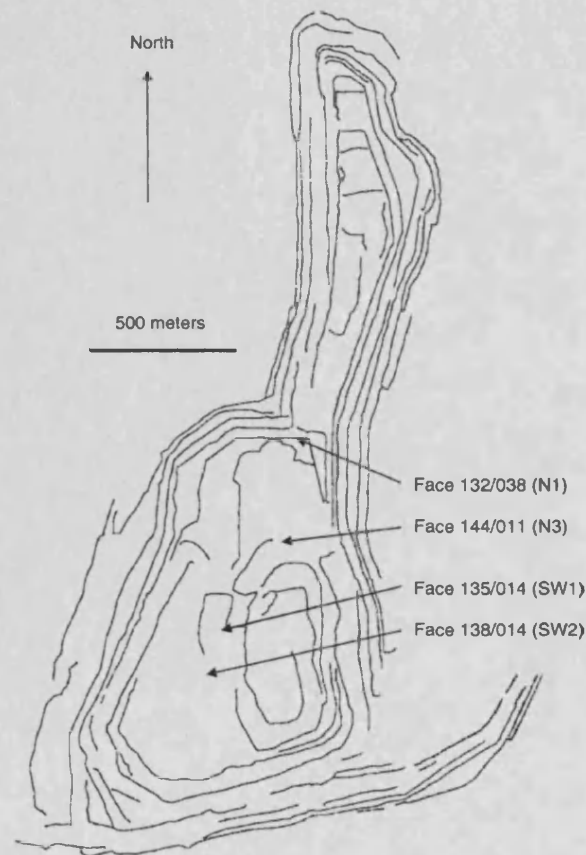


Fig. 4 Wireframe plan view of the Sandsloot open pit in July 2000 showing the locations of the faces mapped and sampled in this study. Solid lines represent the bench tops and the deepest area of the pit (south central area) is approximately 190 m below the level of the outer wall

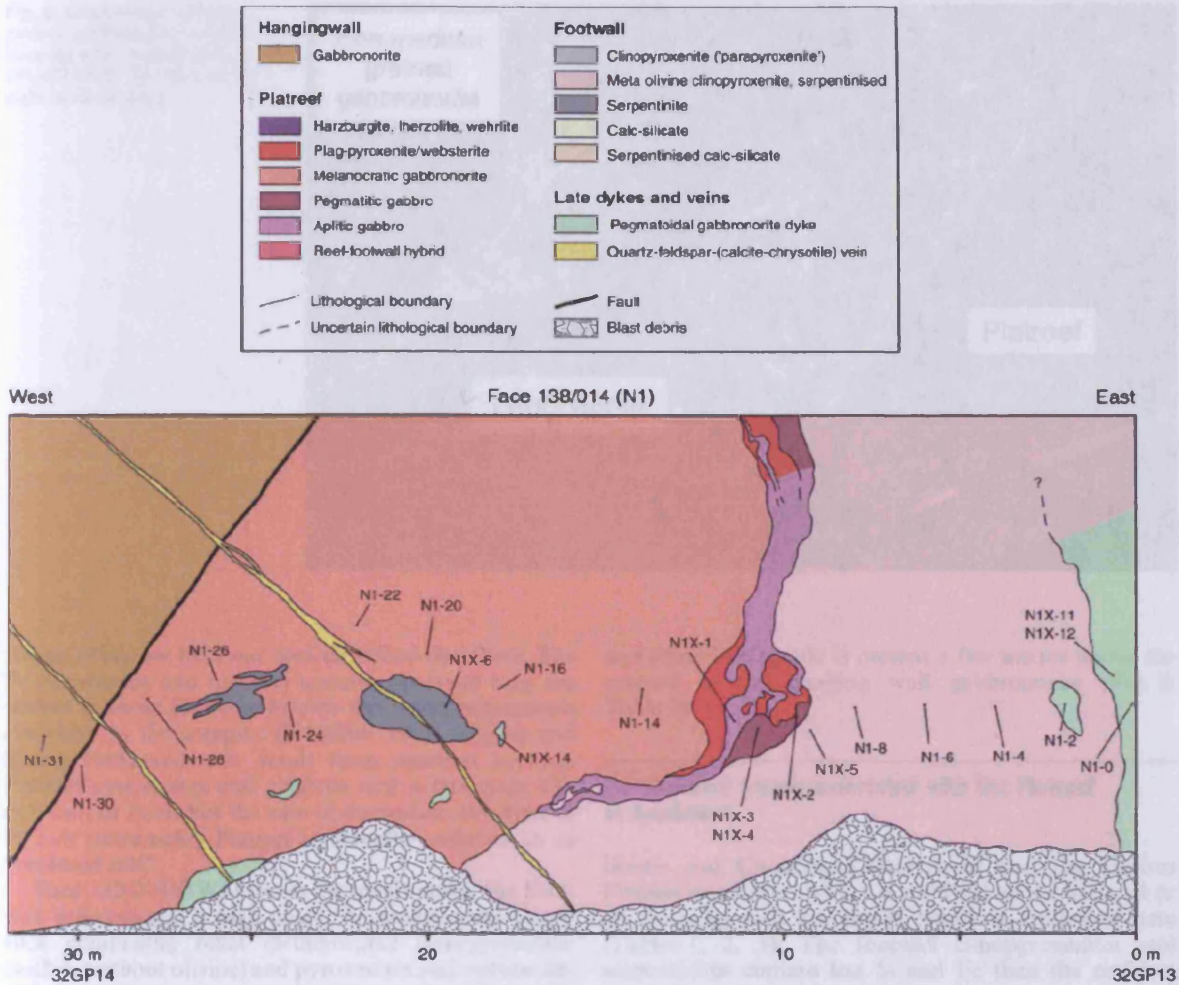


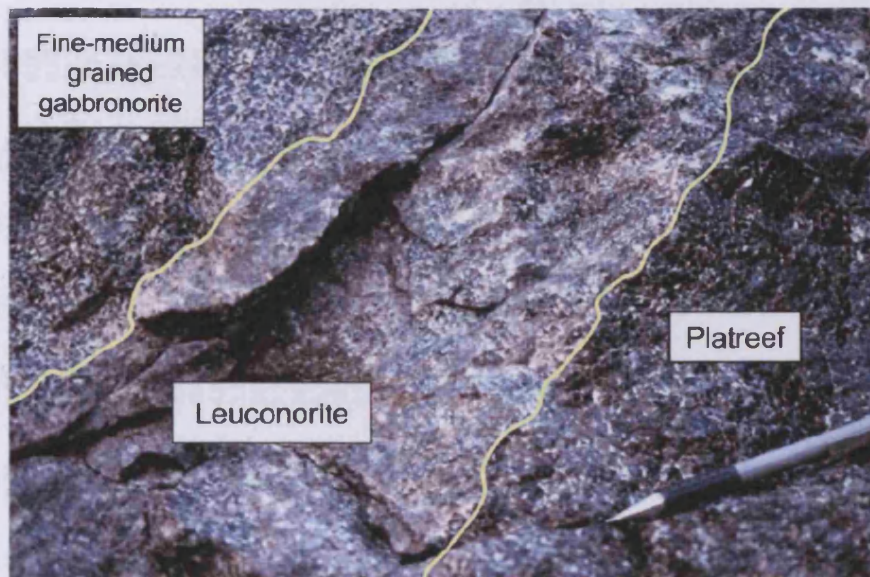
Fig. 5 Dip parallel section through the Platreef on face 132/035 (N1). This shows the major lithologies and the positions of samples taken for petrographic/geochemical analysis. 32GP13 and 32GP14 are the positions of mine survey geopoints

clinopyroxene, and intercumulus plagioclase that may occur as large oikocrysts. Sulphides and PGM are generally restricted to interstitial sites between the cumulate pyroxenes. Chromite, ilmenite, rutile, armalcolite, perovskite, phlogopite and zircon are present as accessories. A pegmatoidal zone of aplitic gabbro and fragmented pyroxenite occurs along the footwall contact where the reef thickens but is absent from thinner reef lower down the face. The contact with the hanging wall in this face is tectonised, and comprises a serpentinitised brittle-ductile shear zone up to 20 cm thick (Fig. 3). The hanging wall is a medium-coarse grained norite with cumulus plagioclase and intercumulus pyroxene (sample N1-31). The Platreef in face 144/011 (N3) appears similar to face N1 and the top contact of the reef was photographed and sampled. Here, instead of a tectonite, there is a planar magmatic contact between the top of

the Platreef and the hanging wall gabbros. The contact is marked by a 10–15 cm thick leuconorite with cumulus plagioclase and orthopyroxene oikocrysts, overlain by a 5 cm thick layer of fine-grained gabbronorite (Fig. 6). The leuconorite and gabbronorite are samples N3X4B and N3X4A in Table 1.

Platreef in the southwest corner of the pit shows important mineralogical and textural differences from the reef exposed to the north. Towards the top contact, Fe-rich olivine is widespread and occurs as a late-stage mineral. It replaces orthopyroxene through many metres of the reef. Plagioclase may also be replaced by Fe-rich clinopyroxene leading to the development of Fe-rich wehrlites, olivine lherzolites and harzburgites and an overall darkening of the rock. These rock types have been noted to the south where the Platreef rests on banded ironstone (Buchanan et al. 1981; Buchanan and

Fig. 6 Leuconorite and fine-grained gabbronorite at the hanging wall contact in face 141/011 (N3). The pen on the right is 12-cm long



Rouse 1984), but have not been described elsewhere. The Fe enrichment and reaction textures observed here are similar to those found in Fe-rich pipes and pegmatoids elsewhere in the complex (Schiffries 1982; Viljoen and Scoon 1985) and may result from reaction between Platreef pyroxenites and gabbros and a late-stage Fe-rich melt or fluid. For the ease of discussion, this type of Fe-rich (ultramafic) Platreef is hereafter referred to as "replaced reef".

Face 135/014 (SW1) shows Platreef cutting the footwall lithologies at a high angle. A serpentinised mixed rock comprising relict metamorphic clinopyroxenite (with or without olivine) and pyroxenites and websterites with igneous textures, (termed as "footwall-reef hybrid") forms the base of the Platreef. The primary Platreef is heavily replaced and mixtures of orthopyroxenites, websterites, gabbronorites and wehrlites are common. The rocks become more pegmatoidal and olivine-rich upwards, grading into Fe-rich olivine ilherzolite close to the hanging wall contact (Fig. 7). The hanging wall for a few metres above the contact is fine-grained gabbronorite with cumulus plagioclase (sample SW1-47).

Face 138/014 (SW2) also shows Platreef cutting the footwall calc-silicates at a high angle to the remnant layering and is similar in some respects to Face 135/014. Olivine in the footwall is heavily serpentinised and these rocks contain an extensive fracture network filled with magnetite and ilmenite. A thick zone of serpentinised hybrid rocks is present at the base of the reef and wehrlite occurs close to the hybrid rocks. This merges upwards into gabbronorite and pyroxenite that become very Fe-rich, but without much development of olivine, close to the hanging wall. A 15-cm wide dark xenolith of websterite (sample SW2-83) that carries high levels of Cr

and some PGE grade is present a few metres above the contact in the hanging wall gabbronorite (Fig. 8; Table 3).

Geochemical trends associated with the Platreef at Sandskoot

Harris and Chaumba (2001) noted that the igneous Platreef was richer in Cr, Co and Fe than the footwall or the hanging wall lithologies, which is replicated here (Tables 1, 2, 3). The footwall clinopyroxenites and serpentinites contain less Si and Fe than the reef but more Ca and Mn. Similarly, the hanging wall norites and gabbronorites typically contain more Si, Al, Na, K, Rb, Sr and Ba than the reef or the footwall. Harris and Chaumba (2001) noted an upward trend of Fe enrichment in their reef samples and in the N1 face, where there is the least evidence of replacement; we find a similar gradual increase in Fe towards the top of the reef. In replaced reef (e.g. face SW1), the Fe enrichment is dramatic and these areas are also enriched in Ti, Mn, Hf and Nb (and sometimes U and Th) relative to primary reef. The plagioclase-rich hanging wall rocks and the cross-cutting pegmatoidal gabbronorite dyke in the N1 face are also characterised by a consistently positive Eu anomaly ($Eu/Eu^* > 1.0$), while the opposite is generally true of the reef and the footwall. As might be expected, footwall-reef hybrid rocks show concentrations of Si, Mg, Ca, Fe, Co and Cr that are intermediate between reef and footwall (Tables 2 and 3) but nevertheless the Cr concentration is a useful indicator for primary reef, hybrid zones and footwall where the lithological relations are ambiguous.

Appendix 5. Geochemistry and mineralogy of the "Critical Zone" in the northern Bushveld

Table 1 Geochemical data for facies N1 and N3

Unit	E195	E205	E227	N1-02	N1-2	N1-4	N1-6a	N1-6b	N1-14	N1-X6	N1-22	N1-24	N1-26	N1-30	N1-31	DH-G	N3X4A	N3X4B
Rock Type	SPT	PPX	FW	DYKE	DYKE	FW	FW	FW	PR	XN	PR	PR	PR	PR	HW	PR	HW	HW
SiO ₂ (wt%)	39.55	46.26	49.40	50.44	48.77	39.61	43.22	37.08	52.55	33.92	49.18	51.86	50.59	51.25	51.87	50.39	51.81	50.85
TiO ₂	0.09	0.26	0.33	0.17	0.18	0.12	0.26	0.07	0.19	0.20	0.20	0.16	0.17	0.14	0.16	0.19	0.20	0.09
Al ₂ O ₃	2.77	3.12	16.52	14.81	16.85	12.87	11.31	8.46	6.42	10.88	4.28	5.19	5.70	4.17	22.63	5.79	17.48	26.64
Fe ₂ O ₃	6.34	9.12	8.00	7.17	8.43	10.52	7.21	14.44	11.52	8.36	15.07	13.96	13.26	13.93	5.56	12.82	9.75	1.95
MnO	0.22	0.57	0.15	0.13	0.14	0.35	0.52	0.42	0.21	0.73	0.26	0.23	0.26	0.23	0.10	0.22	0.14	0.04
MgO	34.39	21.25	8.05	10.58	9.61	17.59	14.09	28.04	22.14	34.18	22.88	23.23	21.19	22.53	11.52	19.74	6.48	1.61
CaO	2.36	15.51	10.73	9.60	10.00	11.76	18.95	1.78	5.20	0.32	4.57	4.18	5.41	4.03	8.83	13.08	11.17	13.08
Na ₂ O	0.01	0.21	2.79	3.76	1.91	0.22	0.05	0.02	0.50	0.02	0.58	0.46	0.91	0.66	2.77	0.26	1.79	3.35
K ₂ O	0.01	0.15	1.99	0.72	1.20	0.50	0.05	0.09	0.24	0.03	0.20	0.14	0.07	0.05	0.52	0.01	1.30	0.79
P ₂ O ₅	0.01	0.03	0.04	0.05	0.02	0.03	0.02	0.02	0.03	0.01	0.03	0.04	0.04	0.03	0.02	0.03	0.00	0.00
LOI	12.98	3.38	2.98	2.84	1.17	5.58	5.64	11.14	0.41	11.90	1.20	0.76	0.56	1.75	1.33	0.87	1.14	0.90
Total	98.73	99.95	100.99	100.26	98.27	99.14	101.30	101.55	99.42	100.55	98.46	100.21	98.16	98.76	101.85	99.13	101.25	99.30
Sc (ppm)	8.12	33.8	18.6	18.4	15.8	26.8	8.2	28.2	28.2	24.7	38.3	13.3	29.7	28.3	30.9	27.8	30.8	5.7
V	44.5	153.2	126.9	128.0	93.4	81.5	133.2	51.0	171.1	51.6	168.5	120.3	130.4	125.1	123.1	135.5	190.9	60.9
Cr	14.4	37.3	485.0	279.9	610.9	198.5	331.9	111.5	1817.4	144.1	1734	1916	1688	3021	462.9	1741	424.0	285.8
Co	42.0	20.4	68.3	44.8	43.9	41.1	55.9	83.1	88.0	35.8	158.1	112.8	110.0	118.0	53.3	98.1	40.9	14.7
Ni	389.8	62.6	289.5	165.1	716.0	253.6	408.1	152.1	1292	64.0	2818	4020	2597	3206	160.4	1736	346.2	56.9
Cu	115.2	69.3	148.7	11.6	310.6	139.3	133.1	227.3	210.1	93.6	1549	1577	885	834.7	74.5	610.1	120.6	79.0
Ga	5.2	5.8	13.5	12.26	14.4	10.7	10.99	15.14	6.71	18.62	5.9	6.3	6.76	4.86	22.9	6.72	18.2	24.64
Rb	0.0	16.2	107.2	36.32	59.7	34.0	1.79	6.24	3.50	1.02	7.2	8.2	1.08	2.74	28.9	2.10	49.9	20.70
Sr	7.7	14.1	280.3	236.0	238.6	164.7	66.3	16.3	101.9	9.5	37.8	54.4	55.4	35.0	332.6	16.9	332.8	385.5
Y	3.2	10.1	7.7	7.1	4.3	3.8	10.2	1.6	5.5	4.4	6.0	5.1	6.5	3.2	5.7	5.7	7.4	2.21
Zr	3.6	24.3	26.0	38.2	32.3	14.0	40.3	16.6	25.4	35.4	11.5	10.0	49.8	10.5	8.8	17.6	11.5	4.31
Nb	0.21	0.73	2.40	0.82	0.83	0.80	3.08	2.66	2.94	2.78	0.48	0.44	0.30	0.26	0.65	0.47	0.4	0.15
Ba	n.d.	8.4	186.3	211.7	217.7	108.9	26.1	16.1	80.0	8.5	23.1	28.3	40.6	35.2	111.2	19.1	149.6	151.1
La	1.50	4.02	6.51	4.16	2.47	3.59	4.21	1.33	2.89	1.28	2.51	1.84	2.17	1.74	4.96	2.97	2.59	4.75
Ce	1.89	9.06	9.45	7.21	5.58	5.86	9.67	2.29	5.73	2.89	5.63	4.88	4.76	2.57	8.33	5.15	5.14	8.33
Pr	0.24	1.32	1.22	0.83	0.68	0.73	1.31	0.26	0.72	0.41	0.73	0.63	0.53	0.27	0.99	0.62	0.66	0.90
Nd	0.92	5.39	4.67	3.74	2.43	2.70	5.56	0.95	2.90	1.84	2.81	2.40	2.41	1.31	3.47	2.96	2.54	3.06
Sm	0.17	1.26	1.06	0.92	0.49	0.55	1.34	0.19	0.61	0.47	0.59	0.51	0.54	0.28	0.62	0.70	0.60	0.46
Eu	0.06	0.27	0.51	0.40	0.49	0.33	0.54	0.11	0.21	0.10	0.16	0.19	0.15	0.09	0.62	0.20	0.34	0.71
Gd	0.24	1.35	1.07	0.94	0.54	0.56	1.50	0.18	0.67	0.51	0.66	0.59	0.59	0.34	0.64	0.86	0.68	0.43
Tb	0.04	0.23	0.18	0.16	0.09	0.09	0.26	0.04	0.13	0.10	0.12	0.10	0.10	0.06	0.11	0.14	0.12	0.06
Dy	0.37	1.51	1.15	1.05	0.61	0.58	1.61	0.23	0.83	0.65	0.81	0.71	0.71	0.47	0.71	1.09	0.87	0.39
Ho	0.09	0.28	0.22	0.21	0.13	0.11	0.33	0.05	0.18	0.14	0.17	0.15	0.14	0.09	0.14	0.24	0.18	0.07
Er	0.35	0.90	0.73	0.65	0.44	0.38	0.86	0.14	0.50	0.39	0.61	0.57	0.48	0.33	0.47	0.76	0.64	0.21
Tm	0.06	0.13	0.11	0.09	0.07	0.06	0.13	0.02	0.08	0.07	0.10	0.09	0.08	0.06	0.07	0.12	0.10	0.03
Yb	0.48	0.81	0.70	0.68	0.46	0.36	0.94	0.20	0.65	0.50	0.68	0.58	0.56	0.43	0.48	0.92	0.69	0.17
Lu	0.09	0.14	0.12	0.10	0.08	0.06	0.19	0.08	0.15	0.13	0.11	0.10	0.07	0.05	0.08	0.14	0.11	0.03
Hf	0.09	0.67	0.67	0.73	0.64	0.36	1.20	0.42	0.60	1.08	0.29	0.22	0.14	0.17	0.20	0.43	0.25	0.09
Ta	0.02	0.07	0.18	0.08	0.07	0.05	0.23	0.18	0.21	0.21	0.06	0.05	0.05	0.03	0.04	0.05	0.01	0.01
Th	0.45	1.08	1.52	0.64	0.57	0.67	1.19	0.37	1.11	0.86	0.95	0.54	0.49	0.34	0.51	0.62	0.39	0.26
U	0.85	0.20	0.37	0.18	0.09	0.11	0.30	0.12	0.29	0.26	0.11	0.13	0.11	0.06	0.06	0.12	0.01	0.02
Eu/Eu*	0.90	0.64	1.45	1.29	2.86	1.81	1.16	1.79	1.02	0.62	0.78	1.05	0.78	0.93	2.97	1.63	4.78	4.78
La/LuN	1.77	3.03	5.85	4.12	3.39	6.66	2.34	1.82	2.01	1.03	2.42	1.98	3.16	3.35	6.48	2.16	2.42	19.42
PGE grade	n/a	n/a	n/a	v. low	n/a	low	n/a	n/a	n/a	n/a	inter	inter	high	high	v. low	inter	inter	v. low
Pt/Pd	n/a	n/a	n/a	0.75	n/a	0.90	n/a	n/a	n/a	n/a	1.04	0.98	1.94	0.93	1.36	1.03	0.91	0.87

Rare earth element values in chondrite used for normalisation come from Taylor and McLennan (1985)
 PGE grade bands based on total Rh + Pt + Pd + Au: < 0.1 ppm = very low; 0.1 - 2.0 ppm = low; 2.0 - 6.0 = intermediate; 6.0 - 10.0 = light; > 10.0 = very high
 Major units: FW footwall; DYKE cross-cutting pegmatoidal dykes; PR primary reef; XN xenoliths; HW hanging wall
 Rock types: SPT serpentinite; PPX paracelino-pyroxenite; CS calc-silicate; GBVRT gabbronorite; PY pyroxenite; VRT norite; WBST websterite; LCNRT leuconorite

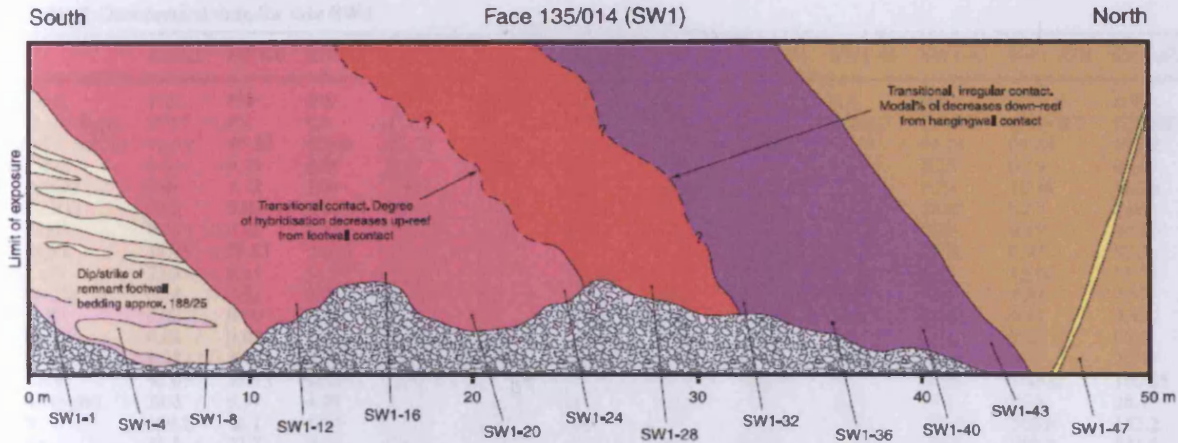


Fig. 7 Slightly oblique section through the Platreef on face 135/014 (SW1). This shows the major lithologies with contacts extrapolated/inferred at height and the positions of samples taken for petrographic/geochemical analysis. The key is as in Fig. 5

Links between the Platreef and the Merensky Reef

Stratigraphic context

The modern consensus stems from Willemsse (1969) and van der Merwe (1976) who followed Wagner (1929) and correlated the Platreef with the Merensky Reef. This interpretation is primarily based on the nature of the rocks immediately above the Platreef. The hanging wall norites and gabbros are visually similar and have similar orthopyroxene compositions to MZ rocks elsewhere in the Bushveld Complex. Von Gruenewaldt et al. (1989) suggested that the Platreef might be correlated with the upper part of the GNPA member (shown in detail in Fig. 9). Evidence cited in support of this includes: the layering of some units and the presence of cumulus chromite and development of a chromitite layer. These are the characteristic features of the UCZ in the eastern and western Bushveld and the MZ is notable for the absence of both. The terms "Critical Zone" and "Main Zone" when applied to the northern lobe effectively refer

to whether the rocks are located above or below the Platreef. The veracity of this assumption will be tested below.

Petrographic similarities between the Platreef and the Merensky Reef

Both units are dominated by cumulus orthopyroxene, with subordinate amounts of plagioclase and clinopyroxene, and carry an assemblage of interstitial sulphides and elevated concentrations of PGE. Buchanan et al. (1981) suggested that pyroxene compositions in the Platreef were the same as in the Merensky Reef (see below for discussion). In places, both units develop pegmatoidal facies. Chromite in the form of one or two chromitite layers is a ubiquitous feature of the Merensky Reef and the highest PGE grades are generally associated with one or both chromitites (Lee 1996; Kinnaird et al. 2002). Chromite occurs as isolated crystals, or as rare pods/schlieren, in the Platreef (Viljoen and

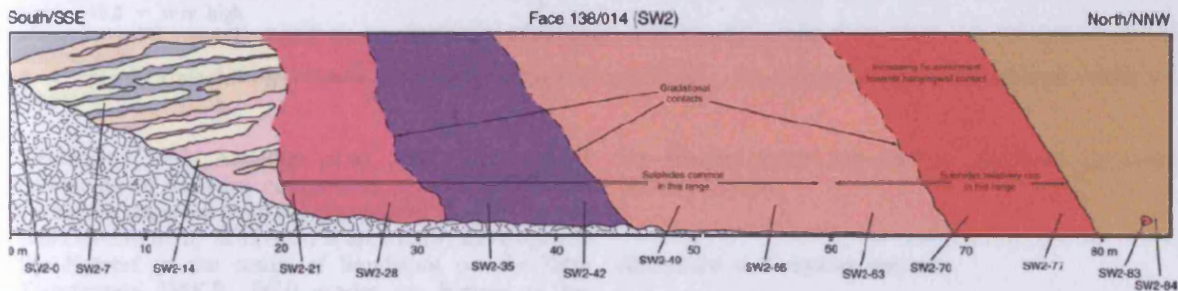


Fig. 8 Oblique section through the Platreef on face 138/014 (SW2). This shows the major lithologies with contacts extrapolated/inferred at height and the positions of samples taken for petrographic/geochemical analysis. The key is as in Fig. 5

Appendix 5. Geochemistry and mineralogy of the "Critical Zone" in the northern Bushveld

Table 2 Geochemical data for face SW1

	SW1-1	SW1-4	SW1-8	SW1-20	SW1-24	SW1-28	SW1-32	SW1-36	SW1-40	SW1-43	SW1-47B	SW1-47A
Unit	FW	FW	FW	HYB	HYB	PR	RR	PR	RR	RR	HW	HW
Rock Type	PPX	CS	CS	n.a	n.a	WBST	LHRZ	PX	HZBG	LHRZ	GBNRT	GBNRT
SiO ₂ (wt%)	43.51	40.24	40.94	44.38	42.66	45.16	44.84	46.55	48.11	44.21	51.44	49.44
TiO ₂	0.42	0.29	0.09	0.62	0.15	0.14	0.18	0.14	0.21	0.23	0.19	0.16
Al ₂ O ₃	6.08	3.32	2.48	5.47	6.27	3.61	3.44	3.70	2.56	3.29	16.48	16.30
Fe ₂ O ₃	8.03	3.89	7.38	13.49	12.86	13.28	19.36	13.43	17.85	22.08	8.83	9.04
MnO	0.35	0.68	0.73	0.31	0.29	0.24	0.33	0.22	0.32	0.38	0.19	0.15
MgO	14.79	29.81	27.00	10.62	18.43	20.63	22.58	23.27	23.46	21.76	6.93	8.55
CaO	23.83	9.61	11.52	24.30	16.05	12.36	6.31	8.99	4.75	6.48	12.06	11.75
Na ₂ O	0.19	0.03	0.01	0.19	0.29	0.67	0.37	0.33	0.10	0.33	2.43	2.52
K ₂ O	0.02	0.00	0.01	0.02	0.46	0.13	0.15	0.13	0.19	0.23	0.41	0.43
P ₂ O ₅	0.03	0.00	0.01	0.03	0.02	0.03	0.05	0.02	0.03	0.04	0.01	0.02
LOI	0.83	10.85	8.28	0.27	4.00	3.09	1.06	1.57	0.52	0.57	1.34	2.27
Total	98.09	98.73	98.45	99.69	101.48	99.33	98.66	98.35	98.12	99.59	100.32	100.65
Sc (ppm)	28.0	5.57	4.90	46.12	26.9	34.8	24.3	30.0	25.8	31.0	37.8	28.1
V	159.2	46.1	47.4	333.4	117.7	129.2	126.5	126.3	145.4	187.9	200.0	152.2
Cr	41.5	27.7	48.3	835.0	601.8	306.5	304.2	306.1	310.4	230.4	292.0	551.5
Co	37.8	11.3	56.4	71.0	92.9	123.3	116.4	134.9	131.3	136.9	48.3	59.1
Ni	1683	189.7	3732	928.3	2286	2156	2769	3921	2804	3390	406.9	376.1
Cu	1448	87.1	2097	675.5	839.0	828.7	764.5	1477	1156	1329	170.5	186.6
Ga	7.6	6.3	4.3	10.2	6.5	4.88	5.50	4.5	5.2	5.6	18.1	15.7
Rb	1.9	-0.1	0.1	3.7	26.3	6.32	5.72	7.3	15.4	11.9	7.3	11.9
Sr	25.5	7.6	7.2	25.6	31.3	47.1	85.5	60.9	34.4	66.1	282.2	233.9
Y	18.2	29.6	14.9	12.3	6.6	6.7	7.9	5.3	6.5	10.3	11.7	8.2
Zr	67.5	7.8	3.0	58.2	12.6	15.7	19.5	10.3	14.0	15.5	5.1	7.0
Nb	1.36	2.08	0.52	1.51	0.61	0.54	0.98	0.49	0.78	0.62	0.03	0.15
Ba	2.1	n.d.	n.d.	1.8	37.7	54.0	85.6	44.2	37.3	52.1	76.6	71.6
La	5.53	6.27	1.93	3.91	1.82	1.90	3.24	1.69	1.82	2.52	1.80	2.04
Ce	15.56	17.57	5.40	9.40	4.61	4.47	6.94	3.46	4.54	6.35	4.03	4.53
Pr	2.26	2.26	0.75	1.43	0.67	0.59	0.87	0.50	0.64	0.97	0.60	0.64
Nd	9.29	8.51	3.10	6.16	2.91	3.06	4.07	2.22	2.67	4.23	2.68	2.75
Sm	2.27	2.11	0.81	1.69	0.74	0.81	0.98	0.56	0.62	1.11	0.75	0.73
Eu	0.61	0.46	0.21	0.42	0.23	0.21	0.28	0.18	0.17	0.29	0.39	0.45
Gd	2.49	2.64	1.19	1.80	0.88	0.96	1.04	0.70	0.72	1.27	0.95	0.86
Tb	0.42	0.54	0.24	0.30	0.16	0.16	0.19	0.11	0.13	0.21	0.18	0.16
Dy	2.64	3.68	1.74	1.86	1.02	1.09	1.23	0.81	0.94	1.48	1.23	1.07
Ho	0.48	0.73	0.37	0.34	0.19	0.22	0.25	0.15	0.19	0.28	0.24	0.21
Er	1.60	2.68	1.44	1.11	0.65	0.64	0.73	0.54	0.68	0.99	0.86	0.72
Tm	0.24	0.43	0.25	0.17	0.09	0.09	0.13	0.08	0.11	0.15	0.14	0.11
Yb	1.45	2.80	1.70	1.11	0.59	0.65	0.80	0.51	0.74	0.99	0.91	0.73
Lu	0.22	0.44	0.27	0.19	0.09	0.08	0.13	0.08	0.13	0.16	0.15	0.11
Hf	1.93	0.27	0.09	1.70	0.32	0.35	0.38	0.26	0.35	0.37	0.21	0.20
Ta	0.12	0.64	0.06	0.09	0.04	0.04	0.09	0.04	0.07	0.05	0.01	0.01
Th	1.63	11.93	1.32	1.45	0.52	0.58	0.86	0.51	0.76	0.71	0.29	0.29
U	0.86	0.95	0.11	0.41	0.10	0.11	0.26	0.04	0.15	0.12	0.00	0.01
Eu, Eu*	0.78	0.60	0.65	0.73	0.85	0.72	0.84	0.86	0.76	0.75	1.40	1.74
La, LuN	2.57	1.48	0.74	2.11	2.08	2.40	2.57	2.13	1.44	1.66	1.28	1.87
PGE grade	v. high	low	v. high	inter	inter	high	inter	high	inter	v. high	low	low
Pt-Pd	0.86	0.65	0.99	0.88	0.67	1.28	0.81	0.74	0.55	0.70	0.95	0.97

Rare earth element values in chondrite used for normalisation come from Taylor and McLennan (1985)

PGE grade bands based on total Rh + Pt + Pd + Au: <0.1 ppm = very low; 0.1-2.0 ppm = low; 2.0-6.0 = intermediate; 6.0-10.0 = high; >10.0 = very high

Major units: FW footwall; DYKE cross-cutting pegmatoidal dykes; HYB footwall hybrid; PR primary reef; RR replaced reef; HW hanging wall

Rock types: PPX para(clino)pyroxenite; CS calc-silicate; GBNRT gabbornite; PX orthopyroxenite; LHRZ lherzolite; HZBG harzburgite

Schürmann 1998; Armitage et al. 2002), but is most commonly an accessory component. A more widespread chromitite (inferred from the presence of chromite at the same level in many drillcores) is apparently developed in the Platreef to the south of Sandsloot on the farm Tweefontein 238KR. PGE grades are highest in the pyroxenite immediately beneath the chromitite and Viljoen and Schürmann (1998) suggest that at this locality

the Platreef bears the greatest similarity to normal Merensky Reef.

Strontium and osmium isotopes

Cawthorn et al. (1985) found a wide range of ⁸⁷Sr/⁸⁶Sr initial ratios in Platreef whole rock samples that they

Appendix 5. Geochemistry and mineralogy of the "Critical Zone" in the northern Bushveld

Table 3 Geochemical data for face SW2

	S2-6	S2-12	S2-18	SW2-14	SW2-28	SW2-35	SW2-49	SW2-77	SW2-83
Unit	FW	FW	FW	FW	HYB	RR	PR	RR	XN
Rock Type	SPPX	SPPX	CS	SPPX	n/a	WHRL	GBNRT	PX	WBST
SiO ₂ (wt%)	40.71	31.57	26.73	34.12	46.60	46.40	48.49	50.03	52.78
TiO ₂	0.12	0.11	0.34	0.29	0.19	0.21	0.21	0.37	0.17
Al ₂ O ₃	3.69	11.32	8.27	17.65	5.37	5.26	5.44	4.35	3.42
Fe ₂ O ₃	11.02	8.79	11.85	7.66	8.83	15.53	16.48	16.95	10.23
MnO	0.54	0.26	0.31	0.26	0.40	0.33	0.29	0.34	0.23
MgO	27.08	20.30	21.95	13.22	23.53	20.27	18.63	16.33	22.59
CaO	7.50	15.98	18.17	20.09	13.09	11.07	8.73	9.65	8.64
Na ₂ O	0.06	0.02	0.10	0.14	0.13	0.44	0.84	0.69	0.37
K ₂ O	0.06	0.00	0.02	0.08	0.03	0.17	0.25	0.05	0.23
P ₂ O ₅	0.03	0.04	0.03	0.02	0.02	0.03	0.06	0.02	0.02
LOI	8.05	10.12	11.68	5.41	2.98	1.02	0.86	0.57	0.93
Total	98.85	98.52	99.45	98.93	101.17	100.73	100.28	99.34	99.61
Sc (ppm)	11.5	3.1	4.8	16.0	20.6	32.3	28.8	48.3	37.4
V	55.7	8.1	28.8	76.6	76.0	137.1	132.9	261.0	157.2
Cr	64.5	20.5	35.9	215.3	777.1	2467	2406	1568	3435
Co	47.2	34.9	8.4	35.0	52.8	122.3	112.9	84.6	80.6
Ni	860.0	764.5	113.2	408.4	1451	3231	2779	559.1	1034
Cu	130.4	201.4	330.3	18.8	372.5	867.8	1395	139.1	198.2
Ga	4.46	21.09	8.77	20.67	6.36	6.75	7.16	7.16	5.2
Rb	2.24	0.06	2.21	1.86	2.01	3.08	13.74	1.34	9.7
Sr	10.8	5.0	3.3	28.7	74.4	101.4	106.9	44.9	38.1
Y	4.8	12.8	10.4	8.0	7.6	9.3	7.7	18.2	6.6
Zr	18.3	15.3	13.2	49.0	31.7	28.0	23.1	46.2	9.9
Nb	0.31	0.23	0.00	3.18	2.75	2.87	1.01	3.61	0.39
Ba	33.3	15.1	15.1	39.7	75.4	84.1	105.2	23.4	33.7
La	2.71	3.64	0.18	3.29	2.17	2.69	3.84	4.27	1.43
Ce	5.76	9.00	0.29	8.17	5.12	6.33	7.82	10.92	3.71
Pr	0.76	1.32	0.04	1.18	0.76	0.94	0.87	1.67	0.55
Nd	3.82	6.80	0.52	4.98	3.41	4.15	4.03	7.66	2.33
Sm	1.00	1.63	0.30	1.15	0.90	1.10	0.93	2.06	0.55
Eu	0.23	0.37	0.08	0.31	0.29	0.35	0.26	0.60	0.18
Gd	1.07	1.69	0.71	1.21	1.02	1.29	1.05	2.36	0.68
Tb	0.17	0.29	0.16	0.21	0.19	0.24	0.18	0.44	0.12
Dy	1.17	1.78	1.24	1.30	1.18	1.47	1.25	2.79	0.86
Ho	0.23	0.36	0.28	0.27	0.26	0.31	0.25	0.60	0.17
Er	0.68	1.02	0.92	0.68	0.65	0.82	0.78	1.62	0.62
Tm	0.10	0.16	0.17	0.10	0.09	0.12	0.12	0.24	0.09
Yb	0.68	1.03	1.13	0.72	0.71	0.91	0.87	1.83	0.61
Lu	0.09	0.16	0.19	0.15	0.14	0.17	0.13	0.33	0.10
Hf	0.36	0.23	0.31	1.60	0.95	0.75	0.55	1.22	0.27
Ta	0.05	0.02	0.01	0.22	0.19	0.20	0.08	0.26	0.03
Th	0.53	0.37	0.19	0.83	0.58	0.75	1.27	1.39	0.49
U	0.19	0.04	0.02	0.22	0.17	0.21	0.39	0.50	0.05
Eu:Eu*	0.66	0.67	0.51	0.79	0.91	0.89	0.80	0.83	0.91
La:LuN	3.00	2.43	0.10	2.32	1.58	1.63	3.10	1.33	1.52
PGE grade	v. low	low	v. low	n/a	n/a	n/a	high	n/a	low
Pt, Pd	2.76	0.55	2.81	n/a	n/a	n/a	1.48	n/a	1.65

Rare earth element values in chondrite used for normalisation come from Taylor and McLennan (1985)

PGE grade bands based on total Rh + Pt + Pd + Au: <0.1 ppm = very low; 0.1-2.0 ppm = low; 2.0-6.0 = intermediate; 6.0-10.0 = high; >10.0 = very high.

Major units: FW footwall; DYKE cross-cutting pegmatoidal dykes; HYB footwall hybrid; PR primary reef; RR replaced reef; HW hanging wall

Rock types: SPPX serpentinised para(clino)pyroxenite; CS calc-silicate; GBNRT gabbonorite; PX pyroxenite; WBST websterite; WHRL wehrlite

ascribed to the effects of contamination by local granite footwall. In a follow-up study, Barton et al. (1986) determined ⁸⁷Sr/⁸⁶Sr initial ratios in orthopyroxene and plagioclase mineral separates and found that most of the radiogenic Sr was hosted by plagioclase and other intercumulus minerals. The lowest ⁸⁷Sr/⁸⁶Sr initial ratio found in orthopyroxene separated from the Platreef was

0.7079, outside the normal UCZ range of 0.7055-0.7065, but within the range of initial ratios determined for the Merensky Reef (e.g. Kruger 1994).

Chaumba et al. (1998) reported initial ¹⁸⁷Os/¹⁸⁸Os ratios for the Platreef that ranged from 0.10974 to 0.20292. The Platreef range encompasses the range of initial ratios found in the Merensky Reef (Os minerals

with $^{187}\text{Os}/^{188}\text{Os}_i \sim 0.94$, and laurite with $^{187}\text{Os}/^{188}\text{Os}_i$ 0.142–0.151; Hart and Kinloch 1989; McCandless and Ruiz 1991). Chaumba et al. (1998) interpret this as indicating that Os in the Merensky Reef and the Platreef came from the same source. On close inspection though, the comparison is less robust than it first appears. Chaumba et al. (1998) only presented the range of initial ratios they found. No information was given on what samples were analysed, their positions within or outside the igneous reef, or which initial ratios came from samples with the most Os. Until more information is available, these Os data are open to multiple interpretations and cannot be used to argue strongly for a link between the Merensky Reef and Platreef.

Differences between the Platreef and the Merensky Reef

There are other lines of evidence that would seem to contradict the stratigraphic link implied in Fig. 3. These are outlined below:

Mineralogy of the "Critical Zone" of the northern lobe

Hulbert (1983) divided the GNPA member into two sub-zones (Fig. 9). The lower sub-zone contains orthopyroxene-clinopyroxene, orthopyroxene-clinopyroxene-chromite and orthopyroxene cumulates with subordinate plagioclase-rich units. The upper sub-zone is dominated by plagioclase cumulates with minor norites. Clinopyroxene is ubiquitous at between 5 and 25 modal%, even where chromite is present, and clinopyroxene is sometimes a cumulus mineral with chromite (Hulbert and Von Gruenewaldt 1985). Clinopyroxene is less abundant in the UCZ elsewhere in the complex (typically < 10 modal%; Cameron 1982; Maier and Barnes 1998) and is never present in a cumulus association with chromite. Unusual orthopyroxene-clinopyroxene-chromite cumulates (at -85 and +10 m; Fig. 9) are only developed where the GNPA member rests on LZ cumulates and are unknown from elsewhere in the complex (Hulbert and Von Gruenewaldt 1985). Chromite in the GNPA member has TiO_2 contents (1.77–3.08 wt%; Hulbert 1983) that are generally higher than UCZ stratiform chromites outside of Fe-rich replacement pegmatoids (e.g. Stumpfl and Rucklidge 1982) and the Ti enrichment increases with stratigraphic height in the GNPA sequence.

Rocks of the upper sub-zone of the GNPA member are also unusual because the basal layers of all of the cyclic units recognised by Hulbert (1983) are plagioclase-only cumulates. The crystallisation order for this part of the sequence appears to be governed by the liquidus order plagioclase-orthopyroxene-clinopyroxene (Hulbert 1983). A few cyclic units with basal plagioclase-rich units are known from the UCZ in the eastern and western Bushveld but even in these, plagioclase is

invariably joined by orthopyroxene or chromite as the cumulus phase (Cameron 1982).

Considering only those cumulates containing > 50% orthopyroxene (in order to minimise the effects of reaction with trapped liquid; cf Cawthorn 1996, 2002), the compositions of cumulus orthopyroxene in the GNPA member range between $\text{Mg}\#_{75-78}$ (Hulbert 1983; Fig. 9). These pyroxenes are systematically more Fe-rich than those in similar UCZ cumulates elsewhere in the Bushveld Complex ($\text{Mg}\#_{78-84}$; Cameron 1982; Naldrett et al. 1986; Eales et al. 1993; Maier and Eales 1994; Cawthorn 2002). The available data show that the cumulus plagioclase compositions in the GNPA member are An_{68-78} (Hulbert 1983). This range overlaps with the lower part of the range of UCZ plagioclase compositions observed in the rest of the complex (An_{68-85} ; Cameron 1982; Naldrett et al. 1986; Kruger and Marsh 1985; Maier and Eales 1994), but not with the upper part of the range.

Mineralogy of the Platreef and the Merensky Reef

The primary Platreef records differences in mineral textures from those commonly found in the Merensky Reef. In the Merensky Reef, the liquidus order is orthopyroxene-plagioclase-clinopyroxene (e.g. Cawthorn 2002). In the mafic units of the Platreef, clinopyroxene either follows orthopyroxene or crystallises concurrently with it, and generally precedes plagioclase, which is usually intercumulus. Contamination of the Platreef with dolomite at Sandsloot may promote clinopyroxene crystallisation (e.g. Harris and Chaumba 2001) but it is important to note that the same crystallisation order also occurs where the footwall comprises rocks other than dolomite. For example, orthopyroxene-clinopyroxene-chromite cumulates occur in the Platreef on Overysel 815LR, where the footwall is granite (Hulbert 1983; D Holwell unpublished data). In this sense, the Platreef shows greater similarity with the orthopyroxene-clinopyroxene cumulates of the GNPA member (which are floored by harzburgites or quartzites) than the Merensky Reef. Chromite also shows important petrographic differences. Chromite is consistently the earliest phase in the Merensky Reef, forming layers and inclusions in pyroxenes, but it is most commonly post-cumulus in the Platreef.

Olivine is an important component of the Merensky Reef in some sectors of the Bushveld Complex. In the western lobe around the Union and Rustenburg sections, olivine (Fo_{79-80}) is common and the reef may be developed as a pegmatoidal harzburgite (Vermaak and Hendriks 1976; Kruger and Marsh 1985; Maier and Eales 1994) but in other areas of the complex, olivine is absent from the Merensky Reef. Primary olivine in the Platreef is more problematic. Van der Merwe (1976; Fig. 3 and p.1341) alludes to olivine (Fo_{84}) in a harzburgite or lherzolite at the base of the Platreef but the locality is not described. High-Mg metamorphic olivine

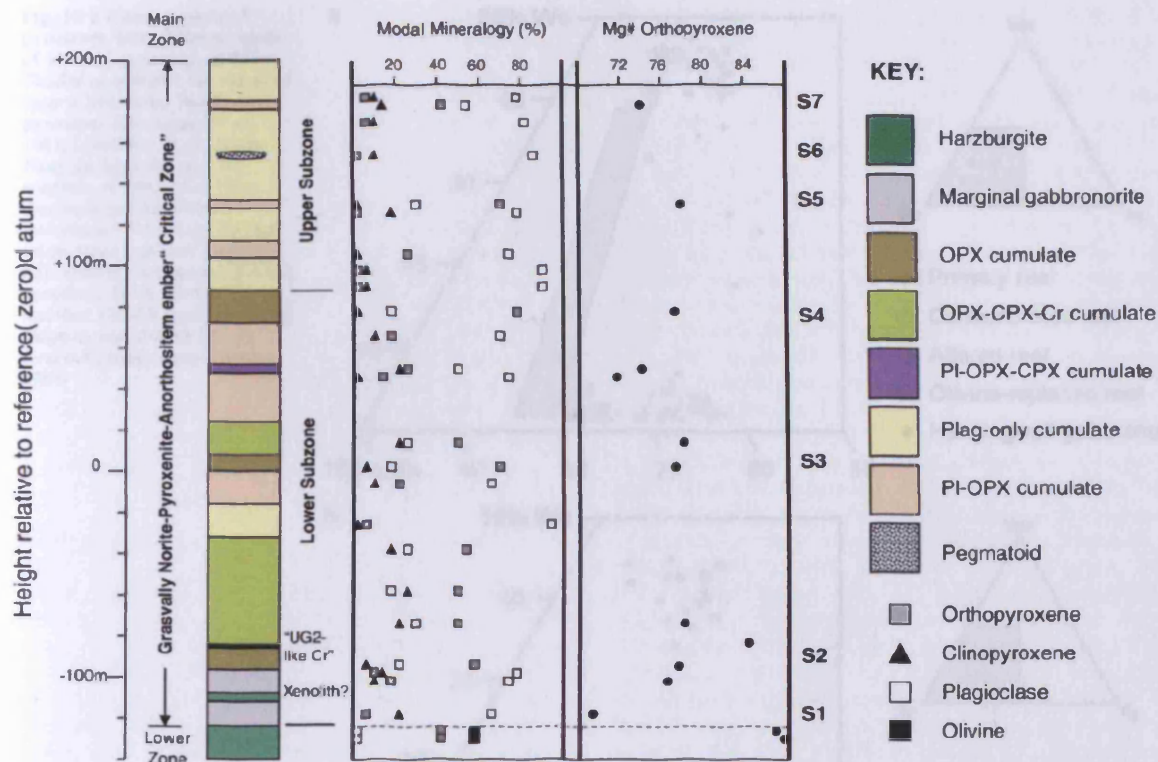


Fig. 9 Summary of the cumulate sequence in the Grasvally Norite-Pyroxenite-Anorthosite member (adapted from Hulbert 1983). Modal mineralogy comprises percentages of olivine (black square); orthopyroxene (grey square); clinopyroxene (black triangle); and plagioclase (white square). Layers indicated with S1-S7 contain

sulphide mineralisation with PGE. The high Mg# of orthopyroxene in association with chromite in the "UG2-like chromitite" is not primary, but the result of reaction (Fe loss) between the pyroxene and spinel (Hulbert 1983)

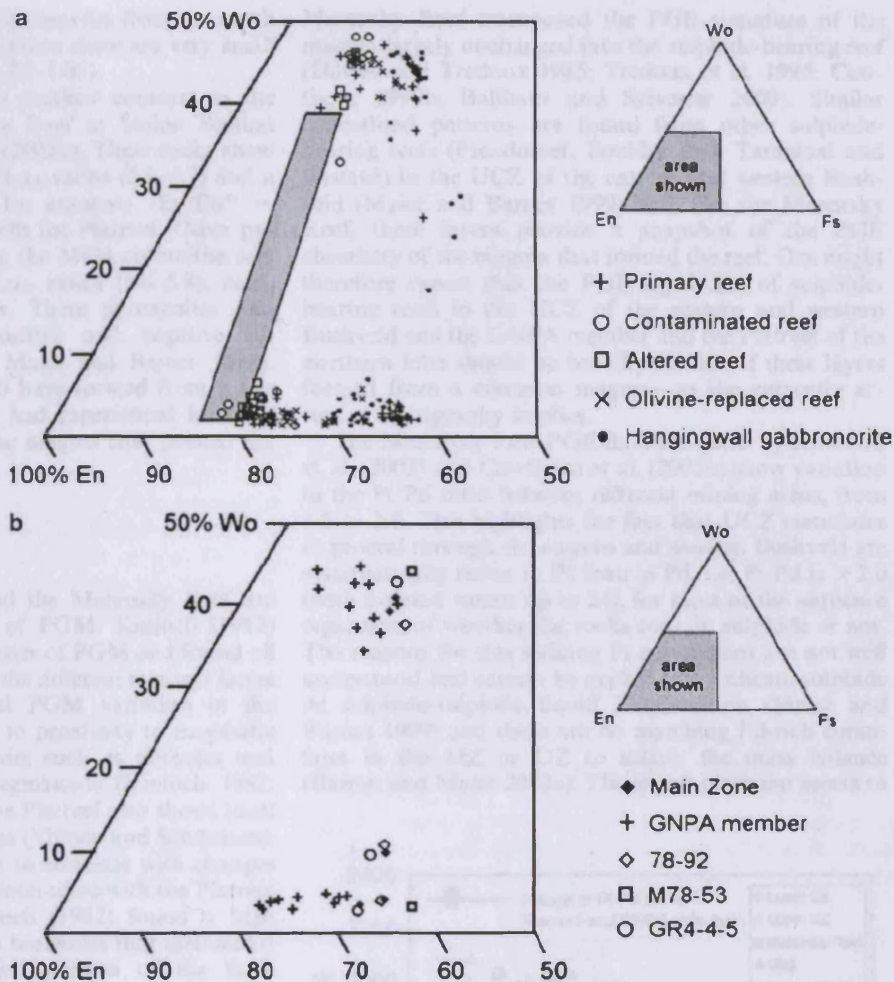
(FO_{82-85}) occurs in the footwall at Sandsloot (Harris and Chaumba 2001; this work) but Kinnaird et al. (2005) also report the presence of igneous harzburgites with magnesian olivine at the base of the Platreef on the farm Macalacaskop 243KR. These rocks may belong to satellite intrusions of the LZ (see Discussion below). Buchanan and Rouse (1984) found Fe-rich olivine (FO_{71}) in a basal "peridotitic" Platreef facies on the farm Turfspruit 241KR which they ascribed to the assimilation of banded ironstones into the reef. Similarly Fe-rich olivine (FO_{64-72}) occurs in replaced reef at Sandsloot. Buchanan et al. (1981) analysed apparently igneous olivine (FO_{75-76}) and this is currently the best (and only) estimate of the composition of primary Platreef olivine.

The most common mineral in the Platreef is orthopyroxene and this allows the most systematic comparison between different localities. Buchanan et al. (1981) studied orthopyroxenes on the farm Tweefontein 238KR where the reef is contaminated by banded ironstone and dolomite. They found pyroxenes with $Mg\#_{74-78}$ in primary reef but more Fe-rich pyroxenes ($Mg\#_{36-42}$) in contaminated units. Orthopyroxenes in the Platreef on Drenthe 788LR and Overysel 815LR, where the reef is

contaminated by granite, gneiss and dolomite (Fig. 1), show a range of compositions with a similar upper limit ($Mg\#_{65-77}$; Gain and Mostert 1982; Cawthorn et al. 1985).

Pyroxene compositions in the Platreef at Sandsloot are complicated by the presence of a reactive footwall that is rich in both Ca and Mg. Our data show a range of orthopyroxene compositions with a main population between $Mg\#_{76-80}$ (Fig. 10) in samples of primary reef. The main population is similar to results obtained by Harris and Chaumba (2001), but smaller sub-populations with $Mg\#_{81-83}$ and $Mg\#_{64-74}$ exist. The high $Mg\#$ population come from a gabbro (N1-26) associated with ragged serpentinite xenoliths (Fig. 4) and from a gabbro (SW2-49) in the southwest corner that has been partially altered to a mixture of tremolite, actinolite, chlorite and sericite. Analyses from N1-26 and SW2-49 are shown as "contaminated reef" and "altered reef", respectively in Fig. 10. In both cases, the Ca contents of clinopyroxenes are higher than expected for igneous pyroxenes (WO_{45-48} ; Fig. 10) and the pyroxene compositions in these samples appear to be affected by local enrichment in Ca and Mg.

Fig. 10 a Compositions of pyroxenes from different types of Platreef at Sandsloot Mine. Shaded area shows the range of typical Merensky Reef pyroxenes (Buchanan et al. 1981; Cawthorn et al. 1985). Note the high En and Wo contents of pyroxenes from contaminated reef where enrichment of Ca and Mg has taken place (see text for more information). b Compositions of pyroxenes from the GNPA member, GNPA member chilled magmas and chilled MZ at Grasvally (data from Hulbert 1983)



The low Mg# population in our dataset comes from samples of replaced reef, located close to the top of the reef in southwest corner of the pit. Fe-rich olivine is common as a replacement for orthopyroxene in many of these rocks and this strongly suggests that the Fe-rich pyroxene composition is not primary. Orthopyroxene in a coarse-grained pyroxenite (SW2-77) at the top of the reef is as Fe-rich as the hanging wall gabbronorite (Mg#₆₄₋₆₆; Fig. 10), but the rock has cumulus orthopyroxene and lacks obvious textural evidence for replacement. It may represent differentiated Platreef that crystallised from a residual melt or which underwent some kind of reaction with the hangingwall liquid.

Based on all the data summarised above, if one accepts Mg#₈₀ and Mg#₇₆ as the upper compositional limits of orthopyroxene and olivine in primary Platreef, then the pyroxene composition is consistent with the GNPA member (Fig. 10). However, the Platreef silicates appear systematically more Fe-rich than their

equivalents in the Merensky Reef (Mg#₇₈₋₈₄ for orthopyroxene and Mg#₇₉₋₈₀ for olivine; Buchanan et al. 1981; Kruger and Marsh 1985; Naldrett et al. 1986; Holwell 2002; Scoon and Mitchell 2002).

Rare earth element geochemistry

Rare earth element data for reef, hanging wall and footwall lithologies at Sandsloot are given in Tables 1, 2, 3. The footwall rocks have a characteristic and sometimes quite pronounced negative Eu anomaly when normalised to chondrite (Eu/Eu* 0.48–0.80) and show a range of LREE:HREE fractionation. La/Lu_N in the footwall varies between 0.09 and 5.89, but most samples fall within the range 1.2–4.0, which overlaps with the narrow range (1.3–3.3) observed in the reef rocks. Small negative Eu anomalies (Eu/Eu* 0.72–0.93) are observed in most of the reef samples, with the exception of some

more plagioclase-rich reef gabbronorites from the north wall (e.g. N1-14 and N1-24), where there are very small positive anomalies ($\text{Eu}/\text{Eu}^* 1.02-1.05$).

These observations are in marked contrast to the melanorites in the Merensky Reef at Union Section studied by Barnes and Maier (2002b). These rocks show a much broader range of La/Lu_N ratios (2.8-5.7) and a more pronounced negative Eu anomaly ($\text{Eu}/\text{Eu}^* = 0.42-0.80$) when compared with the Platreef. Other pyroxenites in the UCZ between the MG4 chromitite and the Bastard Reef show La/Lu_N ratios (1.8-5.8), commonly above Platreef values. These pyroxenites also show more pronounced positive and negative Eu anomalies ($\text{Eu}/\text{Eu}^* 0.6-1.4$; Maier and Barnes 1998). The Platreef would appear to have formed from a less LREE-enriched magma that had experienced less plagioclase fractionation than the magma that formed the Merensky Reef.

PGE mineralogy

The PGE in the Platreef and the Merensky Reef are carried by common groups of PGM. Kinloch (1982) recognised eight major categories of PGM and found all of these in the Platreef and in the different regional facies of Merensky Reef. Regional PGM variation in the Merensky Reef was ascribed to proximity to magmatic feeders and other local factors such as potholes and occurrence of replacement pegmatoids (Kinloch 1982; Kinloch and Peyerl 1990). The Platreef also shows local variation in PGM assemblages (Viljoen and Schürmann 1998) but these changes seem to correlate with changes in the footwall lithology that interacted with the Platreef magma. For example, Kinloch (1982) found a high proportion of Pt sulphides in boreholes that intersected the Platreef on the northern portion of the farm Zwartfontein 818LR and the farm Overysel 815LR, where the footwall is mostly granite. Boreholes on the southern portion of Zwartfontein and samples from the Sandsloot open pit, where the footwall is primarily dolomite, show almost no Pt or Pd sulphides and the assemblage is dominated by Pt and Pd tellurides and alloys (Kinloch 1982; Armitage et al. 2002).

PGE Geochemistry

One of the most striking differences between the PGE deposits of the northern lobe and the rest of the Bushveld Complex is to be found in their noble metal budgets; a feature first noted by Wagner (1929). Davies and Tredoux (1985) were the first to observe that the chondrite normalised PGE pattern of the Merensky Reef was almost parallel to the pattern of high-Mg basaltic sills thought to represent the parental (B1) magma of the Lower Zone and possibly the Critical Zone (Sharpe 1981; Harmer and Sharpe 1985). This similarity has led various authors to infer that the formation of the

Merensky Reef transposed the PGE signature of the magma largely unchanged into the sulphide-bearing reef (Davies and Tredoux 1985; Tredoux et al. 1995; Cawthorn 1999b; Ballhaus and Sylvester 2000). Similar normalised patterns are found from other sulphide-bearing reefs (Pseudoreef, Boulder Bed, Tarentaal and Bastard) in the UCZ of the eastern and western Bushveld (Maier and Barnes 1999) and, like the Merensky Reef, these layers provide a snapshot of the PGE chemistry of the magma that formed the reef. One might therefore expect that the PGE signatures of sulphide-bearing reefs in the UCZ of the eastern and western Bushveld and the GNPA member and the Platreef of the northern lobe should be broadly similar, if these layers formed from a common magma as the currently accepted stratigraphy implies.

The Merensky Reef PGE data compiled by Kinnaird et al. (2002) and Cawthorn et al. (2002b) show variation in the Pt/Pd ratio between different mining areas, from 1.8 to 2.9. This highlights the fact that UCZ cumulates in general through the eastern and western Bushveld are systematically richer in Pt than in Pd, i.e. Pt/Pd is > 2.0 (with isolated values up to 24), for most of the sequence regardless of whether the rocks contain sulphide or not. The reasons for this striking Pt enrichment are not well understood and cannot be explained by silicate-sulphide or sulphide-sulphide liquid fractionation (Maier and Barnes 1999) and there are no matching Pd-rich cumulates in the MZ or UZ to satisfy the mass balance (Barnes and Maier 2002c). The excess platinum seems to

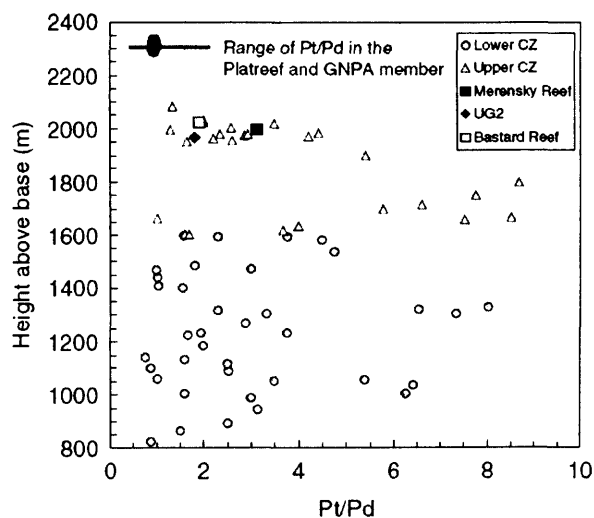


Fig. 11 Variation in Pt/Pd ratios through the Critical Zone in the western lobe (Maier and Barnes 1999) compared with the range (represented by the *bar*) and the mean (represented by the *ellipse*) for the "Critical Zone" and Platreef of the northern lobe (Von Greunewaldt et al. 1989; this work). Very high Pt/Pd ratios in some Critical Zone rocks that are off scale are not shown in the diagram. Note the generally lower Pt/Pd ratios in the northern lobe compared with the Critical Zone elsewhere in the complex.

be a fundamental compositional feature of the magma(s) that fed the UCZ.

Platinum group element ratios for the Platreef and the sulphide-rich reef of the GNPA member are compared with those in sulphide reefs of the UCZ in Table 4. These comparisons indicate that all the sulphide-bearing reefs in the northern lobe are different from those found in the UCZ. The Platreef and all of the sulphide reefs in the GNPA member show greater fractionation of low-temperature PGE (Pt and Pd) from high-temperature PGE (Ir and Ru) and all of them are Pd-rich compared with reefs between the UG2 and the Merensky Reef in the eastern and western lobes. It is important to note that this comparison does not take account of PGE in the footwall. High-grade zones in the footwall at Sandsloot often show even lower Pt/Pd ratios than the main reef (Tables 1, 2, 2), suggesting that there may have been preferential mobilisation of Pd over Pt into the footwall from the proto-reef. The outcome of this would be to raise the apparent Pt/Pd ratio of the Platreef, i.e. the original Pt/Pd ratio of the Platreef before it preferentially lost Pd to the footwall could have been even lower and further removed from UCZ values than it appears currently.

An important primary observation from the northern lobe is that the GNPA member and the Platreef (and silicate rocks with total PGE contents as low as 10ppb; Tables 1, 2, 3) show lower and more restricted Pt/Pd ratios than the UCZ, where Pt/Pd ratios may exceed those in the northern lobe until well above the level of the Bastard Reef (Fig. 11). Whatever the reason for the striking Pt enrichment in the eastern and western lobes during formation of the UCZ, it is not repeated in any of

the sulphide-bearing reefs of the GNPA member, or in the Platreef!

Discussion

Implicit in current models for the evolution of the northern lobe is the idea that UCZ magma entered the northern lobe and formed a sequence of layered cumulates represented by the GNPA member prior to the development of the Platreef (e.g. Van der Merwe 1976, 1998; Von Gruenewaldt et al. 1989). The GNPA member was subsequently covered by mixed UCZ-MZ magma that spread out to the north, interacted with the footwall rocks, and formed the Platreef. If the Platreef is correlated with the Merensky Reef, then introduction of this magma into the northern lobe may be assumed to be coincident with the massive injection of MZ magma that led to the formation of the Merensky Reef and the MZ sequence elsewhere in the complex (e.g. Kruger 2003).

In most tholeiitic magmas, chromite crystallisation terminates before clinopyroxene attains cumulus status due to a reaction relationship between spinel and pyroxene but this reaction is sensitive to oxygen fugacity. The lack of reaction between chromite and clinopyroxene in the orthopyroxene-clinopyroxene-chromite cumulates of the GNPA member led Hulbert (1983) to conclude that the GNPA member magma had an unusually high fO_2 that provided enough ferric iron to stabilise chromite. If this is correct, it follows that the Fe-rich nature of the pyroxenes in the GNPA member cannot be ascribed to fO_2 as, if the GNPA member started with the same composition as the UCZ, a higher

Table 4 Platinum group elements ratios of Upper Critical Zone sulphide-rich reefs and parental magmas (see text for further details)

	Pt/Pd	Pt/Ir	Pd/Ir	Pd/Rh	Source
Eastern and western lobes					
Bastard Reef	3.03	41.8	13.8	3.45	1
Merensky Reef (eastern lobe)	1.57	41.1	26.2	12.9	1
Merensky Reef (western lobe)	1.94	41.9	21.6	8.46	1
Boulder Bed	3.04	32.6	10.7	4.97	2
Tarentaal	4.43	105.6	23.8	5.41	2
Pseudoreef	2.35	37.2	15.9	3.52	1
Northern lobe					
Lower Platreef (Drenthe)	0.81	76	93	18	3, 8
Upper Platreef (Drenthe)	0.65	89	139	58	3, 8
Platreef (Sandsloot)	0.95	96	63	15	4
S7 Norite (top of GNPA member)	0.29	65	230	31	3
S6 Pegmatitic gabbro-norite	0.99	41	41	19	3
S4 Ni-rich leuconorite	0.41	30	73	20	3
S2 Footwall (UG2-like chromitite)	0.43	63	130	19	3
S1 Basal gabbro-norite	0.39	54	140	21	3
Pyroxenite (Unit 36 Lower Zone)	0.34	n/a	n/a	n/a	5, 6
Upper Volspruit (Unit 11 Lower Zone)	0.72	34	47	6.8	3, 7
Parental magmas					
B1 (Lower: Critical Zone)	1.64	56.2	34.3	10	1
B3 (Main Zone)	1.55	77.8	50	15	1

Data sources: (1) Barnes and Maier 2002a; (2) Naldrett et al. 1986; (3) recalculated from Von Gruenewaldt et al. 1989; (4) this work; (5) Hulbert 1983; (6) van der Merwe 1998; (7) R.M. Harmer (personal communication); (8) A.J. Naldrett (personal communication). S1 to S7 refer to sulphide reefs in Fig. 8

fO_2 would be expected to generate more Mg-rich silicates. The lower Mg/Fe ratios observed in the GNPA member are therefore most probably a consequence of a starting magma composition that was more Fe-rich than the UCZ magma.

We have shown above that, apart from the visually similar appearance and the presence of high PGE concentrations, evidence linking the Platreef with the Merensky Reef is not strong. Significant mineralogical and geochemical differences exist between the Platreef and the GNPA member of the northern lobe and the Merensky Reef and the UCZ in the rest of the Bushveld Complex. In contrast, the greater similarities in terms of pyroxene compositions (Fig. 10), crystallisation sequences and PGE signatures between the Platreef and the GNPA member are more consistent with a model whereby these units formed from the similar or related magmas.

The simplest explanation for this apparent paradox is that the Merensky Reef and the Platreef (along with any related pre-reef cumulates) formed from separate magmas with different Mg/Fe ratios and PGE budgets. On the basis of a higher modal clinopyroxene content, the lower Mg# of orthopyroxene and the PGE ratios, the northern lobe rocks formed from a magma that was poorer in Mg, richer in Ca and Fe, was more highly PGE fractionated (greater Pt/Ir and Pd/Ir ratios) and was Pd rather than Pt-dominant relative to the magma(s) that formed the UCZ and Merensky Reef in the eastern and western lobes.

The obvious question is what was this northern lobe magma? The B1 magma of Sharpe (1981), believed to be parental to the Lower and Critical Zones in the eastern and western lobes, is a high Mg basaltic andesite that produces a crystallisation sequence olivine; olivine-orthopyroxene, orthopyroxene, orthopyroxene-plagioclase that is observed in the Lower and Critical Zones (Barnes and Maier 2002a). In contrast, the B3 (tholeiitic) magma believed to be parental to the MZ crystallises plagioclase-orthopyroxene, and then plagioclase plus both pyroxenes (Harmer and Sharpe 1985; Barnes and Maier 2002a). Neither of these magmas on their own can generate the observed crystallisation sequences for the GNPA member or the Platreef.

In order to account for the different PGE ratios, Cawthorn et al. (2002a) proposed that UCZ-type magma similar to that formed the UG2 chromitite in the eastern lobe (which has a Pt/Pd ratio close to unity) could have either flowed northwards or been present in the northern lobe prior to the formation of the Platreef. Cawthorn et al. (2002a) suggest that this magma did not form any chromitite layers and retained its PGE signature until the event that formed the Platreef. This is not supported by the available evidence as the GNPA member contains a chromitite layer as well as thick pyroxenite cumulates with disseminated chromite. The model also fails to explain the Fe-rich nature of the orthopyroxenes, the abundance of clinopyroxene in the GNPA member and why and all the reefs actually have

Pt/Pd ratios lower than unity. In any case, the magma in the eastern lobe became Pt-dominant again at the level of the Merensky Reef. No evidence for this is found in the northern lobe.

Development of the GNPA member

The answer to the question may lie with a marginal member defined by Hulbert (1983) that is developed at the base of the GNPA member where it rests on LZ ultramafic cumulates and Pretoria Group sediments. He suggested that these unusual pigeonite gabbronorites were chilled "Critical Zone" magma or hybrids of chilled magma with LZ or sedimentary footwall melts. Hulbert (1983) suggested that a sample (M78-53) found in the marginal zone above the Pretoria Group might represent the closest match to the initial "Critical Zone" magma composition. Another fine-grained pigeonite gabbronorite (GR4-4-5) developed above LZ cumulates has similar characteristics. The bulk chemistries of these two rocks are compared with estimated compositions of the parental magmas for the Critical and Main Zones in Table 5 and their pyroxene compositions are compared with GNPA member and MZ compositions in Fig. 10. It is clear that both M78-53 and GR4-4-5 lie closer to the model MZ magma than CZ magma.

If this is correct and these rocks represent chilled tholeiitic (MZ) magma, then it offers a possible explanation for the unique orthopyroxene-clinopyroxene-chromite cumulates and the lack of mineralogical or geochemical similarity between the GNPA member and the UCZ in the rest of the complex. Where the marginal member rests on the LZ, Hulbert (1983) cited the fine grain size, the abundance of pigeonite and rapid reversal in orthopyroxene compositions from Mg#₈₄ in the last LZ harzburgite to Mg#₆₇₋₇₁ just above the contact (Fig. 9) as evidence for undercooling and crystallisation of new liquid to form the marginal gabbronorites.

Hulbert (1983) observed at least five cyclic sub-units within the marginal member, each with a fine-grained basal gabbronorite. Skeletal plagioclase crystals with trapped melt and orthopyroxenes with Mg#'s close to the bulk Mg# of the rock (e.g. M78-53) suggest rapid supercooling, which becomes less effective upwards. Each sub-unit shows upward increases in the Mg# of orthopyroxene and in the absolute concentrations of Ni, Cu and PGE, which are most enriched in coarser (sometimes pegmatitic) zones above the fine-grained base of each sub-unit. Hulbert (1983) suggested that the marginal member was emplaced as a series of thin pulses of colder, denser liquid at the base of the magma chamber. Model crystallisation of liquids with M78-53 or GR4-4-5 compositions at 1,500 bars in the PELE programme (Boudreau 1999) produces liquidus temperatures of 1210–1230°C and crystallisation sequences of plagioclase, plagioclase-orthopyroxene, then plagioclase as well as both pyroxenes, which mirror the observed textures. The idealised section given by Hulbert

Table 5 Comparison of fine-grained gabbronorite chills with estimated Critical and Main Zone magma compositions.

Sample Position	GR4-4-5 LZ-GNPA	78-53 Pret-GNPA	B1 (LZ/CZ)	B3 (MZ)	Crit Zone	Main Zone	78-92 GNPA-MZ	N3X4A Plat-MZ	SW1-47B Plat-MZ	SW1-47A Plat-MZ
SiO ₂ (wt%)	52.11	49.97	53.17	50.70	55.87	50.48	53.61	51.81	51.44	49.44
TiO ₂	0.10	0.62	0.36	0.41	0.37	0.71	0.34	0.20	0.19	0.16
Al ₂ O ₃	17.31	15.67	11.36	16.03	12.55	15.79	17.36	17.48	16.48	16.30
FeO	5.34	8.82	10.72*	9.14*	9.15*	11.61*	5.13	n/a	n/a	n/a
Fe ₂ O ₃	1.60	2.12	n/a	n/a	n/a	n/a	1.84	9.75*	8.83*	9.04*
MnO	0.15	0.19	0.20	0.17	0.21	0.18	0.13	0.14	0.19	0.15
MgO	8.86	7.77	14.93	9.21	12.65	7.26	7.42	6.48	6.93	8.55
CaO	11.66	10.91	7.47	11.14	7.29	10.86	11.58	11.17	12.06	11.75
Na ₂ O	2.15	2.15	1.57	2.52	1.53	2.20	2.38	1.79	2.43	2.52
K ₂ O	0.67	0.58	0.17	0.23	0.77	0.16	0.58	1.30	0.41	0.43
P ₂ O ₅	0.02	0.10	0.07	0.08	0.10	0.16	0.04	0.01	0.01	0.02
Sc (ppm)	n/a	n/a	n/a	n/a	41	35	n/a	31	38	28
V	90	232	n/a	n/a	179	182	119	191	200	152
Cr	390	396	1240	205	939	335	317	424	292	551
Co	80	88	n/a	n/a	73	53	66	41	48	59
Ni	184	184	337	162	329	128	128	346	407	376
Cu	75	120	n/a	n/a	58	62	23	121	170	187
Rb	30	20	4	7	27	3	13	50	7	12
Sr	385	353	183	324	170	340	275	333	282	234
Y	7	19	15	n/a	n/a	n/a	13	7	12	8
Zr	6	30	47	20	80	60	39	12	5	7
Source	1	1	2	2	3	3	1	4	4	4

Position key: LZ Lower Zone; MZ Main Zone; Plat Platreef; Pret Pretoria Group; GNPA GNPA member

Sources: (1) Hulbert 1983; (2) Sharpe 1981; (3) Barnes and Maier 2002b; (4) this work

* indicates total Fe as FeO or Fe₂O₃ as appropriate

and Von Gruenewaldt (1986) shows the marginal member developed across the LZ cumulates and over the adjacent Pretoria Group quartzites. In this situation, heat loss would have taken place primarily against the quartzites and a thermal gradient extended laterally from this zone into the liquid overlying the LZ cumulates. General coarsening of units upwards from the contact suggests more effective thermal insulation as the member thickened (Hulbert 1983).

Hulbert (1983) noted that pyroxenes in the marginal member overlying the LZ cumulates were more Mg-rich than those developed in the gabbronorites against the Pretoria Group and that abundant sulphides, high PGE and Cr concentrations were also restricted to the marginal member above the LZ. He argued that these features could only be accounted for by adding some residual LZ melt to the new liquid as the marginal member developed. This may also provide a mechanism to generate the unusual orthopyroxene-clinopyroxene-chromite cumulates associated with the "UG2-like" chromitite (Fig. 9). In addition to the unusual crystallisation order, these units are very rich in Cr (2,500–28,500 ppm) and it is hard to see how to generate them from liquids similar to M78-53 (with < 400 ppm Cr) alone. We suggest that mixing the new tholeiitic liquid with an existing volume of overlying resident LZ-type magma crystallising olivine, orthopyroxene (Mg#₈₄₋₈₈) and chromite could produce a hybrid magma that crystallises orthopyroxene and chromite, followed by orthopyroxene, chromite and clinopyroxene, which mirrors the observed sequence in the lower part of the GNPA member (Fig. 9). Densities calculated in PELE for melts of M78-53 and GR4-4-5 at 1,500 bars are 2.71

and 2.65 g.cm⁻³, respectively, and may be sufficiently high to displace a hotter (> 1,270°C) LZ-type liquid upwards in the manner suggested by Tegner et al. (1993). Undercooling of the resident LZ-type liquid by repeated injections of colder liquid at the base, coupled with gradual heating of the new liquid as thermal insulation of the thickening marginal member becomes more efficient would lower the temperature gradient and the density contrast to the point where the mafic and tholeiitic liquids might mix.

A second cycle with basal orthopyroxenite and orthopyroxene-clinopyroxene-chromite cumulates occurs higher in the sequence at the zero reference, and a third one at + 75 metres is overlain by anorthosite (Fig. 9). These orthopyroxene-rich cumulates are additionally important because they carry sulphides and associated Pd-rich PGE mineralisation. Decreasing volumes of orthopyroxene-clinopyroxene-chromite cumulates and the trend of Ti enrichment in chromite developed with height probably reflect diminishing volumes of mafic magma available for mixing as the chamber becomes swamped with tholeiitic magma. Peck and Keays (1990) have independently proposed a similar process, involving injection of small volumes of gabbroic liquid into a larger volume of ultramafic magma, to explain the development of thin layers of chromite gabbronorite in harzburgites of the Heazlewood River Complex.

We suggest that the explanation for why the orthopyroxene-clinopyroxene-chromite cumulates are unique to the northern lobe is because these two magma types do not mix together in this manner elsewhere in the Bushveld Complex. The process outlined here is similar in some respects to the mixing of ultramafic (U-type) and

tholeiitic (T-type) magmas proposed by Irvine and Sharpe (1986) for the origin of stratiform chromitite and PGE reefs, including the Merensky Reef. The principal difference lies in the nature of the U-type magma and the degree of interaction. The Critical Zone in the eastern and western lobes preserves chemical and isotopic signatures inherited from the LZ and the new, distinctively Pt-rich, magma(s) which hybridised with it during the formation of the UCZ. The base of the UCZ marks the change from olivine-orthopyroxene cumulates to a chromite-orthopyroxene-plagioclase liquidus order, which persists throughout the UCZ, until the introduction of MZ magma coincident with the formation of the Merensky Reef (Kruger 1994), where the last cumulus chromite appears. Mass balance modelling by Barnes and Maier (2002b) suggests that the Merensky event involved ~40% tholeiitic magma mixed with ~60% UCZ-type magma crystallising orthopyroxene and plagioclase.

In the northern lobe, we suggest that there was no distinctive Pt-rich magma and no intermediate stage where the liquidus order shifted from olivine-orthopyroxene to chromite-orthopyroxene-plagioclase. The GNPA member formed by a series of rapid and dramatic interactions between progressively larger volumes of new tholeiitic liquid and a resident LZ-type liquid. In addition, we suggest that the tholeiitic and mafic liquids are derived from different sources with different isotopic signatures (see below) and within a few mixing/quenching interactions following the first introduction of the tholeiitic liquid, the reservoir of mafic liquid was exhausted or it ceased to be supplied to the chamber. Magmatic evolution beyond that point is controlled by the chemistry of the dominant tholeiitic liquid which later formed the MZ of the northern lobe.

Further support for the involvement of tholeiitic magma comes from the rocks at the top contact of the GNPA member. Above a prominent mottled anorthosite which caps the member, Hulbert (1983) found a 1–2-m thick layer of medium-grained gabbro (sample 78 92) with distinctive radiating clusters of acicular plagioclase and inverted pigeonite. He interpreted this as an influx of new MZ magma which supercooled and chilled against the GNPA cumulates. The composition of 78 92 is close to the chilled rocks at the base of the GNPA member (Table 5). This can only be explained if MZ-type magma was involved prior to, during, and after the formation of the GNPA member.

This interpretation apparently contradicts the view that there was major hiatus between the emplacement of the magmas of the LZ and the MZ (Van der Merwe 1978). Field evidence cited to support this is based on apparently transgressive relationships established between LZ intrusives and the Platreef north of Mokopane that are not in dispute, plus the assignment of the GNPA member to a pre-Platreef UCZ, which is disputed. Fundamentally, van der Merwe's model rests on two assumptions; first, that the LZ was fully crystallised (not just the satellite intrusions where the transgressive relationships occur) and second, that the

Platreef and the GNPA member are unrelated to the LZ. The evidence presented above suggests that mafic liquid remained in the Grasvally magma chamber up to the development of the GNPA member and it is possible that supply of magma into the northern satellite chambers ceased while mafic magma continued to enter the Grasvally chamber. The role of LZ magma in the formation of the Platreef is discussed in the next section.

Links between the GNPA member and the Platreef

The exact relationship between the Platreef and the LZ and the GNPA member to the north of the Grasvally area is poorly known and will only be revealed as further exploration takes place on farms between Grasvally and Mokopane. Hammerbeck and Schürmann (1998) indicate that the "Critical Zone" wedges out to the south of Mokopane but Von Gruenewaldt et al. (1989) equated xenolith-rich portions of the GNPA member with the Platreef and implied that one might merge laterally into the other; a proposal supported by the data presented here. Kinnaird et al. (2005) report that north of Mokopane, LZ rocks may occur below the Platreef but the LZ appears to wedge out on the farm Macalacaskop 243KR and the Platreef rests directly on metasedimentary footwall from Macalacaskop northwards to Zwartfontein. Indeed it seems more than a coincidence that the modal mineralogy of the GNPA member orthopyroxene and orthopyroxene-clinopyroxene cumulates (55–60% opx, 15–25% plag, 20–25% cpx), the crystallisation order, orthopyroxene compositions (Mg_{70-78} ; Fig. 10) and Pd-dominant PGE mineralisation are similar to the Platreef at Sandsloot at many of the localities described above. Orthopyroxene-clinopyroxene-chromite cumulates, apparently similar to those that occur in the GNPA member, occur in the Platreef on the farm Overysel 815LR (Hulbert 1983).

It is also possible that the contacts between the GNPA member and the Platreef with the base of the MZ may correlate along strike. At Sandsloot, the unshered contact with the hanging wall MZ gabbros is marked by leuconorite ("mottled anorthosite") and a fine to medium-grained gabbro (Fig. 6). This unit contains traces of inverted pigeonite, PGE grade up to 2.0 g/t, and a PGM assemblage containing laurite (RuS_2) and Pd-bearing pentlandite that is very different from that in the Platreef (Holwell et al. 2004). On Turfspruit 241KR, Kinnaird et al. (2005) observed that the upper contact of the Platreef with the MZ is marked by a prominent mottled anorthosite and on Drenthe 788LR, inverted pigeonite is also found in the MZ immediately above the Platreef (Gain and Mostert 1982). These associations are remarkably similar to the rocks at the contact between the MZ and GNPA member at Grasvally (Hulbert 1983). The chemistry of fine-grained gabbroites from just above the Platreef are compared with a MZ chill against the GNPA cumulates (78 92) in Table 5. These

rocks are separated by ~40 km (Fig. 1) but the match between their major and trace element signatures is striking and suggests that chilled MZ magma may terminate both the GNPA member and the Platreef. The presence of PGE in the MZ basal chill zone further suggests that the quenching of MZ magma may be an important trigger for the development of PGE-rich zones around rafts of disaggregated country rock in the MZ (e.g. on Drenthe 788LR and other farms).

In the light of the above, the finding by Barton et al. (1986) that orthopyroxene separated from the Platreef has an $^{87}\text{Sr}/^{86}\text{Sr}$ initial ratio of 0.7079 may be highly significant. Barton et al. (1986) suggested that even this should be considered an upper limit because of the possibility that the pyroxene separates contained traces of plagioclase with elevated $^{87}\text{Sr}/^{86}\text{Sr}$ initial ratios influenced by late-stage melts or fluids derived from the footwall. The MZ magma in the northern lobe shows $^{87}\text{Sr}/^{86}\text{Sr}$ initial ratios in the range 0.708–0.710 (Barton et al. 1986). Data for the Lower LZ in the northern lobe is lacking but if one assumes that this magma had a similar initial ratio to LZ rocks in the western Bushveld (0.705–0.707; Kruger 1994), then the lowest initial ratio of 0.7079 found by Barton et al. (1986) in the Platreef is consistent with a mixture of MZ-type and LZ-type magmas. In the absence of further geochemical data, particularly REE and isotopes from the GNPA member and elsewhere on the Platreef, the proposed link between the two must be considered possible, but unproven, at this stage. Nevertheless, the similarity is intriguing and underlines the need for further research into these rocks.

Implications for connectivity between the northern lobe and the rest of the Bushveld Complex

Cawthorn and Webb (2001) concluded that the eastern and western lobes were linked throughout the development of the Critical, Main and Upper Zones but that links with other lobes, including the northern lobe, were less certain and had to remain speculative. Kruger (1999, 2003), following the conventional stratigraphy, considered the northern lobe to have been linked with the eastern and western lobes during UCZ and MZ times. In his model, a mixed MZ and UCZ magma flows north across the chamber, overtops the Thabazimbi-Murchison Lineament (locally manifested as the Zebediela and Ysterberg-Planknek Faults; Fig. 1) and flows into the northern lobe, generating the Platreef along the base. LZ-type magma plays no role in forming the Platreef.

This work has shown that the conventional stratigraphic interpretation shown in Fig. 3 is untenable. The "Critical Zone" of the northern lobe, incorporating the "UG2-like" chromitite and Platreef cannot be correlated with the UG2-Merensky Reef package in the rest of the complex. The UCZ-type magma with its high Mg/Fe ratios, chromite-orthopyroxene-plagioclase-clinopyroxene crystallisation sequence and distinctive Pt enrichment did not play a role in the development of the

GNPA member or the Platreef. The orthopyroxene-clinopyroxene-chromite cumulates of the GNPA member and the Pd-dominant PGE mineralisation contained in it and the Platreef are unique to the northern lobe of the complex. Their origin requires different magmatic components.

We interpret the available evidence to suggest that the GNPA member and the Platreef may represent a transitional period where the earliest tholeiitic MZ-type magmas interacted with pre-existing mafic LZ-type magmas. It should perhaps be renamed the Transitional Zone of the northern lobe. The questions of when these two major magma types were introduced into the northern lobe, how their introduction relates to emplacement of magmas in the eastern and western lobes, and how their interaction might have generated the mass of PGE present in the GNPA member and the Platreef all remain unclear at this time and need further research.

In our view, the Merensky Reef and the Platreef formed from compositionally different magmas with different lineages and there is no genetic link between them. The possibility remains that introduction of tholeiitic magma into the northern lobe took place at the same time as into the eastern and western lobes but this cannot be proved unequivocally and a reliable time line cannot be drawn between the Merensky Reef and the Platreef. The "Critical Zone" of the northern lobe is not the Critical Zone as known from the rest of the Bushveld Complex. The former term is confusing and should be discontinued. There may be a reliable link between lobes in the Upper Zone at the level of the Main Magnetite (Fig. 3), but it remains to be established how closely the stratigraphy of the MZ of the northern lobe matches that seen in the rest of the complex. The northern lobe may have been completely separated from the rest of the complex until intrusion of the Upper Zone. The stratigraphy of the northern lobe must be evaluated on its own merits, without premature attempts to fit it into that established elsewhere.

Conclusions

This work has shown that the Platreef and the GNPA member, long thought to correlate with the Merensky Reef and the UCZ elsewhere in the complex, formed from a different magma than that which generated the UCZ in the eastern and western lobes of the complex. The Platreef and the GNPA member show pyroxene compositions that are systematically more Fe-rich and PGE signatures that are more fractionated and more Pd-rich than the Merensky Reef and other reefs of the UCZ. This work demonstrates that UCZ magma, with its characteristic and economically significant Pt enrichment, was not involved in the generation of the Platreef and that there is no compelling evidence linking the formation of the Platreef either genetically or temporally with the Merensky Reef.

Chilled MZ-type magma is preserved at the base and the top of the GNPA member and this unit is suggested to have formed from the mixing of existing LZ-type magma and new tholeiitic MZ-type magma that first intruded along the floor of the Grasvally chamber. Mixing/quenching events produced a series of orthopyroxenites that grade upwards into orthopyroxene-clinopyroxene-chromite cumulates that are unique to this area of the complex. The basal orthopyroxenites are invariably associated with the presence of sulphide and elevated base metal and PGE values. The GNPA member rocks show similarities in terms of mineral chemistries, modal mineralogy, crystallisation sequences, and PGE ratios with Platreef rocks and a compositionally similar MZ liquid is chilled against the top of both the GNPA member and the Platreef. These similarities open up the possibility that the Platreef and GNPA member merge laterally into one another and that both result from interactions between MZ and LZ-type magmas.

On a final note, although we have demonstrated that Wagner's original link between the Platreef and the Merensky Reef may be incorrect, it would be unjust to be overly critical of him. The visual similarity between the two reefs is striking and this, coupled with the apparently unlikely possibility that there could be another fantastically rich platinum horizon in addition to the Merensky Reef, must have played a part in forming his opinion. The fact that the assumed link has remained unchallenged for so long is surely a measure of the immense respect that Wagner's pioneering work still commands 75 years after his death.

Acknowledgements The authors would like to thank the staff at Anglo Platinum's Sandsloot Mine, particularly Alan Bye and Alfred Sarila, for logistical support during the mapping and sampling. Eveline de Vos and Peter Fisher are thanked for their assistance with the ICP and SEM analyses at Cardiff and Terry Williams, John Spratt and Anton Kearsley are thanked for their assistance with analytical work by Paul Armitage at the Natural History Museum. Wes Gibbons and Jock Harmer are thanked for their advice and input. The paper benefited from constructive reviews by Chris Lee and Tony Naldrett. Tony Naldrett also kindly made available his unpublished PGE assays from Drenthe for use in Table 4 and this is greatly appreciated. This research makes new use of Larry Hulbert's remarkable 1983 DSc thesis and re-interprets his work into the GNPA member in the light of new data. The authors would like to thank Wolf Maier for helping us to obtain a copy of this thesis. Key elements of this paper could not have been assembled without Dr Hulbert's original work and we are extremely grateful to have had access to it. We accept full responsibility for our conclusions (and any errors in interpretation), particularly where they differ from the original. Paul Armitage's PhD research was funded by the University of Greenwich. David Holwell's PhD research is funded by the NERC and supported by Anglo Platinum through Industrial CASE project (NER/S/C/2003/11952). PGE analytical work at Cardiff is supported by the Leverhulme Trust (grant F/00407/K to IMcD) and the ICP laboratory is supported by the NERC, through Joint Infrastructure Fund award NER/H/S/2000/00862. Finally, the first author would like to thank Steph and Robbie for their patience and support throughout the completion of this work.

References

- Armitage PEB, McDonald I, Edwards SJ, Manby GM (2002) Platinum-group element mineralisation in the Platreef and calc-silicate footwall at Sandsloot, Potgietersrus district, South Africa. *Appl Earth Science (Trans Inst Min Metall B)* 111:B36-B45
- Ballhaus C, Sylvester P (2000) Noble metal enrichment processes in the Merensky Reef, Bushveld Complex. *J Petrol* 41:545-561
- Barnes SJ, Maier WD (2002a) Platinum-group element distributions in the Rustenburg Layered Suite of the Bushveld Complex, South Africa. In: Cabri L (ed) *The geology, geochemistry, mineralogy and mineral beneficiation of the platinum-group elements*. *Can Inst Min Metall Special Volume* 54:431-458
- Barnes SJ, Maier WD (2002b) Platinum-group elements and microstructures of normal Merensky Reef from Impala Platinum Mine, Bushveld Complex. *J Petrol* 43:103-128
- Barnes SJ, Maier WD (2002c) Platinum-group elements in the Upper Zone of the Rustenburg Layered Suite of the Bushveld Complex: preliminary results from the Bellevue Borehole. In: 9th international platinum symposium, Billings, Montana, (abstract)
- Barton JM, Cawthorn RG, White J (1986) The role of contamination in the evolution of the Platreef of the Bushveld Complex. *Econ Geol* 81: 1096-1104
- Boudreau AE (1999) PELE—A version of the MELTS software program for the PC platform. *Comput Geosci* 25:21-203
- Buchanan DL, Rouse JE (1984) Role of contamination in the precipitation of sulphides in the Platreef of the Bushveld Complex. In: Buchanan DL, Jones MJ (eds) *Sulphide deposits in mafic and ultramafic rocks*. *Inst Min Metall, Lond*, pp 141-146
- Buchanan DL, Nolan J, Suddaby P, Rouse JE, Viljoen MJ, Davenport JWJ (1981) The genesis of sulfide mineralisation in a portion of the Potgietersrus lobe of the Bushveld Complex. *Econ Geol* 76:568-579
- Bye AR (2001) Mining the Platreef. *Appl Earth Science (Trans Inst Min Metall B)* 110:B209-B210
- Cameron EN (1982) The upper critical zone of the Eastern Bushveld Complex - precursor of the Merensky Reef. *Econ Geol* 77:1307-1327
- Cawthorn RG (1996) Re-evaluation of magma compositions and processes in the uppermost Critical Zone of the Bushveld Complex. *Min Mag* 60: 131-148
- Cawthorn RG (1999a) The platinum and palladium resources of the Bushveld Complex. *S Afr J Sci* 95:481-489
- Cawthorn RG (1999b) Platinum-group element mineralisation in the Bushveld Complex - a critical reassessment of geochemical models. *S Afr J Geol* 102:268-281
- Cawthorn RG (2002) Delayed accumulation of plagioclase in the Bushveld Complex. *Min Mag* 66:881-893
- Cawthorn RG, Lee CA (1998) Field excursion guide to the Bushveld Complex. In: 8th international platinum symposium. *Geol Soc South Africa and S African Inst Min Metall*, p 113
- Cawthorn RG, Webb SJ (2001) Connectivity between the western and eastern lobes of the Bushveld Complex. *Tectonophysics* 330:195-209
- Cawthorn RG, Barton JM Jr, Viljoen MJ (1985) Interaction of floor rocks with the Platreef on Overysel, Potgietersrus, northern Transvaal. *Econ Geol* 80:988-1006
- Cawthorn RG, Merkle RK, Viljoen M (2002a) Platinum-group element deposits in the Bushveld Complex, South Africa. In: Cabri L (ed) *The geology, geochemistry, mineralogy and mineral beneficiation of the platinum-group elements*. *Can Inst Min Metall* 54:389-429
- Cawthorn RG, Lee CA, Schouwstra RP, Mellowship P (2002b) Relationship between PGE and PGM in the Bushveld Complex. *Can Mineral* 40:311-328

- Chaumba JB, Harris C, Tredoux M, Reisberg L, Arndt NT (1998) Oxygen, strontium and osmium isotope geochemistry of the Platreef of the northern lobe of the Bushveld Complex, South Africa. In: 8th international platinum symposium, S African Inst Min Metall Symposium Series S18:71-72
- Davies G, Tredoux M (1985) The platinum-group element and gold contents of marginal rocks and sills of the Bushveld Complex. *Econ Geol* 80: 838-848
- Eales HV, Botha WJ, Hattingh PJ, de Klerk WJ, Maier WD, Odgers ART (1993) The mafic rocks of the Bushveld Complex. *J Afr Earth Sci* 16: 121-142
- Gain SB, Mostert AB (1982) The geological setting of the platinoid and base metal sulphide mineralisation in the Platreef of the Bushveld Complex on Drenthe, north of Potgietersrus. *Econ Geol* 77:1395-1404
- Hammerbeck EC1, Schürmann LW (1998) Nickel. In: Wilson MGC, Anhaeuser CR (eds) *The Mineral Resources of South Africa. Coun Geosci Handbook* 16:471-482
- Harmer RE, Sharpe MR (1985) Field relations and strontium isotope systematics of the marginal rocks of the Eastern Bushveld Complex. *Econ Geol* 80:813-837
- Harris C, Chaumba JB (2001) Crustal contamination and fluid-rock interaction during the formation of the Platreef, northern lobe of the Bushveld Complex, South Africa. *J Petrol* 42:1321-1347
- Harris C, Pronost JM, Ashwal LD, Cawthorn RG (2004) Oxygen and hydrogen isotope stratigraphy of the Rustenburg Layered Suite, Bushveld Complex: constraints on crustal contamination. *J Petrol* 46:579-601
- Hart SR, Kinloch ED (1989) Osmium isotope systematics in Witwatersrand and Bushveld ore deposits. *Econ Geol* 84:1651-1655
- Holwell DA (2002) Base-metal sulphide geochemistry of the Merensky Reef, Bushveld Complex. MSc dissertation, Cambridge School of Mines, (unpublished)
- Holwell DA, McDonald I, Armitage PEB (2004) Platinum-group mineral assemblages in the Platreef at Sandsloot Mine, Limpopo Province, South Africa. *Geoscience Africa*, University of the Witwatersrand, 12-16 July 2004 (abstract)
- Hulbert LJ (1983) A petrographical investigation of the Rustenburg Layered Suite and associated mineralisation south of Potgietersrus. DSc dissertation, University of Pretoria, (unpublished)
- Hulbert LJ, Von Gruenewaldt G (1982) Nickel, copper and platinum mineralisation in the Lower Zone of the Bushveld Complex, south of Potgietersrus. *Econ Geol* 77:1296-1306
- Hulbert LJ, Von Gruenewaldt G (1985) Textural and compositional features of chromite in the lower and critical zones of the Bushveld Complex south of Potgietersrus. *Econ Geol* 80:872-895
- Hulbert LJ, Von Gruenewaldt G (1986) The structure and petrology of the upper and lower chromitite layers on the farms Grasvally and Zoetveld, south of Potgietersrus. In: Anhaeuser CR, Maske S (eds) *Mineral Deposits of Southern Africa*. *Geol Soc South Africa, Johannesburg*, 2:1237-1249
- Hutchinson D (2001) The origin and distribution of platinum-group mineralisation in the oceanic upper mantle: a comparison of samples from the Lizard and Troodos ophiolite complexes and dredge samples from the Tonga trench. PhD thesis, Cardiff University, (unpublished)
- Irvine TN, Sharpe MR (1986) Magma mixing and the origin of stratiform oxide ore zones in the Bushveld and Stillwater complexes. In: Gallagher MJ, Ixer RA, Neary CR, Prichard HM (eds) *Metallogeny of Basic and Ultrabasic rocks*. Inst Min Metall, Lond, pp 183-198
- Kinloch ED (1982) Regional trends in the platinum-group mineralogy of the critical zone of the Bushveld Complex, South Africa. *Econ Geol* 77: 1328-1347
- Kinloch ED, Peyerl W (1990) Platinum-group minerals in various rock types of the Merensky Reef, genetic implications. *Econ Geol* 85:537-555
- Kinnaird JA, Nex PAM (2003) Mechanisms of marginal mineralisation in the Bushveld Complex. *Appl Earth Science (Trans Inst Min Metall B)* 112: B206-B208
- Kinnaird JA, Kruger FJ, Nex PAM, Cawthorn RG (2002) Chromitite formation – a key to understanding processes of platinum enrichment. *Appl Earth Science (Trans Inst Min Metall B)* 111: B23-B35
- Kinnaird JA, Hutchinson D, Schürmann L, Nex PAM, de Lange R (2005) Petrology and mineralisation of the southern Platreef: northern limb of the Bushveld Complex, South Africa. *Mineral Deposita* (this volume)
- Kruger FJ (1994) The Sr-isotopic stratigraphy of the western Bushveld Complex. *S Afr J Geol* 97:393-398
- Kruger FJ (1999) The Bushveld Complex unconformity related ore deposits: an isotopic perspective. In: Stanley CJ et al (eds) *Mineral deposits: processes to processing*. Balkema, Rotterdam, pp 737-738
- Kruger FJ (2003) Filling the Bushveld Complex magma chamber: intra-chamber magma dynamics and the generation of giant chromite and PGE deposits. *Appl Earth Science (Trans Inst Min Metall B)* 112: B208-B209
- Kruger FJ, Marsh JS (1985) The mineralogy, petrology and origin of the Merensky Cyclic Unit in the Western Bushveld Complex. *Econ Geol* 80: 958-974
- Lee CA (1996) A review of mineralisation in the Bushveld Complex and some other layered intrusions. In: Cawthorn RG (ed) *Layered intrusions*. Elsevier, Amsterdam, pp 103-146
- Maier WD, Barnes SJ (1998) Concentrations of rare earth elements in silicate rocks of the Lower, Critical and Main Zones of the Bushveld Complex. *Chem Geol* 150:85-103
- Maier WD, Barnes SJ (1999) Platinum-group elements in silicate rocks of the Lower, Critical and Main Zones at Union Section, Western Bushveld Complex. *J Petrol* 40:1647-1671
- Maier WD, Eales HV (1994) A facies model for the interval between the UG2 chromitite and Merensky Reef, western Bushveld Complex. *Appl Earth Science (Trans Inst Min Metall B)* 103: B22-B30
- McCandless TE, Ruiz J (1991) Osmium isotopes and crustal sources for platinum-group mineralisation in the Bushveld Complex, South Africa. *Geology* 19:1225-1228
- McDonald I, Irvine GJ, de Vos E, Gale AS, Reimold WU (2005) Geochemical search for impact signatures in possible impact-generated units associated with the Jurassic-Cretaceous boundary in southern England and northern France. In: Cockell C, Gilmour I, Koeberl C (eds) *Biological Processes Associated with Impacts*. Springer, Berlin, Heidelberg, New York pp 101-131
- van der Merwe MJ (1976) The layered sequence of the Potgietersrus lobe of the Bushveld Complex. *Econ Geol* 71:1337-1351
- van der Merwe MJ (1998) Platiniferous horizons of the Potgietersrus lobe of the Bushveld Complex. In: 8th international platinum symposium. S Afr Inst Min Metall Symposium Series S18:407-409
- Naldrett AJ, Gasparrini EC, Barnes SJ, von Gruenewaldt G, Sharpe MR (1986) The Upper Critical Zone of the Bushveld Complex and a model for the origin of Merensky-type ores. *Econ Geol* 81:1105-1118
- Peck DC, and Keays RR (1990) Geology, geochemistry and origin of platinum-group element-chromite occurrences in the Heazlewood River Complex, Tasmania. *Econ Geol* 85:765-793
- Schiffries CM (1982) The petrogenesis of a platiniferous dunite pipe in the Bushveld Complex: infiltration metasomatism by a chloride solution. *Econ Geol* 77:1439-1453
- Secon R, Mitchell AA (2002) The Merensky Reef at Winnarshoek, Eastern Bushveld Complex: insights from a wide reef facies. In: Boudreau A (ed) 9th international platinum symposium, extd abstracts, Billings, Montana, pp 401-404
- Sharpe MR (1981) The chronology of magma influxes to the eastern compartment of the Bushveld Complex as exemplified by its marginal border groups. *J Geol Soc Lond* 138:307-326
- Stumpfl EF, Rucklidge JC (1982) The platiniferous pipes of the Eastern Bushveld. *Econ Geol* 77:1419-1431
- Taylor SR, McLennan SM (1985) *The continental crust: its composition and evolution*. Blackwell, Oxford

- Tegner C, Wilson JR, Brooks CK (1993) Intraplutonic quench zones in the Kap Edvard Holm layered gabbro complex, East Greenland. *J Petrol* 34: 681-710
- Tredoux M, Lindsay NM, Davies G, McDonald J (1995) The fractionation of the platinum-group elements in magmatic systems with the suggestion of a novel causal mechanism. *S Afr J Geol* 98:157-167
- Vermaak CF (1995) The Platinum-Group Metals—A Global Perspective. Mintek, Randburg
- Vermaak CF, Hendriks LP (1976) A review of the mineralogy of the Merensky Reef, with specific reference to new data on the precious metal mineralogy. *Econ Geol* 71:1244-1268
- Viljoen MJ, Schürmann LW (1998) Platinum-group metals. In: Wilson MGC, Anhaeusser CR (eds) *The mineral resources of South Africa. Coun Geosci Handbook* 16:532-568
- Viljoen MJ, Seoon RN (1985) The distribution and main geologic features of discordant bodies of iron-rich ultramafic pegmatite in the Bushveld Complex. *Econ Geol* 80:1109-1128
- Von Gruenewaldt G, Hulbert LJ, Naldrett AJ (1989) Contrasting platinum-group element concentrations in cumulates of the Bushveld Complex. *Mineral Deposita* 24:219-229
- Wagner PA (1929) *The platinum deposits and mines of South Africa*. Oliver and Boyd, Edinburgh
- White JA (1994) The Potgietersrus prospect - geology and exploration history. In: Anhaeusser CR (ed) *Proceedings XVth CMMI Congress*. S Afr Inst Min Metall, Johannesburg, vol. 3, pp 173-181
- Willemsse J (1969) The geology of the Bushveld Complex: the largest repository of magmatic ore deposits in the world. *Econ Geol Monograph* 4: 1-22

